REPORT UAG-83 PART I

WORLD DATA CENTER A
for
Solar-Terrestrial Physics

SOLAR-GEOPHYSICAL ACTIVITY REPORTS
for
September 7-24, 1977 and November 22, 1977

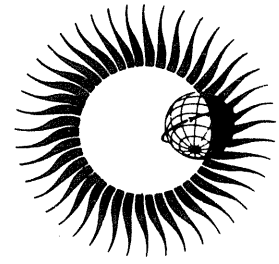

February 1982

WORLD DATA CENTER A
National Academy of Sciences
2101 Constitution Avenue, NW
Washington, D.C. 20418 USA

World Data Center A consists of the Coordination Office and the following seven Subcenters:

COORDINATION OFFICE
World Data Center A
National Academy of Sciences
2101 Constitution Avenue, NW
Washington, D.C. 20418 USA
[Telephone: (202) 334-3359]

GLACIOLOGY (Snow and Ice)
World Data Center A: Glaciology (Snow and Ice)
Cooperative Inst. for Research in Environmental Sciences
University of Colorado
Boulder, Colorado 80309 USA
[Telephone: (303) 492-5171]

METEOROLOGY (and Nuclear Radiation)
World Data Center A: Meteorology
National Climatic Center
Federal Building
Asheville, North Carolina 28801 USA
[Telephone: (704) 258-2850, ext. 381]

OCEANOGRAPHY
World Data Center A: Oceanography
National Oceanic and Atmospheric Administration
2001 Wisconsin Avenue, NW
Page Bldg. 1, Rm. 414
Washington, D.C. 20235 USA
[Telephone: (202) 634-7249]

ROCKETS AND SATELLITES
World Data Center A: Rockets and Satellites
Goddard Space Flight Center
Code 601
Greenbelt, Maryland 20771 USA
[Telephone: (301) 344-6695]

ROTATION OF THE EARTH
World Data Center A: Rotation of the Earth
U.S. Naval Observatory
Washington, D.C. 20390 USA
[Telephone (202) 254-4547]

SOLAR-TERRESTRIAL PHYSICS (Solar and Interplanetary Phenomena, Ionospheric Phenomena, Flare-Associated Events, Geomagnetic Variations, Aurora, Cosmic Rays, Airglow):

World Data Center A for Solar-Terrestrial Physics
Environmental Data and Information Service, NOAA, D63
325 Broadway
Boulder, Colorado 80303 USA
[Telephone: (303) 497-6323]

SOLID-EARTH GEOPHYSICS (Seismology, Tsunamis, Gravimetry, Earth Tides, Recent Movements of the Earth's Crust, Magnetic Measurements, Paleomagnetism and Archeomagnetism, Volcanology, Geothermics):

World Data Center A for Solid-Earth Geophysics
Environmental Data and Information Service, NOAA, D62
325 Broadway
Boulder, Colorado 80303 USA
[Telephone: (303) 497-6521]

World Data Centers conduct international exchange of geophysical observations in accordance with the principles set forth by the International Council of Scientific Unions. WDC-A is established in the United States under the auspices of the National Academy of Sciences. Communications regarding data interchange matters in general and World Data Center A as a whole should be addressed to World Data Center A, Coordination Office (see address above). Inquiries and communications concerning data in specific disciplines should be addressed to the appropriate subcenter listed above.

SUBSCRIPTION PRICE TO UAG REPORT SERIES: $40.00 a year; $23.00 additional for foreign mailing; single copy price varies. Checks and money orders should be made payable to the Department of Commerce, NOAA/NGSDC. Remittance and correspondence regarding subscriptions should be sent to the National Geophysical and Solar-Terrestrial Data Center, NOAA, D63, 325 Broadway, Boulder, Colorado 80303 USA.

WORLD DATA CENTER A
for
Solar-Terrestrial Physics

REPORT UAG-83 PART I

SOLAR-GEOPHYSICAL ACTIVITY REPORTS
for
September 7-24, 1977 and November 22, 1977

compiled by

John A. McKinnon and J. Virginia Lincoln
WDC-A for Solar-Terrestrial Physics
Boulder, Colorado 80303 USA

February 1982

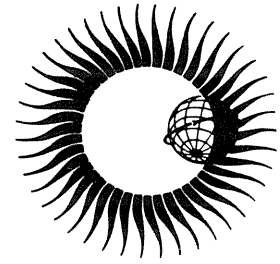

Published by World Data Center A for
Solar-Terrestrial Physics, NOAA, Boulder, Colorado
and printed by

U.S. DEPARTMENT OF COMMERCE
NATIONAL OCEANIC AND ATMOSPHERIC ADMINISTRATION
ENVIRONMENTAL DATA AND INFORMATION SERVICE
Boulder, Colorado, USA 80303

FORWORD

This exhaustive case study of an unusual period of solar-terrestrial activity (September and November 1977) is a truly cooperative international effort. It contains data reports from 116 individuals and groups throughout the world, giving details of the solar activity itself and its consequences in the interplanetary medium and the Earth's vicinity that far exceed those normally exchanged through the World Data Centers. The quantity of data contributed is amazing, yet it probably represents only a modest fraction of what exists. A by-product of this effort is its service as an index to (or perhaps more a reminder of) those groups that are active in monitoring and performing special experiments in the Solar-Terrestrial Physics (STP) disciplines.

The covered period excited the STP community for a number of reasons. It was the first period of outstanding STP activity since the 1976 solar cycle minimum. Of course, a solar minimum happens every 11 years and by itself is not exciting to any but the newest workers in the field, but this was a time of unusual activity for this (or any) stage of the solar cycle. There were two cosmic ray ground level events (GLEs) in September and one in November, with the November increase being the largest since 1960. The Sun was dominated by one active region, McMath 14943, which contained an old cycle spot group that Helen Dodson Prince had contemporaneously termed "ambiguous". The region was 2 days past the west limb when the second September GLE occurred, but the disk at that time was bland. There was therefore an opportunity to study in detail the major interplanetary and terrestrial effects of a solar activity situation that was not complicated, as it usually is, by several possible sources of enhanced solar radiation and particle emission. The phenomena seem to have been well observed and the November 22 events fortuitously came during a planned period of intensive observation, Interval Number 4 of the Study of Traveling Interplanetary Phenomena (STIP).

This was, in effect, a self-declared interval for special study; it was first suggested by Dodson Prince and then by the leaders of the STIP program of SCOSTEP. The plan for a special data compendium was endorsed by the MONSEE Steering Committee of SCOSTEP and a call for contributions was issued by the World Data Center A (WDC-A) for STP in January 1978. The response was literally overwhelming, to a degree that the editorial staff of WDC-A was swamped to the point of embarrassment. We take comfort in knowing that the phenomena were unique, at least thus far in our experiences with STP activity, and so the data reports should not become outdated.

This compilation has been a labor of love for John McKinnon and more recently for the retired long-time leader of WDC-A for STP, J. Virginia Lincoln. They have had much help from Helen Coffey and others in the technical editing of the data reports which were submitted in all variations of the English language. William Winkler, the chief editor for the Data Center, prepared the manuscript for publication, a not inconsiderable job. Others who have helped include Susan Godeaux and Carol Weathers. There has been welcome financial assistance from the U.S. Air Force Geophysical Laboratory. The delay in publication is regrettable, but some comfort can be taken that resources were indeed found in difficult times to complete the project and that the perseverance, especially of Miss Lincoln, prevailed. We think this project will have a lasting influence.

A.H. Shapley
Chair MONSEE Steering Committee
ICSU Scientific Committee on Solar-Terrestrial Physics

TABLE OF CONTENTS

TABLE OF CONTENTS

*Article covers both the September and November events.

Table of Contents (Continued)

Table of Contents (Continued)

1. SOLAR REGION OF SEPTEMBER 7-24, 1977

The Ambiguous Spot Group with CMP September 15, 1977

by

Helen W. Dodson, E. Ruth Hedeman, and Orren C. Mohler
McMath-Hulbert Observatory
University of Michigan

Data Relating to the September 15, 1977 Spot Group

On September 15, 1977, a relatively large spot group crossed the central meridian of the Sun. Its mean area was ≃ 700 millionths of the solar hemisphere and its maximum area was ≃ 1100 millionths. The spot group occurred at a latitude of N08. Polarity measurements at Mt. Wilson indicated a δ and/or γ magnetic classification. Magnetograms at Kitt Peak and Mt. Wilson and spot polarity measurements at the McMath-Hulbert Observatory all showed a primarily east-west orientation for the line separating the two polarities, instead of the usual north-south alignment. In our judgment, in September, which was about 1.5 years after the March and June 1976 minimum values in the smoothed Zurich sunspot numbers, neither latitude nor polarity patterns provided clear guidance for definitely associating the region with the old or with the new solar cycle. Its latitude was relatively "high" for old cycle spots at this time in the cycle and relatively "low" for new cycle membership.

The above spot group (Mt. Wilson spot 19849) was in McMath plage 14943. This spot group and plage returned in October as Mt. Wilson spot 19864 and McMath plage region 14979. During the October transit of the disk, the spot group was again classified by Mt. Wilson primarily as γ or δ, but the magnetograms in SGD [1977] showed that it was located in a large active zone north of the equator with a polarity pattern that can be described either as appropriate for the Northern Hemisphere of cycle 20 or reversed for the Northern Hemisphere of new cycle 21. Again, the measurements do not provide clear guidance to the cycle association for this large and important region. Was it primarily an old cycle spot group or was it a new cycle region with "reversed polarity?"

Development of Comparative Data for Six Solar Minima

Because of the possible significance of this center of activity (plage 14943 in September, with its numerous flares, its large size, and its two associated ground level cosmic ray enhancements) to the general development of the current cycle 21, we have sought additional guidance from recorded evaluations of perhaps similar situations in prior solar cycles. This exploration into the past has produced a compilation of data relating to spot areas, polarities and latitudes and to published cycle evaluations for spots in the years near minimum of six solar cycles going back to 1922. The accumulated data reflect bringing together by latitude and time the polarity determinations and cycle associations assigned by Mt. Wilson Observatory staff, and the measurements of spot area published primarily by the Greenwich Observatory. Close attention has been given to the individual evaluations of "old cycle, reversed polarity" and "new cycle, reversed polarity" published by Dr. Nicholson and his successors at Mt. Wilson. Some of the pertinent facts learned from these summaries are recorded in Table 1.

The September 15, 1977 spot developed approximately a year and a half after minimum values in smoothed Zurich sunspot numbers (March and June 1976) and 2 years 10 months after observations of the first confirmed spot of cycle 21 (November 1974). These time intervals will be used to compare the September 15, 1977 spot with spots near minimum in prior solar cycles.

Study of Spots at ≃1.5 Years after Statistical Minimum

Examination of the data indicated that there is nothing atypical in the occurrence of a spot with mean area >500 millionths of the solar hemisphere within 1.5 years after statistical minimum in sunspot numbers. In the past 54 years (6 minima), there have been approximately 20 such spots within this time limit. In prior years, however, those relatively large spots that did emerge shortly after statistical minimum were all at markedly higher latitudes than the 8° of the September 1977 region. Furthermore, all but one of these large spots (March 1945 at latitude 31°) had polarity measurements appropriate for new cycle membership. Thus there is only one case since 1923 of a spot after statistical minimum with area >500 millionths and with old cycle polarity. The latitude of this unusual spot was so high (31°) that it was confidently evaluated as "new cycle with reversed polarity." This summary indicated that there is no precedent in the last 54 years for the occurrence after statistical minimum of an old cycle spot as large as 500 millionths. These statistics suggest that in the absence of reliable contrary evidence, it would seem appropriate to consider the September 15, 1977 region (and its October return) as a center of activity with new cycle membership, but with reversed polarity.

If McMath plage 14943 at latitude N08 is to be considered as a possible new cycle member, it seems desirable to try to find supporting data in earlier minima for the occurrence of new cycle activity at relatively low latitudes and at comparable times in the cycle. For each minimum since 1923 the reports indicate the occurrence of a small number of new cycle spots with latitudes of ≃11°, or somewhat less, within 1.5 years after statistical minimum. In prior minima these low latitude, new cycle spots were all

Table 1. Summary of Data Related to Spots Near Minimum 1922-1977
(Based on reports by Mt. Wilson and Greenwich Observatories)

Statistical Minimum		First New Cycle Spot		Last Large Old Cycle Spot (A>500)		Last Reported Old Cycle Spot		First Large Spot After Min. (A>500)			First Occurrence of Large Spot (A>500) at <10° Lat.		
Cycle	Date	Month	Lat.	Month	Lat.	Month	Lat.	Month	Lat.	Polarity	Month	Lat.	Polarity
15-16	1923 July,Aug.	-13	31°	- 7	05°	+14	06°	+11	32°	N.C.	+35	08°	N.C.
16-17	1933 Sept.	+ 1	27°	- 7	15°	+20	04°	+ 7	29°	N.C.	+38	07°	N.C.
17-18	1944 Feb.	- 9	40°	- 6	16°	+18	02°	+10	22°	N.C.	+34	06°	N.C.
18-19	1954 Apr.	- 8	53°	-12	10°	+13 +19 N.C.,Rev.Pol.	04° 02°	+ 9	36°	N.C.	+39	09°	N.C.
19-20	1964 Oct.	-13	34°	-12	12°	+19	05°	+17	18°	N.C.	+22 Aug. 1966	07°	N.C.
20-21	1976 Mar.	-16	37°	0	08°	+11	03°	+ 5 Aug. 1976	16°	N.C.	+18 Sept. 1977	08°	?

- = months before minimum
+ = months after minimum
N.C. = new cycle polarity

of small area. According to the data that we have been able to assemble for the last 54 years, the September 15, 1977 spot group is the only center of activity, old or new cycle, with mean spot area >500 millionths and latitude as low as 8° within 1.5 years after "statistical" minimum in sunspot numbers.

Study of Spots at ≃2.8 Years after First Observation of New Cycle Spots

It is possible that the development of a new solar cycle depends more on the time elapsed since the first spot of the new cycle appeared than on the time interval since statistical minimum in smoothed sunspot numbers. The first confirmed spot of cycle 21 on the visible solar hemisphere was observed in November 1974, two years and ten months before the September 15, 1977 spot and plage developed. If one considers the occurrence of relatively large spots within 2.8 years after observation of the first spot of the new cycle, one finds more than 40 such spots with areas >500 millionths in the past six solar minima. Again, they are primarily new cycle spots. Only two of these relatively large spots were of other than new cycle polarity (March 1945 described above, and December 1922). For the years here studied, the occurrence of relatively large spots during the first 2.8 years after cycle onset was a thoroughly usual circumstance. In fact, cycle 21 is perhaps a bit atypical in having developed only two such large spots (August 1976 and September 1977) within this time interval. In this respect, cycle 21 resembles cycle 20.

Study of the lower latitude limit of new cycle activity within 2 years 10 months of cycle onset, shows that without exception, for each of the cycles studied, the lower latitude limit of spots with new cycle polarity has reached 9°. Thus, there is a consistent prior history of new cycle spots, albeit small, near the latitude of the September 15, 1977 spot at the corresponding time after the onset of new cycle phenomena.

In July-September 1924, spots with new cycle polarity were observed in latitudes 5°-6° and were called new cycle regions. It is probable that today these spots would be evaluated as "old cycle, with reversed polarity." They were followed in February 1925 by a new cycle spot at 8°, at a time that was 2 years 8 months after the first observed new cycle region. In all subsequent minima, new cycle spots were observed at latitudes as low as 9° before the passage of 2 years 10 months of new cycle observations. These early low latitude spots, as already mentioned, were all small, whereas the September 15, 1977 spot was relatively large. The earliest prior observation of a relatively large new cycle spot at low latitudes was the long-enduring, stable spot of 1966 that first appeared at latitude N07 in August 1966, two years eleven months after observation of the first new cycle spot in solar cycle 20. This relatively large spot with new cycle polarity at low latitude in the early years of cycle 20 seems to

provide a reasonable precedent for the occurrence of significant new cycle activity at latitudes and and times comparable to those of the September 15, 1977 spot group.

As one reviews the assembled data, one is tempted to ask the difficult question, "When did the last spot of the old cycle occur?" For some minima, perhaps those of 1933 and 1944, there seems to be an acceptable answer. For minima such as those of 1964 and 1976, however, in which the new cycle begins while the old cycle is still relatively active, the question becomes especially hard to answer. In the several years following such minima, the latitudes for members of the two cycles tend to merge. For the minimum of 1976, with its conspicuous overlap of old and new cycles, and with the highest residual activity on record (12.2 in the smoothed Zurich sunspot numbers), it is perhaps not surprising that a large and significant center of activity--the September 15, 1977 spot group--should present ambiguities and possibly reversed polarity. The possibly reversed polarity of this interesting region (especially in the October transit) leads one to ask if reversed polarity is a mere accident in solar "geometry" or if its occurrence perhaps carries some poorly understood significance related to the general development of the solar cycle.

Finally, the September 15, 1977 spot group emerges from the foregoing survey of data with a certain uniqueness. Apparently it is the only spot group in the last 54 years, old or new cycle, with mean area as great as 700 millionths of the hemisphere, to have formed at latitudes as low as 8° within 1.5 years of statistical minimum or 2.8 years after the observation of the first new cycle spot.

In spite of the foregoing effort, ambiguities remain with respect to cycle membership of the large spot with central meridian passage on September 15, 1977. In individual characteristics, it has been preceded by similar phenomena. Taking several characteristics together, we conclude that this spot may be unique in the last 54 years, for it is the only example of a spot with mean area greater than 500 millionths of the hemisphere and maximum area ≃1100 millionths that emerged within 1.5 years after statistical minimum and at a latitude as low as 8°. Could this set of circumstances in any way have contributed to the geophysical effects attributed to this region and its flares? Its relatively high level of activity and low latitude at a time of probably uncomplicated interplanetary structure may have facilitated energetic particle propagation.

REFERENCE

SGD 1977 *Solar-Geophysical Data*, 400 Part I, 30-90, December 1977, U.S. Department of Commerce (Boulder, Colorado, U.S.A. 80303).

Sunspot Motions and Activity in McMath 14943

by

Howard L. DeMastus, Donald F. Neidig, and Philip H. Wiborg
Air Force Geophysics Laboratory
Sacramento Peak Observatory*
Sunspot, NM

We present a photographic record and a partial magnetic photospheric velocity record of the evolution of McMath 14943 for the period September 9-20. We also plot the positions of sunspots for September 10-19 and consider their motions in relation to flare activity in the region.

Data

Photographic data were obtained from the Sacramento Peak Observatory Hα patrol (both line center the Hα ± 1 Å), and from the white light patrol. Morning and afternoon white light photographs (Figure 1a) show the evolution of the active region for September 9-20. The region is shown in greater detail in photographs taken with the Vacuum Tower Telescope on September 13 (Figure 1b).

The photoelectric Doppler-Zeeman Analyzer (DZA) at Sacramento Peak provides unsaturated magnetograms and tachograms. The magnetograms in Figure 2 are displayed here in isogauss contours at levels of $10 \times 2^{n-1}$ gauss ($n = 1, 2, 3 \ldots$). Similarly, the tachogram (line or sight) photospheric velocity levels in Figure 3 are 0.1×2^{n} km/s. Spatial resolution is limited by the size of the scanning aperture, in this case $4.8'' \times 4.8''$. A detailed description of the DZA instrument is given by Dunn [1971].

Sunspot coordinates were measured from both off-band Hα and white light patrol images. In the case of the former the umbrae were measured for longitude and latitude using a Richardson film projector with movable cross hairs interfaced with the Sacramento Peak Sigma 5 computer. The coordinate reduction is based on fitting points at the solar limb; solar ephemerides are applied and the x,y coordinates of the sunspots are translated into heliocentric coordinates, corrected for geocentric parallax. The standard deviation for repeated measurements of coordinates on different film frames is about 0.1 degree for the center of the solar disk (of course, errors increase toward the limb); the error bars plotted in Figure 4 represent two standard deviations. Table 1 keys dates and UT to the points plotted in Figure 4a.

Analysis

There are two principal motions in the active region: the usual stretching, in this case primarily due to the forward motion of spots A, B, C, D, F, L, M, and N (spot A moves forward in Carrington longitude by about 3.5 degrees during September 10-19, and a dramatic counter-clockwise rotation of these same spots centered on (approximately) spot A. The large complex of forward-moving spots which participate in the rotation is not magnetically unipolar; in fact, the neutral line passes between spots D and F. The most rapid angular velocity appears in the motion of B around A, executing a 180-degree rotation in the seven-day period September 10-17, including a 77-degree rotation in the 44-hour period September 14-16.

An examination of the Sacramento Peak Hα patrol record shows that during September 9-11 flares were occurring in the eastern part of the region. McMath 14943 then suddenly became quiet on September 12. Activity resumed on September 13, with flare locations moving westward in the region; during September 16-19 almost all flares occurred near spot A, especially along the neutral line south of A. Presumably the activity in this locality was a response to the increase in shear produced there by the rapid rotation of AB. Activity near spot A was highlighted by large flares on September 16 and 19 (importance 2N and 3B, respectively). Beginning on September 20, flare activity shifted to the north of spot A, in response to newly-emerging spots in that part of the region (compare photograph on September 18-20).

Superposing the tachograms and magnetograms reveals two blue-shifted velocity features which persist during September 13-14; one is located at the northwest of the large preceding spot and the other along the neutral line south of the preceding spot. A large red-shifted area covers the southeastern part of the preceding spot on September 13 and moves to the northwest, displacing the blue-shifted feature there, on September 16. Another prominent red-shifted area spans the neutral line from spots D and F; this feature decreases in size during September 14 and by September 16 covers only the region near spot F. Since McMath 14943 was near disk center during September 13-16 we may interpret the velocities (on these days) mostly as vertical components of the photospheric circulation in the active region. As the region approaches the limb we would expect to progressively observe the horizontal components associated with the sunspot motions in Figure 4. Unfortunately, no tachograms were available after September 16.

*Operated by the Association for Research in Astronomy, Inc., under contract with the National Science Foundation.

The shape of the principal neutral line shows very little change during September 13-14. However, on the magnetogram taken at 2126 UT, September 14, a small feature of negative polarity becomes visible just south of the neutral line across from spot A. The growth of this flux apparently forces the southward diversion of the neutral line, producing the large kink visible in the magnetograms from September 16-18. Thus, in addition to the shearing motion an argument could be made that this emerging flux also played a role in producing the large flares of September 16 and 19. The rotation of AB appears also to drag the neutral line northward around the west of spot A, as seen on magnetograms after September 14.

Table 1. Dates and UT for Sunspot Coordinate Points; each Asterisk Indicates a Datum in Figure 4a for the Particular Spot.

SEPT	UT	A	B	C	D	E	F	G	H	J	K	L	M	N
10	1446	*	*	*			*	*						
10	1812	*	*				*							
10	2250	*	*	*			*	*						
11	1928	*	*	*			*	*					*	*
11	2356	*	*	*			*							
12	1454	*	*	*			*	*					*	*
13	1404	*	*		*	*	*		*				*	*
13	1735	*	*		*	*	*		*				*	*
14	1435	*	*		*	*	*		*					
14	1835	*	*		*		*		*	*				
15	1409	*	*		*	*	*			*				
16	1442	*	*		*		*			*	*	*		
16	1949	*	*		*		*			*	*	*		
16	2243	*					*							
17	1536	*	*		*		*			*	*	*		
17	1832	*	*		*		*			*		*		
18	1545	*	*		*		*			*	*	*		
18	1825	*	*		*		*			*	*	*		
18	2259	*	*		*		*			*		*		
19	1437	*	*		*		*			*		*		
19	1943	*					*							

Reference

DUNN, R.B. 1971 Solar Magnetic Field, IAU Symp. 43 (R. Howard, ed.), p. 65.

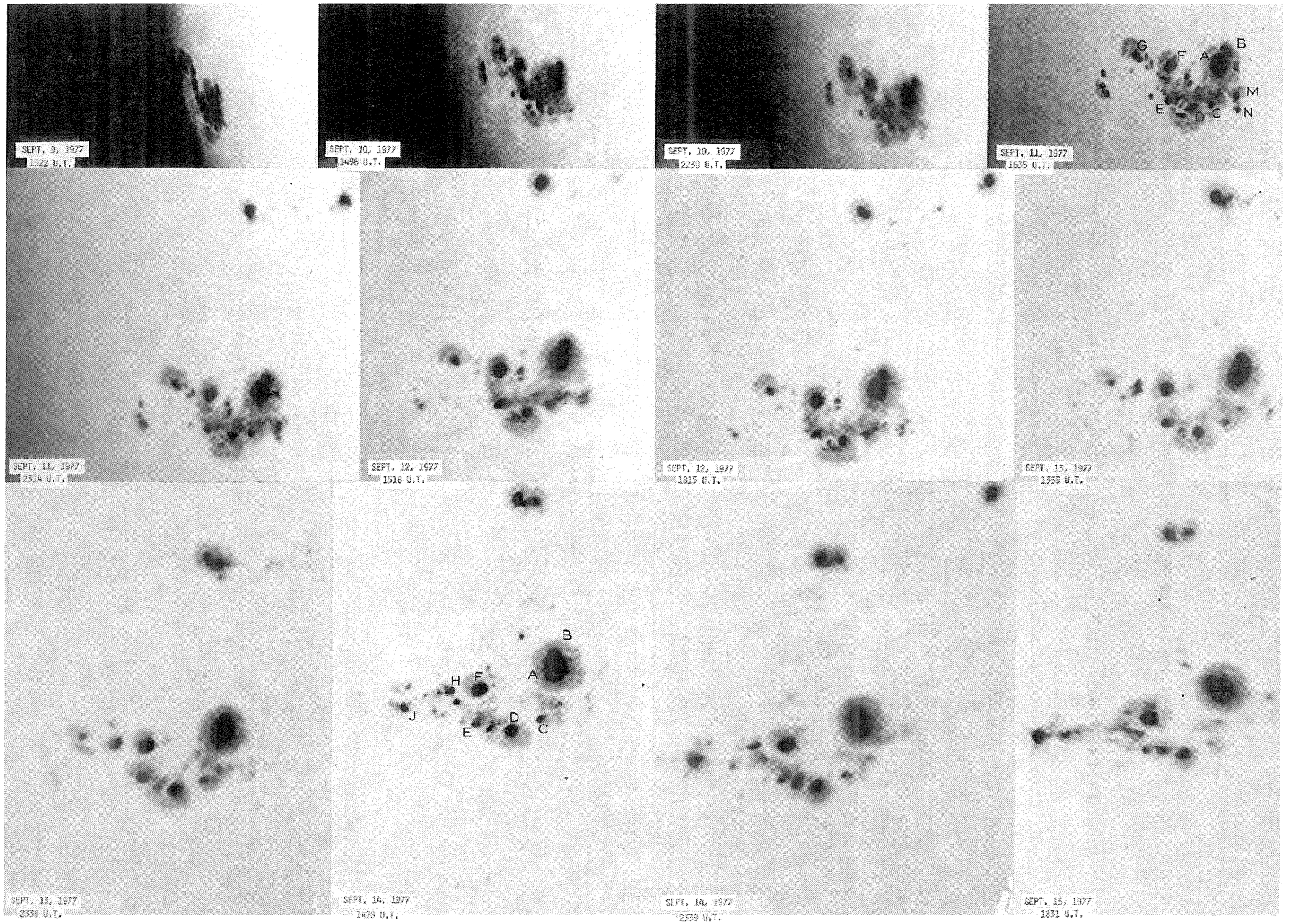

Fig. 1 (a). Sacramento Peak white light patrol (aperture 15 cm, focal length 220 cm) covering the transit of the region. The sunspots identified by letters are plotted for their proper motions in Figure 4.

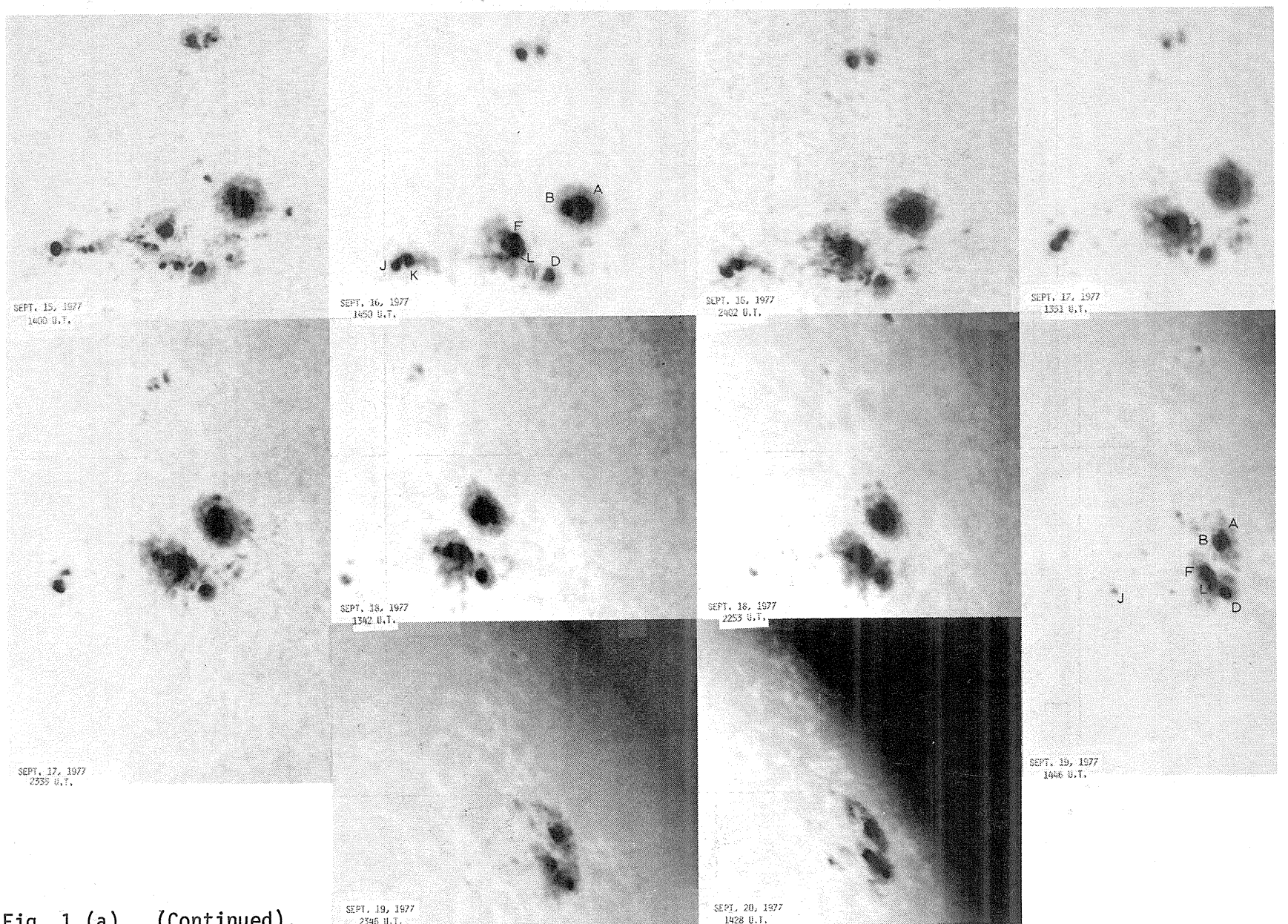

Fig. 1.(a). (Continued).

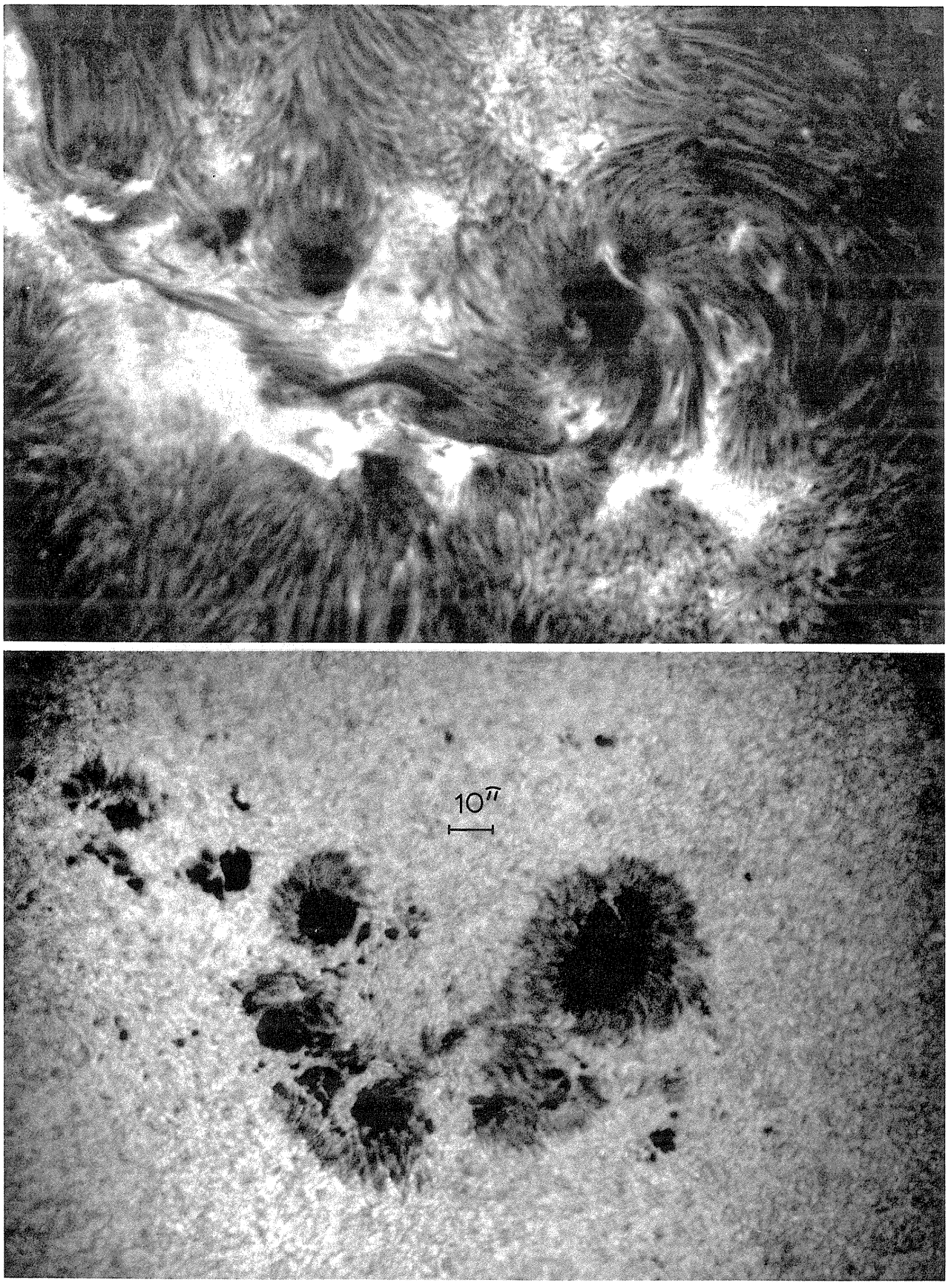

Fig. 1 (b). Vacuum Tower Telescope photographs in Hα and in continuum near Hα, September 13, 2051 UT. As in all figures except 1 (b), celestial north is at the top, west to the right.

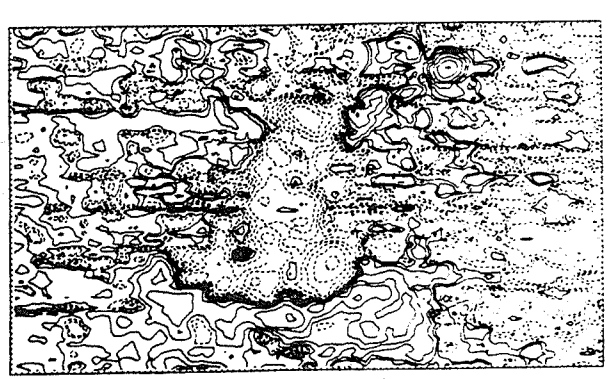

SEPT. 13, 1977
1751 U.T.

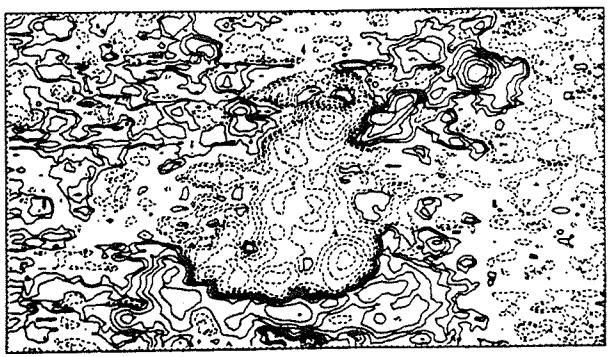

SEPT. 13, 1977
2021 U.T.

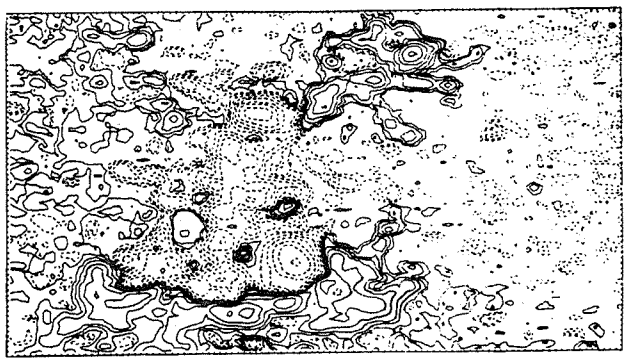

SEPT. 14, 1977
1451 U.T.

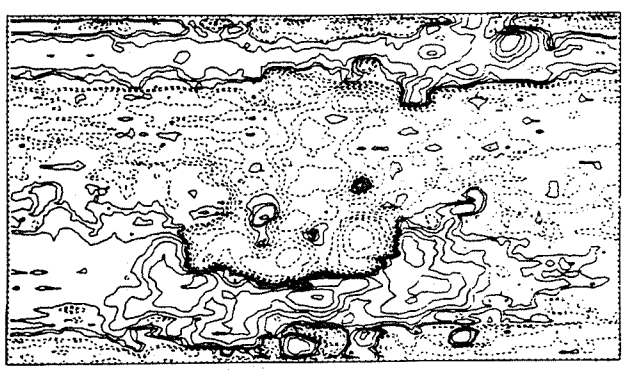

SEPT. 14, 1977
1638 U.T.

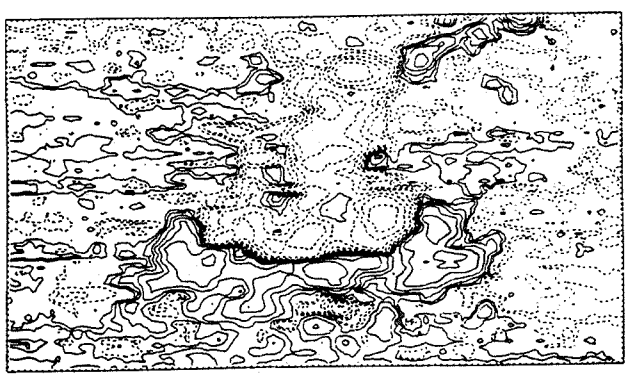

SEPT. 14, 1977
1933 U.T.

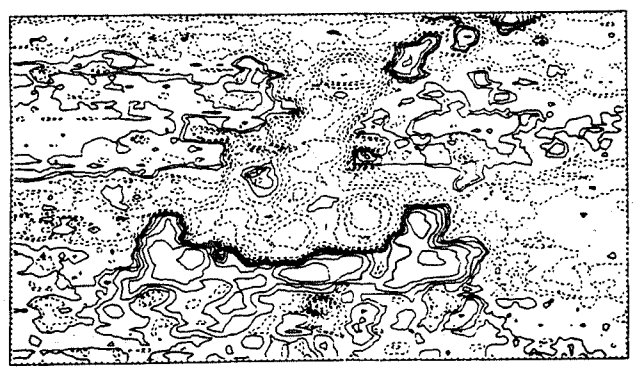

SEPT. 14, 1977
2126 U.T.

Fig. 2. Sacramento Peak DZA magnetograms with isogauss contours $10 \times 2^{n-1}$ gauss (n = 1, 2, 3 . . .) (solid lines (positive) indicate magnetic vector pointing outward). Here, as in Figure 3, the size of the scanning aperture is 4.8 x 4.8; tic-marks are in steps of the scanning aperture dimensions. Note that the vertical and horizontal coordinates are not plotted on equal scales.

SEPT. 16, 1977
2040 U.T.

SEPT. 17, 1977
1615 U.T.

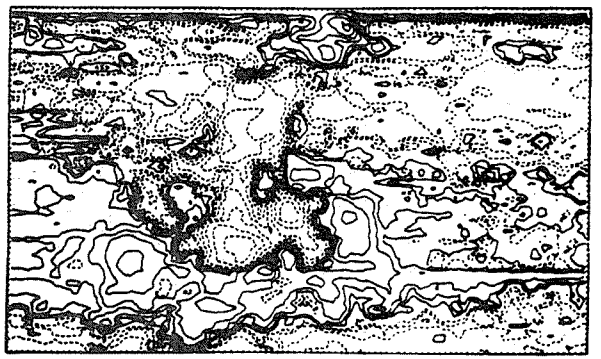

SEPT. 17, 1977
1859 U.T.

SEPT. 18, 1977
1743 U.T.

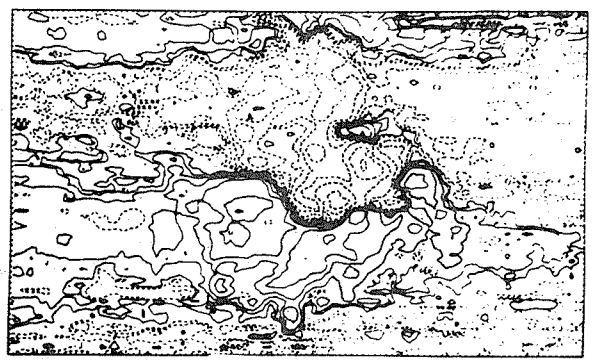

SEPT. 18, 1977
1925 U.T.

Fig. 2. (Continued).

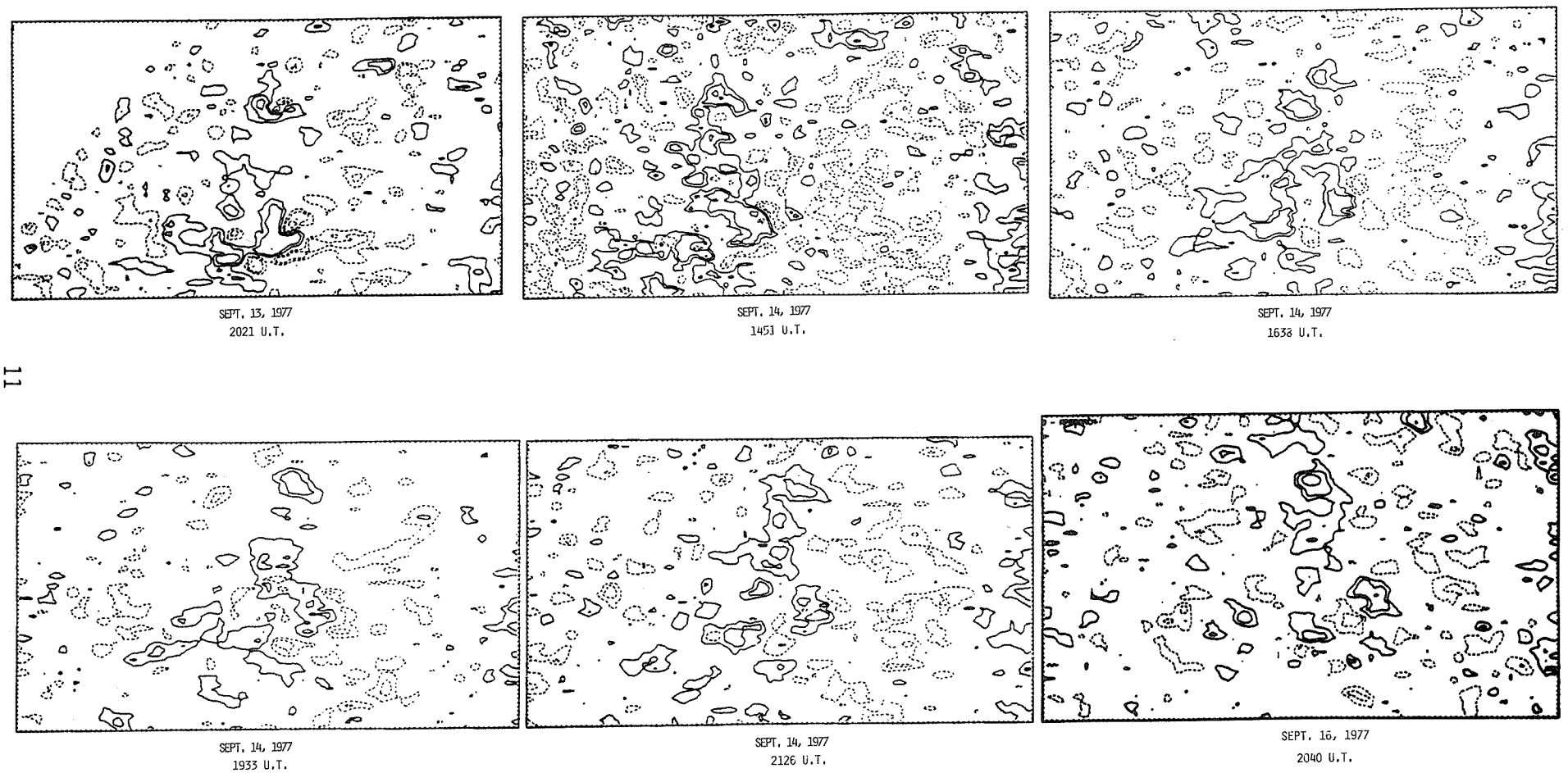

Fig. 3. Sacramento Peak DZA tachograms with velocity contours 0.1 x 2^n km/s (n = 1, 2, 3 . . .) (dashed lines indicate approach).

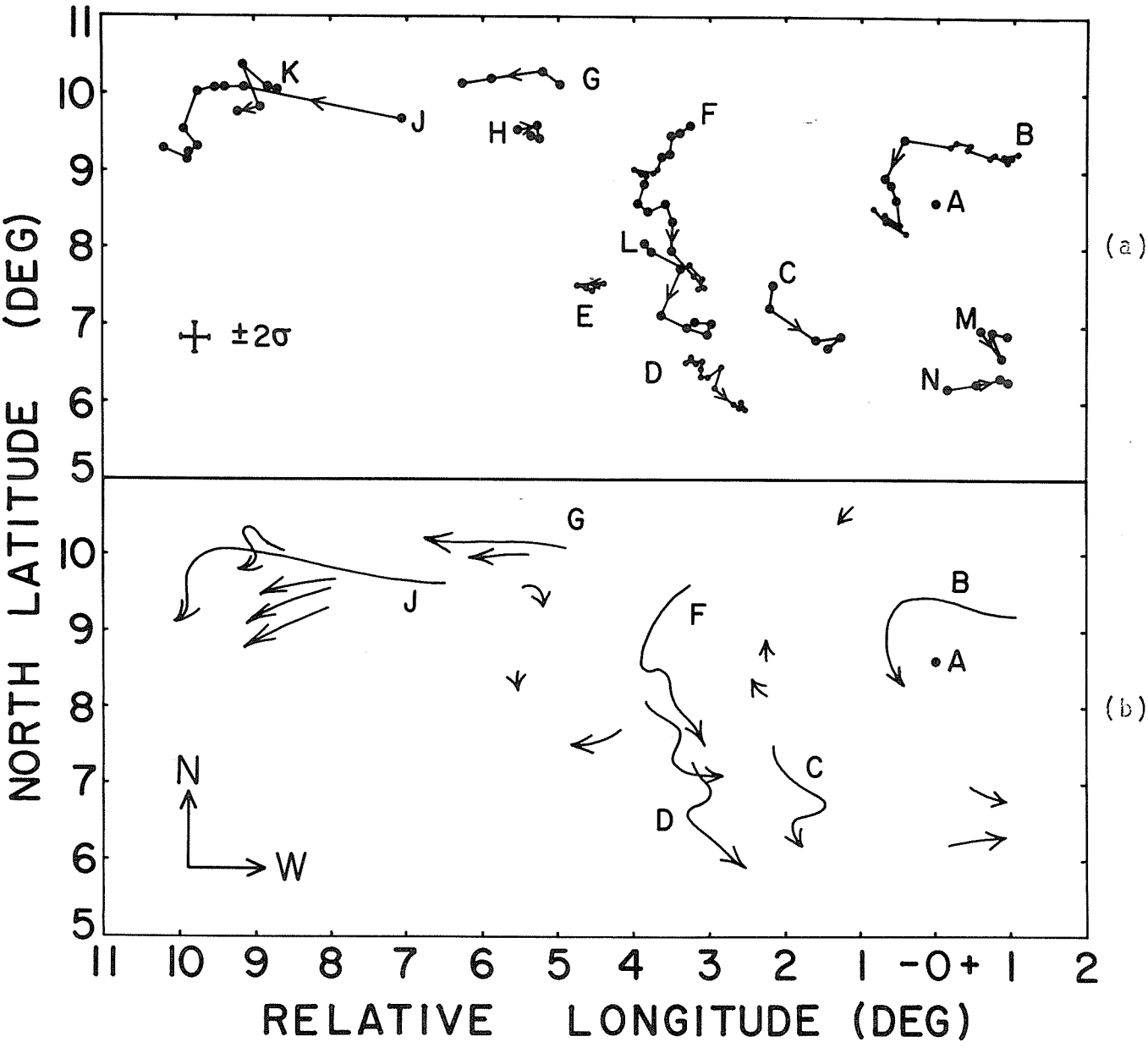

Fig. 4. (a) Umbral centroid positions derived from off-band Hα patrol images. Positions are all relative to spot A which is held constant, although the latitude can almost be considered absolute since the latitude of spot A did not change more than 0.5 degree during disk transit. The dates and UT of each point are given in Table 1. Spots of positive magnetic polarity are: C, D, E, J, K, M, N. Spots of negative polarity are: A, B, F, G, H, L.

(b) Schematic representation of 4a supplemented by white light patrol data, which show a few smaller spots.

Rotation of a Sunspot in the Active Region McMath 14943

by

Z.B. Korobova
Astronomical Institute of the Uzbek Academy of Sciences
Tashkent, U.S.S.R.

Introduction

From white-light photographs of the active region McMath 14943, it is easy to note the rotation of a large stable sunspot in the western part of the group. The sunspot lay in the common penumbra of a magnetically complex sunspot until September 14. Then it separated and became the leader of the group. The spot was crossed by a light bridge during the whole period of the transit of the group. The spot persisted oval in shape until September 17. These two facts made it possible to note the rotation and to measure its angle.

A large series of full disk white light photographs were obtained with 130-mm refractor AFR-3. The image diameter is 75 mm. Four photographs taken September 13, 14, 15, and 16 when the group was in the central zone of the solar disk were selected for accurate measurements.

Figure 1 shows drawings of the sunspot. Nine points were chosen for measurement of the angle of the rotation. Positions 1, 2 are the points of intersection of the longitudinal axis of the sunspot umbra with the umbra-penumbra boundary. Similarly, 3, 4 and 5, 6 are the points for the light bridge and umbra-penumbra and penumbra-photosphere boundaries, respectively. The rest are features of the solar surface confidently identified on the large series of photographs.

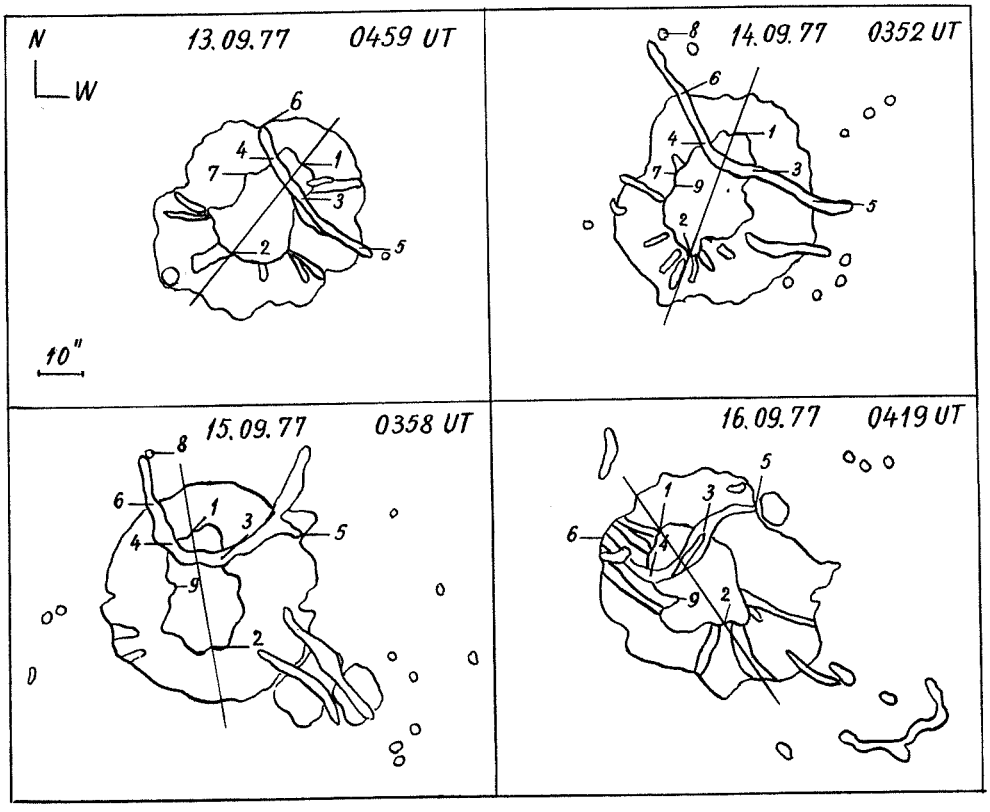

Fig. 1. Drawings of the spot of the active region McMath 14943 for September 13-16. The thin line represents the longitudinal axis of the spot. Figures mark the points used for measuring the spot rotation.

The rectangular positions of these points were measured with a UIM-23 measuring device. Figure 2 shows calculated heliographic positions of the points.

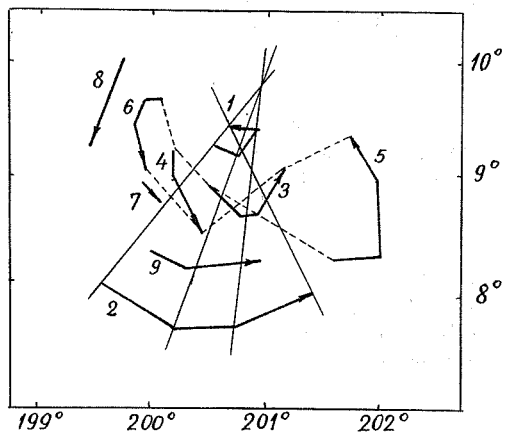

Fig. 2. The shift of the measured points September 13-16. Thick lines indicate the points trajectories. Thin lines indicate the positions of the spot longitudinal axis. Dashed lines join the points of the light bridge for September 13 and 16.

Our results lead to the following conclusions.

(1) The spot turned towards west-north-east-south. Its daily rotation is 19° from September 13 to September 14, 14° from September 14 to September 15, 36° from September 15 to September 16. The total three-day angle is 68°.

(2) The center of the spot rotation did not coincide with its geometrical one and lay somewhere near point 1.

(3) The light bridge noticeably lost its shape, but rotated with the sunspot.

It is to be noted in addition that Figure 1 shows that the directions of the penumbra filaments gradually deviate from radial ones during September 13-16, the deviation being generally opposite to the spot rotation. The same winding of transverse magnetic field lines coinciding in direction with penumbra filaments [Kuklin and Stepanov, 1963] has been discovered by Gopasyuk [1965].

REFERENCES

GOPASYUK, S.I. 1965 *Izv. Krymsk. Astrofiz. Obs. 33*, 100-110 (In Russian).

KUKLIN, G.V. and V.E. STEPANOV 1963 *Soln. Dann.* No. 1, 55-67. (In Russian).

Evolution of Overall Photographic and Isodensitometric Investigation of McMath Plage Region 14943 in Hα and Ca-K Line, September 7-24, 1977 and Associated Geomagnetic and SEA Events

by

E. Soytürk and A. Özgüc
Kandilli Observatory
Istanbul, Turkey

Introduction

September 7-24, 1977 is an interesting interval. For this interval the sunspot group evolution in McMath plage region 14943 in its first passage, Hα and Ca-K filtergrams, the evolution of the plage, isomaps, the energy content of plage, the morphological structure are examined together with observed durations of flares, SEA, and the H component of the geomagnetic field.

Sunspot Observations

The sunspot observations are made from the projected image of the Sun in Kandilli by drawing the sunspots on a white paper 25 cm in diameter. The classification of the sunspot groups is made by the Zurich classification.

It was observed that the umbras in the north part of the group were south polarity (S) and to the south part of the group north polarity (N) both leading and following parts according to Rome Monthly Bulletin No. 233 [1977] until September 13. On September 14 the small (N) polarity sunspot group which emerged north of the leading sunspot moved to the west. It was a complex scene. September 18 small spots increased, then September 19 the sunspot group reached its minimum value in terms of its number of spots (see Fig. 1).

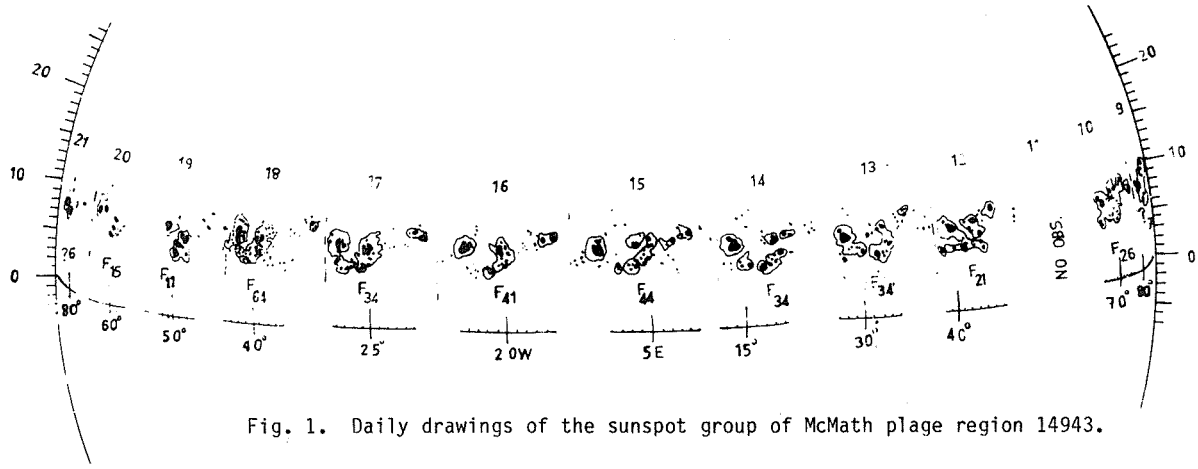

Fig. 1. Daily drawings of the sunspot group of McMath plage region 14943.

Chromospheric Observations

The observations are made by Zeiss Hα (0.25Å) and Halle Ca-K (0.6Å) birefringent filters. Diameters of the Sun images for both are about 20 mm. The isomaps are obtained with a Joyce isodensitracer.

In the calculations of the energy content, the effects of the limb darkening, changes in the atmospheric conditions and foreshortening effects are corrected.

Evolution of Hα and Ca-K Plages

September 8: On this day the visual region of the plage was at N06 E90 (1126 UT). It was observed that the part of the plage reached up to a height of about 8" and had some weak puffs. September 9: The plage was at N07 E84 (1022 UT). You will notice the contour which is separated from the chromosphere by means of 0.09D steps as the boundary of the plage in both Hα and Ca-K isomaps. All properties of the plage which we observed and calculated are presented in Tables 1,2 and 3. The bright patches in the isomaps are examined thoroughly (see Table 2) because of their importance in the evolution of the plage. The patch densities are measured by supposing the undisturbed chromosphere density is 0.0D. The magnetic field strengths are derived from Mt. Wilson magnetograms in Table 2. The patches were located on the south elongations of the leading and the following parts of the sunspot group. September 14: The plage which was located at N08 E16 (0746 UT), contained five patches. These five patches were over the small spot regions which spread out of the large spots with penumbra. This result is confirmed in that the brightest plage regions coincided with the small spots where the magnetic fields are channelized by the big sunspots [Soyturk, 1973]. An undefined tracing of a filament channel was apparent and bisected the plage from east to west.

Table 1. Summary of properties of McMath plage region 14943

Date	Location Carrington Lat.	Long	Meas. Area Millionths Solar Hemisphere		Plage dimensions sec. of arc E-W	N-S	Energy 10^{25} ergs/sec		Max. Density of plage	
Sep			Hα	Ca-K			Hα	Ca-K	Hα	Ca-K
08	N06	203								
09	N07	194	2706	3024	17	6.5	2.31	3.79	0.3D	0.21D
14	N08	198	2230		16	10	2.51		0.35	
16	N09	200	3400	5250	19	10	3.37	11.7	0.40	0.36
19	N10	195	3700	4960	19	10	4.85	10.2	0.54	0.36
20	N11	198	4870	5700	19	10	7.3	17.6	0.63	0.45
21	N13	200	5890	7000	18	7	4.68	19.9	0.18	0.36

Table 2. Properties of bright patches.

Date	Density of the Patches		Magnetic Field Strengths (Gauss)	Polarity	Description of Location in Group
Sep.	Hα	Ca-K			
09	0.3D	0.21D	40	S	Northern
	0.2	0.21	40	N	Southern
14	0.28		80	N	Easternmost
	0.35		40	N	Eastern
	0.28		80	S	Central
	0.21		80	N	Northern
	0.28		40	N	Southern
16	0.4, 0.4, 0.4, 0.36	0.36			Eastern
	0.4, 0.4	0.36			Between spots
	0.27	0.27			Northern
	0.4, 0.36	0.36			Western
19	0.54, 0.48, 0.48	0.36	20-80	N	Eastern
	0.3, 0.24	0.27	20	S	Northern
	0.48, 0.18	0.18	20	N	Western
20	0.63, 0.45	0.45			
21	0.18, 0.18	0.36			

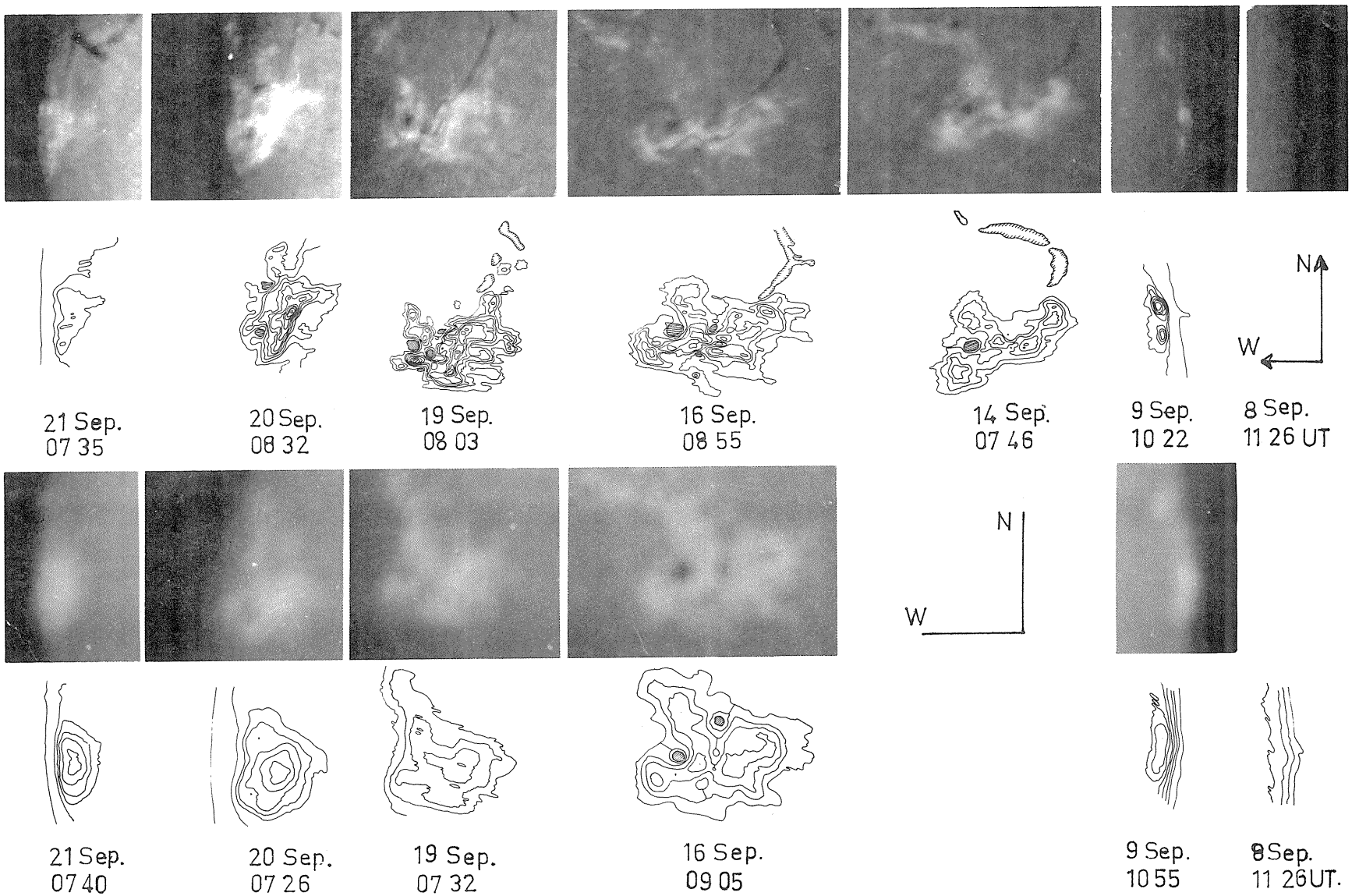

Fig. 2. Hα and Ca-K filtergrams and their isomaps of the McMath plage region 14943.

Table 3. List of observed flares.

Date	Observed UT			Importance
	Start	Max.	End	
Sep.				
19	1010	1044	1206	3B
20	0714	0714	0847	1N
21	0805	0818	0830	SN
	0920	-	-	SN ?
	1040	1100	1115	SN

September 16: The plage appeared at N09 W13 (0855 UT). It was composed of four bright patches in Ca-K. These patches were also spread over the small spot regions.

September 19: The plage was located at N10 W47 (0803 UT). The explanations in detail for this day are given in another part of this report. The plage comprised three bright patches. The big part of the plage area which is also the brightest part was located over the following spots. Between 1010-1206 UT a major flare (3B) and mass motions associated with the flare were observed.

September 21: The plage was located at N13 W79 (0735 UT). The flare started at 1040 UT and was a cone type flare which rose up to 3" height.

Geomagnetic and SEA Perturbations

Tracings of H component of geomagnetic field and SEA for September 7-24 which were recorded at Kandilli are presented in Figures 3 and 4. Table 4 shows hourly and daily mean values of horizontal intensity of geomagnetic field.

Table 4. Hourly Mean Values of Horizontal Intensity of Geomagnetic Field

24000 nT + tabular quantity (in nanotesla)

Istanbul-Kandilli
September 1977

Day	01	02	03	04	05	06	07	08	09	10	11	12	13	14	15	16	17	18	19	20	21	Universal 22	time 23	Mean
07	305	304	303	303	307	300	291	284	285	294	300	305	306	309	307	302	299	297	299	300	299	304	311	309	301
08	303	303	305	312	306	295	282	271	284	279	302	311	318	313	313	308	308	312	309	309	309	318	317	312	304
09	306	304	305	307	300	296	287	272	269	281	290	284	275	284	283	287	281	282	281	293	293	296	298	298	290
10	300	307	305	309	299	292	276	266	260	270	277	274	281	290	287	281	278	281	286	296	290	300	305	297	288
11	296	291	298	291	282	272	263	252	263	263	261	272	281	269	263	261	264	265	272	270	276	281	290	297	275
12	286	287	290	288	289	284	277	268	267	275	282	288	293	292	290	287	285	287	289	278	289	287	304	297	287
D13	292	297	303	302	294	286	269	247	252	268	279	273	266	273	262	243	253	285	244	264	287	271	275	279	274
14	284	295	299	292	287	268	257	252	254	262	270	278	284	288	285	287	289	287	287	287	282	285	287	289	281
15	291	288	290	290	286	279	271	263	260	258	268	283	287	283	282	281	286	291	293	296	295	295	298	297	284
16	296	298	299	301	301	298	281	273	273	283	297	033	311	314	304	292	292	298	301	297	313	304	298	297	297
17	294	294	296	302	303	296	278	254	263	272	279	285	289	291	289	287	292	294	296	296	295	297	297	296	289
18	293	293	292	294	298	296	291	282	283	291	294	293	297	302	297	294	292	294	296	298	297	303	300	301	295
D19	298	301	302	305	307	302	295	285	283	295	303	316	340	294	271	235	222	235	255	283	262	241	253	270	281
D20	271	284	269	274	265	259	245	229	227	213	219	230	230	214	209	205	231	273	259	260	281	292	286	274	250
D21	278	281	283	278	290	265	262	230	232	225	193	251	241	234	255	257	258	261	261	265	277	330	304	266	262
D22	292	279	278	246	265	265	251	248	238	263	259	256	266	241	239	215	249	218	217	228	267	236	249	263	251
23	254	253	255	255	253	251	250	249	258	268	279	279	262	250	265	266	282	245	256	286	279	265	268	273	263
24	268	268	270	267	259	256	256	260	270	266	267	277	277	275	268	263	261	267	270	272	272	292	282	278	269

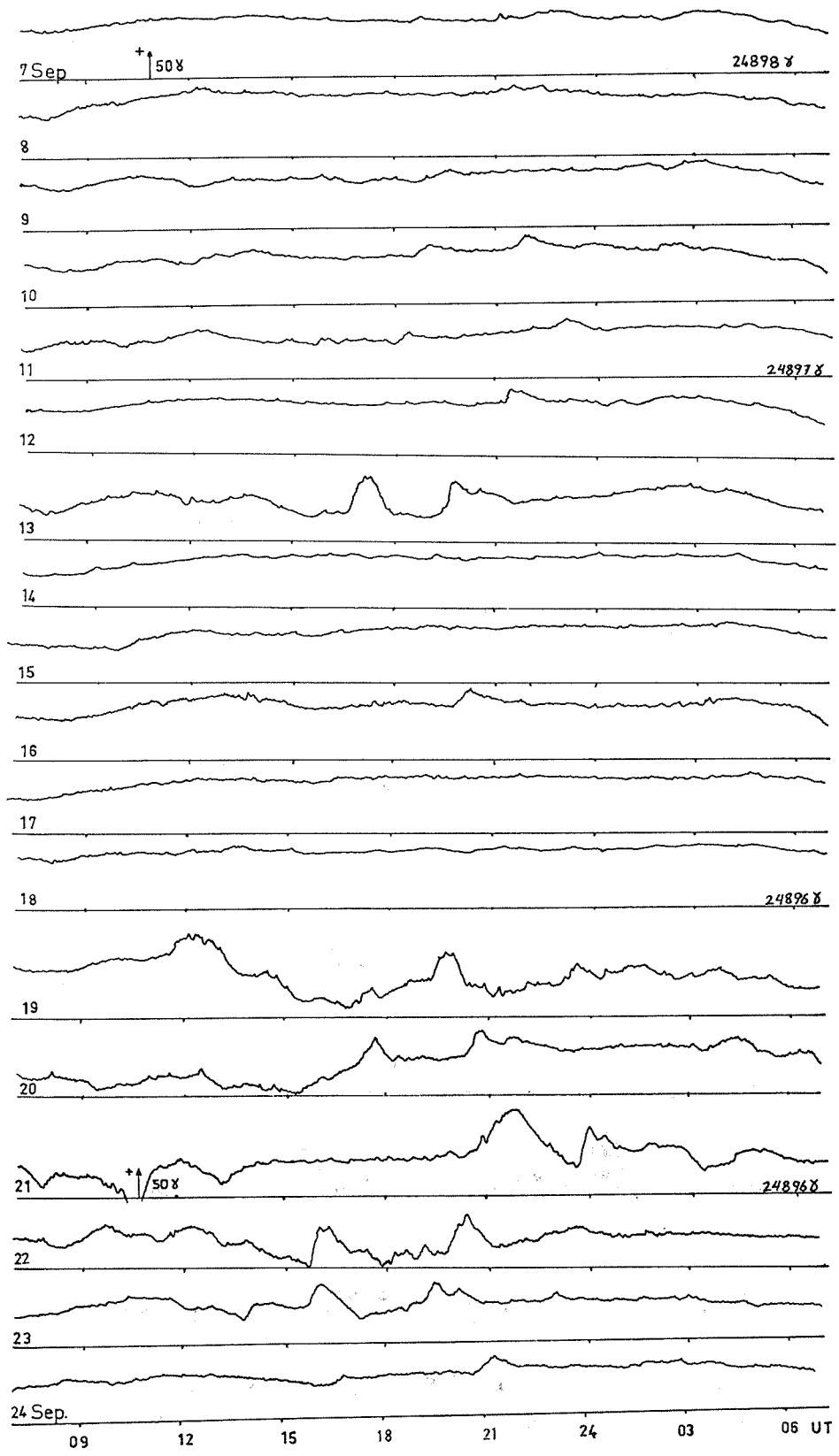

Fig. 3. Daily recordings of H component of geomagnetic field September 7-24, 1977.

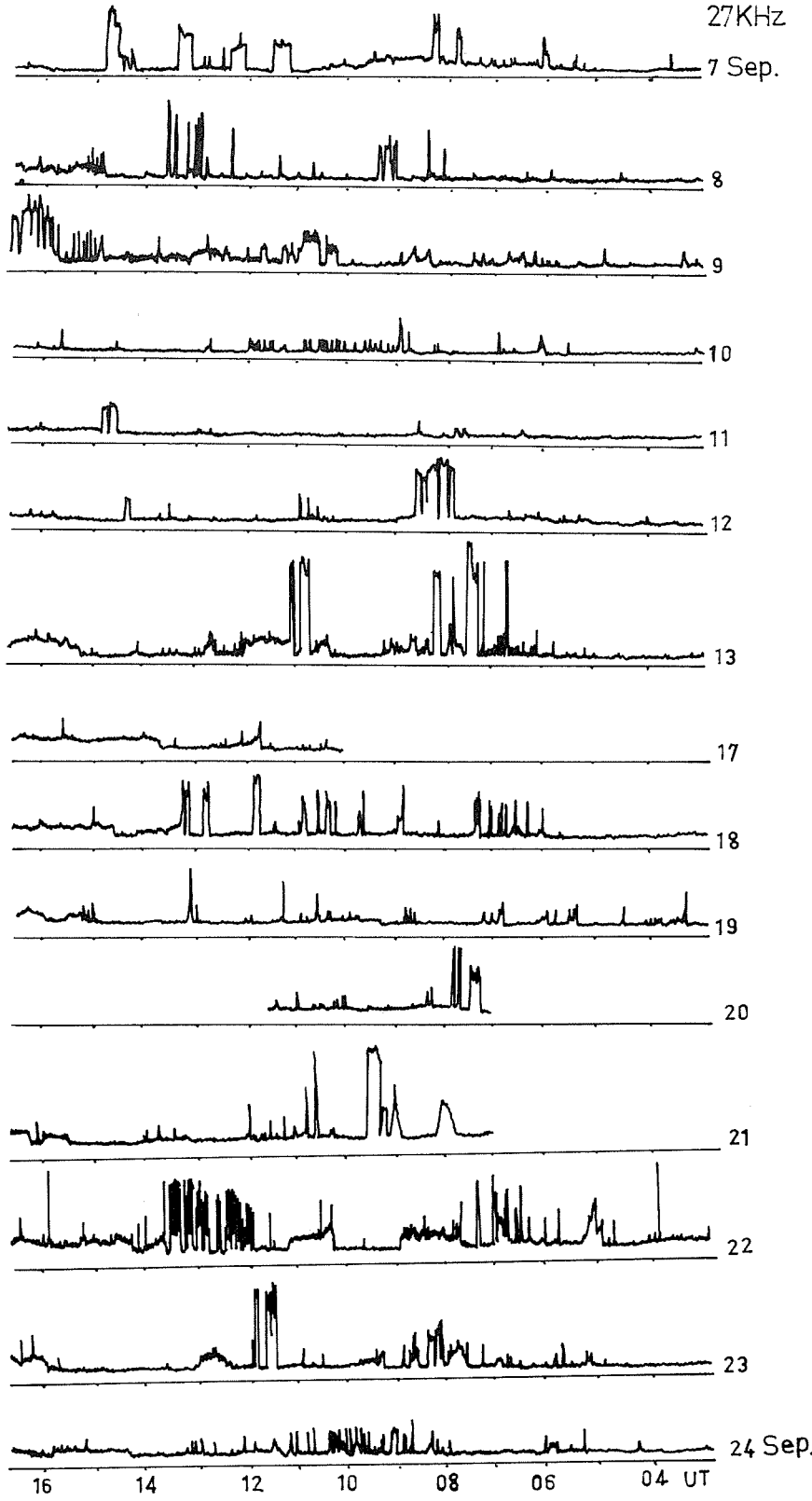

Fig. 4. Daily tracings of SEA recorded at 27 kHz for September 7-24, 1977.

Conclusion

Because of the gap days in our observations between September 7-24, we could not follow the structural evolution of the plage, i.e. the identification of bright patches during the evolution. These patches almost match in H α and Ca-K lines [Soytürk, 1973]. If we compare Table 2 with the classification of the plage by Soytürk according to energies, velocity of development and lifetime, the following results can be seen:

- Active centers in this classification live two rotations.
- The velocity of development for the first three days is about 500-800 millionths of the solar hemisphere per day.
- It reached its maximum area on the tenth day.
- The sunspot group of the plage has 20-35 spots.
- The most probable sunspot evolution is B, D, E, D, C, G or J types.

It is estimated that the plage spent 4-17 days of its lifetime between September 8-21. During these days the plage had almost maximum area and intensity. When the activity of flares decrease the plage conserves its area.

The evolution of the plage shows some differences according to the above mentioned classification. The sunspot group developed to F type and lasted longer than the model mentioned above. It was not seen at the next rotation, so it diminished quicker.

References

ROME 1977 Roma Monthly Bulletin No. 233, Solar Phenomena.

SGD 1977 Solar-Geophysical Data, No. 398-400 Part I, U.S. Department of Commerce, Boulder, Colorado, U.S.A.

SOYTÜRK, E. 1973 Development of Active region in H α and Ca-K line. Thesis part II, unpublished.

Observations of Flares in McMath 14943

by

F. Moriyama
Tokyo Astronomical Observatory
Mitaka, Tokyo, Japan

Introduction

The center of activity, associated with a large sunspot group and designated as McMath 14943, was observed at the Tokyo Astronomical Observatory during its transit of the visible hemisphere from 10 to 21 September 1977. At Mitaka, in addition to patrol programs on a routine basis, high-resolution filtergrams of this active region were obtained in the center as well as in the wings of the Hα line through a Halle birefringent filter (band width 0.5 Å) on a 20-cm equatorial refractor. At Norikura, spectrographic observations were carried out for outstanding events in the region with a Littrow spectrograph fed by a 25-cm coudé coronagraph. A Halle filter with 0.5-A band width tuned to the Hα line center was used for the slit jaw picture. This report gives as brief description of large flares in McMath 14943 as observed at the two sites.

Fig. 1 displays Hα photographs of McMath 14943 in the line center in the wings of ±1.0 Å during its western disk passage. As is clearly seen in these pictures, the configuration of the sunspot group in the central part of the region changed markedly after September 15. During the late hours of September 16 to 20, three large flares were observed by us.

On the slit jaw picture taken at 2111 UT on the 16th (see Fig. 2) the arrangement of filaments in McMath 14943 had somewhat changed compared with the previous day. An arc-shaped filament (D_1) developed on the west of the preceding spot (S_1), and seemed to connect with the pre-existing filament (D_2) running from east to west in the middle of the region. At 2306 UT when the Hα patrol started at Mitaka, a large flare was found in progress in this active region. It consisted of three separate parts: a bright fibril (F_1) covering a large part of the preceding spot, and luminous ropes (F_2) and (F_3) lying along outside the filaments D_1 and D_2, respectively. The flare had passed its maximum brightness, and gradually faded during the next few hours.

Spectrograms in the UV region were obtained for the brightest portions of F_1 and F_3 between 2316 and 2340 UT. H_{11} was the highest Balmer series line that can be seen, and enhancements of metallic lines were not so conspicuous. After 2320 UT, F_3 decreased in brightness from the northern edge, and its width became narrower. The flare seemed to be of two ribbon type, but the lateral movement of bright ropes away from the intervening filament was not evident.

The evolution of the flare in the last phase was seen in high-resolution photographs taken after 0010 UT on the 17th. (Fig. 3-a and 3-b). Although the brightness decreased considerably at 0010 UT, the flare ribbons were still visible in emission even in the wings of Hα ±0.5 Å. Another remarkable feature in this phase is the two systems of Doppler shifted curvilinear filaments. The one (L_1) seemed to be rooted on one side in the penumbra of the preceding spot partly covered by the flare, and on the other side in the bright rope (F_3) outside of the southernmost spot (S_2). The other system (L_2) linked a pore (P) west of S_2 and the remnant of the flare (F_2) in the leading side of the region. Strong positive Doppler effect at both ends of these systems indicates the matter descending into the spots and the flare, and they are believed to be post-flare loops. Bright arcs which can be seen until 0030 UT in the center of Hα might be the tops of the loops (L_1) in emission. Composite drawing of the loops and the dark filaments almost stationary during the flare are made from photographs in the center of Hα and at ±0.5 Å in Fig. 3-b.

On the next day, an importance 1n flare originated in the same region. No observations were made at Mitaka because of unfavorable weather; observations of the event with incomplete time coverage were available at Norikura. The picture at 2107 UT on the 17th (Fig. 4) shows that the general configuration of the filaments and spots associated with the active center did not change appreciably after the end of the previous flare. About 15 minutes later, however, there occurred a noticeable change in the arc-shaped filament (D_1) preceding the leader spot (S_1). The filament became very faint at 0014 UT on the 18th, and Hα plage north of the filament increased in both area and brightness. Unfortunately there was no picture between 0014 and 0033 UT, during which the flare had started. A few bright areas, each irregular in form, were scattered in the west side of the active region. Among them, B_1 (covering the western part of the umbra of S_1) and B_2 (forming along the location of D_1 which had vanished) are most prominent. At first B_1 was most brilliant, and after 0045 UT B_2 became the brightest. On the spectrograms taken at 0041 UT, we can see the Balmer series lines up to H_{14} and also the faint Balmer continuum at B_1 as well as B_2. The flare began to fade from about 0100 UT, and the arc-shaped filament which had disappeared before the onset of the flare reappeared slightly dislocated. It might have slipped out of the filter pass band because of large Doppler shift. At 0120 UT the flare diminished in area and brightness, but still partly covered S_1 and S_2. After then we have no photographs until 0231 UT by which time the flare had ended.

Another importance 2n flare was observed on the 20th in the following side of McMath 14943. As the region approached the west limb, foreshortening interfered with observations of evolution of the region after the 18th. In the early hours of the 20th, small luminous points with short duration appeared sporadically near the umbrae of larger spots. Some examples are illustrated in Fig. 5. After 0130 UT a large dark filament (d_1) extending to the northeast of the active region was activated, and partly disappeared. At 0258 UT a tiny luminous point (b_1) occurred in a plage at the northeast border of the active region, but soon faded away. With a few minutes lag in start time, the plage brightened in two points (b_2 and b_3) on either side of b_1. As time went on these two parts became the principal area of brightness. Almost simultaneously, the region along d_1 and the extension of d_2 (another large filament east of d_1) grew brighter, and two chains of bright points (b_4 and b_5) appeared. The former joined with b_2 into a long bright filament.

At 0309 UT another brightening (b_6) took place in a plage east of the following spot. In the spectrograms obtained at the initial phase of the flare, the Balmer series lines were observed up to H_{13} at b_2 and up to H_{15} at b_6. At the brightest parts the faint Balmer continuum was also recognized. After 0030 UT, b_4 and b_5 began to disappear, while b_2 and b_3 expanded to make wide ribbons, and the flare finally took the shape of a two-ribbon structure. The two bright strands gradually receded, and slowly faded during the next few hours. In the 0539 UT spectrum, a remarkable feature with large radial velocities was observed between the two flare ribbons (Fig. 7). Though distinct loops were not detectable on the slit jaw picture in the center of Hα, this might be the indication of the matter descending into the legs of a loop prominence system connecting the two flare ribbons.

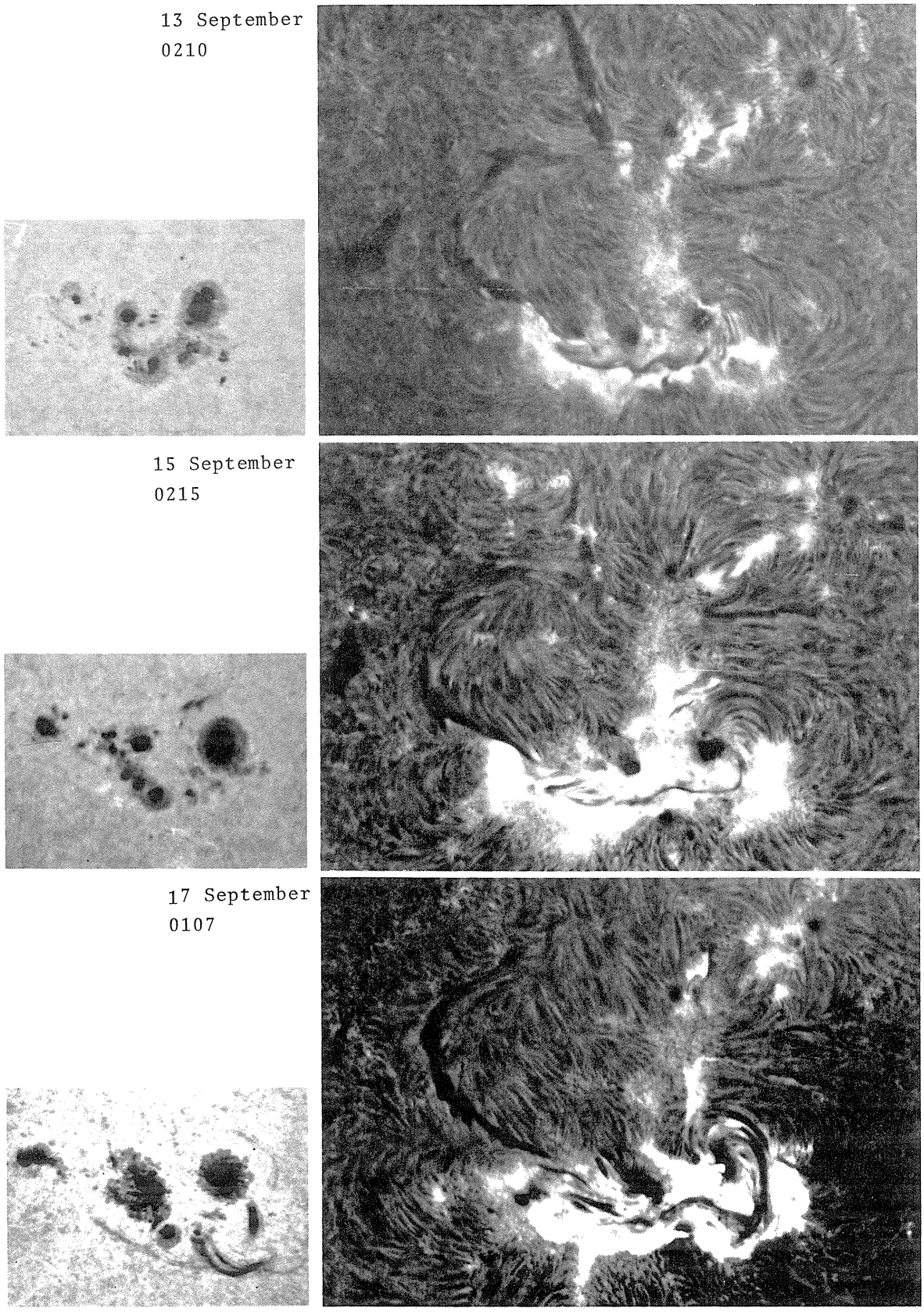

Fig. 1. Evolution of McMath 14943 between 13 and 17 September 1977.

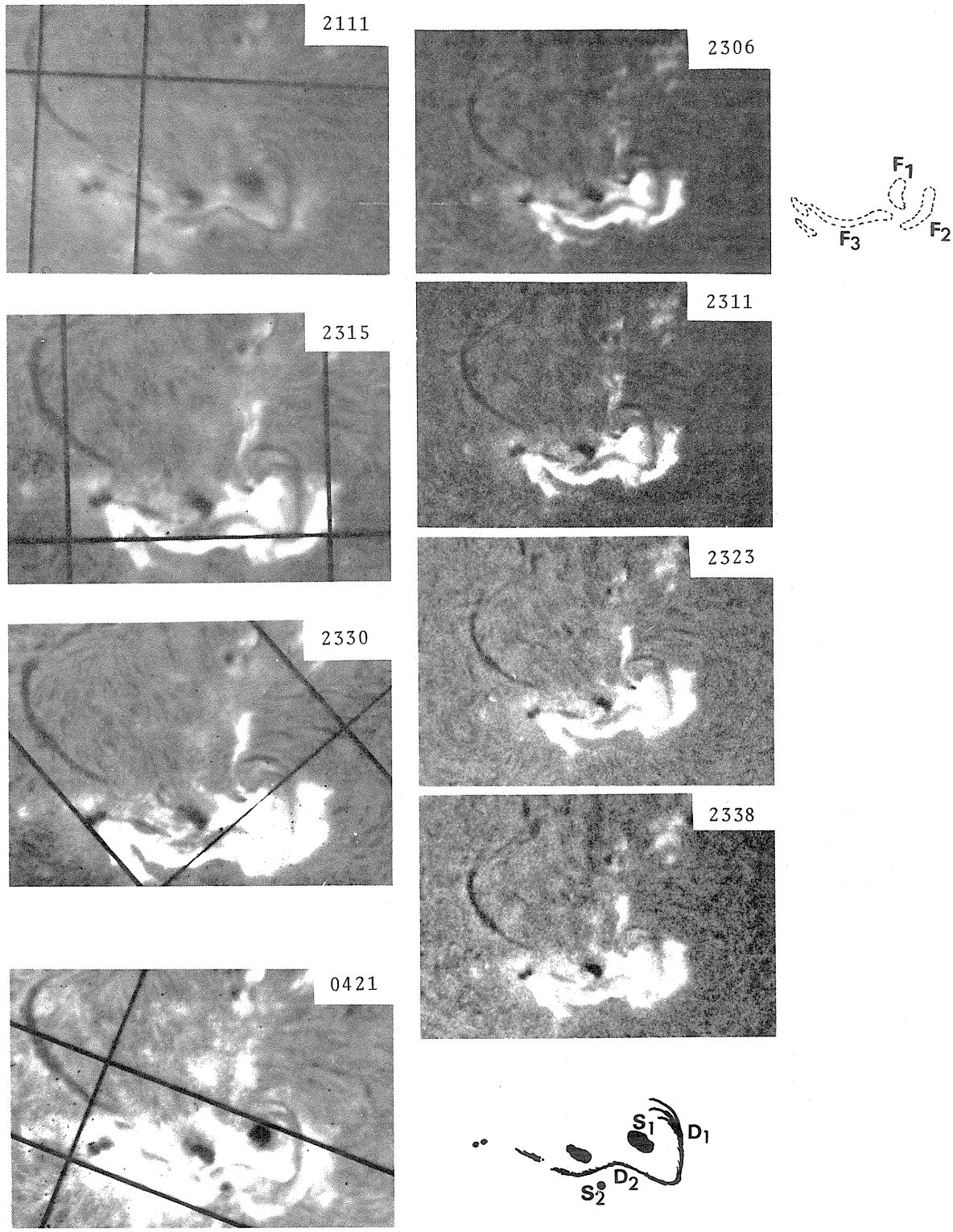

Fig. 2. Flare of 16 - 17 September 1977
Left: slit jaw pictures at Norikura
Right: patrol photographs at Mitaka.

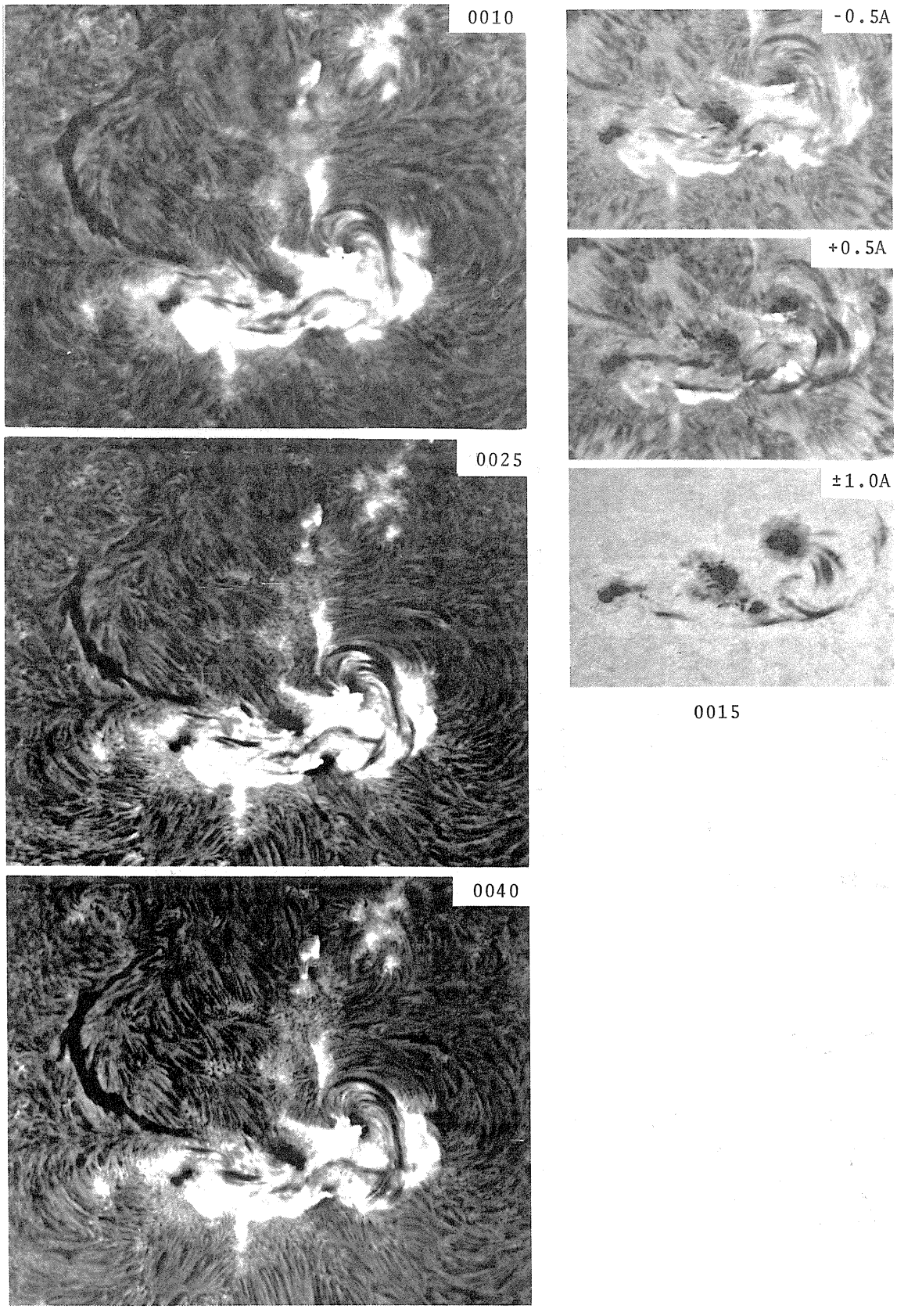

Fig. 3-a. Flare of 16 - 17 September 1977 at the last phase (1).

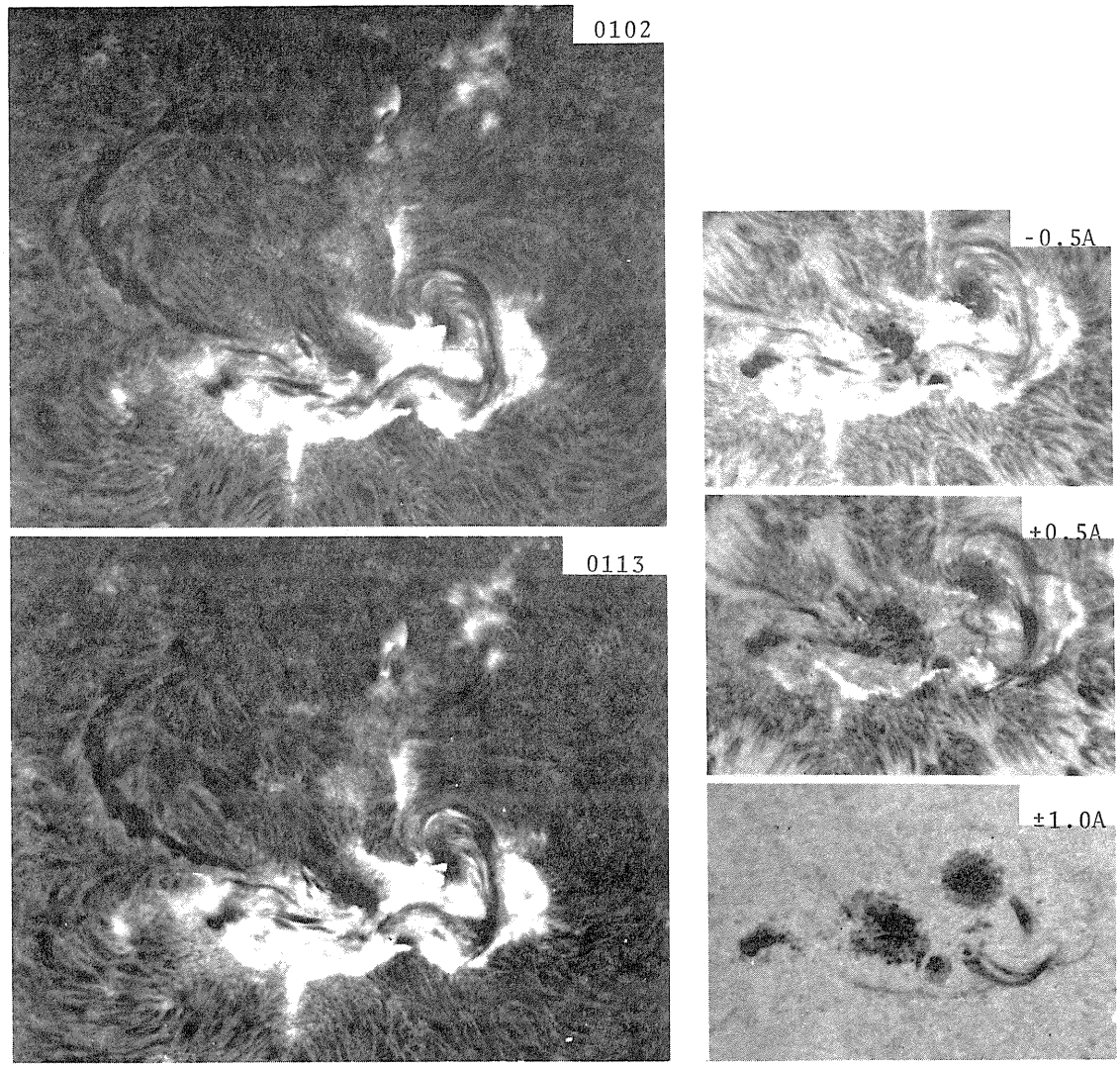

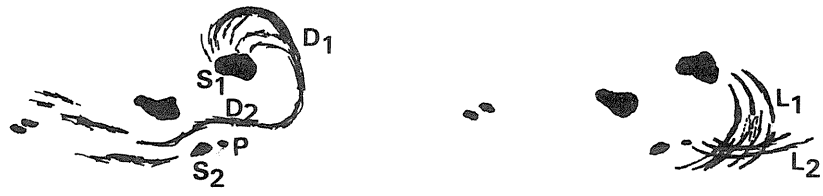

Fig. 3-b. Flare of 16 - 17 September 1977 at the last phase (2).

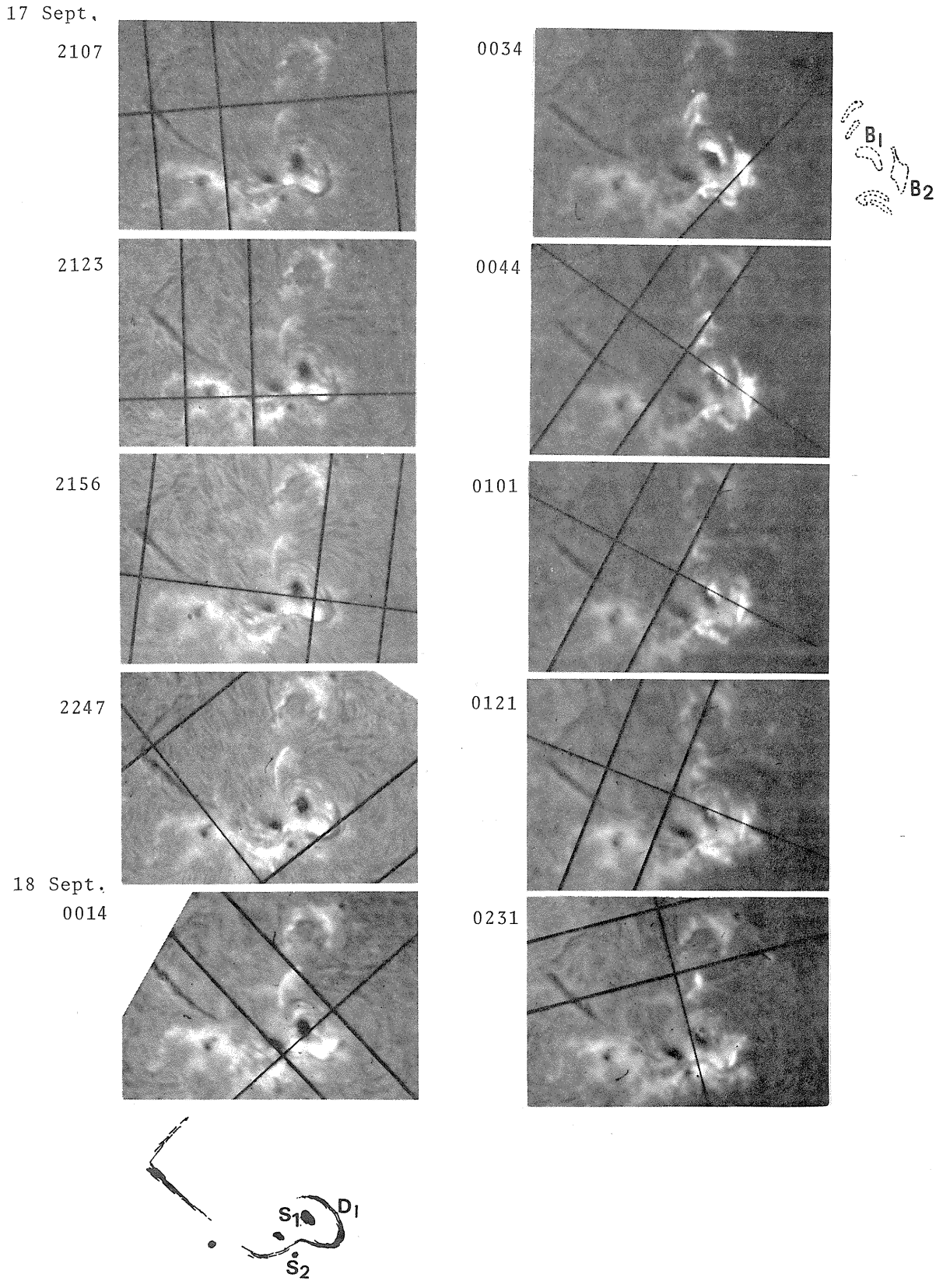

Fig. 4. Flare of September 17, 1977.

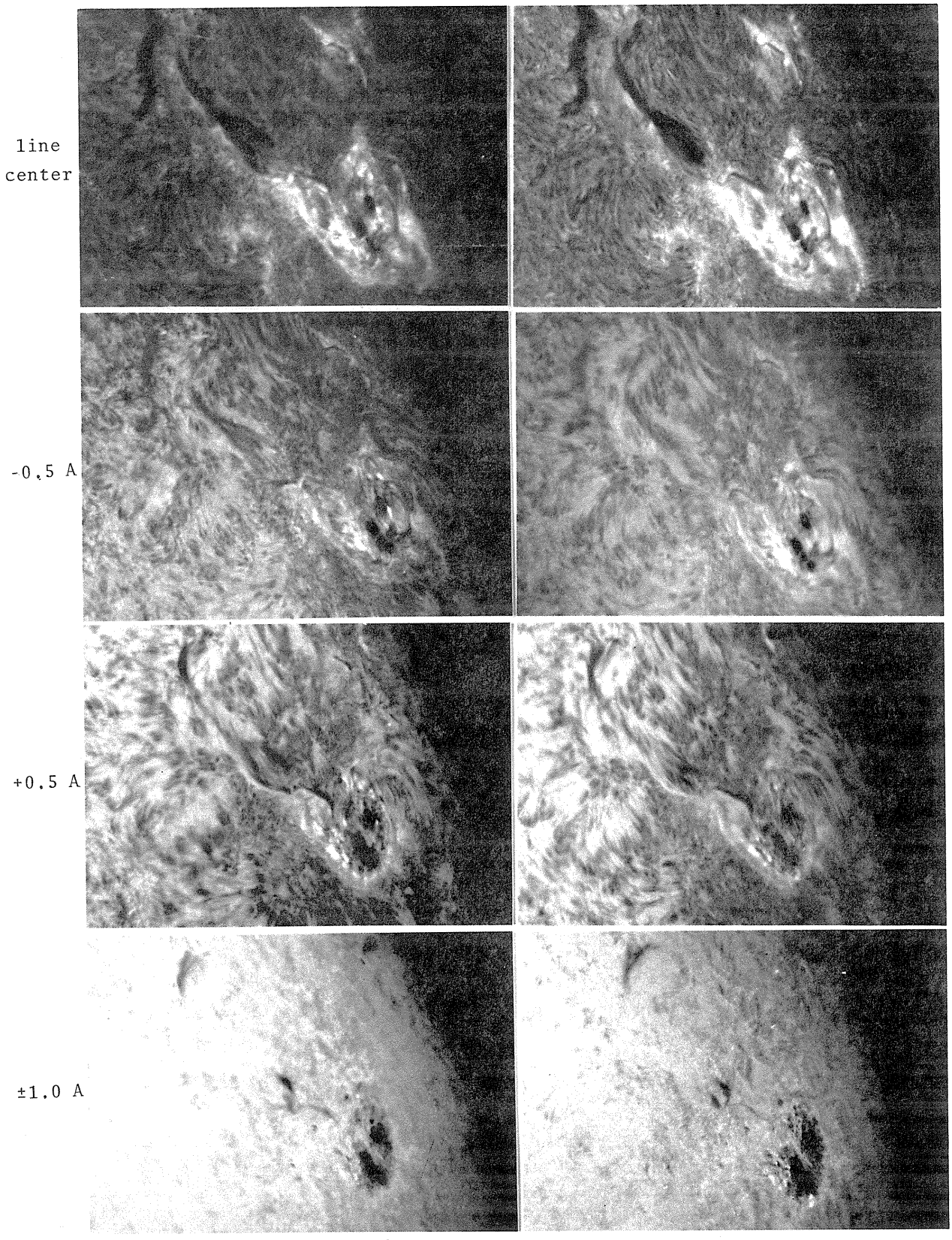

Fig. 5. McMath 14943 before the onset of 2n flare of 20 September 1977.

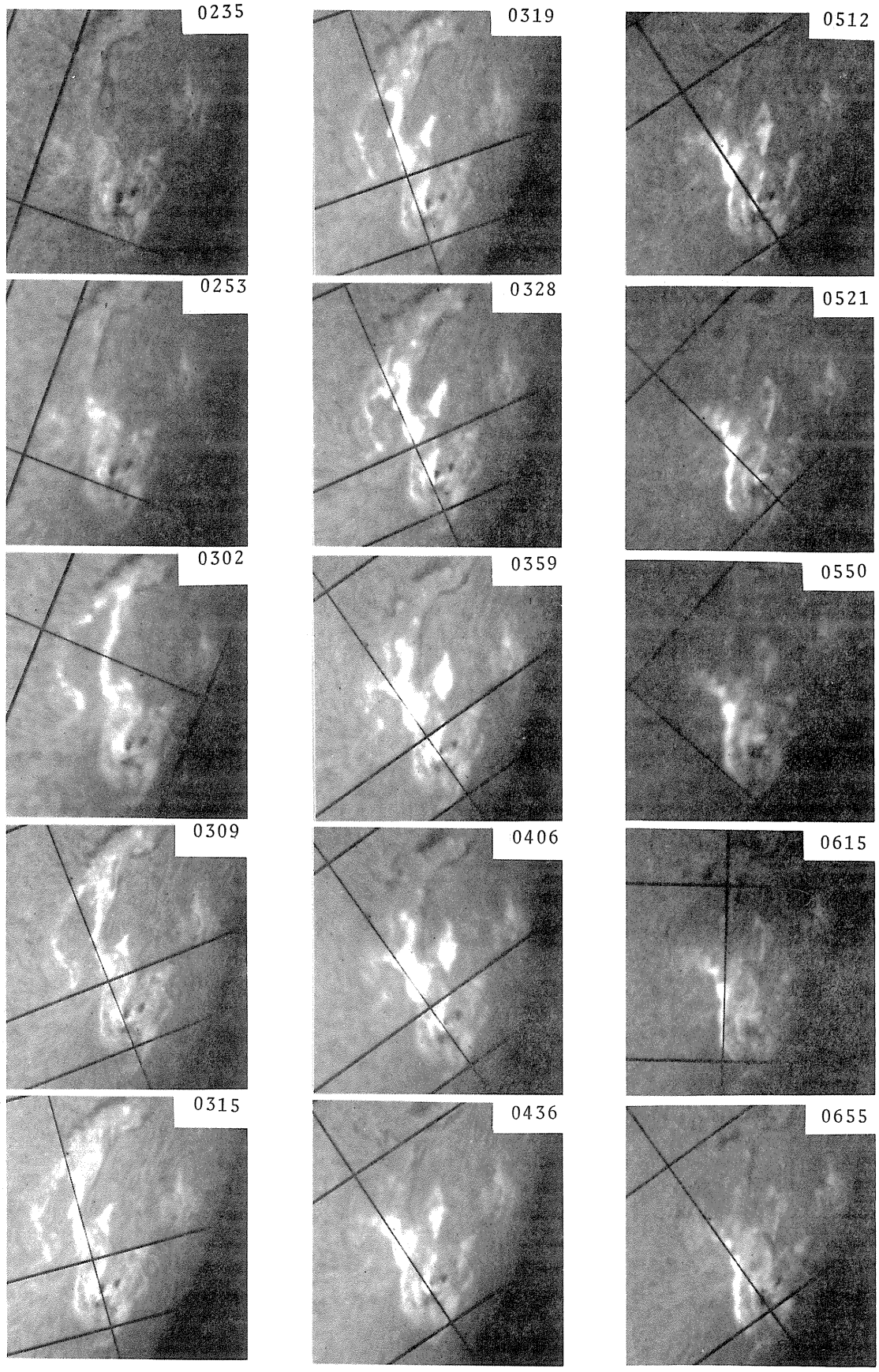

Fig. 6-a. Flare of 20 September 1977.

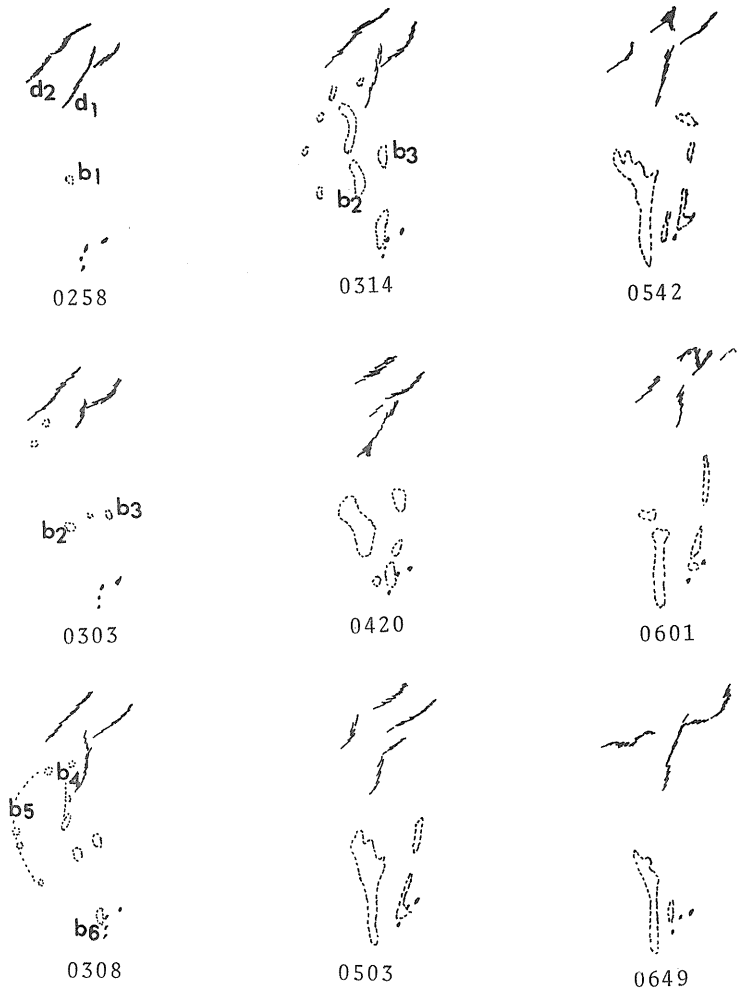

Fig. 6-b. Evolution of Flare of 20 September based on patrol photographs.

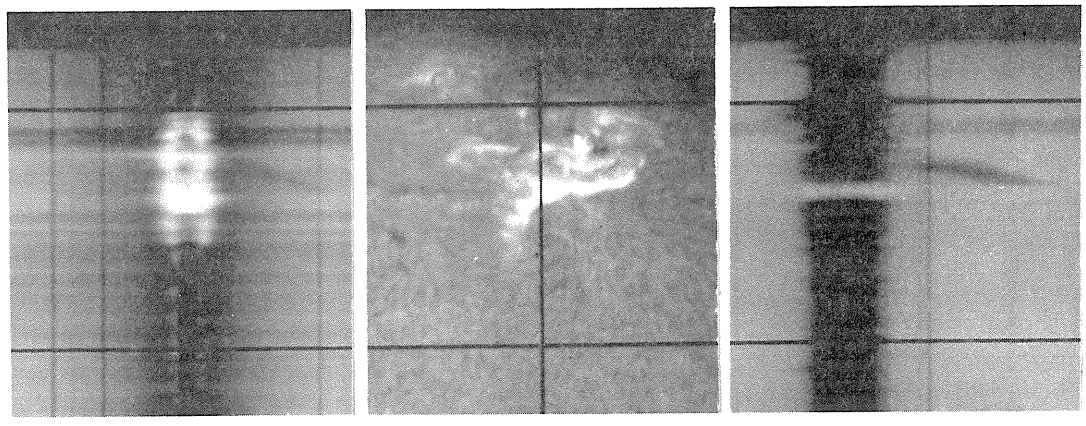

Fig. 7. K and Hα spectra taken at 0539 on 20 September 1977.

The Solar Flare of September 16, 1977, in the K Line of Ca II

by

Daniel Balboa and Francis J. Heyden, S.J.
Manila Observatory
P.O. Box 1231
Manila, Philippines

The flare of September 16, 1977, in McMath Region 14943* occurred in a type E sunspot group, which had an R value of 55, as estimated at Manila Observatory on September 15. The sky over Luzon, or the northern part of the Philippines, was full of scattered clouds and haze from the 13th to the 18th of the month, so that observations were available only through random openings in the clouds.

On September 13 a good photograph of the sunspot group was obtained through a broadband red filter on an orthosensitive film with the 10-centimeter refractor at Baguio--the mountain station north of Manila Observatory. The light bridge across the largest leading spot is present in this photograph shown in Figure 1. It persisted until the flare that followed 3 days later. This photograph of the spot group is the only one obtained during the period.

On September 16, the flare (early morning of the 17th in Manila) was photographed through haze with the spectroheliograph in the K line of ionized calcium. Figure 2 shows the flare as it enveloped the spot group of McMath Region 14943. The flare was observed visually in progress with the H-alpha filter at 16/2300 UT and was photographed with the spectroheliograph at 16/2320 UT. The end occurred at 17/0015 UT. Its position was N08 W21. The 850 millionths area measured by our observers reduced to 9.6 square degrees, thereby classifying the event as an importance 2b.

The telescopes had been in operation at 16/2244 UT. Clouds covered the sun from 16/2344 to 17/0000 UT and again from 17/0029 to 17/0130 UT. The sun was not bright enough for the 35-mm camera on the 30-cm monochromator with the Halle filter to take pictures. From 17/0525 until 17/0610 UT the sky cleared again, but the intervals between passing clouds were too short for a scan in hydrogen light. In all, the telescopes were kept running for 7.5 hours, but the intermittent clearings of the Sun amounted to about 2.2 hours for the entire period.

The Ca II scan of this flare displays unusual involvement of bright plage with spots in the group, showing filamentary ties with only those spots that have north magnetic poles (cf. *Solar Phenomena-Osservatorio Astronomico di Roma,* No. 233, p. 12).

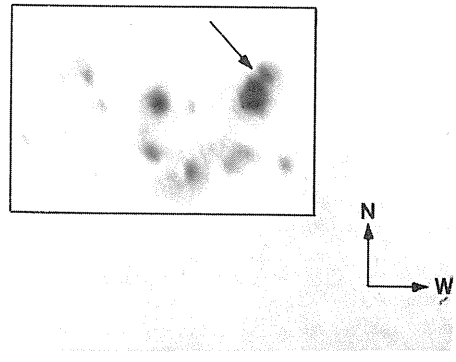

Fig. 1. Box encloses sunspot group associated with McMath Region 14943 (R = 55 on September 15). This photograph was taken on September 13, 1977 at 0105 UT at the Baguio Station of Manila Observatory. Arrow marks light bridge.

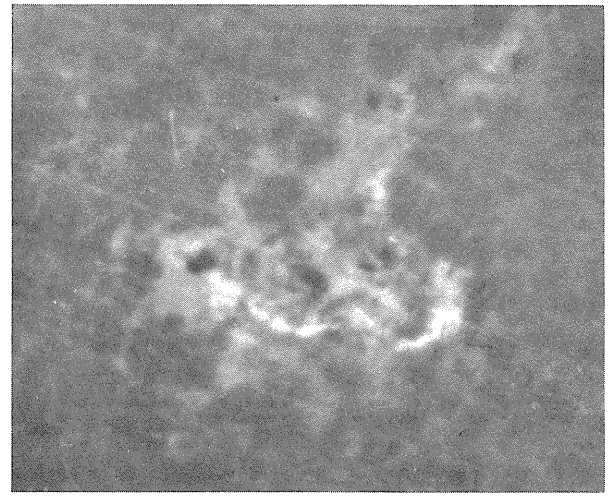

Fig. 2. Spectroheliogram of McMath Region 14943 in the K line of Ca II. This photograph was taken on September 16, 1977, at 2320 UT.

*McMath Region 14943 = Boulder Region 889 = Manila Region 322.

Morphological Structure and Energy Content of Flares of September 19, 1977 in Hα and CaK Line and Associated Geomagnetic and SEA Events

by

Erden Soytürk and Atila Özgüc
Kandilli Observatory
Istanbul, Turkey

Introduction

Between September 7 and 24, 1977 there was a series of interesting solar, ionospheric, and geomagnetic phenomena associated with the transit of McMath region 14943. During its first passage this active center was located around 196° in Carrington longitude and at S08. Throughout its passage many flares occurred in this region; however, the largest and the most intense one (3B) began on September 19, 1977 at 1010 UT, reached its maximum around 1044 UT, and ended about 1206 UT. We believe it was this major flare which caused these prominent ionospheric, geomagnetic, and solar cosmic phenomena on September 19.

Morphology of the Active Region on September 19

McMath plage 14943 located at N09W57 on September 19. According to the sunspot observations of Kandilli this plage comprised an F-type bipolar sunspot group with 11 spots. It will be useful to note that on September 18 the number of spots in this group increased to 64. The plage was photographed at the Kandilli observatory for 10 days on a scale of 10 arcsec mm^{-1} through a Zeiss 0.25Å birefringent filter for Hα and B. Halle 0.6Å birefringent filter for CaK. The isomaps were obtained by a Joyce isodensitracer. Referring to the chromospheric density as 0.00 D, 0.06 D contour, where D marks the plage's boundary, defines an average area of 7,500 millionths in the Hα line and 9,500 millionths of the solar hemisphere in CaK line. The following part of this plage forms the greater part of the region. The shape of the plage is controlled by the filament that existed along the neutral line from September 12 in such a way that it seperated the region into two parts, and also extended beyond it (Fig. 1 first row, frame 2 at the arrows). This filament bisected the U-shaped plage lengthwise. When Hα and are CaK isomaps of this plage examined, there appear to be six bright points [Dizer 1969] (see Figure 1: row 2, column 1 Hα isomaps; and row 3, column 4 CaK isomaps). These bright points match in both the Hα and CaK lines. Since there is a direct relationship between the intensity of CaK brightness and magnetic intensity [Bappu and Punetha 1962], these points can undoubtedly be interpreted as the region which has intense magnetic fields. They are placed at right (points 1-2-3) and left (points 4-5-6) of the filament, to the west and east of it, respectively. Due to some of the bright points' (3-4-4') movement towards the S (displacements away from the filament channel) during the flare, which became more perceptible after the flare and the movement of the plage towards the limb, a slight change was observed in the positions of these bright points. By examination of the last column of Figure 1, though the shape of the plage was conserved in CaK line, we see the plage enlarged and deformed towards the south in Hα.

Morphology and Development of the Flare

By examining the flare isomaps it is deduced that the flare commenced at 1010 UT with the flashing of three points: point 3, in between the leader and follower spots; point 4, to the south of the follower spots; and point 5 at the left of the filament. At 1035 UT point 4' appeared in the penumbra of the following spots, and later this point expanded over and united with point 4. A survey of the isomaps of the flare at its maximum phase (1044 UT), reveals that the flare was basically sharpest at the points numbered 3, 4', and 4. In the isomaps, unclosed contour lines correspond to 0.00 D; every closed contour line separation is equivalent to 0.06 D density difference; and the dotted contour lines are equal to 0.18 D difference in either Hα or CaK isomaps. Supposing chromospheric density is zero, then the density of the flare's maximum bright points equals 1.66 D in the Hα line and 0.72 D in the CaK line. From the isomaps at this phase it is clearly evident that the filament channel which is between points 3 and 4 (4') position remains as it was (Figure 1, row 5, frame 3). In Figure 2 you will find the projections of the flares, drawn from the Hα photographs, taken in 0.5°A steps in the interval of +2°A wings of Hα line. It is also seen that points 3 and 4 (4') feature the most energetic areas with the flare lying along both sides of the filament channel. At 1135 UT the flare fades out; at points 3 and 4 (4') there were some slight brightenings; at point 6 there sere some outstanding bright points similar to flare-like brightenings (FLB). Even at 1206:30 UT, an FLB is visible to the right of the extension of the filament out of the plage. In the CaK line the flare appeared in the same manner with the exception that centers 3 and 4 were not as distinct. Towards the end of the flare brightenings prevailed in centers 5 and 6. Finally we are satisfied with drawing your attention to the fact that in the CaK isomaps before and after the flare, contrary to centers 3 and 4 from which the flare advanced more intensely, the brighter centers have been points 5 and 6 where the flare was weak.

The Energy Content of the Flare

The isomaps obtaining Hα and CaK lines show the different phases of the flare development. The flash energy graphs are illustrated in Figure 2a and b. The additional dotted areas indicate the corrections made according to the intensity of solar center. The total and mean plage energy levels are given in Figure 3. It is understood from the graph, the flare was started at 1010 UT, following a

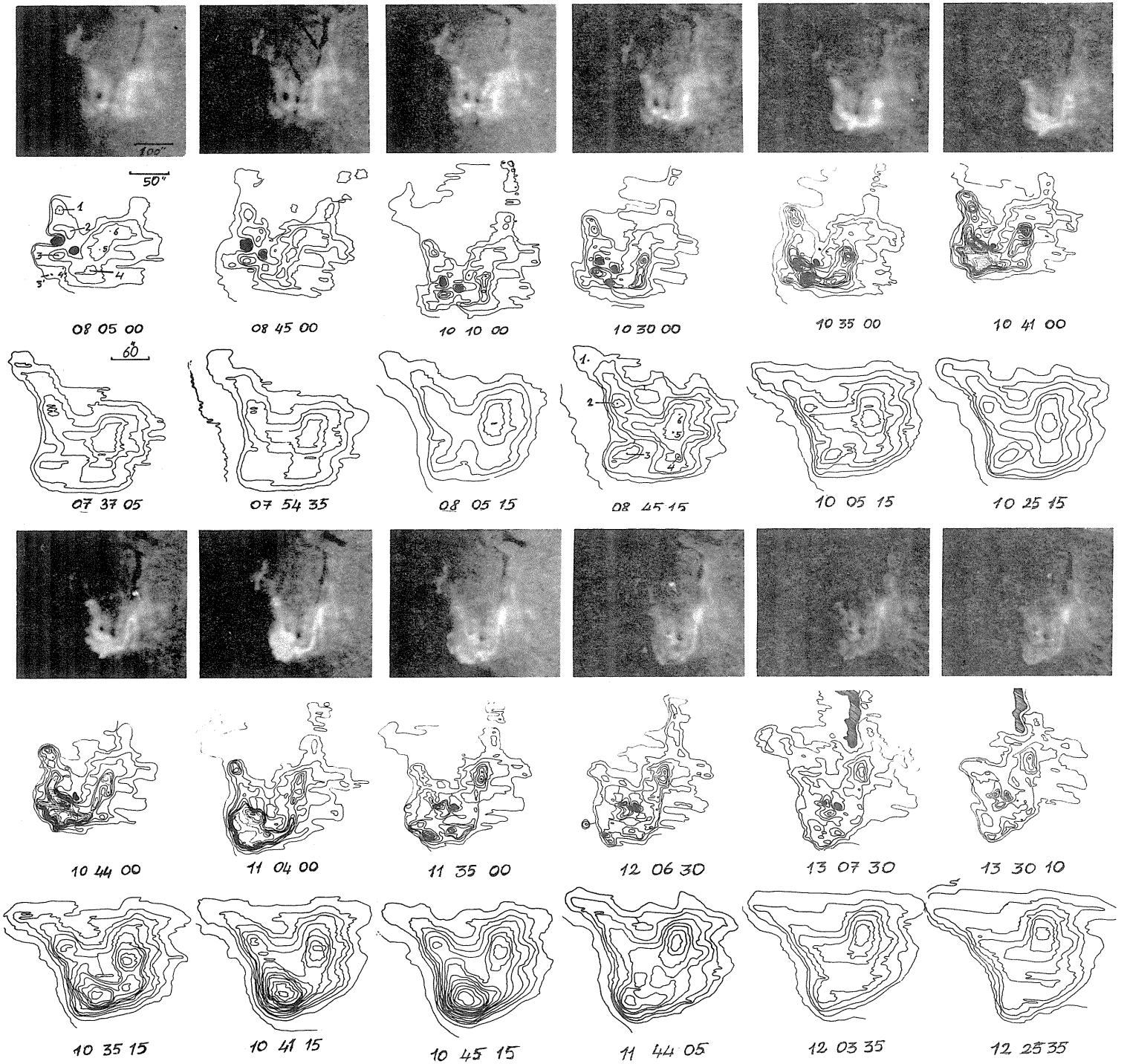

Fig. 1. First row shows Hα Filtergrams and the second and third show the Hα and Ca K isomaps.

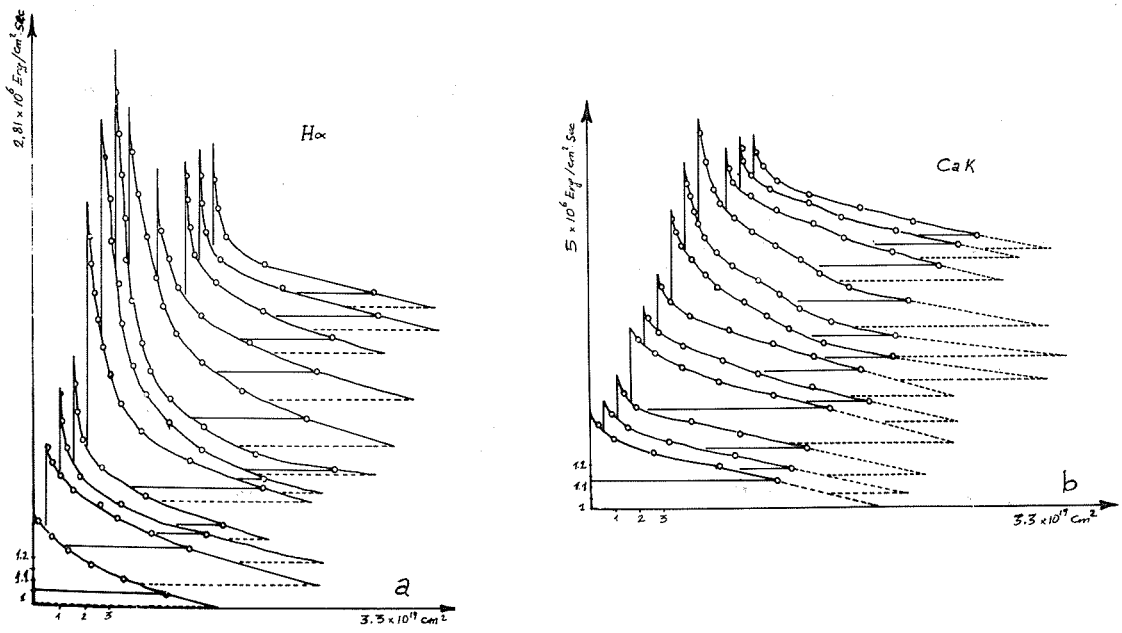

Fig. 2. Graphs a and b exhibit the flash energies in Hα and CaK lines, respectively. The abscissa is the area in terms of cm^2 and the ordinate indicates the density steps. Each graph has its own axis. However, the graphs are not on a time scale but are arranged in order of succession. Effects of the limb darkening and changes in atmospheric conditions are corrected by using dots. So dotted horizontal lines indicate the corrected chromospheric intensities.

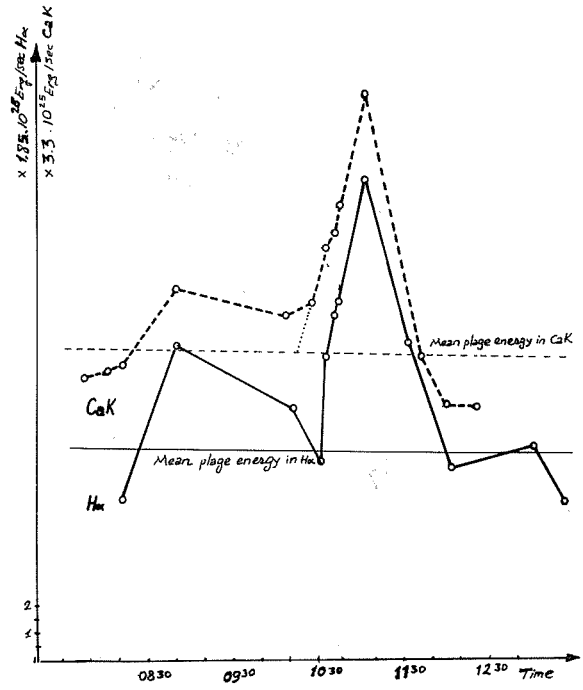

Fig. 3. Total energy of the plage and the flare in Hα and in CaK lines. The abscissa shows the time and the ordinate shows the energy in terms of Erg/sec. The horizontal dashed and full lines show the mean energy of the plage in CaK and in Hα lines, respectively.

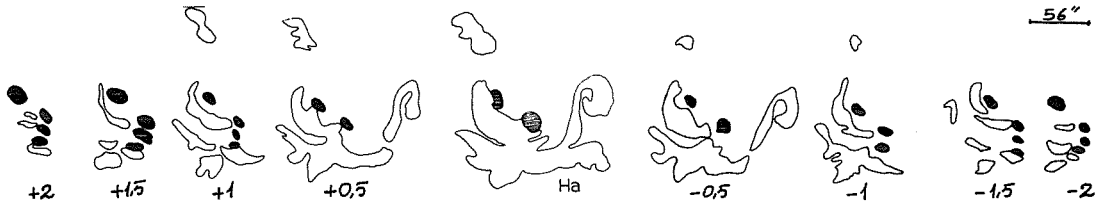

Fig. 4. The appearance of the flare in between ± 2Å wings of Hα at its maximum phase. All of the series were photographed in 30 seconds.

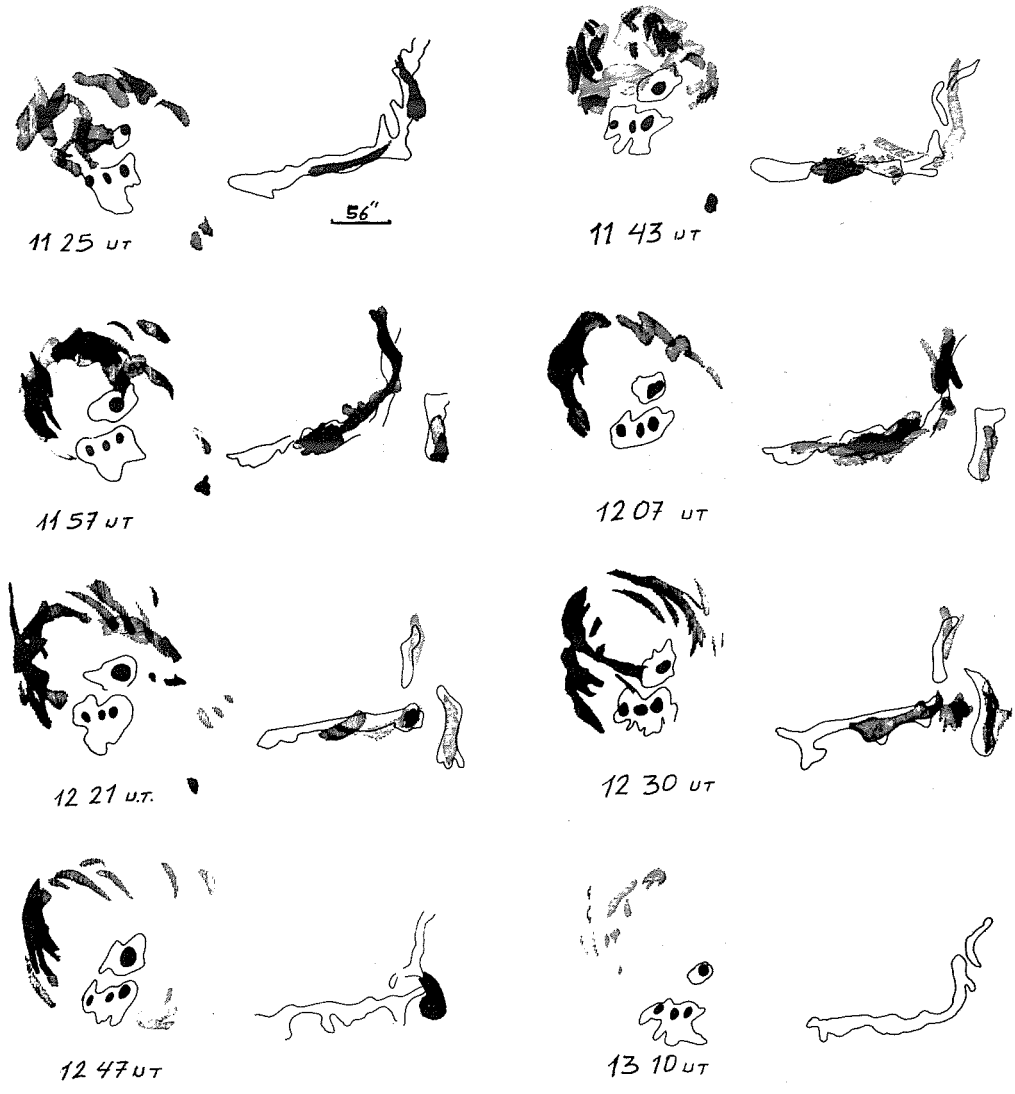

Fig. 5. This is a sketch obtained by drawing the mobile mass region from the photographs taken at different times, with 0.25Å steps, between the wings of ± 2Å of Hα horizontally and vertically, hatched areas represent the red and blue wings. For the regions 1, 2, and over 2 Å, gradually darker hatching is used.

preflare which started around 0830 UT. This was 1010 UT to 1206 UT when the plage energy, exceeding the mean plage energy, as calculated is found to be:

$0.51 \cdot 10^{30}$ Ergs in H α line and
$0.81 \cdot 10^{30}$ Ergs in CaK line.

Mass Motions in Plage Area

During the observation series of photographs, each completed in 30 seconds and taken with 0.25Å steps, observations between the wings of Hα $\pm$2.5Å were recorded in 10 or 20 minute intervals. In these photographs, depending on the speed of the movement and directional perspective some evidence of mass movements have been possible. Fig. 4 is sketched in such a way that, the movements seen up to 1A are loosely spaced lines (horizontal for (+) wing, and vertical (-) wings), and the movements seen up to 2Å are shown in the same manner by closer spaced lines. The movement seen in the over 2Å wings are dark painted areas, the position of the sunspots which are seen over the 2 Å wings and the filament seen at Hα are shown in full lines. Fig. 5 is obtained by superposing 8 wing frames like those in Fig. 4. On a study of Fig. 5, material trapping and mass movements are obvious on an arc which extends from following to the preceding spot with a diameter of 65,000 km and an altitude of 85,000 km. At the same time some waves are evident beyond the plage extension of the filament. Looking at Mt. Wilson magnetograms it seems that formation of a flux tube between the follower and the leader of this sunspot group, is typical. At 1125 UT (near the end of the flare) were seen mass motions as small arcs. At At 1143 UT some mass motions were apparent along an arc of diameter about 30,000 km which as it was observed by us, consisted of three ribbons. The frames taken between the times 1157 and 1230 UT show the most developed state of the arc. However, it was not so clear because of very little inclination with respect to the line of sight. A view was presented that the arc consisted of 4 ribbons, three emerging from the follower and approaching about to the leader spots (see Fig. 5, 1157 and 1230 UT superposed frames) and the one emerged from the leader spot (N polarized) and terminated at an S polarized region near the limb according to Mt. Wilson magnetogram records. In Figure 5 the right side of the arc was seen on the (+) wing and the left side on the (-) wing. It is believed that inside the plage area the speedy particles to which a piece of the diffuse filament joined were trapped by an already existing arc [Kleczek 1969], and they were subjected to the known physical phenomena. At 1310 UT some residuals of the trapped materials were seen. On the other hand the outward extension of the filament splitting the plage seems perturbed because of the flare. Some movements were seen in the direction parallel to and even perpendicular to the direction of sight, particularly at the far end and on the kink of the filament.

SEA and Geomagnetic Events

Fig. 6 shows the records of the H and D components of the geomagnetic field. On the same graph the duration of the flare, as observed from Kandilli Observatory are also marked. The preflare which occurred 0830-0930 UT are not included to the graph. In Fig. 6 although the geomagnetic disturbance, record by H and D component took place between the times 1143 and 1335 UT the flare itself started at 1010 UT, continued until 1206 UT. Thus geomagnetic disturbance commenced 93 minutes before and finished 91 minutes after the flare. Whereas when we place the interval of 1125-1310 UT during which we saw the arc (the perpendicular hatched column), it is seen that it associates with the geomagnetic perturbation. The perturbation was 18 minutes later at the beginning and 26 min later at the end with respect to the arc. The observed arc duration was 115 min while duration of the perturbation was 112 min. It seems doubtful to us whether to consider the arc responsible for the geomagnetic perturbation and for the ground level cosmic ray enhancement. SEA event started at 0935 UT and after reaching a peak at 1040 for 6 minutes, it ended at 1212 UT.

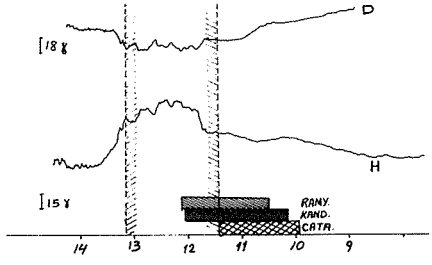

Fig. 6. Geomagnetic variations of H and D components and the flare according to the various observatories are given. The hatched column shows the time interval in which the big arc was observed.

References

DIZER, M. 1969 Isophotal Photometry and Morphological Changes in the Flares., Solar Physics, 10, 416-428.

BAPPU, M.K. and L.M. PUNETHA 1962 Calcium Faculae and Solar Effects, The Observatory, 82, No. 929, 170-171.

KLECZEK, J. 1969 Splintering Loop Prominences, Solar Physics, 7, 238-242.

Combined Observations of a Flare-Producing Region Development on the Sun on September 10 - 20, 1977 at Mt. Sayan Observatory

by

V.V. Kasinskii, A.A. Golovko
Siberian Institute of Terrestrial Magnetism, Ionosphere and
Radio Wave Propagation of the Academy of Sciences
Irkutsk, USSR

Introduction

At the Mt. Sayan Observatory from September 10 to 20, 1977, regular observations of the McMath 14942 and 14943 active regions were conducted.

The complex observations were made with three solar instruments. On the automatic solar telescope using the panorama magnetograph [Grigoriev et al., 1975] regular recordings were performed. Photoheliograms of sunspots in integral light with high resolution (10-15 min each) and drawings of groups as well as the longitudinal magnetic field registrations in the integral image of active regions were done on the second horizontal telescope. On the large coronograph (ϕ = 50 cm, f = 7 m) of Prof. Nikolskii's design (IZMIR) recordings of active regions in the Hα line have been carried out by P. Cotrč (Astronomical Institute of the Czechoslovakian Academy of Sciences, Ondrejov). According to the preliminary information sent by NOAA, Boulder, Colorado (USA), the burst of flare activity in McMath 14943 was very high on September 16, 18, and especially 19, 1977. All flares were visible in X-rays and generated energetic particles. Thus we have obtained preliminary data that when put together may give a definite picture of specific features of the active complex evolution under consideration.

The full list of data obtained by these types of observations is given in Table 1.

Table 1. Summary of Data Obtained on the Mt. Sayan Oberservatory

Type of observation	Date, Time (UT)	Remarks
1. Panoramic magnetograms	11 Sep 0100 - 0242	Time of overlapping by panorama magnetograph is indicated. Scale of magnetogram's area 400" x 600".
	0650 - 0910	
	12 Sep 0110 - 0323	
	13 Sep 0249 - 0630	
	1012 - 1105	
	14 Sep 0055 - 0229	
	0631 - 0937	
	15 Sep 0034 - 0925	
2. H-alpha films	19 Sep 1028 - 1055	The Sun's diameter 130 mm.
3. Photoheliograms of sunspot in the white light	18 Sep 0600 - 0655	
	19 Sep 0032 - 1026	
	20 Sep 0000 - 0115	The Sun's scale 550 mm.
4. Sunspot drawings in white light	15 Sep 0113 - 0303	
	- 0429	
	17 Sep 0005 - 0646	Scale of Sun 550 mm. Only the first moment of drawing is given.
	- 0844	

Morphological Features of McMath 14942, 14943

September 1977 falls on the rising phase of the solar cycle 21 when there is a high probability of interaction between the regions with mixing of polarities. The McMath 14942, 14943 regions emerged on the invisible side of the Sun after August 26, 1977.

The McMath 14943 region with maximum areas 970 millionths (Sept. 17) was the main component. It was at the low-latitude position of N08. Its leader had south polarity 2700 Gs and may thus be assigned as a spot of cycle 20. A smaller component McMath 14942, with area 230 millionths (Sept. 14) can be treated as a satellite group. It was at N16 and its polarity order was normal for sunspots of the new solar cycle 21. The total dimension of the complex was 20° in latitude and 220° in longitude, Fig. 1.

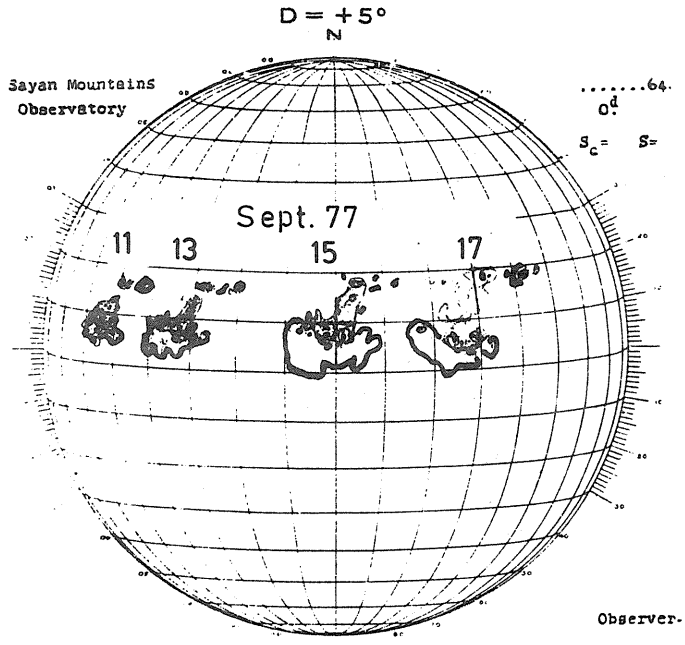

Fig. 1. General picture of development of McMath 14942/43 on Sept. 11-17. The dashed area is S-polarity. Note the EW-direction of the neutral line on Sept. 15.

Similar complexes consisting of the main group and the nearest satellite group have been studied earlier [Kasinskii, 1972, 1973a] where interaction between the components leads to the flare [Rust, 1974] or proton flare situation. The physical relation between the old and newly developed group as is shown by panorama magnetograms was manifested by means of a wide "bridge" of south polarity elongated in the meridional direction (Fig. 1). The sketches in white light have fixed darkenings and pores between the groups similar to dark surges that occur in the chromosphere, Fig. 3.

General Development in the Pre-flare Period of Sept. 11-15, 1977

In that period, observations were most effective and comprehensive.

The main magnetic flux terminated on Sept. 11. After Sept. 11 the panorama magnetograms did not show any significant increase in the flux, although a general expansion of the magnetic flux of the "bridge" took place, Figs. 1, 2. From the beginning of the appearance of the main group in the complex on the visible disk, its unusual magnetic configuration is evident. As a result of evolution, hills of N-polarity took on with respect to S-polarity hills an unusual nearly "vertical" location, and the zero line took on E-W location almost normal to the equator, i.e. turned by 90° to the normal one which according to Rust [1973], is a predictor of a major proton flare. This leads to essential deformation of the zero line and to enhancement of magnetic tensions (grad $H_{\parallel}$) along the filament, Fig. 4.

The general picture of sunspot development shows the following properties. On Sept. 11-12 somewhat quick impulsive changes in configuration are observed: enlargement of size, changes of the shape of nuclei and penumbra perimeters. No new spots have been developed. On Sept. 13-14 only slow evolutionary changes are observed implying divergence and individualization of magnetic poles. On Sept. 14-15 prior to the "flare" stage, the emergence of a new magnetic flux at the center of the group was observed and small spots appeared closer to the following spots (Fig. 1). The leader having two nuclei shows rotational movement with a velocity of 0.8 grad/h. At the same time the magnetic hill adjacent to the leader from SW-side had also shown the rotational motion. This altogether complicated and twisted the zero magnetic line of $H_{\parallel}$.

The satellite McMath 14942 was the ordinary bipolar group of new cycle and did not show any significant features. The emergence of the magnetic flux in it terminated by Sept. 13, Fig. 3.

SEPT. 13, 1977

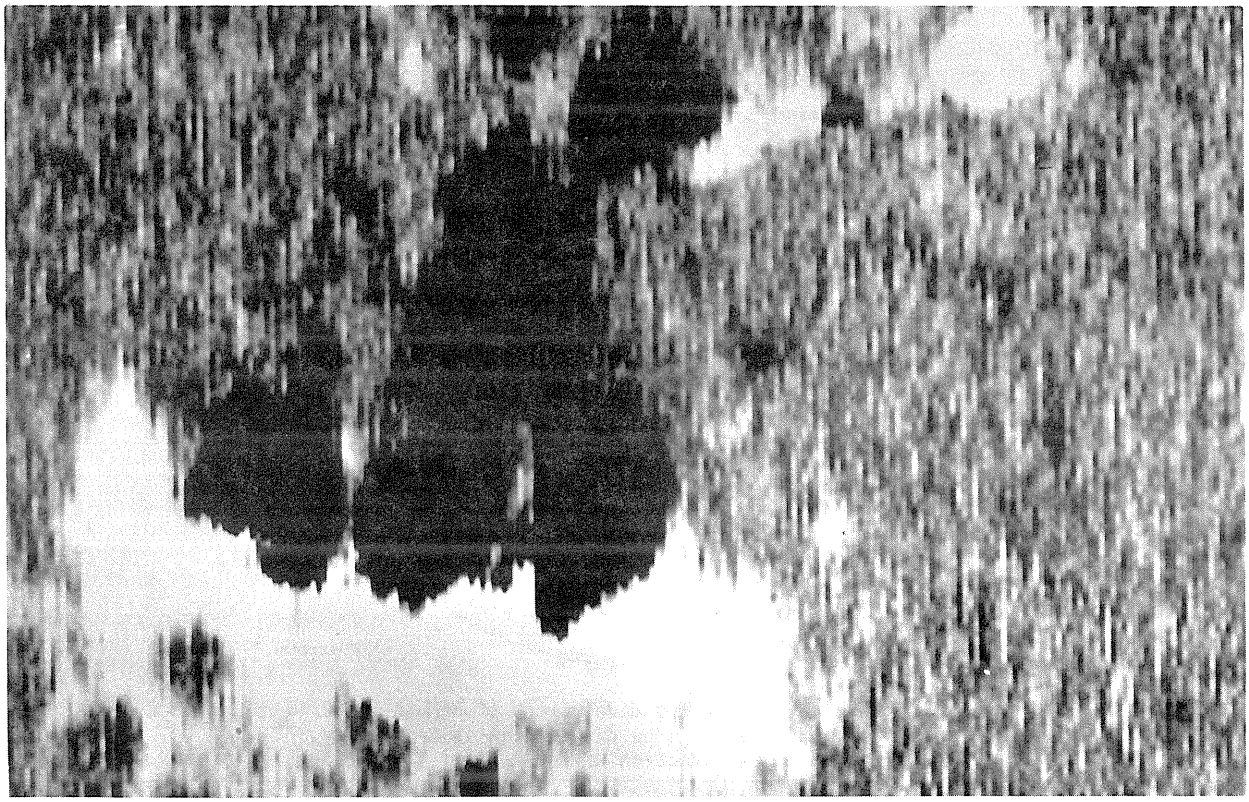

SEPT. 15, 1977

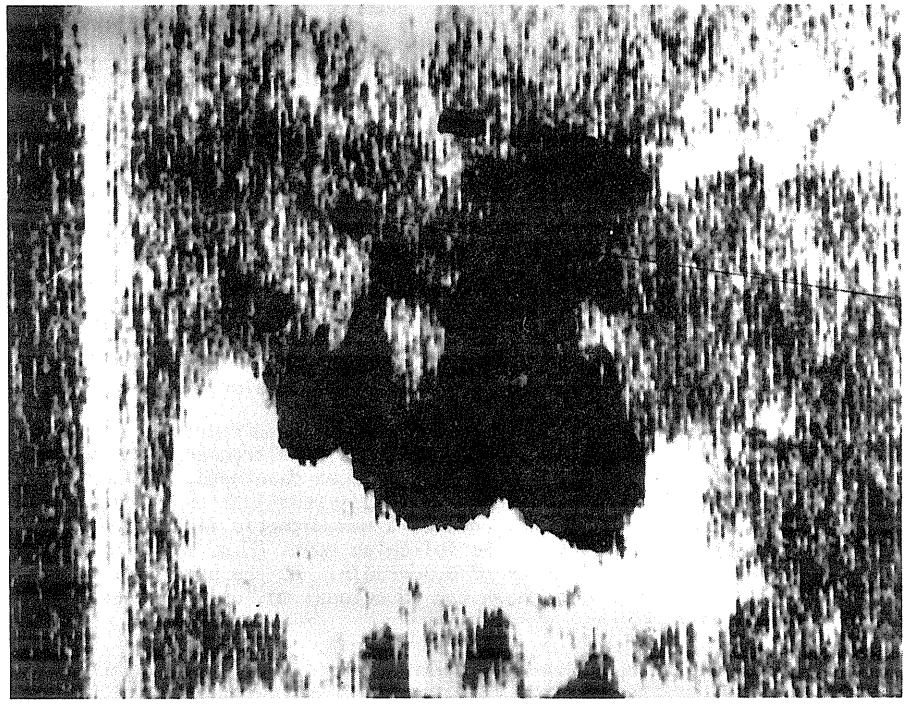

Fig. 2. Two panorama magnetograms, dimensions of 400" x 600", of the large group (center) and the satellite (right-top) on Sept. 13 and 15. The wide bridge (black-south) polarity connects two components of the complex. Zero line $H_{\parallel}=0$ is stretched nearly parallel to the equator, east-right, west-left. One can see black S-polarity is more compact and continuous on Sept. 15 at 0540 UT than on Sept. 13 at 0235 UT.

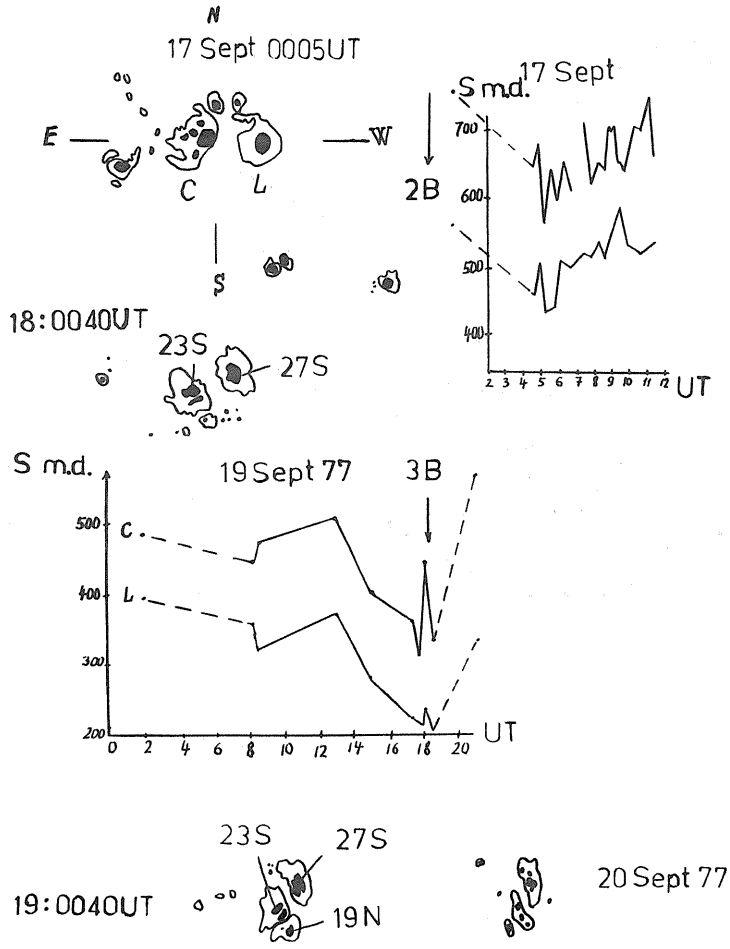

Fig. 3. White-light drawings of Sept. 17-20 and the area development (in millionths of disk) of two large sunspots "C" and "L" after the Sept. 16 flare and before the 3b flare on Sept. 19. It can be seen that the disruption of E-N penumbra of the "C" spot 2 hours later in the Sept. 16 flare and simultaneous decrease in area "C" and "L" spots are just before the 3b (see arrow) flare of Sept. 19.

In selected periods we have recorded the longitudinal field in FeI 5474Å in integral image of the McMath 14943 active region as complex, see figure. Fig. 4 presents the curves of magnetic field changes, or "imbalances of magnetic flux" with time. The curves show the selected impulse enhancement level of imbalance towards the S-polarity with subsequent reduction that begins about 2 hours later. There was no general enhancement of "imbalance flux". On Sept. 15, the signal south polarity of 8 Gs was recorded which is the indication of the common imbalance of flux over the whole complex area. We associate this impulsive signal of magnetograph integral bunch with the general instability or emergence of new flux portions which could lead to alternative overwhelming north or south polarity recorded in the integral light by the magnetograph.

Fig. 4. General position of curved "neutral line" or filament (dark) inside and outside of active region on Sept 19 3 hours before the beginning of a proton flare obtained in the Hα line center.

Evidence for Magnetic Energy Buildup Prior to a Flare

According to Kasinskii [1978] the energy stored in an active region near the filament is directly proportional to the magnetic flux F penetrating the filament, the gradient longitudinal field $H_{\parallel}$ and the square of deviations ε from the line of force of a source-free dipole-like configuration. The energy can be expressed in the following form:

$$E = (\pi^2\mu/4)\vec{F}\cdot(\text{grad } H_{\parallel})\varepsilon^2$$

We can determine the value of the magnetic energy capacity of the region using the observed parameters F and grad $H_{\parallel}$. The flux F determined as the product of the area north (75 square degree) or south (65 square degree) polarity from the magnetograms and B=150 Gs is the mean magnetic intensity recorded on the magnetograms (Fig. 1). This gives $F=BS=1.36\ 10^{22}$ maxwell. For the gradient let us take its value between two spots S 2300 gauss and N 1700 gauss on both sides of the filament, as was the case on Sept. 18. The estimation gives 0.053 gauss/km which can be considered as moderate. For the value let us take a thickness of about 1000 km or the vertical dimension of the filament that are quite comparable. Substituting all the quantities in formula (1) we get:

$$E = 8\text{x}10^{31} \text{ to } 10^{32} \text{ ergs}$$

which is quite appropriate for the flare of Sept. 19. These calculations seem to be supported by the observation of sunspot in white light (large-scale sketches), Fig. 3, showing the energy build-up stages.

The central massive spots in the main group were smashed to pieces on September 15, 0403 UT and consisted of as many as 3-4 consolidating sunspots with general penumbra. Therefore before the large Sept. 16 flare (2228 UT) the process of consolidation of sunspot in the central part of the region is over. At that time the region acquires the maximum magnetic flux and gradients sufficient for the energy supply to the large flare as formula (1) states. The sketches taken just after the beginning of the Sept. 16, 2b importance flare (2 hours later) showed that the center spot had adopted a saw-like shape of the eastern penumbra and a long-stretched train ($\sim$50,000 km) or pores in the NE direction, Fig. 3. Beside this, "C"-spot shows a strong anomalous Wilson effect, while the "regular" leader "L" does not. These facts give evidence in favor of fast changes in the configuration of the large-spot type of "breaking" part of penumbra. Typically, on Sept. 18 at 0040 UT after the flare, the "C" spot shows the normal Wilson effect which exhibits the rehabilitation of the initial configuration.

Pecularities of the Sept. 19 Proton Flare

The proton flare of Sept. 19 began at 1026 UT. Using the cinema H-alpha camera in the focus of the large coronagraph ($D_\odot$ = 130 mm) it was possible to follow the main phase up to 1055 UT. The general view of the flare is given in Fig. 5 at 1035 UT. The flare had a classical character: two long ribbons on both sides of jug-like filament but shifted with respect to each other along the neutral line H_{II} (Fig. 6). The south ribbon was longer in the ES part and wider at its center, where the main body of the flare occurred. In this place, the bright matter of the flare covered almost completely the spot of N-polarity, 1700 gauss. The two ribbons shifted the one to the east and the other to the west together with the central flare's body resembling a crab form (Fig. 7). In the later stage of the main phase there are noticeable systems of bright loops as the bridges over the neutral line. Another interesting feature is the spiral structure near the small N-spots at the ES-quadrant (at 1042 UT) 20 min after the flare's beginning. This is indicative of the curving of the hot plasma similar to funnel motions of fluid. The form of curving resembles a letter S. Similar spiral forms have been found in all flares of the main Zurich spot classes (E,F,G) [Kasinskii, Lyakhov, 1975a]. It can be interpreted as the circular current systems in the crossed electric and magnetic fields, $\vec{E} \times \vec{H}$ [Kasinskii, 1975b]. It is typical that spiral structure in the Sept. 19 flare enhanced 8 min after its appearance, which indicates the short-impulsive manner of the accelerating field $\vec{E}$ in the flare.

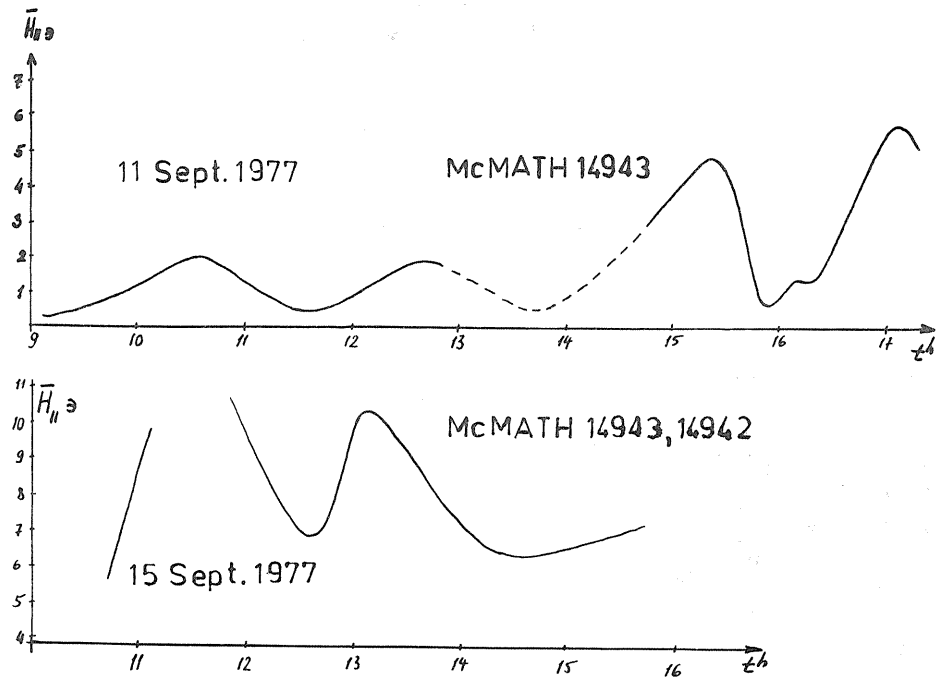

Fig. 5. The pulsations of the magnetic flux from all over the region McMath 14942/43 in flare-quiet period on Sept. 11-15 recorded by magnetograph in the "parallel beam" regime.

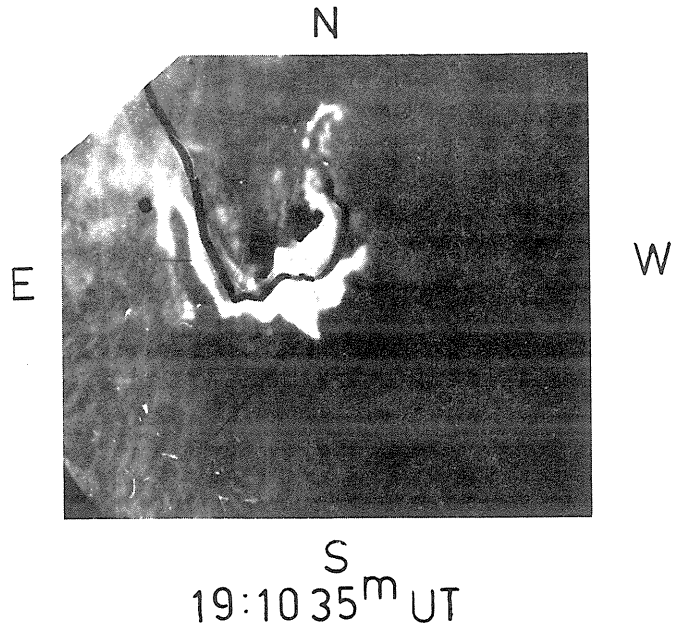

Fig. 6. General localization of two ribbon flares on Sept. 19 along the neutral filament (retouched). The main triangle-like body of flare is indicated by black arrow.

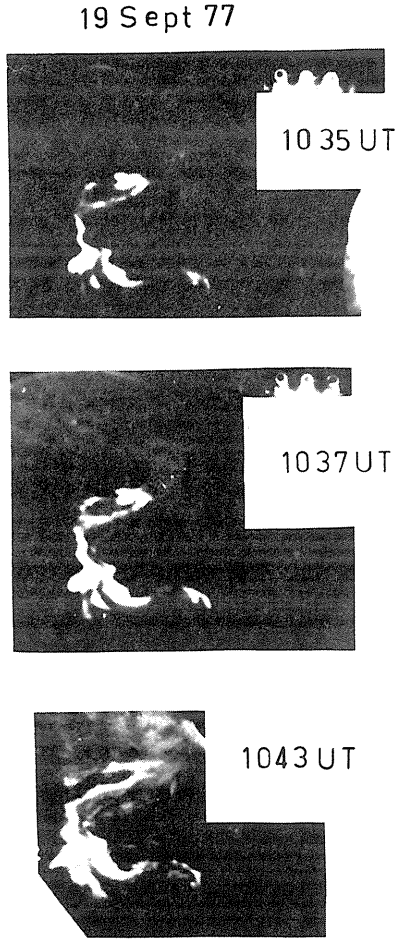

Fig. 7. Three points of development of "crab flare" on Sept. 19 just after the flash-phase. The spiral structure which existed at 1035 and 1037 UT (top) has been enhanced 8 min later (1043 UT).

Conclusions

Having summarized the preliminary analysis of the McMath 14942, 14943 active regions we can make the following conclusions.

1. The regions show a typical slow build-up of magnetic energy (Sept 10-15) which accompanied an enhancement of the magnetic flux F, and possibly the gradients of field, along the neutral line that turned by 90° from its meridional (classic) direction.

2. Registration of magnetic flux of region in integral light with high resolution witnesses in favor of the dynamical instability of separate parts of the magnetic region considered.

3. The release of energy on Sept. 16, 17, 19 has occurred owing to large energy capacity ($8 \cdot 10^{31}$ ergs) of the region, unusual neutral line direction, and some changes in the penumbra of "disrupt-like" manner. The Sept. 19 flare has obtained a spiral structure and this indicates the accelerating field $\vec{E}$ in the main phase.

Acknowledgments

The authors wish to thank Miss L. Ermakova for some of the panorama magnetograms, Dr. P. Cotrc for providing H-alpha films and to all members of Observatory staff for good cooperation.

REFERENCES

KASINSKII, V.V. 1972 On the Large-Scale Interaction between the Chromospheric Flare Generated Sunspots and the Satellite Groups, (in Russian), *Solnechno-zemnaya Fizika, 3,* Moscow, 296-305.

KASINSKII, V.V. 1973a On the Role of the Satellite Groups as the Proton Flare Predecessors, (in Russian) *Issledovaniia po Geomagnetizmu, Aeronomii i Fizike Solntsa, 26,* Moscow, Nauka, 118-128.

KASINSKII, V.V. and LYAKHOV 1975a Spatial Structures of Flare Ribbons in Bipolar Sunspot Groups E, F, G Class, (in Russian) *Issledovaniia po Geomagnetizmu, Aeronomii i Fizike Solntsa, 37,* Moscow, Nauka, 37-45.

KASINSKII, V.V. 1975b S-Structures of some Flares and Possible Topology of an Electric Current in Flat Geometry of a Bipolar Magnetic Field, (in Russian) *Issledovaniia po Geomagnetizmu, Aeronomii i Fizike Solntsa, 37,* Moscow, Nauka, 46-54.

KASINSKII, V.V. 1978 Satellite-Sunspot Phenomena as an Index of Magneto-Hydrostatic Instability of the Chromosphere before Large Flares, Preprint SibIZMIR, No. 14-78, IRKUTSK, 3-10.

KLOTCHEK, N.V., V.M. GRIGORIEV, and V.I. KRUGLOV 1975 Panoramic Solar Magnetograph of Mount Sayan Observatory, (in Russian) *Novaya Tekhnika v Astronomii, 5,* Leningrad, 25.

RUST, D.M. 1973 Estimating the Flare Production Potential of Solar Active Regions from Analysis of Real-Time Magnetic Field Data, *Sac. Peak Obs., E.R.P.,* No. 440.

RUST, D.M. 1974 Observation of Flare Associated Magnetic Field Strength in "Flare Related Magnetic Field Dynamics," NCAR, Boulder, Colorado, p. 243.

Some Characteristics of the Evolution of the Flare-Active Complex Observed in September 1977 (McMath Plages 14942 and 14943)

by

V.N. Ishkov and E.I. Mogilevsky
Institute of Terrestrial Magnetism
Ionosphere and Radiowave Propagation of the Academy of Sciences
(IZMIRAN), Moscow, U.S.S.R.

and

G.S. Minosaynts and S.O. Obashev
Astrophysical Institute of the Academy of Sciences
Kasakh SSR, Alma-Ata
U.S.S.R

The observational data obtained for the complex of flare-active regions McMath 14942 and 14943 at IZMIRAN and the Astrophysical Institute are summarized in Table 1. At IZMIRAN the observations were carried out on a tower solar telescope with birefringent Hα-filter "Opton" (the band of 0.25Å moved over Hα-contour within ± 1.0Å, per 0.25Å). Polarization spectrograms for measuring the sunspot magnetic fields were obtained on the spectrograph of the same solar installation. At the Astrophysical Institute the observations were performed on a high-altitude station (≈3000 m) for coronal observations. a) There a big coronograph was used (D = 53 cm, F = 8 m) for chromospheric observations (Hα-filter "Halle"). The size of the solar image was 160 mm. The observations were made in the center and Hα-wings at 0.5Å. b) Magnetic fields of the active region (a.r.) were observed by means of a vector-magnetograph (the system of Siberian IZMIR) with the use of a horizontal solar telescope ACU-5. c) The intensity of the monochromatic corona in green and red lines was observed by means of a Zeiss coronagraph.

Table 1. Observations of the active complex with the spot groups No. 98 and No. 99 from September 6 to 20, 1977 at IZMIRAN and the Astrophysical Institute

	IZMIRAN			A I		
Date	UT of photographic measurement of magnetic fields of spots	UT of full-disk observations	UT of chromospheric observations	UT of magnetograph data	UT of chromospheric observations	UT coronal observations and wavelength
9/6	-	-	-	-	-	5303A 0336 6374A 0354
9/7	-	-	-	-	-	5303A 0352 6374A 0336
9/9	-	1045-1100	-	-	-	-
9/12	1255-1310	0805-0836	1125-1226	-	-	-
9/13	0932-0945 1510-1520	1435-1444	1446-1507	0400-0900	0433-0720	-
9/14	-	-	-	0330-0900	0244-1029	-
9/15	-	-	-	0345-1010	0258-0945	-
9/16	-	-	-	0400-1000	0316-1005	-
9/17	-	-	-	0330-1030	0423-0928	-
9/18	-	-	-	-	0332-0757	-
9/20	-	1105-1124	1132-1216 1409-1421	-	-	-

The observations performed in IZMIRAN were essentially restricted by weather conditions (successful observations were made on September 13), whereas at the Astrophysical Institute all six days of observations were under favorable weather conditions, which allowed one to get high-resolution filtergrams.

As seen from Table 1, we observed only individual small flares (we were unable to observe the flares of Importance 2 and 3, which occurred on September 16 and 19). But according to our observational data, and those published by different observatories in "Solar-Geophysical Data" [1977] and "Solnechnye Dannye" [1977], one can reveal some distinguishing features in the evolution of those active regions. By using direct and indirect measurements, we tried to determine characteristic properties in the structure and evolution of flare-active magnetic field regions. In the case of indirect measurements use was made of a series of high-quality Hα filtergrams. They made it possible (see, for instance, Zirin [1972] to describe qualitatively the magnetic field distribution in the active regions by using distinctive characteristics in a fine structure of some chromosphere elements, as the basis. For illustration, we show one of our Hα filtergrams (Fig. 1), where the external contours of the magnetic field isogauss are plotted (the observations of [SGD 1977b]).

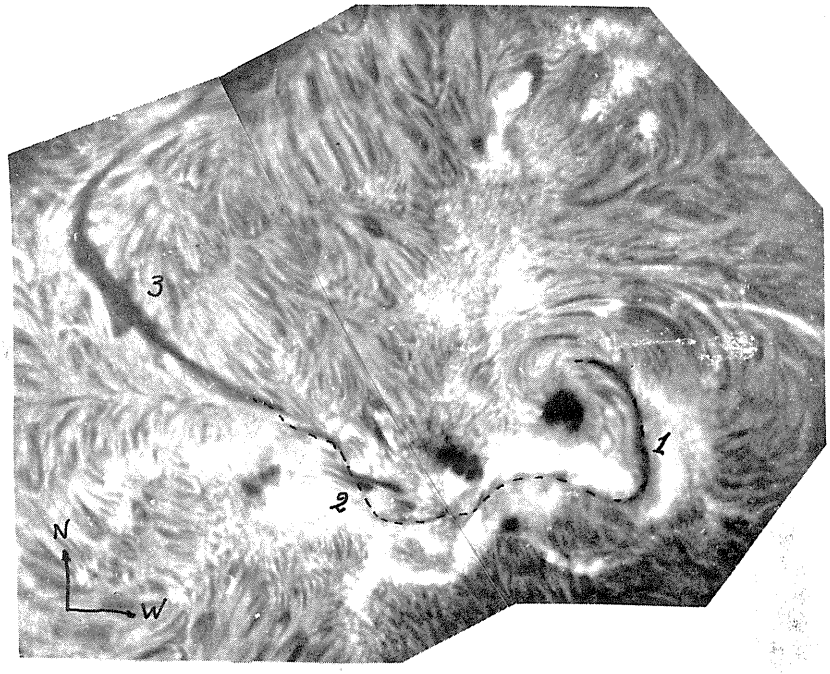

Fig. 1. Hα filtergram of active complex on Sept. 17, 0429 UT. Dashed line indicates the position of longitudinal neutral line.

1 - west path of filaments
2 - arch filament system
3 - east path of filament

A powerful low-latitude varying sunspot group (ϕN8, L200, No. 99 by the "Solnechnye Dannye" number system), and a bipolar group (ϕN16, L208, No. 98), which comprise the active region complex, appeared at the E-limb on September 9, although high activity in the corona (high coronal condensation) for the groups, which are still behind the limb, was observed by us as early as September 6 and 7 (see Table 1). This fact has been confirmed, according to the observational data from [SGD 1977b] and [SGD 1977], by the presence of active regions in the powerful variable X-ray and local radio sources (the observations at 8 mm, 2 cm and 4.4 cm wavelengths, 2 or 3 days before the appearance of groups at the E-limb edge).

Note that the active region was generated in late August in previous Carrington rotation (No. 1658) near the boundary between two supergiant structures (SGS). The active regions McMath 14930 and the studied regions McMath 14942 and 14943 constituted a "boundary zone". To the east and west from those a.r. in the N-Hemisphere, there were extended latitude (120-150°) bands of the S-background magnetic field. The bands were surrounded by extended chains of Hα filaments. Those two supergiant structures appear in synoptic H charts for the Carrington rotations No. 1657-1661, and are illustrated by our review Hα filtergrams on September 3 and 13 (Fig. 2). By studying the complex a.r. in McMath regions 14942 and 14943 one can note the following structural and evolutional distinguishing features in the magnetic fields on the basis of our direct and indirect observations (from the chromospheric structural analysis): a) A large low-latitude sunspot group (No. 99) represented before September 14 the group "δ" of magnetic configuration, that is, within the limits of a complex changing penumbra there were located the spots of S and N polarity (Fig. 3). In subsequent days the group dissipated into spots of the same polarity. The group No. 99 is notable for the fact that the leading spot had S-polarity, which is opposite to the case, that should take place for groups in the current solar cycle. The bipolar group No. 98, on the contrary, had a regular distribution of the magnetic field polarity. The leading spot had N-, and the follower, S-polarity. An "irregular" polarity in group No. 99 has been observed regardless of the N-polarity observable in the west part of McMath 14943. Such a complex distribution of magnetic fields in the group and a.r. resulted in the fact that the boundary

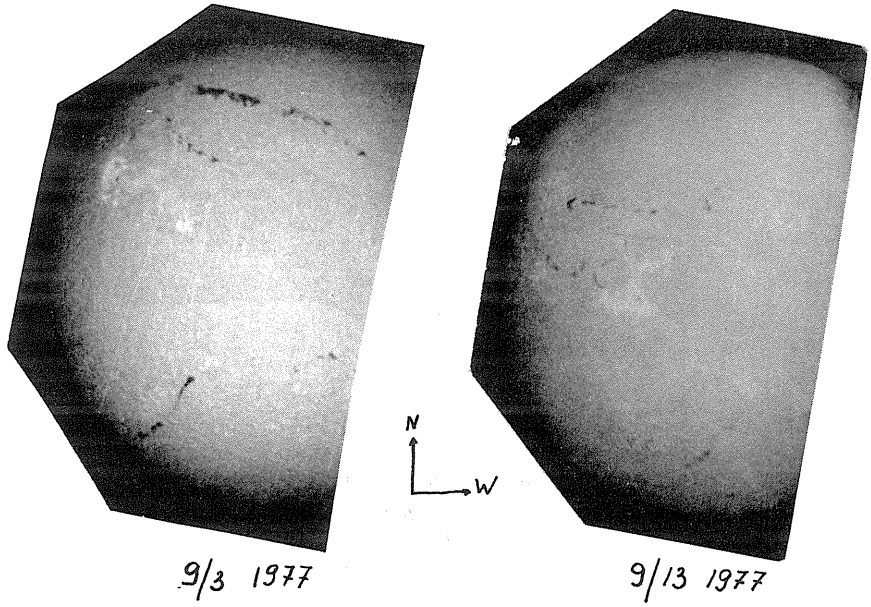

Fig. 2. Review Hα filtergrams in centerline on Sept. 3 and 13.

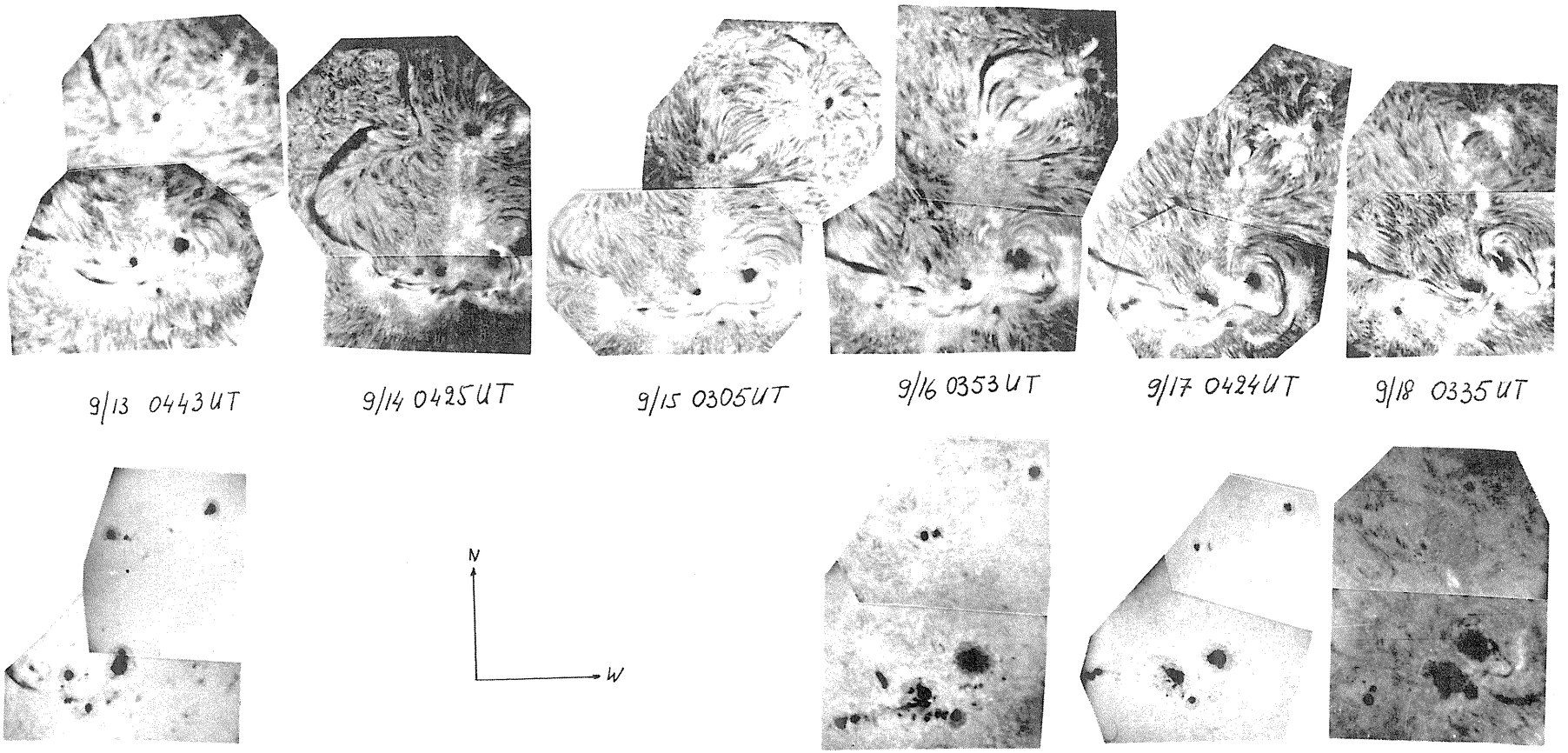

Fig. 3. Synoptic series 9/13 - 9/18 with Hα center above and Hα ±1 Å below.

between magnetic polarity ($B_{\parallel}$=0) and the H_{α} filament located along it, was complex and serpentine-like (Fig. 1). Note that the west (position 1) and east (position 3) parts of the filament enveloping the group, were separated by a system of stable loops and fibrilles (position 2). The latter connected with their ends the opposite-polarity magnetic fields (on both sides of the line $B_{\parallel}$=0). b) Another pecularity of the a.r. 14943 magnetic field and the group No. 99 was the fact that the boundary of polarity ($B_{\parallel}$ = 0) went almost parallel to the Equator during all days of observation. Such a structure in the a.r. field normally corresponds to flare-active regions. From September 15, the magnetic field of S-polarity was slowly wedged in the near-to-the Equator region of N-polarity, which resulted, by September 20, in a separation of the pre-equator a.r. zone into three parts with N-S-N magnetic fields. Such an evolutional alteration in the distribution of a.r. 14943 magnetic field was accompanied by a notable simplification of the structure and field in the group No. 99. These separated two large stable leading spots of S-polarity, whereas small spots and pores of N-polarity in the follower part of the group changed (in number and value). Note that in the subsequent rotation (No. 1660, in October) the same complex structure was preserved in tha a.r. magnetic field distribution for the "irregular" distribution of polarity in the sunspot group. c) An important property of the magnetic field in McMath 14942 and 14943 a.r. complex is the "magnetic bridge", i.e. the meridian region of S-magnetic polarity, which connected the leader part of S-magnetic field in the group No. 99 with the follower part of S-polarity in the group No. 99. From a characteristic chromospheric structure (Fig. 1 and 3) the magnetic field in the region of the "bridge" had a vertical component only, whereas the position of fibrilles and filaments to the west and east from the magnetic bridge indicated the existence of a large-scale vortex structure of the field with a prevailing tangential field component. If one also allows for the "bridge"-symmetrical arch system in the chromosphere available in both groups, then due to Howard et al. [1977] one can assume that in the "magnetic bridge" region there is a "dark corridor" for the X-ray emission separating both active regions.

Our prolonged chromospheric observations during 7 days made it possible to analyze some temporal changes in H_{α} filament, in arch systems and fibrilles, which depict the changes of the magnetic field structure in the chromosphere and corona resulting from the a.r. evolution and chromosphere flares. Without making a detailed description, we shall note only some distinguishing features of those variations. a) Two parts of the filaments (westside - position 1, and eastside - position 3) depicted in Fig. 1, undergo significant alterations under the action of weak flares. For instance, in a small flare of September 16 at 0958 UT there was a noticeable broadening of the filament after 5 min (see Fig. 4). It corresponds to the perturbation from the flare propagating with average velocity 290 km/sec after overcoming such a perturbation the filament occupied again its previous position, and assumed a "quiet" form. The same phenomenon has been observed in the flare-like brightening of September 17 at 0504 UT. Analogous changes were observed in the westside part of the filament. In all cases of flare-like brightening that has been observed in any part of the a.r. complex (in the region of the group No. 98), one observed short-term perturbations of the filament (about a few minutes). Such a high response suggests that the complex contains a mutual (interrelated) structure of magnetic fields, in which the pulsed perturbation propagates from the individual flares. The observed short-term perturbations indicate that the flare-like brightenings give rise to the short-term "elastic deformations" in the magnetic field structure for chromosphere and a.r. corona, as we have already noted for some other powerful active regions [Korobova et al., 1976]. b) One can also follow the evolutional changes in the discrete stable arch system. For instance (see Fig. 1) the large-scale arch two-level system in the active region 14942 changed slowly from September 13 to 16, and on September 17 it practically dissipated. The analogous discrete arch system can be observed in a.r. 14943 at the points marked in Fig. 1 as position 2. The arches remained stable for a few days, although they were subjected to some "elastic" changes after the flares. Being located in the regions, where some new follower spots and pores of N-polarity were generated, and then dissipated, those arches were deformed and stretched along the line $B_{\parallel}$ = 0 by September 18, in the form of a few long thin threads connecting the filament "ends". c) Concurrent with the evolutional changes in the arch systems, which outline the chromospheric - coronal magnetic fields, one observed rather stable (up to a few hours) single and two-level arches typical of the flares. For example, after the flare of Importance 1B, by September 18 (0019-0058 UT) we observed initially (t = 0332 UT) in the red wing ($\Delta\lambda$= +1Å) and in the center of the line, a high arch (see Fig. 3) which entirely dissipated by ~5^hUT. The second flare arch was above the filament, and as the first one, it connected the points with magnetic polarity of the opposite sign.

In conclusion it should be noted that the main variation characteristics of the magnetic field structure in the studied a.r. complex take place mainly in the form of evolutional (slow) changes. Small flares, in our case, resulted in the short-term relaxation changes of the magnetic field structure.

References

HOWARD, R. and Z. SVESTKA — 1977 — Development of a complex of activity in the solar corona, Solar Physics, 54, 65-105.

KOROBOVA, Z.B. V.N. ISHKOV and E.I. MOGILEVSKY — 1976 — On the problem of stability of the structure of magnetic fields in active region as obtained from observations of the chromospheric events dynamics during the flare on August 2, 1972, Solnechnye Dannye, 10, 92-99.

SGD — 1977a — Solar-Geophysical Data, 398, Part 1, U.S. Department of Commerce (Boulder, Colorado, U.S.A., 80303).

SGD 1977b Solar-Geophysical Data, 399, Part 1, U.S. Department of Commerce (Boulder, Colorado, U.S.A., 80303).

SD 1977 Solnechnye Dannye, 9.

ZIRIN, H. 1972 Fine structure of solar magnetic fields, Solar Physics, 22, 34-48.

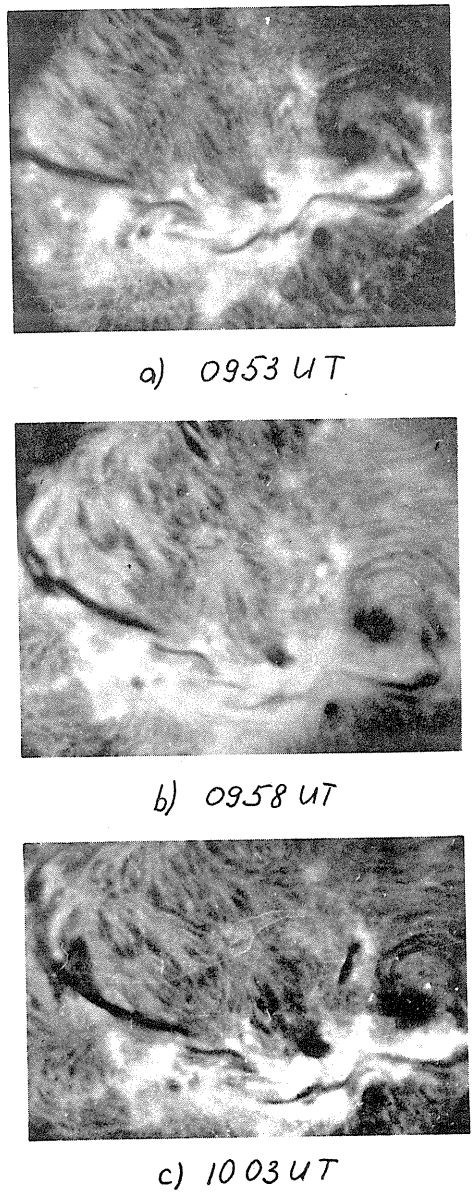

Fig. 4. Hα center sequence of the small flare at 0958 UT, Sept. 16 (a - before, b - at onset, c - after). Note that perturbation from flare east path of filament in ~5 min after the flare beginning.

λ5303A Corona Connected With McMath Plage Region 14943

by

M. Rybansky and V. Rusin
Astronomical Institute of the Slovak Academy of Sciences
Tatranska Lomnica, Observatory Lomnicky Stit, Czechoslovakia

Introduction

The active region connected with McMath plage region 14943 appeared at the eastern limb on September 8, 1977, and went beyond the western limb on September 22, 1977. During its passage across the solar disk it had been very active which can be seen by both the number and importance of the flares and by the geophysical effects (e.g., the Forbush effect on September 11-13 and September 22, 1977).

In the present paper we demonstrate as far as it is possible from the observational data how this region appeared in the intensity of the emission coronal line of λ5303A.

The observations of the emission coronal line of λ5303A according to the international program have been made regularly only at four observatories: Norikura - Japan /NO/, Kislovodsk - USSR /KI/, Wendelstein - FRG /WE/ and Lomnicky Stit - Czechoslovakia /LS/. The observations from different stations differ in the position angle as well as in the absolute value and therefore it is necessary that they be transformed first to a uniform scale. This method is given in detail in the papers by Rybansky [1975 and 1979].

From the different stations we have results for the studied region on the following days.

NO: September 17, 18, 20; October 4, 6, 8, 1977
KI: September 17, 19, 20, 22; October 3, 4, 7, 8, 9, 1977
WE: September 25, 1977
LS: September 24, 26; October 7, 8, 9, 1977.

These measurements allow us to prepare a map of coronal isophotes at the position of this region beyond the western limb. These results are given in Figure 1. The first isophote is 10. Each step between the isophotes is 10. The values of 50 to 100 are given by the heavy line. One unit of the equivalent width of the intensity of the coronal line corresponds to 10^{-7} nm of the continuous spectrum in the middle of the solar disk at the same wavelength. The broken line gives the boundary of McMath plage region at its passage through the central meridian.

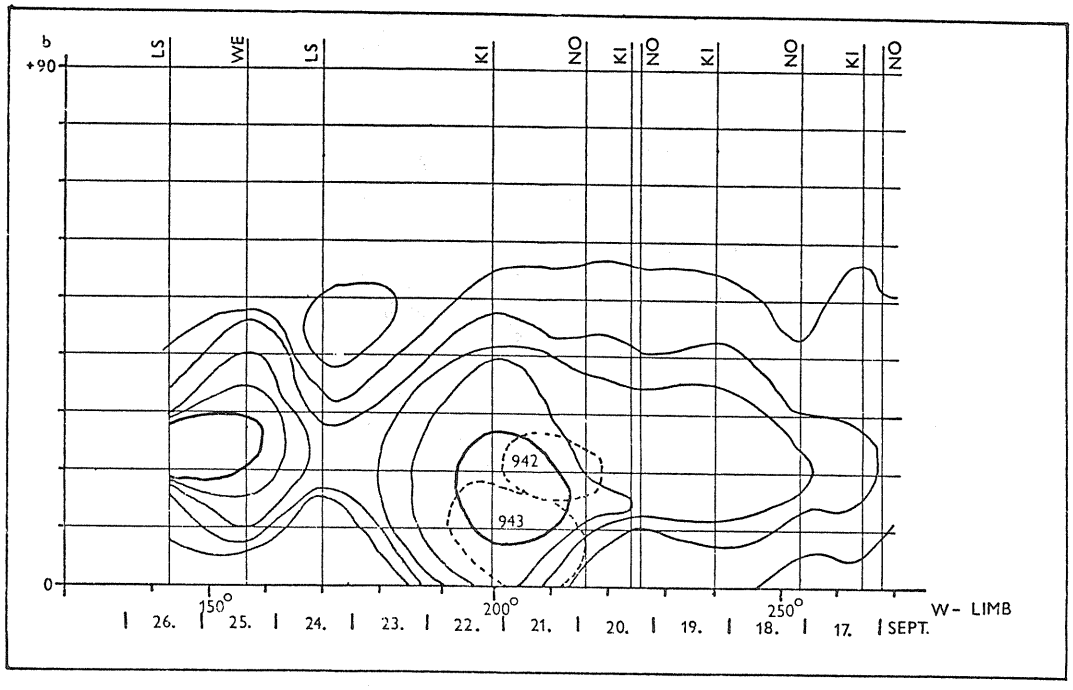

Fig. 1. Brightness of the λ5303A coronal line as function of position of McMath region 14943 beyond the west limb.

In Figure 2 is given a similar map for the eastern limb, when it appeared again on the eastern limb on October 5, 1977. At that time the region was McMath 14979.

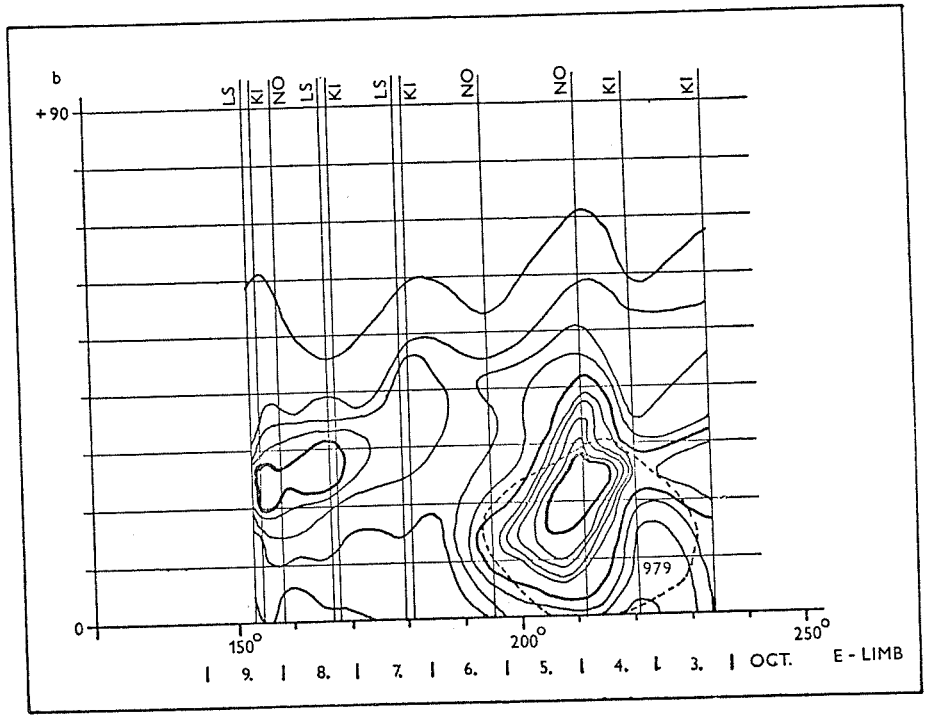

Fig. 2. Brightness of the λ5303A coronal line as a function of McMath region 14979 beyond the east limb.

Detailed morphological pecularities will be investigated after analysis of all data of solar activity connected with this region are available, but a cursory comparison of the maps of coronal intensities with magnetograms from Solar-Geophysical Data [1977a and 1977b] shows that the maximum of coronal intensity is connected to a negative polarity of the magnetic field which lies between two positive polarities.

REFERENCES

RYBANSKY, M. 1975 Coronal Index of Solar Activity, I. Line 5303 A, 1971 and II. Line 5303 A, 1972-73, *Bull. Astron. Inst. Czech., 26,* 367.

RYBANSKY, M. 1979 Coronal Index of Solar Activity, III. Years 1971-76, *Bull. Astron. Inst. Czech., 30,* 104.

SGD 1977a *Solar-Geophysical Data, 399 Part I,* 34-92, November, U.S. Department of Commerce (Boulder, Colorado, U.S.A., 80303).

SGD 1977b *Solar-Geophysical Data, 400 Part I,* 30-90, December, U.S. Department of Commerce (Boulder, Colorado, U.S.A., 80303).

2. SOLAR RADIO EVENTS

Radio Observations from the Voyager 2 Spacecraft

by

Anthony C. Riddle
Radio Astronomy Observatory
University of Colorado
Boulder, Colorado

Introduction

The Planetary Radio Astronomy (PRA) experiment aboard Voyager 1 (described by Warwick et al. [1977], and Lang and Peltzer [1977]) was operating from September 7 through 2000 UT on September 14 and also on November 22, 1977, with about 95 percent data coverage. During this period eight solar bursts were observed. For the remaining period of interest in this UAG report, data coverage was less than 1 percent and has not been analyzed.

Two types of PRA observing modes are utilized in this study. In the fixed frequency mode (about 40 percent of the data) one of three frequencies is observed continuously for 6 sec in both modes of circular polarization. During the period under study two of the frequencies were 308 and 251 kHz, and the third frequency was either 212 or 193 kHz. This mode provides high-time resolution data on solar activity originating at about 1/4 to 1/2 AU from the Sun. In the scanning mode (about 20 percent of the data) the spectrum from 41 MHz to 1.2 kHz is sampled at 200 frequencies each 6 sec. Groups of eight consecutive scans occurred at time intervals separated from 4 to 8 min. This mode defines nicely the time behavior of a burst at frequencies below several hundred kilohertz, but does not provide sufficient samples to define the time behavior at significantly higher frequencies.

During the September events Voyager 1 was essentially at 1 AU from the Sun and event times at the spacecraft may be compared directly with event times observed at Earth. On November 22 Voyager 1 was almost on the Sun-Earth line at 1.5 AU from the Sun. To enable direct comparison with terrestrial data, the times quoted in this paper for November 22 are 4 min earlier than the times the data were observed at the spacecraft.

The time of occurrence of each intensity peak at 308 MHz is listed in Table 1 (the September data from Riddle [1978]) together with the value of peak intensity. Subsidiary maxima are also listed in the case of complex bursts. The time difference between peak intensities for the fixed frequency observations can be interpreted as implying an exciter velocity of about one-sixth the speed of light. The exciter apparently left the surface of the Sun about 10-12 min before the times given in Table 1. This estimate is in good agreement with the start times of the apparently associated bursts seen at higher frequencies (Table 1). The e-folding voltage decay times ranged between 320 and 500 sec at 308 kHz and lengthened to 500 to 800 sec at 212/193 kHz. At no time during any of the bursts could circular polarization be detected at any frequency below 1.3 MHz.

The three most intense events listed in Table 1 correspond to the major solar flares of September 7, 9, and November 22. They are all complex events, clearly observed from 40 MHz to 40 kHz (20 kHz on November 22). For these events the times of peak intensity are plotted as a function of frequency in the figure. Above 300 kHz there are problems resolving the individual peaks because of lack of data in the swept frequency mode. Below 200 kHz the peaks begin to coalesce due to the long decay times. The September 9 event appears to take longer to reach lower frequencies, which is possibly indicative of a slower exciter or smaller electron density gradient in the solar wind. However, for this event the burst profile changes markedly from 308 to 212 kHz; apparently different electron streams are dominating at different times (distances from the Sun).

The September 7 flare event has been compared in detail with the radio spectrum from Culgoora (see acknowledgments). The electron stream causing the first peak observed at 308 kHz could well have been generated at the time of a strong group of Type III's which commenced at 2231 UT and were observed on the spectrum from 500 MHz through 10 MHz. However, the second and stronger peak observed at 308 kHz has no obvious spectral counterpart near 2245 UT. Near that time the spectrum shows strong Type II and Type IV emission from 100 to 20 MHz but no fast drift features. Again the final peak at 308 kHz, observed at 2324 UT, has no obvious spectral counterpart although weak fast drift features are observed from 2245 through 2325 UT in the 120- to 20-MHz range.

It is interesting that the strongest 308-kHz peak on September 7 has no corresponding spectral feature when three of the weakest bursts do have corresponding Type III events (see Table 1).

TABLE 1. BURSTS OBSERVED BY VOYAGER

Date	Time of occurrence and intensity(*) of successive peaks						Spectral data(**)	
	UT	dB	UT	dB	UT	dB	UT Time	Type
7 Sep	1742	29	1749	26				
7 Sep	2241	43	2257	55	2324	48	2229-2235	III GG,V
9 Sep	1643	40	1652	40	1700	43	1636-1642	III G,V
10 Sep	0021	18						
12 Sep	0226	24					0215	III B,W
14 Sep	1610	26					1557-1600	III G
14 Sep	2200	31					2143-2214	III GG,W
22 Nov	1013	49	1019	63	1030	50	1002-1102	IV,N

*The intensity scale has an arbitrary origin.
**From "Solar-Geophysical Data" Prompt Reports [1977] and [1978].

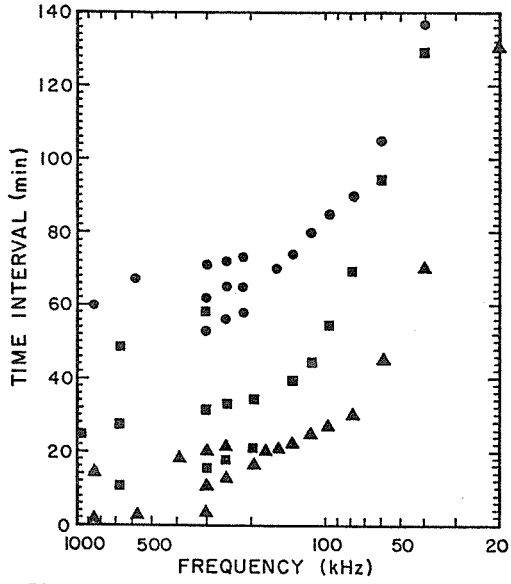

Fig. 1. Time of maxima at various frequencies for the major bursts of Sept. 7 (squares), Sept. 9 (circles) and Nov. 22 (triangles). The timing errors are approximately ±2 min except for data points between 312 and 193 kHz where they are ±1 min.

Acknowledgments

The Planetary Radio Astronomy Experiment is supported by NASA Grant AST 76-81577.

Dr. K. Sheridan of CSIRO Division of Radiophysics, Epping, NSW, Australia, kindly provided an excellent radio spectrum of the September 7, 2200 UT event.

References

LANG, G.J. and R.G. PELTZER 1977 Planetary Radio Astronomy Receiver, IEEE Trans. AES-13, 466-472.

RIDDLE, A.C. 1978 Solar Bursts Observed by Voyager 20 August to 14 September 77. University of Colorado, Radio Astronomy Observatory, Publication PRA-7.

SGD 1977 Solar Geophysical Data, 399 Part I, November, 103-106, U.S. Department of Commerce (Boulder, Colorado, U.S.A., 80303).

SGD 1978 Solar Geophysical Data, 401 Part I, January, 104, U.S. Department of Commerce (Boulder, Colorado, U.S.A., 80303).

WARWICK, J.W., J.B. PEARCE, R.G. PELTZER and A.C. RIDDLE 1977 Planetary Radio Astronomy Experiment for Voyager Missions. Space Science Rev., 21, 309-327.

Microwave Pulsations from a Compact Source Associated with McMath Plage Region 14943

by

V. Gaizauskas and K.F. Tapping
Herzberg Institute of Astrophysics
National Research Council of Canada
Ottawa, Canada K1A OR6

Introduction

During the disk passage of McMath plage region 14943, a search was made for rapid periodic fluctuations ($\sim$1 Hz) in the microwave emissions from solar active regions as an extension to a related study by Tapping [1978]. The 46-m fully-steerable paraboloid at the Algonquin Radio Observatory* was used for this search at a wavelength of 2.8 cm. The half-power beamwidth of this antenna is about 2.7 arc-min. Collaborative optical observations were made with the 25-cm photoheliograph of the Ottawa River Solar Observatory (ORSO) [Gaizauskas, 1976] in an effort to provide optical identifications for time-varying microwave sources.

Radio Observations

On September 12, 1977, a raster scan map was made of the entire solar disk to locate regions of enhanced emission at 2.8 cm. The most significant microwave source was associated with McMath plage 14943 and was found to consist of two parts: a general enhancement over the entire region that reached an antenna excess of about 10^4K over the background level, and a bright core with a peak temperature excess of about 1.1×10^5K. Because the apparent angular diameter of this hot component was identical to the diameter of the antenna beam, it is likely that its true angular size was appreciably less than 1 arc-min. This result is typical of the emission from complex active regions at centimetric wavelengths. [Donati Falchi et al., 1978, and references therein]. No optical activity was reported from McMath 14943 in the time required to complete this scan of the disk.

On September 13, the intense compact source was still present. On this occasion, the pointing of the antenna was optimized on the hot core at 1300 UT. From the antenna pointing, the position of the compact microwave source was found to coincide with the westernmost portion of McMath 14943 (see Figure 1). The accuracy of the pointing was approximately 10% of the beamwidth.

This source was found to be pulsating with a modal frequency of 0.4 Hz and a peak-to-peak amplitude of about 4000 K. These pulsations persisted over the entire observing period of 5.5 h. The measurements were made by taking averaged power spectra with the antenna directed alternately on-source and off-source. Typical on-source and off-source power spectra, each averaged for 10 min, are shown in Figure 2. To minimize possible confusion with output fluctuations produced by changes in the receiver or in the troposphere, power spectra were taken with the receiver looking at (1) the active center; (2) the background solar disk; (3) the solar limb; (4) the discrete point source 3C273; (5) the "cold" sky and (6) the receiver internal cooled termination. For (4), (5) and (6) the receiver gain was increased by 15 dB.

Optical Observations

The optical data on McMath 14943 secured at ORSO on September 11 and 15 consisted of filtergrams taken through a Zeiss birefringent filter (bandpass of 0.25 Å) at 17 wavelength positions centered on the Hα line and spanning the range $\pm$1.4 Å. A sweep in wavelength was completed every 42 or 85 s depending on observing conditions. Full disk images in Hα were supplied for September 12 and 13 by Ramey AFB. The magnetic configuration of the region was obtained from sunspot data published by Rome Astronomical Observatory [Cimino, 1977] and from Kitt Peak magnetograms published in *SGD* [1977].

Discussion

During the few days covered by these observations, McMath plage 14943 was essentially a bipolar region. It had, however, two anomalies: (1) the division between opposite polarities was aligned east-west rather than north-south and the largest leading spot was of following polarity. As seen in the Hα filtergrams in Figure 3, the portion of the "neutral line" filament that ran between the closely clustered sunspots of opposing polarities was similarly aligned roughly east-west. When the "neutral line" filament was examined at high resolution (especially on September 15, Figure 3), it was found to consist of numerous short strands that were inclined to the mean axis of the filament. These short strands presumably interconnected regions of opposite polarity [Prata, 1971], and their inclinations were indicative of strong shears in the magnetic field [Tanaka and Nakagawa, 1973].

---

*The Algonquin Radio Observatory is operated as a national facility by the National Research Council of Canada.

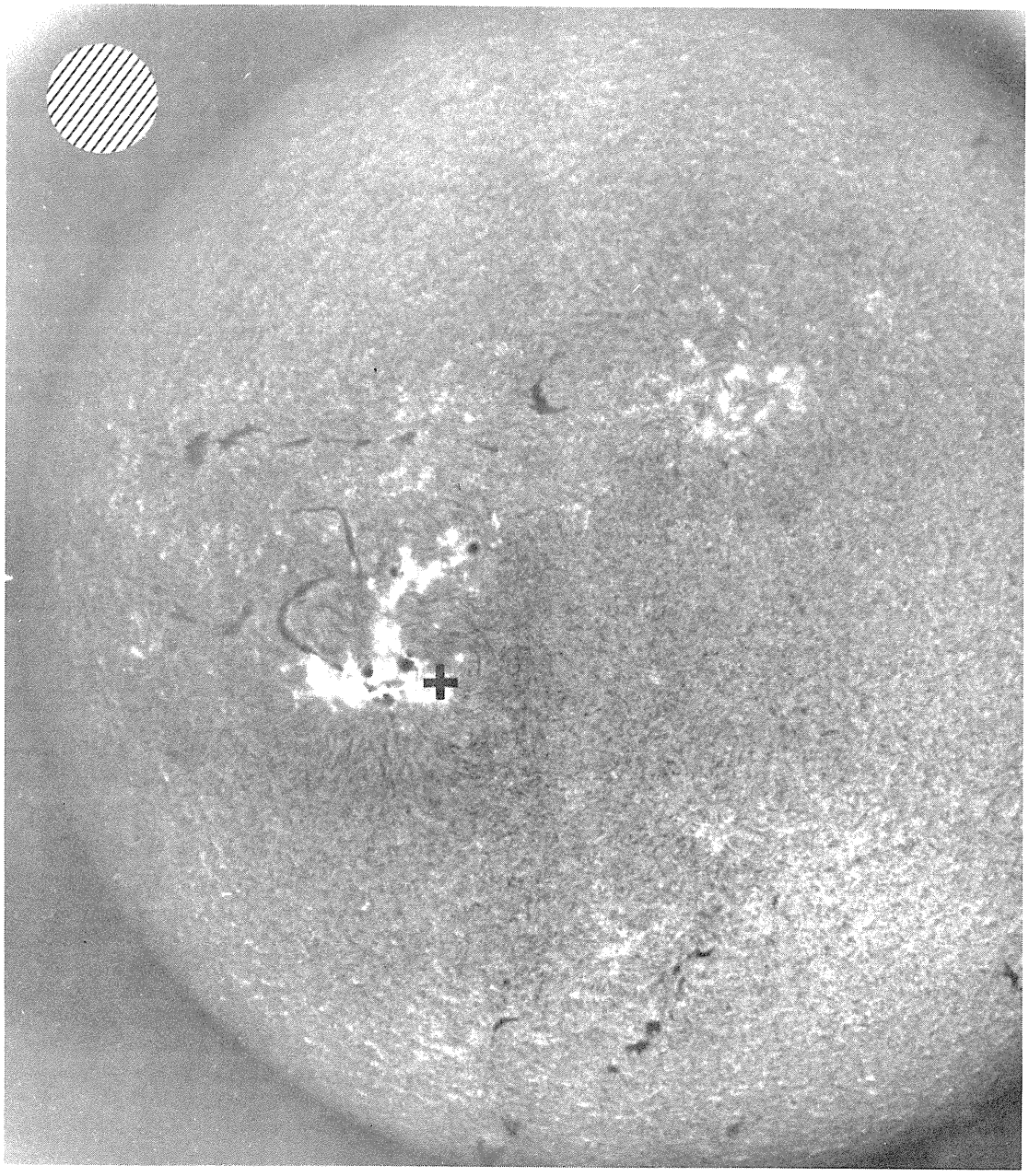

Fig. 1. The cross on the leading plage of McMath region 14943 marks the location of peak intensity from the compact source pulsating at a wavelength of 2.8 cm. The hatched circle indicates the relative size of the antenna beam. The figure is oriented with east at the left and north at the top. This Hα filtergram, taken on September 13, 1977, was supplied through the courtesy of Ramey AFB.

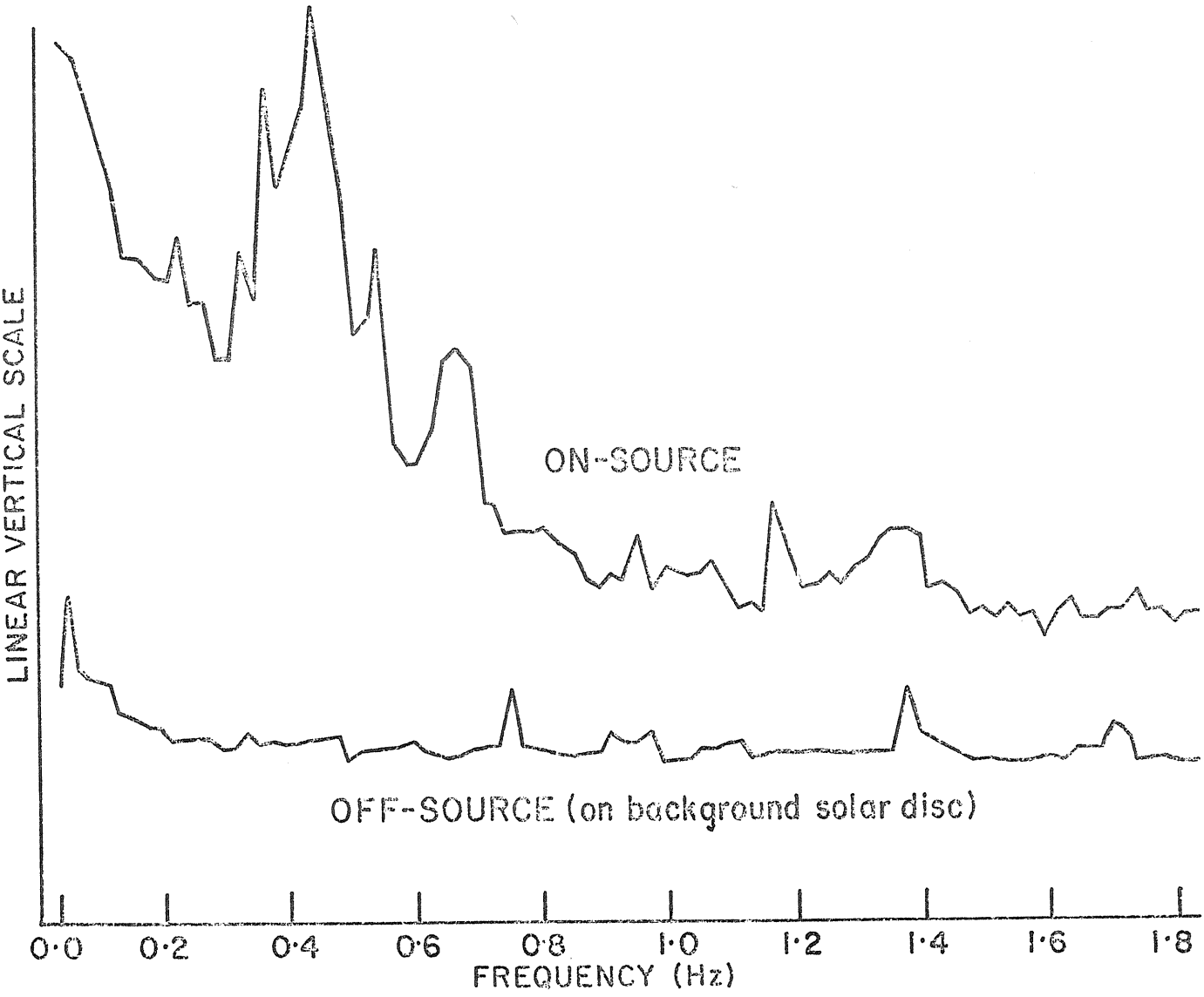

Fig. 2. A typical example of power spectra averaged for 10 min on and 10 min off the pulsating microwave source.

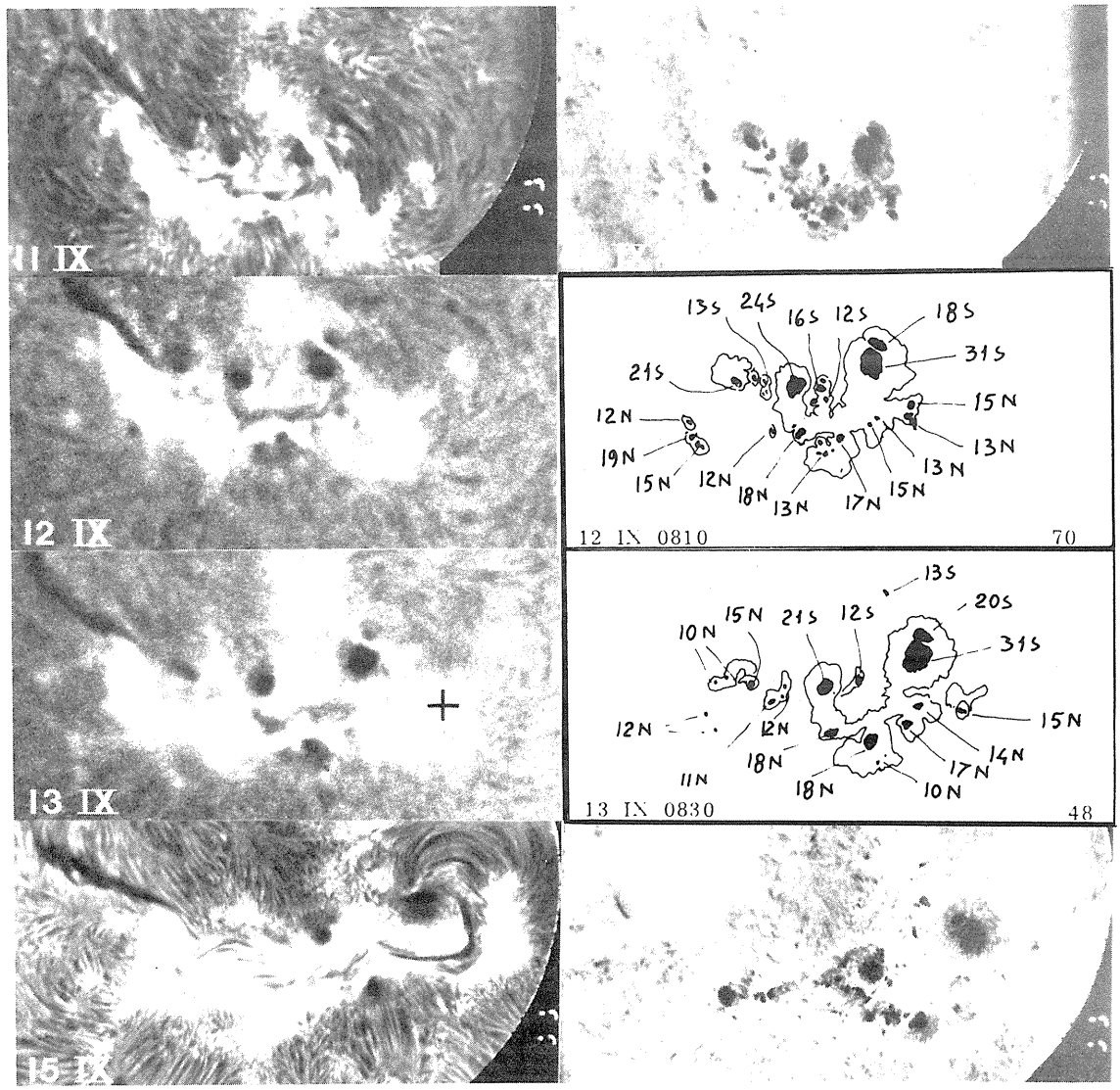

Fig. 3. The panels in the column at left are Hα filtergrams; those in the column at right are either filtergrams at (Hα - 0.9 Å) or sunspot drawings courtesy of the Astronomical Observatory of Rome. The filtergrams for September 12 and 13 are enlarged to the same scale as the ORSO filtergrams from full disk prints supplied by courtesy of Ramey AFB. The cross on the filtergram for September 13 has the same significance as in Figure 1.

We further note that the largest leading spot had a bifurcated umbra with both components of following polarity. The Rome sunspot drawings indicate that these umbral components retained their relative magnetic strengths from at least September 10 to 16, but that their orientation changed in a way suggestive of counterclockwise rotation as seen from above. The preceding-polarity plage, which we have identified as coincident with the microwave source on September 13 (Figure 3), was southwest of the large follower spot on September 11. By September 15 it was due west of that spot. Thus, as the region evolved, the spots gradually spread apart while a substantial portion of the leading section rotated in a counterclockwise sense. This motion opposed the apparent rotation of the region produced by changes in perspective as the Sun rotates.

We conclude that the rotation was real and that the region was attempting to align itself in the normal magnetic configuration, i.e., preceding polarity leading and a neutral line running north-south. It is conceivable that the shears introduced by differential motions of the sunspots within the region created the instabilities responsible for the pulsating microwave emission from the hot, compact source.

REFERENCES

CIMINO, M. 1977 *Solar Phenomena, Monthly Bulletin N. 233,* Osservatorio Astronomico di Roma.

DONATI FALCHI, A., M. FELLI, P. PAMPALONI, and G. TOFANI 1978 The Development and Structure of Bright Active Regions at 2.8 cm, *Solar Physics, 56,* 335.

GAIZAUSKAS, V. 1976 The Ottawa River Solar Observatory, *J. Roy. Astron. Soc. Canada, 70,* 1.

PRATA, S.W. 1971 A Note on Chromospheric Fine Structure at Active Region Polarity Boundaries, *Solar Physics, 20,* 310.

SGD 1977 *Solar-Geophysical Data,* 399 Part I, 34-92, November 1977, U.S. Department of Commerce (Boulder, Colorado, U.S.A. 80303).

TANAKA, K. and 1973 Force-Free Magnetic Fields and Flares of August 1972, *Solar Physics, 33,* 187.

TAPPING, K.F. 1978 Meter Wavelength Pulsating Bursts during the May 21, 1972, Solar Noise Storm, *Solar Physics, 59,* 145-158.

High Resolution Fan Beam Observations of 35 GHz Solar Bursts in September 1977

by

K. Kawabata, H. Ogawa, T. Omodaka, M. Fujishita, and T. Kato
Department of Physics, Nagoya University
Chikusa-ku, Nagoya, 464 Japan

Introduction

The 35-GHz fan beam interferometer at Nagoya has been extended and improved in order to achieve a higher angular resolution and sensitivity. The interferometer can be used for solar observations during almost the whole day and is suitable for observations of outstanding occurrences at millimeter wavelengths. The interferometer also can be used for synthesis of two dimensional brightness distributions of intense stable sources by using whole-day data, when the declination of the Sun is high. Monitoring of the Sun has been carried out by the interferometer since May 1976. The half power beamwidth and the separation between fan beams are 29" and 8'49", respectively, at the meridian transit. A survey of the Sun is done by the method of drift scanning and the sampling time on any point on the solar disk is 35.56 sec/(cos δ cos H), where δ and H denote the declination and the hour angle of the Sun, respectively. The observing site is located on the campus of the Nagoya University (geographic coordinates: 135°58.3'E, 35°8.8'N).

The first violent activity in solar cycle 21 occurred in September 1977 and radio activity was observed by the interferometer. In the present report, we describe the radio activity in McMath Region No. 14943 observed by the interferometer.

Equipment

The new interferometer (Figure 1) is composed of 16 antennas aligned on an east-west line with an equal spacing and the maximum baseline is 5849.1 wavelengths (50.10 m). The block diagram of the interferometer is shown in Figure 2. Antennas used in the interferometer are composed of a fixed paraboloidal reflector (50 cm diameter) with a Cassegrain feed and a steerable plane reflector (110 cm x 60 cm). An advantage of an antenna of this type for monitoring of the Sun is an absence of serious degradation on rainy days [Kawabata, Ogawa, Sofue, and Suzuki, 1974]. The half power beamwidth of the antenna is 69' and the power response decreases 14% at the optical limb of the Sun, when the antenna is pointed at the center of the solar disk.

We use four single mixers coupled with a common local oscillator (Klystron) by directional filters. Image band signals are eliminated by high-pass filters composed of narrow waveguides and

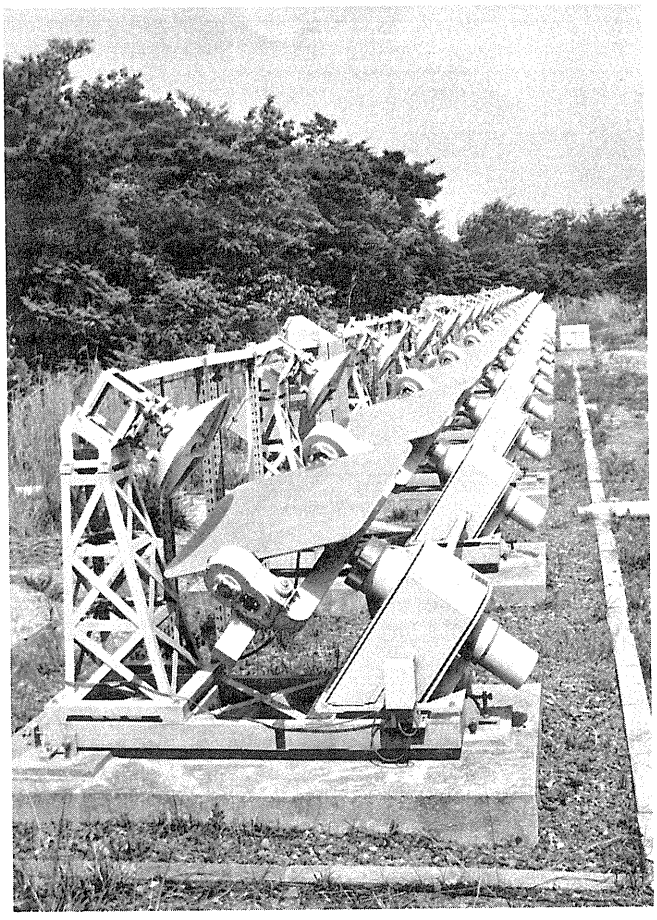

Figure 1. The 35-GHz fan beam interferometer at Nagoya.

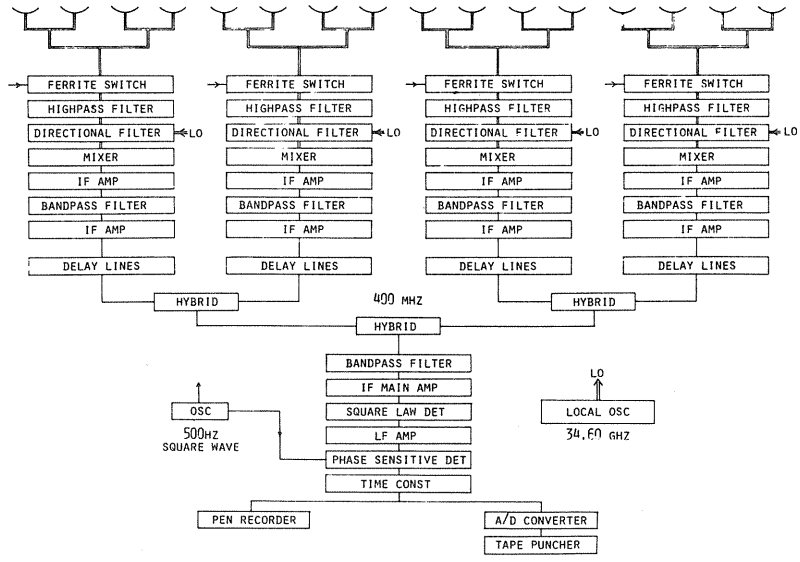

Fig. 2. Block diagram of the 35-GHz fan beam interferometer at Nagoya.

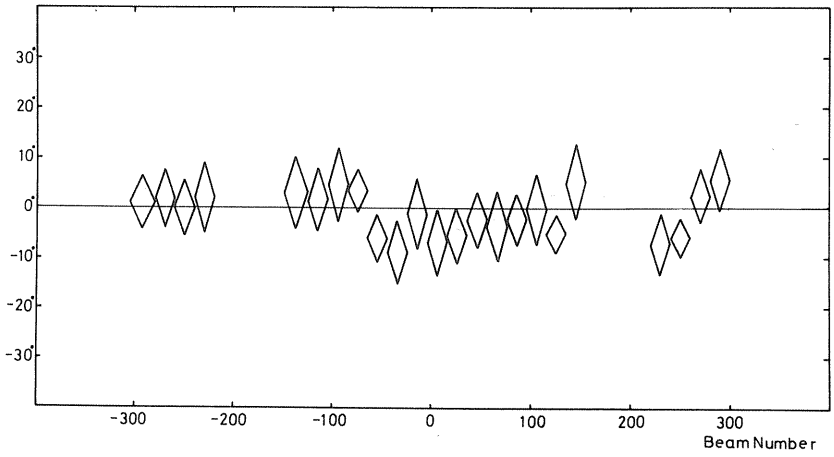

Fig. 3. An example of measurements of phase errors between two adjacent antennas at the middle of the interferometer. Measurements are made by observations of the Sun.

matching sections. The directional filters and the high-pass filters were designed by Dr. T. Otomo, Yokosuka Electrical Communication Laboratory. Oversize rectangular waveguides are used for transmission of signals from the antennas to mixers and from the local oscillator to mixers. The transmission loss of the waveguides is 2.8 dB from an antenna to an RF receiving system and is 6.7 dB from the local oscillator to a mixer. Phases of the local oscillator signals are not controlled but overall phase errors are less then 10°. An example of measurements of phase errors is illustrated in Figure 3. The center frequency of observations and IF amplifiers are 35 GHz and 400 MHz, respectively. We can choose a bandwidth of 80, 16 or 8 MHz. Observations by 80-MHz filters can be done only at around the meridian transit. Observed data are recorded digitally for computer data processing and also by a pen recorder for a quick look.

Observations

Observations of the Sun were carried out by the interferometer normally from 2130 through 0800 UT in the period September 7-24. Intervals of no observations exceeding 10 minutes in the normal time of observations in this period are also noted at the bottom of Table 1. Examples of our records are illustrated in Figure 4. The recorded interference pattern consists of a nearly sinusoidal one and

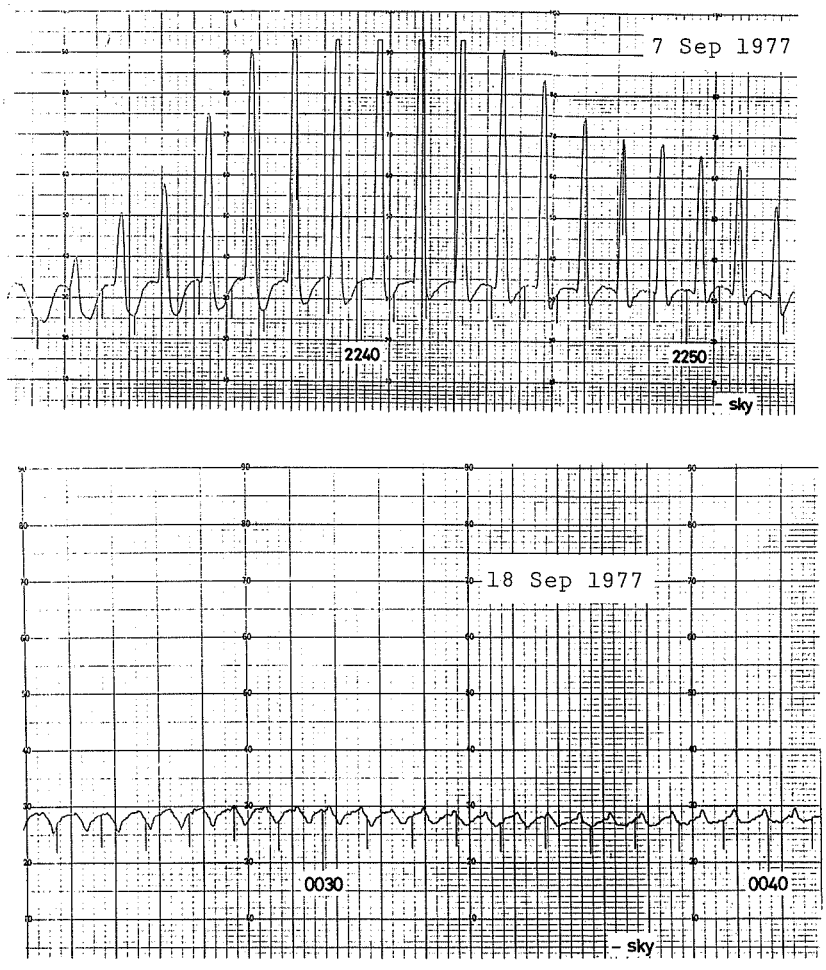

Fig. 4. Records of the 35-GHz fan beam interferometer at Nagoya. The time of observation is indicated in the figure in UT.

spikes. The nearly sinusoidal interference patterns are due to the quiet solar disk and spikes are due to emissions from McMath Region No. 14943. Location of a radio source can be determined by referring to the interference pattern of the quiet Sun with an ambiguity of a multiple of the beam separation. Flux densities of local sources are also determined by comparison with the power response of the quiet Sun, and then the attenuation due to the terrestrial atmosphere is corrected. In this reduction of data, the total flux density of the quiet Sun is assumed to be 2000 s.f.u. Decreases of flux densities due to the decreases of power response of antennas are not corrected in Table 1, or in Figure 5. Changes of terrestrial atmospheric attenuation can be easily discriminated from solar events. Thus reliable data on solar radio emissions can be obtained even for weak radio events with flux densities as low as 5 s.f.u. (0.25% of the emission from the solar disk).

During the period September 7-24, we observed a great burst and three GRF by the interferometer. Interferometer observations of these events are summarized in Table 1. The start time, the time of maximum phase, location and importance of associated Hα flares are also listed in the Table. The time profiles of flux densities at 35 GHz are illustrated in Figure 5. During the time of observations by the interferometer for September 7-24, two 2N flares, four 1N flares, and a 1F flare are reported in *Solar-Geophysical Data*, and all of the 2N flares and two 1N flares were associated with radio events at 35 GHz.

TABLE 1. Outstanding Occurrences
35 GHz September 7-24, 1977

DATE SEPT 1977	TYPE	START TIME UT	TIME OF MAXIMUM UT	DUR. MIN.	PEAK FLUX DENSITY S.F.U.	POSITION ANGLE DEG.	POSITION DISTANCE $R_\odot$	Hα FLARE START UT	Hα FLARE MAX. PHASE UT	Hα FLARE LOCATION		IMP.
7	47 GB	2231	2240	30	1170	79.1	0.99	2255	2321	N10	E90	1N
	29 PBI	2301	2310	70	170	71.9	1.04					
16	20 GRF	2237	2317	90	80	253.3	0.38	2230	2256	N08	W20	2N
18	20 GRF	0023	0100	110	26	246.5	0.43	0020	0040	N08	W38	1N
20	20 GRF	0410	0505	160	35	244.9	0.75	0251	0354	N10	W58	2N

Normal times of observations: 0000-0800, 2140-0000 UT.
Data interruption greater than 10 minutes (date (UT)).
No observation:
7(0100-0800); 11(0730-0800); 12(0055-0120); 14(0700-0710);
15(0720-0740); 18(0710-0800); 20(0720-0800); 22(0725-0740);
24(0720-0800).
Attenuation:
8(0310-0335, 0410-0445, 0510-0520, 0535-0620, 0730-0800, 2140-2255);
9(0005-0030, 0040-0130, 0310-0450, 0518-0528).

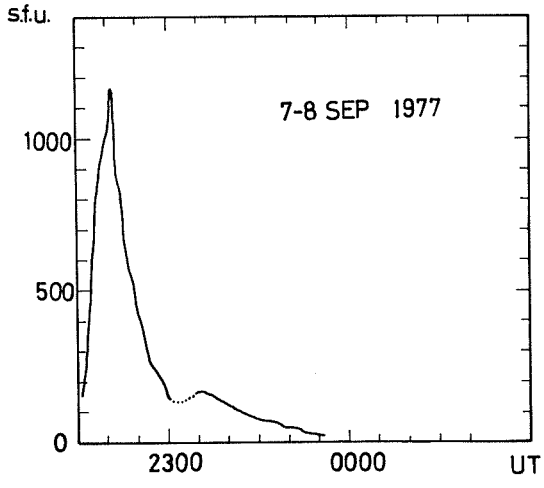

Fig. 5a. Time profile of flux density. Great burst on September 7, 1977.

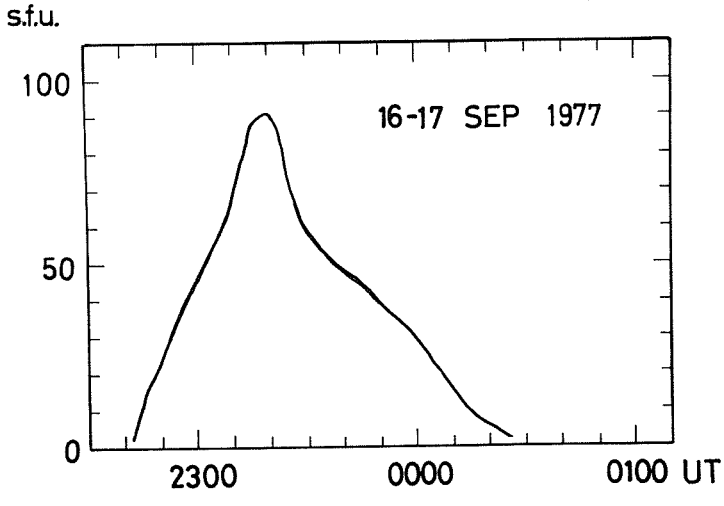

Fig. 5b. Time profile of flux density. Gradual rise and fall on September 16-17, 1977.

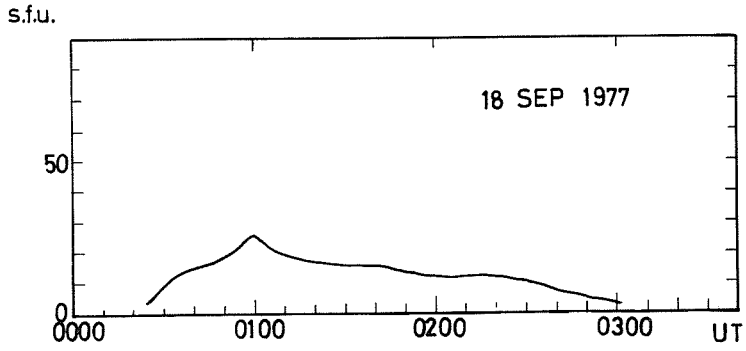

Fig. 5c. Time profile of flux density. Gradual rise and fall on September 18, 1977.

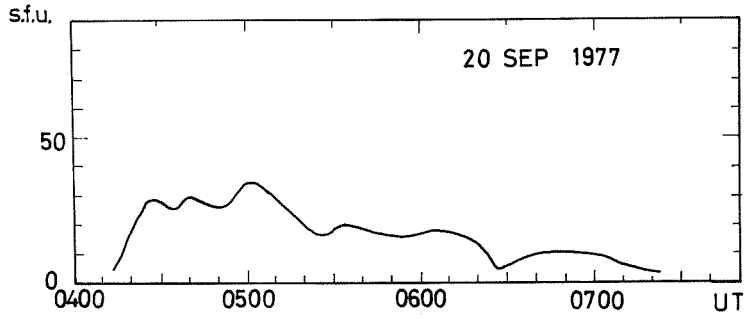

Fig. 5d. Time profile of flux density. Gradual rise and fall on September 20, 1977.

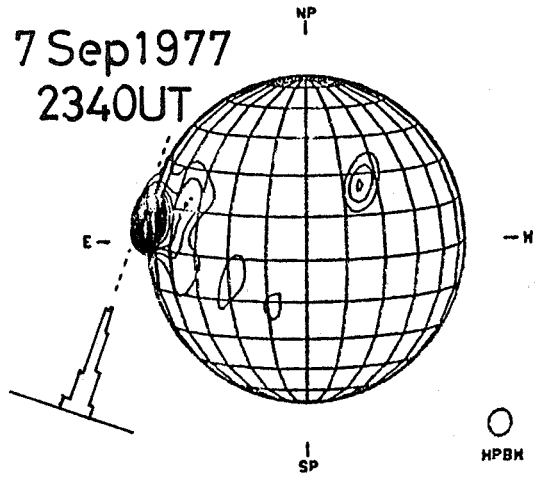

Fig. 6. Comparison of a fan beam scanning of post burst increase of great burst on September 7, 1977, with 8-cm radio map observed at the Research Institute of Atmospherics at the local noon on September 8, 1977.

Great Burst on September 7, 1977

McMath Region No. 14943 had already developed and was very active prior to its appearance at the east limb of the Sun. We observed a very intense outburst which started at 2231 UT on September 7. The outburst is of special interest, because it was produced by an active region behind the limb. The sampling time of the interferometer was about 1 min 20 sec at the beginning of the great burst, because the burst started in the early morning at Nagoya. The scanning of McMath Region No. 14943 at 2231:10 UT indicated the onset of the outburst (Figure 4) with the start and the peak flux density of the radio burst at 35 GHz 24 and 15 minutes earlier than the start of the Hα flare, respectively. We observed 26 outbursts from August 1970 through July 1974 by the old 35-GHz interferometer and 8 outbursts from

from May 1976 through December 1977 by the present interferometer. Most of these 34 outbursts started after the reported starting time of the Hα flare and the time of peak flux density coincided with the time of Hα-flare maximum within several minutes. Only two outbursts were exceptional out of these 34 outbursts. An outburst on May 24, 1972 started at 0658 UT and attained its peak flux density of >6000 s.f.u. at 0702 UT. The radio burst was associated with a 1N flare (N08E85) that started at 0702 UT. The time of maximum phase of the Hα flare was 0715 UT. The time delay of the Hα flare on September 7, 1977 was even longer than the event on May 24, 1972. The time delay of the Hα flare on September 7, 1977 appears to indicate that the flare occurred behind the limb and only the top of flare region was observed after the flare developed. The time profile of flux density at 35 GHz is typical of a great burst and closely resembles in appearance a great burst on the disk on January 24, 1971 and a great burst near the limb on May 24, 1972.

Our observation shows that the distance of the radio source from the disk center is 0.99 + 0.02 $R_\odot$ at the onset, if we assume the latitude of the radio source is the same as that of Hα flare. Observations of the quiet solar disk by the interferometer give the radius of the radio disk as 1.015 $R_\odot$ at 35 GHz. Because the great burst occurred in the active region behind the limb, the height of the radio source must be nearly equal to or higher than the radio limb of 1.015 $R_\odot$. Otherwise, radio waves from the source would be absorbed by the solar atmosphere or spicules between the source and observer. The argument gives the height of the source of the great burst of 7,000-10,000 km above the photosphere. The half power beam width was 2.9-2.6' at the time of the great burst and too large to give the brightness distribution of the burst.

Cheng and Widing [1975] have suggested from observations obtained with the XUV spectroheliograph aboard Skylab that flares result from a plasma instability which also produce localized heating of the hot flare plasma near the top of the loop. The great burst on September 7 started at the time of maximum of X-ray intensity ratio I(0.5-4A)/I(1-8A) obtained with instruments aboard GOES-2. The height of the radio source agrees with the height 4,000-13,000 km given by Cheng and Widing [1975].

Fan beam brightness distribution of the post burst increase can be obtained near the end, because the half power beam width becomes about 1.6'. Figure 6 illustrates a comparison between the fan beam brightness distribution at 35 GHz and the 8-cm radio map obtained at the Research Institute of Atmospherics at local noon on September 8. Restoration by Bracewell method is applied to obtain the fan beam brightness distribution at 35 GHz. If we assume the latitute of the radio source is the same as that of Hα flare, as before, the height of the radio source becomes 0.06 $R_\odot$ (42,000 km). If we assume the radio source is a circular disk of 1.1' diameter, which is equal to the half power width of the brightness distribution in Figure 6, the brightness temperature becomes 1.7×10^5 K.

Gradual rise and fall events

In the intervals September 7-24, three GRF were recorded by the interferometer. The GRF on September 16 was associated with a great burst at frequencies below 9.4 GHz. In the present section, we describe comparisons between our scanning curve and the Hα photograph obtained at the Tokyo Astronomical Observatory. On September 16-17, two Hα flares are reported in the *Solar-Geophysical Data*. The first Hα flare started at 2123 UT and was associated with a precursor of the cm burst. The great burst at cm wave appears to be associated with the second Hα flare which started at 2230 UT. The GRF at 35 GHz started between the onset and the maximum phase of the second Hα flare. The Hα flare was a typical two-ribbon flare. The size of the GRF is approximately the same as the extension of the Hα flare (Figure 7). If we assume the radio source has an elliptical shape with an axial ratio of 2:1 and with a major axis of 1.9', the brightness temperature at 35 GHz becomes 1.8×10^5 K.

The location of the peak brightness at 35 GHz coincided with sunspots located near the center of the active region. Photographs exposed in the wings of Hα line show that the sunspots near the center of the active region developed rapidly between September 15 and 17 [Moriyama 1978]. The interferometer observation appears to show that the great burst at cm wave and the GRF at 35 GHz results from the changing field configuration in this area of the active region.

On September 20, the Hα flare started at 0251 UT near the northwest boundary of the active region and extended toward the southwest [Moriyama 1978]. The GRF at 35 GHz started about 80 minutes after the flare onset, but still earlier than the onset of cm burst. The peak of the brightness at 35 GHz was located near the sunspots at the west end of the active region, in advance of the extension of the luminous area of Hα toward the west (Figure 7). The brightness temperature at 35 GHz is 70,000 K at the time of maximum flux density, if we assume the radio source has a circular shape with 1.4' diameter, which is equal to the half-power width of the fan beam brightness distribution.

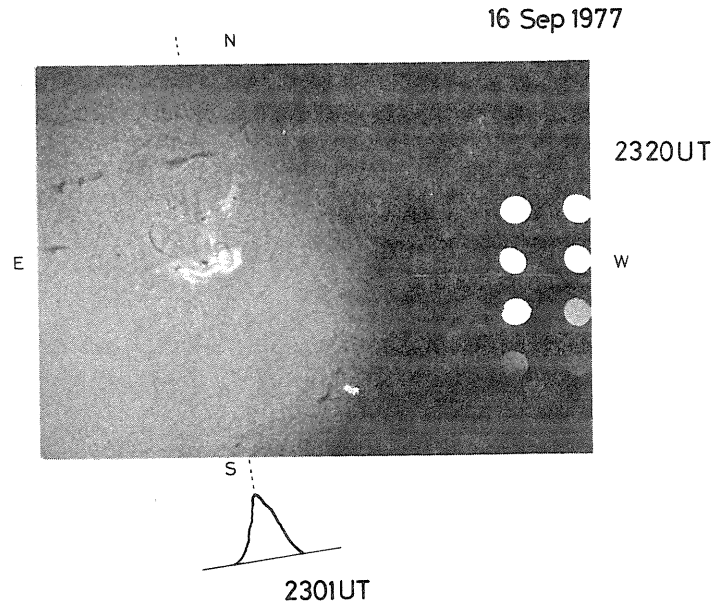

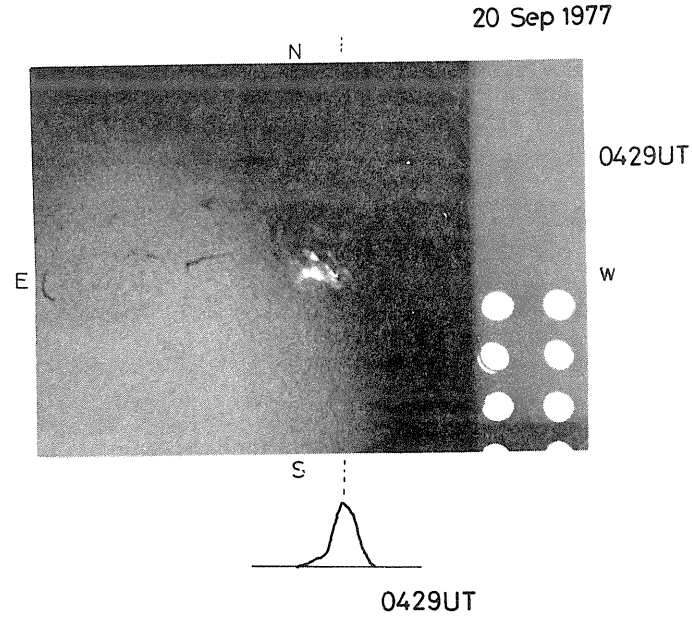

Fig. 7. Comparison between Hα photograph observed at the Tokyo Astronomical Observatory and fan beam scanning curve at 35 GHz.

The authors would like to thank Prof. F. Moriyama, Tokyo Astronomical Observatory and Dr. S. Enome, Research Institute of Atmospherics, for supplying observational data. They would like to acknowledge the assistance of Mr. K. Akita in obtaining observational material.

This work was supported by the Scientific Research Fund of the Ministry of Education 254046 and 942026.

REFERENCES

CHENG, C.H. and K.G. WIDING — 1975 — "Spatial Distribution of XUV Emission in Solar Flares," *Astrophys. J., 201,* 735-739.

KAWABATA, K., H. OGAWA, Y. SOFUE, and I. SUZUKI — 1974 — "The 35 GHz Solar Interferometer at Nagoya," *Publ. Astron. Soc. Japan, 26,* 387-398.

MORIYAMA, F. — 1978 — "Optical Observations of McMath Region 14943," *Solar Terrestrial Environmental Research in Japan, 2,* 1-8.

The McMath Region 14943 Observed at 8.6 mm Wavelength with an Angular Resolution of 3.1'

by

Peter Steffen
Radioastronomisches Institut der Universität
Bonn, Germany

and

Wolfgang Harth
Max-Planck-Institut für Radioastronomie
Bonn, Germany

Introduction

At Stockert Observatory, 40 km away from Bonn, routine observations of the solar radio emission are performed with a parabolic dish of 10 m diameter. Normally all observations with this instrument are made at a frequency of 34.9 GHz (λ = 8.6 mm) from 0700 UT to 1600 UT each day. Here we report on data relevant to McMath region 14943 obtained at this wavelength during the period from September 9-24, 1977.

Although the weather conditions during this period were not good, we are able to present one solar map at 8.6 mm wavelength for nearly every day and, furthermore, for all days some other flux values of the active region.

Telescope and Receiver Characteristics

The 10-m telescope consists of a parabolic dish with a solid surface and is a Cassegrain system. It has an equatorial mount and allows scanning of the Sun in the right ascension direction and also tracking of arbitrary points on the solar surface. Because of the bad weather conditions mentioned above, no tracking observations were made in the observing period reported here. At a wavelength of 8.6 mm the angular resolution of the telescope is 3.1' arc and its aperture efficiency is 0.43.

A Dicke type radiometer with a broadband mixer (Δf = 500 MHz) was used. Including the antenna temperature of the Sun in the system temperature, a temperature resolution of 0.01% of the quiet Sun level was obtained for the entire system during the integration time of 3 sec. With this, under good weather conditions, it is easy to produce solar maps, which show negligible noise.

Solar Maps at 8.6 mm Wavelength

Solar maps were obtained from right ascension drift scans. In order to get a good baseline for the sky level, each scan lasted about 5 minutes. The distance between scans in declination was about 1.3', changing slightly with the solar proper motion in the α, δ - coordinate system. Correction for this motion was made in the first stage of the telescope data reduction, both for right ascension and declination. Thus the data point separation of the solar maps given in Figures 1a/1b and 2 is about 1.3' and 0.75' in δ and α, respectively. Normally only a fraction of the solar surface is scanned, depending on the activity in the solar atmosphere.

The contour lines in Figures 1 and 2 start at a level of 1% above the quiet Sun level, which has been determined numerically. The separation between successive contour lines if 1% up to values of 10%. After that a separation of 2% has been chosen. The maps were plotted using the NOD2 - system library of Haslam [1976]. The arrows indicate whether a relative maximum (counterclockwise) or a relative minimum (clockwise) is enclosed by the contour levels.

From September 8-10 the source McMath Region 14943 was not scanned, but Figures 1a and 1b show the movement of the source between the 11-20. For September 12 and 15 no maps were available, owing to bad weather. On the map for September 21 the 8.6 mm emissive layer of the source has disappeared. A clear double structure can be detected on September 11, 13, 16 and 17. During the other times the source is clearly broader in the direction of its two components, and thus the double structure is also indicated during these times.

For September 13 a series of solar maps specially for McMath region 14943 was produced (Figure 2). It can be seen that the source structure is not constant. Some of these maps show changing flux density and appearance, in particular for the northern component.

Flux Values of McMath Region 14943

To determine the flux density of an active region, all flux values of the source area were integrated numerically. The absolute calibration was carried out using a quiet Sun flux density at 8.6 mm of 2435 sfu (1 sfu = 10^{-22} W m^{-2} Hz^{-1}), obtained from Kuseski and Swanson [1976]. This was done not only for the maps shown in Figures 1 and 2, but also for many other maps of McMath region 14943, obtained during the observing period. The errors in these flux densities are about $\pm$12%, due to the

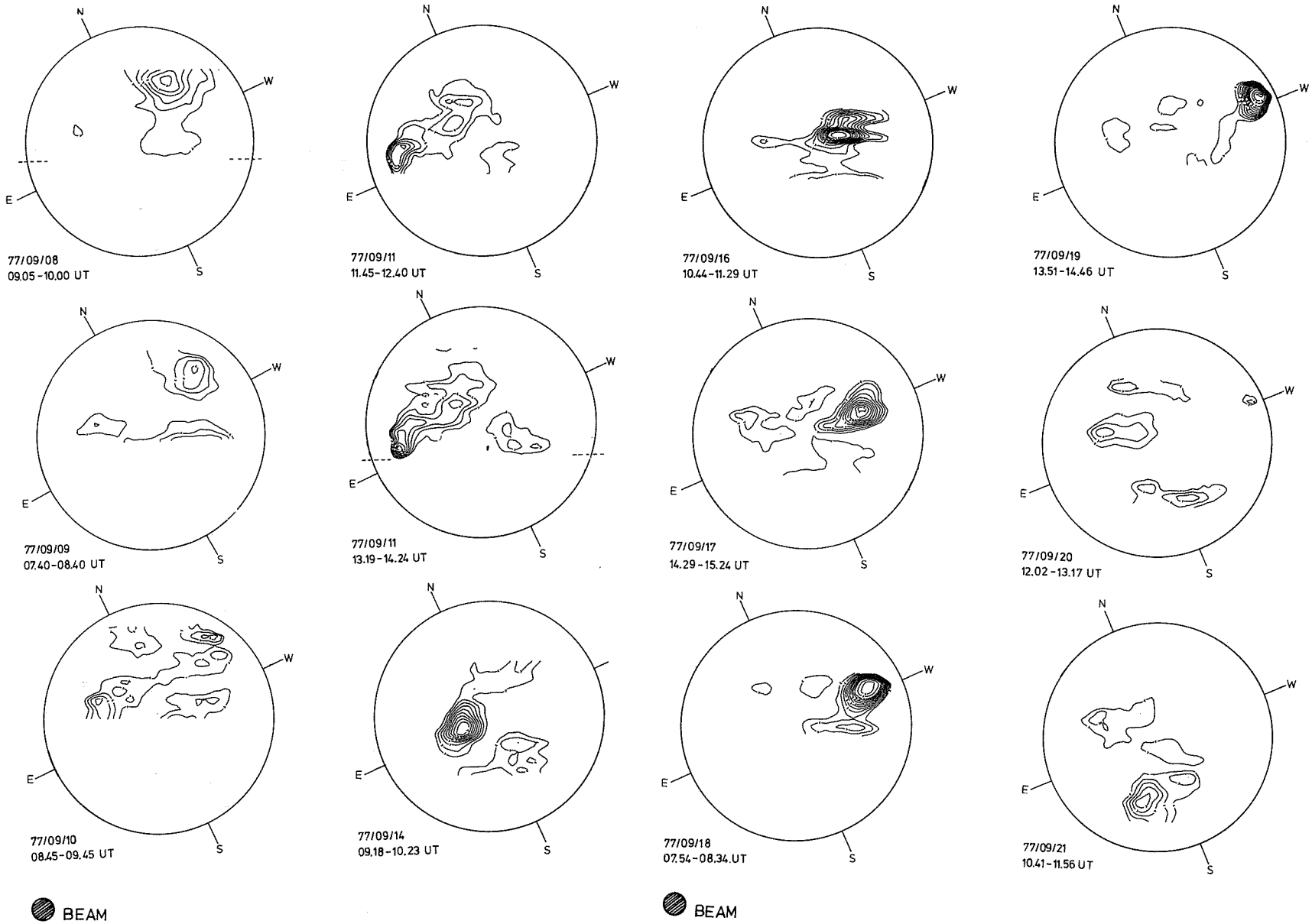

Fig. 1a/ab. 8.6 mm solar maps -- the scanned area is indicated by open contour lines or by dashed lines. Intensities are given in % above the quiet Sun level; separation: 1% from 1-10% and 2% for higher intensities.

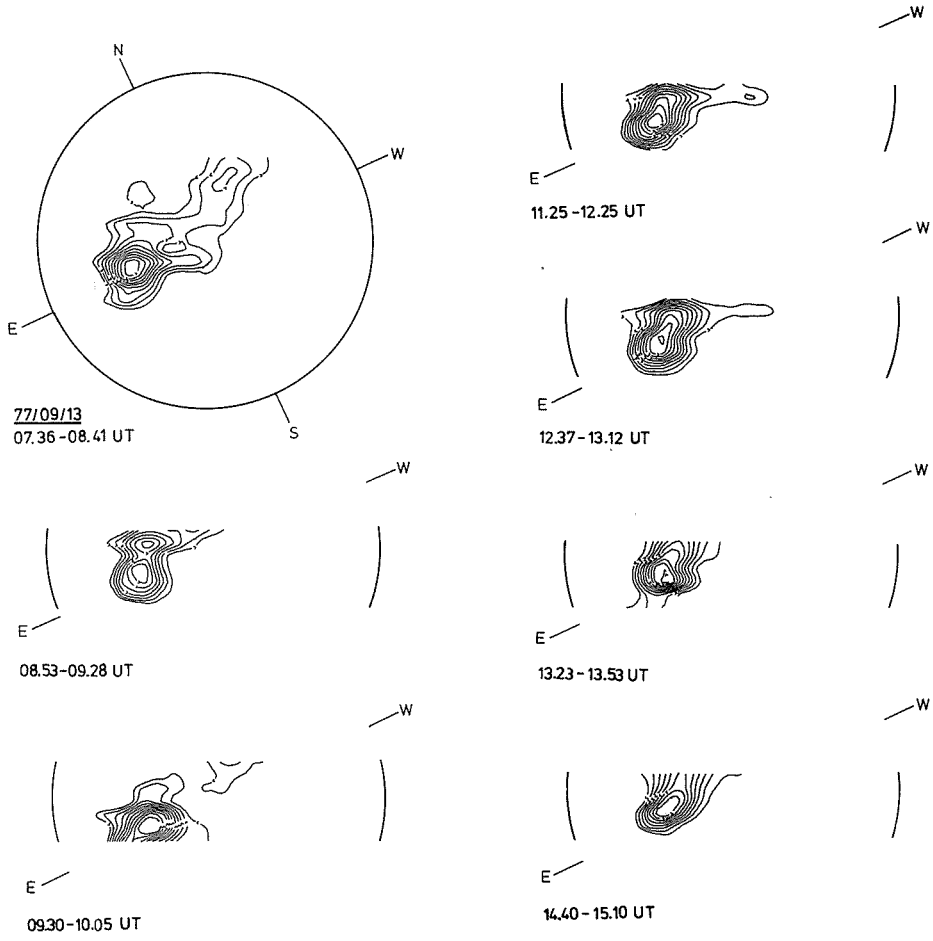

Fig. 2. A series of 8.6 mm maps of McMath region 14943 for September 13.

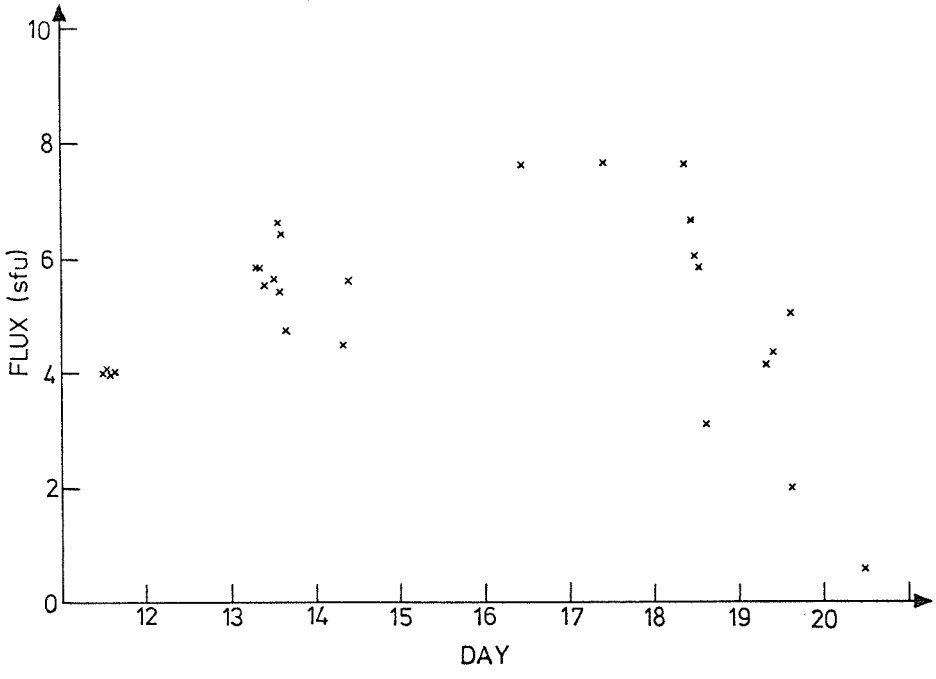

Fig. 3. 8.6 mm flux density of McMath region 14943 versus time (the abscissa tick marks are at 0000 UT of the September date.

flux integration procedure, the quiet Sun level determination, and mainly to the uncertainty in separating the area of the emission from McMath region 14943 from other nearby structures, as, for instance, the broad flat one in the north-west direction of region 14943.

The results of these flux determinations are summarized in Figure 3. Excluding the rapid decrease in flux density on September 18 between 1000 UT and 1400 UT, and in spite of the large errors, an increase in flux from September 11 to 16/17 seems to be indicated, as well as a decrease from 17 to 20. This may be due to the projection effect caused by solar rotation and gives evidence for a flat, disk-like 8.6 mm emissive layer with an optical depth larger than 1 [Christiansen et al., 1960].

References

CHRISTIANSEN, W.N.
D.S. MATHEWSON,
J.L. PAWSEY,
S.F. SMERD,
A. BOISCHOT,
J.F. DENISSE,
P. SIMON,
T. KAKINUMA,
H. DODSON-PRINCE and
J. FIROR
1960 A study of a solar active region using combined optical and radio techniques, *Ann. d'Astrophys., 23,* 75.

HASLAM, C.G.T. 1976 *Technischer Beright des Max-Planck-Institutes fur Radioastronomie Bonn, 34.*

KUSESKI, R.A. and
P.N. SWANSON
1976 The solar brightness temperature at millimeter wavelengths, *Solar Phys., 48,* 41.

Microwave Solar Activities Observed at Toyokawa in September (McMath 14943) and in November (McMath 15031), 1977

by

K. Shibasaki, S. Enome, and M. Ishiguro
Research Institute of Atmospherics, Nagoya University, Toyokawa 442, Japan

A region of high activity appeared on September 7, 1977 on the east limb of the Sun and produced a great burst with high energy proton enhancement in the interplanetary space. In the course of disk passage, several bursts occurred in this region and some of them yielded a high energy proton event and/or GLE (Ground Level Event). The microwave activities of this region observed at Toyokawa are reported here. On November 22, 1977 a large GLE occurred, but we cannot observe the microwave burst associated with this GLE because of sunset at Toyokawa. We, therefore, present only the S-component activity of McMath region 15031.

Observations

Total flux observations at 9.4, 3.75, 2.0, and 1.0 GHz are carried out every day. Collected data are digitized and recorded on a magnetic tape. Sampling interval is 0.1 second for each frequency. East-west solar scans are taken by interferometers at 9.4 and 3.75 GHz from about 0100 UT to 0500 UT. Digital data are taken at local noon (~0300 UT), and the HPBW (half-power-beam-width) at this time is 1.1 arc minutes [Kakinuma and Tanaka, 1963; Tanaka and Kakinuma, 1965; Tanaka et al., 1969]. Pencil beam observations by radioheliograph at 3.75 GHz [Shibasaki et al., 1976] start after the east-west drift scan observations at local noon. The mode of observation is skip scanning [Tanaka et al., 1970]. It takes 20 minutes to take one map. The HPBW is 2'.25 x 2'.25·SEC(ZD), where ZD is zenith distance of the Sun. Parameters of antennas and receivers are briefly listed in the following table.

Table. Parameters of antennas and receivers

	Frequency (GHz)	Antenna ($m\phi$)	τ/HPBW
Polarimeter	9.4	0.8	0.3 sec
	3.75	1.5	0.3
	2.0	2.0	0.3
	1.0	3.0	0.3
Interferometer	9.4	2.0	1.1 arc min.
	3.75	3.0	1.1
Heliograph	3.75	3.0	2'.25 x 2'.25·SEC(ZD)

S-component of McMath region 14943

Figures 1 and 2 show the radioheliograms at 3.75 GHz for the period when the region was visible on the disk. The latitudinal displacement of the region, which is seen in the maps of September 17 and 18, seems not real but instrumental. In Figure 3, we have plotted the evolution of the S-component observed by 3-cm and 8-cm interferometers. The quiet sun was obtained by connecting the most frequent values (modal values) in each bin of 27-day data. Flux variations and the flux ratio (3-cm flux/ 8-cm flux) of the S-component are shown in Figure 4.

S-component associated with McMath region 14943 was first observed after the event of September 7 at microwave frequencies. The flux densities at 3 cm (9.4 GHz) and 8 cm (3.75 GHz) of this S-component on that day were 10.6 and 9.5 s.f.u. respectively. The flux ratio (F3/F8) was larger than unity. During the period September 8 through September 11, dominant features of the S-component are the flux density at both wavelengths increased, the flux ratio kept larger than unity, and the source size at 3 cm became smaller. It is also to be noted that the activity was very high during this period. After September 11, the 3-cm flux started to decrease and the source width at 3 cm became broader. The brightness temperature, therfore, decreased sharply, as seen in Figures 3 and 4, till September 15, when the region passed the central meridian. During this declining phase, the activity was low. The above-mentioned phenomena suggest that the magnetic flux of the region diverged during the declining phase. The field strength became weak to emit gyroresonance radiation at 3 cm, but it was strong enough for gyroresonance emission at 8 cm wavelength at the harmonics of gyrofrequency. After the central meridian passage, the brightness temperature at 3 cm increased gradually and the flux ratio also increased, but kept less than unity. Several great bursts were observed in this increasing phase.

To sum up, high activities of the S-component can be divided into two phases. The first phase began with the appearance of this region and lasted until September 11, during which two great bursts occurred. The second phase was from September 16 through September 20. Five great bursts were observed in this period. Characteristics of the bursts in these two phases will be described in the next

section. As the final remark in this section, interferometric observations of the polarized component (Figure 5) show that the preceding spot has left-handed circular polarization. As this region was in the northern hemisphere of the Sun, the sunspot polarity alignment of this region was reversed from what would normally be expected, if this region belonged to the cycle 21.

Microwave Bursts in McMath Region 14943

McMath region 14943 produced several great bursts in microwave range. Most of them were accompanied by an enhancement of high energy protons in the vicinity of the Earth and two of them were associated with GLE [SGD, 1977, 1978b]. Among these great bursts, we observed the events on September 7, 16, 20, and 24. Figures 6, 7, and 8 show the time profiles of the bursts. The calibration signals are superposed in some of the records. The peak value of the flux for the burst on September 24 was not so large (13 s.f.u. at 3.75 GHz) and there is no report of optical flare [SGD, 1978b]. Temporal coincidence, however, strongly suggests that it was associated with an enhancement of high energy protons and a GLE. It is quite possible that McMath 14943 produced this event well behind the west limb of the Sun, since there was no prominent active region on the disk in these period other than McMath 14943. Unfortunately, the burst on September 24 occurred about 0600 UT, when the interferometers are out of routine observations.

McMath 14943 recurred on October 5 and was numbered McMath 14979. It was not so active as in the previous rotation, but it produced a great burst on October 12, which was accompanied by an enhancement of high energy protons [SGD, 1978c].

The frequency spectra are shown in Figure 9 of the peak flux of each event in McMath 14943. The spectra of these bursts can be divided into two groups. One is low peak frequency group and the other is high peak frequency group. The bursts of the first group with low peak frequency around 5 GHZ occured during the second phase of activity mentioned in the previous section. The bursts of the second group with peak frequency around 10 GHz were observed, with one exception in the first phase of activity. It also suggested from the change of burst spectra that the morphology and/or strength of the magnetic field has changed between the two phases of activity.

S-component of McMath Region 15031

McMath 15031 produced a great burst on November 22 [SGD, 1978a]. This event was not observed at Toyokawa. We describe only the activity of S-component here. This region appeared on November 11 on the east limb of the Sun, but its flux densities were small at 3 and 8 cm. The S-component was remarkable during the period November 18 through November 22, as seen in Figure 10. The gyroresonance emission is regarded effective only during this period.

REFERENCES

Kakinuma, T. and H. Tanaka — 1963 — A high-resolution interferometer for polarization measurement at 9.4 GC/S, Proc. Res. Inst. Atmospherics, Nagoya Univ., 10, 25-33.

Tanaka, H. and T. Kakinuma — 1965 — Improvement of the high-resolution interferometer at 9.4 GC/S, Proc. Res. Inst. Atmospherics, Nagoya Univ., 12, 27-34.

Tanaka, H., T. Kakinuma, S. Enome, C. Torii, Y. Tsukiji and S. Kobayashi — 1969 — A high-resolution quick-scan interferometer for solar studies at 3.75 GHz, Proc. Res. Inst. Atmospherics, Nagoya Univ., 16, 113-126.

Tanaka, H., S. Enome, C. Torii, Y. Tsukiji, S. Kobayashi, M. Ishiguro and M. Arisawa — 1970 — 3-cm radioheliograph, Proc. Res. Inst. Atmospherics, Nagoya Univ., 17, 57-74.

Shibasaki, K., M. Ishiguro, S. Enome, H. Tanaka, C. Torii, Y. Tsukiji S. Kobayashi and N. Yoshimi	1976	λ 8 cm radioheliograms, Proc. Res. Inst. Atmospherics, Nagoya Univ., 17, 57-74.
SGD	1977	Solar-Geophysical Data, 399 Part I, November 1977, U.S. Department of Commerce, (Boulder, Colorado, U.S.A. 80302).
SGD	1978a	Solar-Geophysical Data, 401 Part I, January 1978, U.S. Department of Commerce, (Boulder, Colorado, U.S.A. 80302).
SGD	1978b	Solar-Geophysical Data, 403 Part II, March 1978, U.S. Department of Commerce, (Boulder, Colorado, U.S.A. 80302).
SGD	1978c	Solar-Geophysical Data, 404 Part II, April 1978, U.S. Department of Commerce, (Boulder, Colorado, U.S.A. 80302).

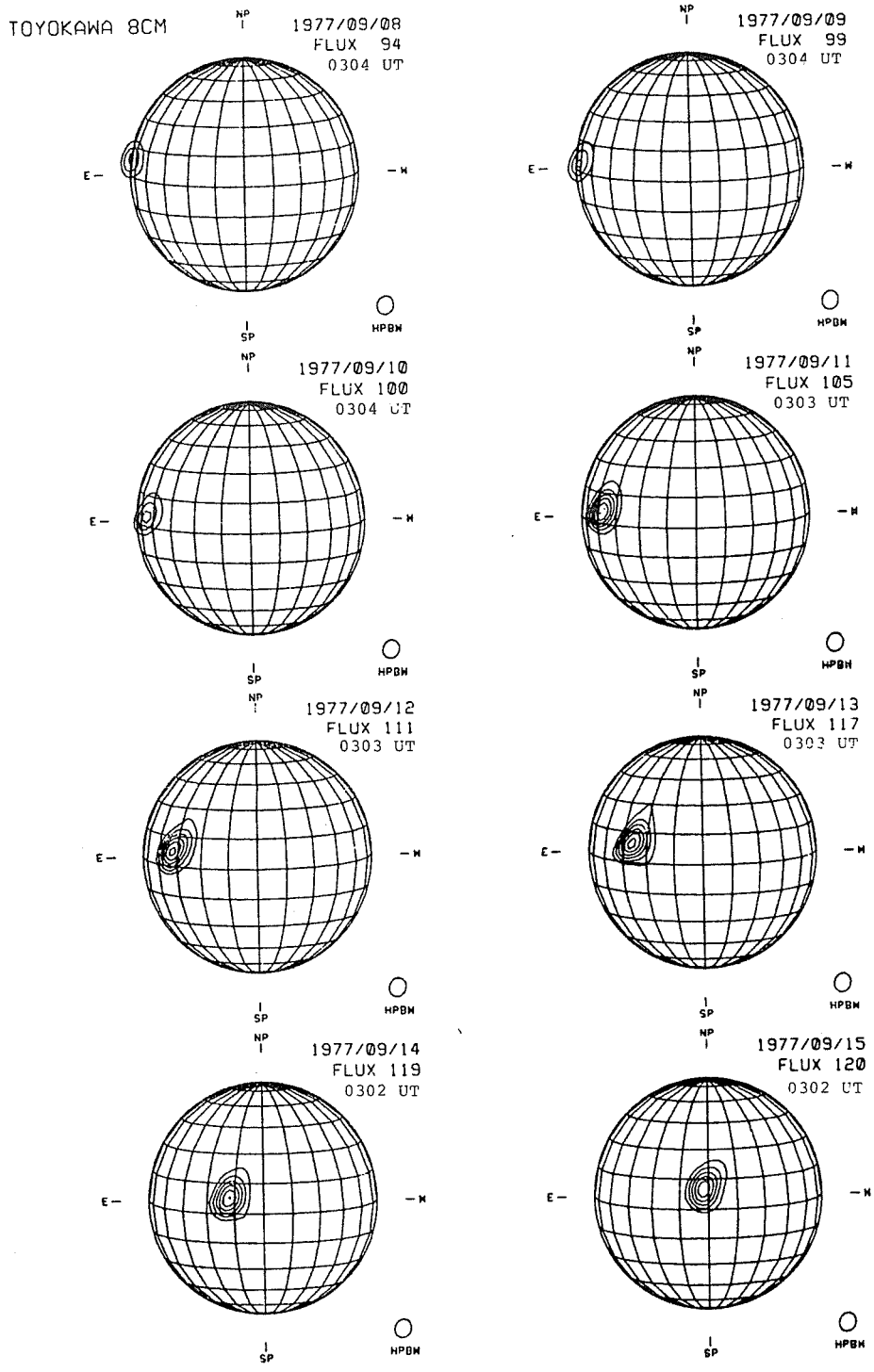

Fig. 1. Radioheliograms. The lowest contour level is 132000 K and the interval is 88000 K.

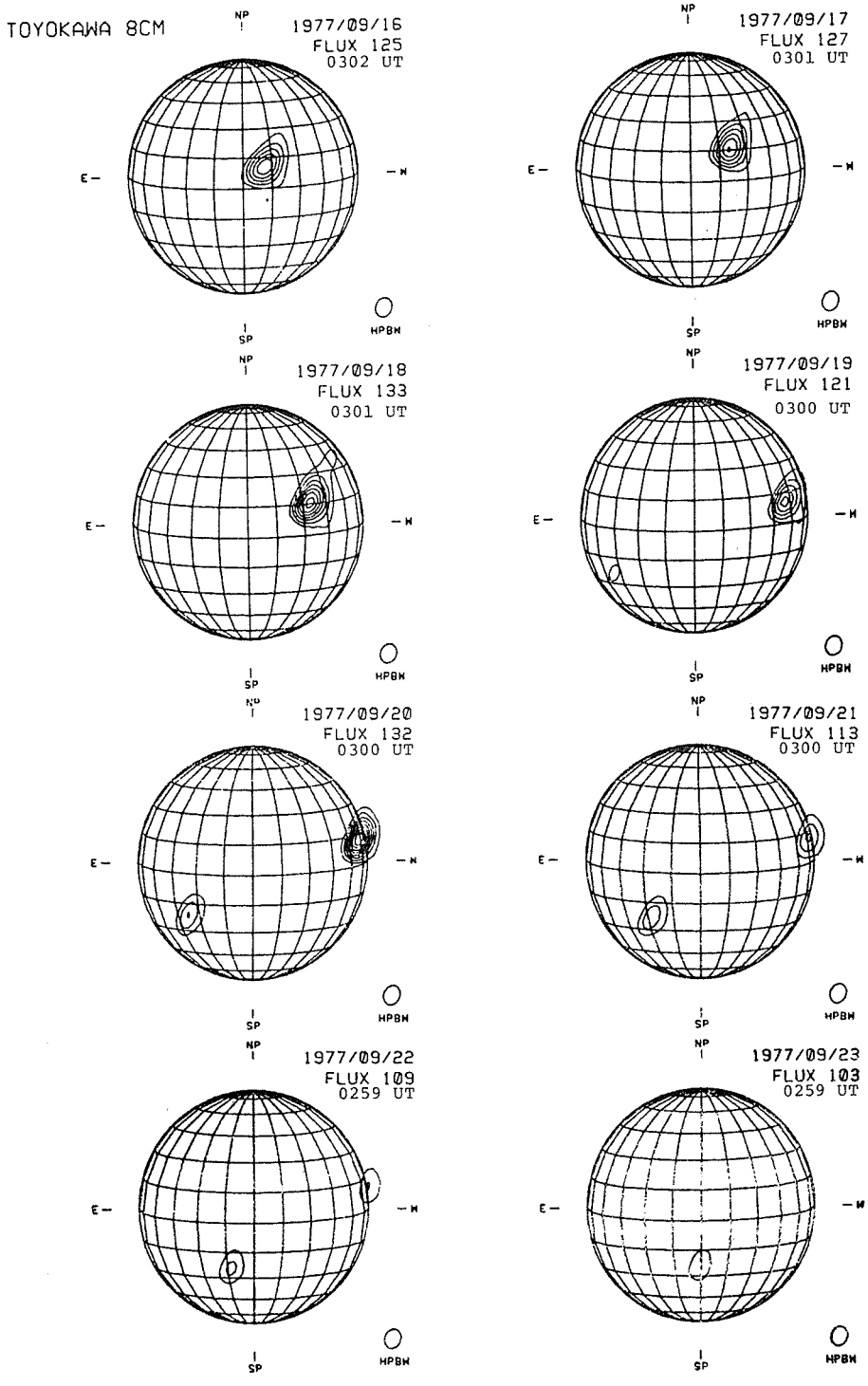

Fig. 2. Radioheliograms. The lowest contour level is 132000 K and the interval is 88000 K.

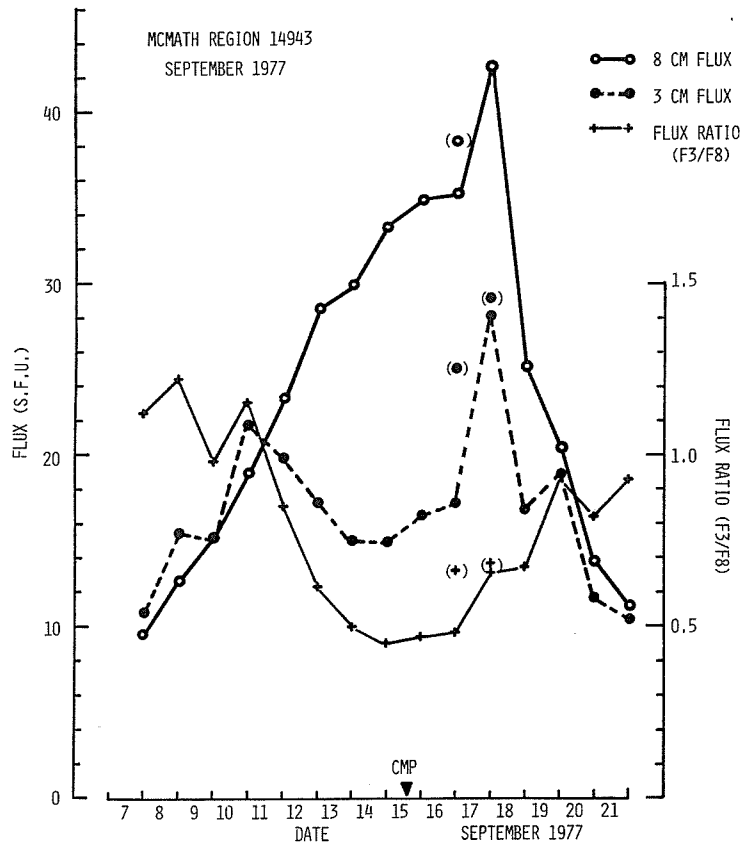

Fig. 4. The variation of S-component flux and the flux ratio for McMath region 14943.

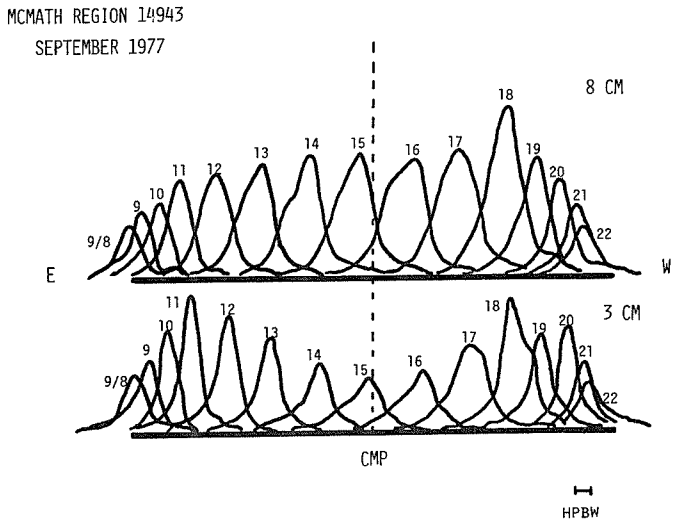

Fig. 3. S-component evolution of McMath region 14943.

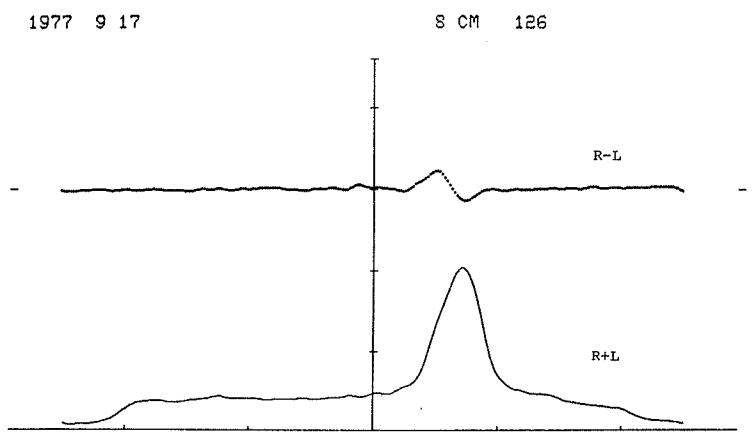

Fig. 5. East-west solar scan on September 17, 1977 at 3.75 GHz.

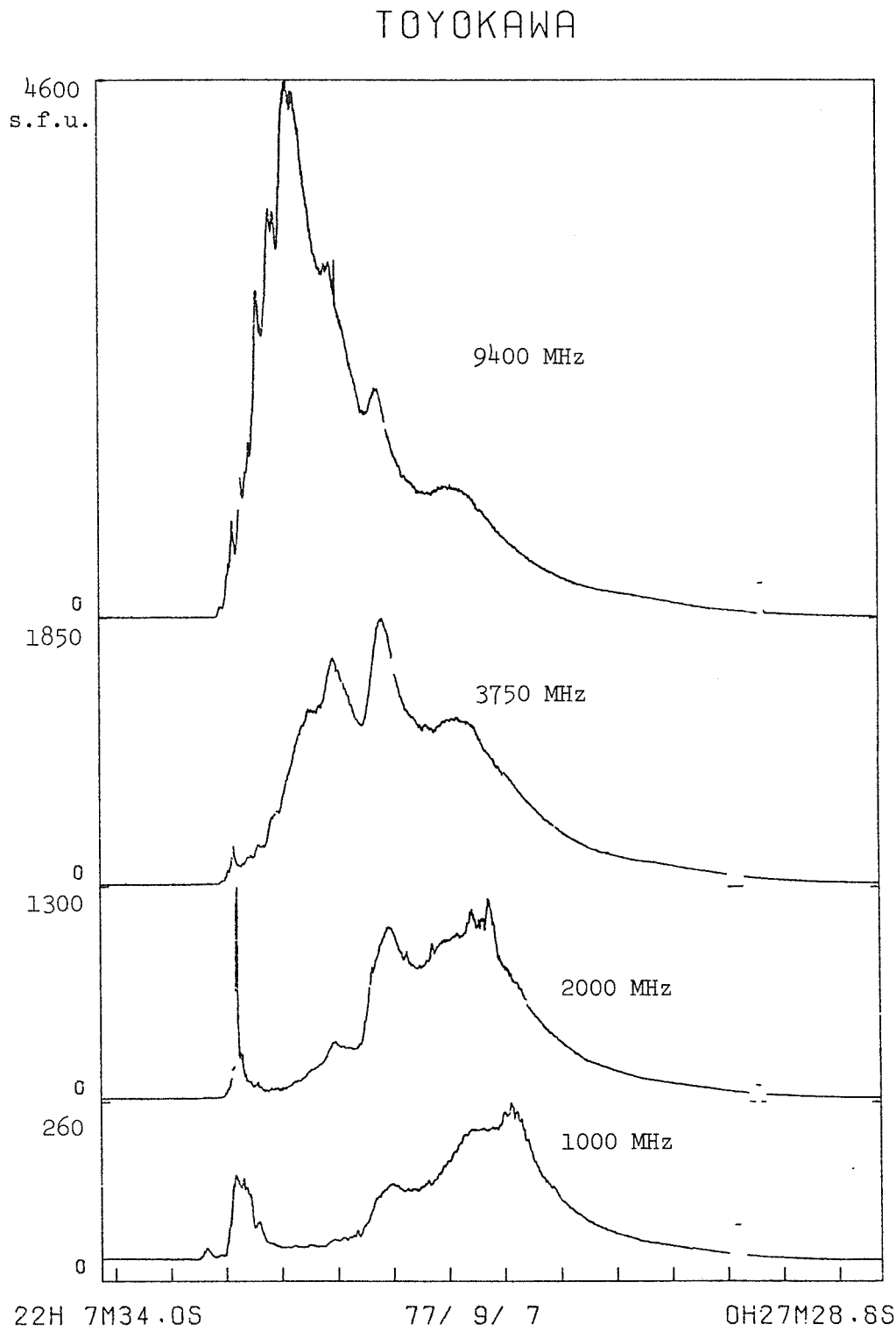

Fig. 6. Time profiles of the burst on September 7, 1977. The vertical scale is linear.

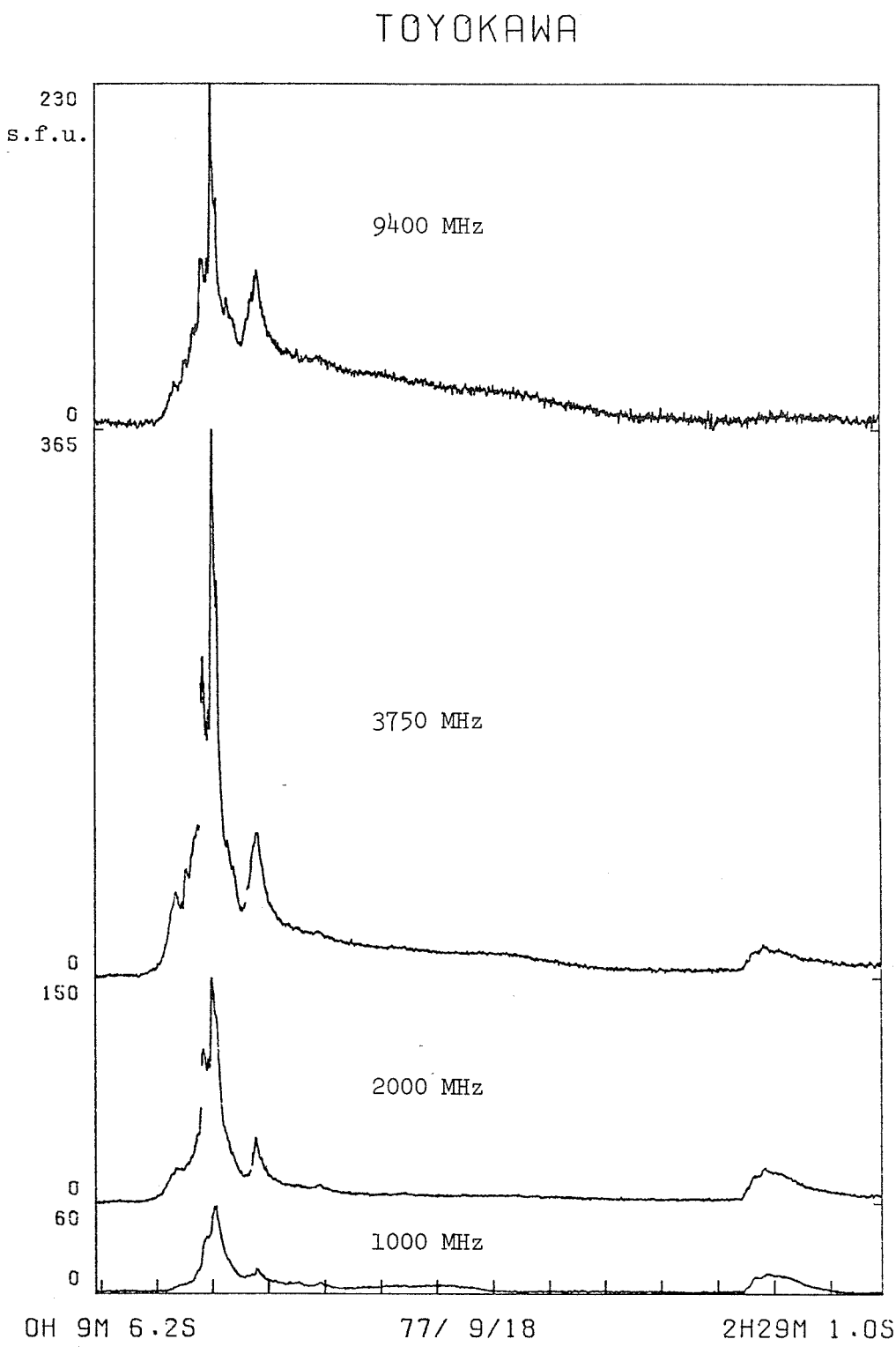

Fig. 7. Time profiles of the burst on September 18, 1977. The vertical scale is linear.

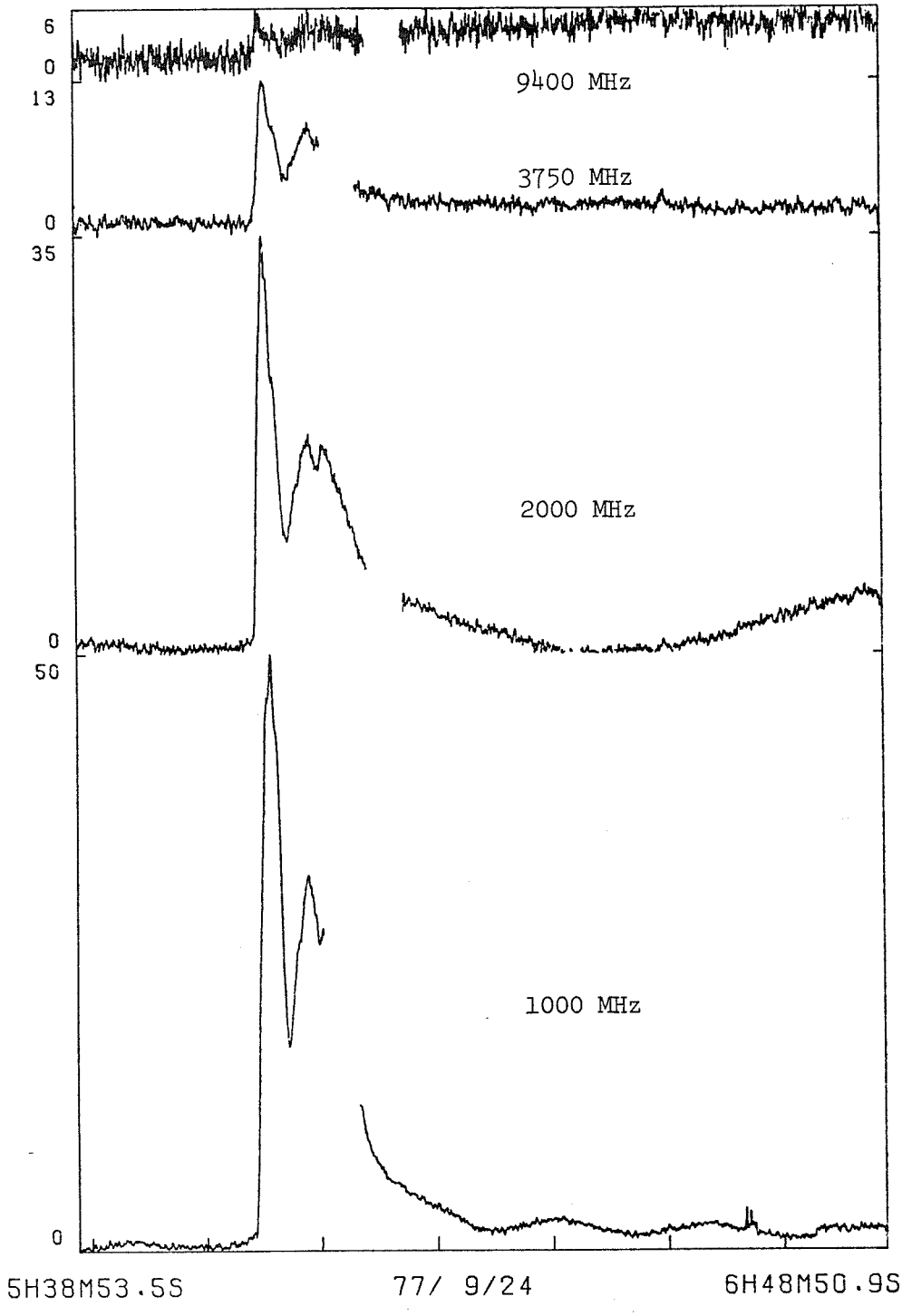

Fig. 8. Time profiles of the burst on September 24, 1977. The vertical scale is linear.

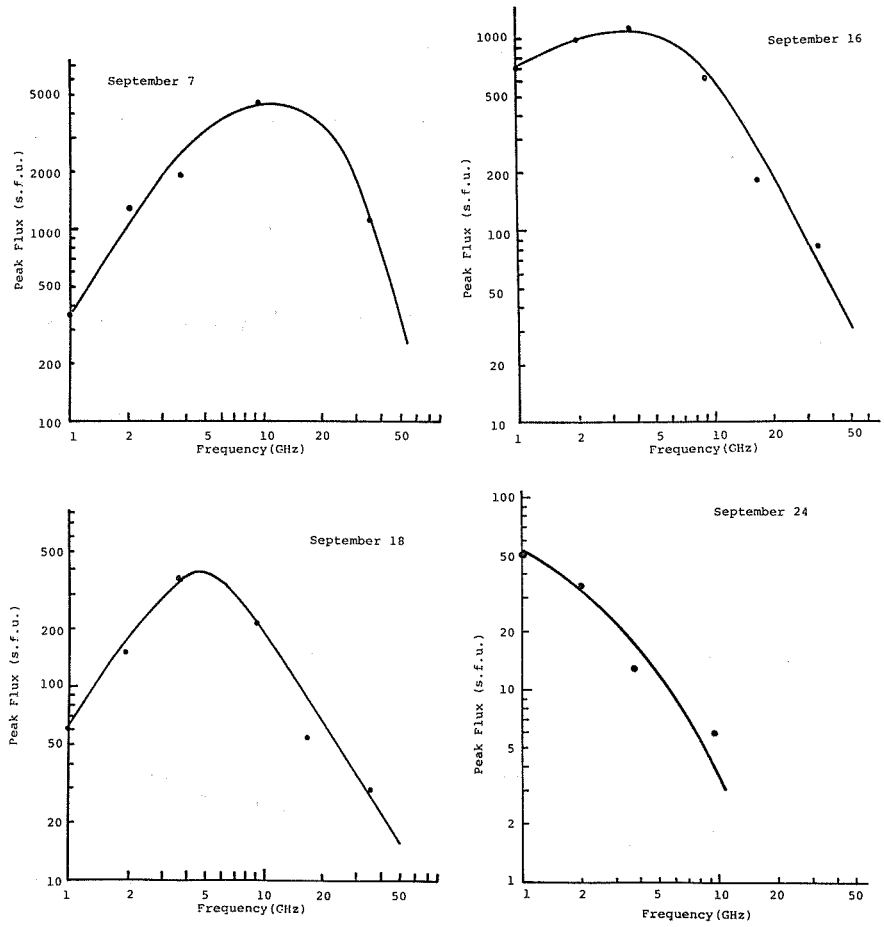

Fig. 9. The frequency spectra of the bursts on September 7, 16, 18, and 24, 1977. Data at 17 GHz is from Nobeyama Solar Radio Station, Tokyo Astronomical Observatory and data at 35 GHz is from Department of Physics, Nagoya University.

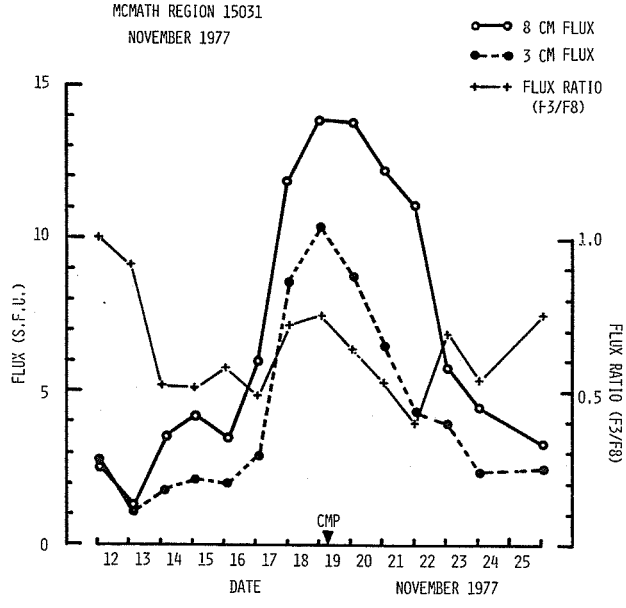

Fig. 10. The variation of S-component flux and flux ratio for McMath region 15031.

Solar Radio Emission at 10.7 cm in the Period of September 7-24 and on November 22, 1977

by

H. Welnowski and J. Hanasz
Polish Academy of Science
Center for Astronomy, Astrophysics Lab.
12/18 Chopin Str.
87-100 Torun, Poland

Daily observations of solar radio emission have been carried out at the Torun Astronomical Observatory (53°05'48"N, 1h 14m 13.1s E), with our total power receiver connected to the half-wavelength equatorially polarized dipole, in the focus of a 1.8 m steerable dish. The Sun is continuously pointed to the axis of the angular pattern of the antenna of 4° HPBW. The receiver noise is recorded with $\Delta S/S_Q = 20$, where ΔS is the fluctuation of the received total flux on the quiet Sun level, S_Q, and occurs when noise in the bandwidth of 12 MHz is detected and smoothed with a time constant of 4 seconds. For the latitude of the observatory the daily observing period is short in November, and for the low elevations of the Sun in autumn some errors of flux density determinations can be due to ground fluctuations and shadows of surrounding trees.

Accompanying SEA (sudden enhancements of atmospherics) observations at 27 kHz, carried out with our equipment at the Torun Observatory are also reported here.

Table 1 shows our daily observing periods for days between the 7th and 24th of Sept. and for the 22nd of Nov. Table 2 lists all the clearly identified events, whose total flux density was greater than 20 s.f.u. (1 s.f.u. = 10^{-22}watts $m^{-2}Hz^{-1}$). The types of outstanding occurrences are classified according to the Solar Radio Emission Instruction Manual for Monthly Reports by Haruo Tanaka, Jan. 1st, 1975.

Table 1. Operating Hours, UT (No Data Interruptions Greater than 15 Min.)

Date	Hours 2800 MHz	SEA - 27 kHz
7-9 Sept.	06-16	all day
10 Sept.	08-16	"
11-12 Sept.	07-16	"
13 Sept.	08-16	"
14 Sept.	no observations	"
15 Sept.	08-16	"
16-24 Sept.	06-16	"
22 Nov.	07-14	no observations

Daily values of solar flux density in s.f.u. are presented in Fig. 1. A gradual increase of mean solar flux from 80 s.f.u. on Sept. 7, to 130 s.f.u. on Sept. 17 and 18 was observed. From Sept. 19 to Sept. 30 an almost constant mean solar flux was observed at the level of 110 s.f.u., which is almost twice the quiet Sun level of 66 s.f.u.. In November daily values of solar flux fluctuated no more than from 91 to 101 s.f.u., and in particular the daily mean for Nov. 22, 97.5 s.f.u., did not differ much from values for other days.

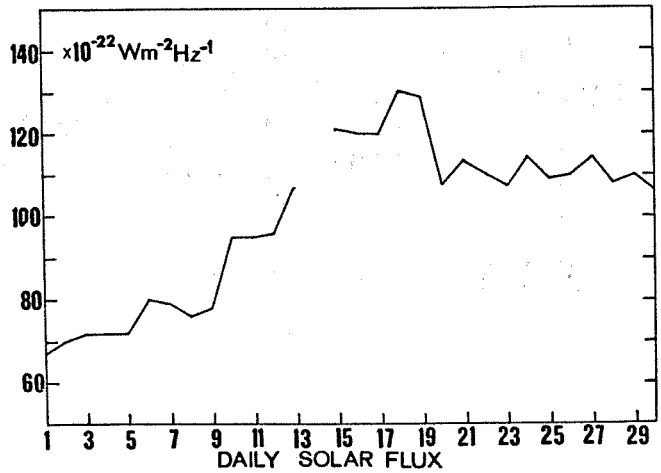

Fig. 1.

Pen records of events contained in Table 2 are shown in Figs. 1-7. Recorded output voltage is scaled to solar flux units, s.f.u., via noise calibration with the standard noise diode and the thermal source.

Table 2. Outstanding occurrences for the period of Sept. 7-24, and Nov. 22, 1977 as observed at 2800 MHz at Turun, Poland.

Date 1977	Type	Start UT	Time of maximum UT	Duration min	Flux density, s.f.u. Peak	Mean	Remarks
Sept. 15	3S	1047	1048	4	25	15	
"	3S	1053	1054	2	18	13	Weak SEA observed
"	41F	1056	1101	11	49	13	
Sept. 16	45C	0738	0740	5	22	8	
Sept. 17	4S/F	0618	0619	4	33	12	
Sept. 19	3S	1033	1034	3	16	11	
"	49GB	1037.5	-	56	≫200	≫200	
	"		1039	0.5	162	-	SEA observed
	"		1127.5	3	133	-	
	29PBI		1134	42	78	53	
"	3S	1136	1137.5	3.5	38	13	
"	46C	1216	1220.5	10	111	55	
"	8S	1234	1234	0.5	31	14	
Nov. 22	28PRE	0951	0958	7	25	12	No SEA observations
"	49GB	0958	-	49	≫260	≫260	Nov. 22
"	29PBI		1047	27	38	16	
"	2S/F	1053	1055	7	67	17	
"	4S/F	1133	1135	4	38	18	
"	4S/F	1137	1139	8	38	16	
"	2S/F	1153	1155	3	29	16	

Description of events

Sept. 15, start: 1047 UT (Fig. 2). The whole group is the first clearly identified event observed at our observatory in the period of interest. The main event is preceded by 2 possible weak simple, S, bursts at 1047 and 1053 UT. The event itself consists of a group of 3 to 4 short duration spike bursts, superimposed on a gradual rise and fall, GRF, of intensity, which lasts for about 10 minutes. The accompanying weak SEA starts at 1041 UT, with maximum 1052 UT, and duration 27 min.

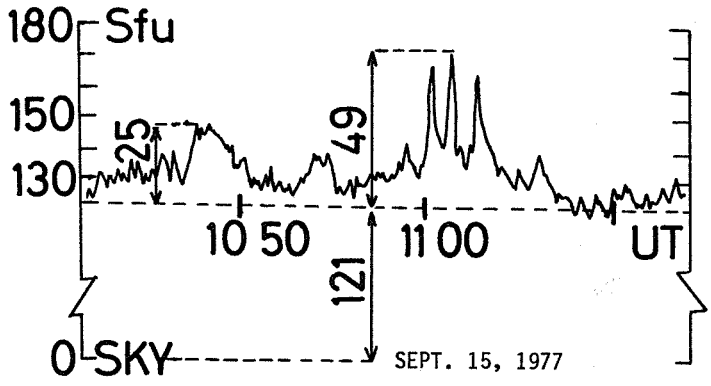

Fig. 2.

Sept. 16, start: 0738 UT, Fig. 3. Weak and short burst.

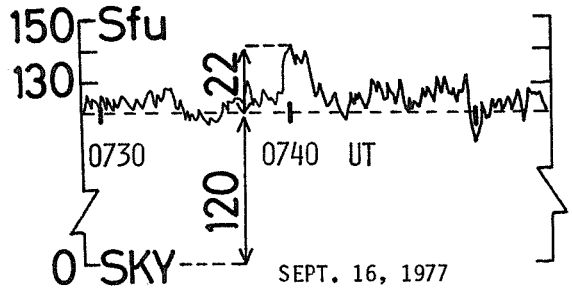

Fig. 3.

Sept. 17, start: 0618 UT Fig. 4. The event is preceded by a little rise of continuum of about 10 to 15 s.f.u. at 0615 UT.

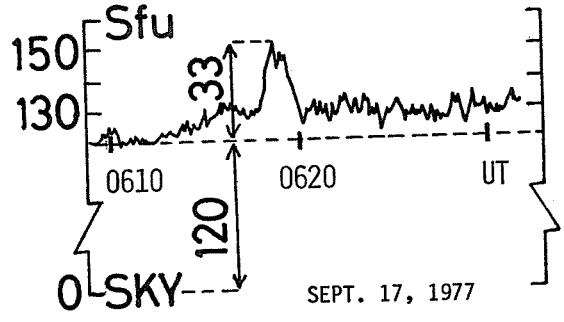

Fig. 4.

Sept. 19, start: 1033 UT, Fig. 5. This is a starting time of a small simple burst, preceding a great burst, GB, whose peak amplitude and time of maximum have not been measured due to a reception at higher sensitivity range. A steep rise of GB is observed at 1037.5, and an off-scale level of 210 s.f.u. is reached at 1040 UT. A little peak of intensity is observed during the rise time at 1039 UT. Another peak, 1128 UT, is observed on the decreasing branch of the event. GB is followed by a post burst increase, PBI, which lasts from 1134 until 1216 UT. A simple burst, S, is superimposed on it at 1137.5 UT. The whole group ends up with a complex burst, C, which starts at 1216 UT and reaches maximum intensity at 1220.5 UT. This is the greatest burst activity, observed with the 2800 MHz equipment at the Torun Observatory since 1974 the start of observations. Accompanying SEA starts at 1029 UT, with maximum 1038 UT, and duration 53 min.

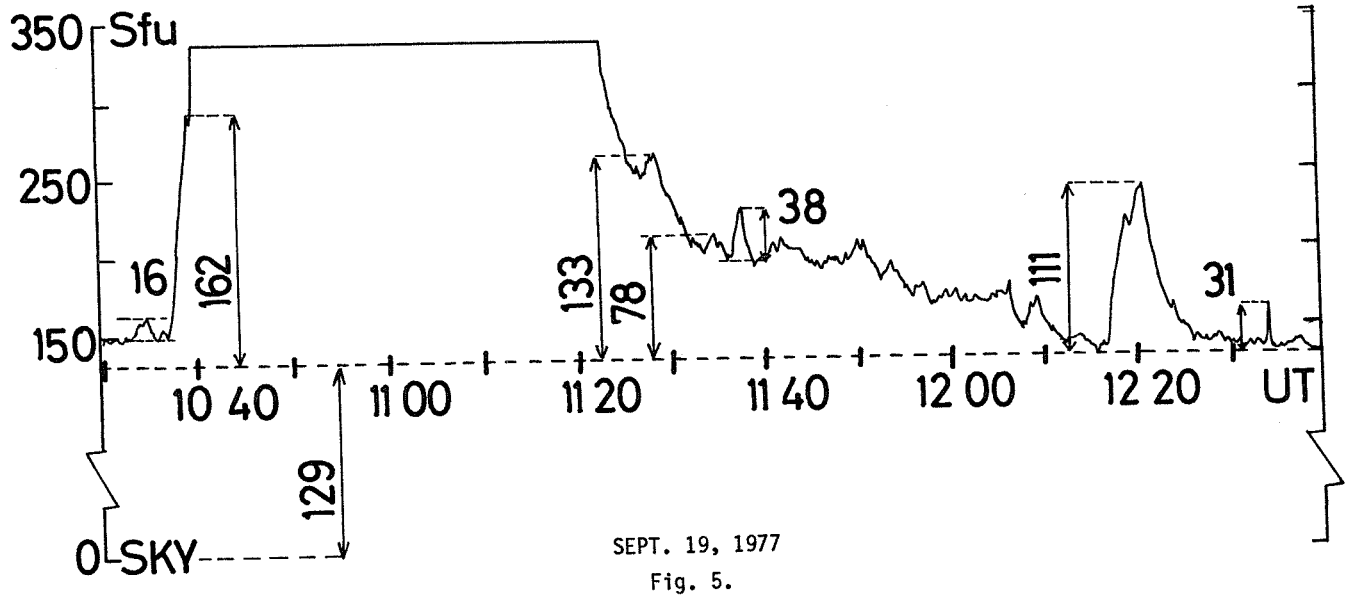

SEPT. 19, 1977

Fig. 5.

Sept. 24, start: 1157 UT, Fig. 6. After 5 quiet days a typical gradual rise and fall, GRF of intensity observed.

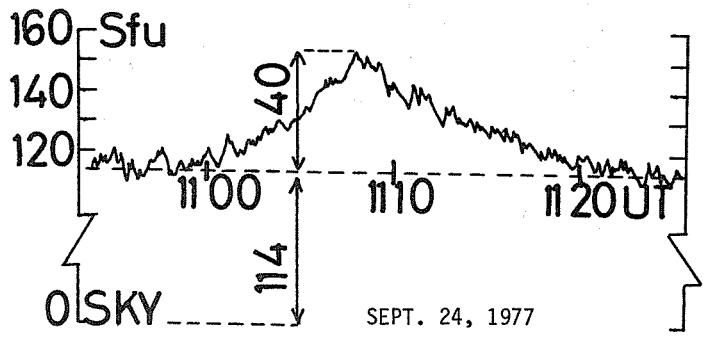

Fig. 6.

Nov. 22, start: 0951 UT, Fig. 7. Another great burst activity, which started with a little precursor, 0951 UT. A steep rise of intensity is observed at 0958 UT and an off-scale level of 350 s.f.u. is reached at 1002 UT. The double structure of this great burst, GB, can be seen, the starting time of the second part being 1022 UT. The post burst increase, PBI starts at about 1047 UT at the level of 38 s.f.u., and lasts until 1114 UT. The simple burst with a little fluctuation S/F is superimposed on the PBI at 1053 UT. The 2800 MHz activity ends up with the 3 simple S/F bursts: at 1133, 1137, and 1153 UT. No SEA observations were possible since the 27 kHz recordings were not being made at that time.

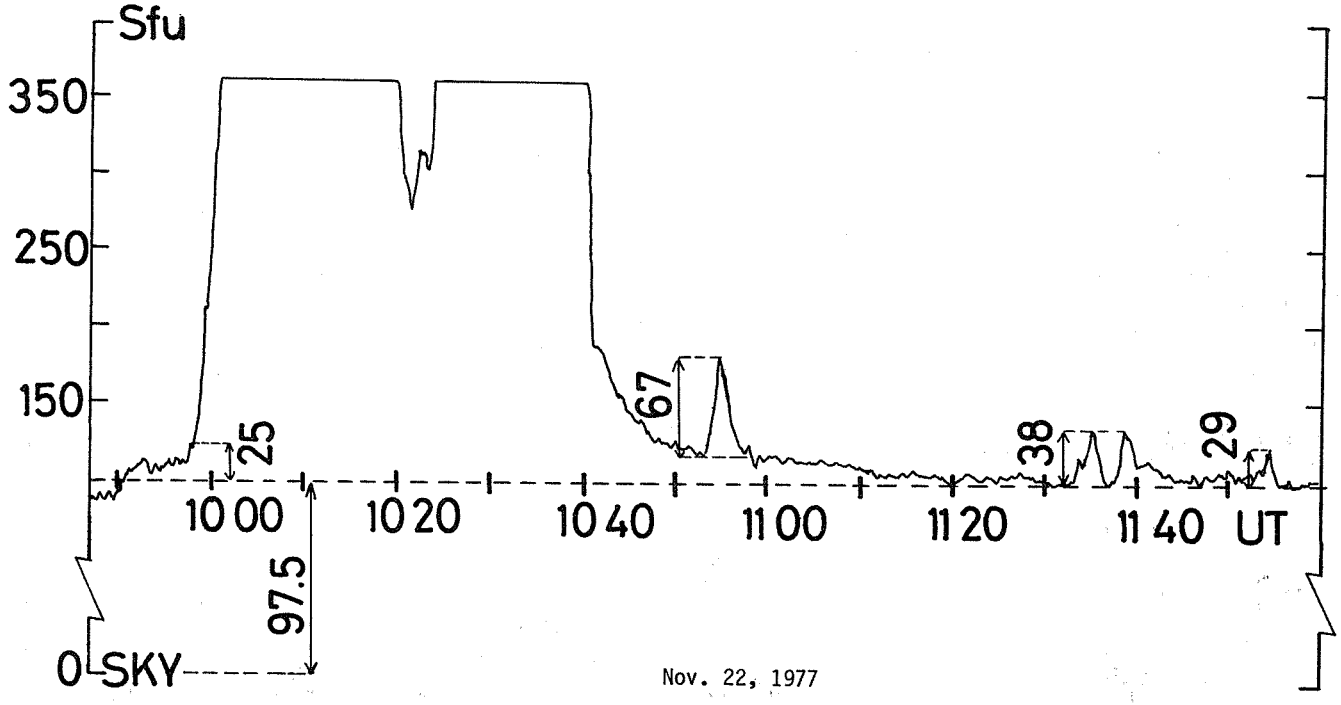

Fig. 7.

A Brief Report on Microwave Emission Associated with McMath 14943 in September 1977 (Flux and Polarization)

by

Pierre Kaufmann
CRAAM/ON/CNPq - Conselho Nacional de Desenvolvimento Científico e Tecnológico
Rua Ceará 290, 01243 - São Paulo, SP, Brasil

ABSTRACT

The active center associated with McMath 14943 and 14942 complex was measured at 7GHz in flux and polarization. A reversal in polarization sense in the observed bursts, when the source was still close to the eastern limb, suggests the occurrence of a significant change in the magnetic field morphology. A 43GHz map of the Sun indicates the active center position on the eastern limb September 10, 1977 (at about 1300 UT).

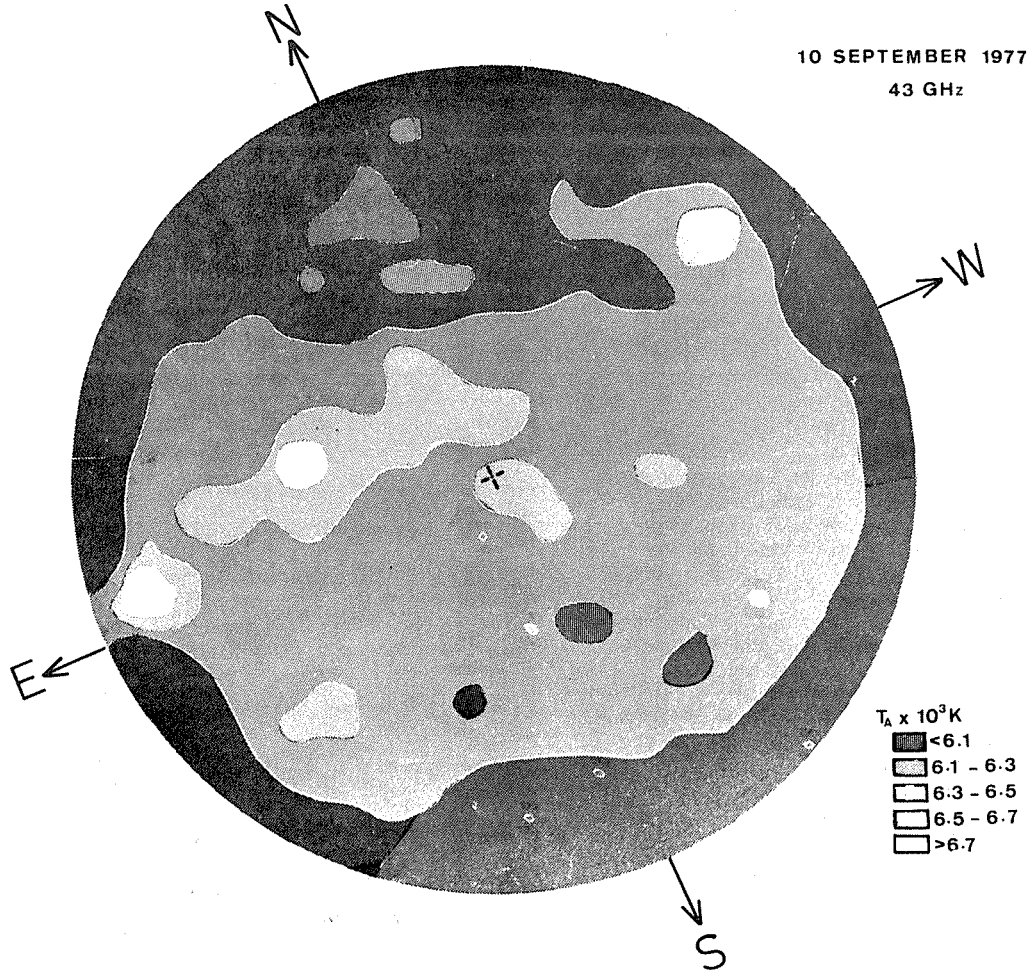

Fig. 1. A 43GHz solar map obtained with a 2'arc beam, using the 45-ft telescope from Itapetinga Radio Observatory. McMath 14943 and 14942 complex is seen at the eastern limb, close to the equator, in the Northern Hemisphere. Units are in corrected antenna temperatures.

We wish to present briefly a number of relevant microwave emission features associated with McMath plage 14943 which might be of interest for other workers concerned with this particular period of solar activity.

In Figure 1 we show a 43-GHz map of the Sun obtained with the 45-ft radiotelescope from the Itapetinga Radio Observatory. It was obtained on 10 September 1977 (at about 1300 UT), and displays McMath 14943 at the eastern limb. The spatial resolution was of about 2'arc. The maximum radio source was located in the Northern Hemisphere, with a corrected antenna temperature close to 7000 K. If we assume that the actual size of the active center is smaller than a few arc seconds [Kundu and Alissandrakis, 1975], we might infer a brightness temperature larger than 3 x 10^6K at 43 GHz.

In Figure 2 we show the development of McMath 14943 as measured at 7 GHz by a patrol solar polarimeter. At the top we indicate the flux from the slowly varying component (continuous line) and peak-fluxes from the measured bursts (vertical bars) in the period 11-20 UT. At the bottom we have the circular polarization associated with the contribution of the S-component (continuous trace) and the polarization at maximum of the bursts measured (vertical bars). Data are missing for 14-16 September.

The appearance of McMath 14943 on the solar disk originated a moderately strong S-component at 7 GHz, weakly polarized in comparison to many S-components analyzed in 1968-1969 [Paes de Barros and Kaufmann, 1972]. It was shown that in that period (i.e., the previous solar cycle) most S-components were left-handed, with a few rare cases of polarization sense reversal after CMP due to magneto-ionic coupling effects [Takakura, 1961]. In one of these cases studied in detail [Scalise Jr. and Kaufmann, 1974] it was shown that the polarization sense of bursts associated to the active center followed the S-component polarization sense.

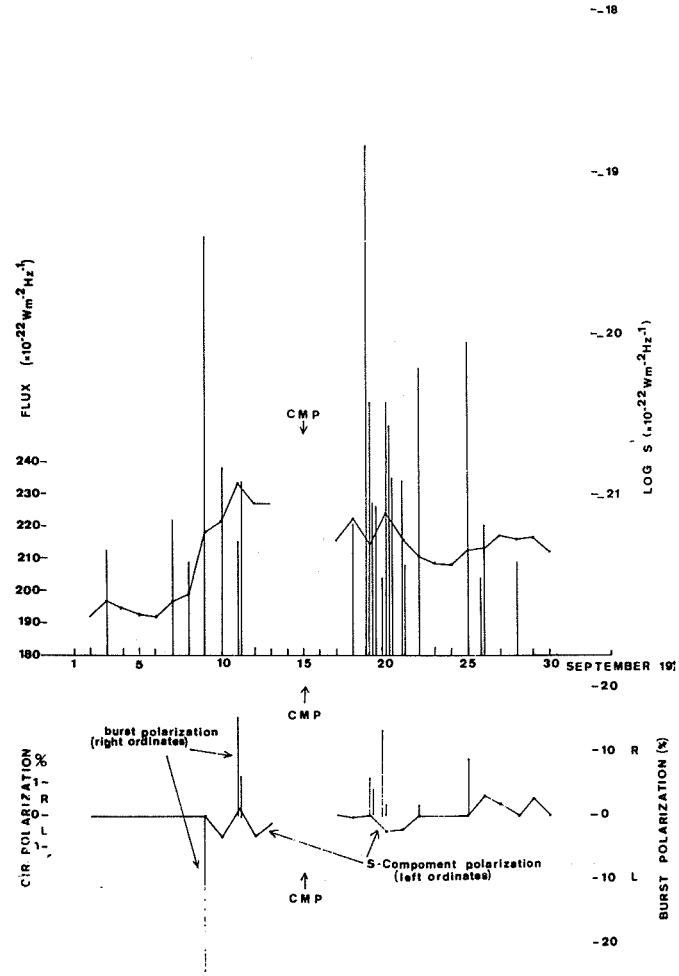

Fig. 2. The development of the S-component associated with McMath 14943, at 7 GHz. At the top we have flux density. The ordinates at left refer to the S-component daily average. The ordinates at right (log scale) refer to the burst's maximum flux (the vertical bars). At the bottom we have the degree of circular polarization (in percent). Ordinates at the left refer to the S-component daily average. Ordinates at the right refer to the polarization degree at the maximum of the burst (vertical bars). CMP: central meridian passage of McMath 14943.

A strong burst was recorded on 9 September 1977 (at 1625.2 UT) in McMath 14943 (approximate flare location N07E87 [SGD, 1977]). It was 23 percent left-handed at the maximum of the event. One unpolarized burst was recorded on 10 September (N05E66) and two right-handed bursts were recorded on 11 September, starting at 1139.4 UT (associated flare location N15E47 or N07E52 [SGD, 1977]), and at 1432.5 UT (flare location N15E48 [SGD, 1977]), respectively. In the following days until the active center completed its rotation across the visible solar disk, there were a number of bursts recorded, some unpolarized, others right-handed (see Figure 2).

These results suggest that there was a clear polarization sense reversal sometime in the period 10-11 September 1977, with the source still rather close to the climb (i.e., at about E$\sim$60). An important change in the magnetic field topology at the source should be required to explain a drastic change in the magneto-ionic propagation and coupling conditions. In terms of previous solar cycle normal polarity [Paes de Barros and Kaufmann, 1972], the active center should have remained left-handed, and a reversal, if any, should only occur after CMP [Takakura, 1961] (i.e., after 15 September).

We gratefully acknowledge Dr. E.J. Reichmann, from NASA Marshall Space Flight Center, who alerted us to the peculiar behavior of McMath 14943, discussing the problem and providing us with optical data. We also acknowledge the help given by P. Iacomo Jr. and C. Laporte from CRAAM. This work was partially supported by São Paulo State research agency FAPESP.

REFERENCES

KUNDU, M.R. and C.E. ALISSANDRAKIS 1975 "Observations at 6 cm of the Solar Active Region," *Nature, 257,* 465-467.

PAES de BARROS, M.H. and P. KAUFFMAN 1972 "On the Long-Term Behaviour of the Circular Polarization from Coronal Condensation Radio Emission at 4.3 cm Wavelength," *Solar Phys., 27,* 203-207.

SCALISE JR., E. and P. KAUFMANN 1974 "Coupling of Microwaves at a Selected Solar Active Centre," *Solar Phys., 34,* 189-191.

SGD 1977 *Solar Geophysical Data,* No. 398, Part 1, Boulder, Colorado, USA.

TAKAKURA, T. 1961 "Limiting Polarization of Solar Microwave Emission," *Publ. Astron. Soc. Japan, 13,* 312-320.

A Group of Highly Polarized Type III Bursts

by

P. Zlobec, C. Zanelli, A. Abrami and U. Koren

Trieste Astronomical Observatory
I 34131 Trieste, Italy

During September 12, 1977, a group of rather strong Type III bursts beginning at 0955:18 UT was recorded (see Fig. 1). The separate left- and right-hand circularly polarized components were registered at the Trieste Observatory at 237 MHz. We are very much indebted to Dr. A.O. Benz for kindly providing us with a copy of the spectrum of this event taken at Dürnten by the Radio Group of the E.T.H. - Zürich.

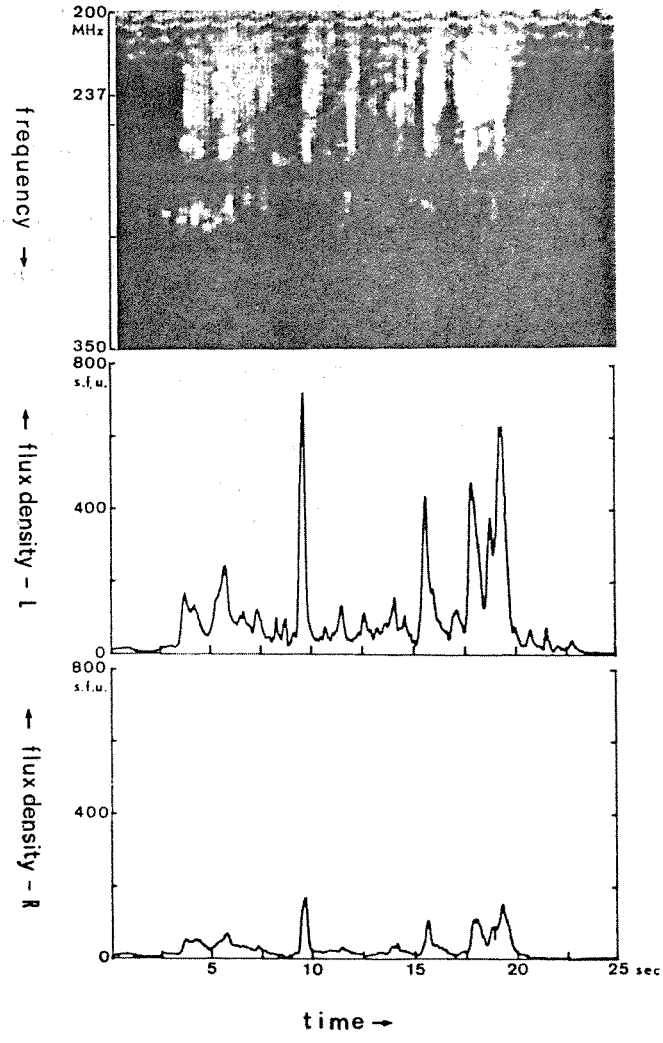

Fig. 1. Frequency versus time behavior and flux density versus time behavior of the September 12, 1977, event that began at 0955:15 UT. In the top panel the position of our observing frequency (237 MHz) is marked. The middle and bottom diagrams report separately the left-hand and right-hand polarized components of the burst group. Radio spectrogram courtesy of the E.T.H. - Zurich Radio Group.

High polarization Type III bursts are quite exceptional [Benz and Zlobec, 1978]. Here they appeared during a day in which the meter-wavelength activity was generally low: just a few weak Type I bursts were present, some of which were strongly polarized in one sense and others in the opposite sense.

Note that in Table 1 the strongest events of the Type III group are polarized about 50 percent or more. The weakest bursts are polarized almost totally, since for some of them it is not possible to see their right-hand component. Such high polarization, low intensity events cannot be Type III bursts; they must be "spike" bursts [Tarnstrom and Philip, 1971]--bursts that are often almost totally polarized and that appear alined with Type III bursts in the frequency-time plane [Zlobec, 1971].

Table 1. Strongest Type III Event; September 12, 1977

Max Time (UT)	Max Flux Density (L+R) (s.f.u.)	Polarization (%L)
0955:18	205	53
19	174	45
21	300	56
24	862	62
26	155	67
29	182	63
30	527	60
32	572	64
33	443	62
34	769	61

The polarization profile of the separate bursts in Figure 1 shows in some cases the so-called "spike polarization" profile [Slottje, 1974; Santin, 1976; Benz and Zlobec, 1978], that is, high polarization at the beginning of the event followed by a decrease in polarization. During the 25-s interval, shown in Figure 1, however, the polarization varies widely. This can be due to a superposition of short duration structures--ones that cannot be distinguished from each other and ones possibly caused by rapid variations within, or by the complex structure of, the active region.

The importance sf flare associated with this event began at 0954 UT, maximized at 1001 UT, and ended at 1028 UT [SGD, 1978]. Its position was N21 E42, placing it nearest McMath plage region number 14943 [SGD, 1978]. This flare erupted east and north of the follower spot associated with McMath region 14943. Furthermore, because the polarity of 14943's spot was south (inward-directed), the entire spot group must have been a member of the new (21st) solar cycle. With these considerations in mind then, we conclude that the emission of the left-hand polarized bursts was in the extraordinary mode.

REFERENCES

BENZ, A.O. and P. ZLOBEC 1978 Correlation between Drift Rate and Polarization in Solar Type III Radio Bursts, *Astron. & Astrophysics, 63,* 137.

SANTIN, P. 1976 The Time and Polarization Profile of Type III Solar Radio Bursts at Meter Wavelengths, *Astron. & Astrophys., 32,* 107.

SGD 1978 *Solar-Geophysical Data,* 403 Part II, 11, March 1978, U.S. Department of Commerce (Boulder, Colorado, U.S.A. 80303).

SLOTTJE, C. 1974 Polarization Fine Structure in Solar Radio-Bursts of Type III on Short Meter Wavelengths, *Astron. & Astrophys., 32,* 107.

TARNSTROM, G.L. and K.W. PHILIP 1971 *Solar Radio Spike Bursts* (Scientific Report UAG R-217, University of Alaska, Fairbanks, Alaska).

ZLOBEC, P. 1971 Polarization of Type I Bursts, in *Proceedings of the 2nd CESRA Meeting,* A. Abrami Ed. (Trieste Astronomical Observatory, Trieste, Italy), p. 101.

Metric Radio Continuum Activity During Disk Passage of Active McMath Region 14943

by

Kunitomo Sakurai
Institute of Physics, Kanagawa University
Rokkakubashi Yokohama 221, Japan

Introduction

The time variation of metric radio continuum activity at 200 MHz during the passage of the active McMath region 14943 across the solar disk is examined by using the data obtained at Hiraiso. During the passage, the continuum activity increased for September 19-20 and 22-23 but, otherwise the activity was very quiet as shown in Figure 1, although the microwave S-component emissions associated with this active region were quite active.

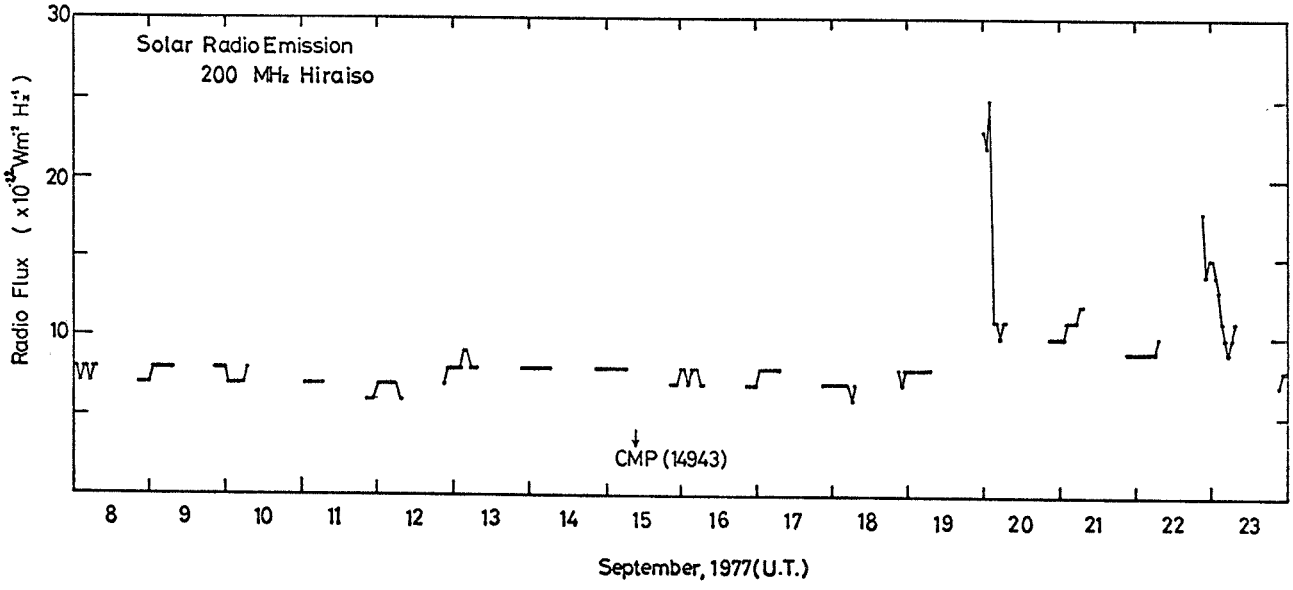

Fig. 1. Metric continuum activity at 200 MHz from September 8 to 23, 1977.

This observed low activity at metric wave frequencies seems characteristically different from the metric continuum as observed for the active McMath regions 14957, 11294 and 11976. The latter regions were quite active and were accompanied by intense microwave S-component emissions. Figure 2 shows the average radio frequency spectrum observed during the passage of the active region under investigation. This indicates that, during its passage, no increase occurred in flux intensity at metric wave frequency even if we take into account the directivity in metric noise continuum emissions as studied by Fokker [1965].

Since it is known that, in the growing phase of an active region, metric continuum activity usually becomes very high in association with both the activation of microwave S-component emissions and the change of sunspot type of the active region into $\beta\gamma$ or γ [Sakurai, 1976a] it is to be expected that the metric continuum activity would be very high for the active McMath region 14943. However, the observations only indicate that activity during its passage remained at the activity level for very quiet conditions as shown in Figure 1, except for the two observed increases which were associated with major solar flares. Thus, it can be said that this active region was quite unusual in metric continuum activity as compared with other active regions ever studied [e.g., Sakurai, 1976a]. Furthermore, this result suggests that the continuous production of energetic electrons responsible for Type III burst storm does not seem to have occurred efficiently. In fact, only a small number of flares of importance greater than 1s were produced in this active region as summarized in Figure 3. According to Sakurai [1971a], the result as shown in this figure conclusively tells us that energetic electron events and Type III burst storms were not efficiently produced from the active region under consideration. This is consistent with the result obtained earlier [e.g., Sakurai, 1971a,b].

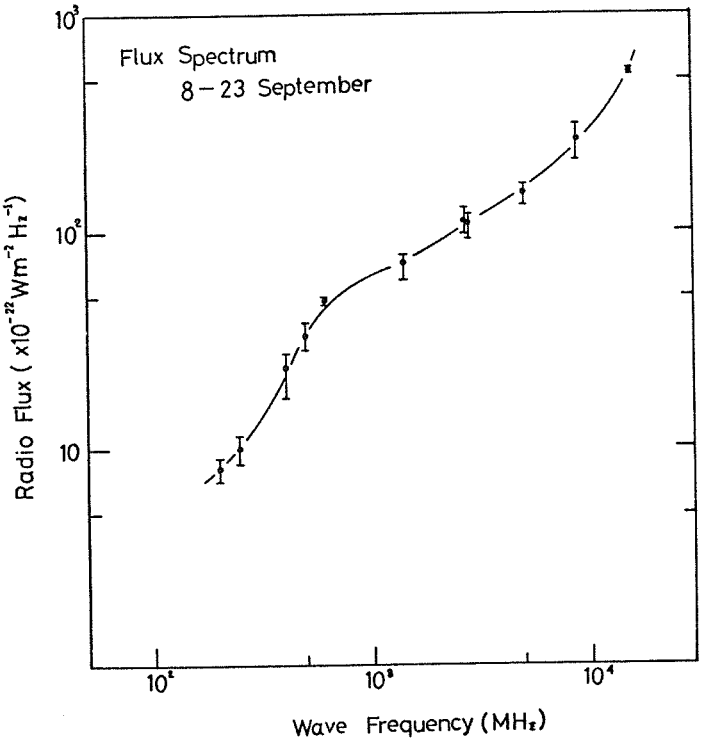

Fig. 2. The average radio flux spectrum during September 8-23, 1977.

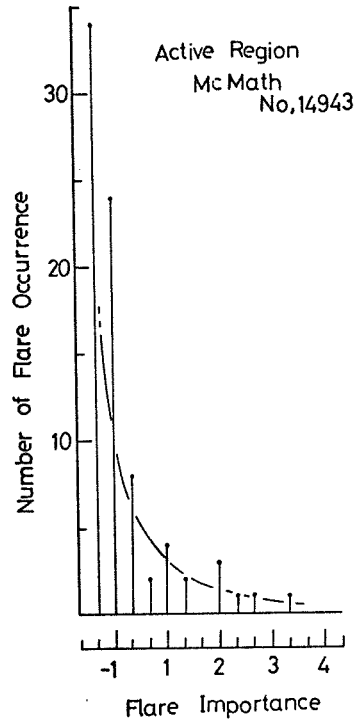

Fig. 3. The distribution of the importance of solar flares associated with the active McMath Region 14943.

The result obtained above shows that metric radio continuum activity remains inactive in cases where the parent active region has already passed through its most active phase in its development even if the sunspot type of this region is $\beta\gamma$ or γ. It can, therefore, be said that the rapid growth of metric radio continuum activity as shown by Sakurai [1976a,b] is only seen in the early phase of the development of active regions associated with active S-component emissions in microwave frequencies. It seems that the active McMath region 14943 may be a typical example for metric continuum activity in the late phase of the life of active regions related to metric radio characteristics.

I wish to thank Mr. K. Muranaga of the Hiraiso Branch, Radio Research Laboratories for supplying the radio records.

REFERENCES

FOKKER, A.D. 1965 "Noise Storms," in *Solar System Radio Astronomy*, p. 171, J. Aarons, Ed. (Plenum Press, New York).

SAKURAI, K. 1971a Energetic electrons associated with solar flares and their relation to type I noise activity, *Solar Phys.*, *16*, 198.

SAKURAI, K. 1971b On the characteristics of the solar active regions responsible for the generation of type III radio bursts at hectometric frequencies in August 1968, *Solar Phys.*, *16*, 125.

SAKURAI, K. 1976a Solar radio continuum storms, *Astrophys. Space Sci.*, *42*, 349.

SAKURAI, K. 1976b Growth of metric noise continuum storms and its relation to the source of Microwave S-emission, *Planet. Space Sci.*, *23*, 1344.

Type II, Moving Type IV, and Pulsating Radio Bursts Arising from McMath Region 14943 During September 1977

by

R.A. Duncan and J.M. Dixon
Division of Radiophysics, CSIRO
Epping, N.S.W., Australia

While crossing the solar disk between September 7 and September 24, 1977, McMath region 14943 repeatedly gave rise to large flares. Three of these flares occurred during Culgoora radioheliograph hours (2240 to 0520 UT) and were recorded as intense Type II/IV outbursts. Although a fourth intense Type II outburst, beginning at 0554 UT on September 24, occurred outside heliograph hours, it was recorded on the spectrograph. No optical flare was associated with this last event [*SGD*, 1978, p.32], and so we suspect that it also arose from region 14943, which was by then 27° behind the west limb.

Table 1 lists some characteristics of these four flares. The maximum of the optical flare on September 7 corresponded to only a Type IIIG radio burst. Probably because region 14943 was then 14° behind the east limb, optical observations missed the main phase of this radio flare.

Table 1. Optical and Radio Data for Large Flares from McMath Region 14943, Sept. 1977

1977 Sept.	Time UT	Flare Phase	Flare Imp.	Flare Pos.	CMD McMath 14943	Radio Type
	2226					SWF
	2229.5					IIIGG,V
	2230					IV
7	2255	Start				
	2315	Max	1N	N10 E90	E104	
	2319					IIIG
	0002	End				
	2123	Start				
	2141	Max	2N	N07 W20	W18	
	2225					IV
16	2229					IIIG
	2232					SWF
	2232.5					II
	0043	End				
	0955	Start				
19	1038	Max	3B	N08 W57	W52	Night-time at Culgoora
	1207	End				
	0250					IV
	0251	Start				
	0310					SWF
20	0315					IV,P
	0315					II
	0354	Max	2N	N09 W59	W62	
	0847	End				
	0554					IIIGG,V
24	0554				W117	IV
	0555					II

Each of the flares occurring on September 7, 16 and 24 ejected large electron, proton and α particle fluxes into interplanetary space [*SGD* op. cit., pp. 37-41]. Because the flare on September 20 produced the most energetic radio outburst, one would suspect that it also ejected protons and α particles. This cannot be clearly established, however, because this flare had been preceded only 17 h earlier by an even larger flare, and interplanetary particle fluxes were thus already high [*SGD* op. cit., pp. 32, 37-41].

More detailed descriptions of some aspects of these radio events have been published elsewhere [Smerd, 1977; Stewart et al., 1978; Duncan, 1978]. Of particular interest are color film records of the spectro-polarimeter [Suzuki and Sheridan, 1977]; these cannot be satisfactorily reproduced in this report, but they are shown by Smerd [1977] for the September 20 event. Using radio spectrograph and radioheliograph data, we briefly summarize here the four events.

Figure 1 shows radio spectra of the four events. The terms we use to describe these spectra have been defined by Wild and Smerd [1972]. In these spectra one may see the following characteristics:

(1) strong initiating Type III,V (electron beam) bursts on September 7 and 24;

(2) Type II (shock-wave) spectral bands in all four events;

(3) Type II fundamental and harmonic bands on September 7 and 16 and less clearly on September 24;

(4) Type II herring-bone structure on September 7; and

(5) Type II secondary band splitting on September 16 and 20.

Between 2319 and 2320 UT on September 7 (not shown in Figure 1), a second Type III burst occurred. It was this event that most closely corresponded to the maximum of the optical flare (Table 1).

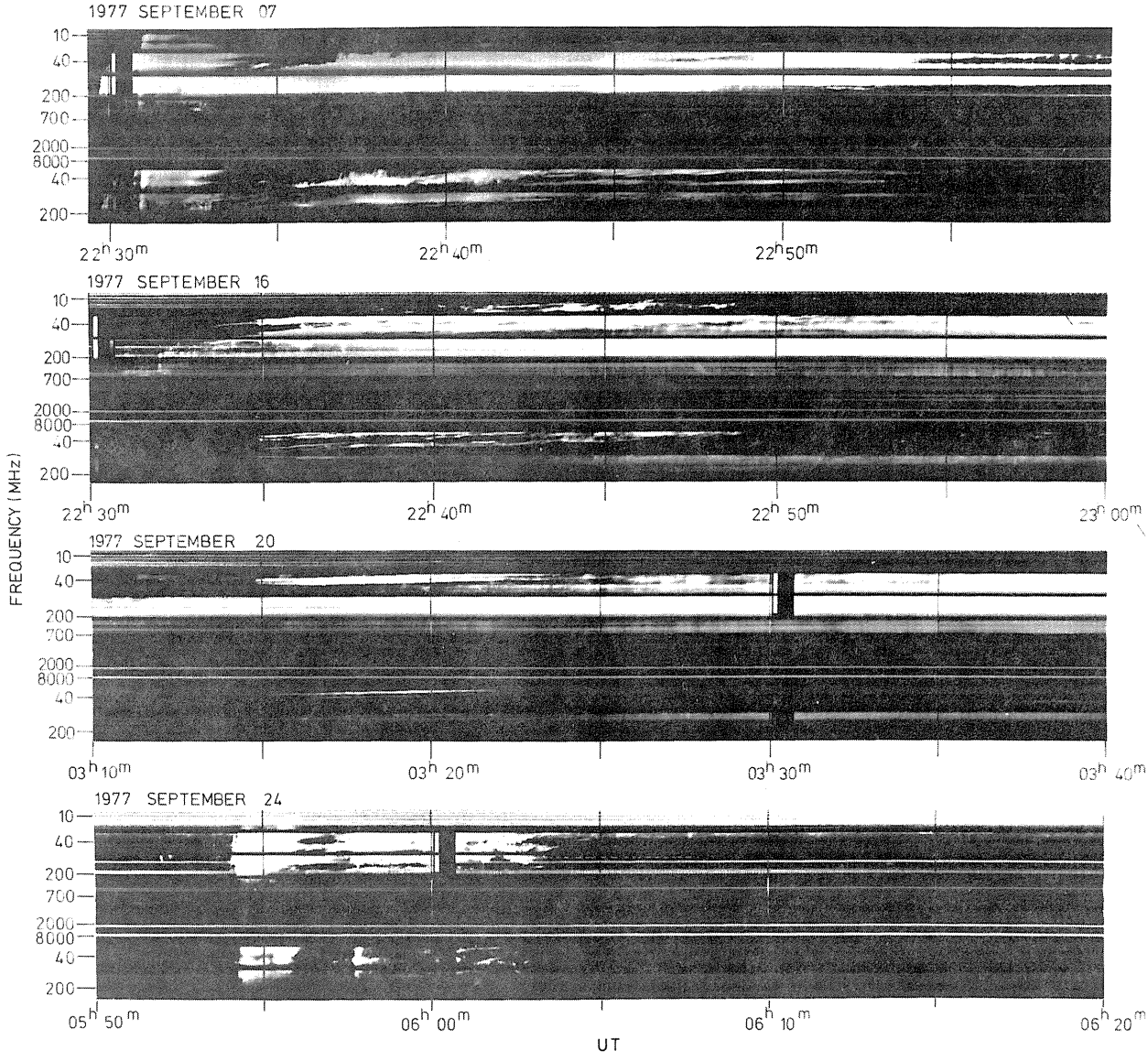

Fig. 1. Dynamic radio spectra taken at Culgoora of the four September 1977 solar flares. Each spectrum is recorded twice, once at high sensitivity (top) and once at low sensitivity (bottom). The thin horizontal white lines result from broadcast interference; the wider horizontal dark bands denote gaps between the receiver bands.

All four radio bursts were accompanied by continuum (Type IV) radio emission. On September 20, between 0315 and 0340 UT, this continuum showed strong, somewhat irregular pulsations with an average period of about 2 s.

Figure 2 shows half-peak-power source contours for times early (on left) and late in the Type IV phase of the events. All three events recorded on the heliograph showed bipolar structure with a right-hand polarized source (R) to the north and a left-hand polarized source (L) to the south. We discuss, in turn, these northerly and southerly sources.

In all three events the northerly source was long-lived and right-hand circularly polarized. This polarization increased with time and reached almost 100% before the sources faded.

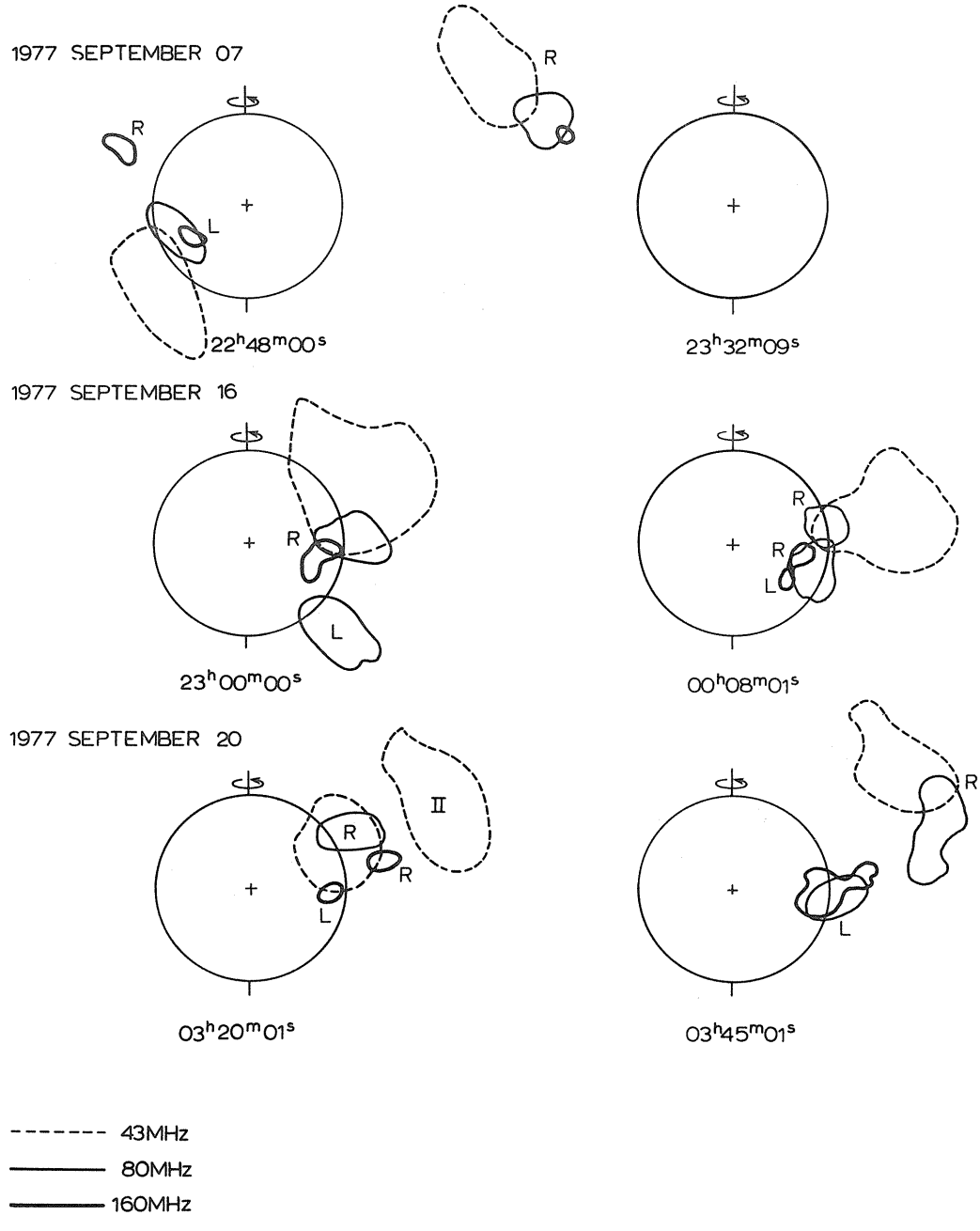

Fig. 2. Half-peak-power contours of solar radio sources observed with the heliograph. Contours are shown for three observing frequencies, 43.25, 80 and 160 MHz.

In the two limb events, September 7 and 20, the northerly source moved outwards, reaching final projected heliocentric radial distances of 2.4 $R_\odot$ (September 7) and 3.4 $R_\odot$ (September 20). The September 16 source showed no such outward movement. Nevertheless, Hα Doppler studies of this event [*SGD* op. cit., p. 13] did show outward motion, so possibly the radio source moved outward along the line of sight.

The southerly source of September 7 was continuously detectable for only the first 5 min of the Type IV phase of the event; it was then very weakly left-hand circularly polarized. It was later detected twice for short periods with 30% left-hand polarization. In the other two events, September 16 and 20, the southerly sources, like the northerly sources, were long-lived. On September 16 the left-hand polarization of the southerly source was high but difficult to measure reliably. On September 20 the left-hand polarization of the southerly source remained almost constant at about 60%.

No movement of the southerly sources was observed. The September 7 source was too short-lived to reveal any movement. The September 16 southerly source, in its lack of outward movement, resembled the corresponding northerly source. The September 20 southerly source, in addition to its lack of movement, showed a lack of dispersion of height with observing frequency (Figure 2). That the magnetic field lines were directed toward the Earth may explain both the lack of movement and lack of dispersion. On the other hand, from a comparison we made of this event with similar events in successive months, it seems likely that the southerly sources were truly stationary.

Strong, but not conclusive evidence suggests that the pulsations seen in the spectra on September 20 (Figure 1) originated in the southerly source. Both this source and the pulsations were left-hand polarized, and they attained maximum flux density and amplitude at about the same time, namely 0330 UT.

On the evidence shown in Figure 2 alone, sources early and late in the events cannot easily be related to one another. The full second-by-second heliograph data do, however, unambiguously establish these relationships, which are indicated by the labels on Figure 2. In particular, on September 20, the progenitor of the 43-MHz contour marked "R" at $03^h45^m01^s$ was the contour marked "R" at $03^h20^m01^s$, and not as one might think the contour marked "II". This "R" source moved outward continuously from its early to its late position.

The "II" source in Figure 2 only appeared transiently during the passage of the Type II burst on the spectrum (Figure 1). That the Type II source should appear so much higher than the Type IV(R) source at the same time is perhaps surprising. A similar pattern occurred during the September 7 event (earlier than the $22^h48^m00^s$ frame shown in Figure 2). Here the Type II source appeared approximately midway between the northerly (R) and southerly (L) sources. The patterns suggest that the continuum sources represented the feet, and the Type II source the helmet, of a magnetic loop. Late in the September 20 even a faint radio-emitting loop could be seen connecting the R and L sources (Figure 3). This again suggests that the radio sources lay at either end of a magnetic loop.

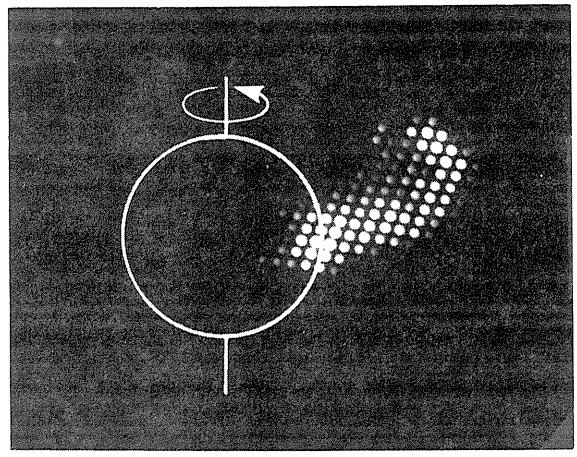

Fig. 3. The 80-MHz heliograph display on September 20, 1977 at $03^h48^m01^s$ UT. At this time the continuum sources (cf. Figure 2) had begun to fade, thus leaving the bridge connecting them relatively brighter.

REFERENCES

DUNCAN, R.A. 1978 Heliograph Observation of Both Fast Drift (Type III) and Continuum (Type IV) Solar Emission from the One Source High Above the Solar Limb, *Proc. Astron. Soc. Aust., 3,* issue 4, 253-256.

SGD 1978 *Solar-Geophysical Data,* 403 Part II, March 1978, U.S. Department of Commerce (Boulder, Colorado, U.S.A. 80303).

SMERD, S.F. 1977 Research Activities in Radio Astronomy 1975-1977, prepared for URSI, (Division of Radiophysics, CSIRO, Sydney, Australia).

STEWART, R.T., R.A. DUNCAN, S. SUZUKI, and G.J. NELSON 1978 Observations of High Brightness Temperatures in Moving Type IV Solar Radio Bursts, *Proc. Astron. Soc. Aust., 3,* issue 4, 247-249.

SUZUKI, S. and K.V. SHERIDAN 1977 Observations of the Circular Polarization of Fundamental and Harmonic Type III Bursts Throughout the Frequency Range 24 to 220 MHz, *Radiofiz., 20,* 1432.

WILD, J.P. and S.F. SMERD 1972 Radio Bursts from the Solar Corona, in *Ann. Rev. Astron. Astrophys., 10,* (Annual Reviews Inc., Palo Alto, California) pp. 159-196.

The Dissipation Pattern Associated with McMath Region 14943 During September 1977

by

H.W. Urbarz
Astronomical Institute of Tübingen University
Weissenau Station
7980 Rasthalde
Ravensburg, GFR

Introduction

The parameters of McMath region 14943 are plotted together with the time sequence of flares and associated radio bursts. These events are briefly discussed in context with proton emission and associated Type II/IV bursts. Those of September 16 and 19 were observed at Weissenau.

The parameters of McMath region 14943 during E-W transit available from Solar-Geophysical Data are plotted in Figure 1. Figure 2 shows the total number of flares and associated radio bursts, while Fig. 3 and 4 shows the time sequence of the flares and radio bursts occurrence. The region produced 9 flares of Imp 1 or higher (5 of these associated with Type II/IV bursts) and about 70 subflares. A revised list of radio bursts was used to avoid multiple reporting, based on some criteria of burst type identification. The region exhibited was of magnetic D-configuration at the time of E-limb passage, when the first group of events occurred. Due to limb position it is uncertain if the plage and spot areas were growing or were already at high values. The sudden jump of both parameters is probably due to the observation conditions. However, the sunspot number increased up to Sept. 15. During the decay phase of the magnetic configuration, of both the spot area and spot count, the event rate increased again from September 19 to 22. Furthermore there were 4 Importance 1 flares from Sept. 8 to 10 and 4 large importance flares in the decay phase starting on Sept. 19. Thus Figures 1, 3 and 4 show the capability of energy storage and release which is an essential feature of the spatial magnetoplasma structure of this region during its E-W transit.

Table 1 shows a list of the flares associated to Type II/IV bursts and polar riometer and near Earth satellite data on energetic protons and ions and spectra of maximum radio fluxes. The following is found from association of the radio and particle data.

1. The compound Type II/IV bursts are associated with larger flares (Imp $\geq$1)

2. Proton-events are found delayed by a few hours but no ground level events have been reported.

Table 1. McMath Region 14943 proton-events during Sept. 1977

Flares				Radio-Bursts	Riometer-PCA			Proton-events: Particle Fluxes by Satellite Monitors	Start Date UT			Comments to the Spectra of Max Absolute Fluxes of Type-IV Burst from Outstanding Occurrences
Date	Max UT	Pos.	Imp Start-End	Type from spectral observation	Date	Start UT	Max UT		Protons to 80MeV	Alphas to 90MeV	Electrons 1-5 MeV	
07	2315	N10E90	1N 2229-2252	IIIGG/V, dm,m,dkm	09	9^h	16^h 0.3dB	gradual rise of counting rate long duration	08 6^h30	08 0^h	08 0^h	max: 10 GHz, 3.10^3 sfu, no m-wave fluxes available
09	1634	N09E84	1N 1629-1738	IIIGG,m,dkm				superposition with previous event, weak second max	11-12	11-12		max: 20 GHz, 5.10^3 sfu, increased with frequency, no m-wave fluxes available
16	2141	N07W20	2N 2225-2252	IIIG, m IIm, dkm IV dm, m				steep max of count rate	17 0^h	17 0^h	17 0^h	max: 1.5 GHz, 2.10^3 sfu, decreased to 3.5 GHz, no fluxes available below 500 MHz, two more branches with maxima below 1 GHz
19	1038	N09W57	3B 1031-1130	IIm, observed only IVm at m-Waves	19	11^h45 21^h30 4.5 dB		steep max	19 8^h30*	19 13^h	19 11^h	max: 3 GHz, $1.1.10^3$ sfu, no m-wave fluxes reported, one more branch with max at about 15 GHz
20	0345	N09W59	2N 0250-0330	IVdm,m,P II m IIIG m								
24	Not observed position behind W-limb		0552-0605	IVdm,m IIm IIIGG/Vm,dkm				steep max	24 8^h30	24 5^h30	24 10^h	max: 1 GHz, 40 sfu, steep slope to lower frequencies up to 10^3-4.10^3 sfu, two branches, extremely low cm fluxes, high m-fluxes

*This value is two hours before the flare start due to inaccuracy of the graph used.

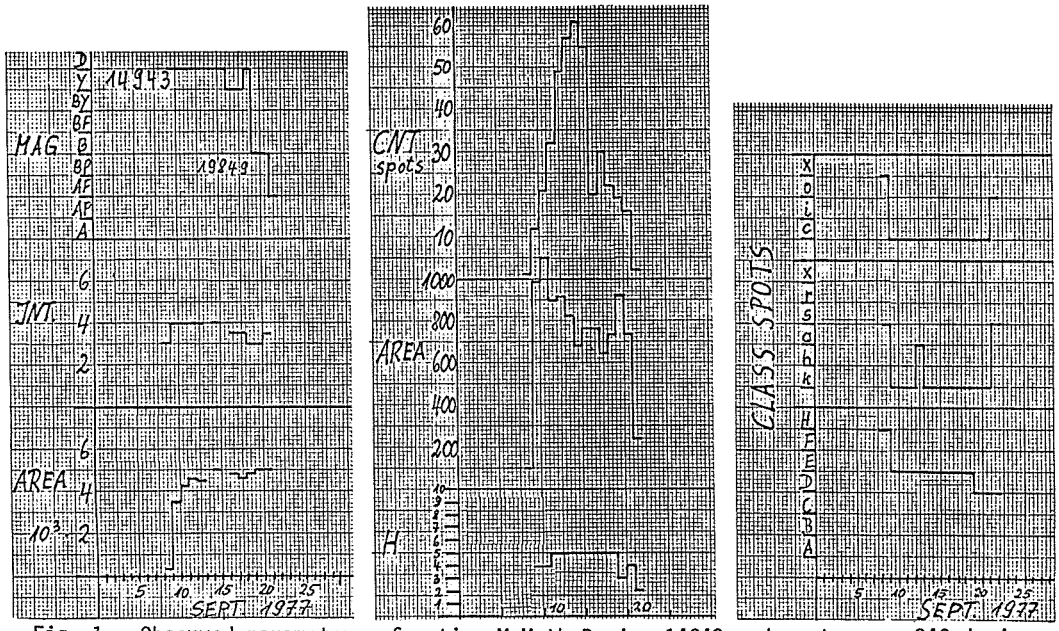

Fig. 1. Observed parameters of active McMath Region 14943 and spot group 849 during Sept. 1977.

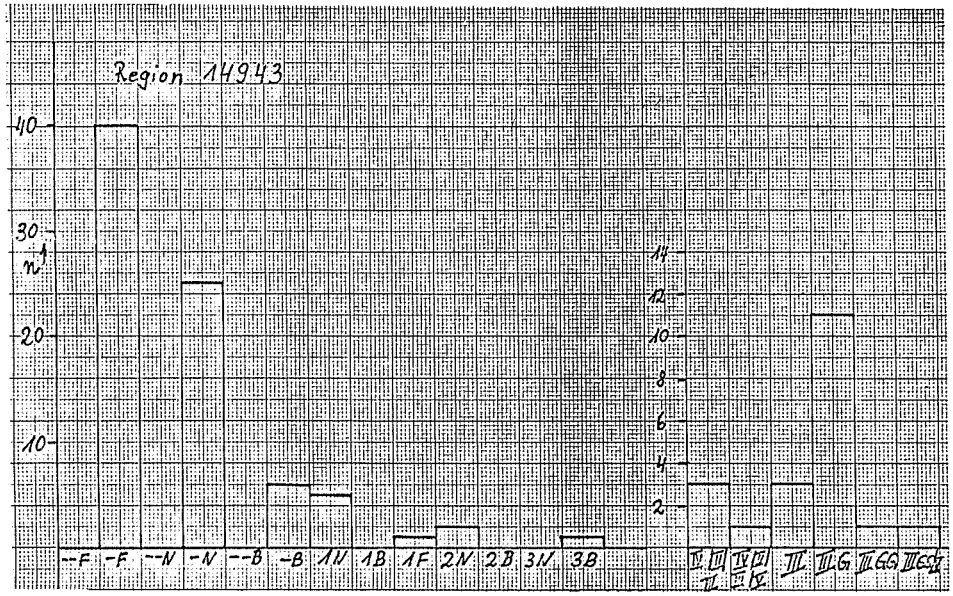

Fig. 2. Number of flares of different importance classes that occurred in McMath Region 14943 during Sept. 7-19, 1977 (confirmed list of Solar-Geophysical Data).

Number of radio bursts of different types associated with McMath Region 14943 flares.

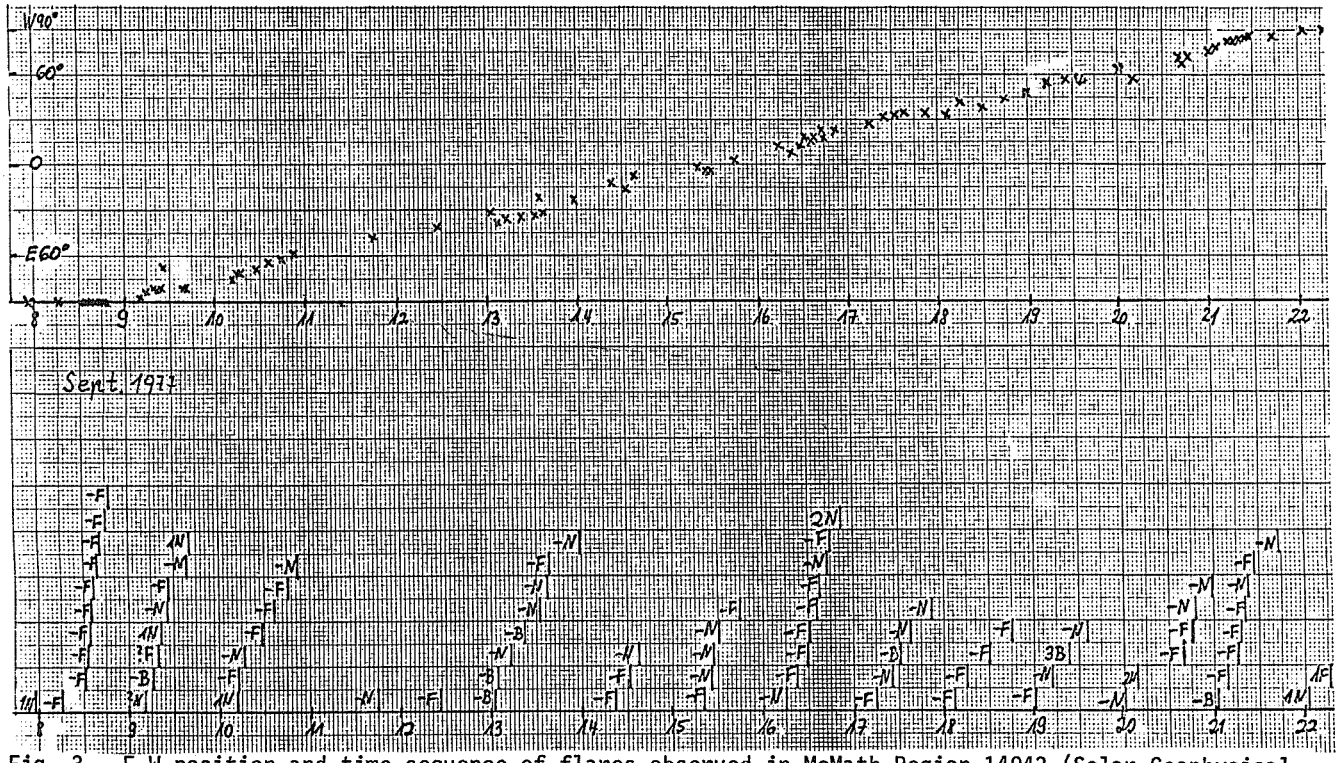

Fig. 3. E-W position and time sequence of flares observed in McMath Region 14943 (Solar-Geophysical Data, confirmed list).

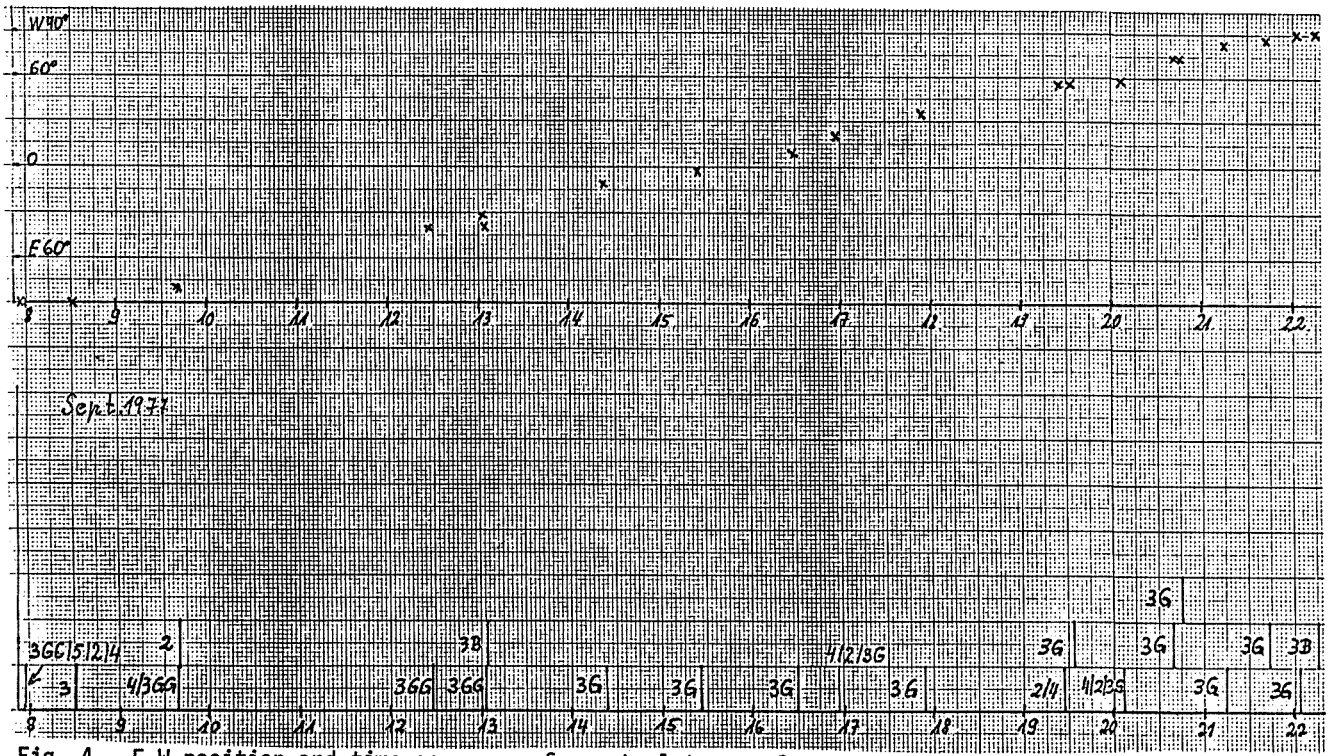

Fig. 4. E-W position and time sequence of spectral types of radio bursts associated with the flares from Figure 3 (Solar-Geophysical Data, spectral observations).

The following features are shown of the events listed in Table 1. The Sept. 7 E-limb event showed near by earth enhancements of energetic electrons, protons and heavier particles, as did the other events. The curve of the counting rate is stretched in time and shows a gradual onset. The first maximum being delayed by about 1.5 days and there is a second one after about 5 days due to the Sept. 9 event. This response is due to particle diffusion normal to the interplanetary sector field. The Sept. 16 event shows a sudden onset and steep maximum indicating direct propagation of the particles, the fastest have travel times of about 1.5h. Similar features are shown by the Sept. 19 event, a travel time of one to 3 hours is found, but the graph gives low accuracies. The count rate of the Sept. 20 event is evidently superposed, suggested by the maximum being widened by one day. The Sept. 24 event is suggested to start from behind the W-limb, the curve is somewhat stretched but has essentially the form of both the earlier events. This may suggest a forward diffusion by the interplanetary magnetic field. On the beginning of Sept. 27 there is an interesting dip in all of the curves which suggests an ex-solar origin. It is worth noting that relativistic electrons have been reported together with heavier particles all showing similar responses of counting rates thus indicating the same propagation mechanism. Previously the production of highly energetic electrons has been indicated during proton-events by associated broad band Type IV bursts.

From the plots of the absolute maximum radio fluxes, not included here, the complete V-Spectra could not be verified. The high m-wave fluxes expected from the spectral observations could not be found due to missing data. The synchrotron emissivity curves at GHz frequencies however were found in all of the cases, except in the Sept. 7 event, where only a few flux values were available. The GHz maxima of the first two events are at 10 and 20 GHz, respectively, in the following cases near 1 to 3 GHz. Thus, theory indicates that the product of the expression f_{max} B E^2 is different in these cases where f_{max} equals frequency of maximum flux, E equals electron energy, and B equals magnetic field in the burst source. The Sept. 24 event may be associated clearly with a Type II/IV event, however, no flare was reported at the time in question. The suggested position of the flare in question is at 20 to 30° latitude behind the W-limb. Though not definitely identified in region 14943, an association may be assumed. An interesting feature of the absolute flux spectrum deserves special attention. The m-wave fluxes reported, rise to several 10^3 sfu, but cm fluxes were extremely low, about 10 sfu. Furthermore, two spectral branches delayed by about 5 min were observed. The interpretation of this feature is a Type-IV source at low coronal heights with flux maximum at 1 GHz, and the concommittant m-wave Type IV source located at great height which together would yield a V-Spectrum, if the event had occurred on the visible disk. It was inferred previously that both the Type IV burst sources forming the broad band Type-IV bursts with V-spectrum of maximum flux values, do occur at different coronal heights [Urbarz, 1970]. The event discussed here shows direct evidence of this suggestion. Theoretical consideration may lead to some estimate on the magnetic field strengths and electron energy in both bursts sources.

Fig. 5 shows the beginning of the dynamic spectrum of the Type-II/IV event of Sept. 16. The Type-II with harmonic precedes the Type-IV by a few minutes, showing typical patch structure suggesting strong coronal inhomogenities of the density and magnetic field [Korolev et al., 1972, Chernov et al., 1975, Urbarz et al., 1977]. There is a sudden rise to high fluxes at 1042.6 UT in the m/dkm waves, ascribed to the Type-IV burst onset rather than a Type-III, because fluxes remain high for about 20 min. This feature sometimes observed for Type IV m-bursts is due to the injection of relativistic electrons into a coronal magnetic trap. There is some connection with the second stage of an acceleration mechanism of protons and ions discussed recently.

Some remarks are made here on the radio event of Sept. 9 associated with an Importance 1 flare (see Table 1). Table 2 gives the spectral reports with corrected WEIS data (WEIS 30-160 and 540-1000 MHz), (DURN 130 to 1000 MHz).

Table 2

Sept. 9 event from Spectral observations (Solar-Geophysical Data)

	dm	m	dkm	spectral type
WEIS 1629.5	-1636	1635-1721		IV
DURN 1629	-1738	1629-1738		IV
SGMR			1639-1656	IV
DURN 1629	-1630	1629-1630		IIIG
HARV		1633		IIIG
WEIS		1633-1633.7		IIIG
WEIS		1635-1654		IIIGG
HARV		1636-1642	1636-1642	IIIG/V
HARV		1638-1647	1636-1647	II
HARV			1643-1651	II

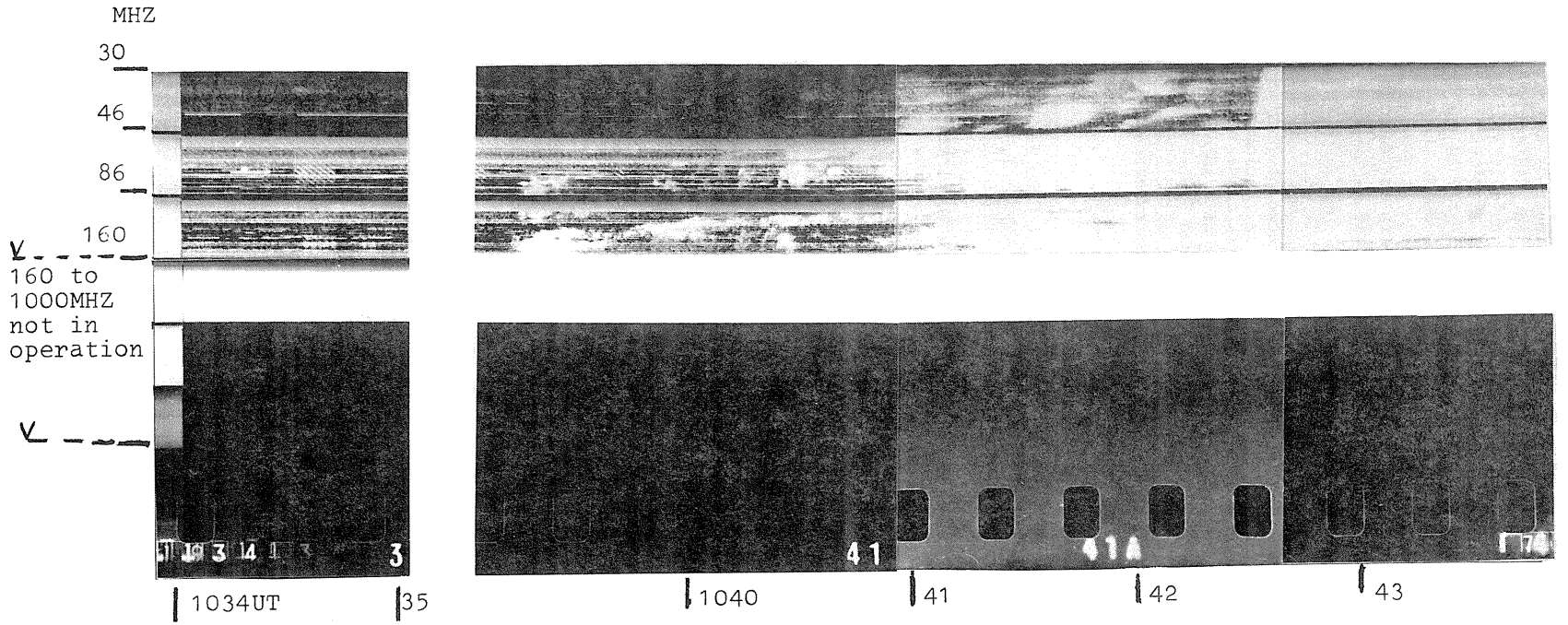

Fig. 5. First part of the dynamic spectrum of the Type II/IV event at m-waves associated with an IMP 3B flare (Sept. 19, 1977, see Table 1). The Type II burst starts at 1039 UT with harmonic and shows patch structure. At 1042.6 UT there is a sudden onset to high fluxes of the m-dkm continuum in channel 1, while at higher frequencies the superposed continuum starts about 2 min earlier.

Without considering a detail the WEIS spectral record it is found that a dm-m-dkm-Type IV-event is clearly identified by 3 stations. The WEIS record shows a flux decrease at higher frequencies going below sensitivity limit at about 140 MHz, a Type III event was found by two stations preceding the Type IV m start by 2.5 min. The latter, however, was superposed by Type III activity as found from the EIS spectrum. The Type IV/III event, was classified by one station as IIIG/V/II on m-waves. Evidently a Type II event on m- and dkm waves was present as reported by two stations. This evidently had the effect of masking the Type IV event on the HARV m-wave record and may be due to the fact that the time span of recording film is about one half of the span at WEIS and DURN. From the plot of maximum fluxes versus frequency one finds 5.10^3 sfu on 2 GHz and with high fluxes at m-waves inferred from the dynamic spectra a complete V-spectrum may be suggested. A comparison with the data in Table 1 shows similar overall features as with the other 6 proton-events listed in Table 1.

Summary

The comparison of data shows that McMath region 14943 produced at least 5 typical proton events of medium energy associated with Type II/IV radio bursts. It may be concluded that such events occur in a standardized manner in well defined sequences of processes in the Spatial Magnetoplasmastructures intercepted by D-configurations of active regions. The forming of a second floor magnetic coronal trap and production of relativistic electrons and ions and broadbanded Type IV emission with V-spectra, sometimes with several spectral branches due to multiple injections exhibits the characteristic dissipation patterns of these regions. In the regions considered the events were distributed over a half of a solar rotation.

REFERENCES

CHERNOV, G.P., O.S. KOROLEV and A.K. MARKEEV — 1975 — Observations of a Complex Solar Radio Burst with Fine Structure on 3 May 1973, *Solar Phys.*, *44*, 435-446.

KOROLEV, O.S., A.K. MARKEEV, V.V. FOMICHEV and I.M. CHERTOK — 1974 — Type II Solar Radio Bursts with Patch Structure, *Sov. Astron.*, *17*, No. 6, 776.

URBARZ, H.W. — 1970 — Comparison of Dynamic Radio Spectra of the Sept. 2, 1966 Complex Burst Recorded at Culgoora and at Weisseman, *Solar Phys.*, *13*, 458-461.

URBARZ, H.W., V.V. FOMICHEV and I.M. CHERTOK — 1977 — Fine Structure of the Type II Solar Radio Burst on May 3, 1973, *Sov. Astron.*, *21*, No. 1, 77-81.

Solar Radio Bursts of Spectral Types II and IV During September 1977

by

Alan Maxwell
Harvard Radio Astronomy Station
Fort Davis, Texas

Abstract. Data on solar radio bursts of spectral Type II, recorded at Fort Davis, Texas, over the band 25-320 MHz for the month of September 1977 are presented, together with information from other radio observatories on solar radio bursts of spectral Types II and IV. The relation of the radio bursts to the arrival of high-energy electrons and high-energy protons at the vicinity of earth is examined.

In terms of radio outbursts of spectral Types II and IV, the month of September 1977 seems to have marked the commencement of the major upswing in solar radio activity for the current sunspot cycle. (No solar radio bursts of spectral Types II and IV were recorded at Fort Davis during the twelve-month period September 17, 1976 through September 5, 1977. There were 5 Type II and 3 Type IV bursts in the 12 months preceding September 17, 1976 and there have been a large number of Type II and type IV bursts since September 5, 1977.

During the month of September 1977, the frequency range of the solar dynamic spectrum analyzers operated at the Harvard Radio Astronomy Station, Fort Davis, Texas, was 25-320 MHz and the observing hours were approximately 1300 - 2245 UT, daily throughout the month. Details of the equipment have been given elsewhere [Thompson, 1961; Maxwell, 1971].

Figure 1 presents the spectral records taken at Fort Davis for the four major solar radio outbursts recorded during that month: on September 5 commencing at 1951 UT; September 7 commencing at 2230; September 9 commencing at 1636; and September 16, commencing at 2234. Note that, on the spectral record for September 5, 1977, the vertical strokes are caused by lightning flashes from a local thunderstorm.

Table 1 presents complete information on solar radio bursts of spectral Types II and IV as reported by various observatories throughout the world, for the month of September 1977. The data for the table were taken from Solar-Geophysical Data, No. 399, Part I (Prompt Reports for September 1977), and No. 403, Part II (Comprehensive Reports for September 1977), published by the NOAA Environmental Data and Information Service, Boulder, Colorado. As far as can be ascertained, the coverage of the Sun by radio spectral equipment was virtually 100 percent complete for that month. The table also gives optical information, taken in $H\alpha$, on the solar flares associated with these major radio bursts, together with radio information taken by fixed-frequency receiving equipment operating in the microwave band (data recorded at 2800 MHz, or at nearby frequencies).

There are eight events listed in the Table. For event No. 1, a Type II burst reported by Weissenau on September 5, 1977 from 0921-0935 UT, and for event No. 2, a Type II burst reported from Fort Davis on September 5 from 1954-2002, no optical flares were reported and no microwave bursts were reported by radio observatories operating fixed-frequency equipment. In this connection, it may be noted that all the optical flares associated with the radio bursts listed in the table originated in McMath plage region 14943; but on September 5 this region was still about 20° behind the East limb (the attenuated nature of the Type II burst recorded at Fort Davis on September 5 further suggests that the radio burst may have been generated by a flare behind the limb). For event No. 8, bursts of Types II and IV reported from Culgoora on September 24 from 0552-0605, no optical flare was reported. Again, if these bursts originated from a flare in McMath Region 14943, the region would at that time have been about 20° behind the West limb.

Figure 2 compares the data on the major solar radio bursts with data on high-energy electrons (energies in the range 1-5 MeV) and high-energy protons (energies in the range 14-80 MeV), recorded in the vicinity of the Earth by equipment on the IMP 7 and 8 satellites during September 1977. Note that the solar radio outbursts on September 7, 16, 19 and 24 immediately preceded large increases in the high-energy electron and proton fluxes recorded on September 8, 17, 19 and 24.

The close relation between solar radio bursts of Types II and IV and the arrival, about 15 to 30 min later, of large fluxes and high-energy electrons and protons near the Earth again reminds us of the possibility that the high-energy particles may have been accelerated in the outward moving shock fronts associated with the Type II bursts. The small increase in the flux of high-energy protons, commencing early on September 12, may have been associated with the arrival at the Earth of the Type II shock observed on September 9, 1629 UT.

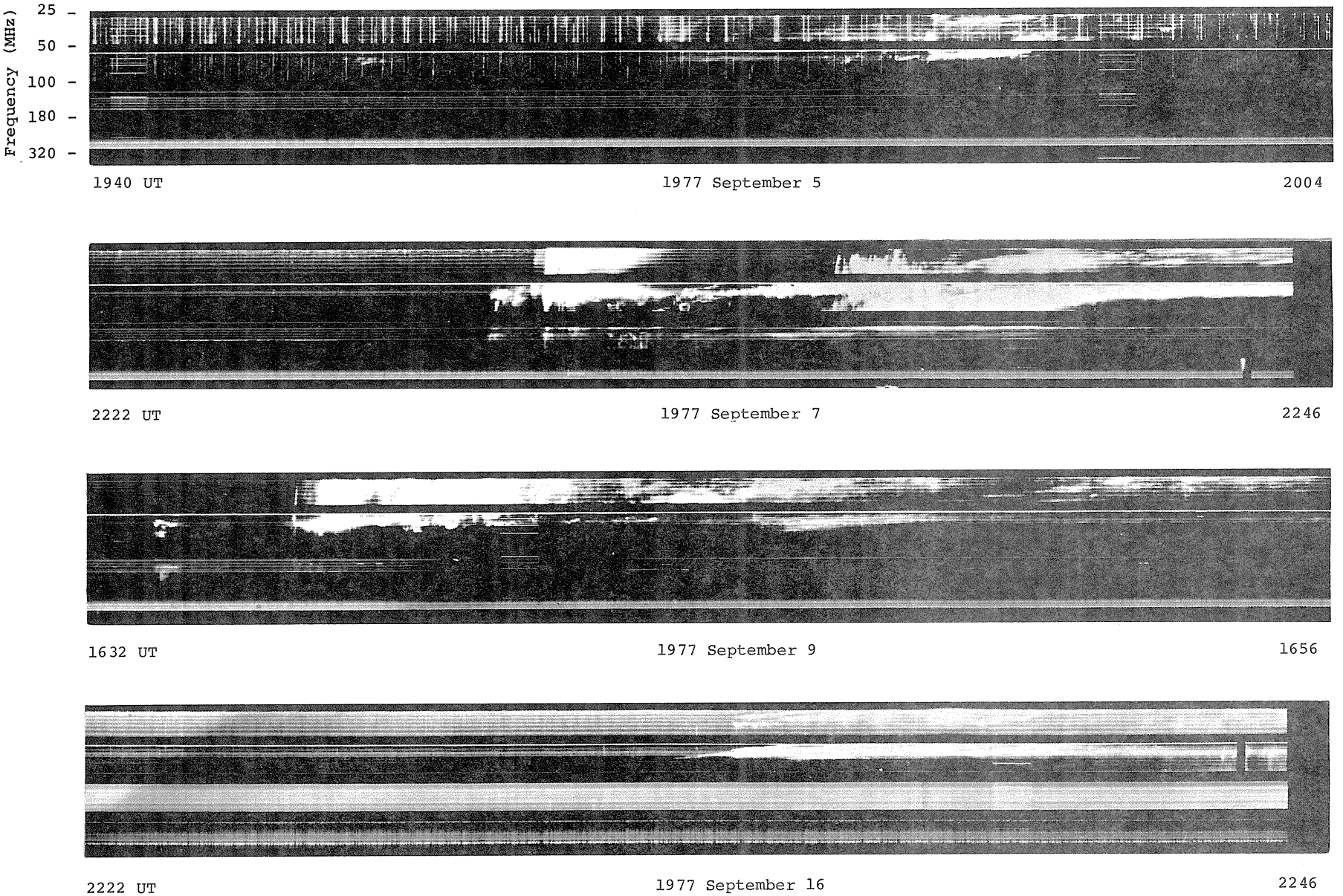

Fig. 1. Solar radio bursts of spectral Type II recorded at the Harvard Radio Astronomy Station during September 1977.

Table 1

Solar radio bursts of spectral Types II and IV during September 1977
(24-hr coverage), associated microwave bursts, and Hα flares

Event No.	1977 Sep	Radio Bursts of Spectral Types II and IV											Microwave Burst (fixed-frequency)					Hα Flare					
		dm band			m band			dkm band			Spectral Type	Recording Station[1]	Observ. freq. (MHz)	Start (UT)	Duration (min)	Max Int (sfu)[5]	Recording Station[4]	Start (UT)	Max (UT)	End (UT)	Heliograph. Coords	Imp	Recording Station[6]
		Start (UT)	End (UT)	Int	Start (UT)	End (UT)	Int	Start (UT)	End (UT)	Int													
1	05				0921	0935	1				II	WEIS	-	-	-	-		No flare reported					
2	05				1954	2002	3	1954	2002	3	II	HARV	-	-	-	-		No flare reported					
3	07	2230	2245	1	2230	2345	3	2240	2252	3	IV	CULG	2800	2228	112	1370	OTTA	2258 E	2320	0002	N12 E90	1N	CULG
		2231	2238	2	2231	2330	2	2240	2325	2	II	CULG											
					2232	2246	3	2239	2246	3	II	HARV											
4	09				1629	1721	3				IV	WEIS	2800	1625	154	1100	OTTA	1630	-	1900 D	N07 E87	2B	MCMA
		1629	1738D[2]	3	1629	1738D	3				IV	DURN											
								1636	1657	3	IV	SGMR											
					1638	1647	3	1636	1647	3	II	HARV											
								1643	1651	3	II	HARV											
5	16	2225	2240	2	2230	2400	2				IV	CULG	2695	2220	155	1480	PENT	2123	2141	2230 D	N08 W20	1N	CULG
					2232	2252	2	2237	2252	2	II	CULG						2230	2256	0050	N08 W20	2N	CULG
					2234	2242	3	2235	2241	3	II	HARV											
								2235	2246	2	II	SGMR											
	17	0000	0050	2	0000	0025	2				IV	CULG											
					0025	0430	1				IV	CULG											
6	19				1035		3				II	DWIN	2695	1031 E[3]	75 D	1133	SGMR	0955 E	1045	1125 D	N05 W57	3B	CATA
					1038	1044	3				II	WEIS											
					1032	1130	3				IV	WEIS											
					1048	1105	2				IV	DWIN											
7	20	0250	0410	2	0255	0525	2				IV	CULG	2000	0245	85	87	TYKW	0251	0354	0742 D	N10 W58	3N	CULG
					0315	0330	2				II	CULG											
8	24				0552	0605	3				IV	WEIS	2000	0554	15	35	TYKW	No flare reported					
		0554	0605	1	0554	0724	1				IV	CULG											
					0555	0605	2				II	CULG											

[1]CULG = Culgoora
DURN = Dürnten
DWIN = Dwingeloo
HARV = Harvard
SGMR = Sagamore Hill
WEIS = Weissenau

[2]Intensity scale defined in Solar Geophysical Data, Explanatory Text (NOAA-EDIS);

[3]D = after, E = before

[4]OTTA = Ottawa
PENT = Penticton
SGMR = Sagamore Hill
TYKW = Toyakawa

[5]1 sfu = 10^{-22} W $m^{-2}Hz^{-1}$

[6]CATA = Catania
CULG = Culgoora
MCMA = McMath

Acknowledgements. The high-energy electron and high-energy proton data shown in Figure 2 are taken from Solar-Geophysical Data, No. 403, Part II (NOAA-EDIS, Boulder, Colorado), and are reproduced by kind permission of Dr. E. Stone, California Institute of Technology, and Dr. T. von Rosenvinge, NASA-GSFC, respectively.

References

MAXWELL, A. 1971 The Harvard Radio Astronomy Station, Solar Phys., 16, 224.

THOMPSON, A.R. 1961 Spectral Observations of Solar Radio Bursts: I. Receiving Equipment, Astrophys. J., 133, 643.

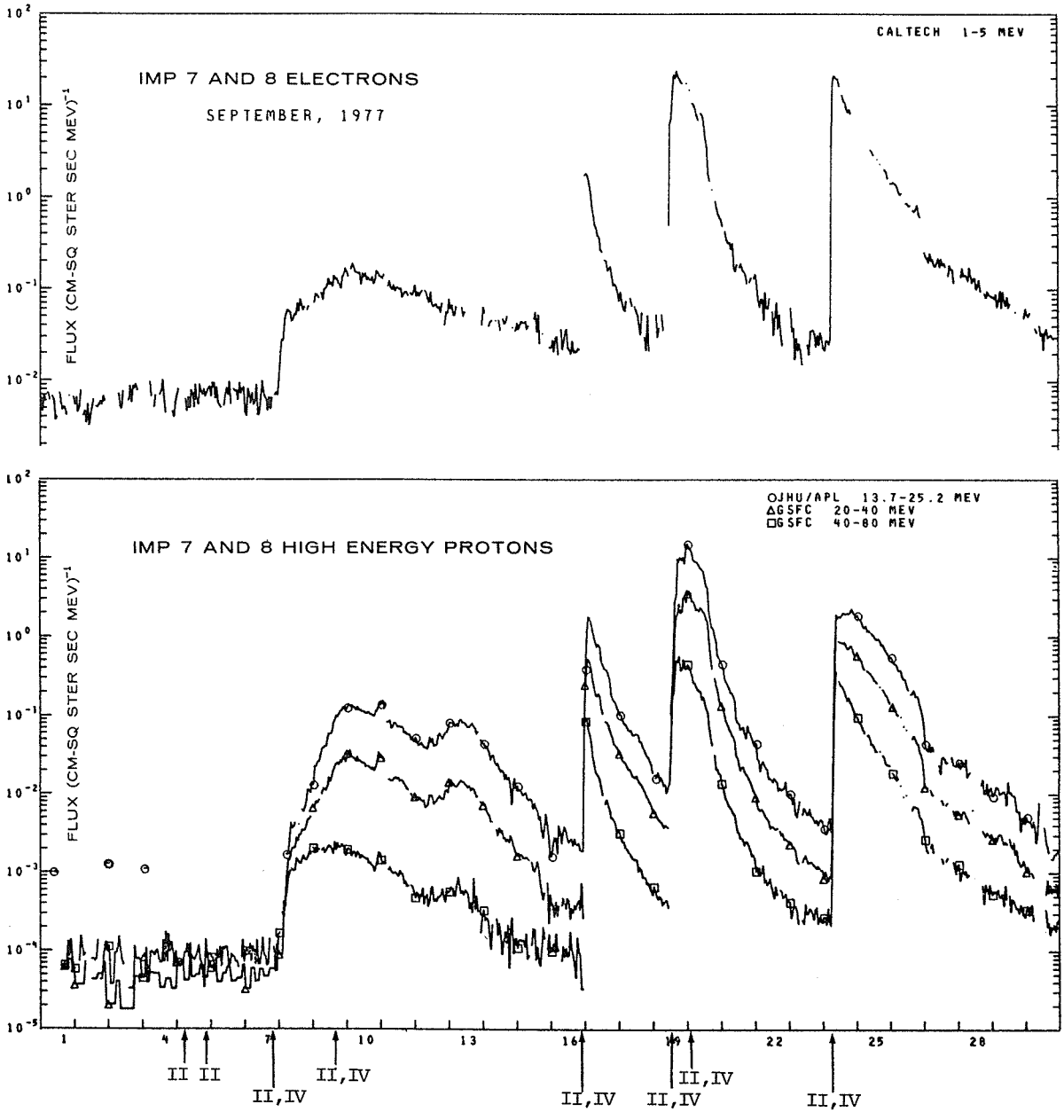

Fig. 2. Relation of high-energy electron and proton fluxes detected on IMP 7 and 8 to solar radio bursts of spectral Types II and IV recorded at various observatories during September 1977.

Type IV Events Observed at Trieste during September 7-24 and November 22, 1977

by

C. Zanelli, P. Zlobec, A, Abrami and U. Koren
Trieste Astronomical Observatory
I 34131 Trieste, Italy

Introduction

Two Type IV events were detected at our Observatory in the period September 7 to 24: the first one on September 9, from 1629 to 1705 UT, was observed on 237 MHz only, because the observing time on our 408 MHz interferometer ended at 1315 UT. The second one on September 19, from 1035 to about 1200 UT has data on 237 MHz and 408 MHz available.

Observations at both frequencies were obtained for the November 22 event also. A description of the events follow in the next sections. All times are quoted in UT, all flux densities in s.f.u. (1 s.f.u. = $10^{-22}Wm^{-2}Hz^{-1}$).

Our data at 237 MHz are converted automatically from analog recordings via a scanner-voltmeter device to a HP 2100A computer that produces the plots like those in this paper [Lampi, Santin and Zlobec, 1977]. Our data at 408 MHz are digitized manually from paper tracings.

The September 9 event

a) Environment

The flare originating this event is classified in Solar-Geophysical Data [March 1978, No. 403, Part II) with the following characteristics:

Start 1630 Maximum 1634 End 1703 Position N08 E84 Importance 1N

The sunspot group in which the flare took place was just crossing the E-limb and only the preceding spot was visible. This spot had a S-magnetic polarity [Magnitnje polja olnecnjih platen - bulletin Solnecnje Dannje No. 9, 1977] and this, together with the low latitude value classes the group as belonging to the old (20th) cycle.

McMath region number is 14943.

b) Description of activity at 237 MHz

At this frequency the event begins at 1629 and continued at least to 1705 (end of observing time).

After the initial rise in the background flux, three small groups of unpolarized bursts take place:

Start	1632.3,	Duration	0.3 min,	Maximum	1632.5,	Flux Density 85 s.f.u.,	Polariz. ∿ 0%
	1633.6		0.9		1633.9	145	∿ 0%
	1635.1		0.6		1635.3	80	∿ 0%

A period about 6 min long of slightly enhanced continuum (about 20 s.f.u. above quiet Sun) follows without bursts.

A gradual structure (duration >1 min) takes place at 1642. It is strongly R-hand polarized and marks the beginning of the polarized part of the event. In fact, in a short group of bursts that follow, the first burst is zero polarized, the second one 43% R, the third one 82% R. Data for this group are:

Start 1644.3, Duration 0.3 min, Maximum 1644.5, Flux Density 60 s.f.u.

Another long lasting structure, strongly R polarized, begins at 1700 and lasts to the end of our observing time (1705).

Mean values of flux density and polarization percent over 10 min intervals covering the event are given below: (Attention should be drawn to the fact that we have subtracted the pre-event flux density amount.)

Start 1623 UT,	Mean Flux Density	7 s.f.u.,	Mean Polarization 0%
1633		23	0%
1643		12	9% R
1653		13	35% R

No peculiar structure (oscillations, absorptions) was detected. The R-hand polarization in the conditions specified under (a) above implies ordinary mode of emission.

The September 19 event

a) Environment

The flare originating this event is classified in Solar-Geophysical Data (March 1978 No. 403 Part II) with the following characteristics.

Start 0955 Maximum 1038 End 1207 Position N08 W57 Importance 3B

The sunspot group in which the flare took place is the same as for the September 9 event and the same considerations about leading polarity and cycle are valid. The position of the group on our drawings is N07 W52.

McMath region number is 14943.

b) Description of activity at 237 MHz (Figure 1)

At this frequency the event begins at 1035 and ends gradually at about 1200.

A short group of Type III bursts acts as a precursor to the major event, starting about 40 min before the latter:

Start 0950.3, Duration 1.4 min, Maximum 0950.5, Flux Density 300 s.f.u., Polariz. 8% L

At 1035 a rise in background flux density begins, with some short-duration, low-intensity structure superimposed (e.g. at 1038.5).

Later a stronger structure appears as a rise-and fall with weak, irregular activity over it; the whole structure grows out of the rising part of the major event, making the determination of its beginning and end times rather uncertain: possible values are 1038 as starting time, 1043 as end. Maximum flux density is reached at 1040.2 with 250 s.f.u., and at this time the polarization is 5% L. At the end of the structure, the polarization goes back to 5% R, that is the mean level before and after the event.

From 1043 onward the main part of the event develops.

The flux density rises irregularly with several maxima and pecular structures (see below); while the polarization reverts to L after 1044 and remains so (with fluctuations) until 1106; after this moment it returns R, growing up to ∿40% R, and then decreasing to ∿0 during the slow final decrease of the flux density; when the latter has gone back to the pre-event level, the polarization is again 5% R (1123). The maximum L-hand polarization value is reached just before the final inversion (at 1106): the value is about 50% L.

Type I-like activity consisting in strongly L-polarized bursts is superimposed on a more constantly varying polarized continuum during the "L-polarized phase" of the event. When the impulsive activity ends abruptly (as at 1059), the polarization drops rapidly to lower values. On the contrary, the presence of the structure at 1045 (that raises the flux density of a factor about two) causes no change in the polarization, thus suggesting this structure to have originated in the same region as the continuum.

As peculiar variability we may note:

At 1046 -a minute of irregular pulsations (period ∿2 sec); from 1057.7 to 1050.8 -totally L-polarized regular oscillations [Abrami and Koren, 1978] (period ∿0.2 sec) (see Figure 2).

Mean values of flux density and polarization percent (without background) over 10 min intervals covering the event are reported below:

Start 1033,	Mean Flux Density 67 s.f.u.,	Mean Polarization	1% L
1043	104		32% L
1053	67		22% L
1103	21		9% L
1113	9		43% R
1123	6		7% R
1133	4		29% R
1143	2		51% R

The L-hand polarization in the conditions specified under (a) above implies extraordinary mode of emission.

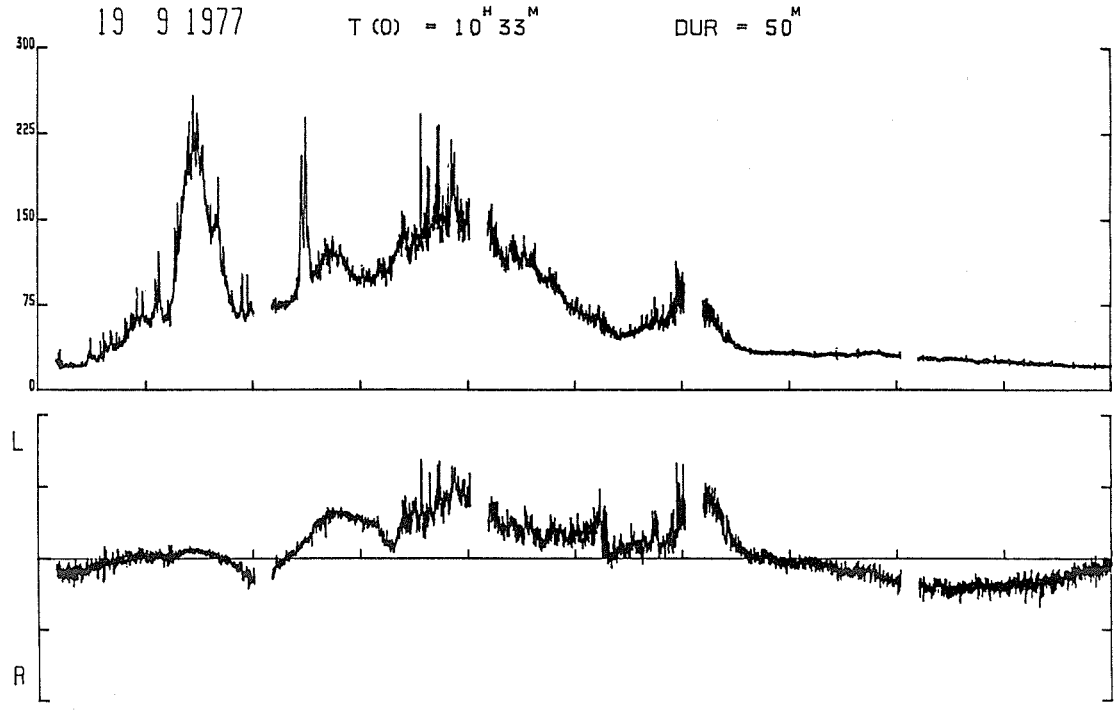

Figure 1. Plots of flux density (upper diagram) and polarization percent (lower diagram) at 237 MHz versus time, for the event of September 19. T(0) indicates the starting time; the flux density scale is graduated in s.f.u., while the polarization scale marks correspond to 100% L, 50% L, 0, 50% R, 100% R. Gaps in the tracings every 10 min are due to our digitization system. Flux density and polarization are both inclusive of quiet Sun background, while the data we report in the text have been corrected for it.

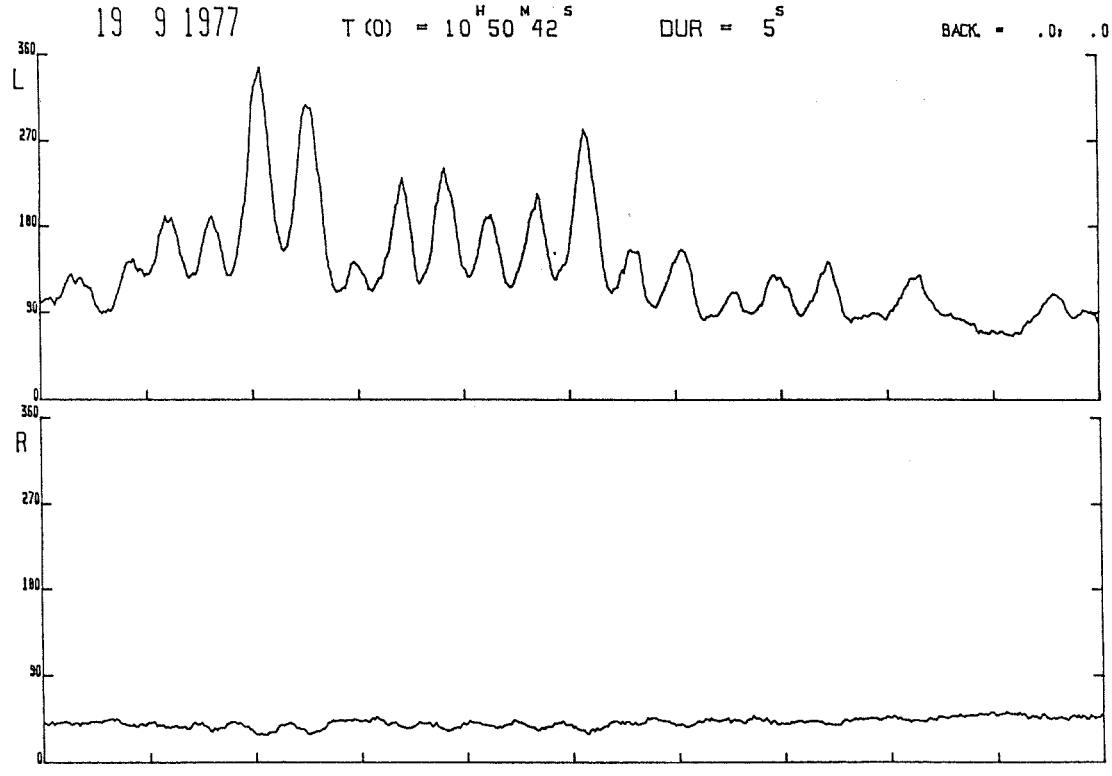

Figure 2. Plots of flux density of the L-hand (upper diagram) and respectively the R-hand polarized part of the emission (lower diagram) at 237 MHz, versus time, for an interval of the September 19 event showing regular oscillations. Ordinate scales are in s.f.u.; marks on the time scales represent 0.5 sec intervals.

c) Description of activity at 408 MHz

At this frequency the event begins at 1028 and ends at about 1200.

A rise in the flux density reaches a first maximum at 1037; then the flux density lowers and remains almost constant (about 100 s.f.u.) until 1102. Finally it decreases gradually until the end.

The average of position measurements [Koren and Zanelli, 1978] over the whole period of the event is W14'.3±0'.5, so this position is further west than the photospheric group.

The November 22 event

a) Environment

The flare originating this event is classified in Solar-Geophysical Data (December 1977 No. 400 Part I) with the following characteristics:

Start 0945 Maximum 1007 End 1105 Position N23 W40 Importance 2B

The sunspot group in which the flare took place has a N-magnetic polarity leading spot (Magnitnje polja solnecnjih pjaten - bulletin Solnecnje Dannje No. 11, 1977) and this together with the rather high latitude value classes the group as belonging to the new (21st) cycle. The position of the group on our drawings is N23 W37.

McMath region number is 15031.

b) Description of activity at 237 MHz (Figures 3 and 4)

At this frequency the event begins at 1001 and ends at about 1300.

From 1001.3 the flux density begins to rise, with unpolarized Type I-like bursts superimposed; at 1003.1 there is a peak - probably a Type III burst - that reaches 1500 s.f.u., unpolarized.

From 1004.1 to 1006.7 a distinctive hump takes place; at its maximum (1006.0) it attains about 1200 s.f.u.. The polarization is about 16% L for the whole duration of this structure. According to the conditions specified under (a) above this implies ordinary mode of emission.

Apart from the mentioned hump, the first 15 min of the event are $\sim$ 0 or very weakly L-polarized: from 1017 the polarization rapidly turns to R-hand and grows to 100% R about 1020. During the development of the event the polarization decreases irregularly and reaches a minimum about 1048 where the flux density is almost equal to the pre-event value.

The strongest part of the event develops from 1017 to 1048: from 1017 to 1026 a series of rise-and-falls of about 200 s.f.u. is observed, then there follows a rapid growth and a plateau (1028 to 1034) of about 800 s.f.u. over which strong variability is superimposed (amplitude of this variability is 150 to 200 s.f.u. above the plateau). The polarization is almost constant for the whole plateau, about 50% R.

At 1034.5 a strong peak grows out of the plateau reaching the maximum flux density level of the whole event ($\sim$1600 s.f.u., with a 35% R polarization); the duration of this peak is about 2 min.

Low activity (200 s.f.u. downward) follows until 1048, when a minimum of flux density and polarization takes place.

The last (decreasing) phase of the Type IV event looks divided in a series of low intensity humps (Figure 4), at least three of which are detectable on our recordings, their maximum flux density being lower and lower, polarization higher and higher, with time:

Start 1048,	End 1107,	Maximum 130 s.f.u.,	Polariz. at Maximum 57% R
1108	1131	$\sim$35	$\gtrsim$90% R
1133	1145	$\sim$10	$\sim$100% R

Other bursts resembling those above, but so low as to be barely distinguishable from the background and detectable with a certain ease only on polarization recordings, have maxima at 1155 and 1223 - their polarization is still very strong R.

Mean values of flux density and polarization percent (without background) over 10 min intervals covering the main part of the event are reported below:

Start 1001,	Mean Flux Density 392 s.f.u.,	Mean Polarization 12% L
1011	106	27% R
1021	425	62% R
1031	559	44% R
1041	56	43% R

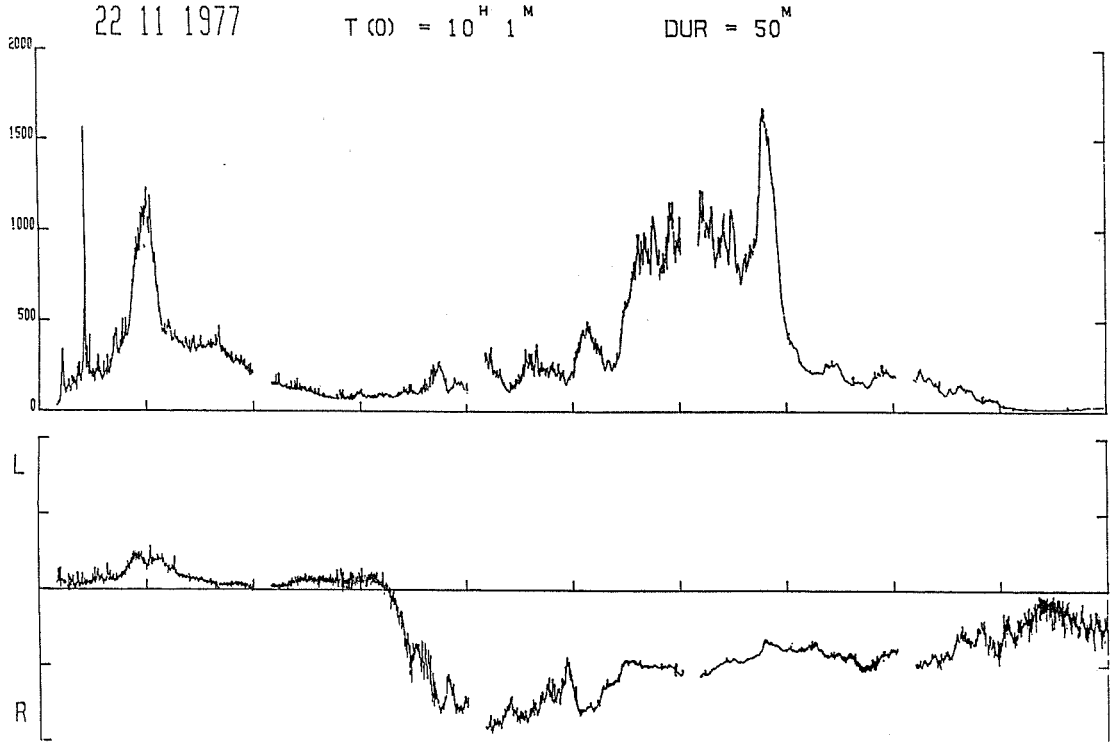

Figure 3. Plots of flux density (upper diagram) and polarization percent (lower diagram) at 237 MHz versus time for the first part of the event of November 22. See caption to Figure 1 for comments.

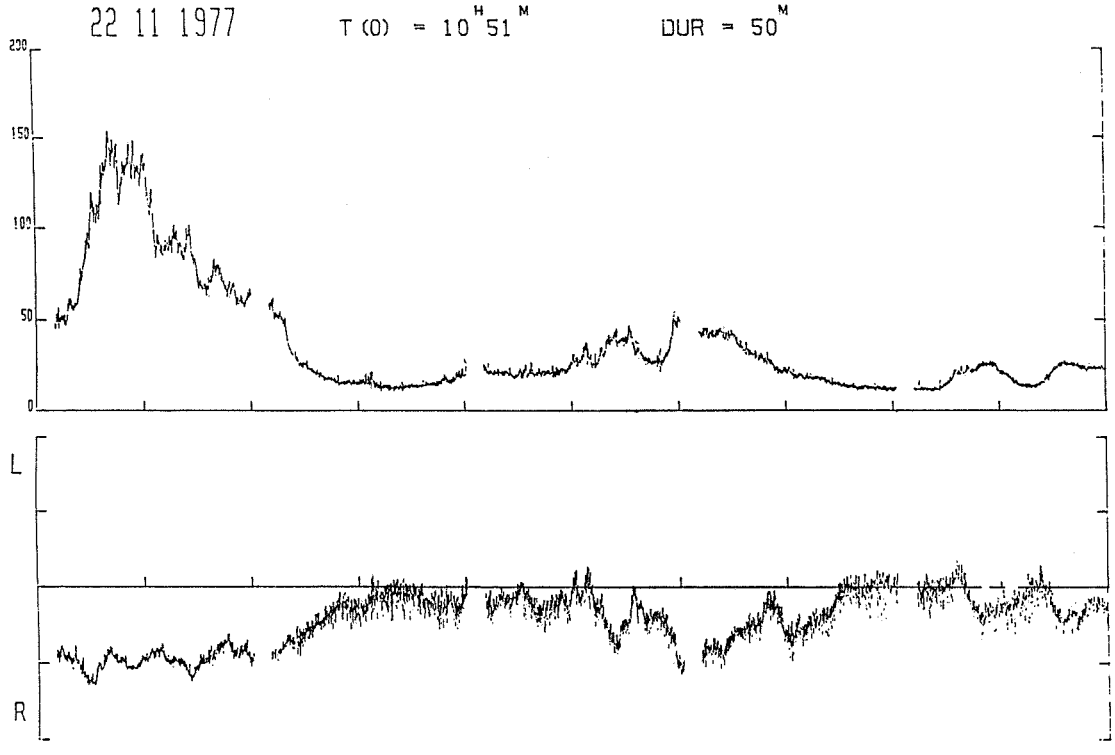

Figure 4. Plots of flux density (upper diagram) and polarization percent (lower diagram) at 237 MHz versus time for the second part of the event of November 22. Note different flux density scale from Figure 3. See caption to Figure 1 for comments.

Start 1051,	Mean Flux Density	80 s.f.u.,	Mean Polarization 56% R
1101		9	51% R
1111		17	32% R
1121		13	46% R
1131		8	29% R
1141		2	30% R
1151		4	34% R
1201		2	30% R
1211		3	21% R

No peculiar structure was detected. The R-hand polarization of the main event in the conditions specified under (a) above implies extraordinary mode of emission - we recall that the first part of the event showed evidence of ordinary emission. We did not observe at 408 MHz a displacement of the source between the time in which the emission was in the L- and R-sense of circular polarization.

c) Description of activity at 408 MHz

At this frequency the event begins at 0959 and ends at ~1200.

A rapid rise of the flux density is followed by a rather flat maximum from 1005 to 1010. About 1016 a low intensity rise-and-fall takes place, then from 1017 to 1046 there is a very strong event (certainly over 1000 s.f.u.).

A series of weaker rise-and-falls follows:

Start 1049,	End 1104,	Maximum Flux Density >650 s.f.u.	
1115	1129	∿100	(2 maxima)
1133	1143	∿120	(3 maxima)
1153	1158	very weak	

The position of the source is rather constant at least from 1000 to 1031 and its value is W7'.5±0'.5, so this position is further west than the photospheric spot group.

References

ABRAMI, A. and U. KOREN 1978 Pulsating Structures in Type IV Solar Radio Events, Astron. & Astrophys. Supplements, (in press).

KOREN, U. and C. ZANELLI 1978 Metodo di elaborazione di radio eventi solari da interferogrammi, Mem. SAIt, (in press).

LAMPI, L., P. SANTIN and P. ZLOBEC 1977 Eventi di tipo III ad alta risoluzione temporale registrati all' O.A.T.; descrizione della strumentazione per l'acquisizione e reduzione dei dati polarimetrici, Mem. SAIt, 48, 231.

Observations of the Radio Source Associated with McMath Region 14943 in the Millimeter Wave Range

by

S.L. Domnin, V.A. Efanov, I.G. Moiseev and N.S. Nesterov
The Crimean Astrophysical Observatory, USSR

The development of the local source associated with McMath Region 14943 was traced from Sept. 15 to Sept. 21, 1977, during the routine solar radio observations carried out at the Crimean Astrophysical Observatory. Measurements were made using a 22-m radio telescope at wavelength 13.5 mm with simultaneous registration of Stokes parameters I and V. The total emission was measured too at 8 mm on Sept. 19 and 20. Because the main beams of the antenna patterns at 8 and 13.5 mm were displaced in the azimuth plane, the radio source was scanned simultaneously at both wavelengths by switching the receiver alternately between the two signals.

Average parameters of this radio source, measured at 13.5 mm at its quiet stages, are listed for each day of observation in Table 1 in the following sequence: the time of measurement, the total flux density (F), the degree of circular polarization (P), and the angular dimensions calculated from the right ascension (ϕ_α) and declination (ϕ_δ) scans under the assumption that the source had a Gaussian shape. In Table 1 and in what follows the source antenna temperature and hence its flux density was determined under the assumption that the brightness temperature of the quiet Sun was 8000 K at 8 mm and 8900 K at 13.5 mm (our determination during 1973-1976 by comparison with the Moon). We did not take into account in our data processing position of the source with respect to the solar limb.

Table 1. Parameters of the Radio Source at 13.5 mm

Sept. 1977 observation	F (s.f.u.)*	P (%)	ϕ_α (arc min)	ϕ_δ (arc min)
15.35	11.8	3.1	3.6	1.8
16.4	13.2	4.6	3.3	1.5
19.33	11.4	1.5	2.8	2.7
20.38	12.8	-	1.8	1.5
21.2	4.5	-	-	-

*s.f.u. = solar flux unit = 10^{-22} Wm^{-2} Hz^{-1}

Two radio bursts were observed in the emission of the source on September 19 and 20 at both wavelengths in their decreasing phases only. Time dependences of the flux densities, angular dimensions and spectral indexes (α) of the radio source during these two bursts are presented with a dotted line for 8 mm and a solid line for 13.5 mm in Figures 1 and 2. The two diagrams show the following burst characteristics: (a) the flux density and spectral index declined slowly but with secondary variations, (b) the flux density oscillated in the range 8-16 s.f.u. with a quasi-period of about 40-50 min, (c) the dimensions of the radio source did not change noticeably during the Sept. 20th event, while the source dimension in right ascension increased by about 40 arc sec for 50 min on Sept. 19, (d) the spectral indexes of the source in the 8 to 13.5 mm range remained the same during the slow decreasing phases, as observed before in the case of a quiet local source related to a spot group [Efanov et al., 1972].

Taken together, these four attributes suggest that a similar emission mechanism existed during the two different stages of the radio source described here. Moreover, a circular polarization degree in both bursts not exceeding 1.5% may be explained by the complex multipolar structure of the spot group [SD, 1977], the differently polarized components of which were possibly not resolved.

REFERENCES

EFANOV, V.A., A.G. KISLYAKOV and I.G. MOISEEV 1972 Slowly Varying Component Spectrum of the Solar Radio Emission at Millimeter Wavelengths, *Solar Physics, 24,* 142-153.

SD 1977 *Solnechnie Dannie, N 9.* (In Russian)

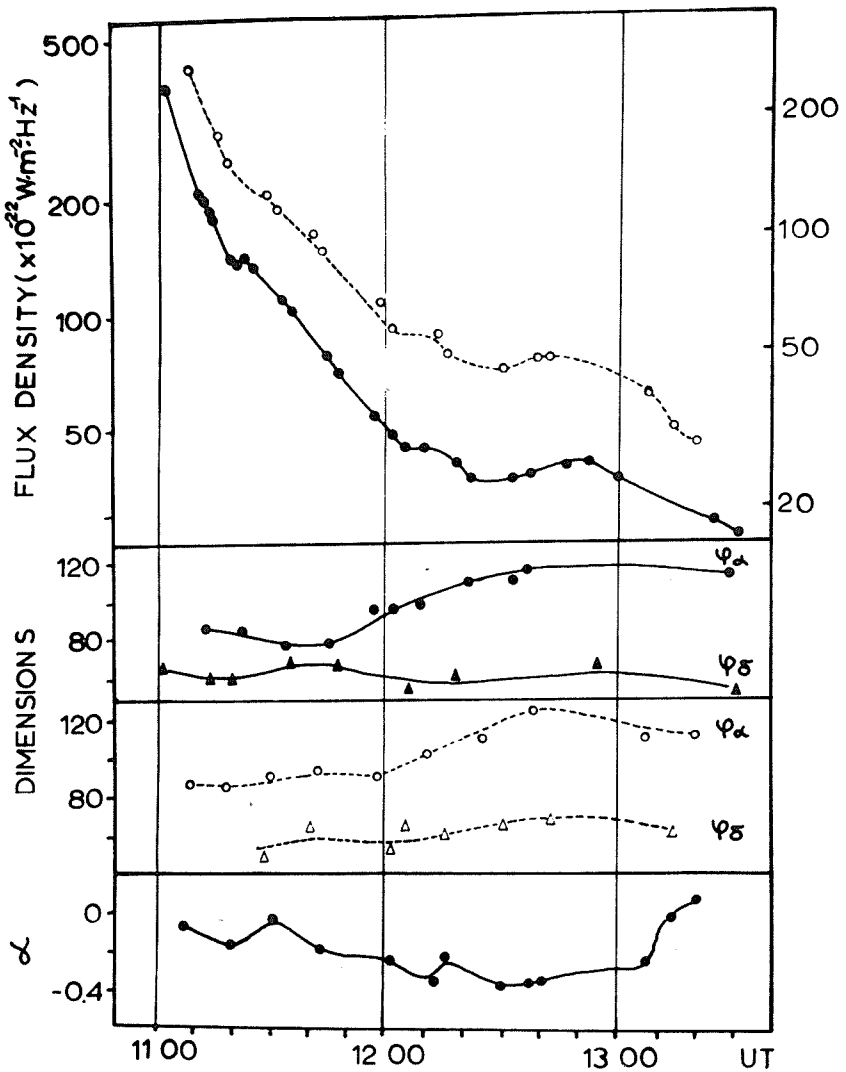

Fig. 1. The outburst of Sept. 19, 1977 measured at 8 mm (dotted lines) and 13.5 mm (solid lines) with the 22-m radio telescope of the Crimean Astrophysical Observatory. The 8-mm flux density scale appears along the right side of the top panel.

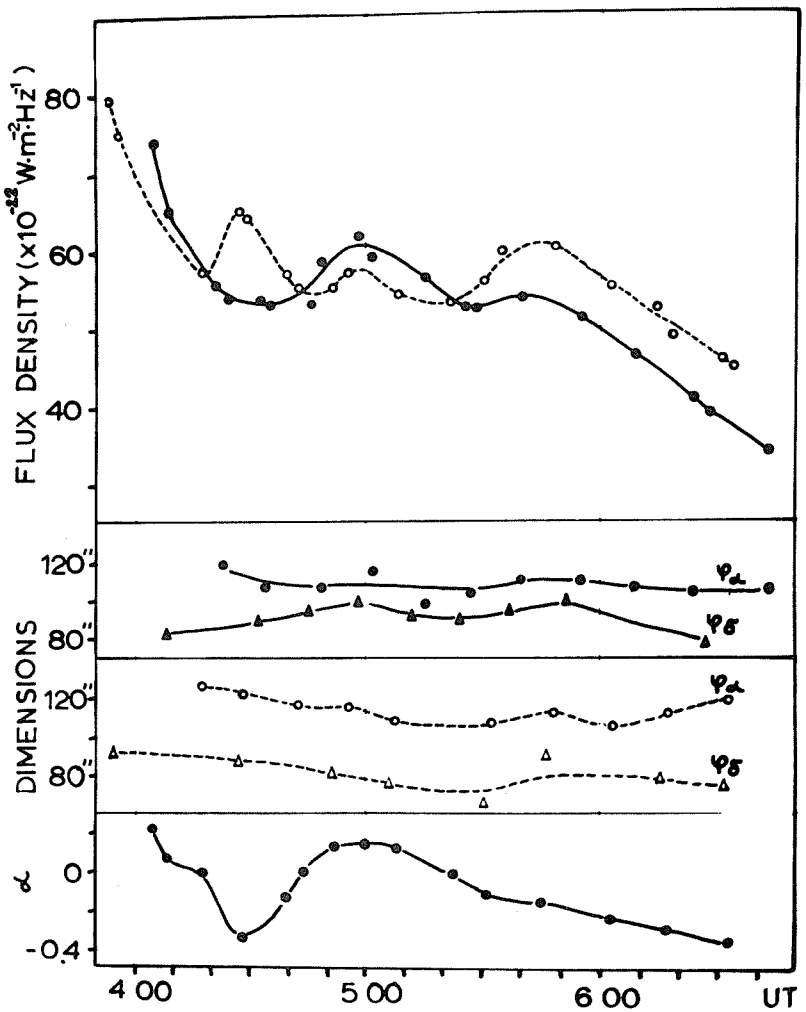

Fig. 2. The outburst of Sept. 20, 1977 measured at 8 mm (dotted lines) and 13.5-mm (solid lines) with the 22-m radio telescope of the Crimean Astrophysical Observatory.

The Large Flare and Associated Radio Burst of September 19, 1977

by

C. Alissandrakis
Department of Astronomy
University of Athens, Greece
and
D. Dialetis and T. Prokakis
National Observatory of Athens
Athens, Greece

In this note we describe the 3b flare and its associated centimeter-wavelength burst, which occurred in McMath Region 14943 on September 19, 1977. The active region was in its first rotation and produced several small flares as well as a 2n flare on September 16. The associated sunspot group became more compact on September 19, consisting of two large spots with multiple umbrae and several smaller spots. The magnetic configuration was bipolar with umbrae of both polarities. The maximum field strength was between 1100 and 1500 gauss [*SGD*, 1977a].

Our observations of the event include Hα patrol photographs obtained with a Halle filter on the Razdow telescope (D = 25 cm, f = 225 cm) of the National Observatory of Athens as well as radio patrol observations at 6 cm (4495 MHz) obtained at the same observatory. The flare was photographed at the center of Hα on Kodak SO-392 film.

The flare started around 1027 UT at N08W57 and ended after 1200 UT. We selected for further processing nine frames, beginning before the start of the flare to well after its maximum. The photographs were scanned with the observatory's Joyce-Loebl microphotometer, which produced contour lines of equal film density of the active region (see Figures 1-9).

The evolution of the flare is also shown in Figure 10, where we have marked the points of flare emission on the isodensity map of Figure 1. We have also drawn on Figure 10 the approximate position of the neutral line of the photospheric magnetic field deduced from the Mt. Wilson magnetogram [*SGD*, 1977b]. The flux of the 6 cm emission as a function of time is shown in Figure 11.

The flare started in a number of small bright kernels that were located in the vicinity of the neutral line (see Figures 2 and 10). The start of the radio emission closely corresponds to the beginning of the flare. The radio emission had a first maximum at 1032 UT, corresponding to the flash phase of the flare. The bright region in the eastern part of the flare (Figure 10) reached maximum intensity at 1037 UT, which corresponds to the primary maximum of the radio emission. The flare's subsequent decay was accompanied by a change in form, and eventually it evolved into a bright streak, loop-like in shape (see Figures 3-9; the location of the streak at 1106 UT is also marked on Figure 10).

The western part of the flare (Figure 10) attained maximum intensity around 1043 UT, followed by an expansion of the bright emission regions. At the same time that the emission patches moved away from the neutral line, one patch covered a major sunspot umbra (spot 1 in Figure 10). The umbral coverage started around 1053 UT (Figure 6) and reached maximum near 1106 UT (Figure 8). It may be associated with a secondary maximum in the radio emission at 1100 UT.

A third emission region, in the northwest portion of the group (Figure 10), emerged between 1043 and 1053 UT (see Figures 5 and 6). Its appearance may be associated with the radio emission peaks between 1046 and 1053 UT. It was located close to a bright portion of the pre-flare plage, which had brightened at the beginning of the flare and had disappeared completely by 1043 UT.

While some of the kernels developed in situ, other kernels showed some motion. We have already mentioned the motion of the bright point that covered the umbra; other bright points both in the western and eastern parts of the flare moved in directions away from the active region with apparent speeds up to 30 km/sec. Arrows mark the direction of their motion in Figure 10. From our observations we cannot tell whether this was a real motion of material or a subsequent brightening of adjacent stationary regions.

REFERENCES

SGD 1977a *Solar-Geophysical Data, 399 Part I,* 96, November 1977, U.S. Department of Commerce, (Boulder, Colorado, U.S.A. 80303).

SGD 1977b *Solar-Geophysical Data, 399 Part I,* 70, November 1977, U.S. Department of Commerce, (Boulder, Colorado, U.S.A. 80303).

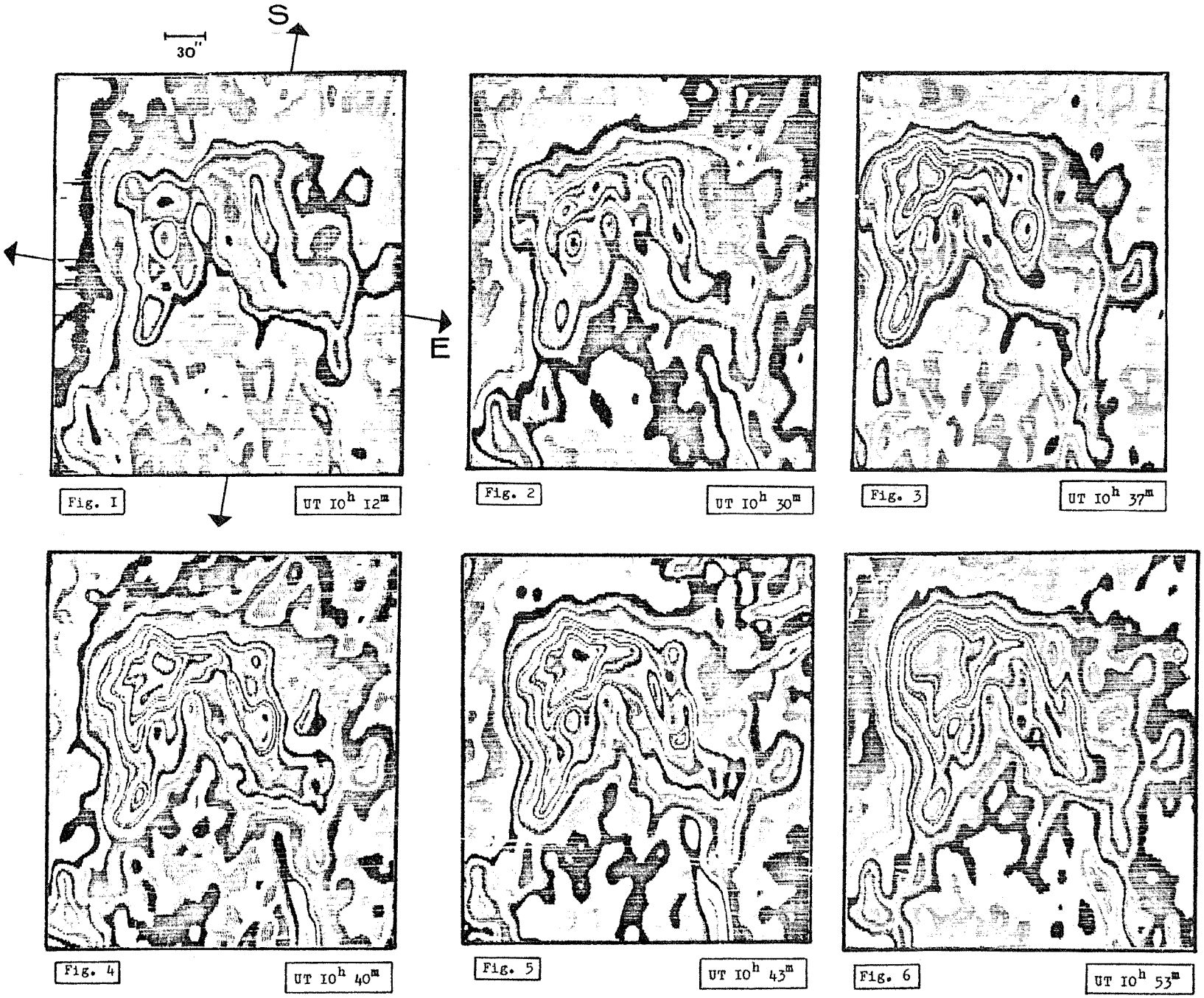

Figs. 1-6. Isodensity maps of McMath Region 14943 on September 19, 1977, before and during the 3b flare.

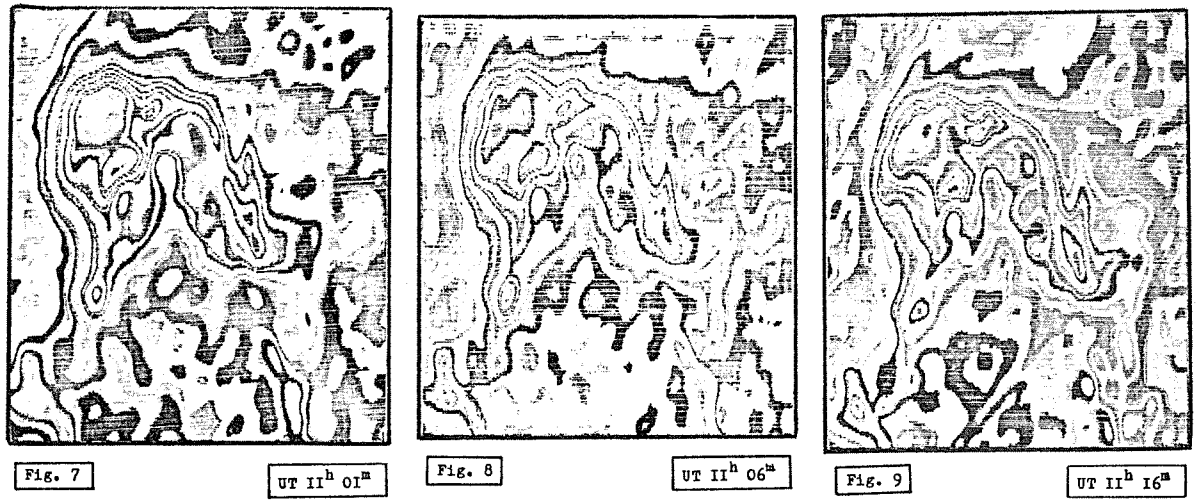

Figs. 7-9. Isodensity maps of McMath Region 14943 on September 19, 1977, before and during the 3b flare.

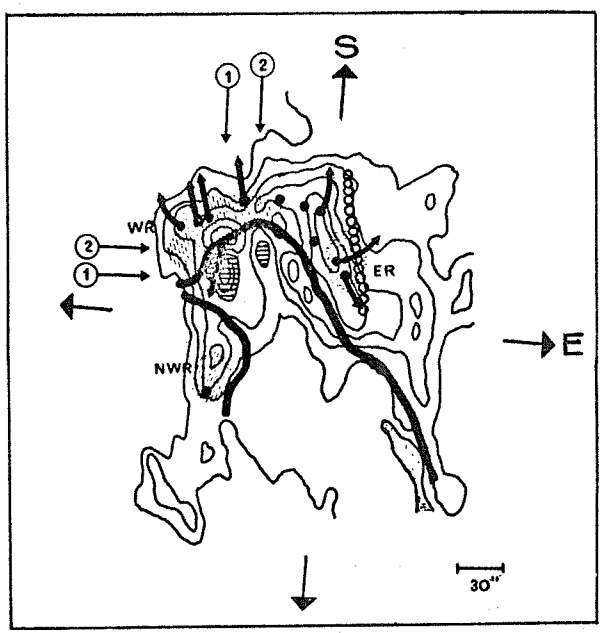

Fig. 10. Contour lines of the active region at 1012 UT. The heavy line shows the approximate position of the neutral line of the photospheric magnetic field. Black dots show the positions of flare kernels; arrows denote the direction of their motion. Open circles show the location of the bright streak at 1106 UT mentioned in the text.

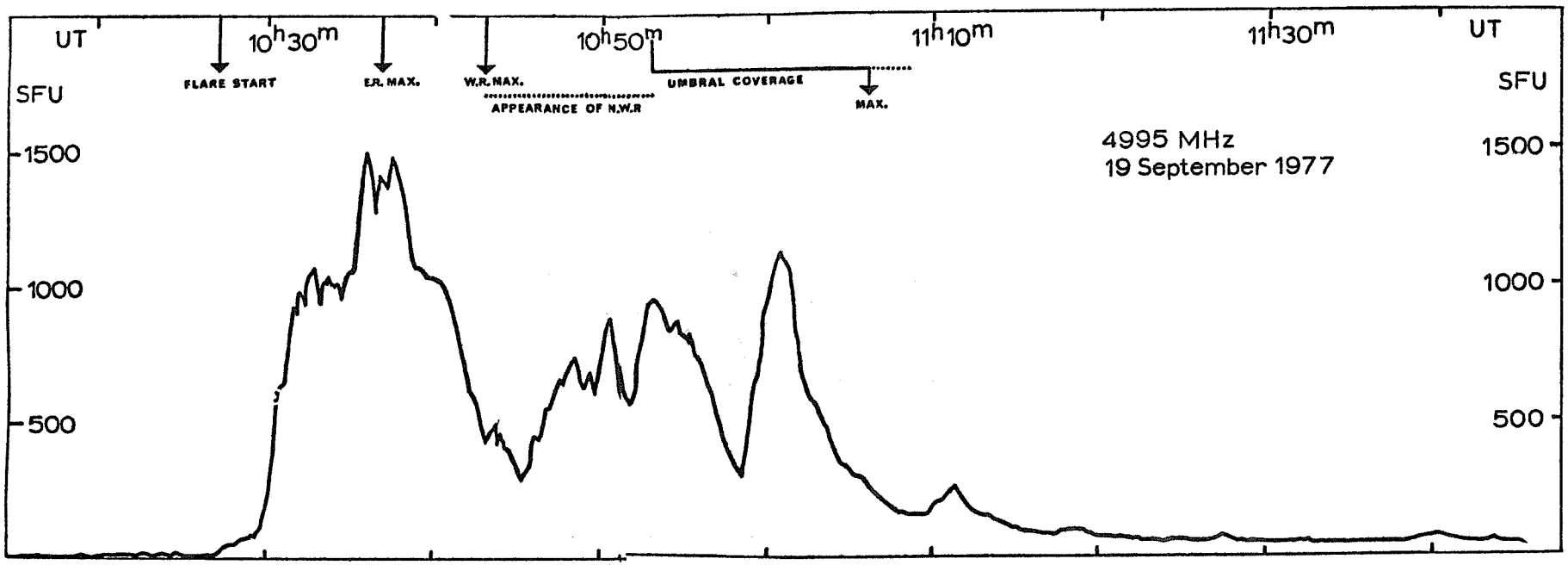

Fig. 11. Time profile of the 6-centimeter (4995 MHz) radio burst associated with the 3b flare of Sept. 19, 1977, that began about 1027 UT near N08W57. (1 s.f.u. = $10^{-22}Wm^{-2}Hz^{-1}$).

Observations of the Radio Burst on September 19, 1977 at IZMIRAN

by

L. M. Bakunin, G. P. Chernov, V. V. Fomichev and A. K. Markeev
Solar Radio Laboratory, IZMIRAN, Moscow, USSR

This report describes the characteristics of radio emission associated with the solar proton flare of September 19, 1977, on the basis of radio observations at IZMIRAN. Observations were made with radiometers at 202 and 3000 MHz and with spectrographs in the ranges 45 - 90 MHz [Markeev, 1961] and 180 - 230 MHz [Markeev and Chernov, 1971].

At the fixed frequencies 202 and 3000 MHz the burst has a complicated form (Figure 1). At γ = 10 cm the time profile of emission consists of more than 10 separate bursts lasting from 2 to 10 min (dashed lines indicate the moments when the 3000 MHz radiometer was off scale during registration with high sensitivity). The onset of radio burst at 3000 MHz (about 1027 UT) began about 5 min before the onset at 202 MHz. One can see also that the moments of the maximum intensity at these two frequencies do not coincide. At 3000 MHz an I_{max} of about 1100 s.f.u. was observed at 1101 UT, and at 202 MHz an I_{max} of about 110 s.f.u. was observed at 1041 and 1053 UT.

The dynamic spectra of the outburst in the range 45 - 90 MHz are shown in Figure 2. The analysis of the spectra shows that the given event is a complex set of Type II, III, and IV bursts.

The Type II burst consists of two groups of individual bands with different frequency drifts at frequencies <70 MHz. The first group lasts from 1037 to 1044.8 UT. It is difficult to determine the frequency drift at the beginning of the burst because the bands divide into numerous blobs arranged irregularly in the frequency-time plane. The most clear frequency drift appears in the interval 1041.2 to 1042.4 UT and equals $\sim$0.12 MHz/sec in the range 65 - 55 MHz. In terms of the plasma hypothesis the indicated drift velocity corresponds to a shock wave propagating through the corona with a velocity $\sim$700 km/sec. Individual elements or blobs, composing the fine structure of the Type II burst, have a bandwidth of 2 - 4 MHz and a duration of 2 - 5 sec.

The second group of drifting bands occurs in the interval 1053.8 to 1054.5 UT. Some bands analogous to the first group exist in this second group, but all of them have slow frequency drifts (values between 0.03 and 0.05 MHz/sec).

The different spectral properties of the bands of the two groups and the time delay between them suggest that each was connected with a different shock wave. Moreover, the individual bands with different frequency drifts in the first group may be also connected with independent shock waves propagating with different velocities or in different directions.

A Type IV radio burst was observed mainly at frequencies >70 MHz. In the time period in which the drifting bands of the first group are observed, the Type IV burst consists of a continuum component with significant intensity variations. The time scale of these variations is 3 - 30 sec. The most clear pulsations with τ = 20 - 30 sec are visible on the dynamic spectra from 1048 to 1053 UT. After 1055 UT the intensity of these variations decreases and fluctuations of shorter period become dominant.

An analogous evolution intensity variation takes place in the range 180 - 230 MHz (Figure 3). The pulsations with $\tau \sim$ 2-10 sec are visible before 1043 UT, then disappear; they are replaced by numerous short-lasting, spike-bursts with duration $\leq$ 0.2 sec. The peculiarity of these spike-bursts is their narrow bandwidth. The full frequency range covered by these bursts is equal to 10 MHz or less. In addition the spike activity is visible mainly near the maximum intensity of the Type IV burst, i.e., between 1050 and 1054 UT (see Figure 1). Pulsations coincide in time with the Type II burst at lower frequencies.

Another kind of fine structure evident in the Type IV radio event is the fiber burst (Figure 3). A system of two fiber bursts is visible between 1055:40 and 1055:46 UT; a single fiber burst lies between 1056:08 and 1056:10 UT. Each fiber burst drifts from high frequencies to low ones at a rate of 2.5 MHz/sec and covers a frequency range $\leq$ 10 MHz. The instantaneous bandwidth of these fiber bursts is about 2 MHz and is less than the roughly 5 MHz frequency interval between the pair at 1055:40 - 1055:46 UT. On the fixed frequency record at 202 MHz, the fiber bursts are identified by the arrow in Figure 1. The maximum intensity of these bursts is about 20 s.f.u. Although the time resolution of the records does not permit us to investigate the time profiles of these bursts, we can suppose on the basis of the dynamic spectra that a weak decrease exists in the background continuum before the increase in intensity associated with the fiber bursts occurs.

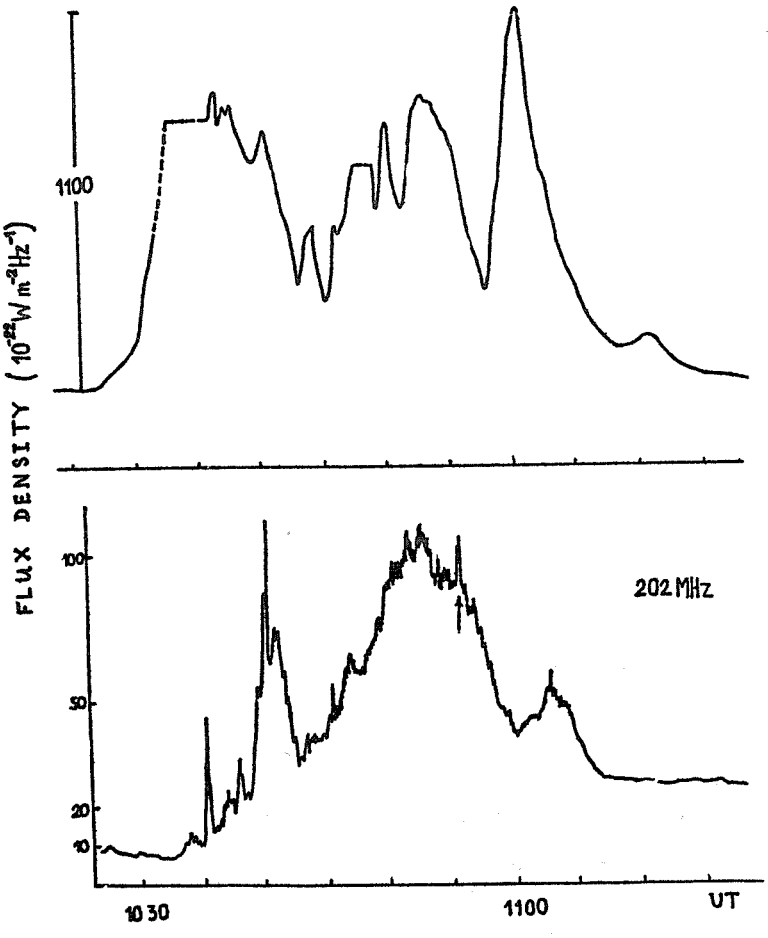

Fig. 1. Single frequency flux records of the outburst on September 19, 1977, at 202 and 3000 MHz. Arrow marks fiber bursts observed on the 180 - 230 MHz spectrograph.

A coupling of Langmuir waves and whistlers probably generates the fiber burst. The frequency interval between the neighboring maxima in emission and absorption is equal to the whistler frequency, i.e., $\Delta\omega - \omega_w \sim (0.25 - 0.5)\ \omega_H$ [Kuijpers, 1975]. Taking the observed value $\Delta\omega \sim 2.5$ MHz, one can obtain the magnetic field strength in the radio source as $2\text{-}4 \times 10^{-4}$T.

It should be noted in conclusion that unlike other Type IV bursts with fine structure, the September 19, 1977, event was observed against a weak background continuum of about 100 s.f.u.

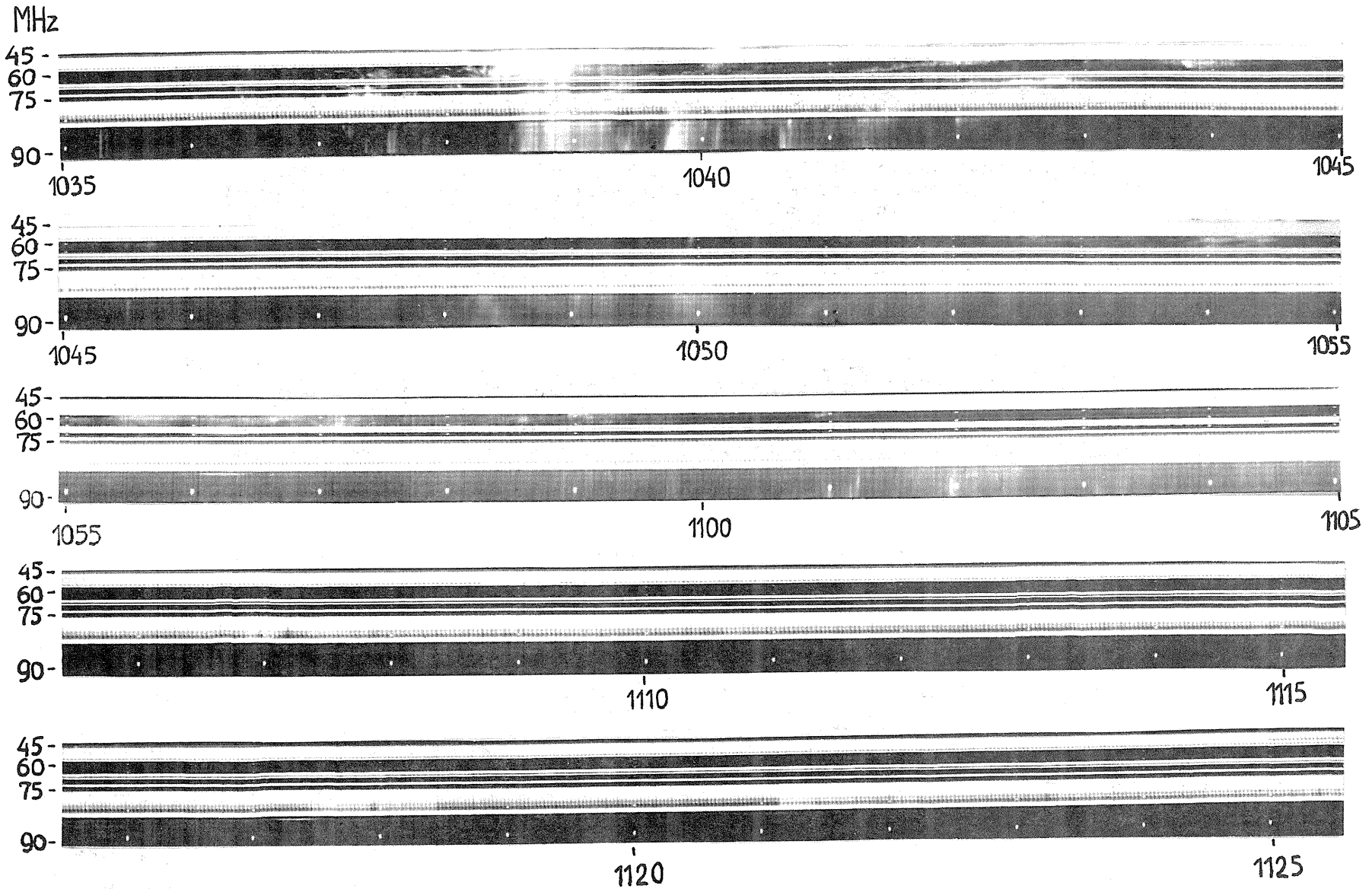

Fig. 2. Dynamic spectra of the outburst on September 19, 1977, in the range 45 - 90 MHz.

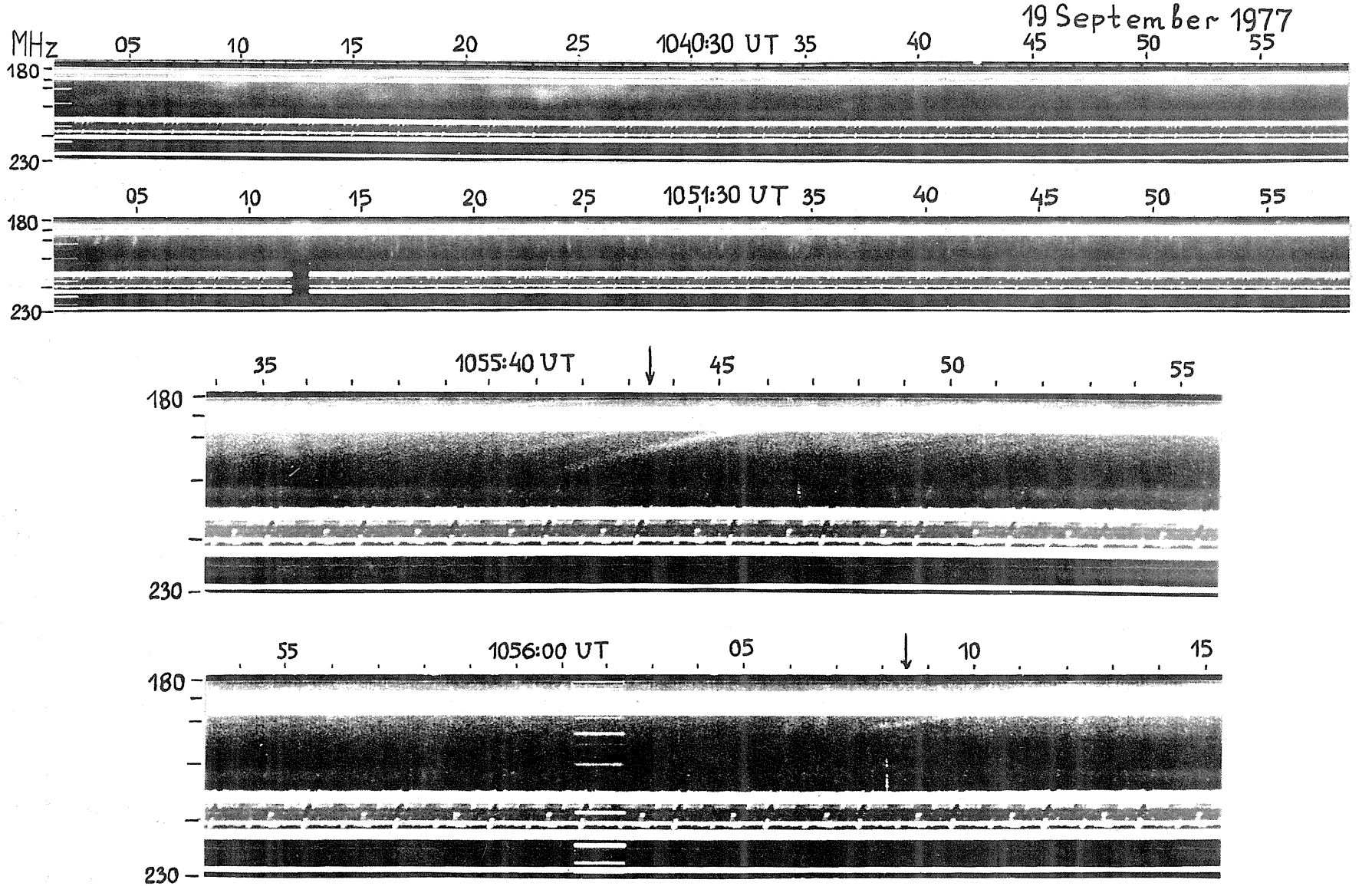

Fig. 3. Dynamic spectra with high time and frequency resolution of the outburst on September 19, 1977, in the range 180 - 230 MHz. Arrows mark the two fiber burst groups.

REFERENCES

KUIJPERS, J. 1975 Generation of Intermediate Drift Bursts in Solar Type IV Radio Continua through Coupling of Whistlers and Langmuir Waves, *Solar Phys.*, *44*, 173-193.

MARKEEV, A. K. 1961 The Apparatus for the Observations of the Enhanced Solar Emission in Range 45 - 90 MHz, *Geomagnetizm and Aeronomy*, *1*, 999-1002. (in Russian)

MARKEEV, A. K. and G. P. CHERNOV 1971 Observations of Solar Radio Bursts with High Spectral Resolutions, *Soviet Astron.*, *14*, 835-838. (in Russian)

Solar Radio Bursts of September 7 and 16, 1977

by

Victor L. Badillo
Manila Observatory
P.O. Box 1231
Manila, Philippines

Conspicuously increased solar activity was manifested with the appearance of McMath Plage Region 14943. In the period September 7-24, 1977, the greatest solar radio bursts were recorded at the Manila Observatory on September 7 and 16. These bursts on five fixed frequencies are depicted in Figures 1 and 2. Associated sudden increases in energetic electrons and protons were detected by satellites [SGD, 1978a].

The burst on the 7th occurred from a source on the east limb; the burst on the 16th had its source at W20. In Figure 1 the maximum intensity occurs progressively later with decreasing frequency. This observation is strengthened by Table 1, which lists published values of frequencies and times of maximum [SGD, 1978b]. On the other hand, the same published list shows a maximum that occurs at 2233 UT, almost simultaneously at the following frequencies: 200, 245, 410, 606, 1415, 2000, and 35000 MHz. In Figure 2 the time of maximum for four of the five frequencies occurs at the same time, 2308 UT. This is also the published time for frequencies 606 MHz and greater. The burst-associated flare on September 16 had a reported importance 2n; that on the 7th had a reported importance 1n. This latter event may have been larger, since the east limb may have occulted parts of the flare area. It is interesting to compare the two radio bursts, considering the difference in meridian distance of their sources. From the satellite data, plasma clouds moved radially outward in each case. But in the limb radio burst one could more easily follow the upward moving plasma, as it progressively excited lower frequencies.

This research was sponsored by Air Force Geophysics Laboratory.

Table 1. UT Times (t) of maximum intensity at various frequencies (f) in MHz

f	t	f	t	f	t
35000	2231	4995	2246	1415	2314
15400	2236	3750	2258	1000	2321
9400	2241	2695	2300	606	2326
8800	2243	2000	2317		

REFERENCES

SGD 1978a *Solar-Geophysical Data, 403 Part II*, 36-41, March 1978, U.S. Department of Commerce, (Boulder, Colorado, U.S.A. 80303).

SGD 1978b *Solar-Geophysical Data, 403 Part II*, 22-26, March 1978, U.S. Department of Commerce, (Boulder, Colorado, U.S.A. 80303).

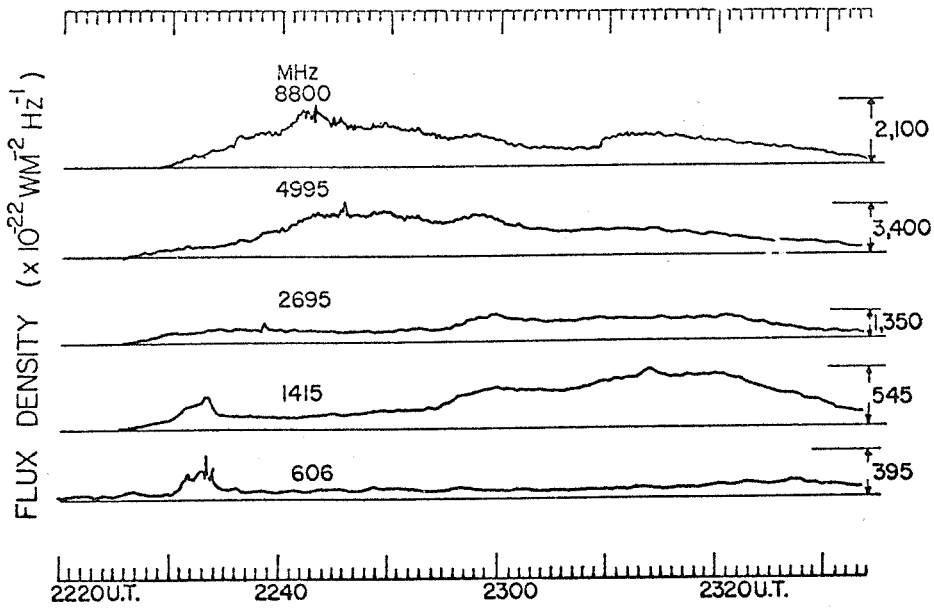

Fig. 1. Radio burst observed on September 7, 1977, at Manila Observatory.

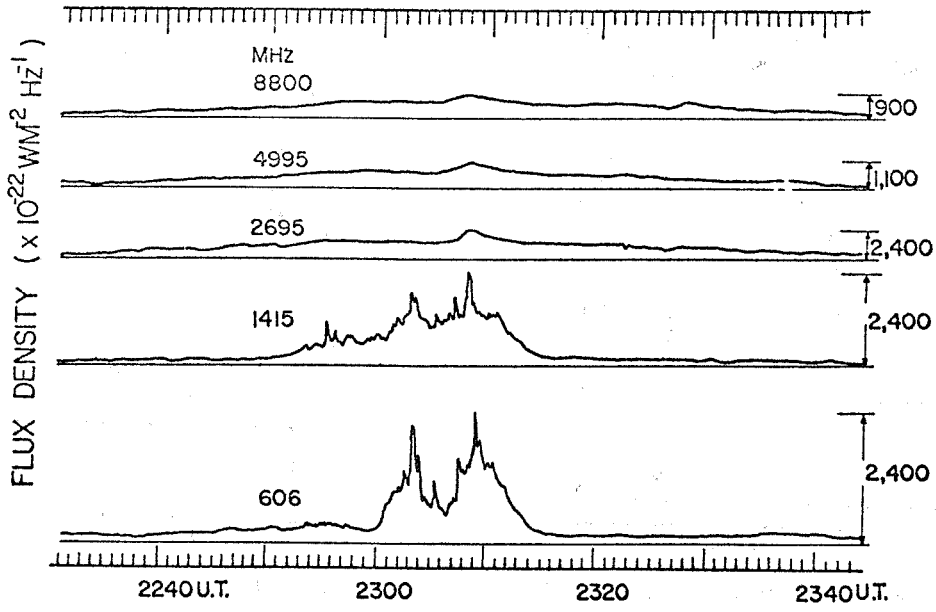

Fig. 2. Radio burst observed on September 16, 1977, at Manila Observatory.

Solar Radio Emissions of 100, 200, 500, and 9500 MHz Observed at Hiraiso

by

K. Ohbu, K. Muranaga, S. Isozaki, A. Mitobe, T. Isobe, and E. Ohuchi
Hiraiso Branch, Radio Research Laboratories
Nakaminato, Ibaraki, Japan

Three interesting examples of radio bursts in McMath plage region 14943, observed at Hiraiso during the period September 7 to 24, 1977, are shown in Figures 1 to 3. The figures present total flux and polarization ratios, where the polarization ratios are scaled linearly and the total flux logarithmically. (Note the fast fluctuations recorded on 200 MHz on September 16 and 20, for they may reflect instability in the equipment.)

On September 7 (Fig. 1) the radio bursts of 100 and 200 MHz began with a sharp rise about 2232 UT; were followed by strong variations; and became right-handed circularly polarized when the intense fluctuations decayed. Apparently it was a Type II burst, because neither a polarized component nor a weakly polarized component was recorded during the several tens of minutes after the start of the burst.

The polarized component of 100 MHz changed from right-handed to left-handed about 2400 UT on September 16 (Fig. 2). This change occurred while the flux was stable. This phenomenon may be interpreted as radiation from a moving source.

Figure 3 shows a complex burst superposed on a noise storm between 0250 and 0515 UT. A typical 30-MHz riometer burst was observed in connection with the event (Fig. 4). According to a report from Culgoora, a Type II burst occurred at 0315 UT over the low-frequency portion of the spectrum. A Type IV burst was observed between 0320 and 0515 UT at 43, 80 and 160 MHz.

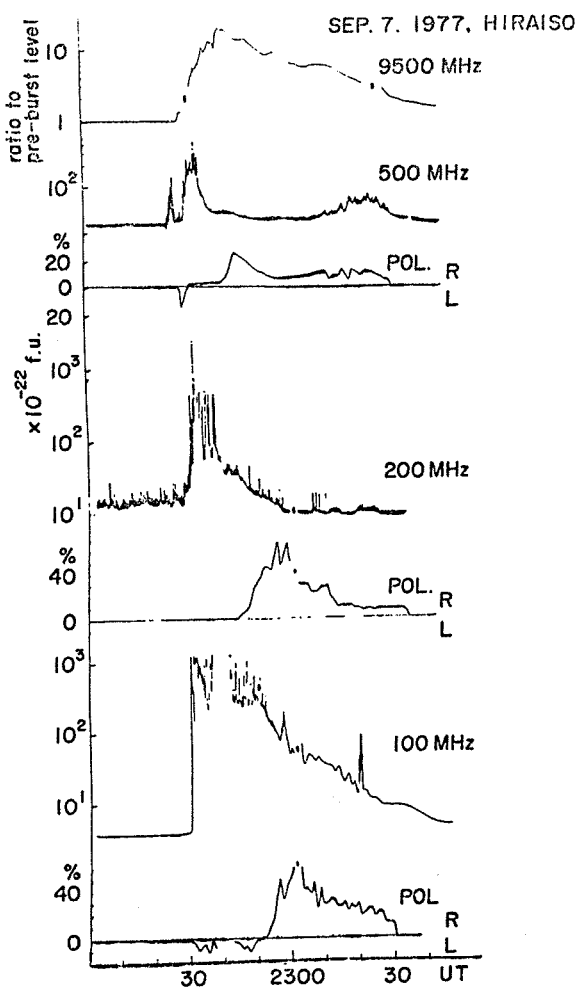

Fig. 1. Radio burst at 100, 200, 500 and 9500 MHz on September 7, 1977, Hiraiso, Japan.

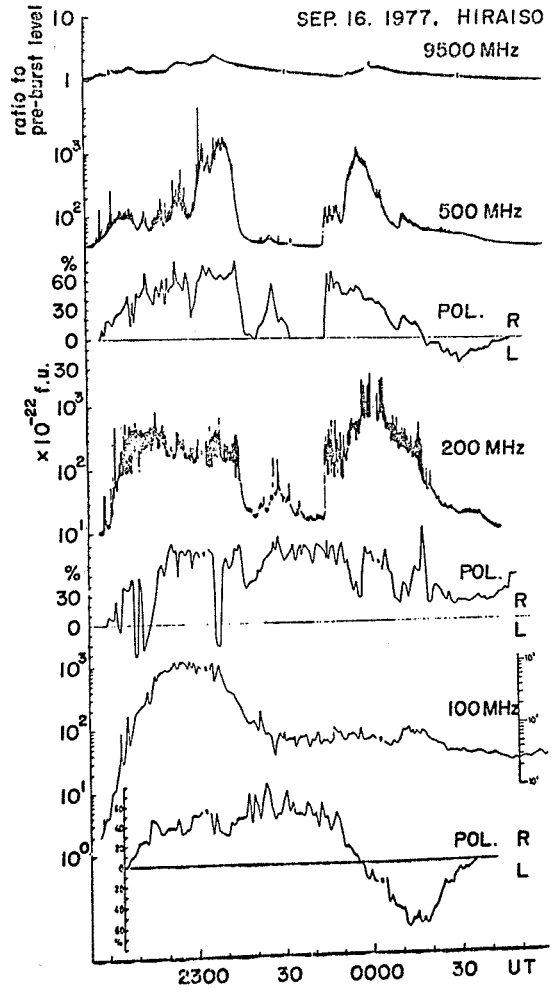

Fig. 2. Radio burst at 100, 200, 500 and 9500 MHz on September 16, 1977, Hiraiso, Japan.

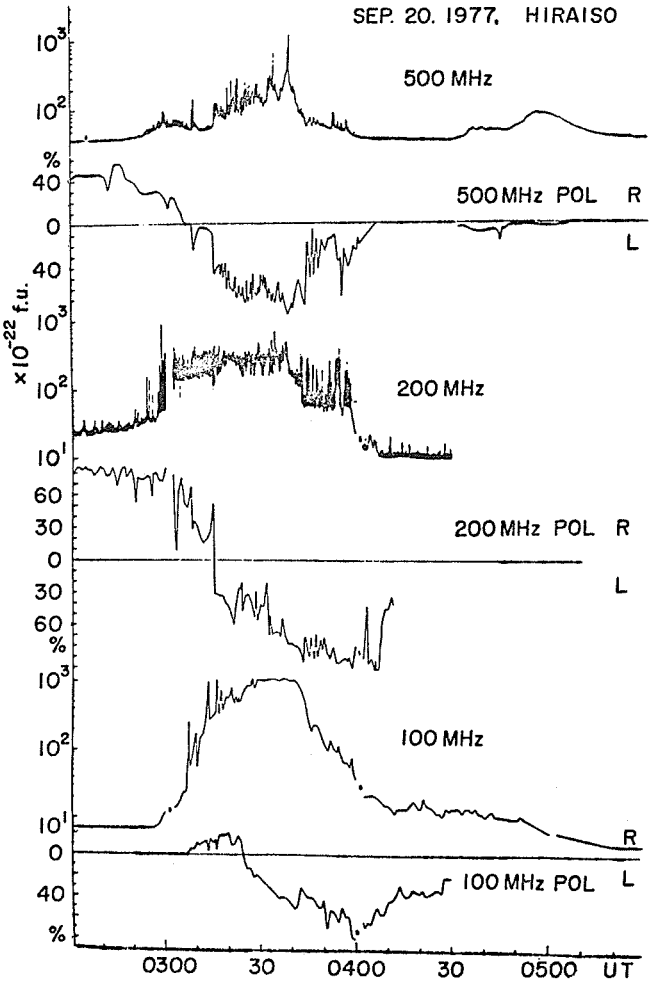

Fig. 3. Radio burst at 100, 200, and 500 MHz on September 20, 1977, Hiraiso, Japan.

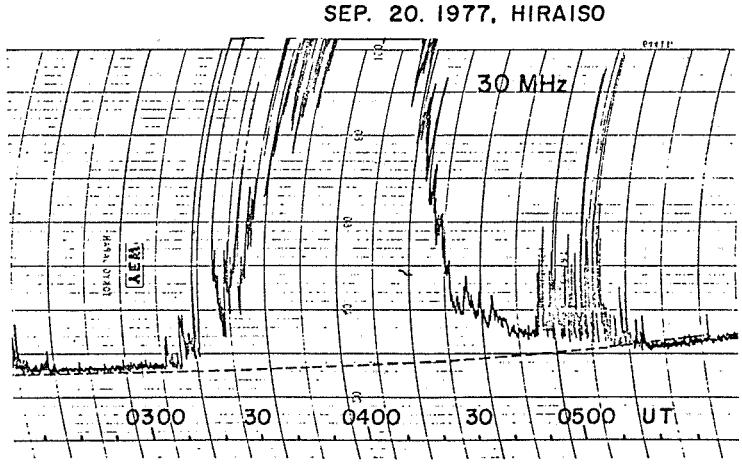

Fig. 4. Riometer record at 30 MHz on September 20, 1977, Hiraiso, Japan

Solar Activity in September 1977 and on November 22, 1977 as Observed at 127 MHz

by

Kazimierz M. Borkowski
Institute of Astronomy, Nicolaus Copernicus University
87-100 Torun, Poland

Introduction

The results presented here are based on the routine solar observations at 127 MHz carried out in Torun since 1958. The main purpose of this patrol is to measure a continuum solar radio emission. However, some distinctive events produced by the active Sun can be measured with satisfactory accuracy. As this frequency band is one of the lowest systematically reported, it may be of interest to have its data for periods of special study. The data are provided in the form of a table of outstanding occurrences and drawings. To allow one to use the detailed records a short description of the observing technique is given.

A note is made of an error discovered recently in the absolute flux scale, a systematic underestimation of this long enduring 127-MHz data series, which may be of importance in view of prevailing discrepancies in the meter wave solar flux determinations.

Instrument

Daily observations of 127-MHz solar radio emission are made at the Astronomical Observatory of the Institute of Astronomy, Nicolaus Copernicus University in Piwnice, with an interferometer consisting of two antennas. The 23.74-m (10.06 wavelength) baseline of the interferometer has the equatorial coordinates of 93.26° and 2.64° in hour angle and declination, respectively. The geographical coordinates of the observing site are 53.0966°N and 18.5544°E. Both antennas are linearly polarized in the baseline direction. The receiver input is switched between the antennas and dummy load, and the differential signal is recorded in an analog form on two paper strips with the speed of 16 cm/h. A detailed description of the receiving system can be found in Borkowski et al. [1975].

Observations and Data Reduction

An observing day usually covers about 7 hours around local noon, from 0700 or 0800 to 1400 or 1500 UT. Daily records consist of 16 to 18 interference fringes with maxima spaced 23 minutes around noon to 45 minutes around sunrise/sunset. Solar flux is measured in each of the fringes and then is averaged to give hourly or daily means. The fringe heights are converted into flux density units accounting for receiver nonlinearity, actual gain, and antenna power pattern. The latter is roughly the fourth power of the cosine of the hour angle. Daily calibrations, as in Figure 3, are made to check on stability of the gain and linearity of receiver. The flux of the Sun is referred to that of the Cas A assuming its density of 1.40×10^{-22} $W \cdot m^{-2} \cdot Hz^{-1}$ at 127 MHz in the second half of 1977.

A considerable error has been found recently in the procedure of absolute flux determination [Borkowski, 1978]. The error arose through the influence of another strong radio source Cyg A on the observation of Cas A resulting in higher flux observations during transit of Cas A; this subsequently led to underestimation of the flux scale. It exists in all our results reported since 1973, and probably also in earlier observations. This problem is under investigation. However, a factor of approximately 1.2 should be used for the flux values reported from Torun in the last few years, including this report.

Results

Though our measurements are believed to have a relative error of about 5-10%, normally we report 3-hourly and daily mean fluxes rounded to integers of 10^{-22} $W \cdot m^{-2} \cdot Hz^{-1}$, i.e. with uncertainty up to 30%. Here, in Figure 1, we present more accurate mean values found for each hour in the period 0700 or 0800 to 1300 or 1400 UT. The mean flux around 1200 UT is indicated with the smaller bar on the bottom scale, and the horizontal bars placed next to the chains of hourly means show the daily means calculated as the average fringe fluxes within 0900 and 1400 UT.

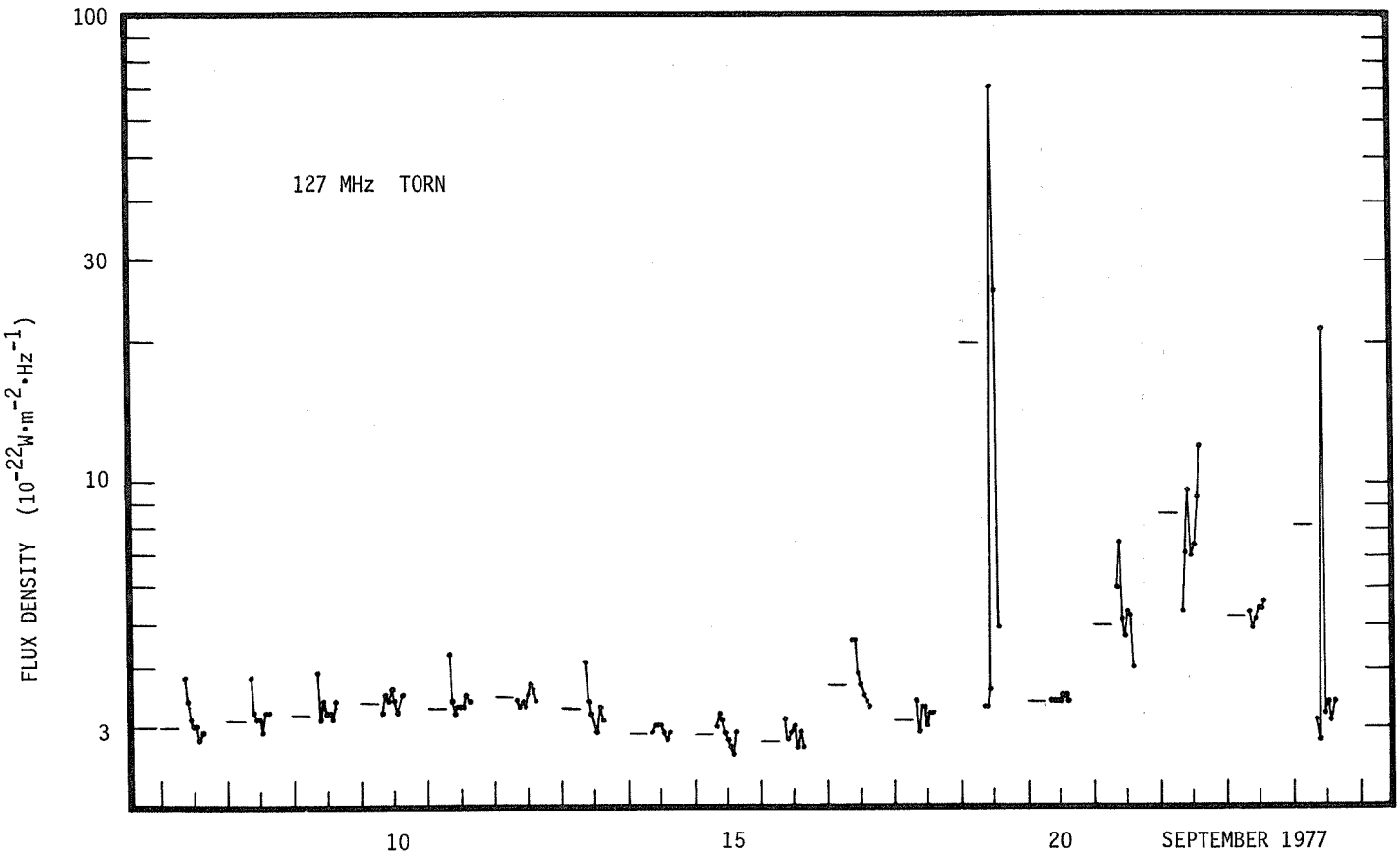

Fig. 1. Variations of the solar continuum radio emission at 127 MHz for Sept. 7-24, 1977. Hourly and daily means for 0900 to 1400 UT are shown by points and horizontal bars, respectively.

Worth noticing is the slow rise and fall of continuum solar emission at 127 MHz which reached its maximum on Sept. 10 to 12 at a level of 15 and 20% higher than on Sept. 7 and 16, respectively. These variations as well as those for Sept. 17 to 24 are well correlated with the variations of energetic solar particle fluxes as measured by IMP 7 and 8 [*SGD*, 1978].

The evaluation of distinctive events from our interferometric records is usually difficult due to the decrease of the observed flux of the Sun in the fringe nulls as well as due to frequent man-made interference. The resultant burst descriptions may contain inaccurate or even false values. To avoid reporting misleading data, customarily we list only the most important and evident bursts. More complete and reliable data can be gained by comparison with other frequency or spectral observations. This was done for the period Sept. 7 to 24, 1977, and the results are given in Table 1. The list is the ordinary monthly report for that period [*SGD*, 1978]. The format of tabulation is the same as in *SGD*. In the rightmost column of the table there are names (using *SGD* abbreviations) of stations whose observations are correlated with the events [*SGD* 1977, 1978]. No effort was made to correct previously evaluated data describing events of Sept. and Nov. 1977; therefore they are not included in Table 1.

TABLE 1. Outstanding Occurrences Sept. 7-24, 1977

DATE /UT/	TYPE	START TIME	TIME OF MAXIMUM	DUR. MIN.	FLUX DENSITY PEAK	FLUX DENSITY MEAN	REMARKS
7	41 F	0722.0	0736.3	20 U	130 U		CRIM
	4 S/F	1245.2 U	1245.5	4 U	8		WEIS, SGMR
9	45 C	1047.5	1049.7	3	18	4.5	DWIN
	1 S	1101.1	1101.3	0.3	7	3	DWIN
10	40 F	1053.8	1054.0	0.4	2.7	0.5	WEIS
11	8 S	0926.4	0926.5	0.3	33	16	WEIS
	5 S	1006.6	1006.8	0.4	4.7	1.5	DWIN
	45 C	1008.6	1009.0	1.5	15	2.5	WEIS
	45 C	1046.2	1046.3	0.5	120	25	DWIN, POTS, IZMI
	8 S	1348.4	1348.5	0.2	63	30	DWIN, WEIS
	1 S	1430.0	1430.1	0.1	3.3 U		WEIS, HARV/SUNSET
12	1 S	0745.3	0745.4	0.2	6.2	2.1	WEIS
	45 C	0821.7	0822.3	0.7	70	12	DURN
	1 S	0827.9	0828.0	0.3	5.0	1.3	WEIS
	45 C	0955.0	0955.4	0.7	200 D		POTS, TRST, DURN
13	43 NS	0757.0	0832.5	70 U	85		DWIN, WEIS
	1 S	1258.0	1258.0	0.1	0.8		DWIN, WEIS
	8 S	1415.5	1415.7	0.4	20 U		DWIN
14	7 C	0935.3	0935.4	0.6	11	2.7	WEIS
			0935.7		13		
15	5 S	1020.4	1020.7	0.5	22	5.6	DWIN, WEIS
	45 C	1049.2	1049.7	1.2	45	7	DWIN, WEIS
16	8 S	0912.9	0913.4	0.7	11	1.7	DWIN, GORK
18	7 C	1133.5	1133.6	0.5	2.4	1.2	WEIS
19	41 F	0645	0648.6	4	40 D		TRST, GORK, IZMI, WEIS / PEAKING
	1 S	0950.4	0950.4	0.4	3.7	1.8	TRST, HARS, DWIN
	45 C	1215.1	1215.3	0.5	140		GORK, WEIS, SGMR
	45 C	1225.9	1226.1	1.4	380	75	DWIN, GORK, WEIS
22	41 F	0631 E	0631.2	2 D	27		HIRA, GORK CALIBRATION
	46 C	1358.2	1359.4	4.6	300 D		ONDR, BOUL, DURN, DWIN / PEAKING
23	2 S/F	1257.5	1257.6	0.6	9	3	DWIN
	41 F	1311.7	1314.6	3.2	41		DWIN
24	45 C	0553.8	0554.6	6.9	200 D		DURN, CULG, WEIS
			0600.5		20 D		SUNRISE
	45 C	1230.3	1230.7	1.1	110	25	WEIS, SGMR

Unit of flux density is 10^{-22} $W \cdot m^{-2} \cdot Hz^{-1}$

Figures 2 and 3 show prominent bursts of Sept. 19 and Nov. 22, 1977, together with the data necessary to reduce them. To find the flux density at the maximum of a fringe one has to use the scale on the ordinate axis and then multiply the resultant flux by the factor shown below the fringe. For fluxes measured above the sloped part of the fringe this factor should be increased according to the shape of the fringe, which may be approximated by a single cycle of sinusoid plus unity.

The described evaluation of flux fails, however, for the record of Nov. 22 due to strong disturbances caused by ground reflections. The received signal does not reach the sky background in the nulls of interferometer pattern. Therefore in Figure 3 only a very rough approximation can be made.

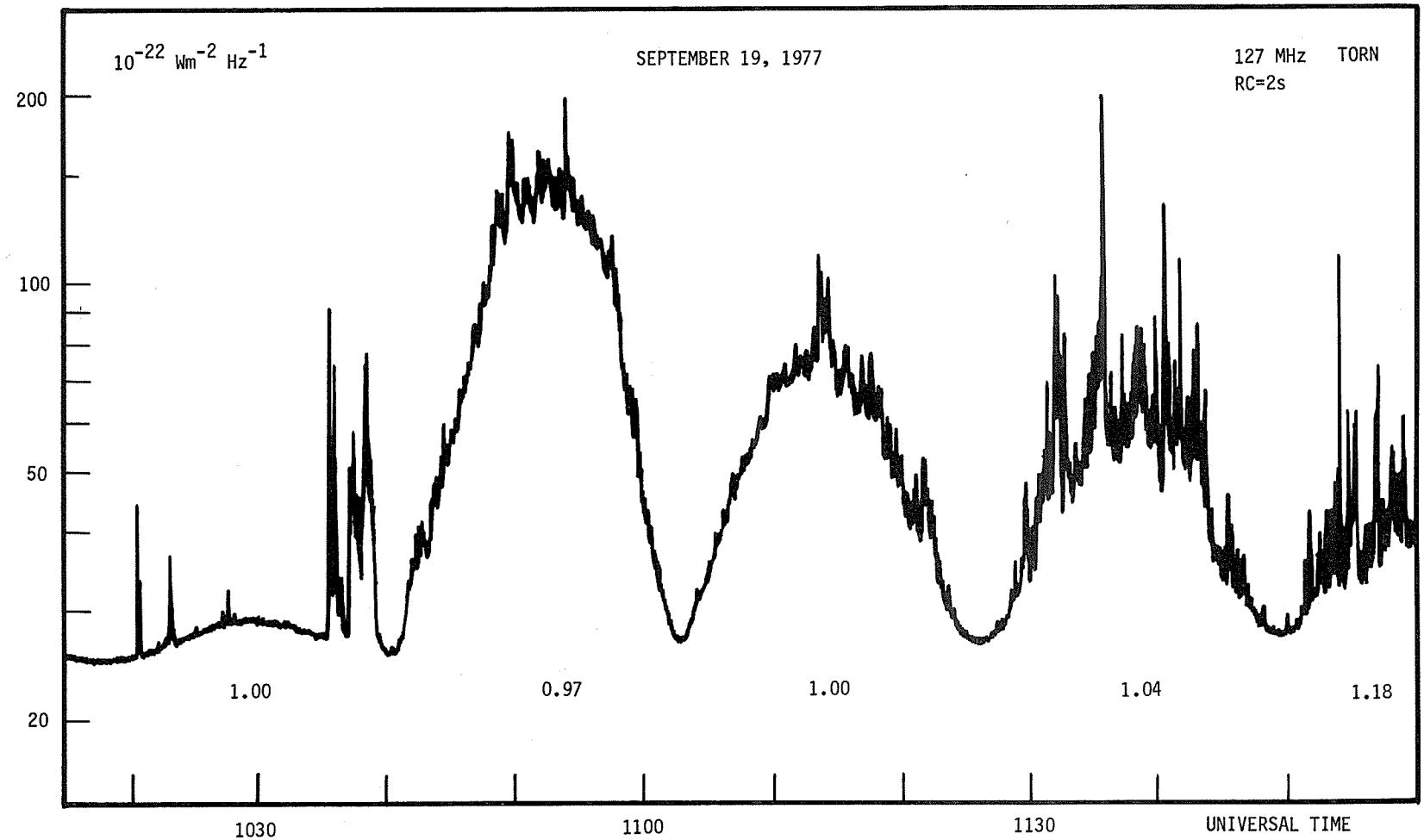

Fig. 2. Interferometric record of solar flux at 127 MHz on Sept. 19, 1977. The numerical values below the fringe maxima are weighting factors to be applied to the ordinate scale. The record was made with the integrating time constant RC=2s and high frequency bandwidth of 230 kHz.

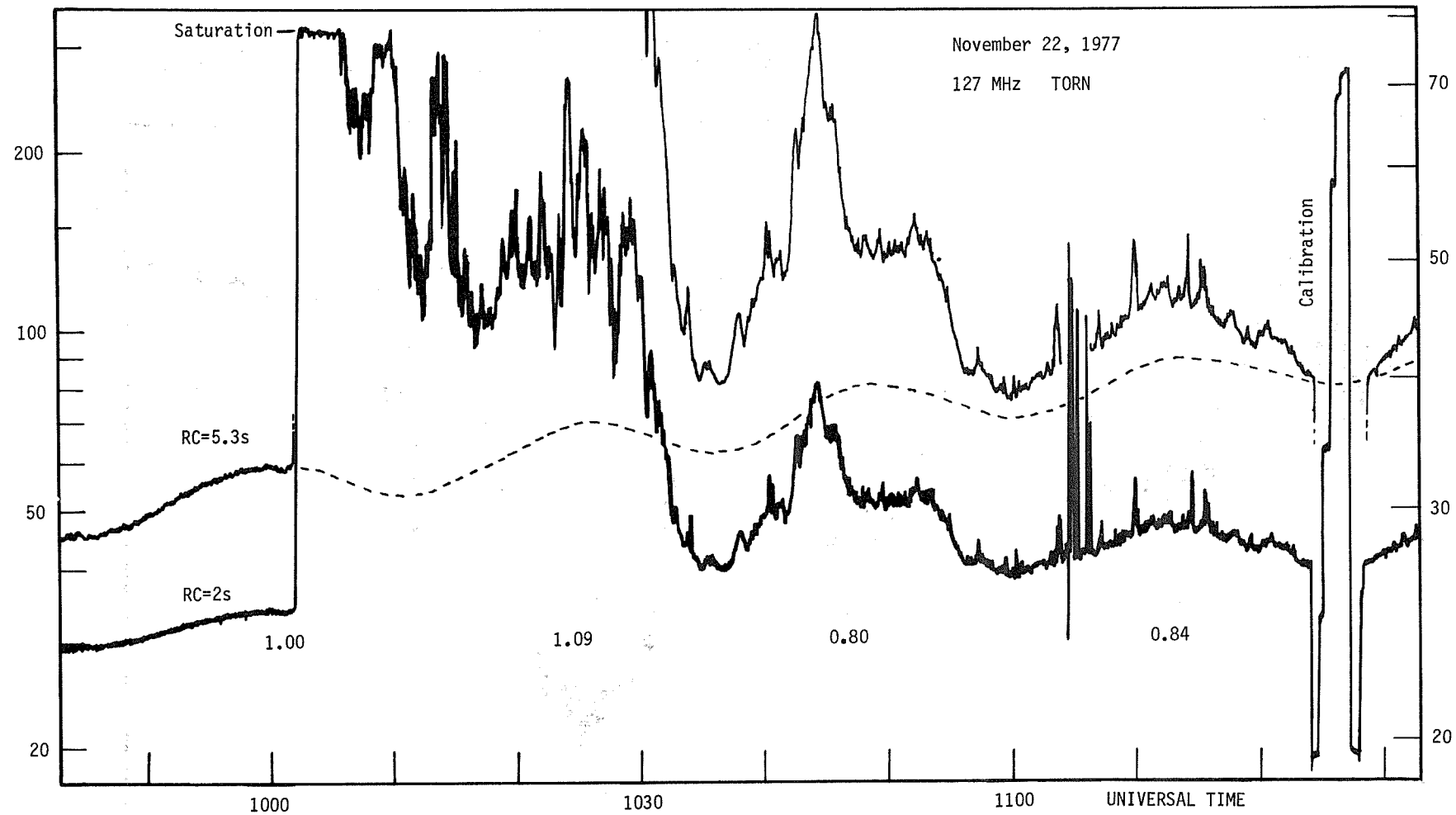

Fig. 3. Stacked interferometric records of the great burst observed on Nov. 22, 1977. The leftside flux scale refers to the lower record and the rightside scale to the upper, which was made with the higher sensitivity, RC=5.3s, and amplitude resolution. The dashed line shows an approximate level of a quiet Sun plus background flux for the upper curve, reconstructed based upon the respective part of the record of Nov. 23, 1977.

REFERENCES

BORKOWSKI, K. M. 1978 Thesis (in preparation).

BORKOWSKI, K. M., S. GORGOLEWSKI, and J. USOWICZ 1975 Interferometer for Observation of the Sun at 127 MHz, *Postepy Astronomii, 23,* 141-151 (in Polish).

SGD 1977 *Solar-Geophysical Data,* 399 Part I, 102-112, November 1977, U.S. Department of Commerce, Boulder, Colorado, U.S.A. 80303.

SGD 1978 *Solar-Geophysical Data,* 403 Part II, 22-41, March 1978, U.S. Department of Commerce, Boulder, Colorado, U.S.A. 80303.

Some Aspects of the Continuous Radio Emission of the Solar Events of September 19 and November 22, 1977

by

H. Aurass, A. Böhme and A. Krüger
Akademie der Wissenschaften der DDR Zentralinstitut für solar-terrestrische Physik
(Heinrich-Hertz-Institut)
DDR-1199 Berlin-Adlershof

Introduction

This report summarizes the observations of two solar Type IV radio bursts derived from the program of single-frequency total-flux and polarization measurements carried out at the Observatory for Solar Radio Astronomy of the Heinrich-Hertz-Institut at Tremsdorf near Potsdam. The investigated events, separated by a period of only 2 months, belong to different 11-year cycles of solar activity and offer a nice opportunity to study various burst characteristics, which are displayed by means of synthetic spectral and polarization diagrams supplemented by tables summarizing the main phases and components of the burst development. Our conclusions refer mainly to the continuous part of the radio emission. A discussion of drift bursts and spectral fine structures will be omitted.

The Event of September 19, 1977

The radio event was associated with a flare (3b) in McMath Plage Region 14943 in the northwest quadrant of the Sun (N05 W57). The low latitude and magnetic structure of the related spot group indicated an active region belonging to the old cycle (No. 20) of solar activity.

The gross structure of the radio burst and main components are visible in the spectral diagram of Figure 1 and outlined in Table 1. The observing frequencies used are marked by horizontal lines in the spectral and polarization diagrams.

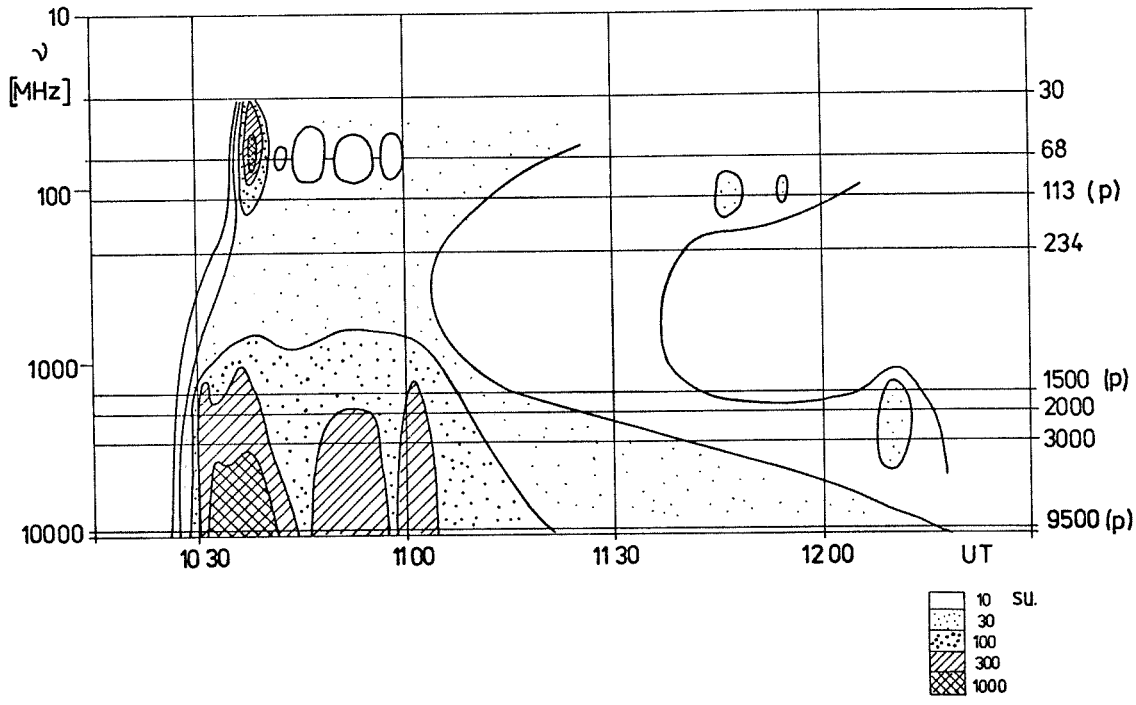

Fig. 1. Spectral diagram of the September 19, 1977, Type IV burst.

Table 1. Main Phenomena of the Radio Event of September 19, 1977

No.	Phase	Start (UT)	Observed Range (MHz)	Type	Remarks
1	Gradual	0900	3000	Preflare	
		1022	9500	Preflare	Superposed fluctuations of polarization?
2	Impulsive	1027	9500-1500	μ burst	
3	Explosive	1028	1500	IVdm	Fluctuations
		1030	9500-1500	IVμ1	Spectral maximum at $\gtrsim$ 9.5 GHz.
		1031 -1035	234-30	(II,III); IVm(A,B?)	Relatively weak emission.
		1045	9500-1500	IVμ2	Maximum ~ 3 GHz
4	Recovery	1115	Whole range	(μ, IVmB?)	

In spite of its proton efficiency, the radio part of the event of September 19, 1977, was comparatively weak, especially in the meter wavelength region. More than 1 hour before the onset of the impulsive phase, a gradual increase in the microwave flux can be noted. At 1022 UT, i.e., about 5 min before the impulsive onset, fluctuations in polarization appear weakly at 9.5 GHz. They are, however, not clearly expressed in the whole-Sun flux density. The most extended, stronger parts of the whole radio event are found in the microwave region where the burst exhibits a very complex morphology. At least two phases may be distinguished: the first lasting from about 1030 to 1045 UT and the second from 1045 to 1115 UT. The first phase comprises the main impulsive and explosive burst components and is characterized by both high intensity in the short cm range and (right-hand polarized) fluctuations in the short dm range. Different peaks show different spectral flux maxima, referring to different particle energies, locations and magnetic fields. The polarization is weak (right-hand) at 9.5 GHz, corresponding to the normal appearance of microwave emission from the northwest quadrant of the Sun during Solar Cycle No. 20 (see Figure 2). At 1.5 GHz the circular polarization shows reversals in time and

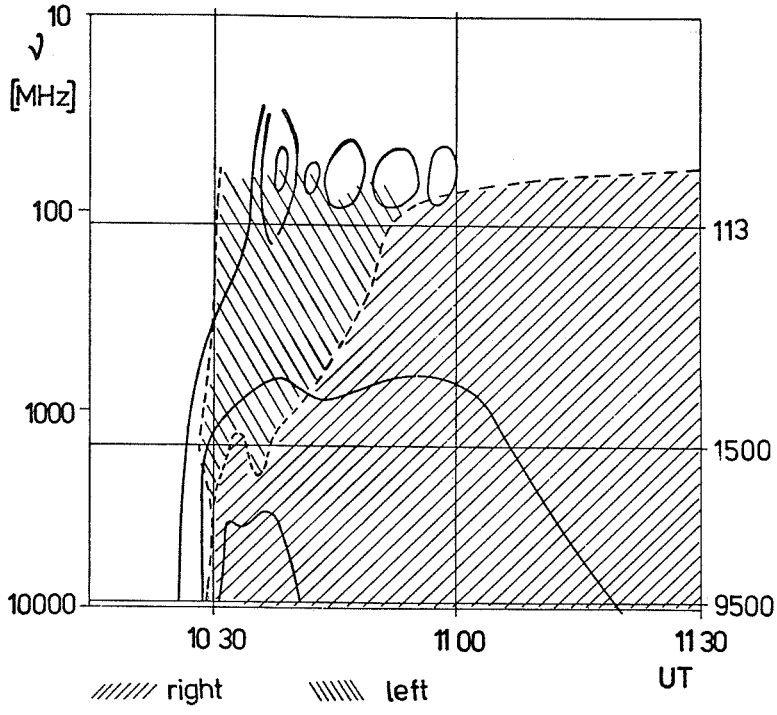

Fig. 2. Circular polarization diagram of the September 19, 1977 Type IV burst. Hatch marks inclined to the right indicate right-hand polarization; those inclined to the left indicate left-hand polarization.

frequency, as is frequently observed in this region, indicating a complex source structure. The reversal of the polarization from right to left probably corresponds to an increase in the effective source height during the lifetime of the event [Krüger, 1976].

In the meter range, the Type IV burst is only weakly developed. Therefore a classification (e.g., distinction between Type IVmA and IVmB components) is difficult to achieve. Noise storm activity is missing (probably because of the source distance from the central meridian). Characteristic flux spectra at 1038 UT during the maximum of the explosive phase are shown in Figure 3. For the main phenomena of the event refer to the compilation of Table 1.

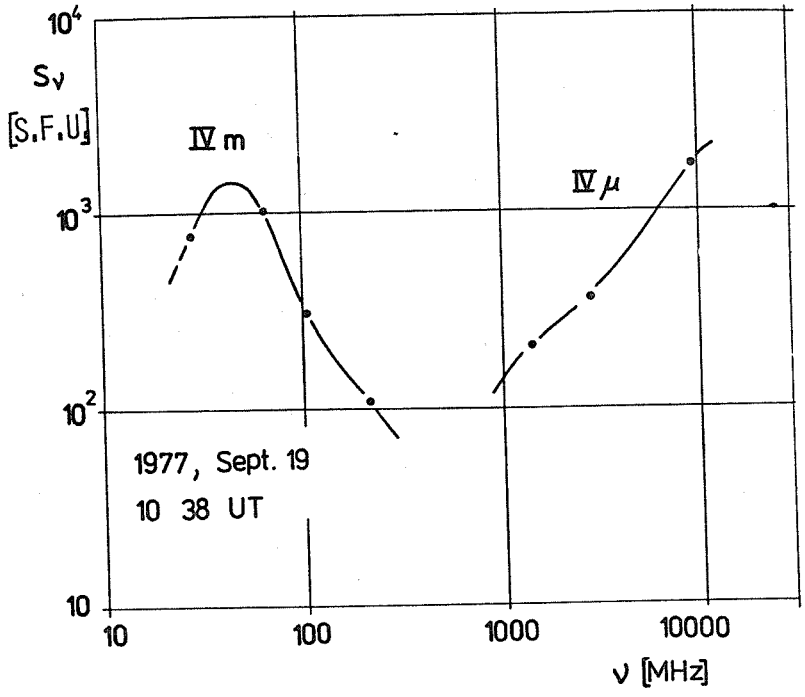

Fig. 3. Characteristic flux spectra at 1038 UT during the maximum of the explosive phase of the September 19, 1977 Type IV burst.

The Event of November 22, 1977

The corresponding flare position was about N23 W40 in McMath Plage Region 15031, indicating activity from the new solar cycle No. 21. The main radio features are outlined below.

Following a short precursor of about 10 min duration, the impulsive and explosive phases (separated by different gradients of the time profile of flux and polarization at a fixed frequency) began suddenly, as demonstrated in Figure 4 and Table 2. Temporal shifts of the maximum peak flux at different microwave frequencies are to be noted. As typical for strong solar events, second and third parts of the Type IVμ/dm burst component followed with a characteristic time scale of about 15 to 20 min. On the average the later parts exhibit a softer spectrum than the earlier parts.

The circular polarization was comparatively strong and left-handed at 9.5 GHz and reversed (preferably right-handed) at 1.5 GHz, as is usual for a source located in the northwest quadrant of the Sun in an odd-numbered 11-year cycle (cf., Figure 5). Decimetric fluctuations are strongly developed in the second part of the event, which peaked at about 1033 UT.

Almost simultaneously with the onset of the explosive phase in the microwave region, a strong emission at meter wavelengths, classified as Type IVmA (1) [Akinyan et al., 1971] or flare continuum [Wild, 1970], can be identified. The related steep radio spectrum (Figure 6) is of high interest and warrants a more detailed discussion.

The circular polarization was mainly right-handed at 40 and 113 MHz, whereas at 778 MHz the degree of polarization was almost zero. Subsequent Type IVmB and continuum storm components only developed weakly.

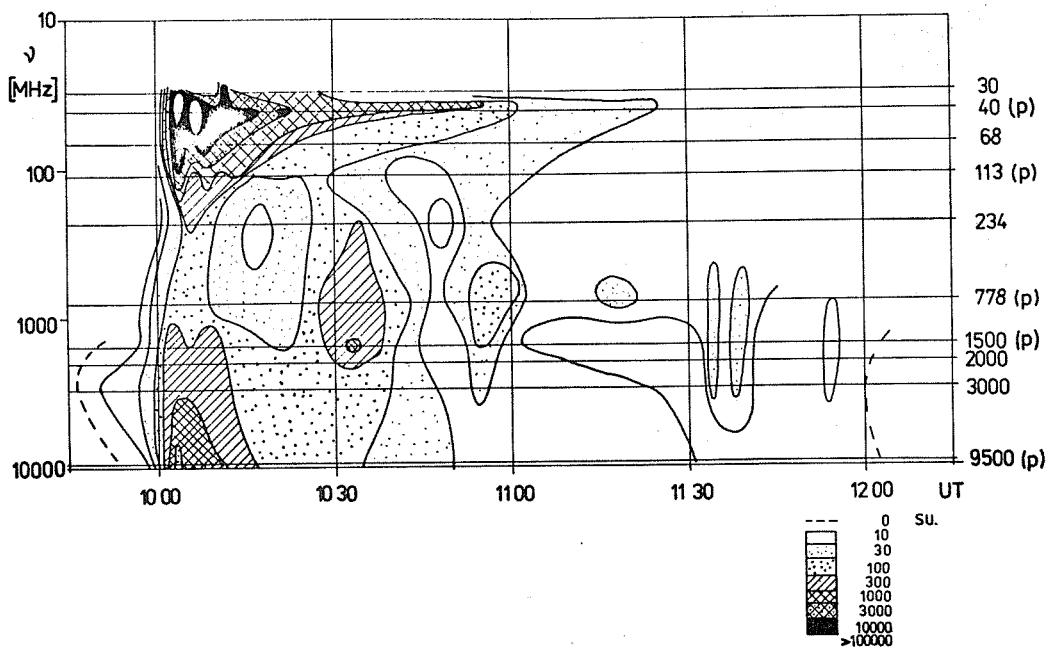

Fig. 4. Spectral diagram of the November 22, 1977 Type IV burst.

Table 2. Main Phenomena of the Radio Event of November 22, 1977

No.	Phase	Start (UT)	Observed Range (MHz)	Component	Remarks
1	Precursor	0947	3000-1500	μ burst	
2	Impulsive	0958	9500- 778	μ burst	
3	Explosive	1001	9500- 778	IVμ(1)	Spectral maximum at 9.5 GHz
			234- 40	(III,II2)IVmA	"Flare continuum."
		1022.5	9500- 778	(IVμ2)IVdm	Short dm fluctuations.
		1050	3000- 778	(IVμ3/dm)	Weak pulse.
4	Recovery	1100	Whole range	(μ, IVmB?)	

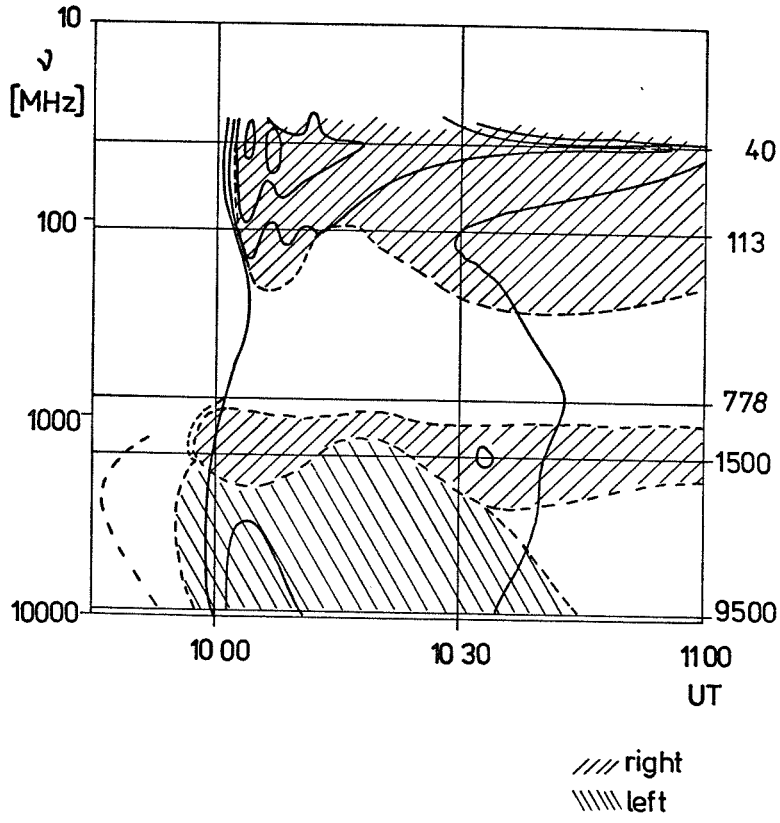

Fig. 5. Circular polarization diagram of the November 22, 1977 Type IV burst. Hatch marks inclined to the right indicate right-hand polarization; those inclined to the left indicate left-hand polarization.

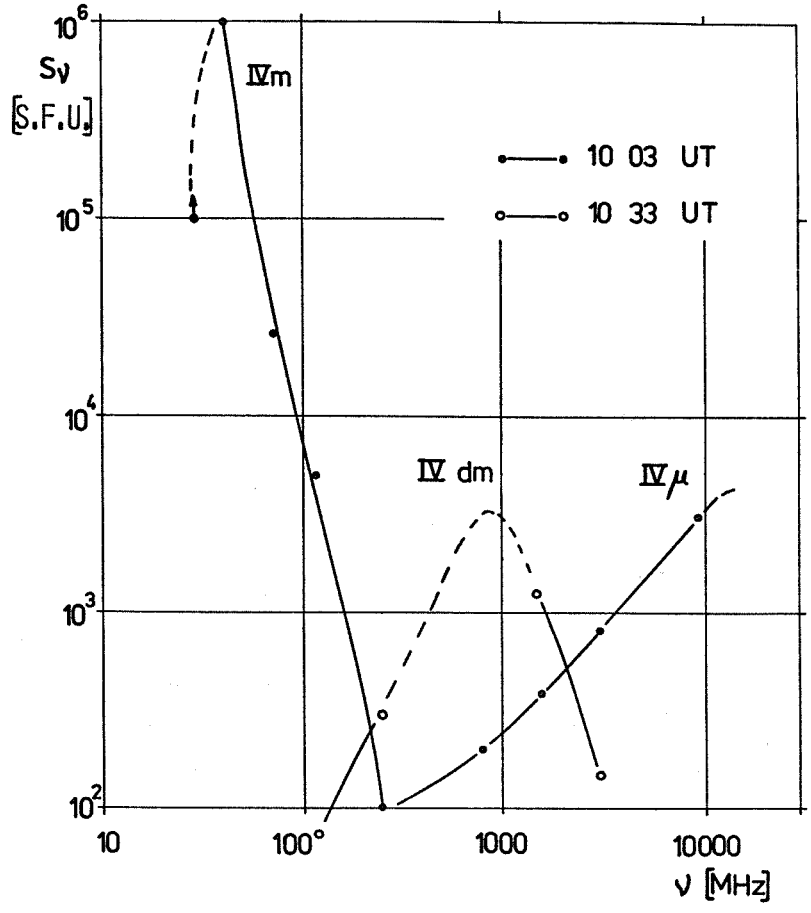

Fig. 6. Characteristic flux spectra at 1003 and 1033 UT during the explosive and maximum phase of the November 22, 1977 Type IV burst.

Conclusions

Apart from the general tendencies of the development of large burst events associated with proton flares (e.g., occurrence of the combination of Type IV and Type IVmA components), both bursts discussed here exhibit a number of minor differences and similarities. Differences concern the solar cycle number and the particular time-frequency pattern of single phases both in total flux and in polarization. Similarities are due to the position in the northeast quadrant of the Sun, the occurrence of dm fluctuations, the weak appearance of Type IVmB and noise storm components, and the generally complex source structure. As is evident from both events, the dm fluctuations can occur at different stages of the event and are not necessarily related to the first or second part of the explosive phase of radio emission.

REFERENCES

AKINYAN, S.T., E.I. MOGILEVSKY, A. BÖHME and A. KRÜGER — 1971 — Spectral features of large type IV bursts and interrelation to solar-terrestrial phenomena, *Solar Phys., 20,* 112-121.

KRÜGER, A. — 1976 — A study of circular polarization of solar microwave burst emission, *Phys. Solariterr., Potsdam, 1,* 7-16. (In German)

WILD, J.P. — 1970 — Some investigations of the solar corona: The first two years of observation with the Culgoora radioheliograph, *Proc. Astron. Soc. Australia, 1,* 365-370.

3. SPACE OBSERVATIONS

Satellite Positions and Conjunctions: September 7-24 and November 22, 1977

by

D. M. Sawyer, R. H. Hilberg, M. J. Teague, and J. I. Vette
IMS/Satellite Situation Center
Code 601, Goddard Space Flight Center
Greenbelt, Maryland 20771 U.S.A.

Introduction

The International Magnetospheric Study/Satellite Situation Center (IMS/SSC) has developed a variety of techniques for displaying the positions and orbital characteristics of satellites performing measurements related to magnetospheric physics. This service involves both predicted and achieved positions of many geocentric satellites, as well as heliocentric satellites orbiting within 1 AU. With the extension of these techniques to other heliocentric satellites, similar services can be provided to scientists studying interplanetary phenomena. Some of these techniques are shown here, giving a brief picture of the satellite positions during the intervals September 7-24 and November 22, 1977. Further details regarding the SSC and its services can be found in *Sugiura and Vette* (1977) or directly from the SSC.

High-Altitude Geocentric Satellites

The positions of a number of high-altitude geocentric satellites (those with apogees above 12 R_E) have been displayed in a number of coordinate systems related to the study of the magnetosphere. Emphasis has been placed on times when they enter the magnetopause, the bow shock, the geomagnetic tail near the neutral sheet, and the cusp. One concise representation is a daily bar chart giving a semi-quantitative picture of each satellite's location, including boundary crossings, and the region of space the satellite is traversing. An example of this type of display is given in Figure 1 for November 22, 1977. Similar charts, using the IMS standard time axis of 1 cm/h have been published in IMS/SSC Report No. 7 (1976) and IMS/SSC Report No. 10 (1977), which contain charts for the high-altitude satellites for 1977.

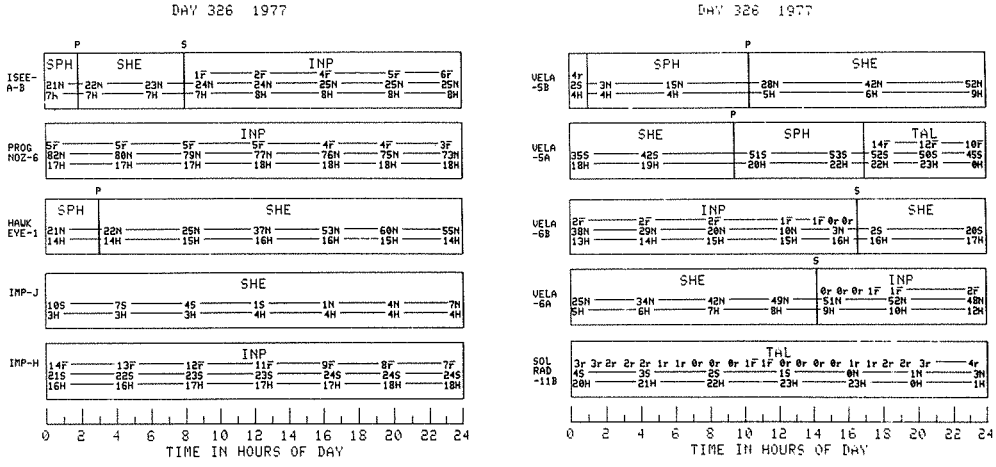

Fig. 1. Bar chart giving positions of 10 satellites for day 326, 1977 (November 22, 1977). This chart indicates the region of space for each satellite and denotes when the satellites cross the magnetopause (P) or the bow shock (S). Local time and latitude are given for each satellite. When a satellite is interplanetary, the distance from the bow shock in Earth radii is given. When a satellite is in the tail, the distance from the neutral sheet is given. For full details, see IMS/SSC Report No. 10.

A more condensed form of bar chart is given in Figure 2, which shows the regions traversed by nine satellites during the period September 7-24, 1977. In this display, the bow shock is denoted by an S and the magnetopause by a P. The numbers above the symbols give the hour of day of the model magnetopause crossings; the numbers below the symbols model bow shock crossing times. Times of bow shock crossings of the Vela satellites are not shown because data acquisition is now generally confined to the magnetotail. On this scale, it is not possible to label each region or to provide the other parameters given in Figure 1. The region of space being traversed by each satellite is identified by the line in the center of its bar: a solid line represents the interplanetary medium, a dotted line the magnetosheath, and a dashed line the magnetosphere. When the complete period between two magnetopause crossings is in the magnetotail the symbol, TAL, is given. If a satellite comes within 2 R_E of the nominal position of the neutral sheet, an asterisk identifies this period. The times of neutral sheet encounters are listed in Table 1.

Table 1. Neutral Sheet Passes, Days 250-267 and 326 (September 7-24 and November 22, 1977)

Satellite	Date	Entry Time DOY/h	Exit Time DOY/h
Vela 6B	Sept. 9	252/1.0	252/3.4
Solrad 11B	11	254/7.0	254/23.8
Vela 6A	15	258/1.0	258/1.7
Solrad 11B	16	259/18.4	260/0.4
Solrad 11B	21	264/20.1	265/1.1
Solrad 11B	Nov. 22	326/3.3	326/18.4

Low- and Medium-Altitude Geocentric Satellites

There are 19 active low- and medium-altitude satellites that carry experiments useful for obtaining magnetospheric data. The orbit characteristics of these satellites are given in Table 2. Satellites that are known not to be collecting data during this period have been excluded from this list. The experiments carried on these spacecraft are listed in IMS/SSC Report No. 9 (1977). The most useful way to concisely present the orbital positions of these satellites is the bar chart illustrated in Figure 3. This bar chart covers the period 0900-1030 on September 21, 1977 for eight low-altitude satellites, three geostationary satellites, and ESA/GEOS. The coordinates are geocentric solar magnetic with the top line of each satellite showing radial distance, the middle line giving latitude, and the bottom line giving the magnetic local time. The local time values are quantized into bins of 1-h duration for the near-polar orbiting satellites with the bin boundaries chosen to emphasize passes along a magnetic meridian. Magnetic equator crossings are indicated by an asterisk. The symbol m following the R denotes the maximum or minimum value, while the same symbol following an N or S denotes the maximum geomagnetic latitude the satellite attains on that particular revolution. The decimal point is positioned at the time of the indicated variable. In the space above each satellite, the symbols have the following meanings:

1. Above ESA/GEOS, the coordinated numbers give the time when the numbered satellite is on the same magnetic flux tube as ESA/GEOS. For the other satellites, the letter G symbolizes the magnetic conjunction with ESA/GEOS.
2. W. denotes entry into the plasmasphere.
3. .W denotes exit from the plasmasphere.
4. ------ denotes traversing the plasmasphere.
5. C denotes passage of 5 min or more through the cusp.

Table 2. Orbital Characteristics For Low- and Medium-Altitude Satellites

Satellite Name	Epoch (DD/MM/YY)	Period (min)	Incl (deg)	Perigee (km alt)	Apogee (km alt)	Longitude (deg E)
AE-C	09/07/77	92.4	68.0	385	399	
AE-E	06/07/77	90.2	19.6	281	284	
ATS 5	07/09/77	1436.0	4.3	35779	35789	-69.5
ATS 6	14/09/77	1436.3	0.9	35773	35808	-139.9
Cosmos 900	30/03/77	94.4	83.0	460	523	
DMSP-F1	31/08/77	101.5	98.6	819	846	
DMSP-F2	31/08/77	101.5	99.1	801	868	
GEOS 1 (ESA)	31/08/77	718.2	26.5	2046	38330	37.3/-142.7
GMS	31/08/77	1436.2	1.1	35771	35804	139.6
GOES 2	22/08/77	1436.2	0.7	35787	35790	-74.7
ISIS 1	31/08/77	128.2	88.4	577	3518	
ISIS 2	31/08/77	113.6	88.1	1358	1428	
NOAA 4	31/08/77	114.9	101.5	1447	1461	
NOAA 5	31/08/77	116.2	102.0	1507	1522	
SMS 2	31/08/77	1436.2	0.0	35777	35801	-135.1
Solrad 10	31/08/77	94.5	51.0	421	568	
S3-2	31/08/77	97.5	96.2	223	1061	
S3-3	31/08/77	176.1	97.5	234	7829	
TIP 1	31/08/77	100.6	90.0	738	840	

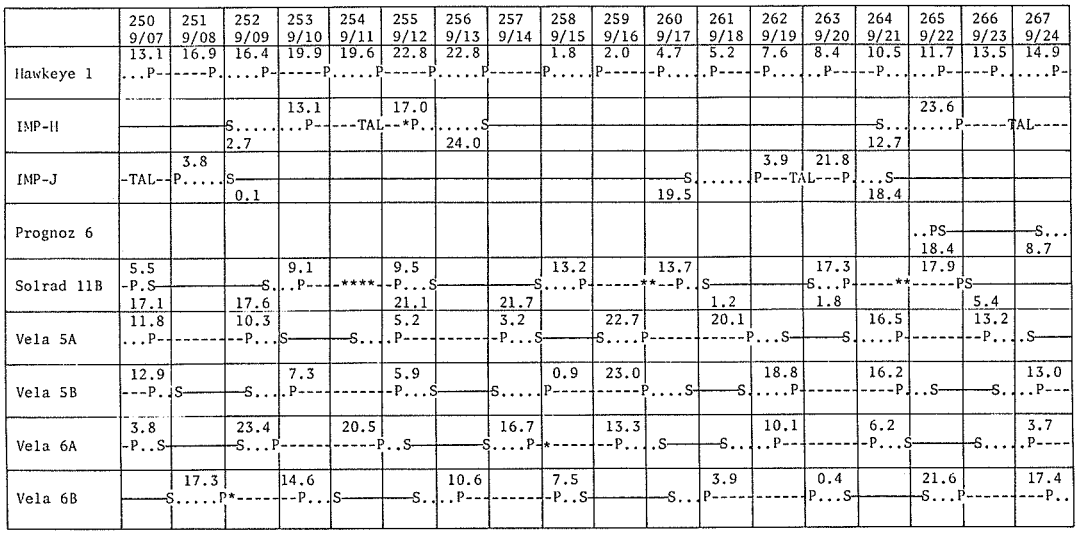

Fig. 2. Bar chart showing locations of nine satellites during September 7-24, 1977. Solid, dashed, and dotted lines represent the interplanetary medium, the magnetosphere, and the magnetosheath regions, respectively. Numbers above these lines give the hour of day of magnetopause crossings, identified by a P. Numbers below these lines give the hour of day of bow shock crossings, identified by an S.

Table 3. Conjunctions of Heliocentric Satellites and Earth During the Interval September 7-24 and November 22, 1977

Satellite Name	Day 253 9/10 Long. (deg)	Corotation Delay (days)	Radial Distance (AU)	Day 261 9/18 Long. (deg)	Corotation Delay (days)	Radial Distance (AU)	Day 266 9/23 Long. (deg)	Corotation Delay (days)	Radial Distance (AU)	Day 326 11/22 Long. (deg)	Corotation Delay (days)	Radial Distance (AU)
Helios 1	136.2	8.99	0.743	139.3	8.86	0.662	142.9	8.86	0.605	319.9	-4.63	0.649
Helios 2	163.6	11.30	0.797	165.0	11.06	0.724	166.9	10.96	0.671	351.0	-2.56	0.592
Pioneer 6	25.5	1.53	0.919	26.4	1.66	0.932	26.8	1.72	0.939	26.4	1.90	0.983
Pioneer 8	163.7	12.38	1.028	163.4	12.39	1.035	163.2	12.39	1.039	157.0	12.11	1.079
Pioneer 9	14.9	0.86	0.946	15.1	0.94	0.960	15.1	0.98	0.967	11.8	0.78	0.977
Pioneer 11	146.5	5.91	5.712	139.3	5.56	5.753	134.8	5.34	5.778	79.2	2.61	6.086
Voyager 1	1.5	0.16	1.011	3.9	0.42	1.028	5.2	0.60	1.045	358.1	2.25	1.515
Voyager 2	6.3	0.54	1.016	8.3	0.81	1.041	9.2	0.98	1.063	359.1	2.39	1.530
Remarks	Radial Alignment of Helios 2 and Pioneer 8 (within 0.2° 9/7-9/12)			Radial Alignment of Helios 1 and Pioneer 11			IMF Alignment of Pioneer 9 and Voyager 2			Radial Alignment of Earth, Voyager 1, and Voyager 2 (within 1°)		

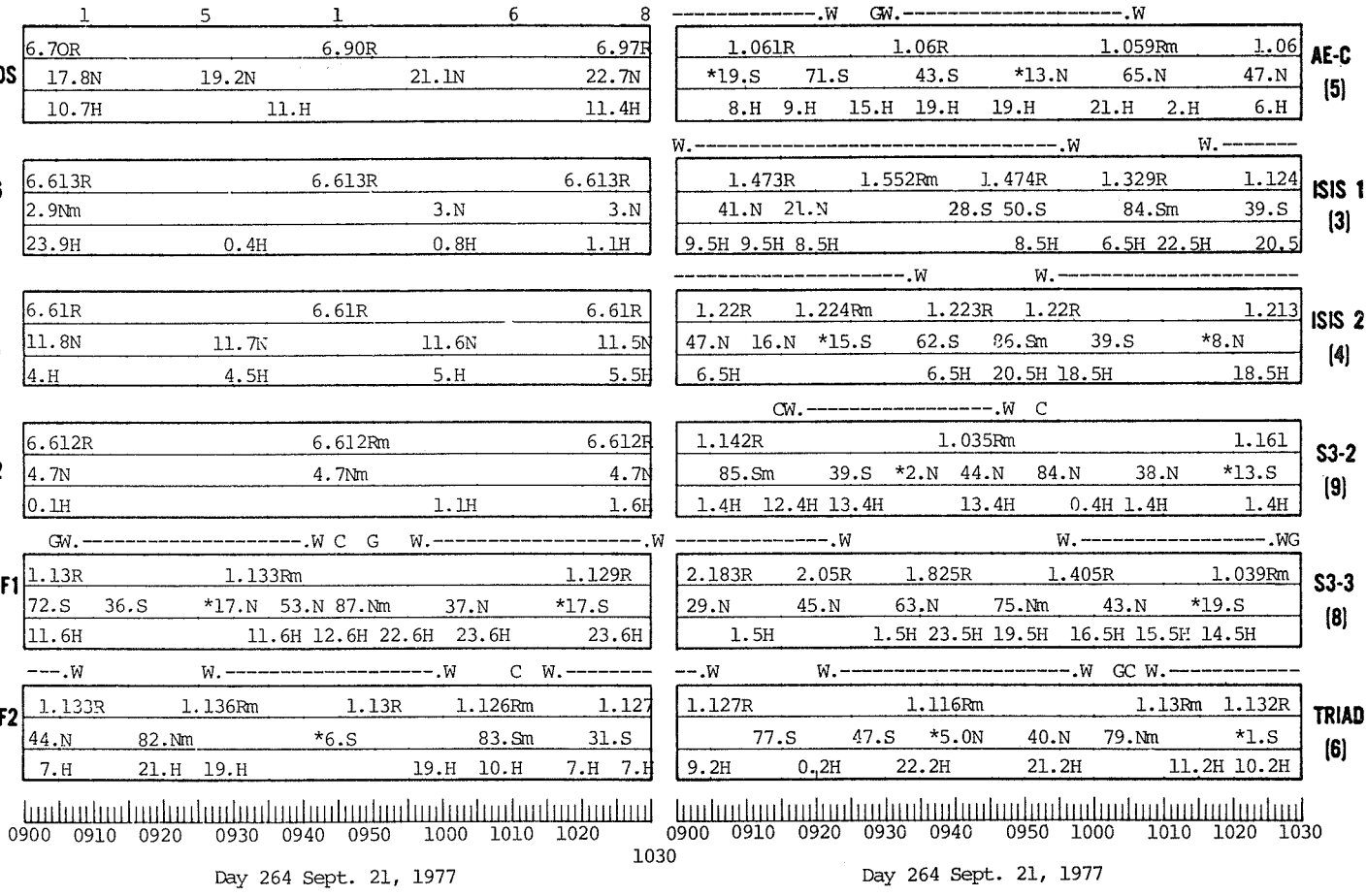

Fig. 3. Bar chart displaying 12 low-altitude satellites for a 90-min period on day 264. The numbers above the ESA-GEOS bar represent conjunction times with the seven low-altitude satellites, and the G represents the times of conjunctions with ESA-GEOS. W. represents entry into the plasmasphere, and .W represents exit from the plasmasphere. A cusp crossing is marked with a C. The top line of data is radial distance, the middle line is latitude with an * marking equatorial crossing times, and the bottom line of data gives local time. An m following N, S, or R represents a minimum or maximum.

Heliocentric Satellites

The positions of eight artificial heliocentric satellites are shown in Figure 4. Radial position projected onto the ecliptic plane is shown as a function of longitude measured with respect to the Earth during the interval September 7 through November 22, 1977. Pioneer 7 is not shown because it was turned off on February 10, 1976, and Pioneer 10 was too far from the Sun to be conveniently shown on this scale. Model corotation delay time curves are shown for a 400 km/s solar wind velocity.

Potentially interesting conjunctions among these satellites are listed in Table 3. On September 10, Helios 2 and Pioneer 8 were radially aligned. Because of their slow relative azimuthal motion, this alignment held approximately for several days. On September 18, Helios 1 and Pioneer 11 were radially aligned. On September 23, Pioneer 9 and Voyager 2 were on the same interplanetary magnetic field line. Finally, on November 11, Voyager 1 and 2 and the Earth were within 1° of radial alignment. Another characteristic of the relative positions of these spacecraft is the azimuthal coverage provided during the September interval. One group is spread over the range 0° to 28° longitude, while the other group is spread over the range 133° to 169° longitude. These distributions could be very useful in determining the azimuthal extent of the interplanetary disturbances. It should be noted that during this whole interval, IMP-H or IMP-J provided continuous interplanetary coverage in the near Earth region except during 6 h on September 21.

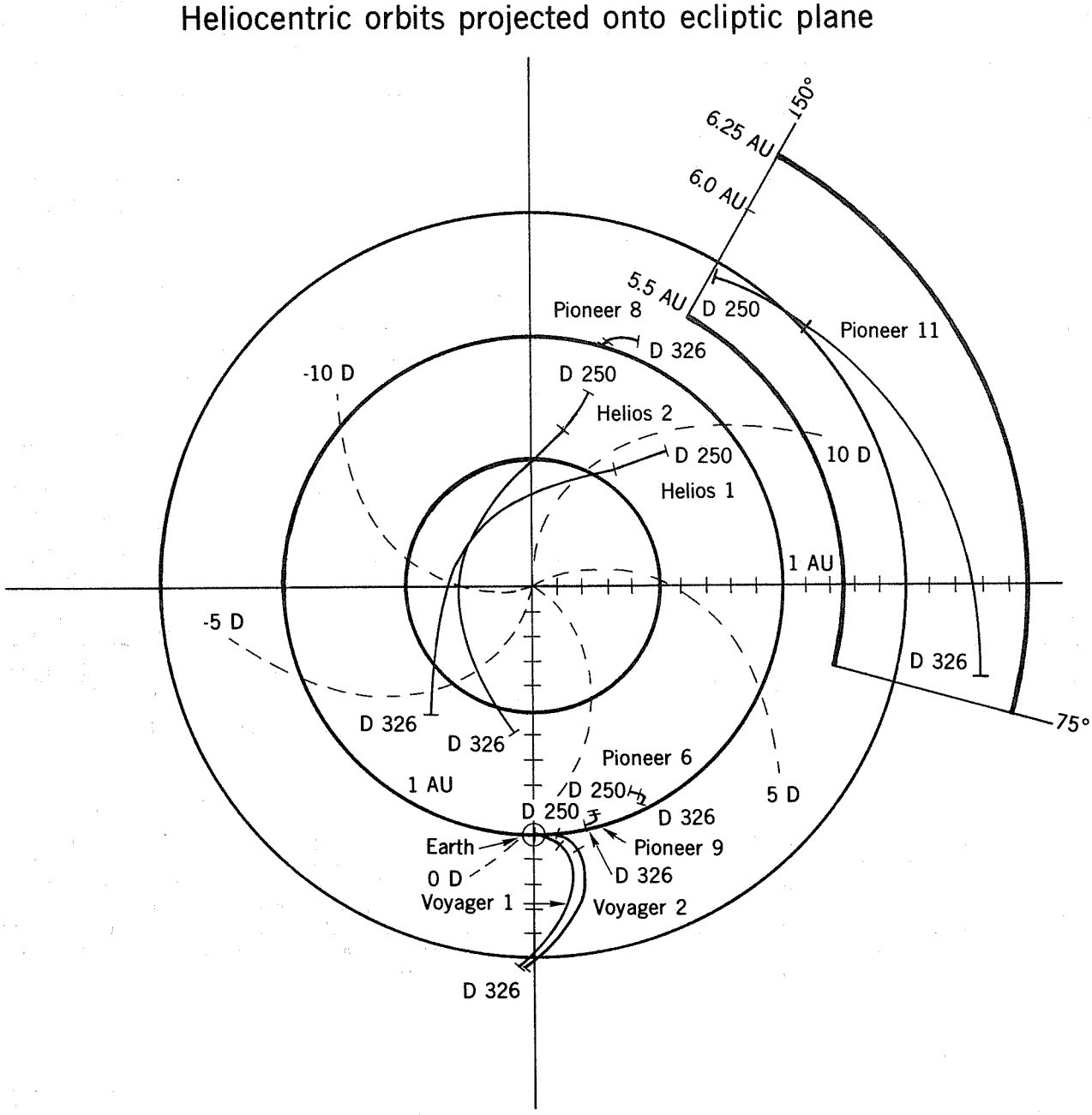

Fig. 4. Heliocentric orbits projected onto the ecliptic plane. Radial distance (in AU) is plotted as a function of longitude relative to the Earth. The dashed curves give corotation times in days.

Concluding Remarks

The approximate locations of 37 satellites during the period September 7-24 and November 22, 1977 have been shown. Four potentially interesting heliocentric alignments have been identified. Those desiring more details regarding these positions should contact the IMS/Satellite Situation Center.

REFERENCES

SUGIURA, M., and J. I. VETTE	1977	"The IMS Satellite Situation Center", *Trans. AGU, 58,* 70-74.
IMS/SSC Report No. 7	1976	Daily Summary for IMS High-Altitude Satellites, Days 1-181 1977 (October 1976), WDC-A, National Space Science Data Center, (GSFC, Greenbelt, MD 20771 U.S.A.).
IMS/SSC Report No. 9	1977	IMS Directory of Spacecraft and Experiment Scientific Contacts (January 1977), WDC-A, National Space Science Data Center, (GSFC, Greenbelt, MD 20771 U.S.A.).
IMS/SSC Report No. 10	1977	Daily Summary for IMS High-Altitude Satellites, Days 182-365 1977 (August 1977), WDC-A, National Space Science Data Center, (GSFC, Greenbelt, MD 20771 U.S.A.).

Pioneer 11 Observations of September-October 1977 Solar Particle Events at 5.8 AU

by

J. A. Van Allen
Department of Physics and Astronomy
The University of Iowa
Iowa City, Iowa 52242, USA

Observations

One-hour averaged counting rates of detectors G, A, and C of the University of Iowa instrument on Pioneer 11 are shown as a function of time in Figure 1 for the period 12 September -- 11 October 1977. At the mid-time of that period the heliocentric polar coordinates of the spacecraft were r = 5.80 AU, Φ = 135°, and Θ = 80°, referenced to the equinox and north ecliptic pole. The two events shown in Figure 1 are quite distinctive in our data, being the most intense since the event of 30 March 1976. Because of the isolation of these major interplanetary events, it seems safe to attribute them to the major solar flare activity of mid-September [Solar-Geophysical Data 1977, 1978]. The approximate times of distinctive discontinuities in the counting rates of G and A are marked and labeled in Figure 1 with hour and date of occurrence. In the absence of solar wind and magnetic field data at Pioneer 11, as of the date of writing, no detailed interpretation of these features can be given.

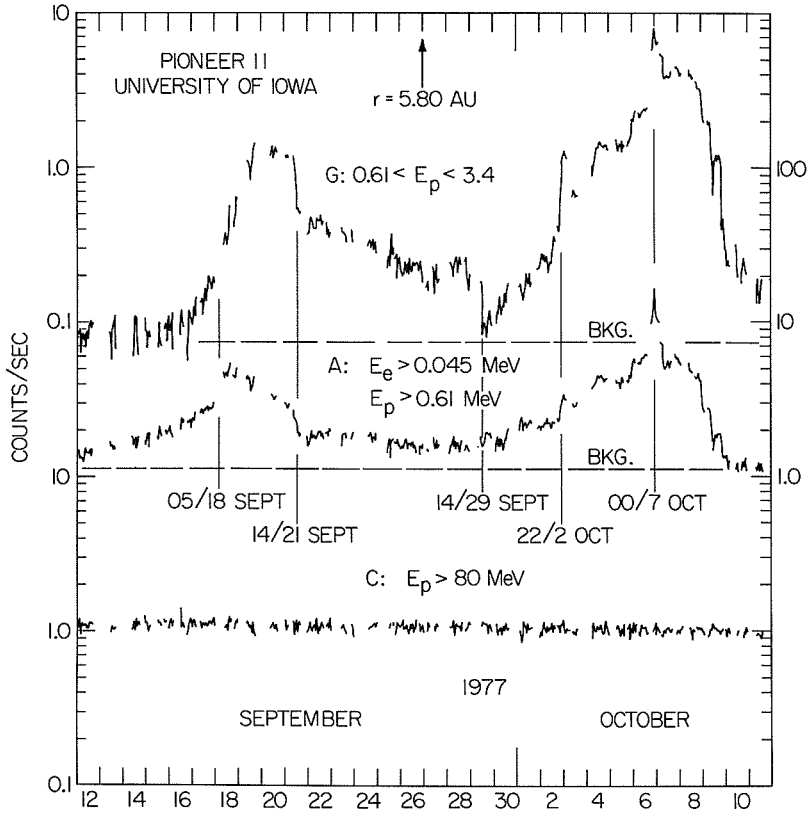

Fig. 1. Counting rates of detectors G, A, and C on the University of Iowa instrument on Pioneer 11, September 12 to October 11, 1977.

Detectors and Nature of the Data

Detector G is a thin (29 μm), single element, totally depleted silicon detector with an effective area of 0.12 cm^2 and a reciprocal unidirectional geometric factor of 24.7 $(cm^2\ sr)^{-1}$. [See Pesses et al., 1978 for further instrumental details.] The axis of its conical collimator is perpendicular to the rotational axis of the spacecraft which is kept pointed continuously at the earth to within 1° and therefore lies approximately in the ecliptic plane. Hence, the "spin plane" of the detector's axis is nearly perpendicular to the spacecraft-sun line. During the period of interest the rotational period of the spacecraft was 7.759 seconds. When the interplanetary magnetic vector $\vec{B}$ lies along the nominal

archimedean spiral (Figure 2) the detector's axis scans nearly the full range of pitch angles α. Detector G responds to protons $0.61 \leq E_p \leq 3.41$ MeV, alpha particles $0.23 \leq E_\alpha \leq 16.8$ MeV/nucleon, and heavier ions in corresponding energy ranges; but it is quite insensitive to electrons of any energy. If the response of the detector is attributed entirely to protons, the unidirectional intensity j in the above energy range is given in $(cm^2\ s\ sr)^{-1}$ by

$$j = 24.7\ (G - 0.074)\ . \qquad (1)$$

In (1), G is the counting rate in counts s^{-1} and the subtractive correction is the mean rate caused by an in-flight calibration source of Am^{241} as determined during the quiet periods 21 August -- 4 September and 16 October -- 5 November 1977.

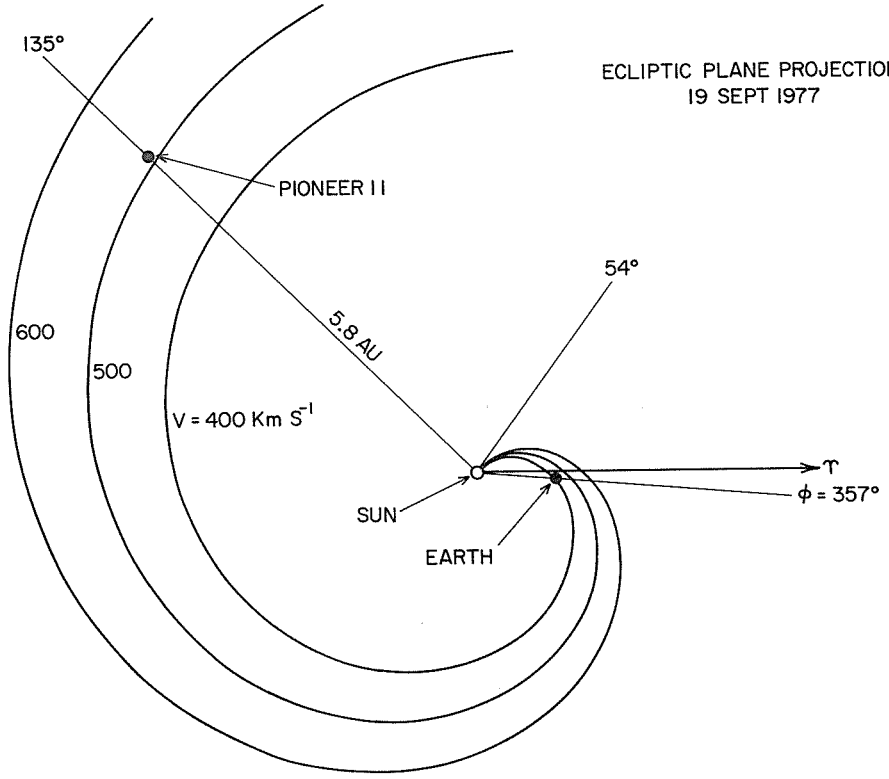

Fig. 2. Ecliptic plane projection for Sept. 19, 1977, showing Pioneer 11's position along the nominal archimedean spiral of the solar wind for particle stream speeds of 400, 500 and 600 km s^{-1}.

Detector A is a thin window Geiger tube with the axis of its physical collimator parallel to that of G. Its reciprocal unidirectional geometric factors are 50.8 and 58.9 $(cm^2\ sr)^{-1}$ for protons and electrons, respectively. It responds to protons $E_p > 0.61$ MeV (and heavier ions) and to electrons $E_e > 0.045$ MeV.

For pure proton irradiation, the integral unidirectional intensity for $E_p > 0.61$ MeV is given in $(cm^2\ s\ sr)^{-1}$ by

$$j = 50.8\ (A - 1.125)\ . \qquad (2)$$

In (2), A denotes the counting rate in counts s^{-1} and the subtractive correction is the mean counting rate during the quiet periods specified above. The omnidirectional sensitivity of detector A is similar to that of the fully shielded detector C with a threshold of $E_p = 80$ MeV and $E_e = 21$ MeV. As judged by the plot of C (lower panel of Figure 1) such higher energy particles make no significant contribution to A during the events under study.

At the intense peak near 0000 UT of 7 October, the respective maximum half-hour averaged counting rates are:

$$A = 17.5 \text{ counts } s^{-1}$$

$$G = 7.80$$

Hence $j(E_p > 0.61 \text{ MeV}) = 830 \text{ (cm}^2 \text{ s sr)}^{-1}$ if there is no contribution to A by electrons and $j(0.61 < E_p < 3.41 \text{ MeV}) = 190 \text{ (cm}^2 \text{ s sr)}^{-1}$. The apparent differential spectral index for protons (assuming no electron contribution to A) is $\gamma = 1.15$. At 1 AU, a value of γ in the range 2-3 is more common [Innanen and Van Allen, 1973]. Hence the proton spectrum in this event is either extraordinarily flat in the energy range $E_p \sim 1$ MeV or there is a significant admixture of electrons. I consider the latter possibility more likely but the generally similar time histories of the counting rates of detectors A and B favor the former. A detailed study of the respective angular distributions from G and A may resolve the ambiguity.

The remainder of the discussion deals only with the unambiguous data from detector G.

Some Details of the Observations

The most distinctive feature of the University of Iowa observations is the brief intense peak at about 2330 UT on 6 October (labeled 00/7 OCT in Figure 1). This peak is tentatively identified with the solar flare of importance 3B from McMath Plage region 14943 starting at 0955 UT on 19 September at N08° W57° [Solar-Geophysical Data, 1978]. The gross geometry of the situation is shown in Figure 2, with nominal archimedean spirals for three solar wind speeds (400, 500, and 600 km s^{-1}) drawn through the flare site. There is seen to be a quite good magnetic connection between the flare, the earth, and Pioneer 11. For a solar wind speed of 500 km s^{-1}, the arc length of the archimedean spiral from the center of the sun to Pioneer 11 is 16.0 AU.

A further examination of the nature of the counting rate peak near 00/7 October is made by studying the angular distributions of protons before, during, and after the peak. In Figure 3 are shown three diagrams of the sums of anisotropy vectors (k, δ) of protons $0.61 \leq E_p \leq 3.41$ MeV derived from our half-hour averaged data fit to the first order harmonic expression:

$$j(\varphi) = M [1 + k \cos (\varphi - \delta)] . \qquad (3)$$

The roll angle φ of the detector axis is measured from the ascending node of the equatorial plane of the spacecraft on the ecliptic plane (an approximately inertial direction). Particles detected at $\varphi = 0°$ are moving counterclockwise in the ecliptic plane as viewed from the north ecliptic pole (i.e., nominally toward the sun); at $\varphi = 180°$, clockwise in the ecliptic plane (i.e., nominally away from the sun); at $\varphi = 90°$, southward; and at $\varphi = 270°$, northward. The maximum value of $j(\varphi)$ in equation (3) occurs at $\varphi = \delta$.

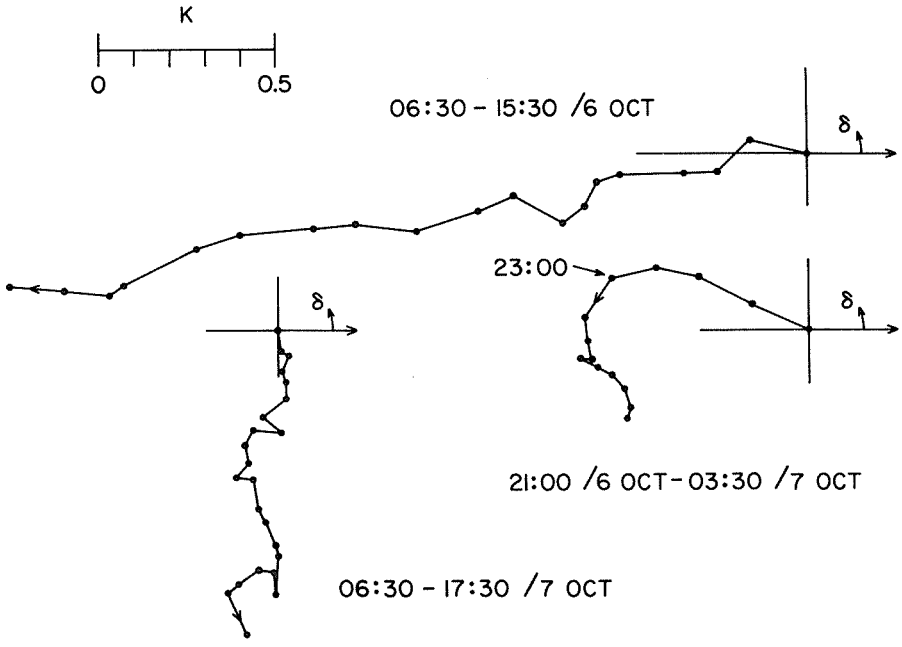

Fig. 3. Angular distribution of protons measured on detector G before, during and after the intense peak at about 2330 UT on Oct. 6, 1977. The three diagrams show the sums of anisotropy vectors (K,δ) of 0.61 to 3.41 MeV protons.

As seen in Figure 3, during the period 0630-1530 UT/6 October considerably before the major peak, there is a relatively smooth flow of protons away from the sun nearly in the ecliptic plane with a mean anisotropy vector:

$$\langle k \rangle = 0.13$$
$$\langle \delta \rangle = 190^\circ . \quad (4)$$

For the period 2100-2300 UT/6 October, immediately before the peak:

$$\langle k \rangle = 0.15$$
$$\langle \delta \rangle = 165^\circ . \quad (5)$$

A decided change in δ occurs in the half-hour following 2300 and for the period 2300 UT/6 October -- 0330 UT/7 October:

$$\langle k \rangle = 0.04$$
$$\langle \delta \rangle = 277^\circ . \quad (6)$$

This apparent northward flow of protons continues for the subsequent period 0630-1730 UT/7 October:

$$\langle k \rangle = 0.04$$
$$\langle \delta \rangle = 264^\circ . \quad (7)$$

Because of the distinctive peak in the counting rate curve of G (at 2330 UT/6 October) and the associated discontinuous change in direction and magnitude of the anisotropy vector, I tentatively identify this event with the passage of a blast wave past the spacecraft. The total time delay from the start of the 19 September flare is 17 days 13.6 hours. Assuming that the blast wave propagates hemispherically from the flare site, the apparent mean velocity over the 5.80 AU radial distance is:

$$\langle v \rangle = 570 \text{ km s}^{-1} . \quad (8)$$

The corresponding, presumptive association of the terrestrial SCC at 2044 UT/21 September implies an apparent mean velocity over 1 AU of

$$\langle v \rangle = 707 \text{ km s}^{-1} . \quad (9)$$

The tentative nature of the foregoing remarks is evident. Further work on these events will be done as more data are assembled.

Acknowledgment

This work has been supported in part by the Ames Research Center/NASA under contract NAS2-6553.

REFERENCES

INNANEN, W. G., and J. A. VAN ALLEN 1973 Anisotropies in the interplanetary intensity of solar protons $E_p > 0.3$ MeV, J. Geophys. Res., 78, 1019-1035.

PESSES, M. E., J. A. VAN ALLEN, and C. K. GOERTZ 1978 Energetic protons associated with interplanetary active regions 1-5 AU from the sun, J. Geophys. Res., 83, 553-562.

SGD 1977 Solar-Geophysical Data, Nos. 398-399, Part I, October-November 1977, National Oceanic and Atmospheric Administration (Boulder, Colorado 80302, USA).

SGD 1978 Solar-Geophysical Data, No. 403, Part II, National Oceanic and Atmospheric Administration (Boulder, Colorado 80302, USA).

Voyager 1,2 Plasma Wave Observations for the September 1977 Storm Period

by

F.L. Scarf
TRW Defense and Space Systems Group
Redondo Beach, California

and

D.A. Gurnett, W.S. Kurth, and R.R. Shaw
University of Iowa
Iowa City, Iowa

Introduction

The significant interplanetary disturbances of September 1977 occurred soon after the launches of Voyager 1 and Voyager 2, and both spacecraft were still sufficiently close to Earth that the available information is relevant for many solar-terrestrial studies. Recently Bridge et al. [1978] and Acuna et al. [1978] summarized the Voyager 1 and 2 plasma and magnetic field observations for the period September 20-23, 1977. In this brief report, we present a preliminary description of the corresponding plasma wave observations for September 20 (Voyager 2) and for September 21 (Voyager 1 and 2). A more detailed analysis of the wave observations for the entire period, along with plasma and field correlations, will be presented elsewhere.

Background

Each of the Voyager plasma wave instruments utilizes a balanced electric dipole with 7-meter effective length. In cruise, the sensor output is processed with a 16-channel spectrum analyzer covering the range 10 Hz to 56 kHz. The time for a single 16-channel spectral scan ranges from a minimum of 4 sec to a maximum of 96 sec. The Voyager spectrum analyzers do not sample continuously, however, since only two log compressors are used for the full spectral coverage, and there is no peak detection or sample and hold capability. Details of the instrumentation and a full description of the planetary science objectives are given in a recent report by Scarf and Gurnett [1977].

The near-Earth spacecraft trajectories and some aspects of the in-flight plasma wave sensitivity are summarized in Figure 1. Both spacecraft were launched toward the dawn terminator, and for many days in this region the low-energy charged particle instruments and the magnetometers detected intermittent burst of ions and upstream MHD waves from the Earth's magnetosphere [Krimigis et al., 1978]. It appears that these burst events were also associated with detection of upstream ion acoustic waves [Kurth, Gurnett and Scarf, 1978], but in this near-Earth region there were many quiescent intervals that allowed us to evaluate the in-flight sensitivity. We found that the Voyagers are exceptionally quiet spacecraft in the frequency range of interest, and this yields unprecedented sensitivity for short wavelength electric field measurements having $f \lesssim 56$ kHz.

A comparison of the Voyager in-flight threshold levels with corresponding data from Helios-2, IMP-8 and ISEE-1 is contained on the right side of Figure 1. These threshold electric field curves are computed assuming that in all cases the sensor effective length, $\ell(\text{eff})$ [7 m for Voyager, 15 m for Helios-2, 61 m for IMP-8 and 100 m for ISEE-1] is small compared to a half wavelength, so that $E(\text{min}) = \phi(\text{min})/\ell(\text{eff})$ is the measured minimum voltage amplitude on the sensor. This means that the comparison of Figure 1 is valid as plotted only for those waves having $\lambda >> 200$ m.

Even for these longer wavelength oscillations it can be seen that the Voyager sensitivity is exceptional. For instance, in the 30-50 Hz frequency range, the Voyager threshold is approximately 1,000 times lower than that for Helios-2, almost two orders of magnitude lower than the IMP-8 threshold, and approximately equal to the measured threshold for ISEE-1 [Gurnett et al., 1978]. This result could never have been attained if the various in-flight thresholds were associated with detection of the same voltage noise signal from each of the spacecraft or from the essentially identical plasma wave preamplifier systems. In these cases, we would expect to find $E(\text{min}) \times \ell(\text{eff}) \approx$ constant, a result which is actually satisfied fairly well only in the narrow spectral range near 10 kHz.

Of course the relation $E(\text{min}) \times \ell(\text{eff}) \approx$ constant is roughly applicable for all frequencies above about 1 kHz, and we conclude that the truly exceptional aspect of the Voyager sensitivity develops only in the $f \lesssim 1$ kHz region. For instance, when we consider the differences in sensor effective length, we find that $\phi(\text{min, Voyager}) \approx \phi(\text{min, Helios-2})/2000$ at $f = 30$ Hz, and $\phi(\text{min, Voyager}) \approx \phi(\text{min, ISEE-1})/14$ at $f = 10$ Hz. These low noise levels on Voyager are undoubtedly associated with the imposition of an electrostatic cleanliness specification leading to a Faraday shield around the spacecraft, and to the absence of solar arrays which frequently couple noise to the plasma; even before the launch of Voyager, Scarf and Gurnett [1977] discussed the good prospects for a quiet in-flight environment based on the unique characteristics of these RTG-powered spacecraft.

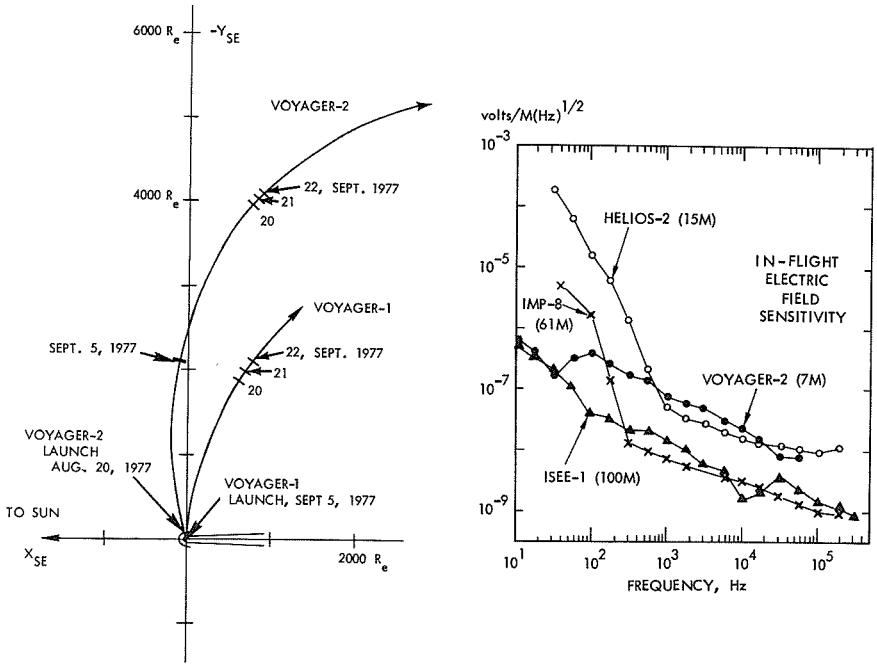

Fig. 1. Left-hand panel: Near-Earth trajectories for Voyager 1, 2: Right-hand panel: Comparison of in-flight threshold levels for several recent investigations utilizing balanced electric dipoles. These levels are computed using $E = \phi/\ell(\text{eff})$, where ϕ is the measured antenna voltage and $\ell(\text{eff})$ is the effective length (given in parentheses). This comparison is strictly valid only for waves having $(\lambda/2)$ large compared to 100m, the ISEE-1 effective antenna length.

The Voyager-2 Plasma Wave Observations

Changes in interplanetary plasma conditions associated with the September storms were first detected on Voyager 2 at 0506 UT on September 20, and Figure 2 shows all of the related plasma wave measurements for the first 12 hours of September 20 and for another interesting 12-h period on September 21. Throughout these intervals both Voyagers were transmitting at their lowest data rates, leading to completion of one spectral scan every 96 sec.

Acuna et al. [1978] identified the initial discontinuity [0506 UT September 20] as a fast forward shock, with a jump in B from 3.6γ to 7.8γ. Thus after 0506 UT, the electron cyclotron frequency was 218 Hz, and we identify the enhanced post-shock noise in all channels up to and including the 178-Hz one as whistler mode turbulence [the few isolated very intense noise bursts in the 10-Hz and 17.8-Hz channels (such as those near 0710, 0800, 1010, 1215 UT on September 20, and 1655 UT on September 21) are thought to be associated with plasma sheath noise impulses as bursts of hydrazine gas are emitted from the attitude control system and then ionized]. On September 21, the discontinuity at 1625 UT yielded an abrupt increase in B to more than 35γ [Acuna et al., 1978], so that the electron cyclotron frequency rose to 980 Hz, just as the enhanced noise appeared in the 311-, 562-, and 1-kHz channels. Once again, the observations are consistent with detection of whistler mode waves in all channels having $f < f_c^-$ for an extremely long period (many hours and days) following the passage of the discontinuity. However, Figure 2 shows also that the onset of turbulence can be quite gradual (as on the 20th) or extremely abrupt (as on the 21st).

Figure 2 shows that very intense and impulsive higher frequency waves were also detected in association with all three discontinuities. These waves are thought to be short wavelength ($\lambda \gtrsim 2\pi\lambda_D$, where λ_D is the Debye length) Doppler shifted ion sound waves (of the type discussed by Gurnett and Anderson [1977], Kurth et al. [1978] and others), and a preliminary analysis supports this interpretation. For instance, just after 0506 UT on September 20, the MIT plasma probe data yielded $V \simeq 380$ km/sec, $N \simeq 20$ cm^{-3}, $T_+ \simeq 2.5 \times 10^4$ K (J. Sullivan and H. Bridge, private communication) so that f_p^+ (the rest frame ion plasma frequency) was 935 Hz and the proton Debye length was 2.5 m. However, for $T_- \simeq 10^5$ K, the electron Debye length is near 5 m and in this case the Doppler shift, $\Delta f = kV \cos(k,V)$, has a peak value $[\Delta f(\text{max})]$ of $V/(2\pi\lambda_D) \simeq 12$ kHz, thus it is easy to explain the observed signals in all the channels up to and including the 17.8-kHz one, in terms of ion sound wave detection.

Note that $\lambda/2 \simeq 15\text{M} > \ell(\text{eff})$ for Voyager, so that the amplitude determination made with this short antenna is not in question. However, for $\ell(\text{eff}) \gtrsim 15\text{M}$, as it would be for the other sensors discussed above, it is clear that one would have to use $E \simeq 2\phi/\lambda$, rather than $E \simeq \phi/\ell(\text{eff})$ for these very short waves.

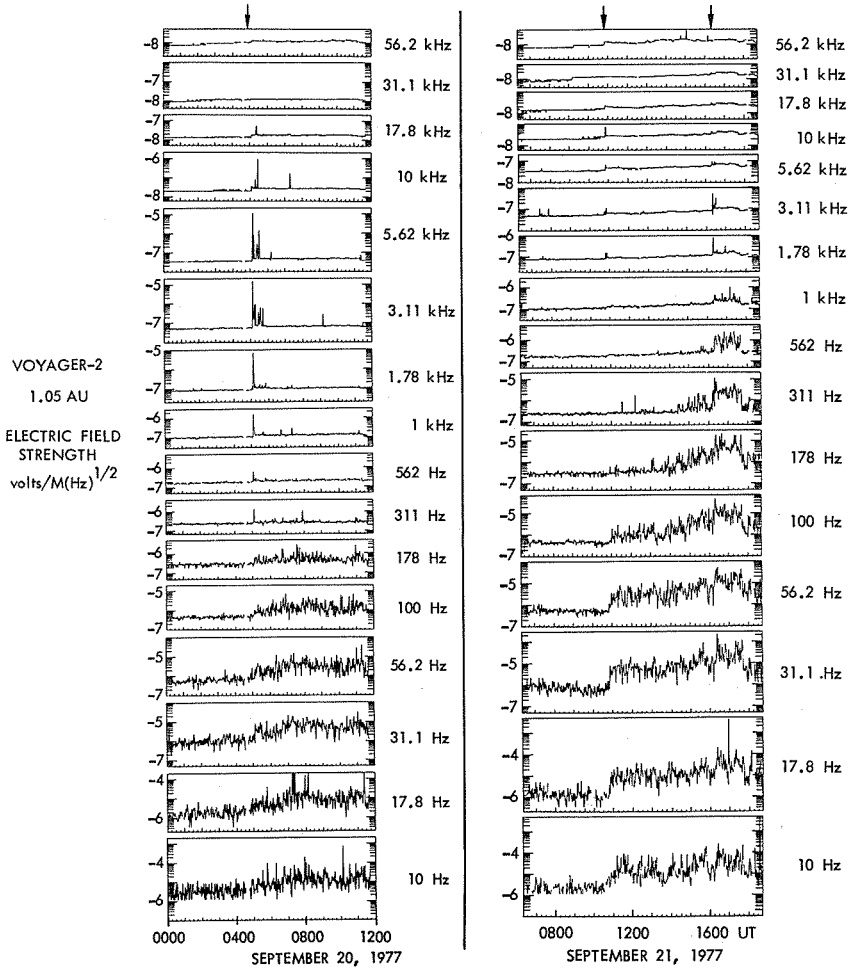

Fig. 2. The Voyager 2 plasma observations for two interesting 12-h intervals, during which three interplanetary discontinuities were detected.

The top two or three panels in Figure 2 show another interesting phenomenon: enhanced levels of high frequency waves (thought to be electron plasma oscillations) were detected for periods extending many hours after passage of the initial shocks. This suggests that the post-shock electron distributions were significantly non-Maxwellian.

Voyager 1 Plasma Wave Observations

On September 20, the Voyager 1 tracking was incomplete and the discontinuity corresponding to the initial 0506 UT Voyager 2 shock was detected near a tracking gap. Therefore, we concentrate on the September 21 discontinuities near 0530 and 1625 UT (another discontinuity was detected at 2220 UT on the 21st). Figure 3 can be used to contrast responses in four Voyager 1 channels with the corresponding channel responses on Voyager 2, and it can be seen that the two instruments measured extremely different wave phenomena on these days. For example:

a) There is no evidence on Voyager 1 for the intense whistler mode noise enhancement detected in the 311-Hz channel on Voyager 2 following the 1625 UT discontinuity.

b) The Voyager 1 discontinuity at 1630 UT appears to signal onset of a quiet period in the 3.1-kHz channel, rather than onset of an interval with enhanced turbulence.

c) The initial Voyager-1 noise increase at 31 Hz (0530 UT) is smooth and gradual in contrast to the abrupt rise in turbulence detected before 1100 UT on Voyager 2.

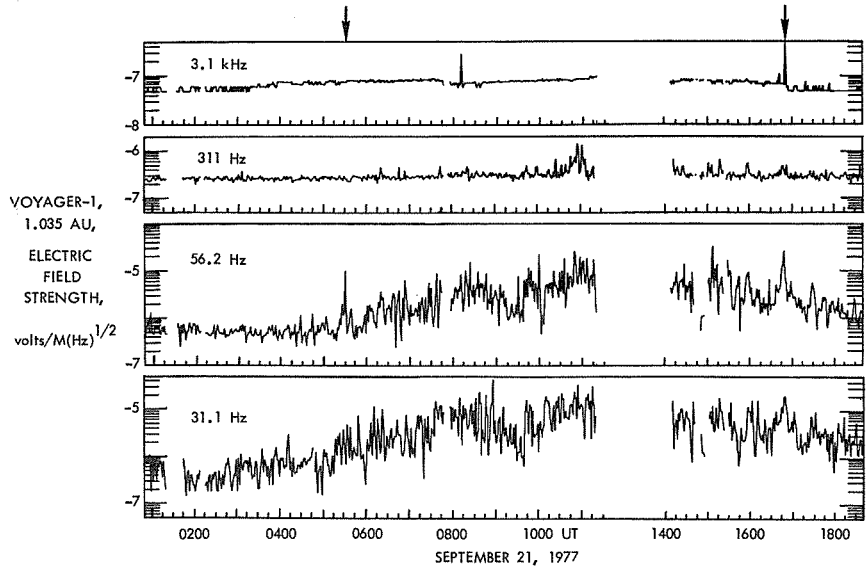

Fig. 3. Some Voyager 1 wave observations for comparison with corresponding plots in Figure 2.

Summary

The September 1977 events provided the first direct information on the response of the Voyager plasma wave instruments to changing interplanetary conditions. We find the first direct confirmation that the intense low frequency electric field turbulence represents detection of whistler mode noise, with f ranging up almost to f_c^-. This Voyager identification is made by noting how the upper frequency of the broadbanded turbulence varies with variations in f_c^-. In fact, the electric field amplitudes can also be related to the earlier Helios 1, 2 measurements of magnetic amplitudes for whistler mode waves [Neubauer et al., 1977] using E = cB/n, where n is the computed index of refraction for whistlers. Although we have no direct simultaneous comparisons, the range of Voyager E-field levels does appear to be quite compatible with levels expected using the Helios measurements of magnetic components.

We also find evidence that the impulsive noise burst with $f_p^+ < f < f_p^-$ are indeed Doppler-shifted ion sound waves, and that enhanced levels of electron plasma oscillations are detected for long periods after passage of the shock. These wave measurements also suggest that the local conditions at Voyager 1 and 2 differed greatly during this time period, although the spacecraft-to-spacecraft separation was relatively small (less than 0.1 AU) at this time.

Acknowledgments

The authors thank Dr. J. Sullivan and Dr. H. Bridge of MIT for providing information on the plasma parameters, and they have also benefited greatly from discussions with Dr. S. Krimigis, Dr. M. Acuna, and Dr. R. Lepping. The research was supported by NASA through JPL Contracts 954012 (TRW) and 954013 (Iowa).

References

ACUNA, M., et al. 1978 Magnetic Field and Plasma Observations of the Interplanetary Shocks and Flows during Sept. 20-23, 1977, EOS,59, 369.

BRIDGE, H., et al. 1978 Observation of Changes in the Interplanetary Medium Associated with McMath Plage Region 14943, EOS,59, 369.

GURNETT, D.A. and R.R. ANDERSON 1977 Plasma Wave Electric Fields in the Solar Wind: Initial Results from Helios 1., J. Geophys. Res.,82, 632.

GURNETT, D.A. F.L. SCARF R.W. FREDRICKS and E.J. SMITH 1978 The ISEE-1 and ISEE-2 Plasma Wave Investigation, IEEE Trans. Geosci. Electron., GE-16, No. 3, 225-230.

KRIMIGIS, S.M., et al. 1978 Observations of Particle Bursts and Upstream Waves from the Magnetosphere at >400 R_e with the Voyager 1 Spacecraft, EOS,59, 366.

KURTH, W.S. D.A. GURNETT and F.L. SCARF 1979 High Resolution Spectrograms of Ion-Acoustic Waves in the Solar Wind, J. Geophys. Res., 84, 3413-3419.

NEUBAUER, F.M. G. MUSMANN and G. DEHMEL 1977 Fast Magnetic Fluctuations in the Solar Wind - Helios 1, J. Geophys. Res.,82, 3201.

SCARF, F.L. and D.A. GURNETT 1977 A Plasma Wave Investigation for the Voyager Mission, Space Sci. Rev's.,21, 289.

Observations of the Aurora in the Far Ultraviolet From "Kosmos - 900" Data

by

K.I. Gringauz*, L. Martini**,
M.M. Shutte*, and A.I. Puolokainen*

The extreme ultraviolet region of auroral emission spectrum ($\lambda \leq 1350$Å) has remained relatively unexplored because of the inaccessibility to ground-based observations and the experimental difficulties of such measurements and limited number of rocket and satellite experiments.

In this paper the preliminary results of observations of auroral emissions within the wavelength band λ 1050-1340Å are given. The experiment was carried out on board the satellite "Kosmos-900" launched on March 30, 1977, to the almost circular polar orbit (h ~500 km, inclination 83°). The results refer to September 20-22, 1977.

To record the auroral emission within the band $\Delta\lambda$ = 1050 to 1340Å the photometer was installed along the longitudinal spacecraft axis so that its entrance window was directed toward the Earth.

An ionization chamber with the electrodes and an MgF_2 entrance window [Martini et al., 1972] installed coaxially was used as a photometer.

Nitrogen oxide, NO, was used as a gas filler. Its electro-negative properties were beneficial for a large value of the work function of the cathode material that made it possible to realize a chamber quantum efficiency of up to 80% within the wavelength band [Carver et al., 1964].

The ionization current was measured by means of a two-scale direct current amplifier with a time constant of 0.14 sec., with two individual outputs to the telemetry transmitter. The range of the recorded currents was 10^{-13} to 10^{-10}A.

The photometer spectral sensitivity, determined by the potential of the photoionization filler NO and by the threshold of radiation absorption of MgF_2 entrance window, matched the wave band 1050 to 1340Å.

A special collimator, consisting of an aluminum tube as the diaphragm system, was installed to protect from scattered radiation.

Absolute sensitivity characteristics of the sensor are known from preflight laboratory calibrations.

Table 1 gives some basic parameters of the photometer.

TABLE 1. Parameters of the Kosmos-900 Photometer

Spectral sensitivity band	1050 - 1340Å
Effective area	0.31 cm^2
View angle	22°
Geometric factor	0.036 cm^2 ster
Quantum efficiency	0.5
Absolute calibration factor	5 kR/volt

Telemetry data indicating normal performance of the instrument came until late April 1978. It is expected that the instrumentation will successfully operate in the future.

*Space Research Institute, Academy of Sciences, USSR.
**Electronics Institute, Academy of Sciences, GDR.

A fixed three-axis orientation of the spacecraft, providing the directivity of the photometer entrance window to the Earth with an accuracy of several degrees, allowed continuous observation of both the dayside and nightside glows of the atmosphere in the ultraviolet wave band.

Based on absolute calibration in the spectral band of 1050 - 1340Å, radiation of the intensity of ≥ 0.25 kR could be reliably recorded. Taking into account the results of previous measurements [Miller and Fastie, 1968; Chubb and Hicks, 1970; Hicks and Chubb, 1970; Part et al. 1977], it is known that the photometer must record auroral emission at the following wavelengths: atomic oxygen λλ1306, 1305, 1302 Å; Lyman alpha - H Lyα - 1215, 6 Å; atomic nitrogen λ1200 Å.

Observational Results

The results described hereafter refer to September 20-22, 1977, when "Kosmos-900" moved along a meridional plane going from 2^h to 14^h, crossing the auroral regions in the Northern and Southern Hemispheres near dusk and dawn magnetic local time.

Figures 1 and 2 give the data for two complete revolutions of the spacecraft during each of which it crossed the auroral latitudes twice.

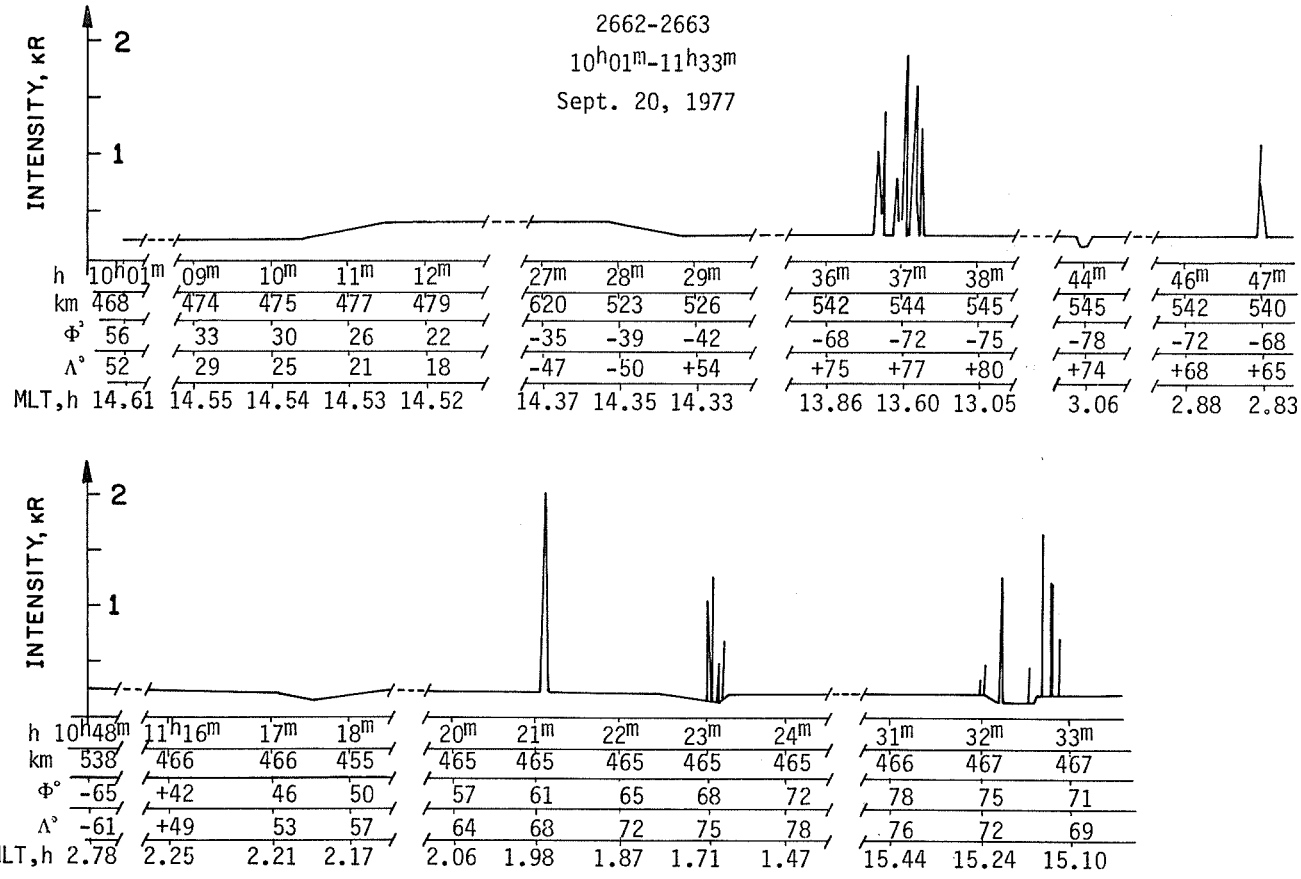

Fig. 1. Observations of aurora within the wavelength band 1050 - 1340° on September 20, 1977.

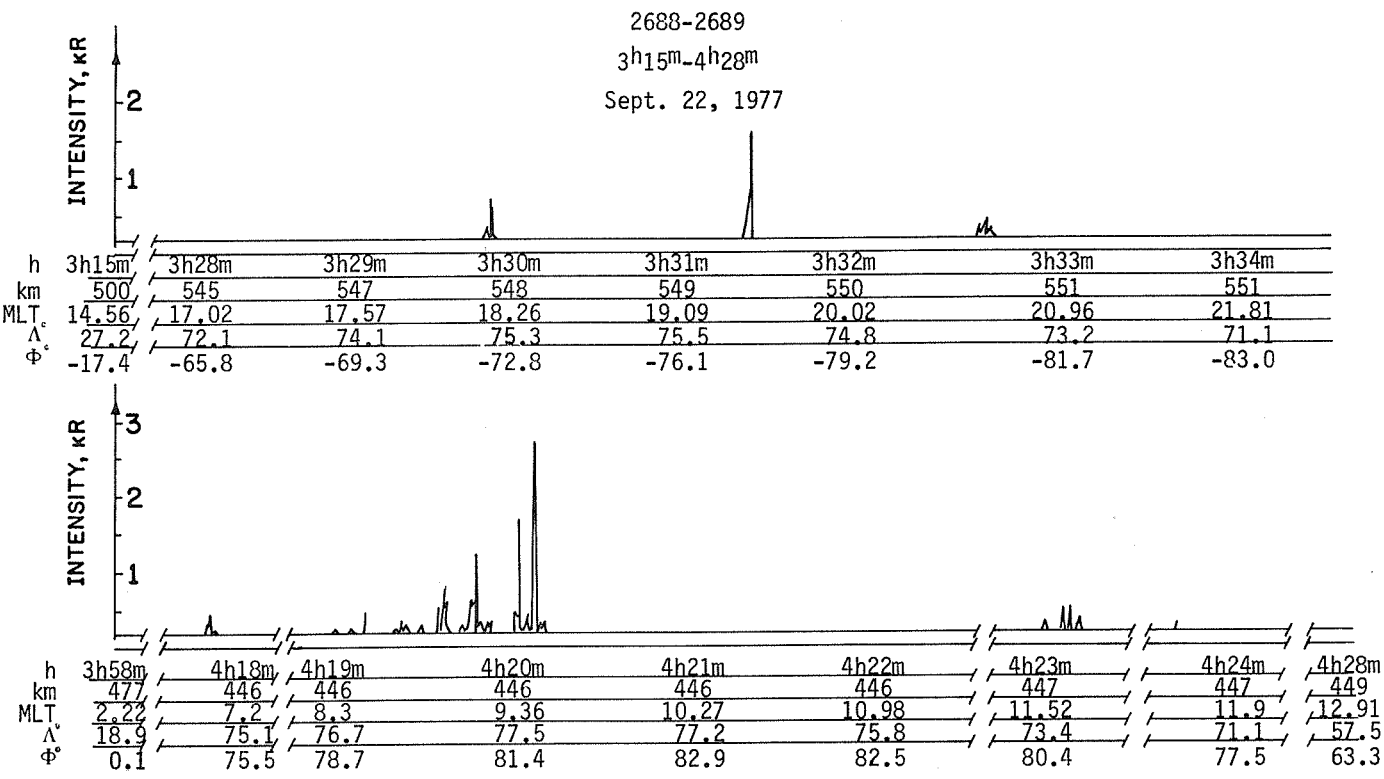

Fig. 2. Observations of aurora within the wavelength band 1050 - 1340Å on September 22, 1977.

It should be noted that during the flight the level of the scattered radiation background was practically constant. On the illuminated and dark parts of the orbit and in most cases its value was close to that of the noise level of the direct-current amplifier (~2-3% of sensitive scale, i.e. ~ 0.10 - 0.15 kR). It can be assumed that such a low sensitivity to scattered radiation was reached due to the use of the entrance collimator, as compared to other experiments [Chubb and Hicks, 1970; Hicks and Chubb, 1970].

As seen in Figures 1 and 2 the photometer signals were above the background only at the polar oval latitudes along the entire orbit, including the polar cap regions.

It can be noted that the intensity of the emissions observed on the dark parts of the orbit was sufficiently less than that on the illuminated ones. The spatial characteristics of these emissions, which extend from 1.5° to 10° in invariant latitude, are fairly complicated. Two structures can be considered: a large-scale structure with two regions of higher intensity spaced from ~100 km to ~1000 km and a fine scale, multipeak structure indicating substantial time variations with intensity maxima every several fractions of a second.

It can be noted that the double structure was less evident on the shadowed parts when the radiative intensity was lower.

Figure 3 gives an example of the structure of the emissions recorded on September 20, 1977, in

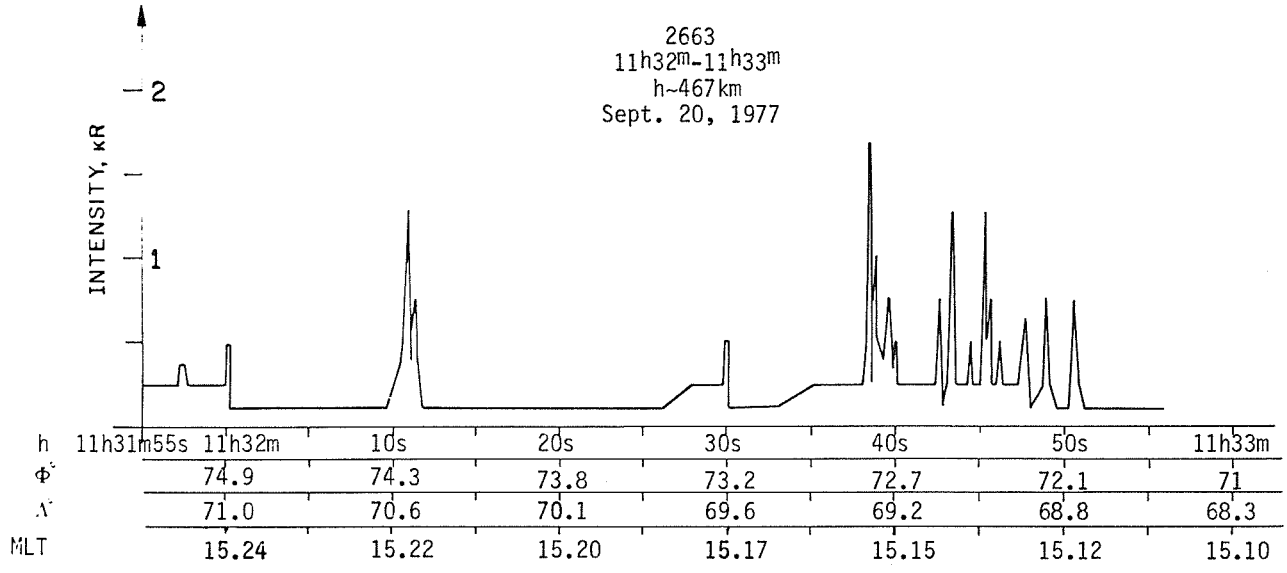

Fig. 3. Photometer readings on September 20, 1977

the Northern Hemisphere at the invariant latitudes Λ_0=75°-71.5°, at 15^{h}MLT, with a 5-msec rate of telemetry data transmission.

Two regions of higher intensity are distinct, one recorded 20 sec after the other, i.e. at a distance of 150 km. The structure of the intensity maxima within the limits of each region is not regular; peak amplitudes and their duration vary from 0.3 to 3 kR and from 0.1 to 5 sec, respectively; the intensity growth from minimum to maximum is fairly sharp.

Discussion of the Data

As it has been noted above, the emissions recorded by the photometer could be caused by Lyman-α emission, by the quartet of nitrogen lines at λ1200Å and λ1134Å and by the triplet of oxygen emissions at λ1304Å.

Chubb and Hicks [1970] have shown that the photometer with spectral sensitivity λ1050-1340° and relative efficiency to emission λ1304Å equal to ~1/4 as compared to that for λ 1215.6Å. In our case the efficiency at the λ 1304Å line is not higher than 1/5 of the efficiency at the λ 1215.6Å line [Martini, Shutte et al. 1972]. On the other hand, the contributing oxygen and nitrogen lines and the 1304Å emissions of the stable oxygen atoms triplet should be the strongest emissions. First, atomic oxygen (1304Å) is much more abundant in the ionosphere than atomic nitrogen and second, of the pertinent oxygen lines, only the 1304Å emission requires excitation from the ground state without spin change [Barth and Schaffner, 1970]. Therefore we can assume that the observed emission was basically Lyman-α. The sharp intensity increase is the evidence for the discrete character of these auroral arcs.

Our assumption that Ly-α emission is the main contributor in the spectral region 1050-1340Å should mean in turn that the recorded emission was excited by fast protons. Besides the display of the so-called large-scale structure with the distinct maxima of intensity is the evidence for not one but at least two sources of excitation [Chubb et al. 1970; Hultqvist, 1974] which can differ in the type of particles and in their energy. Variations in the intensities and extension of these regions can be observed; namely, the maxima from the equator-ward region are more intense and occupy larger areas (Figure 3). This allows us to assume that fluxes of precipitating protons and electrons were the sources of excitation and that, in accordance with theory [Taylor et al.,1965 and Eather, 1967], the proton precipitation regions are shifted toward the equator and are spaced ~100 to 500 km from the electron precipitation regions.

We hope that after more comprehensive investigation of the data we shall be able to distinguish the electron and proton sources of excitation, by analyzing the amplitudes of the intensity maxima of these auroral arcs and their relative positions.

It should be also noted that in our case the display of the double structure was observed both in the dusk and in the dawn sectors, as opposed to the results of the OGO-4 measurements [Chubb et al. 1970].

REFERENCES

BARTH, C.A. and S. SHAFFNER — 1970 — "Ogo 4 Spectrometer Measurements of the Tropical Ultraviolet Airglow," *J. Geophys. Res.*, *75*, 4299-4306.

CARVER, J.H., P. MITCHELL and E.L. MURRAY — 1964 — "Molecular Oxygen Density and Lyman-absorption in the Upper Atmosphere," *J. Geophys. Res.*, *69*, 3755-3756.

CHUBB, T.A. and G.H. HICKS — 1970 — "Observations in the Aurora in the Far Ultraviolet from OGO 4," *J. Geophys. Res.*, *75*, 1290-1311.

EATHER, R.H. — 1967 — "Auroral Proton Precipitation and Hydrogen Emissions," *Rev. Geophys.*, *5*, 207-210.

HICKS, G.T. and T.A. CHUBB — 1970 — "Equatorial Aurora/airglow in the Far Ultraviolet," *J. Geophys. Res.*, *75*, 6233-6248.

HULTQVIST, B. — 1974 — "Rocket and Satellite Observations of Energetic Particle Precipitation in Relation to Optical Aurora," *Ann. Geophys.*, *30*, 223-257.

MARTINI, L., N.M. SHUTTE, K.I. GRINGAUZ and B. STARK — 1972 — "The Measurements of Solar Ly-α intensity by Unoptical Methods on the Rocket 'Vertical-1'," *Kosmicheskie Issledovanija X*, 255-260.

MILLER, R.E., W.G. FASTIE and R.C. ISLER — 1968 — "Rocket Studies of Far-ultraviolet Radiation in an Aurora," *J. Geophys. Res.*, *73*, 3353-3365.

PARK, H., P.D. FELDMAN and W.G. FASTIE — 1977 — "The Extreme Ultraviolet (750-1230°) Spectrum of an Aurora," *Geophys. Res. Let.*, *4*, No. 1, 41-44.

TAYLOR, H.E. and E.W. HONES, Jr. — 1965 — "Adiabatic Motion of Auroral Particles in a Model of Electric and Magnetic Fields Surrounding the Earth *J. Geophys. Res.*, *70*, 3605-3628.

Interplanetary Scintillation Observations of Flare-Generated Shock Waves in September 1977

by
T. Watanabe, T. Kakinuma, H. Washimi and M. Kojima
The Research Institute of Atmospherics, Nagoya University
13-Honohara 3-chome, Toyokawa, 442 Japan

Observations

The operating frequency of our three aerials placed at Toyokawa, Fujigane and Sugadaira is about 69 MHz. The solar wind speed is estimated under the assumptions of elliptical diffraction patterns and radial flow of the solar wind. The interplanetary scintillation (IPS) level which is a measure of the amplitude of density fluctuations in the solar wind plasma is also estimated. In our case, the IPS level is the mean square of the intensity fluctuations (variance) normalized by the galactic background noise level. Figure 1 shows the lines of sight to scintillating radio sources of 3C225, 3C230, 3C237 and 3C298 on Sep. 20, 1977. Daily plots of the solar wind speeds and the IPS levels obtained by the IPS observations of these four radio sources are shown in Figure 2.

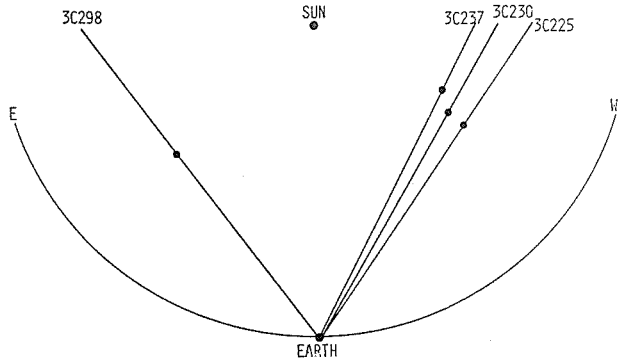

Fig. 1. Locations of the lines of sight to scintillating radio sources on Sep. 20, 1977. Each line of sight is projected onto the ecliptic plane. A dot on each line of sight represents the position of the closest approach to the Sun.

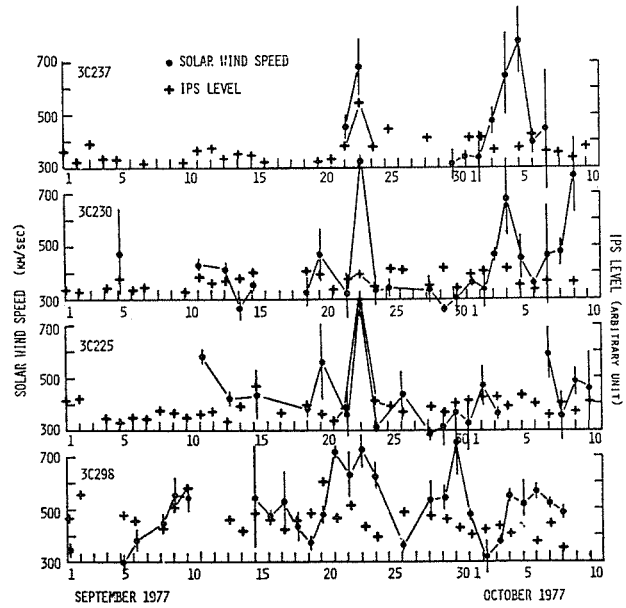

Fig. 2. Daily plots of the solar wind speeds and the IPS levels during the interval from Sep. 1 to Oct. 10, 1977.

Sep. 7 - Sep. 15, 1977

The McMath active region #14943 produced Type II - IV radio bursts at the east limb at 2230 UT on Sep. 7 and at 1629 UT on Sep. 9 (Solar-Geophysical Data). Although no related geomagnetic storms have been reported, we find indications of interplanetary shock waves generated by these flares in our IPS data of the solar wind. As shown in Figure 1, we monitored the interplanetary space to the east of the Sun-Earth line by IPS of 3C298 during this interval. Rather high-speed and turbulent solar wind was observed on Sep. 9 and Sep. 10. These enhancements can be attributed to the shock waves generated by the solar flares on Sep. 7 and Sep. 9 respectively. The lower limit of the mean propagating speed of the preceding shock wave between the sun and the line of sight to 3C298 (0.6 AU) is estimated to be 790 km/sec. In case of the following shock wave, the estimated shock speed is about 1850 km/sec. The IPS observations suggest that the main bodies of these shock waves were confined to the east of the Sun-Earth line.

Sep. 16 - Sep. 21, 1977

During this interval, various solar-terrestrial events were reported. The geomagnetic storms took place on Sep. 19 and Sep. 21 (Solar-Geophysical Data). For provisional purposes, the following associations between the Type II - IV radio bursts and the sudden commencements of geomagnetic storms are proposed.

Shock No.	II - IV	SC
1	16/2225	19/1140
2	19/1031	21/2043

We cannot find clear evidence of shock 1 in our IPS data. On the other hand, rather high speed solar wind of 450 - 550 km/sec was detected by the IPS observations of 3C225 and 3C230 on Sep. 20. This increase in solar wind speed can be attributed to shock 2 though the IPS level was not enhanced. The estimated shock speed between the Sun and the line of sight to 3C225 (0.6 AU) is about 1900 km/sec. The mean shock speed between the Sun and the Earth (SC) is about 730 km/sec. Strong deceleration of shock 2 is suggested if we assume an isotropically expanding shock wave.

Another solar flare accompanied by the Type II - IV radio bursts was reported on Sep. 20. There exists no unambiguous indication of the flare-generated shock wave in our IPS observations.

Sep. 22 - Sep. 25, 1977

Very sharp rise in the solar wind speed up to 800 km/sec was detected by the IPS observations of 3C225, 3C230 and 3C237 on Sep. 23. The increase in IPS level was very prominent in the data from 3C225 and 3C237. These phenomena strongly suggest the existence of a flare-generated shock wave. No geomagnetic storm SC was reported on Sep. 23 and 24. An increase in the solar wind speed from about 540 km/sec to 620 km/sec on Sep. 23 observed in the solar wind data obtained by IMP 7 and 8 (Solar-Geophysical Data). A sharp rise in the flux of low energy protons and a deep minimum in the neutron flux were observed on Sep 23. These terrestrial events suggest the arrival of the shock wave at the Earth on Sep. 23. During the interval from Sep. 20 to Sep. 25, the principal portion of the line of sight to 3C298 was immersed in a corotating high-speed stream. We cannot find clear evidence of the shock wave in the IPS data of 3C298. It is concluded that the main body of this shock wave was confined to the region west of the Sun-Earth line.

Since observed flow speed of the post-shock plasma at about 0.6 AU from the Sun was very high (800 km/sec), the responsible solar flare is considered to have occurred on Sep. 22. Several weak solar flares took place in the active region of #14943. At present, we cannot decide the relevant solar flare because neither Type II nor Type IV radio burst was observed on Sep. 22.

Solar Protons in the Earth's Magnetosphere during the Period from September 19 to 22, 1977

by

B.A. Tverskoy, E.N. Sosnovetz, L.A. Darchieva, T.A. Ivanova,
Yu.V. Kutuzov, and L.V. Tverskaya
Institute of Nuclear Physics, Moscow State University
Moscow 117234, USSR

Considered in the present report are some experimental results of observations of solar cosmic ray proton fluxes in the Earth's magnetosphere during the event of September 19-22, 1977. The data from the Cosmos-900 and 842 satellites are used. The circular orbits of the satellites were inclined at $\approx 83°$ and are at an altitude of $\approx$ 500 km for Cosmos-900 and $\approx$ 1000 km for Cosmos-842. The periods of the satellites orbiting around the Earth were 94.4 min and 105 min, respectively. Because of its smaller orbital period, at individual moments Cosmos-900 flew through one of the polar regions simultaneously with Cosmos-842. This fact made it possible to isolate spatial inhomogeneities in the solar cosmic ray distribution against the background of temporal variations.

Cosmos-900 carried numerous instruments for detecting the various types of radiations, in particular a differential spectrometer of low-energy protons and integral p-n detectors for measuring the proton fluxes with $E_p \geqslant 1$ MeV, $E_p \geqslant 10$ MeV, and $E_p \geqslant 30$ MeV.

The design and operating principle of the differential proton spectrometer were the same as those of the instrument flown earlier on the Molniya-1 satellite [Vernov et al, 1972]. The measured energy ranges, characteristics, and geometric factors of the detectors whose readings are used here are presented in Table 1.

Table 1.

No.	Parameter:	Energy range	Thickness of detector, (μm)	Geometric factor, cm^2.ster.	Thickness of shielding
1	UR26	50-80 keV	100	$8.4.10^{-3}$	-
2	UR27	80-130 keV	"	"	-
3	UR28	130-205 keV	"	"	-
4	UR29	205-315 keV	"	"	-
5	UR30	315-500 keV	"	"	-
6	UR49	1-3 MeV	37	3.10^{-1}	7 μmAl
7	UR8	10-50 MeV	1000	5.55	0.5 mmAl
8	UR9	30-50 MeV	1000	9.85	4 mm Al

Cosmos-900 was permanently oriented with one of its axes towards the Earth's center and with the other along the velocity vector. The differential spectrometer detector and UR49 counter were directed perpendicular to the radius-vector from the Earth's center and measured the proton fluxes perpendicular to the magnetic force line at high geomagnetic latitudes. The UR8 and UR9 axes were directed upwards from the Earth center but the counters were practically global since they measured the proton fluxes within an angle of $\approx 180°$. The UR8 and UR9 counters were identical, the only difference was in the area and the thickness of spherical passive shielding.

The n-p detector flown on Cosmos-842 measured the 1-3 MeV protons and had a 1.46 cm^2.ster geometric factor. The effective angle of proton detection was $\sim 150°$. Cosmos-842 was not oriented and, therefore, its n-p detector measured the mean directed proton flux.

Fig. 1 shows the time dependence of solar protons with $E_p \geqslant 1$ MeV, $E_p \geqslant 10$ MeV, and $E_p \geqslant 30$ MeV at night hours MLT on geomagnetic latitudes $\geqslant 75°$ (the polar plateau region). Shown in the lower part of the figure are the position of the equatorial boundary Λpeq of the solar cosmic rays penetration into the night auroral zone according to the data of the $E_p \geqslant 1$ MeV protons; the Dst-variation [Solar-Geophysical Data, 1977] is also shown. The crosses and dots indicate the Cosmos-900 and 842 results, respectively. The proton intensity level corresponding to the auroral zone plateau level was taken as the penetration boundary. The downward arrows indicate the points at which the true latitude of the equatorial boundary could not be determined because of the auroral zone merging with the $E_p \geqslant 1$ MeV proton radiation belt. Good agreement between the boundaries at individual moments as determined for the perpendicular proton flux (Cosmos-900) and global proton flux (Cosmos-842) should be noted.

The event of September 19-22, 1977 was one in the series of solar cosmic ray increases observed from September 12 to 27. The event began as a gradual increase in the $E_p \geqslant 1$ MeV proton flux up to a level of $\approx 5.10^1$ $cm^2.S^{-1}ster^{-1}$ at $\sim$0645 UT on September 19, 1977 according to the Cosmos-842 data in the southern polar cap against the background of the previous increase. The higher-energy proton fluxes were first observed from Cosmos-900 in the southern polar cap at $\sim$1105 UT on September 19; the

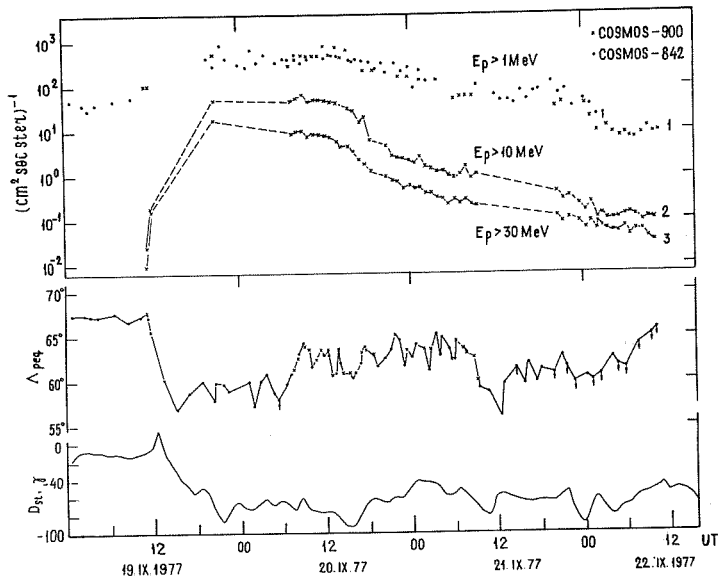

Fig. 1. Time history of the proton fluxes with Ep≥1, 10, 30 Mev averaged over the polar cap (upper panel); equatorial boundary of solar protons and penetration into the night auroral zone Λpeq and Dst value (lower panel).

$E_p \geqslant 10$ MeV and $E_p \geqslant 30$ MeV proton fluxes being $\approx 2.5 \cdot 10^{-2}$ $cm^{-2}s^{-1}ster^{-1}$ and $\approx 10^{-2}$ $cm^{-2}s^{-1}ster^{-1}$, respectively. At $\sim$2040 UT the fluxes in the southern polar cap reached $\sim 5.10^{1}$ $cm^{2}s^{-1}ster^{-1}$ and $\sim 2\cdot10^{1}$ $cm^{-2}s^{-1}ster^{-1}$, respectively. According to the Cosmos-842 data in the northern polar cap, the maximum value of the $E_p \geqslant 1$ MeV proton flux was $\sim 10^{3}$ $cm^{-2}s^{-1}ster^{-1}$ at $\sim$2140 UT on September 19. According to the Cosmos-900 data, starting with $\sim$0430 UT on Septmber 22 the $E_p \geqslant 1$ MeV proton flux did not change and was $8.10°cm^{-2}s^{-1}ster^{-1}$.

The discussed event was accompanied by a moderate magnetic storm consisting of several successive disturances. The maximum Dst variation was -94 γ at $\sim$1600 UT on September 20. The decrease in the equatorial H-component of the Earth's magnetic field (Dst-variation) is due to development of the ring current which changes the magnetic field topology, changing, in its turn, the boundary of solar proton penetration.

The discussed storm is featured, however, by intense disturbances in the night auroral zone. This is in particular indicated by significant fluctuations of the equatorial boundary of penetration of solar cosmic ray protons on the night side against the background of a more gradual change of the Dst-variation. For example, the boundary of the $E_p \geqslant 1$ MeV proton penetration was observed at $\sim$1515 UT on September 19 at latitude $\approx 57°$ ($L \approx 3.35$) at Dst = - 35 γ, and at Dst = - 8 γ at latitude $\approx 60°$ ($L \approx 4$) at 2130 UT on September 19. Even more variations were noted in the position of the polar boundary of solar cosmic ray penetration which were closely associated with the changes of the plasma sheet thickness.

The solar cosmic ray increase of September 19-22, 1977 was featured by significant and fairly pronounced gradients of proton intensity during the passages through the polar regions not only in the auroral zone, but also in the polar plateau region, up to $E_p \geqslant 30$ MeV.

The data of two simultaneously operating satellites show that such gradients are of spatial nature. Figs. 2 and 3 show the intensity profiles of solar cosmic ray protons detected during simultaneous flight of Cosmos-900 and 842 over the southern polar region. At $\approx$2032.5 UT on September 19 at latitude $\approx 71.3°$ and MLT $\approx$ 18 hr, Cosmos-900 detected an abrupt decrease in the 315 to 500 keV and $E_p \geqslant 1$ Mev proton fluxes which lasted until 2036 UT when at latitude $\sim 75°$ at MLT $\approx$ 2230 Cosmos-900 left the decreased intensity zone. During orbit 5837 at $\approx$ 2040 UT (Curve I in Fig. 3), Cosmos-842 also traversed the equatorial boundary of the decreased intensity zone at latitude $\approx 75°$ at MLT = 2230 and left the zone at MLT $\approx$ 22 hr at $\approx$ 2041 UT at latitude $\approx 78°$. On orbit 5838 in the Northern Hemisphere at$\approx$2140 UT at latitude $\approx 78°$, Cosmos-842 again traversed the polar boundary of the zone at MLT $\approx$ 0050 (see Fig. 3, curve II).

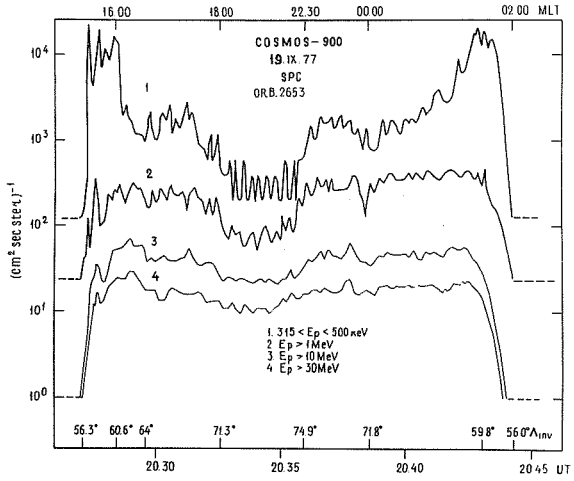

Fig. 2. Proton fluxes for four different energies from south polar pass (orbit 2653 Cosmos 900).

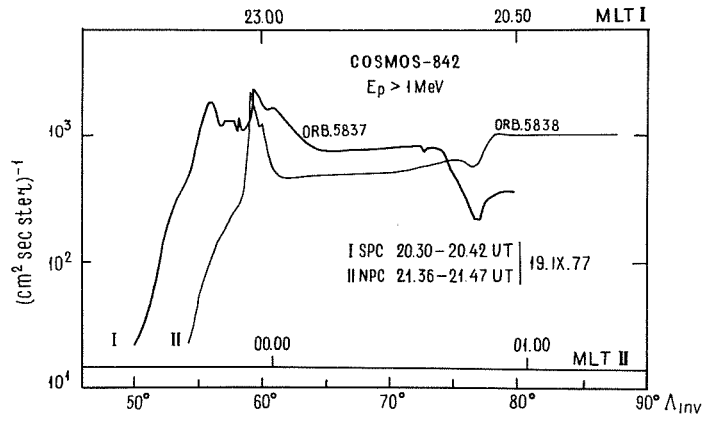

Fig. 3. 1 Mev proton flux for two consecutive polar passes of Cosmos 842 vs. invariant latitude.

Thus, the zone of decreased intensity of the solar cosmic ray protons was recorded from ≈ 2032 UT to ≈ 2140 UT on September 19, 1977 and extended in MLT from 18 hr to ∿01 hr. The equatorial boundary was at ≈71.3° at MLT ≈ 28 and at ≈ 75° at MLT ≈2230 hr. The high-latitude boundary in both hemispheres was at ∿78°. It can be seen from Fig. 2 that region was characterized by less significant, but still sufficiently marked gradients of the E_p ⩾10 MeV and E_p ⩾30 MeV proton intensities. These results favor the assumption that the magnetospheric tail contains large-scale structures with pronouncedly different characteristics which affect the propagation of solar cosmic ray protons in a wide energy range from E_p ≈400 keV to E_p ≈30 MeV.

Fig. 4 shows the differential proton energy spectra according to the Cosmos-900 data.

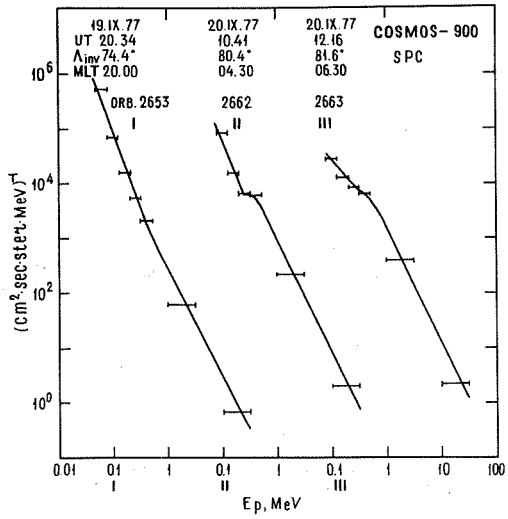

Fig. 4. Solar proton spectra, Cosmos 900 data.

Spectrum I has been obtained in the intensity minimum recorded from Cosmos-900 and 842 at 2034 UT on September 19, 1977 (see Fig. 2). At E_p > 400 keV, the three spectra are similar and may be approximated by the power law function $J(E)nE \sim \gamma$ with exponent γ =2. The main differences are observed at E_p <400 keV where the proton spectrum softens with decreasing invariant latitude.

When the spectrum at E_p=50-400 keV is approximated by the power law function, the exponent $\gamma \simeq 3$ at latitudes 74.4° and 80.4°, and γ=1.5 at 81.6°. The change of the spectral form at E_p ≈ 300 keV may be due to either the different nature of particles or a consequence of various effects of the electronic and magnetic fields of the magnetosphere on the solar cosmic ray protons in the said energy ranges.

References

VERNOV, S.N., V.P. BORODULIN, M.I. PANASYUK, I.A. RUBINSHTEIN, I.A. SAVENKO and E.N. SOSNOVETS — 1972 — Observations of Low-Energy Protons from Molniya-1 Satellite in July-August 1970, Cosmicheskie issledovnija, 10, 376.

SGD — 1977 — Solar-Geophysical Data, 398 (U.S. Department of Commerce, Boulder, CO 80303.)

Solar Proton Data at Geostationary Orbit during September 19-26, 1977

by

Tsuyoshi Kohno
Meteorological Satellite Center
Nakakiyoto, Kiyose
Tokyo, Japan

Large flux increases of solar protons were observed during the September 1977 solar flare events by the Space Environment Monitor on board the Geostationary Meteorological Satellite (GMS-"HIMAWARI"). The "HIMAWARI" is in geostationary orbit at 140°E and the local midnight of the satellite is 1440 UT. The channel names and their characteristics are shown in Table 1. The directions of the center of all fields of view are perpendicular to the satellite spin (100 rpm) axis which is parallel to the Earth's axis.

Hourly averaged fluxes of each channel are shown in Fig. 1. Two sharp increases can be seen in channels of P3 - P7 and A1 - A5. The hourly energy spectra of protons in build-up phase of September 19 are shown in Fig. 2. Spectral change in this phase can clearly be seen here. Assuming the power law spectra as

$$J(E)dE = J_0 E^{-\gamma} dE,$$

the value of γ changes from 0.7 (1200-1300 UT) to 1.6 (1900-2000 UT) and J_0 changes from 6 to 1500 protons/cm^{2}sec·sterad·Mev (E: in MeV) in the same period.

Table 1

Channel Name	Particle Type	Energy Range Mev	G-factor cm^2·st
P1	proton	1.2 - 4	0.0421
P2	proton	4 - 8	0.0421
P3	proton	8 - 16	0.0421
P4	proton	16 - 34	0.389
P5	proton	34 - 80	0.389
P6	proton	80 - 200	0.389
P7	proton	200 - 500	0.389
A1	alpha	9 - 70	0.0421
A2	alpha	30 - 70	0.0421
A3	alpha	65 - 170	0.389
A4	alpha	130 - 250	0.389
A5	alpha	320 - 370	0.389
EL	electron	> 2	0.389

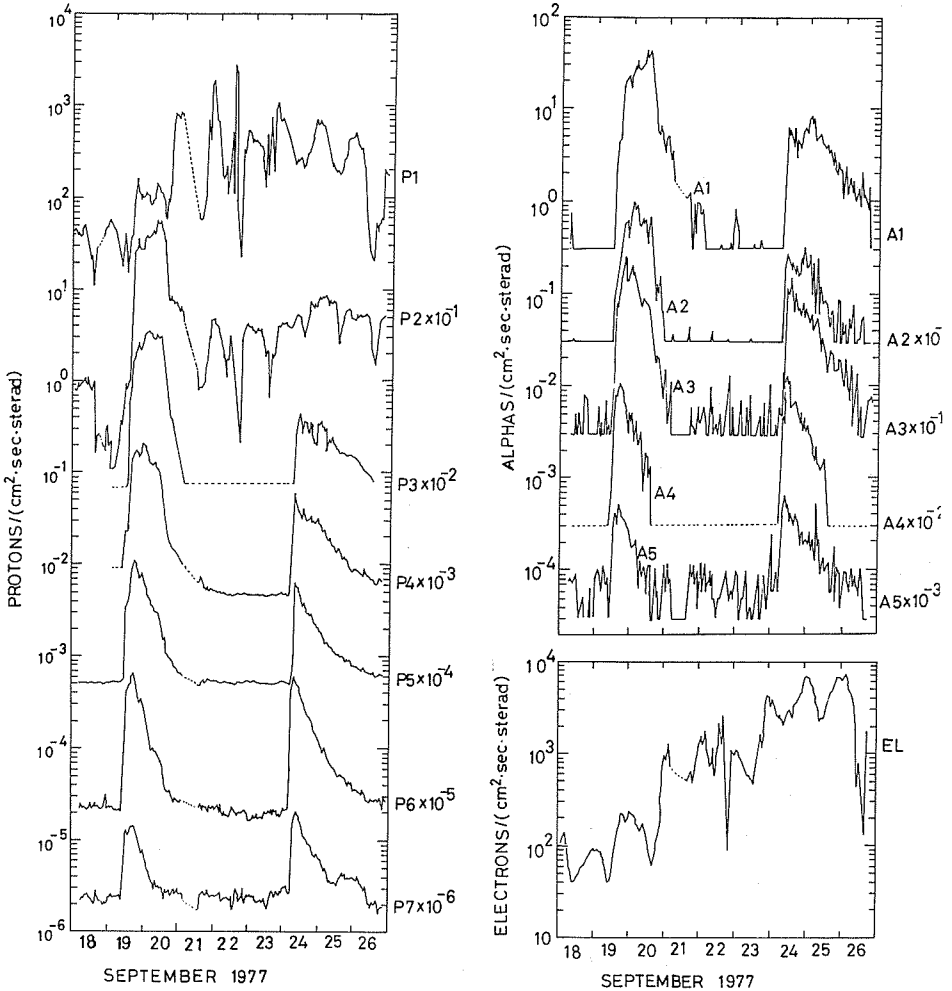

Fig. 1. Hourly averaged fluxes of protons, alphas and electrons observed by "HIMAWARI". Offset magnitudes given to avoid too much overlap are indicated at the right hand side of each channel name. These values are actual counting rates except P3 and A4, where there are relatively high noise levels and the plotted values were obtained by subtracting the noise level from the actual counting rate.

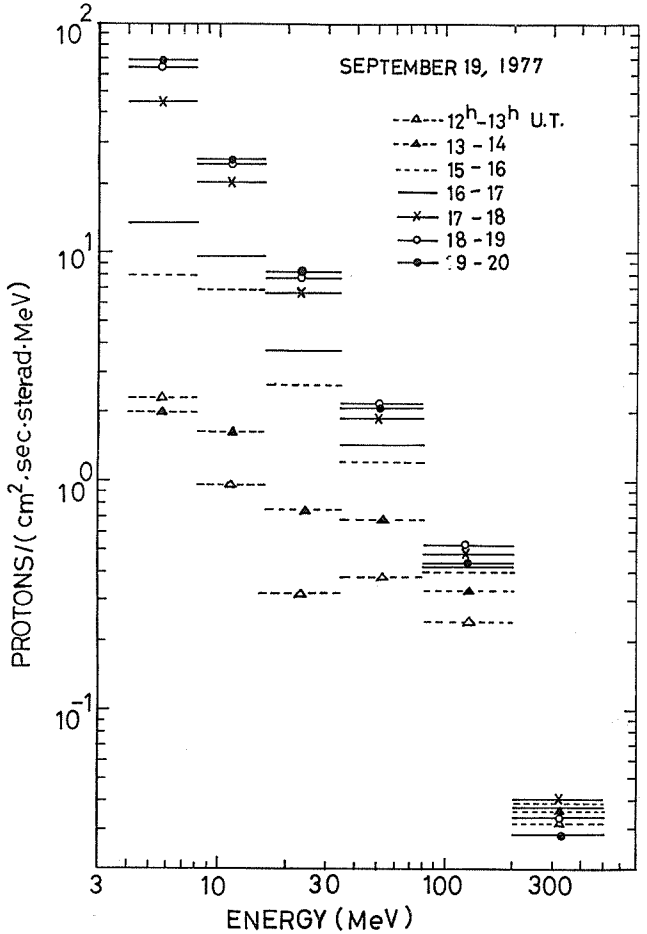

Fig. 2. The hourly energy spectra of protons in build-up phase of September 19, 1977. Data of P1 (1.2 - 4 MeV) were excluded from this figure simply because of the ambiguity of discrimination between "solar proton" and "background flux" that exists steadily in the vicinity of geostationary orbit in this energy range.

Results of Relativistic Particle Measurements in September 1977 with Cerenkov Detector Onboard Cosmos-900 Satellite

by

E.V. Gorchakov, V.A. Iozenas, M.V. Ternovskaya
Institute of Nuclear Physics, Moscow State University
Moscow 117234, USSR

A global multichannel Cerenkov detector with large geometric factor (g ~900 cm^2ster for lower threshold) was installed on Cosmos-900 satellite to obtain information about the intensity and dynamics of fast charged particles in the Earth's vicinity.

A plexiglass spherical radiator of a 30-cm diameter was used as the Cerenkov radiation source in the instrument. Twenty channels of the instruments detected singly charged particles with $Z \geq 2$, 3, 4, 5, 6, 7 and 8.

Cosmos-900 was launched on March 30, 1977, in an almost circular orbit with an altitude of ~500 km. The angle of orbit inclination to the equatorial plane was 83°. At the time of this writing the instrument has been in operation for ~ 6000 hours. Information for September 17, 20, 21, 22, 23, 27, 28, 29 and 30, 1977, has been processed for a single parameter corresponding to the lower threshold. For September 19 the information from thresholds I, IV, V, and XVI obtained during 12 orbits of the satellite has been processed. Figure 1 shows the plots of the counting rates (cts/s) for three channels of protons and electrons as a function of geographic latitude. These are channel I ($E_p \geq 450$ MeV, $E_e \geq 10$ MeV, G~9000 cm^2 ster); channel IV ($E_p \geq 500$ MeV, $E_e \geq 15$ MeV, G~7200 cm^2 ster); and channel V ($E_p \geq 550$ MeV, $E_e \geq 20$ MeV, G~6200 cm^2 ster). Results for channel XVI ($Z \geq 3$, $E_Z \geq 700$ MeV/nucleon) are also plotted. The longitude of satellite traversal of the geographic equator, λ_E, is shown near the vertical lines. The time of day corresponding to the satellite traversal of the equator is also shown. The plots presented for the three orbits are characteristic of all 12 orbits. The latitude dependence of cosmic ray intensity obtained by us agrees in general with earlier measurements [Vernov et al., 1969; George, 1970]. For the first threshold, the counting rate on the plateau in the high-latitude region (ϕ~60°) is about 10 times the counting rate near the equator. For threshold XVI, the equator-to-high latitude counting rate ratio is ~1/4. The counting rate in channel XVI near high latitudes is ~1/300 that in channel I. The small intensity maxima (~5-10% counting rate excess over the counting rate at higher latitudes), which are noticeable near geographic latitudes of 60° are probably associated with either the outer radiation belt or the albedo particles [Gorchakov and Severinov, 1976; Murayama, 1967]. Such maxima are most pronounced on the dayside of the orbits. For the higher-threshold channels, the maxima are less marked. Besides that, the latitude dependence of the intensity for different channels exhibits the characteristic features, which are probably associated with the lower threshold channels' detection of electrons to a higher degree than the higher-threshold channels. Strong maxima of the intensity associated with the Brazilian anomaly can be seen south of the equator on the plots for the orbits intersecting the equator near the geographic longitudes S43.6° and S67.3°. In those locations, the counting rate for the first threshold may be ~15 times that of the plateau, while the higher thresholds of the instrument fail to detect the increased intensity in those regions. Preliminary calculations that included computing the geometric factors of various channels for the power exponent γ and determining the rate of decrease of the differential counting rate in the first three presented channels, have give γ = 0.4, 1.1 and 3.1 for the geomagnetic equator, polar latitudes, and Brazilian anomaly, respectively. These characterize the rigidity of the particle energy spectrum for those locations. It can be seen from the data obtained that the counting rate for the lower threshold near the South Pole is about 5% in excess of that near the North Pole. The difference disappears for higher thresholds. Near the geomagnetic equator, the counting rate for the lower threshold suffers periodic variations after each half-orbit. When the satellite traversed the equator from south to north, the counting rate was 10-20% as high as that for the traversal from north to south. This phenomenon is probably associated with the geometry of the instrument position relative to the object and with the east-west asymmetry of cosmic ray intensity.

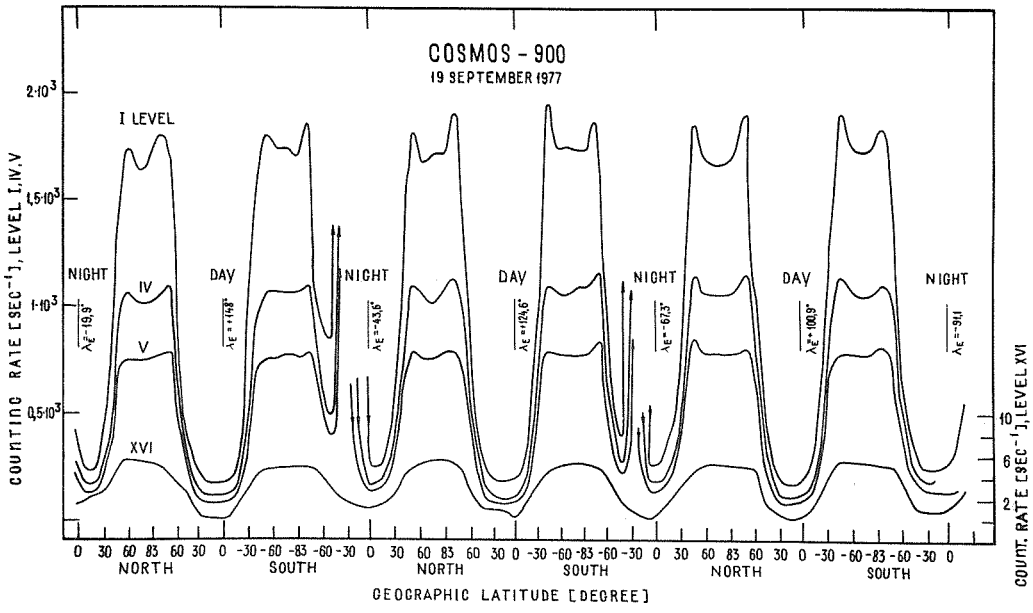

Fig. 1. Latitude dependence of counting rate (cts/s) for channels I, IV and XVI of the Cerenkov detector on Cosmos 900, September 19, 1977.

The data for September 1977 are of interest because the conditions in space during this period reflect the solar activity effect on cosmic rays and the Earth's magnetosphere. On September 7, 9, 16, 17, 19 and 24 many solar flares were observed [*SGD*] which produced the cosmic ray intensity increases detected by neutron monitors and our instrument.

Figure 2 presents the time dependence of the values of the counting rate near the North and South Poles and near the geomagnetic equator for the lower threshold from September 17 to September 30. The figure also shows the daily averages of the Deep River neutron monitor. It can be seen from the plots of Figure 2 that the cosmic ray intensity was approximately at the same level from September 17 to the 21st. The strong decrease in the intensity on September 22 and 23 was associated with a Forbush-effect from the solar flares of September 16 and 17. The intensity decrease was ~21% relative to the recovered value on September 30. According to the data of the Deep River neutron monitor, the daily average cosmic ray intensities decreased by ~6%. The maximum decrease for the hourly data was ~11%, i.e. it was approximately 2 times smaller than the Cosmos 900 data. As was noted earlier [Gorchakov et al., 1976], the same difference was observed between the Forbush-decreases detected from the Mars-2, Mars-4 and Mars-7 space probes and with the Deep River neutron monitor.

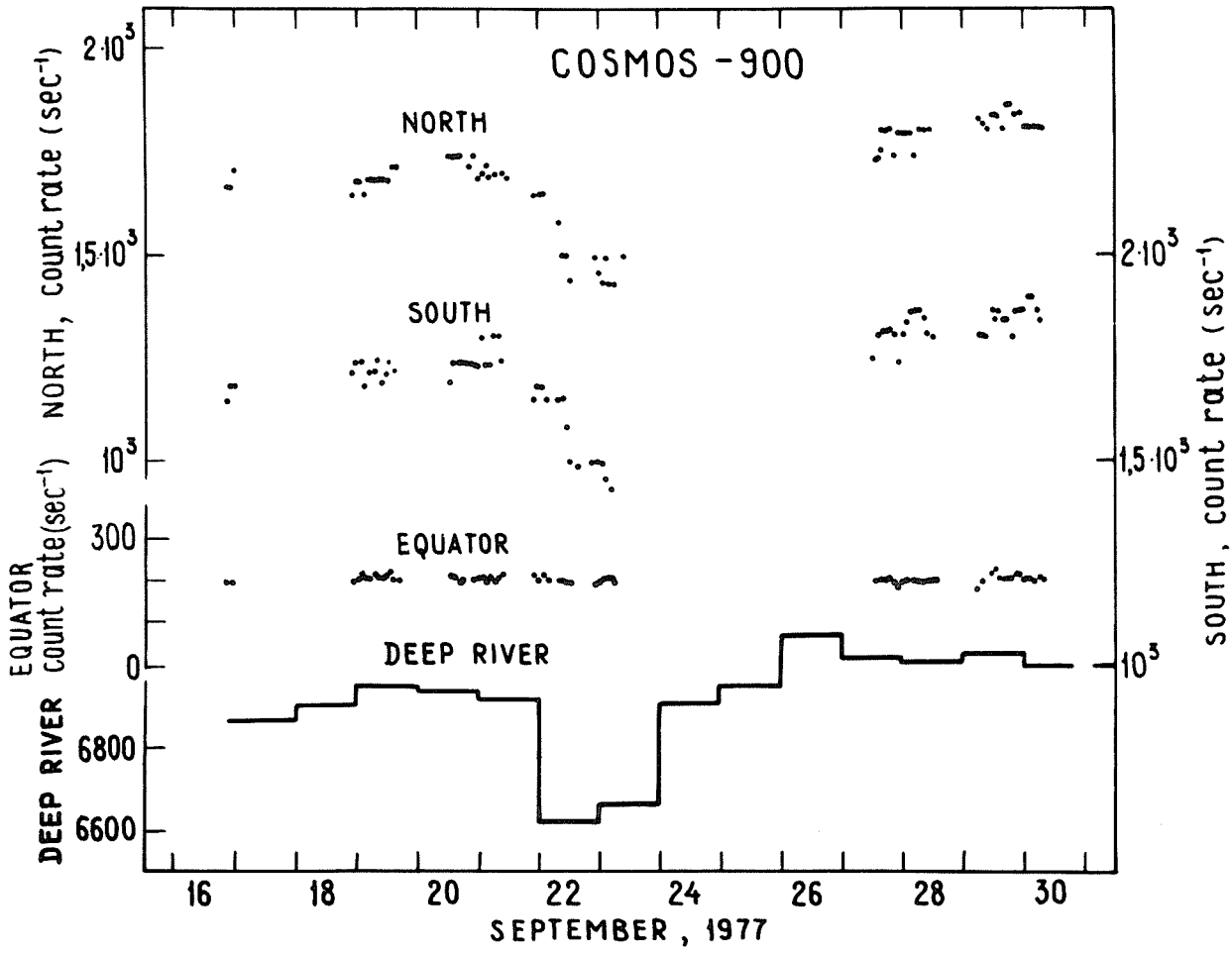

Fig. 2. Time dependence of counting rate (cts/s) on Cosmos 900 for channel I of the Cerenkov detector in polar regions and near the geomagnetic equator. Also shown are the readings of the Deep River neutron monitor for September 16-30, 1977.

It should be noted in Figure 2, that the processing of the data for September 23, on the basis of a higher time resolution, shows the existence of very sharp intensity maxima on the higher-latitude side. Such peaks extended 1.5-2° in latitude. The intensity was ~12% of the nondisturbed level. The existence of such peaks was indicated in work by Anderson et al. [1968] where the relationship of their occurrence frequency with the Kp-index was noted and the cause of peaks was related to the 1-10 MeV electron injection from the outer radiation belt.

Acknowledgment. The authors are indebted to A.E. Chudakov and B.A. Tverskoy for continuous support and interest in the work and to G.G. Zenchev, O.V. Rukosneva, Z.S. Shershukova, V.G. Afanasiev, and K.G. Afanasiev for their assistance.

REFERENCES

ANDERSON, H.R., P.D. HUDSON and J.F. MCCOY 1968 "Observations of POGO Ion Chamber Experiment in the Outer Radiation Zone," *J. Geophys. Res., 73,* 6285-6297.

GEORGE, M.J. 1970 "Observations of the Cosmic Ray Knee with a Polar Orbiting Ionization Chamber," *J. Geophys. Res., 75,* 3159-3165.

GORCHAKOV, E.V., P.P. IGNATIEV, V.A. IOZENAS, T.E. SHVIDKOVSKAYA, V.A. YAKOVLEV, I.V. GETSELEV, V.I. TKACHENKO, G.P. LYUBIMOV, N.N. KONTOR and N.G. GALACHIEV 1976 "Cosmic Ray Measurements in September 1973, from Mars 4, 5, 7 Space Probes," *Space Research, 14,* 65.

GORCHAKOV, E.V. and V.I. SEVERINOV 1976 "Accumulation of Albedo Particles in the Earth Magnetic Field," *Geomagn. i Aeron., 16,* 706.

MURAYAMA, T. 1967 "Measurement of Primary and Albedo Cosmic Rays on a Polar Orbiting Satellite." *Planet. Space Sci., 15,* 1169-1180.

SGD 1977 *Solar-Geophysical Data,* No. 399-Part 1, November 1977, NOAA, Boulder, CO 80303.

VERNOV, S.N., E.V. GORCHAKOV, I.V. GETSELEV, P.P. IGNATIEV and M.V. TERNOVSKAYA 1969 "Results of Measurement of Fast Charged Particles by Satellite 'Cosmos-137,'" *Space Research, VII,* 273.

The Measurements of the Positive Ion Concentration at the Height 500 km on September 16, 1977, Based on Cosmos-900 Satellite Data

by

V.D. Ozerov
Space Research Institute
Academy of Sciences of the USSR
Moscow, USSR

Introduction

Satellite data of the positive ion concentration are given, measured at a height of ~500 km during the evening and night hours of September 16, 1977. These measurements are based on the use of a spherical ion trap with floating potential on the outer grid. The pecularities of the latitude distribution regions of ionization at the height of ~500 km are noted. The characteristic features of the ionized-region disturbances are described.

According to the suggestion that the compressional waves are the cause of the ionization disturbances, the wave-like compression rate and possible amplitudes of oscillatory velocities of the plasma are estimated on the basis of the characteristic quasicycloidal distortion of the waveform of the ionic trap collector current. The point and integral methods of such an estimation are described. The steep front irregularities created by the intense compressional waves with a high compression rate are considered the probable cause of the range spread type of spread F.

The Cosmos-900 satellite was launched on March 30, 1977 into an orbit with parameters as follows: initial period of revolution 94.4 min, apogee 523 km, perigee 460 km, orbit inclination 83°. The apparatus to measure the positive ion concentration (n_i) by spherical ion traps with floating potential on the outer grid aborad Cosmos-900 is now working.

Supposing ionospheric plasma to be motionless, n_i can be calculated by the equation

$$n_i \simeq \text{const } I/V_T$$

where I is the current flowing in the ionic trap collector circuit; I is proportional to the flux density of the ion flow met by the ion trap; V_T is the satellite velocity.

This method enables us to make instantaneous measurements of n_i with minimal requirements to the information possibilities of the telemetric channels. In this report we give the results for the n_i measurements on September 16, 1977 from 1916 to 2232 UT, as plotted in Figures 1-3, and also some peculiarities of the next n_i measurements.

The period from September 7 to 24, 1977 is characterized by the high level of energetic solar proton events and accompanying magneto-ionospheric disturbances. The magnetic storm ($1-\leqslant Kp \lesssim 4+$) was registered from 0600 UT on September 16, 1977 to 1500 UT on September 17, 1977. The sudden commencement of the ionospheric disturbance was registered from 2129 UT on September 16, 1977 to 0416 UT on September 17, 1977. At 2330 UT on September 16, 1977 one noted a growing flow of solar protons with energies 40-500 MeV by means of the apparatus aboard the SMS-2 satellite [SGD].

The Characteristics of the Main Latitude Regions of the n_i Distribution Based on Cosmos-900 Data

The equatorial anomaly region, the main mid-latitude trough region, and the high-latitude region have clear distinctions (see Figure 1). The day-side equatorial anomaly region possesses the highest values of n_i. As a rule, the shape of the n_i distribution consists of two maxima with a shallow minimum between them. However, we recognize an atypical exception to this rule: on September 16, 1977 at 2248-2304 UT (~15 LT) the n_i distribution in this region had only one maximum and the fall of n_i was located at the place of the usual second maximum. More essential changes of the n_i distribution can take place in the night-side equatorial region where the equatorial mean level of n_i can be lower, compared with the level of n_i at the edges of the region (see Figure 2). The mid-latitude ionization trough has a gently sloping low-latitude boundary and a steep sloping high-latitude one. The minimal values of n_i can be $n_{i\,min} \sim (2\text{-}3)\cdot 10^3$ cm^{-3}. The high-latitude region is characterized by the moderate mean level of $n_i \sim 10^5$ cm^{-3} and by nonmonotonic disturbances of n_i which occurred the most frequently.

The Peculiarities of the Latitude Distribution of the Ionization Disturbances

The night-side high-latitude region ($\Lambda \sim 60\text{-}80°$) is mostly subject to invasions of energetic charged particles and precipitated soft electrons, and therefore distinguishes itself by the highest level of disturbance. Relative day amplitudes of the n_i oscillations are esentially lower (see Figure 1), 1920-1928 UT (05-15 LT). Disturbances of n_i mostly have comparatively small scales; however, a superposition of small-scale n_i disturbances and large-scale ones can also be observed (see Figure 1, about 2009-2022 UT), and also Figures 2 and 3. The changes of n_i values in the night-side low-latitude region sometimes can be so obvious that the n_i distribution can acquire the form of a large-scale wave-like structure (Figure 2). The mid-latitude trough region distinguishes itself by a sufficiently high level of small-scale n_i fluctuations.

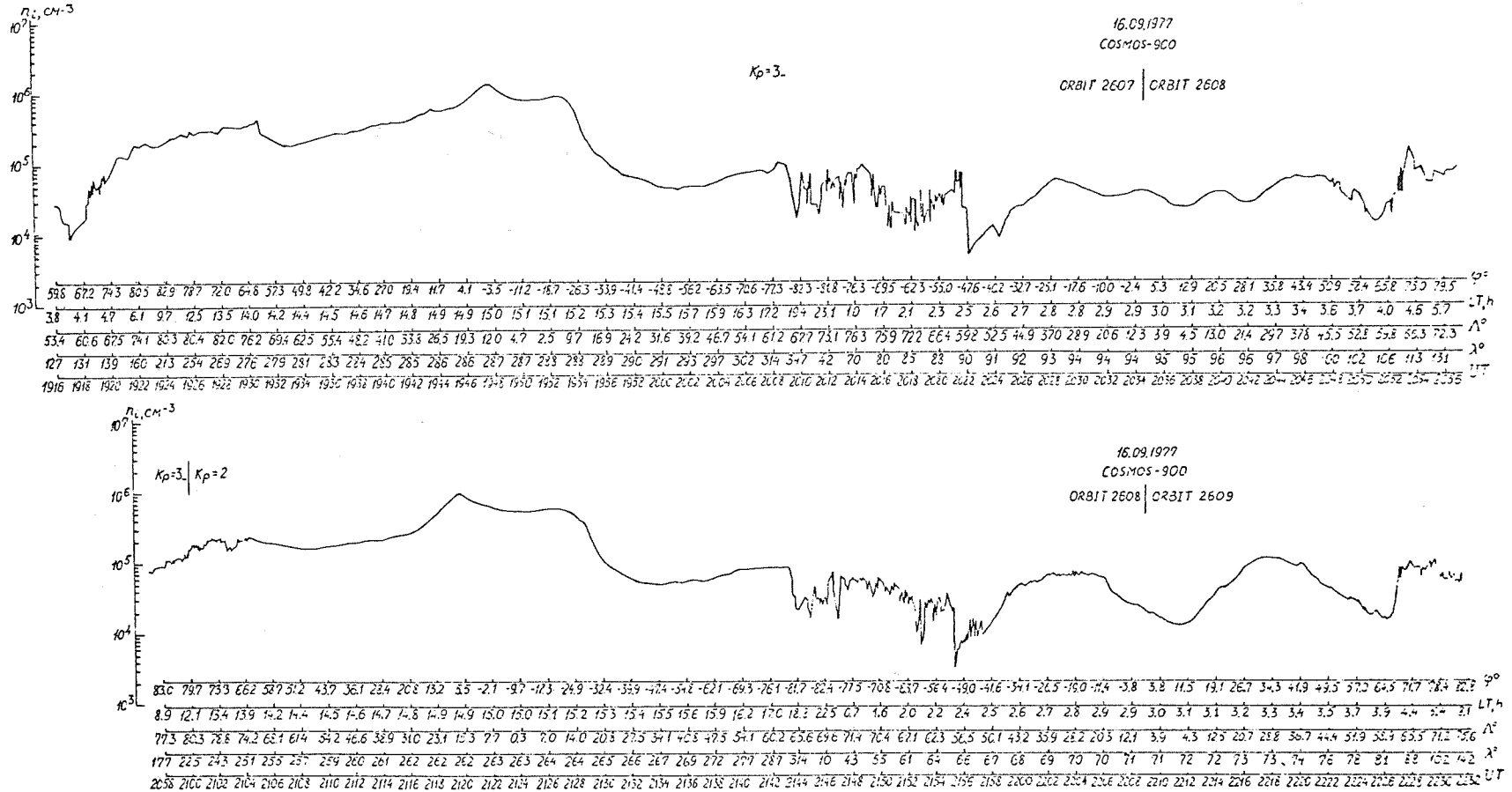

Fig. 1. The experimental data of positive ion concentration from the ion trap measurements on orbits 2607-2609 of the Cosmos 900 satellite at a height of ~500 km on September 16, 1977.

φ is the geographic latitude;
LT is the local time;
Λ is the invariant latitude,
λ is the geographic longitude;
UT is the universal time.

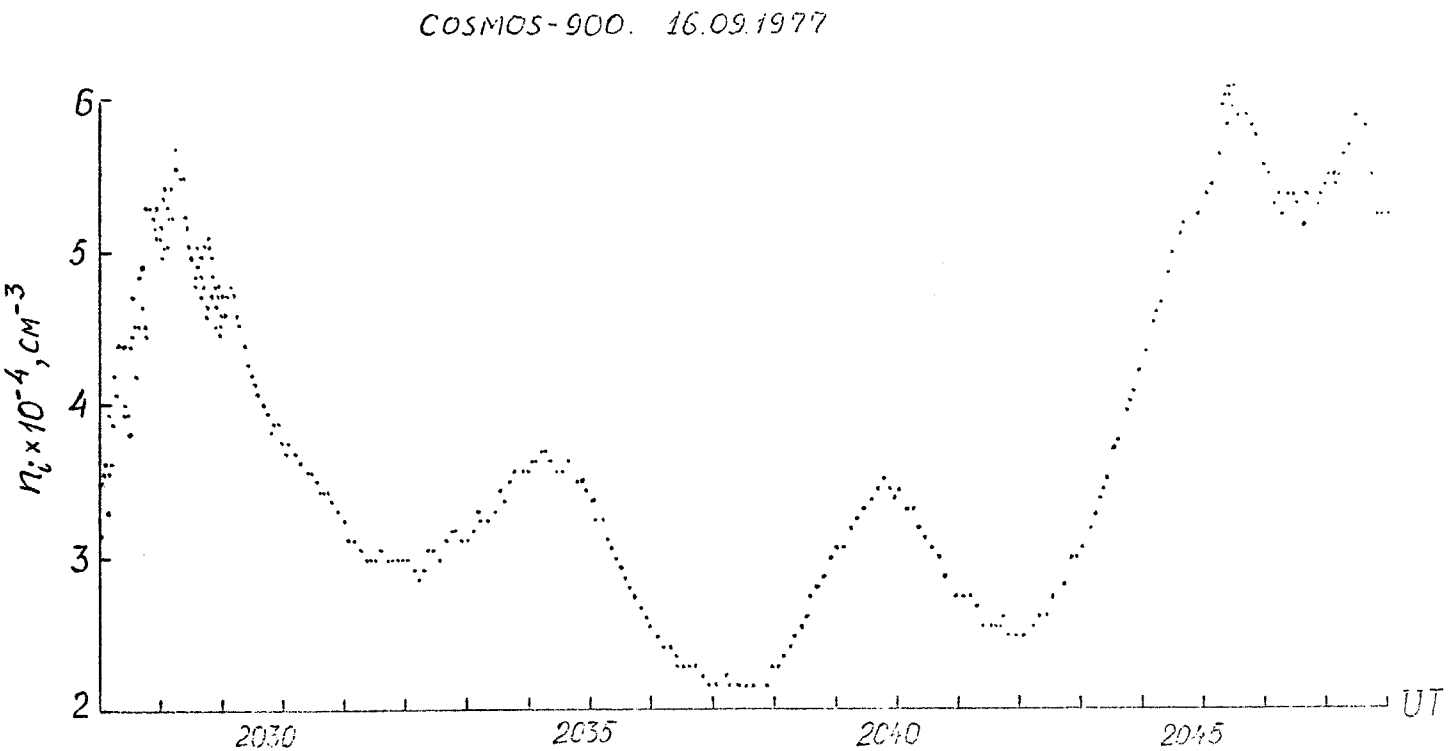

Fig. 2. The waveforms of the ionization disturbances in the night-side low-latitude ionosphere at a height of ~500 km on September 16, 1977.

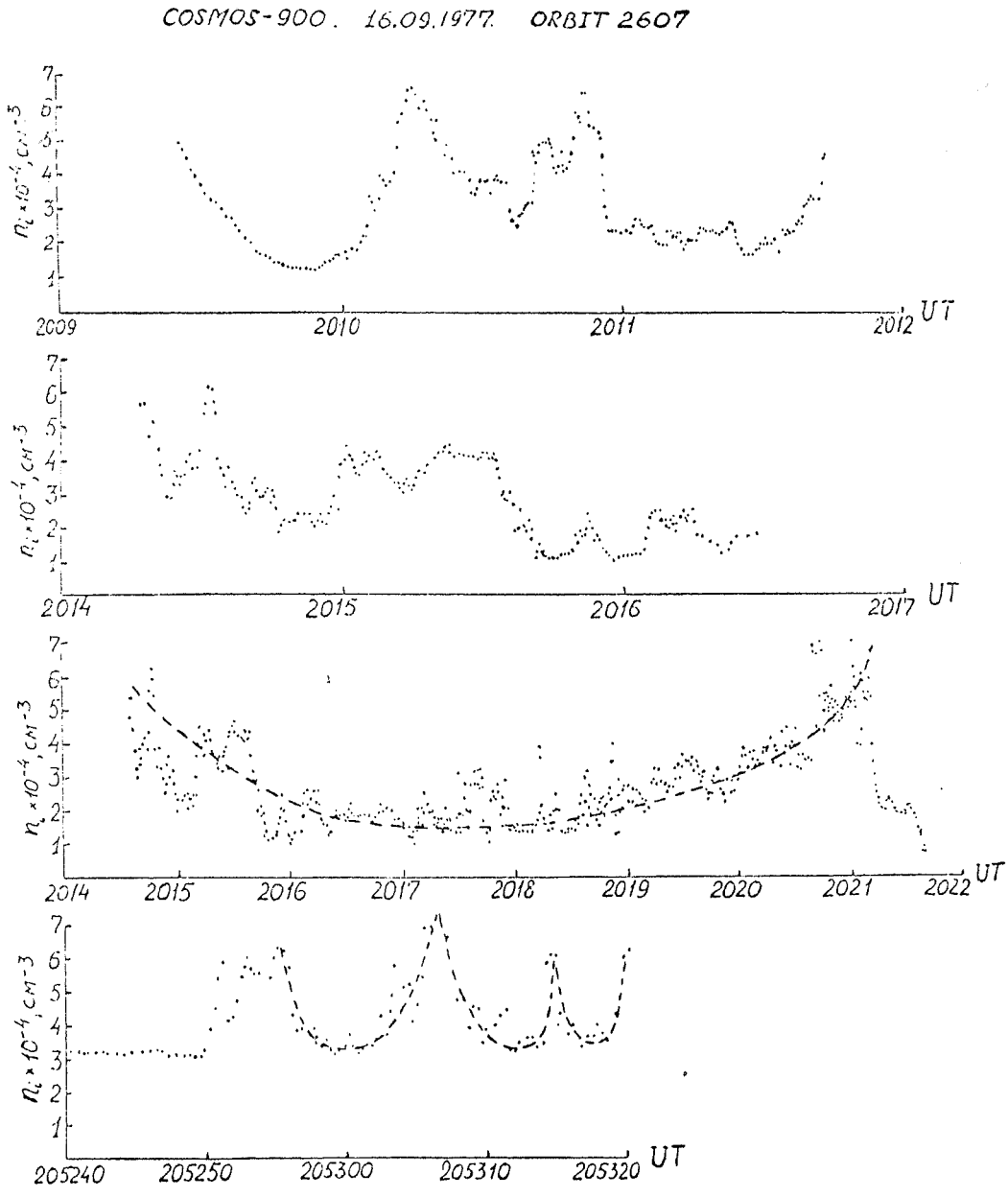

Fig. 3. The waveforms of the ionization disturbances in the night-side high-latitude ionosphere at a height of ~500 km on September 16, 1977.

The Characteristic Properties of and Possible Reasons for n_i Fluctuations in the Low-latitude and Equatorial Regions

The exploration of waveforms of the n_i disturbances showed that the majority of the n_i disturbances have a quasicycloidal waveform (see Figures 2 and 3). This conclusion is in accordance with much data by previous probe measurements (i.e., on board the Third Soviet Satellite, Cosmos-378, Intercosmos-8 satellites, and others). The theoretical analysis showed that the intense particle oscillations in compressional waves, even when of the simplest sinusoidal regularity of the particle displacements from their equilibrium positions, give rise to oscillations of the concentration and particle flux density with a characteristic quasicycloidal waveform with a slightly flattened "bottom" [Ozerov, 1975, 1976 and 1977] (such a waveform was named "acoustoid" [Ozerov, 1977]). The question about the measure of influence of the oscillating particles' velocity on the results of the measurements arises. The physical measure ζ for the quasicycloidality of the disturbance waveform characterizes the intensity of the wave-like compression of the plasma. It is determined as the scalar product of the wave vector ($\vec{k}$) by the amplitude displacement ($\vec{a}$) of the particles from their equilibrium position. The value of ζ can be evaluated by relating either the half-width (C) of the sharp extreme of the concentration or the flux density oscillation waveform, to the half-width D of the blunt opposite extreme.

The dimensionless values for the particle concentration (n_i/n_0), the displaced flux density ($J'i/J_0$) (see Appendix IIA), and the oscillatory velocity ($\tilde{v}_i/v_0$) of particles oscillating in a simple harmonic compressional wave in a homogeneous medium are plotted in Figure 4a. Here $\tilde{v}_i/v_0=-\sin W$: $W = \omega t-\vec{k}\vec{x}$ is the oscillation phase, ω is the oscillation frequency, t is the time, $\vec{x}$ is the vector coordinate for the equilibrium position of oscillating particles; $\ell = dw/dt$; $\ell_0=\omega-\vec{k}\vec{V}$; $\vec{V}=-\vec{V}_T$ is the speed of the plasma flow relative to the ion trap;

$n_i/n_0 = \frac{1}{1+\zeta\sin W}$ (according to the continuity equation);

$\partial n_i/\partial t + \operatorname{div} n_i\tilde{\vec{v}}_i=0$ where $\tilde{\vec{v}}_i=-\vec{a}\omega\sin w$); and $J'_i/J_0=\ell/\ell_0=n_i/n_0$. The solid lines correspond to the case $\zeta=0.8$ and the dotted ones correspond to the case $\zeta = 0$ (the case $\zeta = 0$ is shown as a limiting one for very small values of ζ and corresponds to a pure diametrical wave which does not create the concentration oscillations).

W is related to t by the equation $W-\zeta\cos W=\ell_0 t$. This relation is obtained by multiplying the equality $\vec{X}_T=\vec{X}+\vec{a}\cos W$ ($\vec{X}_T$ is the vector coordinate of the trap and of the particles registered by it.) made scalar by $\vec{k}$, then by differentiation of the equation with respect to t, and by integrating $dw/dt=\ell=\ell_0/(1+\zeta\sin W)$ [Ozerov, 1975]. The curve $\zeta = \zeta(C/D)$ plotted in Figure 4b allows us to evaluate ζ on the basis of the C/D value.

This is the point (local) method to evaluate ζ. For computer calculations the integral method to evaluate ζ is more convenient. This method is based on the linear connection between the square (S) of a period of the oscillating particle concentration (or of the particle flux density or as in this case, of the collector current I) waveform profile; height (H) of this profile (from its foot); oscillation period (T); and the value of ζ as follows:

$$S/(H\cdot T) = (1-\zeta)/2.$$

Hence, $\zeta = 1-2S/(H\cdot T)$ (see Appendix IA).

Evaluations of ζ on the basis of the data in Figure 2 lead to the values $\zeta\sim 0.11$-0.15: these values of ζ are in approximate accordance with the relations among n_i values belonging to the maxima (n_i, max, exper) and to the minima (n_i, min, exper.) of the corresponding oscillation quasiperiod:

$$\frac{n_i,\ \text{max, exper.}}{n_i,\ \text{min, exper.}} \approx \frac{1+\zeta}{1-\zeta} = \frac{n_i,\ \text{max, theor.}}{n_i,\ \text{min, theor.}}$$

(the values n_i, max, theor. and n_i, min, theor. correspond to the continuity equation). This fact indicates the reliability of the suggested reason for the quasicycloidal waveform of the oscillations of I. It also shows that the oscillations of the ion velocities, $\tilde{v}_i$, give sufficiently small contribution to the oscillations of the current I, which is proportional to the ion flux density in the frame of the satellite: $J_i=n_i\cdot v_i\simeq n_i|\vec{v}+\tilde{\vec{v}}_i|$ (see Appendix IIA).

Revelation of the irregularities with steep fronts of n_i growth (similar to the curves plotted in Figures 2-4a and caused by intense compressional waves) is possibly directly connected with the appearance of the range spread type of spread F [Poljakov et al., 1968].

Intense wavelike n_i disturbances in low-latitude and equatorial regions can be caused by the gradient drift instabilities and waves caused or supported by gradients of the plasma concentration, plasma temperature, and the mean mass number of plasma ions (e.g., regions with a complex ionic composition of the plasma, as for example in the trough region).

The n_i Fluctuations in High-latitude Regions

Data plotted in Figure 3 lead in some cases to essentially greater values of ζ, reaching $\zeta \sim 0.3$-0.6. Also the relation of the extremes of n_i is often very different from the calculated values of ζ. This fact indicates the influence of ionic oscillatory velocity; its amplitude estimation leads in some cases to the values of $v_0/V_T \sim 0.3$-0.4, smaller values of ζ being often accompanied by the greater

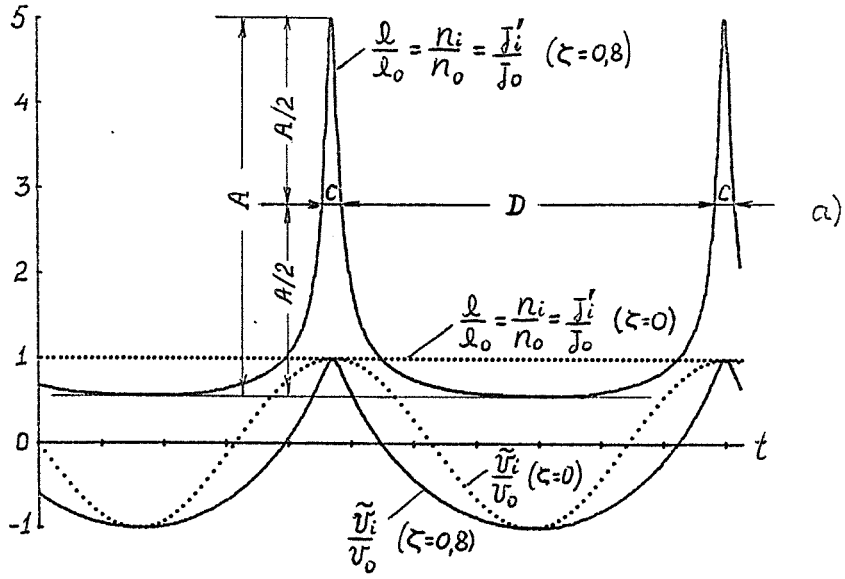

Fig. 4a. The theoretical waveform of concentration, velocity and particle flux density disturbances in a simple intense harmonic compressional wave.

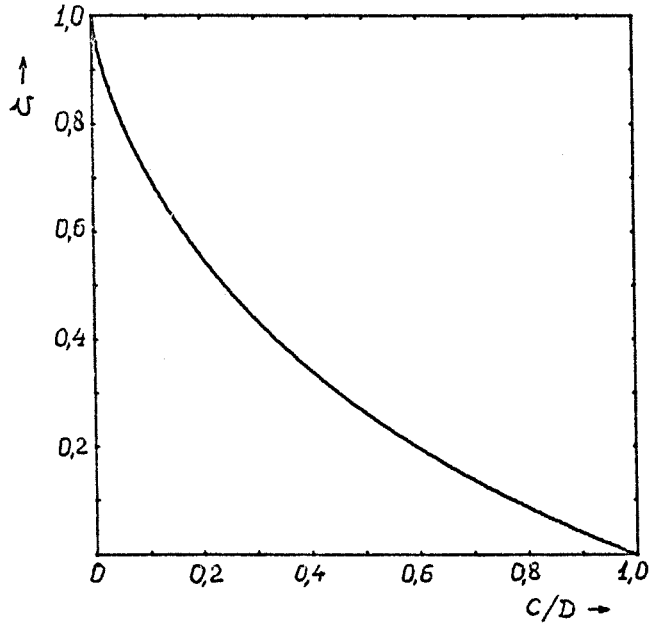

Fig. 4b. The relation of the parameter ζ to the geometric factor C/D which characterizes the theoretical waveform of concentration and flux density disturbances of oscillating particles.

values of v_0/V_T and vice versa. The oscillatory ionic velocities in high-latitude irregularities were found due to other indications from ion traps installed on board Intercosmos 8 [Serafimov et al., 1976]. Consideration of the oscillatory ionic velocity can lead to changes in recorded amplitudes of n_i oscillations by 150 and sometimes 200-300 percent (see Table 1).

Table 1

UT	$J_{i,max}/V_T$ cm^{-3}	$J_{i,min}/V_T$ cm^{-3}	ζ	V_0/V_T	$n_{i,max}$ cm^{-3}	$n_{i,min}$ cm^{-3}	$J_{i,max}/V_T - J_{i,min}/V_T$ $n_{i,max} - n_{i,min}$
2010	6.6×10^4	1.3×10^4	0.34	0.44	4.6×10^4	2.3×10^4	2.3
2010:15-2010:50	6.6×10^4	3.2×10^4	0.40	0.13	7.5×10^4	2.8×10^4	0.7
2011-2012	6.6×10^4	1.9×10^4	0.48	0.09	6.1×10^4	2.1×10^4	1.17
2014-2022	6.8×10^4	1.5×10^4	0.55	0.16	6.0×10^4	1.7×10^4	1.25

Appendices

IA. The Grounds of the Point and Integral Methods of ζ Estimation.

1. The Point Method. The phases $W = W_m$, corresponding to the value $n_i = n_{i,m}$ (the mean arithmetic value of n_i extremes), satisfy the equation

$$\frac{n_{i,m}}{n_0} = \frac{J_{i,m}}{J_0} = \frac{1}{1+\zeta\sin W_m} = \frac{1}{1-\zeta^2} \quad \text{or} \quad W_m = \arcsin(-\zeta) \quad \text{or} \quad W_m \mp \zeta\sqrt{1-\zeta^2} = \ell_0 t_m = Z_m$$

(the sign " - " corresponds to the condition

$$\frac{\pi}{2} + 2\pi q \le W_m \le \frac{3\pi}{2} + 2\pi q;$$

the sign " + " corresponds to the condition

$$\frac{\pi}{2} + 2\pi q \ge W_m \ge -\frac{\pi}{2} + 2\pi q, \quad q = 1, 2, 3, \ldots).$$

The differences $\Delta_1 Z$ and $\Delta_2 Z$ between the neighboring values of Z_m correspond to the values C and D of the half-widths of the neighboring opposite extremes of oscillating parameters n_i/n_0 and J_i/J_0 (see Figure 4a).

Hence

$$\frac{\Delta_1 Z}{\Delta_2 Z} = \frac{\pi - 2(\arcsin\zeta + \zeta\sqrt{1-\zeta^2})}{\pi + 2(\arcsin\zeta + \zeta\sqrt{1-\zeta^2})} = \frac{C}{D} \qquad \text{or} \qquad \arcsin\zeta + \zeta\sqrt{1-\zeta^2} = \frac{\pi}{2}\,\frac{1-C/D}{1+C/D}$$

(see Figure 4b).

2. The Integral Method. The square S of one period of the curve

$$\frac{n_i(t)}{n_0} = \frac{1}{1+\zeta\sin W(t)}$$

between its minimum and maximum levels equals the integral of the difference

$$\frac{1}{1+\zeta\sin W} - \frac{1}{1+\zeta}$$

Taking into consideration the relation

$$W - \zeta\cos W = \ell_0 t = \frac{2\pi t}{T}$$

or

$$dw/dt = \frac{2\pi}{T}\,\frac{1}{1+\zeta\sin W}$$

we have

$$S = \int_{t_1}^{t_1+T}\left(\frac{1}{1+\zeta\sin W} - \frac{1}{1+\zeta}\right)dt = \int_0^{2\pi}\frac{1}{1+\zeta\sin W}\cdot\frac{T}{2\pi}(1+\zeta\sin W)\,dW - \frac{T}{1+\zeta} = T\cdot\frac{\zeta}{1+\zeta}.$$

The height H of this curve (from its top to its bottom) equals the difference between the neighboring opposite extremes:

$$H = \frac{1}{1-\zeta} - \frac{1}{1+\zeta} = \frac{2\zeta}{1-\zeta^2}$$

Hence

$$\frac{S}{HT} = \frac{1-\zeta}{2}; \quad \zeta = 1 - \frac{2S}{HT}$$

IIA. The Estimation for the Contribution of Ionic Oscillatory Velocity to the Flux Density

If $|\tilde{v}_i| \ll V_T$ then $v_i \simeq V_T$ and the flux density

$$J_i = n_i \cdot v_i \simeq n_i \cdot V_T$$

differs from the corresponding n_i value only by the constant multiplier V_T. Consequently, by the oscillations of n_i in a simple harmonic compressional wave and by

$$|\tilde{v}_i| \ll V_T ,$$

the relation of the extremes of n_i, which are equal to

$$n_{i,\,max}/n_{i,\,min} = \frac{1+\zeta}{1-\zeta} ,$$

must coincide with the experimental relation of J_i extremes and ζ can be estimated on the basis of the waveform of J_i.

Let us consider another case when the condition

$$|\tilde{v}_i| \ll V_T$$

is not satisfied. Let

$$\vec{\tilde{v}}_i = -\vec{v}_0 \sin W , \quad \vec{J}_i = n_i \vec{v}_i = -n_0 \frac{\vec{V_T} + v_0 \sin W}{1 + \zeta \sin W}$$

($\vec{v}_0 = \vec{a}\omega$ is the amplitude of the oscillatory velocity $\vec{\tilde{v}}_i$, n_0 is the equilibrium value of n_i). Hence

$$J_i'/J_0 = \left|\vec{J}_i + \frac{\vec{v}_0}{\zeta} n_0\right| \Big/ \left(\left|\frac{\vec{v}_0}{\zeta} - \vec{V_T}\right| n_0\right) = \frac{1}{1+\zeta \sin W} = \frac{n_i}{n_0}$$

In other words the oscillations of the J_i value, even if the latter is displaced by a constant and divided by a constant, must have the waveform which is similar to that of the n_i oscillations.

Consequently in this case the value of ζ can also be estimated on the basis of the J_i waveform. However the displacement of J_i as a constant in the value of J_i'/J_0 must lead to another relation of the extremes of J_i. The most intense oscillations of J_i must happen when the ion velocity oscillates along the vector $\vec{V_T}$ and for all that the phase velocity of the wave is opposite to $\vec{V_T}$. Then the extremes of J_i are equal to the following:

$$J_{i,\,max} = n_0 V_T \frac{1+v_0/V_T}{1-\zeta} , \quad J_{i,\,min} = n_0 V_T \frac{1-v_0/V_T}{1+\zeta}$$

This fact leads to the lower value of estimation of v_i and to the corresponding estimated values of n_0 and the real n_i extremes:

$$v_0 \sim V_T \left| \frac{2J_{i,\,max}(1-\zeta)}{J_{i,\,max}(1-\zeta) + J_{i,\,min}(1+\zeta)} \right| , \quad n_0 \sim \frac{J_{i,\,max}(1-\zeta) + J_{i,\,min}(1+\zeta)}{2V_T} , \quad n_{i,\,min}^{max} = \frac{n_0}{1 \mp \zeta} .$$

References

OZEROV, V.D. 1975 Preprint No. D-201. Space Research Institute. Academy of Sciences, Moscow, USSR.

OZEROV, V.D. 1976 Space Research XVI, ed. by M.J. Rycroft, Academie-Verlag, Berlin, pp. 479-484.

OZEROV, V.D. 1977 In: Trudy Meschdunarodnogo simpoziuma po fizike ionosfery, magnitosfery and solnechnogo vetra, Ed. by G.L. Gdalevich and S. Pinter. Geophysical and Astronomical Institutes of the Slovak Academy of Sciences, Hurbanovo.

POLJAKOV, V.M., L.A. SCHCHEPKIN, E.S. KAZIMIROVSKII and V.D. KOKOUROV 1968 Ionosfernye protsessy, Nauka, Siberian department, Novosibirsk, p. 398.

SERAFIMOV, K.G., I.S. KUTIEV, A.Z. BOCHEV, TS. P. DACHEV, K.I. GRINGAUZ, V.V. AFONIN, G.L. GDALEVICH, V.F. GUBSKY, V.D. OZEROV and YA. SCHMILAUER — 1976 — Space Research XVI. Ed. by M.J. Rycroft, Academie-Verlag, Berlin, pp. 465-469.

SGD — 1977 — Solar-Geophysical Data, No. 399, Pt. 1 (U.S. Dept. of Commerce, Boulder, Colorado)

HUDSON, M.K. and M.C. KELLEY — 1976 — The Temperature Gradient Drift Instability at the Equatorward Edge of the Ionospheric Plasma Trough, Journ. Geophys Res., 81, 3913-3918.

Observations of Solar Energetic Particles in Interplanetary Space from from September 24 to 26, 1977 Onboard Prognoz-6 Satellite

by

V.G. Kurt, Yu.I. Logachev, S.P. Ryumin,
V.V. Ratnikov, V.G. Stolpovsky, and I.P. Shestopalov
Institute of Nuclear Physics, Moscow State University
Moscow 117234, USSR

Presented here are the results of measurements of the solar proton and electron fluxes detected with the instruments developed at the Institute of Nuclear Physics of the Moscow State University and flown on Prognoz-6 satellite during the event of September 24, 1977. Prognoz-6 was launched on September 22, 1977 into a strongly extended elliptic orbit with $\sim$200,000-km apogee and $\sim$65° inclination to the equatorial plane. The data presented were for intervals when the satellite was beyond the Earth's magnetosphere. More detailed description of the experiment can be found in Grigoryan et al. [1978] and Kurt et al. [1978] and will also be published in Grigoryan et al. [1978].

Equipment

Table 1 lists the characteristics of the energetic charged particle detectors flown on Prognoz-6. Some methods of particle detection onboard Prognoz-6 were described earlier and the relevant references are indicated in Table 1. We shall dwell here on only two methods.

Table 1. Characteristics of detectors

Detector method	Species, (MeV)	Direction of particle acceptance relative to the Earth-Sun lines (degrees)	Geometric factor ($cm^2 sr$), angular aperture (degrees)	Time resolution of measurements (sec)	References
1. Gas-discharge counter, backscattering	electrons $E_e>0.03$	0	10^{-1} 160	10	Grigorov et al. 1974
2. Gas-discharge counter under active shelding, difference method	electrons $E_e>0.03$	45	$7\cdot10^{-2}$ 46	160	Zeldovich et al. 1974
3. Proportional gas-discharge counter	electrons $E_e \sim 0.01$-0.03	45	10^{-2} 46	160	Kolesov et al. 1978
4. Single n-p counter, $l \approx 50$ mcm, $d \approx 5$ mm, without active shielding	protons $E_p \sim 1.4$-5.8	45	1.2 90	10	
5. Open n-p counter under active shielding with a magnet to discriminate electrons (l=200 mcm, d=5mm)	protons $E_p \sim 0.07$-0.13 $E_p \sim 0.13$-0.22 $E_p \sim 0.22$-0.39 $E_p \sim 0.39$-0.98 $E_p \sim 0.98$-10	45	$6\cdot10^{-2}$ 20	160	
6. Wide-angle n-p telescope	protons $E_p \sim 7.7$-20 $E_p \sim 20$-50	45	4.0 90	160	
7. Gas-discharge counters under passive spherical shielding	E_p >100	global	3.8	300	
	E_p > 30, E_p > 3	global	3.8	300	
	E_p > 15, E_e > 0.5	global	3.8	300	

The first method was used to measure the ∿0.07-10 MeV proton spectrum and flux. An open silicon junction counter of ∿200 mcm thickness and ∿5 mm diameter with instrumental noise below 10 keV was used as the detector. The protons were discriminated in the given energy range with a CsI (Tl) anti-coincidence scintillation counter surrounding the detector. Besides that, the <500 keV electrons were discriminated using a magnetic filter with an effectiveness close to 1. Thus, the parasitic countings in measurements of small proton fluxes may have been due only to inefficincy of the anti-coincidence counters for high-energy particles and bremsstrahlung quanta with energy release above the detection threshold.

The second method was used to measure the protons in the 7-10 MeV range. A wide-angle telescope of two junction counters of ∿1 mm thickness and ∿18 mm diameter, shielded with ∿5 mg/cm^{2}Al, was used as the detector. The discrimination thresholds and the system of selection of events in the telescope permitted the countings due to electrons and high-energy cosmic ray nucleons and nuclei to be excluded with an efficiency of ∿95%. A fairly wide particle acceptance cone (∿90°, to insure a given aperture) gave some uncertainty in the upper limits of the energy ranges indicated in Table 1 (the table presents the data for particle passages perpendicular to the detector surface). However, the uncertainty does not exceed ∿30%.

Such detectors have made it possible to obtain rather detailed data for plotting the flare particle spectrum, while application of different methods of particle detection in given energy ranges has improved the reliability of the data. It can be seen from Table 1 that some detectors on Prognoz-6 have a sufficient aperture at a given measurement frequency to discriminate the effects of the first arrival of particles from the flare to 1 AU.

Observational data

Fig. 1 shows the hourly counting rates for the electrons with E_e ∿10-30 keV (proportional counter, parameter e1), E_e >30 keV (backscattering detector, parameter e2), E_e 0.3-3 MeV (Zhemo-C2 telescope data from the same satellite, see [Grigoryan et al., 1978], parameter e3), and protons with E_p ∿1.4-5.8 MeV (single n-p counter, parameter p). It can be seen from Fig. 1 that the particle flux increased after the flare by a factor of 10^2-10^3.

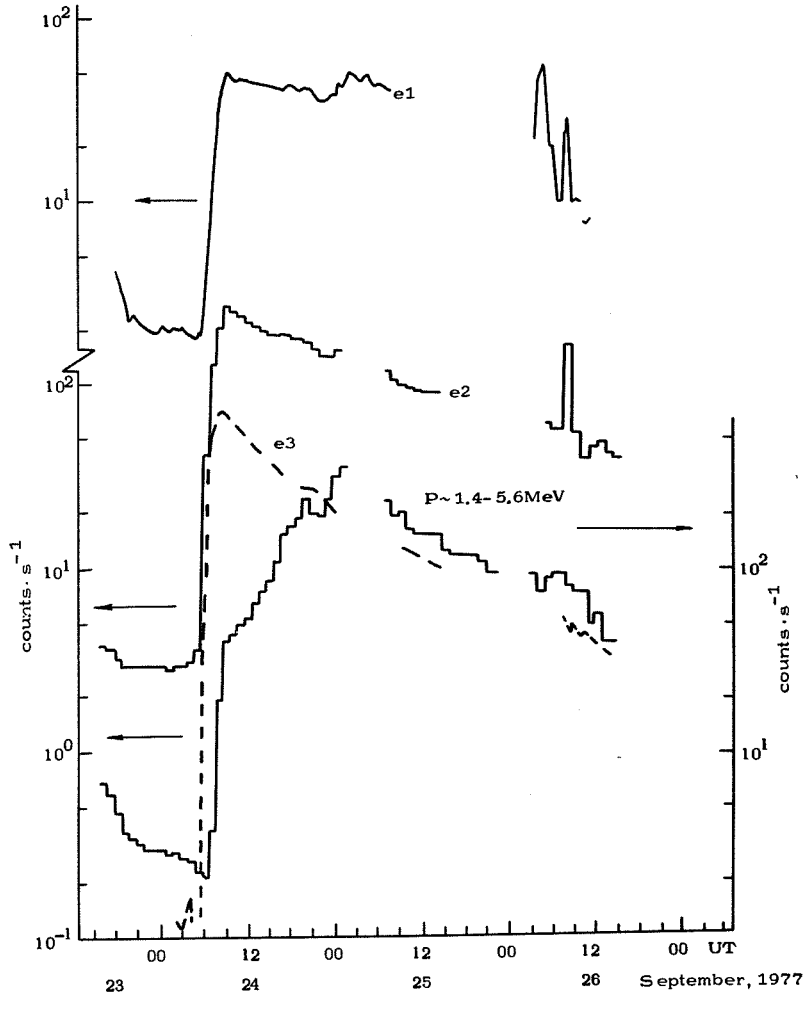

Fig. 1. Counting rates of monitor detectors: E_e 10-30 kev, E_e 0.3-1.3 MeV, E_p 1.4-5.8 MeV for the event of September 24, 1977.

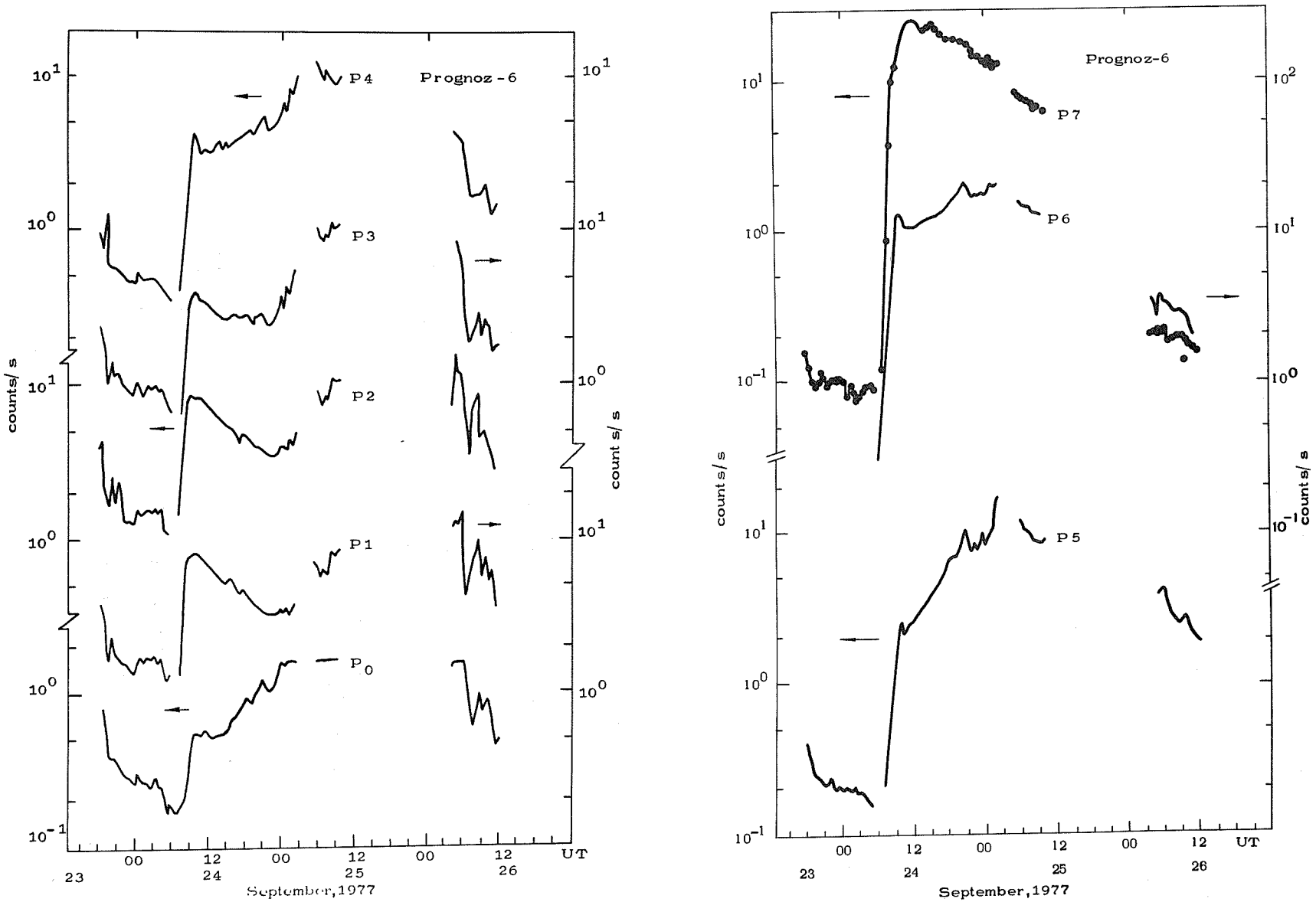

Fig. 2. Proton counting rates for the event of September 24, 1977.

Fig. 2a,b shows the 30-min mean counting rates for protons with E_p >100 keV (proportional counter, parameter p0), E_p ~0.07-0.13 MeV (open n-p counter, parameter p1), E_p~0.13-0.22 MeV (the same, parameter p2), E_p ~0.22-0.39 MeV (the same, parameter p3), E_p~0.39-0.98 MeV (the same, parameter p4), E_p ~0.98-10 MeV (the same, parameter p5), E_p~7.7-20 MeV (wide-angle n-p telescope, parameter p6), E_p ~20-50 MeV (the same, parameter p7). The discontinuity in the time dependences of particle fluxes at 0500-0600 UT on each day is associated with switching of the detectors to calibration mode. The discontinuity in the time dependence for September 25-26 is due to the satellite traversal of the Earth's magnetosphere.

It can be seen from Figs. 1 and 2 that the counting rates in all the proton channels (except for p7) began to grow almost simultaneously with the counting rates in the electron channels and reach their maximum at 0800-0900 UT on September 24. The maximum in the proton channel counting rates is due to the finite effectiveness of the detectors for the high-energy electrons and the relativistic and subrelativistic protons. Estimates show that the contribution from the ≥500 keV electron fluxes to the open n-p counter counting rate (parameters p1-p6) may reach ~0.5-1.5 particle/cm^2 s sr in the given flare. In principle, it is somewhat difficult to estimate the parasitic counting rate due to high-energy electrons and protons and the bremsstrahlund radiation, and such estimates fall beyond the scope of this note. The relevant calculations are being carried out.

Besides that, it cannot be excluded that at 0800-0900 UT on September 24, the particle fluxes from the flare and those associated with some corotating structure were simultaneously detected. An indication of detection of such a structure can be seen in Fig. 3 showing the counting rates for some proton and electron detectors measured at a resolution not worse than 150s. The detectors were so selected that the initial phase of particle increase could be seen for particles of various energies. A slow increase of particle flux, associated probably with the corotating structure, can be noted in Curves 2, 3, 6 of Fig. 3.

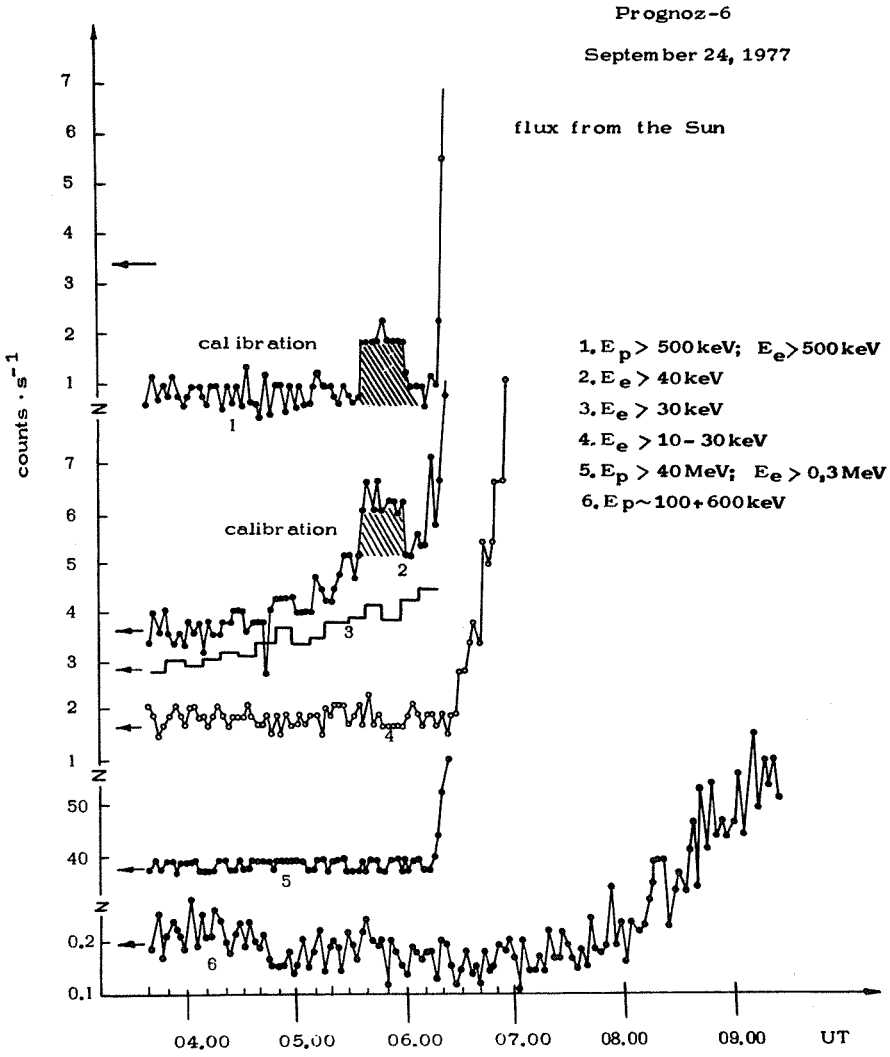

Fig. 3. Initial phase of the increase in the particle fluxes of various energies detected after the flare of September 24, 1977 (0548-0555 UT).

It can be seen from Fig. 3 that the relativistic particles reached the Earth orbit not earlier than at ∿0603 UT (Curves 1, 5) and that the electrons with energies >30 keV and ∿10-30 keV reach the Earth orbit later, in accordance with their velocity.

Fig. 4 shows the time dependence of the counting rates of the gas-discharge counters measuring the particles within a solid angle ∿2π in solar direction. The data have been averaged over a period of ∿ 300s.

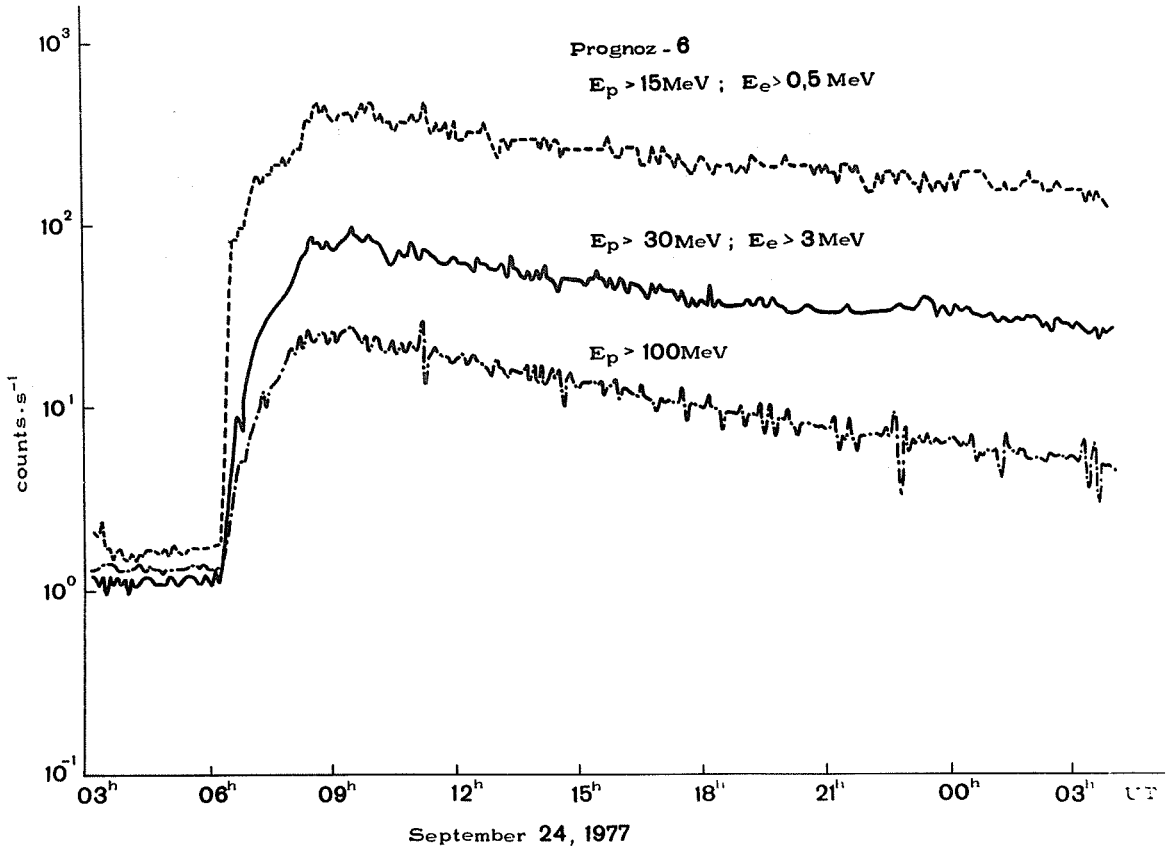

Fig. 4. Counting rates for high-energy protons for the event of September 24, 1977.

It can be seen from Fig. 4 that the shape of the time dependences is close to a diffusive form, excluding for the initial phase. The abrupt increase in the counting rates of the >15 MeV and >30 MeV proton counters is due to detection of relativistic and subrelativistic electrons and bremsstrahlung.

References

GRIGOROV, N.L. V.G. KURT, et al. 1974 "An experiment to study electrons of solar origins by the Prognoz satellites", Kosmicheskie Issledovanya 12, No. 1, 67-73.

GRIGORIAN, O.R. et al. 1978 to be published in Proceedings of IX Leningrad International Seminar.

GRIGORIAN, O.R. et al. 1978 to be published in Kosmicheskie Issledovania.

KOLESSOV, G. Ya. et al. 1978 Kosmicheskie Issledovania, 16, 148.

KURT, V.G. et al. 1978 Presented at XXI COSPAR Meeting, paper II-2.5. Innsbruck 29 May - 10 June 1978.

Energetic Charged Particles from McMath Region 14943 Observed with IMP 7

by

P. R. Briggs, T. P. Armstrong, J. L. Price and R. B. Decker
University of Kansas
Lawrence, Kansas 66045 USA

Introduction

The data set presented here was collected by the Charged Particle Measurement Experiment (CPME) aboard the IMP 7 Earth-orbiting spacecraft. The instrument consists of a solid-state telescope, whose hardware details are described elsewhere [Sarris *et al.*, 1976; Armstrong and Krimigis, 1976]. In addition, particle flux measurements made by the Low Energy Charged Particle experiment (LECP) aboard the outbound Voyager 2 spacecraft have been used to corroborate events identified by IMP 7 [Krimigis *et al.*, 1978].

The CPME detector measures energetic electrons, protons, alpha particles, medium nuclei, and iron group nuclei in several kinetic energy passbands; the relevant information on the channels being used in this study appears in Table 1. All data for this paper take the form of spin-averaged, channel-integrated count rates in counts per second (c/sec).

The IMP 7 spacecraft has a nominal orbit of about 35 R_E; because of the high solar particle fluxes during the period of study, magnetospheric contribution to the low-energy proton and electron channels is minimal.

Table 1. IMP 7 CPME Charged Particle Passbands

Particle Type	Channel Designation	Energy (MeV/nuc)	Geometric Factor (cm^2 sr)
Electrons	E4	0.22 - 2.5	1.51
Protons	P2	0.50 - 0.97	1.51
	P4	1.85 - 4.50	1.51
	P8	25.2 - 49.5	0.32
	P11	190 - 500	0.32
Alphas	A3	1.74 - 4.30	1.51
	A5	11.5 - 26.0	0.32
	A6	26.0 - 52.0	0.32
Mediums	Z1	0.77 - 3.2	1.51
	Z2	1.60 - 3.2	1.51
Iron Group	Z3	3.35 - 7.6	1.51

Solar Activity Sept. 7-24, 1977

The important solar and terrestrial events during the visible disk passage of McMath Region 14943 appear in Table 2 [*SGD*, 1977a&b]. Those events that seem to be associated with particle flux modulations as seen by IMP 7 have been indicated in the last two columns.

Figure 1 is a histogram time profile of protons, alpha particles and medium nuclei count rates, where the averaging interval is 3 hours. We have used the day-of-year (DOY) convention for the time axis; for example, DOY 251 is Sept. 8, and DOY 260 is Sept. 17, 1977. Enhanced activity due to McMath Region 14943 appears to begin around day 251. This plot also reveals the two large flare events marked by arrows on Sept 16 (DOY 259) and Sept. 19 (DOY 262).

In Figure 2 we display the Sept. 16 event in greater detail. The graph covers a 24-hour period with major tick marks every 4 hours. We have plotted 5-min average histograms with ± 1 standard deviation error bars. The particle onset is most evident in the 25-50 MeV proton passband (P8).

Table 2. Important Solar-Terrestrial Events, Sept. 7-24, 1977

DOY	UT	Hα	X-ray	McMath No.	Radio	Ionosphere	IMP 7
250	2225				GB,SWF,IV		
	2258	N12 E>90	✓	14943?		SID(2+)	✓
252	1020	1b N09 E79		14943			
	1604	2b N10 E80	✓	14943		SID(2),PCA	
	1610				GB,SWF,IV		
	1626				IV		
259	2120	2b N08 W22		14943	IV	SID(2)	✓
	2125				GB		
260	2140	2b N07 W21		14943			
261	1905					sfe	
262	1031				GB		
	1045	3b N09 W49	✓	14943	IV	SID(3),PCA	✓
	1143					ssc	✓
263	<0429	2n N11 W57		14943	IV	SID(2)	
	0605	1b N08 W60		14943			
264	2044					ssc	
265	1400					PCA	
267	<0600				IV		✓

Figure 3 shows a similar detailed look at the Sept. 19 event; a 3b flare at N09 W49 began at 1045 UT, and a shock ssc (possibly associated with the Sept. 16 flare) occurred at the Earth about 1143 UT. The low-energy particles (P2, P4, A3, and Z2) seem to show the effects of a pre-shock particle pileup, while the high-energy protons (P8) mark the onset of flare particles at 1 AU. (Sun-Earth particle transit times suggest that the initial low-energy flare ejecta should have arrived at 1 AU sometime after 1200 UT.)

In addition to the above events, a large flux enhancement occurred on Sept. 24 (DOY 267); Hα flare patrol coverage was incomplete before the event, but a Type IV radio signature was observed at approximately 0600 UT. In Figure 4 we display the 5-min average histogram for this day. The count rate increase appears to have originated in solar flare activity, and the two most likely McMath region candidates for the flare site are No. 14943 just behind the west limb and No. 14952 at S24 W20.

For the period Sept. 7-20, 1977, Table 3 lists 3-hour average count rates for electrons (E4), relativistic protons (P11), medium-energy alpha particles (A5), low-energy medium nuclei (Z1) and iron group nuclei (Z3). A histogram plot of these channels has been displayed in Figure 5. Cosmic ray background for channels E4 and P11 is approximately 0.2 and 0.1 c/sec, respectively.

During this period, the LECP experiment aboard the outbound Voyager 2 (at about 1.05 AU) recorded the general activity enhancement as well as the three major flare events on Sept. 16, 19 and 24.

Acknowledgments

This research has been supported in part by NASA under Task I of contract #N00017-72-C-014 with the Department of the Navy.

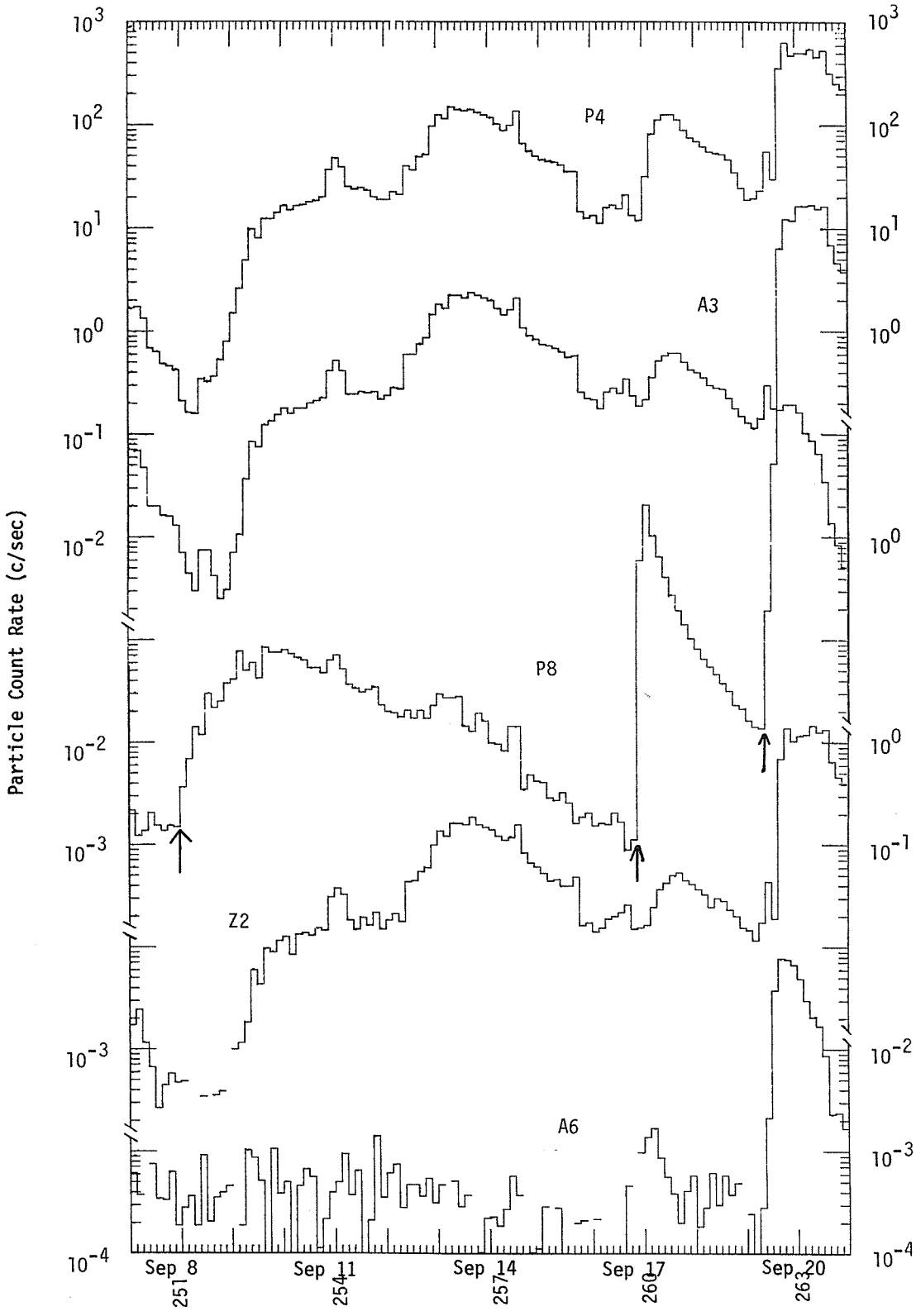

Fig. 1. Histogram time profile of protons, alpha particles and medium nuclei count rates in which the averaging interval is 3 hours. Arrows on the P8 channel mark the onset of enhanced count rates on Sept. 8 and the two large flare events on Sept. 16 and 19.

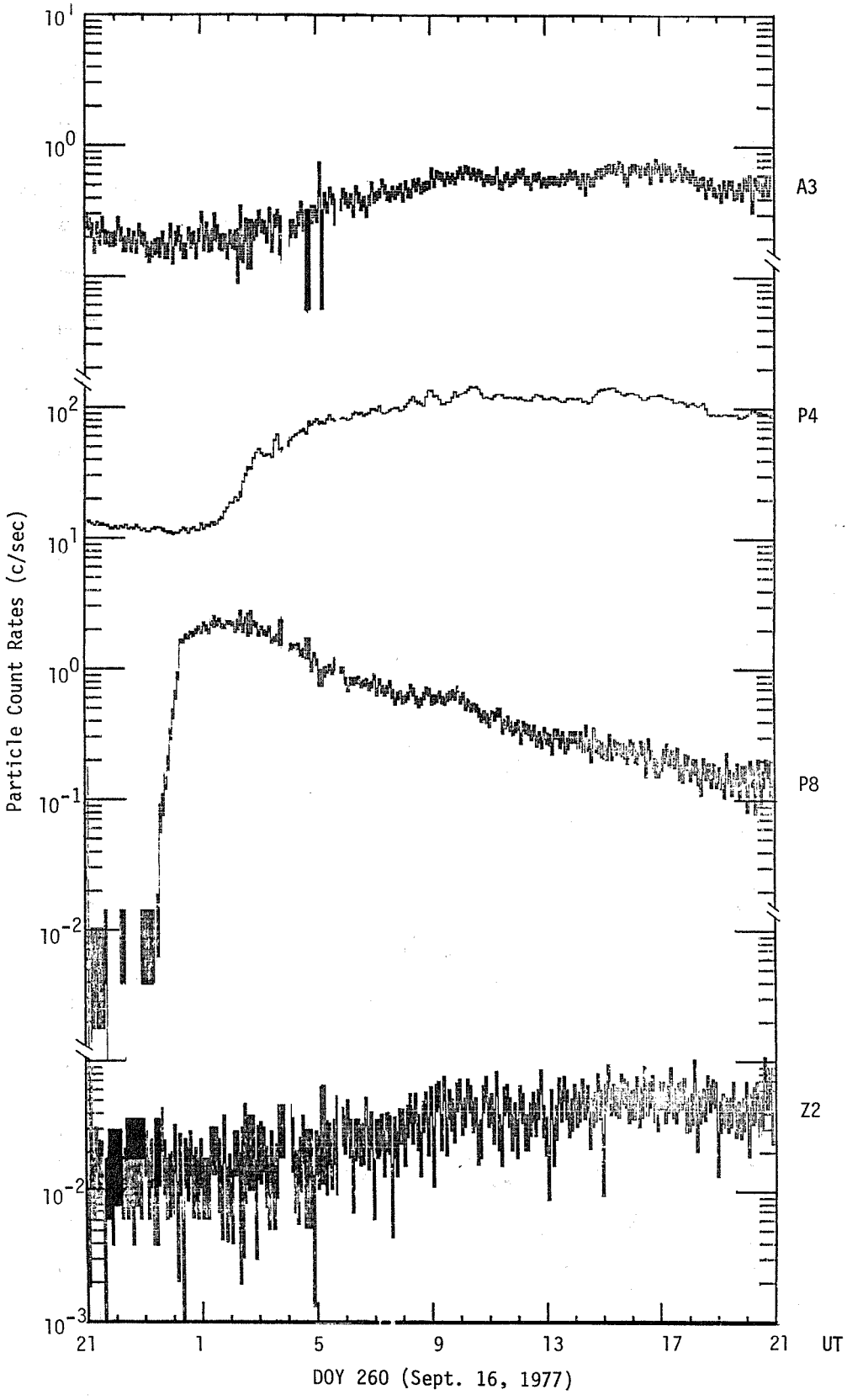

Fig. 2. The Sept. 16, 1977 event in greater detail. Each histogram consists of points averaged over 5 min with ± 1 standard deviation error bars. The graph covers a 24-hour period.

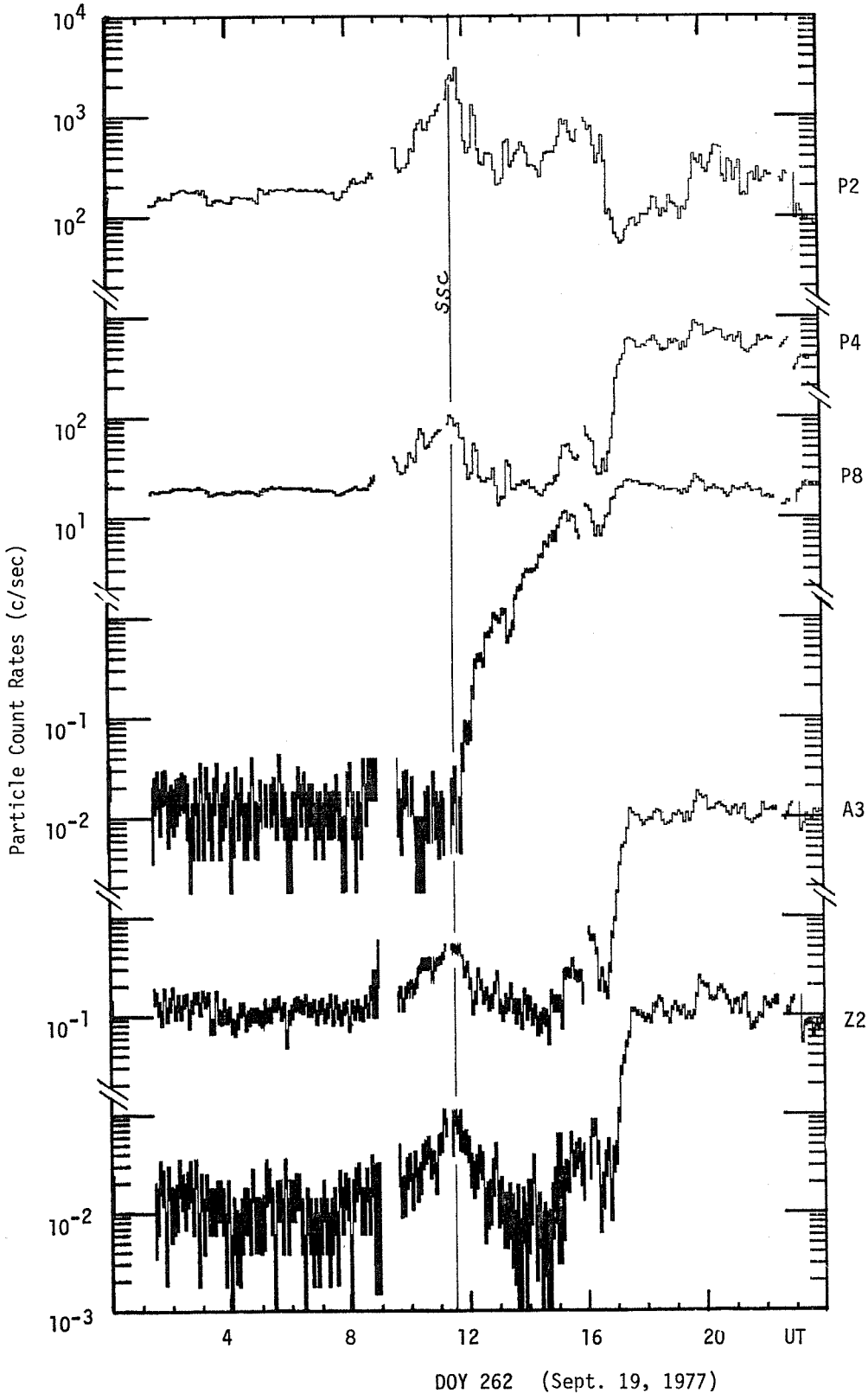

Fig. 3. The Sept. 19, 1977 event in greater detail. Each histogram consists of points averaged over 5 min with ± 1 standard deviation error bars. The graph covers a 24-hour period. A vertical line marks the shock ssc possibly associated with the Sept. 16 flare. The low-energy particles (P2, P4, A3 and Z2) seem to show the effects of a pre-shock particle pileup, while the high-energy protons (P8) mark the onset of flare particles at 1AU.

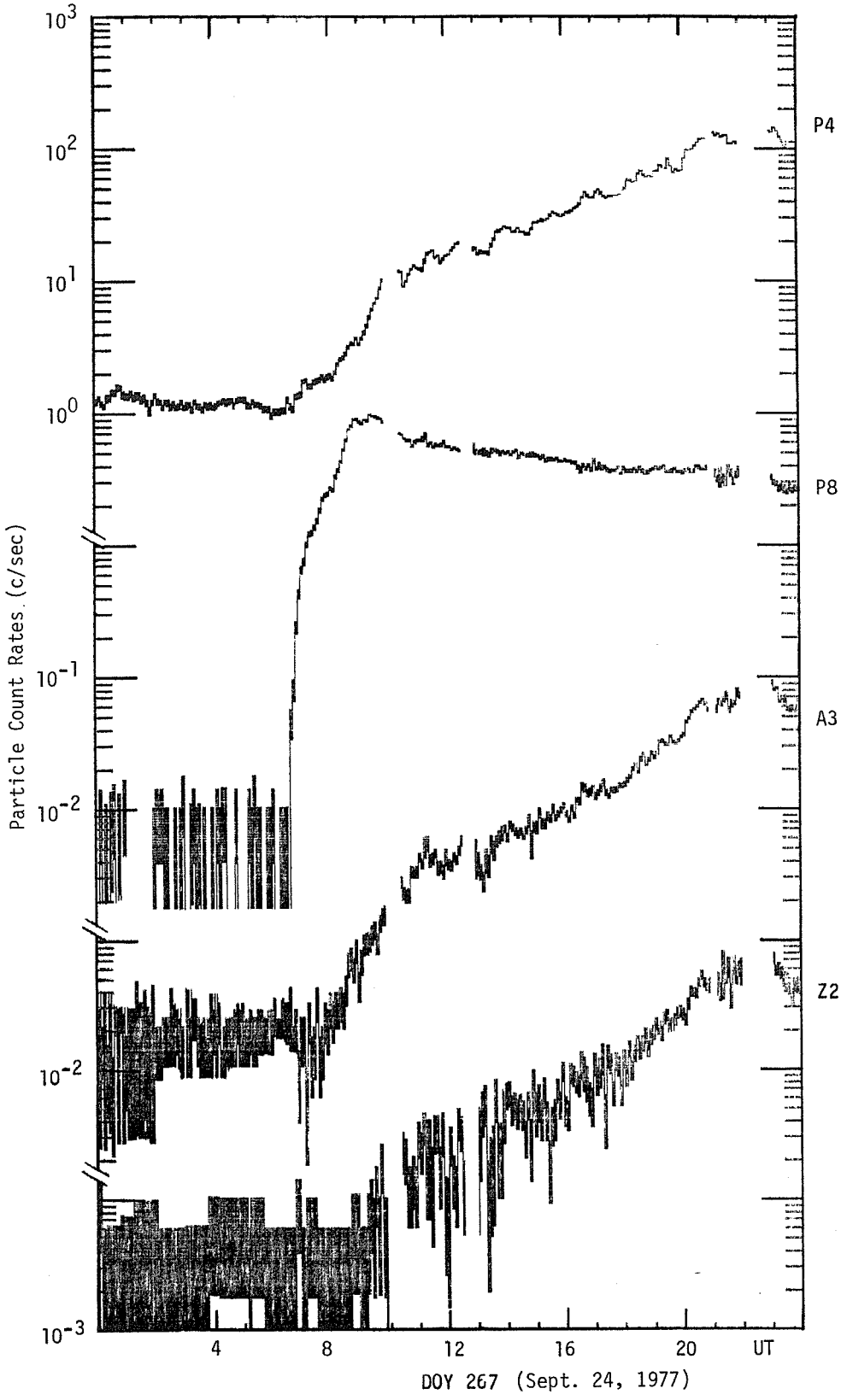

Fig. 4. Five-minute average histograms for the Sept. 24, 1977 event. The count rate increase appears to have originated in solar flare activity. The two most likely McMath Region candidates for the flare site are No. 14943 (just behind the west limb) and No. 14952 at S24 W40.

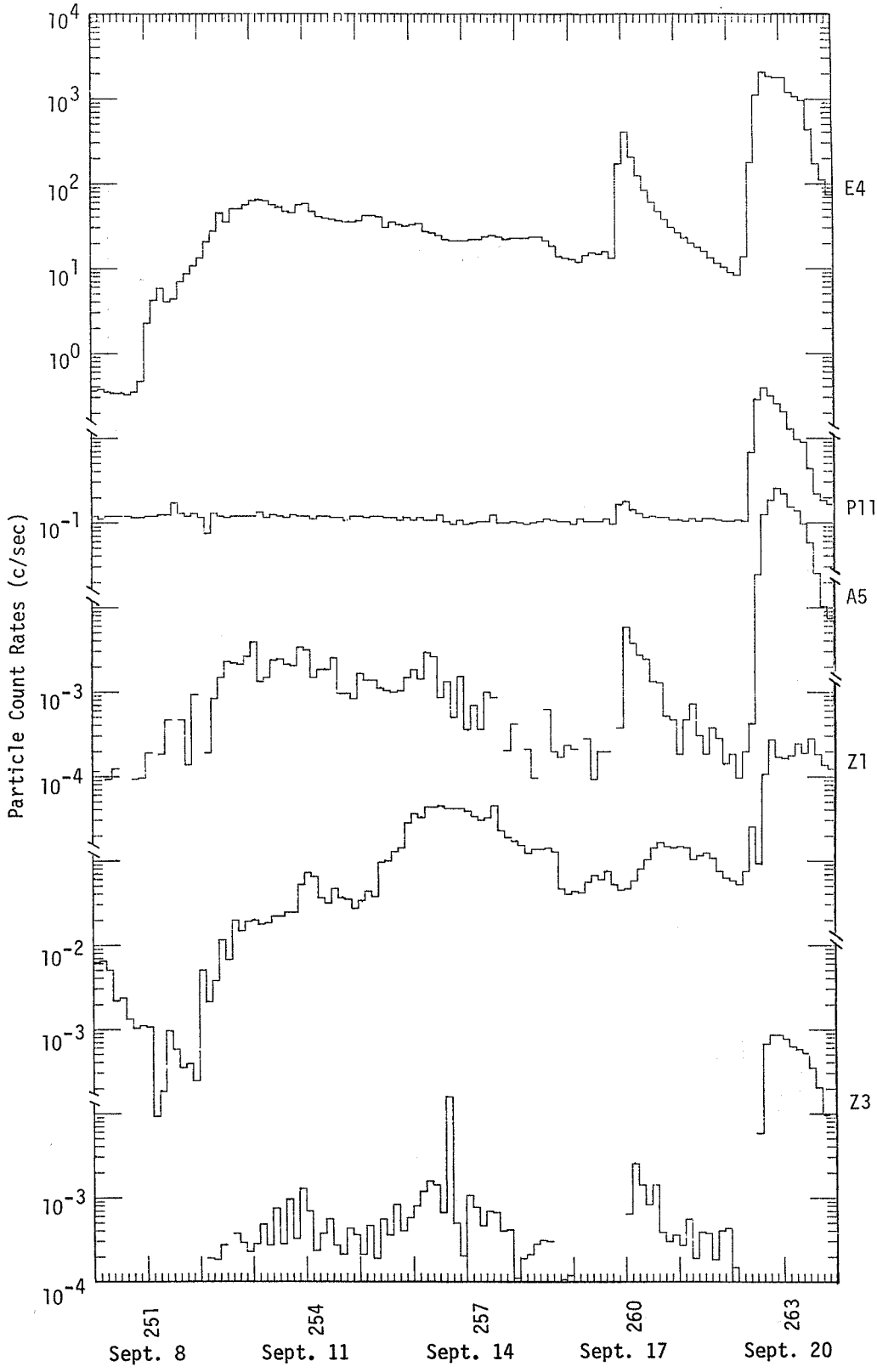

Fig. 5. Histogram of 3-hour average count rates of electrons (E4), relativistic protons (P11), medium-energy alpha particles (A5), low-energy medium nuclei (Z1) and iron group nuclei (Z3) for the period Sept. 7-20, 1977. Background count rates for channels E4 and P11 are approximately 0.2 and 0.1 c/sec, respectively.

Table 3. Three-hour Average Count Rates, September 7-20, 1977

DOY	HR	P11	P11 UNC	A5	A5 UNC	E4	E4 UNC	Z1	Z1 UNC	Z3	Z3 UNC
250	3	0.118	0.596E-02	0.114E-03	0.114E-03	0.371	0.106E-01	0.635E-02	0.139E-02	0.000	0.000
250	6	0.112	0.560E-02	0.000	0.000	0.374	0.102E-01	0.652E-02	0.134E-02	0.000	0.000
250	9	0.120	0.681E-02	0.925E-04	0.925E-04	0.346	0.114E-01	0.512E-02	0.139E-02	0.000	0.000
250	12	0.118	0.762E-02	0.122E-03	0.122E-03	0.338	0.126E-01	0.218E-02	0.981E-03	0.000	0.000
250	15	0.118	0.718E-02	0.000	0.000	0.343	0.122E-01	0.237E-02	0.990E-03	0.000	0.000
250	18	0.118	0.618E-02	0.000	0.000	0.333	0.104E-01	0.132E-02	0.655E-03	0.000	0.000
250	21	0.116	0.689E-02	0.925E-04	0.925E-04	0.347	0.118E-01	0.104E-02	0.656E-03	0.000	0.000
251	0	0.117	0.575E-02	0.956E-04	0.956E-04	0.476	0.115E-01	0.113E-02	0.552E-03	0.000	0.000
251	3	0.119	0.587E-02	0.193E-03	0.193E-03	2.28	0.254E-01	0.108E-02	0.531E-03	0.000	0.000
251	6	0.121	0.579E-02	0.000	0.000	4.24	0.342E-01	0.925E-04	0.925E-04	0.000	0.000
251	9	0.123	0.585E-02	0.185E-03	0.131E-03	5.85	0.404E-01	0.185E-03	0.131E-03	0.000	0.000
251	12	0.125	0.695E-02	0.478E-03	0.373E-03	4.03	0.358E-01	0.977E-03	0.457E-03	0.000	0.000
251	15	0.173	0.359E-01	0.000	0.000	4.40	0.189	0.592E-03	0.342E-03	0.000	0.000
251	18	0.128	0.692E-02	0.473E-03	0.408E-03	6.87	0.503E-01	0.350E-03	0.285E-03	0.000	0.000
251	21	0.119	0.694E-02	0.136E-03	0.136E-03	8.67	0.587E-01	0.389E-03	0.315E-03	0.000	0.000
252	0	0.128	0.108E-01	0.927E-03	0.656E-03	10.8	0.102	0.247E-03	0.247E-03	0.000	0.000
252	3	0.114	0.159E-01	0.000	0.000	13.1	0.170	0.497E-02	0.317E-02	0.000	0.000
252	6	0.761E-01	0.276E-01	0.191E-03	0.191E-03	20.7	0.169	0.210E-02	0.633E-03	0.191E-03	0.191E-03
252	9	0.127	0.593E-02	0.832E-03	0.476E-03	27.6	0.888E-01	0.379E-02	0.102E-02	0.185E-03	0.185E-03
252	12	0.119	0.730E-02	0.147E-02	0.827E-03	45.5	0.147	0.116E-01	0.216E-02	0.277E-03	0.223E-03
252	15	0.117	0.116E-01	0.225E-02	0.159E-02	35.2	0.189	0.680E-02	0.285E-02	0.000	0.000
252	18	0.120	0.841E-02	0.224E-02	0.115E-02	51.3	0.180	0.195E-01	0.338E-02	0.379E-03	0.379E-03
252	21	0.120	0.593E-02	0.211E-02	0.775E-03	50.2	0.125	0.150E-01	0.209E-02	0.297E-03	0.253E-03
253	0	0.121	0.640E-02	0.264E-02	0.943E-03	56.2	0.145	0.193E-01	0.259E-02	0.230E-03	0.230E-03
253	3	0.119	0.590E-02	0.393E-02	0.108E-02	63.4	0.142	0.195E-01	0.240E-02	0.289E-03	0.232E-03
253	6	0.131	0.952E-02	0.135E-02	0.694E-03	64.7	0.220	0.181E-01	0.355E-02	0.486E-03	0.432E-03
253	9	0.115	0.565E-02	0.148E-02	0.619E-03	62.1	0.137	0.186E-01	0.227E-02	0.277E-03	0.227E-03
253	12	0.125	0.594E-02	0.235E-02	0.798E-03	56.2	0.131	0.219E-01	0.248E-02	0.750E-03	0.443E-03
253	15	0.120	0.577E-02	0.243E-02	0.812E-03	52.3	0.126	0.218E-01	0.246E-02	0.279E-03	0.279E-03
253	18	0.114	0.604E-02	0.213E-02	0.794E-03	47.5	0.125	0.247E-01	0.280E-02	0.958E-03	0.553E-03
253	21	0.125	0.678E-02	0.203E-02	0.838E-03	45.6	0.132	0.243E-01	0.295E-02	0.322E-03	0.264E-03
254	0	0.119	0.593E-02	0.334E-02	0.975E-03	55.6	0.133	0.530E-01	0.394E-02	0.130E-02	0.621E-03
254	3	0.121	0.600E-02	0.316E-02	0.940E-03	57.5	0.138	0.722E-01	0.463E-02	0.710E-03	0.445E-03
254	6	0.113	0.626E-02	0.149E-02	0.687E-03	47.4	0.131	0.654E-01	0.475E-02	0.237E-03	0.167E-03
254	9	0.120	0.581E-02	0.187E-02	0.725E-03	40.8	0.109	0.369E-01	0.322E-02	0.374E-03	0.320E-03
254	12	0.119	0.576E-02	0.186E-02	0.717E-03	38.8	0.106	0.320E-01	0.299E-02	0.558E-03	0.385E-03
254	15	0.115	0.978E-02	0.258E-02	0.151E-02	37.8	0.170	0.469E-01	0.598E-02	0.277E-03	0.160E-03
254	18	0.115	0.605E-02	0.981E-03	0.537E-03	36.1	0.109	0.367E-01	0.342E-02	0.210E-03	0.210E-03
254	21	0.106	0.106E-01	0.959E-03	0.554E-03	34.7	0.206	0.355E-01	0.669E-02	0.440E-03	0.311E-03
255	0	0.119	0.649E-02	0.836E-03	0.532E-03	35.7	0.114	0.273E-01	0.310E-02	0.363E-03	0.210E-03
255	3	0.121	0.615E-02	0.166E-02	0.713E-03	36.5	0.108	0.340E-01	0.323E-02	0.212E-03	0.150E-03
255	6	0.115	0.566E-02	0.140E-02	0.622E-03	41.9	0.110	0.431E-01	0.346E-02	0.466E-03	0.347E-03
255	9	0.120	0.579E-02	0.140E-02	0.605E-03	42.0	0.110	0.381E-01	0.327E-02	0.190E-03	0.134E-03
255	12	0.118	0.576E-02	0.113E-02	0.561E-03	40.1	0.108	0.957E-01	0.517E-02	0.570E-03	0.306E-03
255	15	0.116	0.571E-02	0.104E-02	0.531E-03	30.4	0.941E-01	0.991E-01	0.527E-02	0.371E-03	0.253E-03
255	18	0.117	0.685E-02	0.986E-03	0.604E-03	34.7	0.120	0.127	0.713E-02	0.843E-03	0.570E-03
255	21	0.107	0.907E-02	0.105E-02	0.652E-03	32.5	0.156	0.142	0.103E-01	0.406E-03	0.406E-03
256	0	0.115	0.812E-02	0.148E-02	0.923E-03	32.0	0.137	0.283	0.126E-01	0.579E-03	0.482E-03
256	3	0.106	0.605E-02	0.182E-02	0.793E-03	32.3	0.107	0.366	0.112E-01	0.797E-03	0.482E-03
256	6	0.115	0.627E-02	0.145E-02	0.701E-03	34.0	0.110	0.329	0.106E-01	0.119E-02	0.605E-03
256	9	0.108	0.589E-02	0.290E-02	0.969E-03	27.7	0.965E-01	0.437	0.119E-01	0.158E-02	0.715E-03
256	12	0.106	0.554E-02	0.265E-02	0.861E-03	26.1	0.880E-01	0.436	0.112E-01	0.145E-02	0.636E-03
256	15	0.125	0.280E-01	0.873E-03	0.410E-03	24.2	0.317	0.451	0.543E-01	0.678E-03	0.361E-03
256	18	0.103	0.276E-01	0.133E-02	0.133E-02	21.9	0.496	0.423	0.738E-01	0.161E-01	0.137E-01
256	21	0.959E-01	0.128E-01	0.509E-03	0.228E-03	21.1	0.193	0.424	0.267E-01	0.509E-03	0.227E-03
257	0	0.108	0.589E-02	0.155E-02	0.680E-03	21.6	0.846E-01	0.417	0.116E-01	0.207E-03	0.207E-03
257	3	0.975E-01	0.587E-02	0.359E-03	0.293E-03	21.5	0.873E-01	0.395	0.119E-01	0.107E-02	0.605E-03
257	6	0.101	0.591E-02	0.710E-03	0.502E-03	22.0	0.877E-01	0.344	0.109E-01	0.791E-03	0.522E-03
257	9	0.103	0.534E-02	0.370E-03	0.316E-03	22.0	0.786E-01	0.300	0.911E-02	0.462E-03	0.345E-03
257	12	0.104	0.558E-02	0.993E-03	0.526E-03	23.3	0.843E-01	0.325	0.979E-02	0.695E-03	0.263E-03
257	15	0.125	0.280E-01	0.873E-03	0.410E-03	24.2	0.317	0.451	0.543E-01	0.678E-03	0.361E-03
257	18	0.999E-01	0.845E-02	0.000	0.000	23.4	0.131	0.228	0.129E-01	0.407E-03	0.407E-03
257	21	0.100	0.786E-02	0.206E-03	0.146E-03	21.7	0.116	0.191	0.109E-01	0.420E-03	0.297E-03

Table 3. Three-hour Average Count Rates, September 7-20, 1977 (continued)

DOY	HR	P11	P11 UNC	A5	A5 UNC	E4	E4 UNC	Z1	Z1 UNC	Z3	Z3 UNC
258	0	0.102	0.809E-02	0.427E-03	0.361E-03	22.5	0.120	0.171	0.106E-01	0.113E-03	0.113E-03
258	3	0.100	0.658E-02	0.000	0.000	22.8	0.100	0.152	0.811E-02	0.191E-03	0.135E-03
258	6	9.975E-01	0.101E-01	0.214E-03	0.214E-03	23.0	0.156	0.124	0.112E-01	0.214E-03	0.214E-03
258	9	0.987E-01	0.529E-02	0.953E-04	0.953E-04	23.4	0.822E-01	0.138	0.627E-02	0.281E-03	0.227E-03
258	12	0.104	9.806E-02	0.000	0.000	23.8	0.124	0.139	0.959E-02	0.314E-03	0.181E-03
258	15	0.110	0.114E-01	0.626E-03	0.626E-03	21.4	0.165	0.142	0.134E-01	0.304E-03	0.215E-03
258	18	0.107	0.121E-01	0.197E-03	0.197E-03	18.3	0.143	0.127	0.118E-01	0.000	0.000
258	21	0.105	0.698E-02	0.171E-03	0.171E-03	13.8	0.808E-01	0.463E-01	0.463E-02	0.109E-03	0.109E-03
259	0	0.102	0.789E-02	0.238E-03	0.238E-03	13.3	0.900E-01	0.401E-01	0.506E-02	0.119E-03	0.119E-03
259	3	0.976E-01	0.793E-02	0.216E-03	0.216E-03	12.8	0.896E-01	0.435E-01	0.518E-02	0.000	0.000
259	6	0.111	0.670E-02	0.000	0.000	11.9	0.703E-01	0.429E-01	0.427E-02	0.000	0.000
259	9	0.105	0.541E-02	0.279E-03	0.225E-03	14.1	0.632E-01	0.569E-01	0.398E-02	0.933E-04	0.933E-04
259	12	0.105	0.543E-02	0.929E-04	0.929E-04	15.4	0.664E-01	0.664E-01	0.432E-02	0.000	0.000
259	15	0.105	0.900E-02	0.198E-03	0.198E-03	14.7	0.109	0.601E-01	0.700E-02	0.000	0.000
259	18	0.110	0.126E-01	0.197E-03	0.197E-03	15.8	0.141	0.751E-01	0.101E-01	0.000	0.000
259	21	0.963E-01	0.815E-02	0.000	0.000	13.5	0.100	0.517E-01	0.605E-02	0.000	0.000
260	0	0.167	0.689E-02	0.381E-03	0.259E-03	170.	0.228	0.455E-01	0.363E-02	0.000	0.000
260	3	0.178	0.985E-02	0.592E-02	0.181E-02	411.	0.612	0.470E-01	0.507E-02	0.643E-03	0.454E-03
260	6	0.143	0.783E-02	0.375E-02	0.128E-02	205.	0.334	0.586E-01	0.500E-02	0.255E-02	0.105E-02
260	9	0.128	0.604E-02	0.270E-02	0.867E-03	122.	0.204	0.796E-01	0.473E-02	0.142E-02	0.636E-03
260	12	0.117	0.573E-02	0.243E-02	0.790E-03	82.5	0.159	0.104	0.541E-02	0.845E-03	0.470E-03
260	15	0.118	0.580E-02	0.133E-02	0.609E-03	60.5	0.137	0.145	0.639E-02	0.143E-02	0.634E-03
260	18	0.116	0.589E-02	0.130E-02	0.604E-03	47.6	0.122	0.166	0.704E-02	0.395E-03	0.270E 03
260	21	0.114	0.591E-02	0.514E-03	0.393E-03	37.3	0.108	0.150	0.676E-02	0.302E-03	0.245E-03
261	0	0.109	0.561E-02	0.462E-03	0.290E-03	30.6	0.958E-01	0.143	0.642E-02	0.369E-03	0.261E-03
261	3	0.107	0.544E-02	0.185E-03	0.131E-03	26.1	0.864E-01	0.149	0.643E-02	0.277E-03	0.160E-03
261	6	0.103	0.615E-02	0.469E-03	0.296E-03	22.7	0.911E-01	0.142	0.710E-02	0.560E-03	0.449E-03
261	9	0.110	0.776E-02	0.730E-03	0.376E-03	20.0	0.106	0.105	0.755E-02	0.191E-03	0.135E-03
261	12	0.104	0.558E-02	0.302E-03	0.248E-03	17.5	0.730E-01	0.115	0.586E-02	0.394E-03	0.339E-03
261	15	0.111	0.572E-02	0.187E-03	0.132E-03	16.0	0.689E-01	0.123	0.601E-02	0.372E-03	0.263E-03
261	18	0.110	0.556E-02	0.381E-03	0.259E-03	13.4	0.618E-01	0.106	0.547E-02	0.186E-03	0.186E-03
261	21	0.107	0.568E-02	0.283E-03	0.229E-03	11.4	0.588E-01	0.749E-01	0.474E-02	0.413E-03	0.348E-03
262	0	0.105	0.550E-02	0.141E-03	0.141E-03	10.2	0.544E-01	0.630E-01	0.426E-02	0.430E-03	0.348E-03
262	3	0.105	0.593E-02	0.185E-03	0.131E-03	8.89	0.547E-01	0.578E-01	0.442E-02	0.147E-03	0.147E-03
262	6	0.108	0.553E-02	0.966E-04	0.966E-04	8.32	0.487E-01	0.530E-01	0.388E-02	0.946E-04	0.946E-04
262	9	0.103	0.672E-02	0.200E-03	0.200E-03	13.6	0.773E-01	0.748E-01	0.576E-02	0.000	0.000
262	12	0.678	0.136E-01	0.415E-03	0.293E-03	181.	0.247	0.251	0.905E-02	0.000	0.000
262	15	2.80	0.346E-01	0.246E-01	0.287E-02	0.112E+04	1.14	0.920E-01	0.620E-02	0.582E-02	0.119E-02
262	18	3.93	0.341E-01	0.126	0.602E-02	0.206E+04	1.50	1.06	0.163E-01	0.673E-01	0.429E-02
262	21	3.13	0.295E-01	0.187	0.721E-02	0.184E+04	1.50	2.76	0.276E-01	0.860E-01	0.489E-02
263	0	2.51	0.373E-01	0.258	0.117E-01	0.179E+04	1.84	1.70	0.306E-01	0.851E-01	0.689E-02
263	3	2.02	0.352E-01	0.224	0.116E-01	0.175E+04	2.07	1.64	0.313E-01	0.775E-01	0.681E-02
263	6	1.27	0.188E-01	0.152	0.649E-02	0.121E+04	0.881	1.78	0.222E-01	0.630E-01	0.418E-02
263	9	0.977	0.245E-01	0.136	0.882E-02	0.109E+04	1.27	2.48	0.363E-01	0.584E-01	0.574E-02
263	12	0.891	0.178E-01	0.971E-01	0.588E-02	962.	0.922	1.94	0.266E-01	0.524E-01	0.437E-02
263	15	0.431	0.132E-01	0.579E-01	0.479E-02	440.	0.524	2.80	0.335E-01	0.358E-01	0.375E-02
263	18	0.220	0.176E-01	0.252E-01	0.574E-02	172.	0.547	1.83	0.526E-01	0.206E-01	0.588E-02
263	21	0.183	0.902E-02	0.104E-01	0.211E-02	111.	0.236	1.39	0.249E-01	0.969E-02	0.206E-02
264	0	0.168	0.731E-02	0.744E-02	0.152E-02	75.4	0.163	1.26	0.202E-01	0.998E-02	0.180E-02

REFERENCES

ARMSTRONG, T. P. and S. M. KRIMIGIS — 1976 — Interplanetary Acceleration of Realativistic Electrons Observed with IMP 7, *J. Geophys. Res.*, *81*, 677-682.

KRIMIGIS, S.M., T. P. ARMSTRONG, W. I. AXFORD, C. O. BOSTROM, C. Y. FAN, G. GLOECKER and L. J. LANZEROTTI — 1978 — Energy Spectra, Composition and Anisotropy Measurements from ~ 20 keV to >30 MeV Onboard the Voyager Spacecraft, Invited paper presented at the Spring Meeting of the American Geophysical Union, April 19, 1978, Miami Beach, Florida.

SARRIS, E. T., S. M. KRIMIGIS and T. P. ARMSTRONG — 1976 — Observations of Magnetospheric Bursts of High-Energy Protons and Electrons at ~ 35 R_E with IMP 7, *J. Geophys. Res.*, *81*, 2341-2355.

SGD — 1977a — *Solar-Geophysical Data*, Part I, October 1977, U.S. Department of Commerce (Boulder, Colorado, U.S.A. 80303).

SGD — 1977b — *Solar-Geophysical Data*, 399 Part I, November 1977, U.S. Department of Commerce (Boulder, Colorado, U.S.A. 80303).

Thermal Plasma Data Near The Plasmapause From *S3-3* For September 19-21, 1977

by

F.J. Rich
Research Center, Regis College, Weston, Massachusetts 02193

R.C. Sagalyn and P.J.L. Wildman
Space Physics Division, U.S. Air Force Geophysics Laboratory
Hanscom AFB, Massachusetts 01731

The thermal plasma instruments on board the *S3-3* satellite were able to monitor the response of the plasmapause and the thermal plasma just inside the plasmapause to the storm events September 19-21, 1977. Similar to other storm time observations, the plasmapause moved to lower invariant latitudes and the plasma near the plasmapause was heated.

S3-3 is a polar-orbiting satellite with an apogee/perigee of 8000/240 km and an orbital period of approximately 3 h. During quiet times, data are acquired during one full orbit every 12 to 48 h. During this magnetic storm, the satellite was operated continuously from 1600 UT on Sept. 19, 1977, to 2400 UT on Sept. 21, 1977. A duty cycle of 2 h "on" and 1 h "off" allowed recorded data to be transmitted to ground stations. Typical invariant latitudes and altitudes of the satellite during "on" periods are shown in Figure 1. The thermal plasma experiments on board *S3-3* consist of (1) a set of passive planar ion traps designed to measure the thermal ions with densities greater than $10/cm^3$ and the bulk velocity, and (2) a spherical Langmuir probe to measure the thermal electron densities and temperature. The electron probe is limited to ambient densities greater than $10^3/cm^3$ because of photoelectrons created by sunshine on the probe.

The thermal plasma instruments detect the plasmapause at altitudes greater than about 1500 km in the nighttime sector as a rapid decrease in density with increasing invariant latitude near an invariant latitude of 60°. Below 1500-2000 km in the nighttime sector and below 2000-3500 km in the daytime sector, the ionosphere plasma obscures the plasmapause signature. All data shown in this report were obtained at altitudes near apogee and at magnetic local times (MLT) near 0200 h.

Figure 2 shows the position of the plasmapause as observed by *S3-3*. The bars, marking a range of latitudes for the plasmapause, are used to denote the region from the beginning of the density decrease to the end of observable thermal plasma. A long bar indicates that the density drop is much more gradual, i.e., the density gradient is smaller than the drop in density denoted by a short bar. The long bar near 0730 UT on Sept. 19, 1977, before the geomagnetic storm, is typical of observations during quiet times. The plasmapause is near 60° invariant latitude and extends across several degrees of latitude. With the onset of the geomagnetic storm, the plasmapause goes to lower latitudes owing to compression and to erosion of the outer layers of the plasmasphere. On Sept. 19, 1977, the intensive satellite coverage did not start until a couple hours after the storm sudden commencement (ssc) event, so that the effects of compression and erosion cannot be separated. On Sept. 21, 1977, the ssc event occurred at 0030 UT, but no significant change in the plasmapause was observed until about 0500 UT.

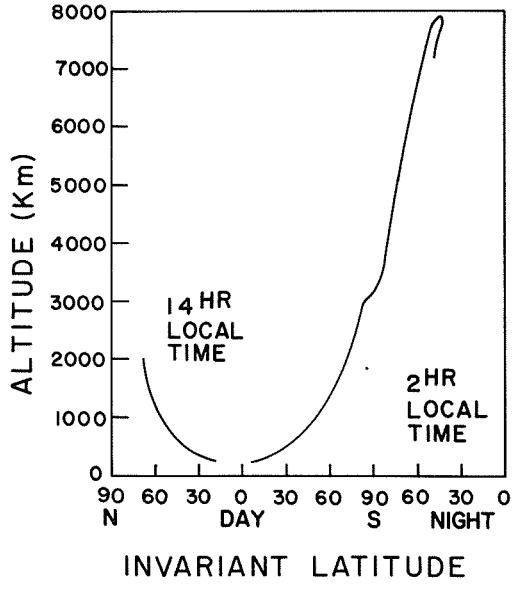

Fig. 1. Typical coverage of invariant latitudes and altitudes during the *S3-3* "on" cycle during Sept. 19-21, 1977.

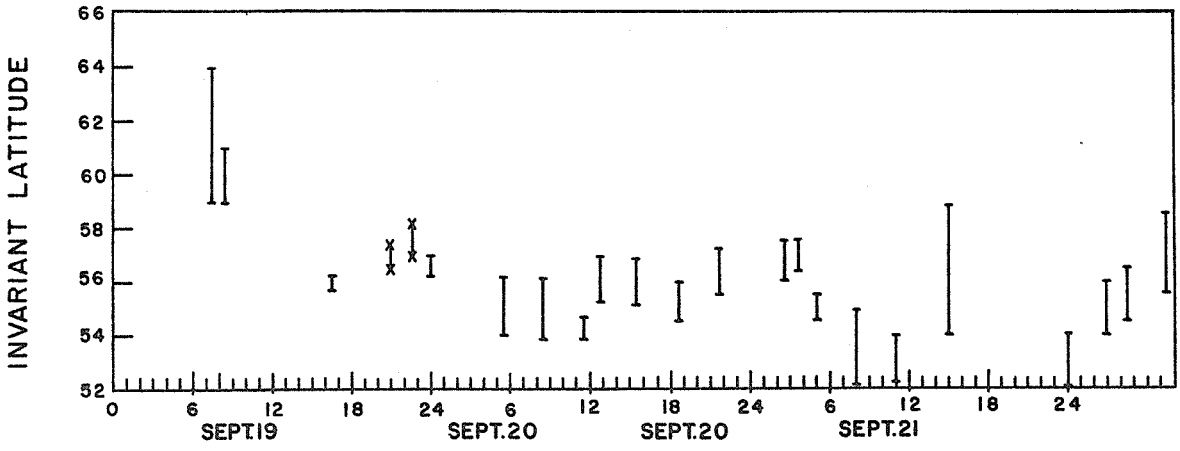

Fig. 2. Position of the plasmapause near 0200 MLT as observed by the *S3-3* satellite.

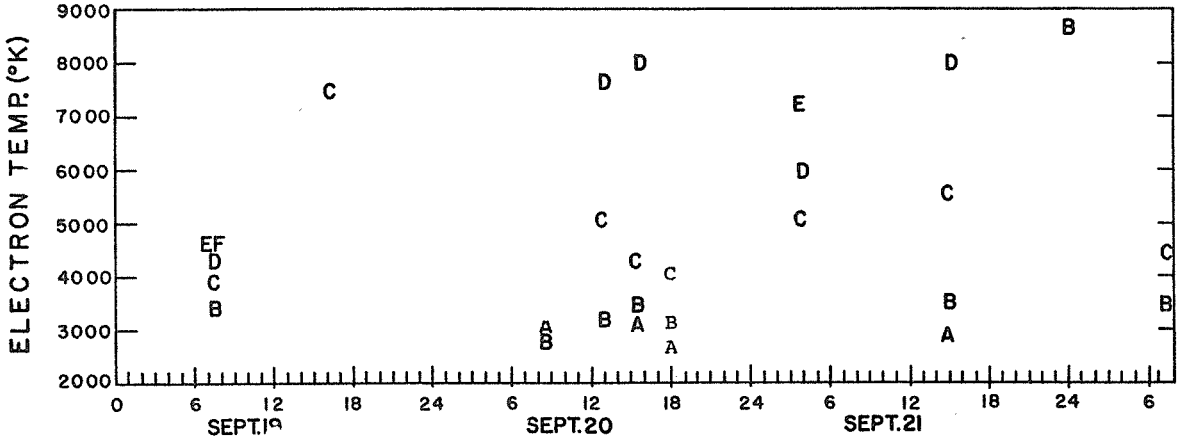

Fig. 3. Latitude profile of thermal electron temperatures near the plasmapause at 0200 MLT. See text for key to letter codes.

Since compression events should be simultaneous with the ssc event, and since erosion due to enhanced magnetospheric convection requires several hours to affect the plasmapause position near 0200 MLT [Medillo et al., 1978], we suggest that almost all of the observed change in the plasmapause position was due to erosion by enhanced magnetospheric convection. The two lines terminated by asterisks at 2100 and 2230 UT on Sept. 19, 1977, are observations of detached plasma-filled tubes of flux that have been separated from the plasmasphere as part of the erosion process [Chen and Grebowski, 1974]. The plasmapause itself was not observed on these orbits because of incomplete data coverage.

During a geomagnetic storm, the thermal plasma near the plasmapause is heated because of its interaction with the ring current system in the equatorial plane [Rees and Roble, 1975]. To show the heating, the temperature profiles of as many orbits as possible are shown in Figure 3 with the use of a letter code. The code is A = 48 to 50° invariant latitude, B = 50 to 52°, C = 52 to 54°, D = 54 to 56°, E = 56 to 58° and F = 58 to 60°. For a few orbits, the thermal electron temperatures could not be processed in time for this report.

The temperature profile observed near 0730 UT on Sept. 19, 1977, is typical of quiet time profiles observed when the foot of the field line is in darkness in both hemispheres. As previously observed by Rao et al. [1978], the electrons are strongly heated after the onset of each major storm event, and the temperatures decline over a period of several days.

REFERENCES

CHEN, A.J. and J.M. GREBOWSKI 1974 Plasma Tail Interpretation of Pronounced Detached Plasma Regions by OGO-5, *J. Geophys. Res., 79,* 3851-3855.

MENDILLO, M., C. CHACKO, F. LYNCH, and P.J.L. WILDMAN 1978 Attempt to Predict Trough/Plasmapause Boundaries in Real Time, in *Effect of the Ionosphere on Space and Terrestrial Systems,* J. M. Goodman, ed. (U.S. Government Printing Office, Washington, DC 20402) 411-422.

RAO, L.D.V., WM. J. BURKE, M. KANAL, and R.G. SAGALYN 1978 INJUN 5 Low Energy Plasma Observations During a Major Magnetic Storm, *J. Geophys. Res., 83,* 3217-3225.

RESS, M.H. and R.G. ROBLE 1975 Observation and Theory of the Formation of Stable Auroral Red Arcs, *Rev. Geophys. Space Phys., 13,* 201-242.

Nighttime Electron Temperature at 500 km from Cosmos-900 Satellite on September 16-28, 1977

by

V.V. Afonin*, K. Kubat**, N.F. Smirnova*, and Ja.Smilauer**

Introduction

The results of electron temperature (T_e) measurements by a RF-electron temperature probe aboard the Cosmos-900 satellite for September 16-28, 1977, are given. Cosmos-900 was launched on March 30, 1977, into an almost circular (perigee 460 km, apogee 523 km) high-latitude (i = 83°) orbit. The satellite was fully stabilized with one of the axes directed along the velocity vector. T_e was measured with a plane differential RF-probe DET mounted together with a plane RPA PL-40A at the end of the velocity oriented boom. The technique of T_e measurements is given by Hirao and Oyama [1961] and Afonin et al. [1973, 1975]. A detailed description will be given elsewhere. The results below correspond to dark sections of the satellite orbits. This is because of the negative body potential of the satellite also measured by DET being lower than the lower limit of input impedance transformer ($R_{in} > 3\ 10^{10}\Omega$) linearity equal -6V.

Results

This paper is based on T_e measurement results for 36 nighttime ionosphere passes at an altitude 500 km for September 16-28, 1977. Most of the passes are given in Figure 1. The numbers on each curve are date (on the left), number of orbit (on the right) and UT, MLT and geographic longitude of the equator (in the middle). The points on the curves with values of L=5, 3, 2 and 1.5 both in the Southern and Northern Hemispheres are connected with dashed lines. All curves are aligned at L=3 in the Southern Hemisphere. The MLT values on each curve are almost constant with the exception of the ends of the passes, which occurred close to the magnetic poles (orbits 2608, 2609, 2654 and 2669). During some of the orbits the satellite passed all the specific ionospheric zones including the polar caps.

Figure 2 gives Kp and Dst values for the period of measurement. The vertical bars along the abscissa of the Figure indicate the passes under discussion. The ends of each curve in Figure 1 correspond to the shadow-light boundary intersections with the exception of orbits 2607, 2611 and 2654, the right ends of which are limited by the ends of the measurement runs.

The curves shown on the left and the lower curve on the right of Figure 1 describe T_e behavior during 24 hours on September 16, 1977, a day which was relatively quiet in accordance with Figure 2. The other curves on the right of Figure 1 were measured during a number of substorms September 19-28, 1977.

The main feature of T_e behavior on September 16 is the quiet, smooth shape of the curves. In low and middle latitudes T_e is remarkably stable and slowly rises from the Southern Hemisphere to the Northern one. For L=2, T_e values are 1200 K - 1400 K in the south and 1800 K - 2000 K in the north. In the L>2 region the T_e behavior is more complicated. There are always higher T_e values in the L=3-5 interval. Although in the lower part of Figure 1 T_e does not attain a maximum value, it starts to rise at L=2-2.5 for all passes in the Southern Hemisphere. A similar, although lower "amplitude", rise of T_e in the Northern Hemisphere is obvious on the passes which are symmetrical in L (see, for example, orbits 2600-2602). On passes 2604-2610 T_e decreases in the L=5-7 region and rises again in L>7 region, the main precipitation zone (auroral zone). As a rule, in a "gap" between the subauroral enhancement and auroral zone, T_e values are about the same as in middle latitudes before the subauroral enhancement, although they are in some passes 2-3 times greater (i.e., orbits 2608, 2610). On passes 2605, 2607, 2608 there is a polar cap depression in T_e values polarward of the auroral maxima. There are usually strong fluctuations of T_e poleward from the "gap".

On September 19 a sudden ring current intensity enhancement occurred which was not very strong (Dst=-90γ). This ring current continued until September 28 in a series of bursts. Pass 2648 occurred just before the storm and pass 2654 during the main phase of the storm. Before the storm T_e was strongly rising for L=3-5. Although the T_e is not evident from the curves it must be located at L≥5. During the main phase the T_e peak moved to L=3 and its width decreased drastically down to ΔL=0.3-0.5. On the next curve shown (pass 2669 on the next day) the T_e peak position was the same but its magnitude had increased. This increase seems to be a result of the next burst of the ring current intensity. During all the following passes when the ring current intensity was almost constant the T_e peak position was practically invariant. The start of the T_e rise was at L=2.5, and the peak width had increased. During pass 2775 an additional but lower magnitude T_e peak at L=2.2 is superimposed on the main T_e peak. This additional T_e peak is also evident on passes 2774 and 2776 (not shown in Figure 1). The lower L-values of the beginning of the T_e rise on passes 2777 and 2778 seem to be caused by this "midlatitude" peak of T_e.

---

*Space Research Institute of Acadmy of Sciences of the USSR
**Geophysical Institute of Academy of Sciences, Czechoslovakia

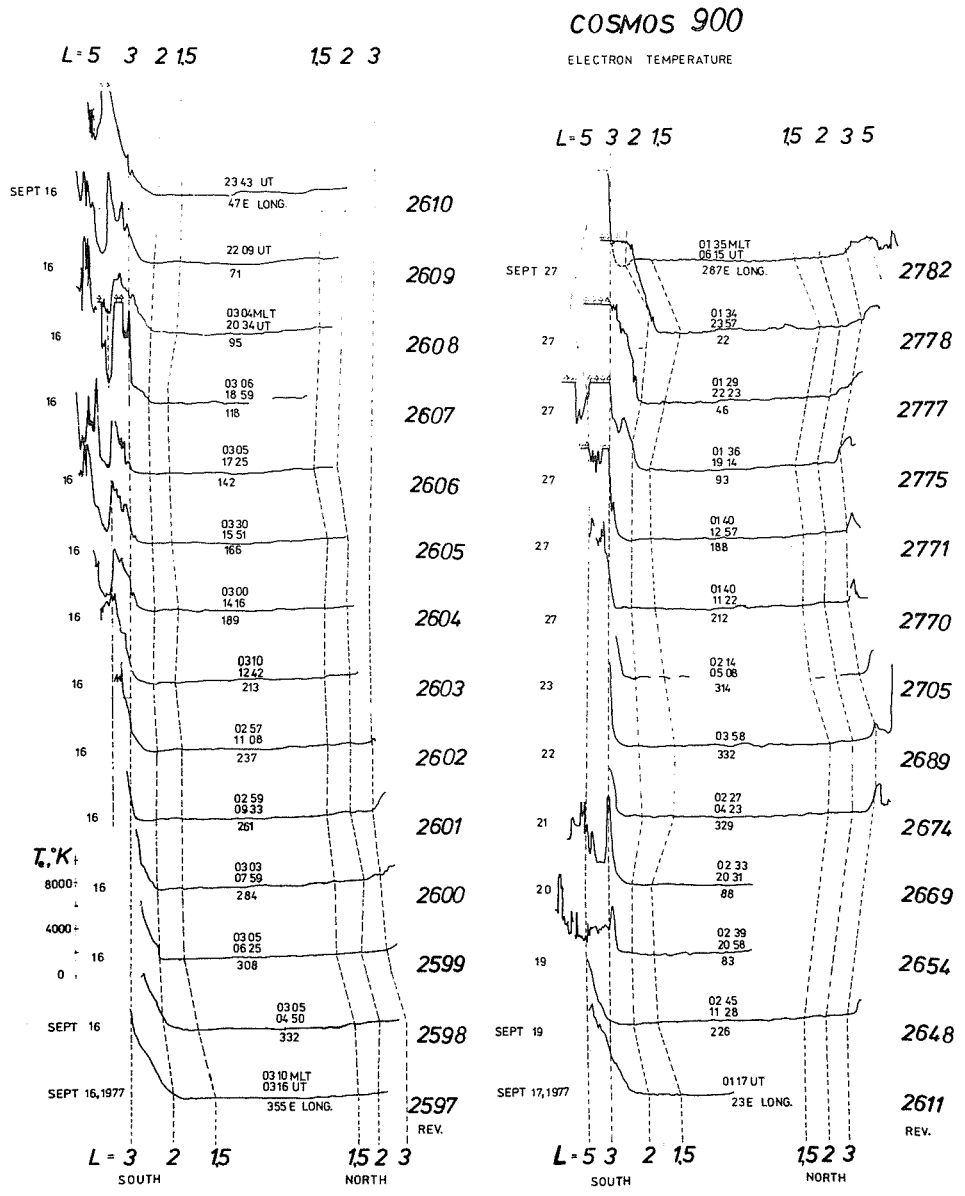

Fig. 1. T_e observed by Cosmos-900 on passes 2597-2782 from Sept. 16-27, 1977.

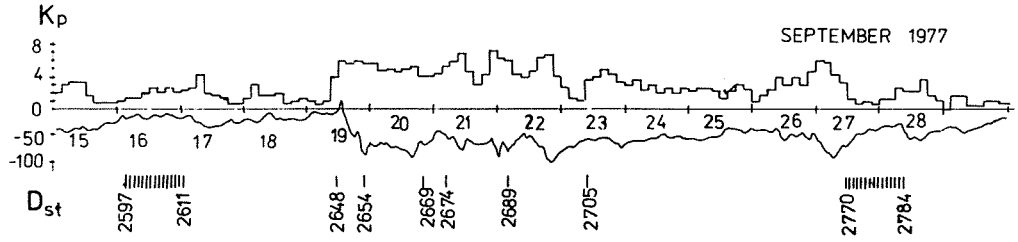

Fig. 2. Kp and Dst for Sept. 15-29, 1977 with times of passes of Cosmos-900 indicated.

Discussion

The above are the first published results on T_e from the Cosmos-900 satellite. The data must be analyzed in comparison with simultaneous data from the other experiments on the satellite, so this paper is mainly descriptive. However, the following features of T_e behavior should be noted.

The subauroral (in the region of the main ionospheric trough) T_e enhancements were observed mainly in disturbed conditions [Raitt, 1974 and Mayer and Chandra, 1975]; their presence during quiet conditions was noted [Brace and Theis, 1974 and Miller, 1970]. The subauroral T_e peaks are related to the often observed SAR-arcs in that latitude region, and the generally accepted mechanism of their occurrence is the energy transfer from the ring current particles [Rees and Roble, 1975]. The details of the mechanism are not fully understood. At least it includes ion cyclotron waves generated in the region where the ring current overlaps with the plasmasphere, the energy of which is transferred to the plasmasphere electrons through heat conduction to ionospheric electrons [Cornwall et al., 1971; Williams and Lyons, 1974; and Joselyn and Lyons, 1976].

The subauroral T_e peaks during quiet periods from the Cosmos-378 satellite and the Intercosmos-8 satellite were discussed by Afonin and Smilauer [1976] and Afonin et al. [1978], where it was shown that the peaks were observed not only in disturbed periods but almost continuously during quiet times; and that an after-effect of the isolated magnetic substorm in the plasmasphere was observed for five days. Afonin and Smilauer [1976] showed the marked role in the formation and maintenance of the subauroral T_e peaks played by the "hot zone" of the plasmasphere recently discovered by the Prognoz satellites [Gringauz and Bezrukikh, 1977]. Afonin and Smilauer [1976] also showed that the qualitative behavior and morphology of the hot zone coincide with the behavior of T_e in the ionosphere. In many papers (e.g. [Hulqvist et al., 1976]) it was shown that there is a maximum of the ion cyclotron wave growth rate in the L=2.7-4 region, i.e., in the region of overlap of the plasmasphere and the ring current. The data from Figure 1 for the quiet period (September 16) confirm this conclusion [Afonin and Smilauer, 1976] of the almost continuous presence of the subauroral T_e peaks, and support the ion cyclotron interaction of the ring current and the plasmasphere as the main cause of the subauroral T_e peaks. Figure 3 shows the simultaneously measured T_e and n_i values for pass 2654 during the maximum phase of the September 19, 1977 substorm; n_i was measured with the plane RPA PL-40A mounted close to the DET sensor on the same boom. Figure 3 shows that the position and the shape of the T_e peak correspond to the trough in n_i. Poleward of the trough and the T_e peak, the T_e values are about a factor of two higher than on the equatorward side and are strongly fluctuating. Poleward of the T_e peak this two-fold increase agrees with n_i increase as seen in Figure 3. The n_i values also strongly fluctuate in the region. This is where intense precipitation of the energetic particles seems to occur in the region.

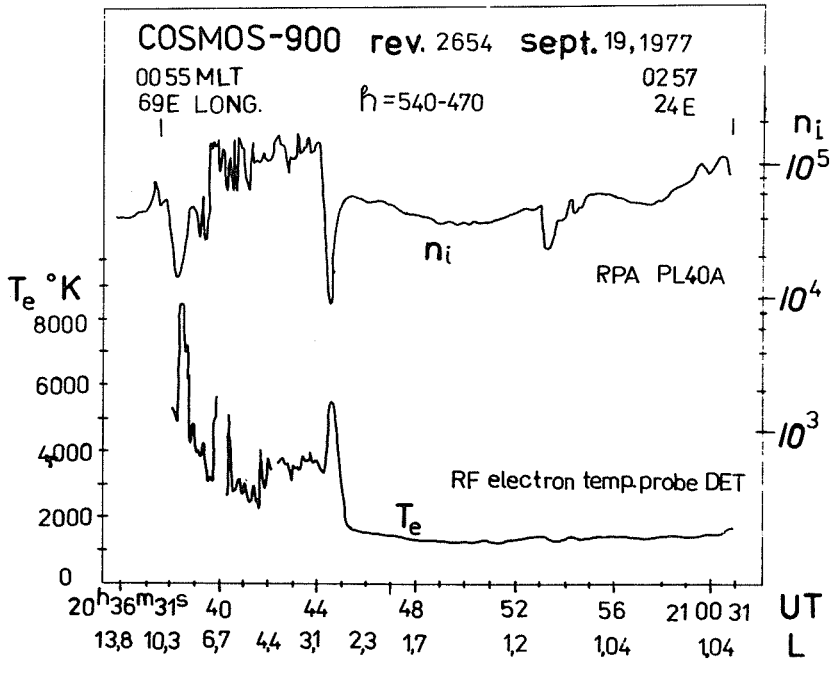

Fig. 3. T_e and n_i for Cosmos-900 pass 2654 during Sept. 19, 1977 substorm.

Without giving the details let us note that particular attention should be paid to the obvious "amplitude" asymmetry north-south during the period under discussion, and to the above midlatitude T_e enhancements at L=2.2. Relative to the former it should be noted that at the times of the T_e enhancement observations, the solar zenith angles were always greater than 110°; the magnetically conjugate heating cannot be responsible for the observed difference.

The midlatitude T_e enhancements were observed on the ESRO-1A, Explorer-31 and ISIS-2 satellites [Brace et al., 1974]. This phenomenon was specially considered by Smilauer and Afonin [1976] for the Intercosmos-14 data; the anisotropy of T_e was also measured on the satellite. According to Smilauer and Afonin [1976], during January 11 - February 2, 1976 strong (more than twofold) anisotropic T_e enhancments were observed on L=1.45-2.1 and h=1600-1700 km. The "amplitude" of these enhancements decreased with time. After a gap in the satellite operation until Feb. 24, 1976, this phenomenon was not observed. The most possible reason for these midlatitude T_e enhancements according to Smilauer and Afonin [1976] is the heating by the waves with frequencies of some hundreds of Hz generated in the equatorial region of the plasmasphere.

In conclusion we want to note that this experiment is a part of the ionospheric complex of instruments aboard the Cosmos-900 satellite which was designed and flown under the guidance of Prof. K.I. Gringauz, whose continuous and fruitful assistance is greatly appreciated.

References

AFONIN, V.V., G.L. GDALEVICH, K.J. GRINGAUZ, Ta. KAINAROVA and Ta. SHIMILAUER — 1973 — Ionospheric Studies Conducted by the Satellite Intercosmos-2. III. Ionospheric Electron Temperature Measurement by the High-Frequency Probe Method, Cosmic Research, 11, 225-234.

AFONIN, V.V., G.L. GDALEVICH and S.M. SHERONOVA — 1975 — Investigations in the Ionosphere on Kosmos 378 8 Results of T_e Measurements with an HF-Probe and a Langmuir Prove, Geomagn. and Aero., 15, 489-491.

AFONIN, V.V. and Ia. SMILAUER — Proceedings of Intercosmos Symposium on the Earth Ionosphere and Magnetosphere, Kaluga, 1976, in press.

AFONIN, V.V., O.P. KOLOMIYTSEV and Yu. G. MIZUN — 1978 — Satellite Measurement of Electron Temperature and its Behavioral Characteristics in the Region of the Main Ionospheric Valley, Geomagn. and Aeron., 18, 290-292.

BRACE, L.H. and R.F. THEIS — 1974 — The Behavior of the Plasmapause at Mid-Latitudes: Isis 1 Langmuir Probe Measurements, J. Geophys. Res., 79, 1871-1884.

BRACE, L.H., E.J. MAIER, J.H. HOFFMAN, J. WHITTEKER and G.G. SHEPHERD — 1974 — Deformation of the Night Side Plasmasphere and Ionosphere During the August 1972 Geomagnetic Storm, J. Geophys. Res., 79, 5211-5218.

CORNWALL, J.M. F.V. CORONITI and R.M. THORNE — 1971 — Unified Theory of SAR Arc Formation at the Plasma-pause, J. Geophys. Res., 76, 4428-4445.

GRINGAUZ, K.I. and V.V. BEZRUKIKH — 1977 — Plasmasphere of the Earth, Geomagn. i. Aeronom., 17, 523-533.

HIRAO, K. and K. OYAMA — 1971 — Electron Temperature Observed with the Langmuir Probe and Electron Temperature Probe, J. Geomagnet. Geoelect., 23, 161-167.

HULQVIST, B., W. RIEDLER and H. BORG — 1976 — Ring Current Protons in the Upper Atmosphere within the Plasmasphere, Planet. Space Sci., 24, 783-797.

JOSELYN, J.A. and L.R. LYONS — 1976 — Ion Cyclotron Wave Growth Calculated from Satellite Observations of the Proton Ring Current During Storm Recovery, J. Geophys. Res., 81, 2275-2282.

MAYER, E.J. and S. CHANDRA — 1975 — The SAR Arc Event Observed During the December 1971 Magnetic Storm, J. Geophys. Res., 80, 4591-4597.

MILLER, N.J. — 1970 — The Main Electron Trough During the Rising Solar Cycle, J. Geophys. Res., 75, 7175-7181.

RAITT, W.J. 1974 The Temporal and Spatial Development of Mid-Latitude Thermospheric Electron Temperature Enhancement During a Geomagnetic Storm, J. Geophys. Res., 79, 4703-4708.

REES, M.H. and R.G. ROBLE 1975 Observations and Theory of the Formation of Stable Auroral Red Arcs, Rev. Geophys. Space Phys., 13, 201-242.

SMILAUER Ia. and V.V. AFONIN Proceedings of Intercosmos Symposium on the Earth Ionosphere and Magnetosphere, Kaluga, 1976, in press.

WILLIAMS, D.J. and L.R. LYONS 1974 The Proton Ring Current and its Interaction with the Plasmapause: Storm Recovery Phase, J. Geophys. Res., 79, 4195-4207.

Spatial Distribution of Solar Cosmic Ray Fluxes in the High-Latitude Zones of the Earth's Magnetosphere during the Events of September and November 1977

by

M.N. Nazarova, N.K. Pereyaslova and I.E. Petrenko
Institute of Applied Geophysics, Hydrometeorological Service of the USSR, Moscow

We investigated spatial distributions of proton fluxes registered in polar zones by the Meteor-2 Satellite during the solar cosmic ray events of September and November 1977. Meteor-2 observed several intensive events during this early-cycle 21 enhancement of solar activity. On page 208 of this volume. Avdyushin et al. [1978] compare Meteor-2 temporal and spectral proton flux characteristics observed during this same period with several geophysical parameters. They also describe the Geiger and scintillation counters the satellite carries to measure proton and electron fluxes at comparatively high energies.

By comparing proton fluxes at energies greater than 5, 15, 25, 40 and 90 MeV, which were measured in the northern and southern polar zones of the Earth's magnetosphere, we established the asymmetry during the flux's rise to maximum and at its maximum. The asymmetry between the two polar fluxes grew to as much as 30-40% and showed a strong dependence on the sign of the radial component of the interplanetary magnetic field. This regularity was established for events in the 20th solar cycle by Mikirova et al. [1976], Pereyaslova et al. [1976] and Fennel [1973], and it continued to hold for the events described here.

During the September 1977 solar particle injections, the distributions over the polar zones were practically uniform. On September 20, however, at 0930 UT, the greater than 40-MeV proton profile contained a peak within geomagnetic latitudes (Φ) $\simeq$ 75-77° on the day side of the Earth's magnetosphere (cusp region). Figure 1 shows the spatial distribution of the proton flux with E_p>40 Mev during the satellite's flight over the southern polar cap.

During the maximum of the event of November 22-24, 1977, a two-step distribution of proton fluxes at all energies (>15, 25, 40 and 90 Mev) over both the northern and polar zones was recorded. This stepwise signature persisted for 3 hours--between 1300 and 1600 UT. An invariant geomagnetic latitude of about 78° marked this sharp transition zone between 6 and 8 o'clock local magnetic time for all measured proton energy channels. Figures 2, 3 and 4 show profiles of proton fluxes with E_p>15, 25, 40 and 90-Mev energies over the northern and southern polar zones. Note that the height of the "step" in the morning sector exceeds that of the evening sector by 20-40%, and it does not depend on proton energy.

REFERENCES

AVDYUSHIN, S.I., N.K. PEREYASLOVA, Yu.M. KULAGIN, M.N. NAZAROVA, I.E. PETRENKO, S.T. AKINJAN, V.V. FOMICHEV and I.M. CHERTOK	1978	Observations of Solar Cosmic Rays and Radio Bursts in September and November 1977, this issue, p. 208.
MIKIROVA, N.A., N.A. MIKRYUKOVA, M.N. NAZAROVA, N.K. PEREYASLOVA and I.E. PETRENKO	1976	Spacial Distribution of Solar Cosmic Rays in the Earth's Magnetosphere, Izv. Akad. NAUK SSSR Ser. Fiz., 40, 471-476.
PEREYASLOVA, N.K., M.N. NAZAROVA, S.M. MANSUROV and L.G. MANSUROVA	1976	Some Patterns in the Relation of Solar Cosmic Rays in Polar Regions with the Sector Structure of the Interplanetary Magnetic Field, Geomagn. and Aeron. (USA), 16, 238-240.
FENNEL, J.F.	1973	Access of Solar Protons to the Earth's Polar Caps, J. Geophys. Res., 78, 1036-1046.

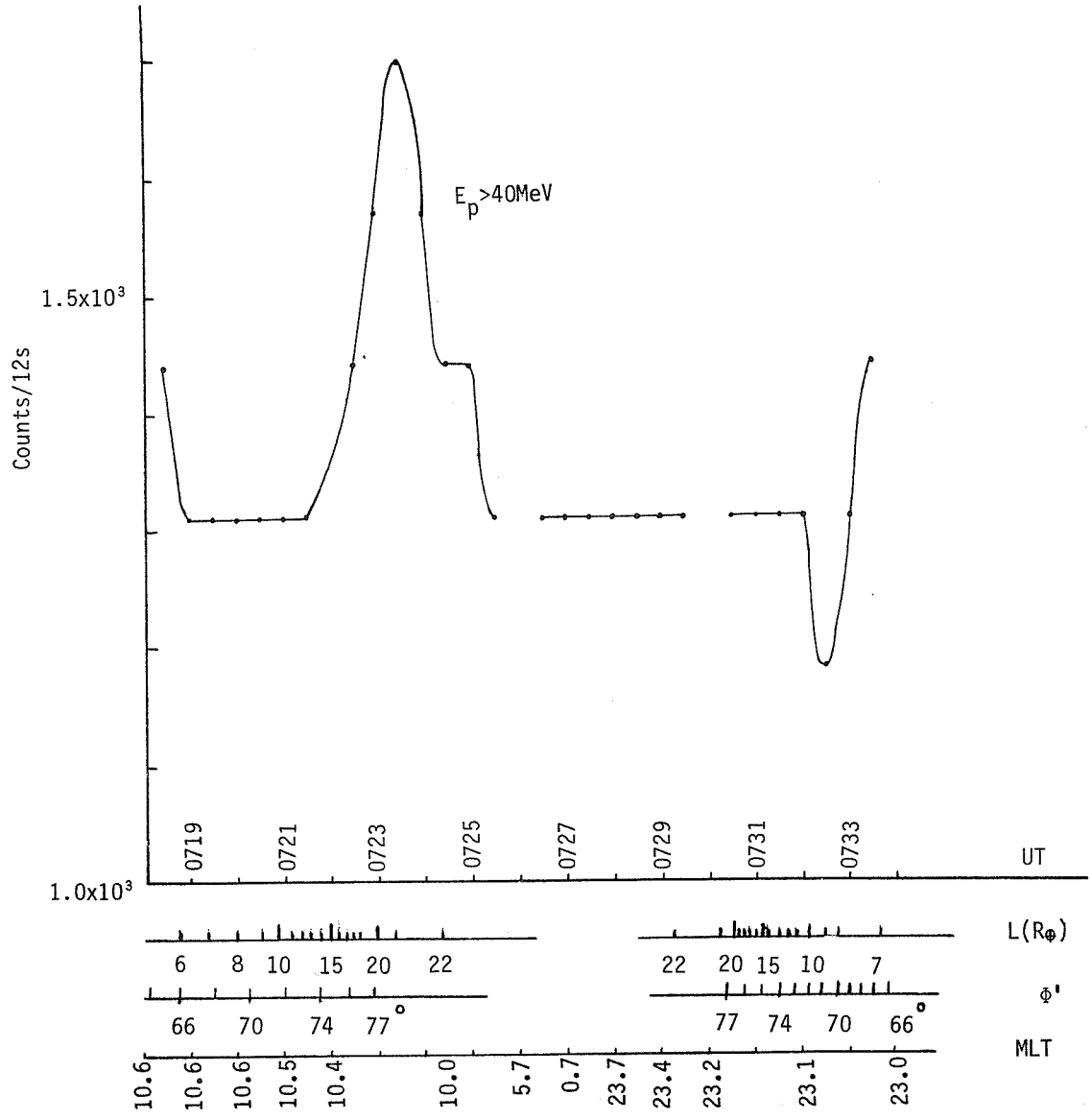

Fig. 1. Proton flux profile with energy E_p>40 MeV over the southern polar cap on September 20, 1977, as measured by Meteor-2. Along the x axis we have plotted the ranges in Universal Time, the McIlwain L parameter, invariant geomagnetic latitude and magnetic local time covered by the satellite during this pass.

Observations of Solar Cosmic Rays and Radio Bursts in September and November 1977

by

S.I. Avdyushin, N.K. Pereyaslova, Yu.M. Kulagin,
M.N. Nazarova and I.E. Petrenko
Institute of Applied Geophysics
Hydrometeorological Service of the USSR, Moscow

and

S.T. Akinjan, V.V. Fomichev and I.M. Chertok
IZMIRAN, Moscow

ABSTRACT

Solar cosmic ray fluxes measured by the *Meteor* Satellite during the periods September 14-27 and November 22-26, 1977, are presented. Integral spectra of protons with energies 5-90 MeV are calculated. Data on proton fluxes are compared with some heliogeophysical phenomena. A quantitative diagnosis of proton fluxes according to radio burst characteristics is made.

Instrumentation

Meteor-2 was launched on January 7, 1977, and has the following orbital parameters: perigee = 892.9 km, apogee = 932.1 km, inclination = 81.3°, and initial period of rotation = 103 min. The radiometric equipment of *Meteor-2* includes a set of detectors (Geiger and scintillation counters), which allow densities of charged particle fluxes to be recorded in various energy ranges and in several memory and information output devices. The radiation equipment provides the record and storage of data concerning radiation fields along the orbit of *Meteor*. A set of detectors, included in an equipment complex, permits measurement of proton and electron fluxes with comparatively high energies. The characteristics of detectors based on Geiger counters (SBM counters) installed behind hemispherical screens of various thickness are given by Avdyushin et al. [1977]. A scintillator was used to record protons with energies Ep>90 MeV. Its form approximates a sphere of radius 25 mm, and it connects with the FMT-58. The scintillator was screened within the solid angle 2π by a brass screen ~9 g/cm^2. The discrimination amplitude level of output impulses corresponds to the energy released by ~5-MeV electrons, thus providing isolation from electron drag radiation. The amount of housekeeping information telemetered from different detectors is not the same and varies from 24 to 48 sec; the time of averaging in a single measurement cycle is 12 sec for any detector.

Observations

Data on proton intensity of solar and galactic cosmic rays were obtained by *Meteor-2* from particle flux measurements in the polar zones of the Earth's magnetosphere within the range of invariant latitudes $\Phi' > 67\text{-}72°$.

The counting rates of detectors on invariant latitudes $\Phi' > 67\text{-}72°$ remain constant, forming a plateau. Proton intensity values are obtained by averaging the 12-sec measurements in a deep polar zone. Averaging time of data is 5-15 min, depending on the satellite trajectory. The mean values of proton flux intensities relate by time to the middle of the plateau.

The September 14-17, 1977, period. In the period of September 14-17, proton fluxes considerably exceeding the background level were recorded at energies Ep>5 MeV. The integral proton fluxes for energies Ep> 5, 15, 25, 40 and 90 MeV and spectrum rigidity index variation with time are given in Figure 1. The same figure shows 3-hour values of the magnetic disturbance index Kp, magnetic storms, chromosphere flares, and the sign of the interplanetary magnetic field [*SGD*, 1977]. As is seen from Figure 1, several cosmic ray events were observed in September 17-18, 19-22 and 24-27. Table 1 gives the main temporal and spectral characteristics of these events as well as data on the flares that were obviously the sources of the observed proton fluxes.

The September 17-18, 1977, period. Proton fluxes recorded during September 17-18 were generated in the flare of 2b importance observed at Palehua in Hα on September 16 at 2140 UT. Reported coordinates were N07 W21, placing it in McMath Region 14943. The flare was accompanied by severe radio bursts of Types II and IV. In the interval from 2125 to 2135 UT an X-ray burst was observed in the range of 1-8Å (~9x10^{-3} ergs/cm^{2}sec). A 6-hour ionospheric disturbance of importance 2 [*SGD*, 1977] occurred as well.

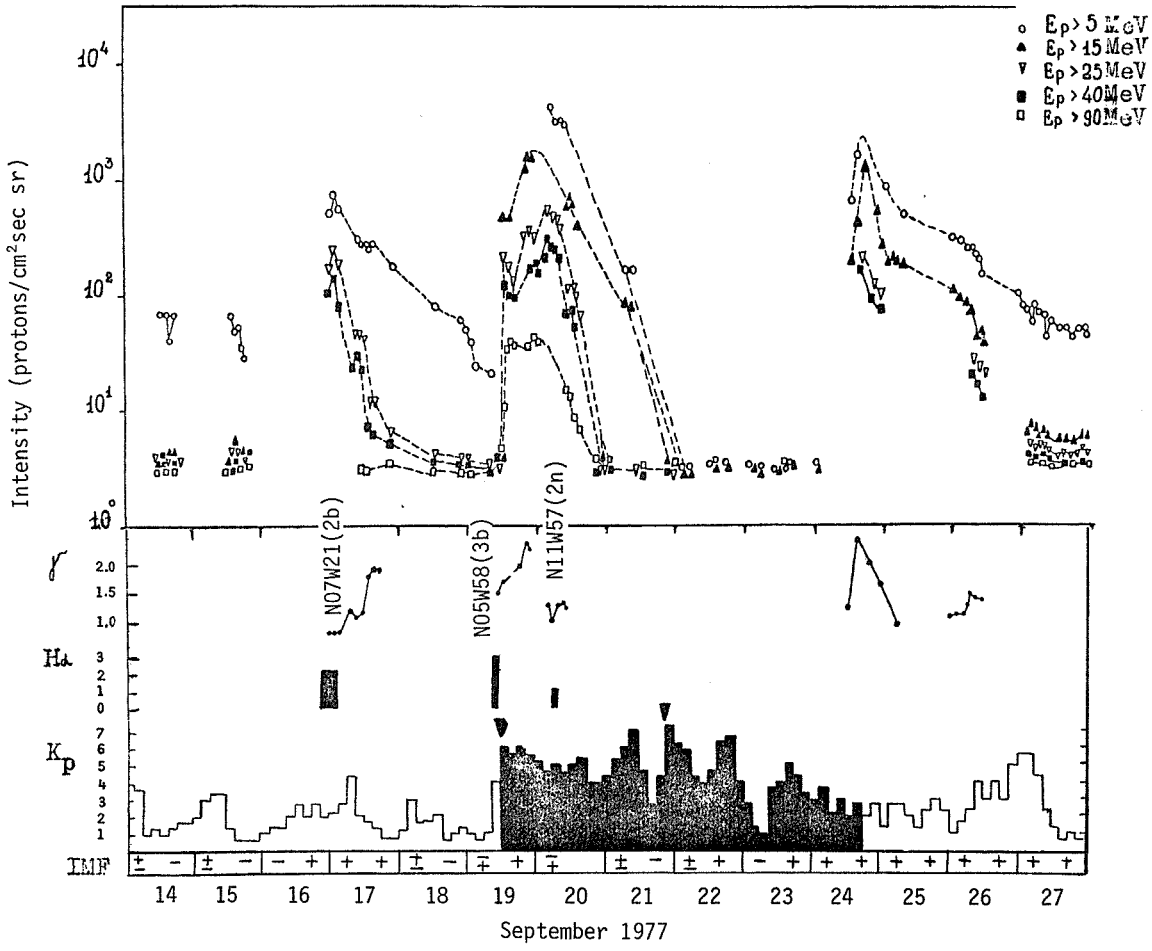

Fig. 1. Temporal distribution of proton fluxes, index of spectrum rigidity, and several heliogeophysical parameters measured during the solar cosmic ray events in September 1977.

Table 1. Characteristics of Proton Events in September 1977

Date Sept. 1977	Maximum (UT Hr)	Energy Ep (MeV)	Max Flux I $(cm^2 sec\ sr)^{-1}$	Max Spectrum Index	Flare in Hα (McMath Region 14943) Data 1977	Start Max End (UT)	Imp	Location	Station
14	16	5	5.41						
17	02	5	63.7	0.8	16	2140	2b	N07 W21	Palehua
		25	18.3			2307			
		40	11.1		17	0215			
19	12	15	39.8	1.5	19	0955	3b	N05 W57	Catania
		25	15.9			1045			
		40	10.4			1125			
		90	3.18						
20	05	5	358.	1.3	20	0429	2n	N11 W57	Mitaka
		25	39.8			-			
		40	19.9			0650			
24	17	5	159.	2.2	24	-	-	N10 W130	-
		15	119.						
		25	16.7						
		40	12.7						
		90	2.87						

The spectrum of particles within the energy range of 5-90 MeV is approximated by $I = I_0 E^{-\gamma}$. The power index of the maximum of the September 17 event was $\gamma = 0.8$, i.e., the particle spectrum was rigid; when the intensity decreased, a gradual softening of the spectrum took place.

The September 19-22, 1977, period. The second significant rise in proton flux intensities was a solar cosmic ray event recorded on September 19-22. The flux increase began simultaneously with a magnetic storm sc observed at 1138 UT on September 19. These proton fluxes were injected by the importance 3b flare Catania reported on September 19 at 0955 UT near N05 W57 and in the same active area as before, namely, McMath Region 14943. The flare was accompanied by intensive radio bursts of Types I, II, III and IV; a considerable increase in X-ray flux; and a sudden ionospheric disturbance of importance 3 and 3-hour duration.

The temporal profile of proton flux in the whole energy range was characterized by great intensity oscillations. These oscillations can result from the evolution of the magnetic storm and the frequent variation of the IMF sign near Earth. It is also possible that the insignificant increase of proton flux in the range 5-40 MeV at about 5 o'clock was connected with the proton injection from the importance 2n flare of September 20. According to the Mitaka Station report, this flare began at 0429 UT near N11 W57 in McMath Plage Region 14943. The event was accompanied by radio bursts of Types II and IV and an SID of 2 importance.

During this event the spectrum rigidity index γ was 1.5 at the first maximum on September 19; the spectrum gradually softened at the second maximum on September 20 to 1.3. This increase in gamma testifies to the existence of an additional proton injection from another source. On September 22-23 a background level of radiation was recorded in the whole energy range.

The September 24-28, 1977, period. The solar cosmic ray event observed on September 24-28 obviously connected with a flare that took place in McMath active region 14943 on September 24, when it was behind the limb. An intensive radio burst of Types II and IV in the centimeter and decimeter ranges occurred at 0552 UT [*SGD*, 1977].

Maximum proton fluxes were recorded near Earth at 1600-1700 UT on September 24. By September 27 the proton flux intensity with energy >15 MeV had decreased to the background level while the proton intensity in the 5-15 MeV range remained high. Observations of high energy cosmic rays by the Apatity neutron monitor on the September 24 showed a sharp increase of intensity of up to ~8% [Ivanov, 1978].

The November 21-25, 1977, period. In November 1977 a new intensive event of solar cosmic rays was registered (see Figure 2). Against the background of practically no solar activity and a quiet geophysical situation, a sharp proton flux increase commenced within a broad energy range observed not only by satellite but by neutron monitor (Apatity station gave an amplitude ~15%) [Ivanov, 1978]. Proton flux values with energies E_p>5, 15, 25, 40 and 90 MeV are given in Table 2.

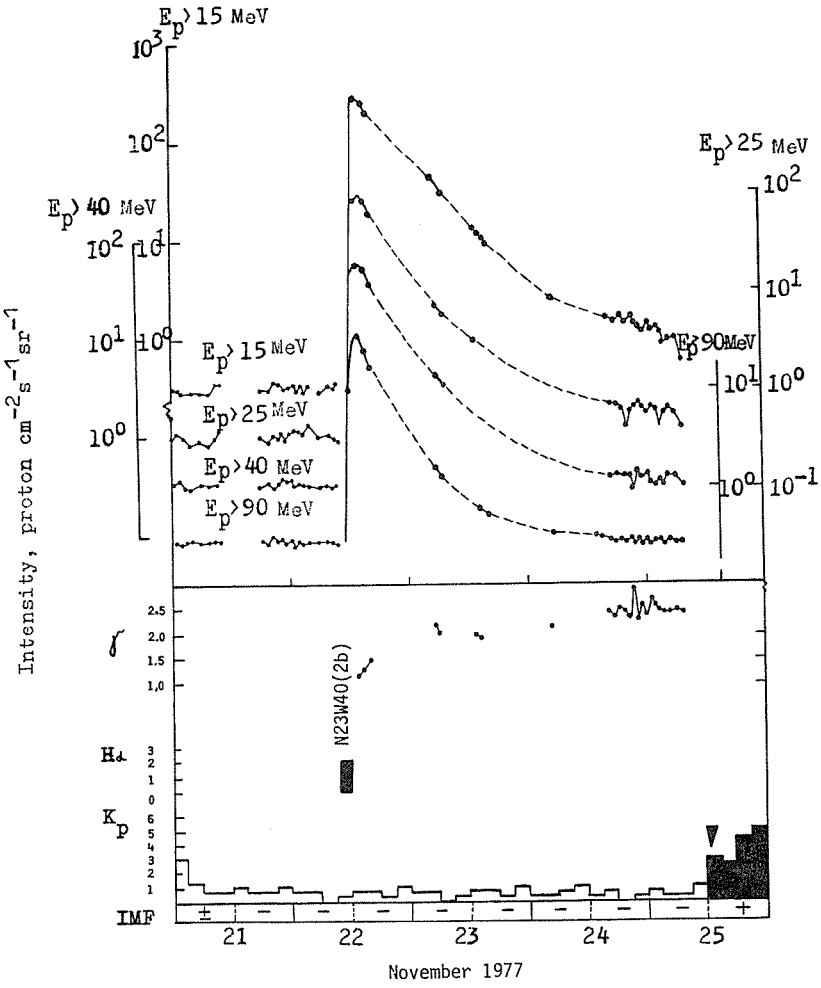

Fig. 2. Temporal distribution of proton fluxes, index change of spectrum rigidity and some heliogeophysical parameters in solar cosmic ray events in November 1977.

Table 2. Proton Fluxes Measured on the *Meteor* Satellite During the Period November 21-25, 1977

Date Nov. 1977	Time (UT)	Lat.	J (protons/cm²sec sr)					Date Nov. 1977	Time (UT)	Lat.	J (protons/cm²sec sr)				
			E_p>5	E_p>15	E_p>25	E_p>40	E_p>90				E_p>5	E_p>15	E_p>25	E_p>40	E_p>90
21	0056	N	-	0.32	0.31	0.33	0.28	23	0507	S	-	54.1	7.48	4.12	1.48
	0148	S	-	0.31	0.33	0.35	0.27		1345	S	-	13.2	3.22	-	0.93
	0237	N	-	0.29	0.32	0.32	0.27		1434	N	-	11.6	-	-	0.63
	0421	N	-	0.28	0.27	0.30	0.28		1529	S	-	10.9	-	-	0.64
	0601	N	-	0.28	0.29	0.33	0.28		1617	N	-	9.71	-	-	0.54
	0744	N	-	0.27	0.25	0.31	0.28								
	0833	S	-	0.35	0.31	-	0.28	24	0516	S	-	2.63	-	-	0.34
	0926	N	-	0.34	0.35	0.32	0.28		1346	S	-	-	-	-	0.33
	1854	S	-	0.29	0.32	0.31	0.28		1435	N	-	-	-	-	0.31
	1945	N	-	0.29	0.28	0.36	0.27		1715	S	16.0	1.73	0.77	0.41	0.30
	2039	S	-	0.35	0.31	0.30	0.31		1806	N	14.6	1.54	0.67	0.41	0.29
	2129	N	-	0.35	0.30	0.33	0.28		1900	S	17.6	1.64	0.62	-	0.30
	2222	S	-	0.31	0.34	0.37	0.29		1948	N	12.1	1.50	0.41	0.44	0.29
	2312	N	-	0.31	0.29	0.36	0.28		2044	S	13.9	1.56	0.57	0.41	0.30
									2134	N	11.8	1.50	0.64	0.37	0.28
22	0006	S	-	0.33	0.33	0.36	0.28		2236	S	12.0	1.39	0.68	0.44	0.29
	0056	N	-	0.28	0.36	0.32	0.28		2319	N	10.1	1.22	0.59	0.40	0.28
	0149	S	-	0.31	0.36	0.33	0.28								
	0239	N	-	0.29	0.33	0.33	0.28	25	0012	S	10.7	1.40	0.56	0.43	0.29
	0420	N	-	0.32	0.42	0.32	0.28		0100	N	9.44	1.30	0.60	0.35	0.28
	0602	N	-	0.28	0.31	0.32	0.28		0152	S	9.98	1.32	0.61	0.33	0.28
	0746	N	-	0.33	0.32	0.32	0.28		0243	N	8.60	1.18	0.41	0.37	0.28
	0833	S	-	0.30	0.31	0.32	0.28		0335	S	11.31	0.91	0.55	0.33	0.28
	0927	N	-	0.33	0.29	0.32	0.27		0425	N	7.58	0.92	0.58	0.40	0.28
	1343	S	-	281.0	86.0	56.8	32.5		0606	N	6.44	0.97	0.56	0.42	0.29
	1435	N	-	266.0	81.2	51.1	25.0		0749	N	6.06	0.52	0.42	0.33	0.28
	1619	N	-	201.0	57.2	35.8	16.2								

The appearance of protons was caused by the flare evolution on November 22 at 0945 UT. Haute Provence reported a 2b importance flare in McMath active area 15031 with coordinates N23 W40. The flare was accompanied by an X-ray burst in the 1-3Å range that maximized at 1.6×10^{-2} ergs/cm^{2}sec and a radio burst of Type IV of importance 3 [*SGD*, 1977].

Rapid access of particles to the Earth is explained by the close position of the flare to the basis of the Sun-Earth magnetic force line. The flux profile corresponds to a particle diffusion distribution along this connecting magnetic line of force. At the maximum the registration of proton fluxes in the 15-90 MeV energy range yielded a $\gamma \sim 1.2$. As is seen from Figure 2, during the decrease phase, a gradual softening of the spectrum occurred, and that by November 25, γ equaled 2.5.

Proton Flux Quantitative Diagnosis. A quantitative diagnosis has been carried out of proton flares that took place in September and November 1977. This diagnosis uses radio burst characteristics connected with a particular flare on the solar disk to make a prediction of proton flux parameters expected on Earth. In this case flares which occurred in the past are analyzed; however, the calculation of proton flux parameters for them and the comparison of calculated values with observed ones are of a considerable interest, since such an approach demonstrates the possibilities of proton flare diagnosis according to radio bursts. If there were operative data on radio bursts, flare diagnosis could be realized in real time. The procedure worked out by Akinjan et al. [1977c] is used for the proton flux parameter calculation. Parameters of microwave bursts, particularly the maximum intensity at a fixed frequency (S_ν), are used initially to characterize the number of particles accelerated in a flare. The estimation of particle release from the flare region is calculated from meter radiation component data (Types II and IV bursts). The technique takes into account the considerable influence of flare heliolongitude on the parameters of proton fluxes that reach the Earth and also on the character of their relation to radio bursts.

The general character of calculated temporal profiles is approximately the same as shown in Figure 1. The main parameter of the flare diagnosis is the maximum intensity of proton fluxes in the vicinity of Earth. The estimation of this parameter for protons with energies Ep>10; 30 and 60 MeV was made here, proceeding from the values of maximum radio burst intensity at 3 and 9 GHz, i.e., from S_3 and S_9. Corresponding expressions for the intensity functions and longitudinal attenuation are given in papers by Akinjan et al. [1977a and b, 1978]. The required data on meter microwave bursts were taken from *SGD* [1977] and *HHI Solar Data* [1977]. Observational data available from IZMIRAN [Bakunin et al., 1978] were also used.

Data on flares and corresponding radio bursts as well as calculated values of proton maximum intensity with energies Ep>10, 30 and 60 MeV are given in Table 3. The proton intensity calculated by parameter S_9 is given in parentheses. Observed proton fluxes are given, interpolated to the same energy range on the basis of proton flux data with Ep>15, 25, 40 and 90 MeV taken from *Meteor*.

Table 3. Radio Bursts and Calculated and Measured Proton Flux Values

Flares			Radio Bursts			Maximum Proton Flux Intensity (protons/cm^{2}sec sr)					
						Calculations			Observations		
Data 1977	Max (UT)	Location	S_3 (10^{-22}W/m^{2}Hz)	S_9	Meter Component	E_p>10	E_p>30	Ep>60	Ep>10	Ep>30	E_p>60
Sept. 7	2255	E90	1500	2080	Intense	Lower limit		0.01	No data		
9	1645	N07 E87	1100	4580	Intense	Lower limit		0.01	No data		
16	2307	N07 W21	1500	----	Weak	6.82	8.4	4	34.8	12.6	7.1
19	1045	N08 W57	1100	2000	Intense	118 (131)*	28 (31)*	14 (12.4)*	132	32.4	13.1
Nov. 22	1007	N23 W40	1220	3300	Intense	152 (190)*	34 (45)*	16.3 (18.4)*	355	80	40

* Computed from the maximum intensity at 9 GHz (S_9).

Flares of September 7 and 9 took place behind the eastern limb and near it, respectively. Taking into consideration the screening effect for these flares, we believe it is possible to estimate the lower limit of proton intensity near Earth, in case we have values that are outside the detection limits. This reflects the considerable role of solar longitude in attenuating the proton flux from eastern flares. As far as the flare behind the limb on September 24, 1977 is concerned, proton fluxes resulting from it cannot be accurately calculated from the data available.

According to the data given in Table 3 for the rest of the flares, which were located on the disk, a quantitative diagnosis gives satisfactory results: calculated proton flux values differ from the observed ones by a factor of 1 to 3. On the whole we can conclude that proton fluxes from the flares for a given period could be calculated in advance with sufficient accuracy under real-time conditions if there are operative radio burst and flare data.

REFERENCES

AKINJAN, S. T., V. V. FOMICHEV and I. M. CHERTOK 1977a — Opredelenie Parametrov Solnetshnikh Protonov v Okrestnosti Zemli po Radiovspleskam. I. Funktsiya Intensivnosty, *Geomagnetizm i Aeronomiya, 17,* 10.

AKINJAN, S. T., V. V. FOMICHEV and I. M. CHERTOK 1977b — Opredelenie Parametrov Solnetshnikh Protonov v Okrestnosti Zemli po Radiovspleskam. II. Funktsiya Dolgotnogo Oslableniya, *Geomagnetizm i Aeronomiya, 17,* 177-183.

AKINJAN, S. T., V. V. FOMICHEV and I. M. CHERTOK 1977c — Opredelenie Parametrov Solnetshnikh Protonov v Okrestnosti Zemli po Radiovspleskam. III. Vremennie Opornie Funktsii, *Geomagnetizm i Aeronomiya, 17,* 596-602.

AKINJAN, S. T., M. M. ALIBEGOV, V. D. KOZLOVSKII and I. M. CHERTOK 1978 — Kolitshestvenaya Diagnostika Protonnikh Vspishek po Kharakteristikam Radiovspleskov na 9 GHz, *Geomagnetizm i Aeronomiya, 18,* 410.

AVDYUSHIN, S. I., N. K. PEREYASLOVA, Yu. M. KULAGIN, M. N. NAZAROVA and I. E. PETRENKO 1977 — Observations of Solar Cosmic Rays by "Meteor" Satellite in March - May 1976, *Report UAG-61,* Collected Data Reports for STIP Interval II, 20 March - 5 May 1976, 157-164, (NOAA, Boulder, Colorado 80303, U.S.A.)

BAKUNIN, L. M., T. P. CHERNOV, V. V. FOMICHEV and A. K. MARKEEV 1981 — Observations of the Radio Burst on September 19, 1977 at IZMIRAN, *Report UAG-83,* this issue, p.121.

BAKUNIN, L. M., T. P. CHERNOV, A. A. GNESDILOV and O. S. KOROLEV 1981 — The Fine Structure of the Complex Type II - IV Radio Burst on November 22, 1977, *Report UAG-83,* this issue, p.484.

HHI Solar Data 1977 — *HHI Solar Data,* 28, September-November 1977, Adlershof, Berlin, DDR.

IVANOV, K. G. 1974 — Viyavlenie Tangentsialnikh i Kontaktnikh Razrivov po Izmereniyam v Solnetshnom Vetre, *Geomagnetizm i Aeronomiya, 14,* 8.

IVANOV, K. G. 1978 — *Kosmitsheskie dannie,* Sentyabr, Noyabr, 1977.

SGD 1977 — *Solar-Geophysical Data,* 398-401, Part I, October-December 1977, U.S. Department of Commerce, (Boulder, Colorado, U.S.A. 80303).

X-ray Observations of the September/November 1977 Solar Events

by

J.A. Williams and R.F. Donnelly
Space Environment Laboratory
NOAA Environmental Research Laboratories
Boulder, Colorado 80303, U.S.A.

Introduction

This paper presents solar X-ray observations from the SMS-2 and GOES-2 geosynchronous satellites. The ½-4 Å and 1-8 Å instruments have been described by Unzicker and Donnelly [1974]. The SMS-2 results are now archival data at NOAA's World Data Center A for Solar-Terrestrial Physics, Boulder, Colorado. The GOES-2 data are still preliminary results and therefore are presented only for flares when no SMS-2 data were available.

The solar flares of September 1977 produced the first large group of major X-ray bursts of Solar cycle 21. These bursts reached X class category [$\Phi(1\text{-}8\ \text{Å}) \geq 10^{-4}\text{Wm}^{-2}$ above the Earth's atmosphere] as defined by Baker [1970]. The last large groups of X-class events were observed during the declining years of solar cycle 20, in July and September 1974 and in August 1975. The present solar, cycle 21, includes the events of March and April 1976.

Observations

The major flares of September 1977 originated from one region (McMath plage region 14943). Three of these were in the X-category; the largest, and X-3, occurred on September 19 at 1027 UT. X-ray descriptions of these major eruptions are contained in Table 1. Data for the X-class flare of November 22, 1977 at 0950 UT are also included.

In Table 1 the start time for each channel was measured as the time when the flux for that channel first rose to 10% above the background level. The average rate of rise of the flare was measured from 10% above the main background level of emission to either 90% of the peak flux or, if applicable, to the point where there is a marked decrease in the rate of increase of the flux near the peak. In those cases where "precursor" events occurred, e.g. Figure 1, or two or more main phases of growth occurred, the rate of flux increase was determined from the final rise to the main peak. The duration of the peak is determined as the amount of time needed for the flux to rise from 95% of the maximum, pass through maximum, and decay to 95% of maximum.

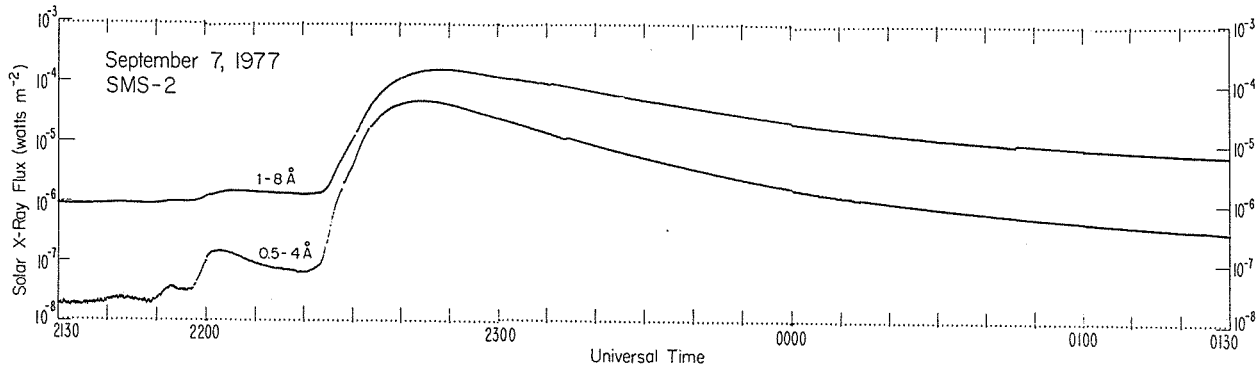

Fig. 1. Solar X-rays from SMS-2 Sept. 7, 1977.

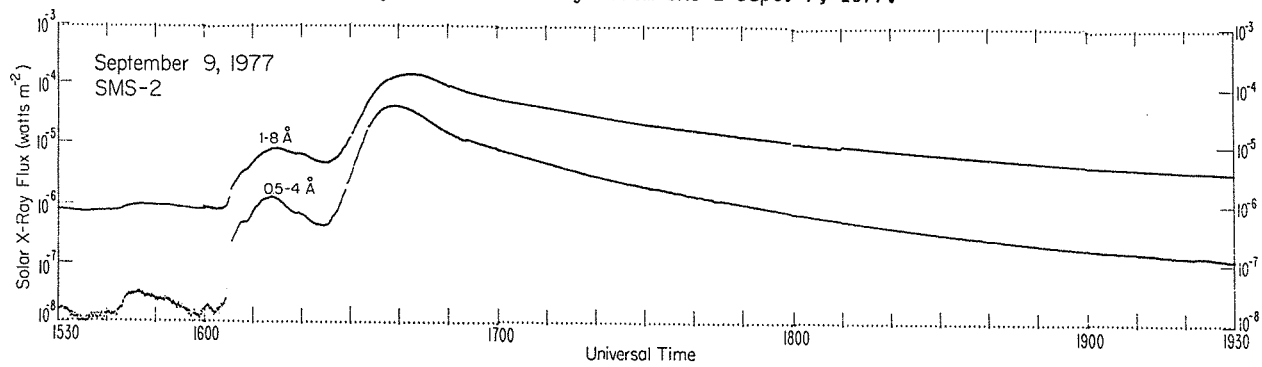

Fig. 2. Solar X-rays from SMS-2 Sept. 9, 1977.

Table 1. Major Flares During September/November 1977

Event Date	Start Time (UT) .5-4 A	Start Time (UT) 1-8 A	Average Leading Edge Rise Rate $\Delta\phi/\Delta t$ ($Wm^{-2}m^{-1}$) .5-4 A	Average Leading Edge Rise Rate $\Delta\phi/\Delta t$ ($Wm^{-2}m^{-1}$) 1-8 A	Peak Time (UT) .5-4 A	Peak Time (UT) 1-8 A	Maximum Flux Φ_{max} Wm^{-2} .5-4 A	Maximum Flux Φ_{max} Wm^{-2} 1-8 A	Duration of peak (min) .5-4 A	Duration of peak (min) 1-8 A	Exponential Decay Time Constant (τ) (min) .5-4 A a	.5-4 A b	1-8 A a	1-8 A b	Amplitude Difference (Wm^{-2}) at the times of Peak of .5-4 A	Amplitude Difference (Wm^{-2}) at the times of Peak of 1-8 A	Level drops to 10^{-6} 1-8 A	Time Ratio .5-4A / 1-8A = .1 UT	Flare Duration Time (UT) 1-8 A
9/ 7/77	2150	2158	$3.1x10^{-6}$	$8.3x10^{-6}$	2244	2248	$5\ x10^{-5}$	$1.8x10^{-4}$	5	4	23.1	74.6	40.6	134.8	$1.2x10^{-4}$	$1.3x10^{-4}$	1100	2338	13 hr 10 min
9/ 9/77	1604	1605	$2.3x10^{-6}$	$8.8x10^{-5}$	1639	1642	$4.5x10^{-5}$	$1.6x10^{-4}$	4	7	20.4	139.8	42.6	109.7	$9.5x10^{-5}$	$1.2x10^{-4}$	0220 (9/10/77)	1720	10 hr 15 min
9/16/77	2126	2124	$3.6x10^{-5}$	$2.0x10^{-6}$	2256	2304	$1.3x10^{-5}$	$7\ x10^{-5}$	14	15	29.0	51	42.2	69.1	$5.7x10^{-5}$	$5.7x10^{-5}$	0523 (9/17/77)	2340	7 hr 59 min
9/18/77	0012	0016	$1.5x10^{-7}$	$1.2x10^{-6}$	0041	0045	$4.3x10^{-6}$	$2.8x10^{-5}$	9	11	27.9	75.3	45.27	274.9	$1.8x10^{-5}$	$2.4x10^{-5}$	>0600	0102	6 hr 39 min
†9/19/77	1027	1027	$3.2x10^{-6}$	$8.5x10^{-5}$	1052	1055	$5.2x10^{-5}$	$3.0x10^{-4}$	7	6	15.0	68.3	20.8	61.5	$2.2x10^{-4}$	$2.4x10^{-4}$	1335	1120	3 hr 8 min
9/20/77	0247	0249	$8.1x10^{-8}$	$6.4x10^{-7}$	0348	0356	$4.5x10^{-6}$	$3.9x10^{-5}$	26	41	136.4	49.3	184.9	179.8	$3.3x10^{-5}$	$3.5x10^{-5}$	>1630	0437	13 hr 45 min
11/22/77	0950	0948	*$1.9x10^{-6}$	*$1.3x10^{-5}$	1005	1007	$1.8x10^{-5}$	$1.1x10^{-4}$	2	2	5.52	27.7	16.6	35.7	$7.2x10^{-5}$	$9.4x10^{-5}$	1320	1023	3 hr 47 min

†Values obtained from GOES-2 satellite. Ouput of the GOES-2 satellite was found to be 15% lower than that of SMS-2. GOES-2 data was corrected to be equivalent to SMS-2 levels. All other values are from SMS-2 satellite.

*Flare exhibited a distinctive step in its rise where the first slope was considerably steeper than final rise to maximum. Initial rise of 1-8 A had a slope of $7.6x10^{-7}$watts/m^2-min whereas the .5-4 A had a slope $\geq 1.3x10^{-7}$watts/m^2-min. Initial increase in flux obtained a level of approximately 1/3 of the maximum amplitude.

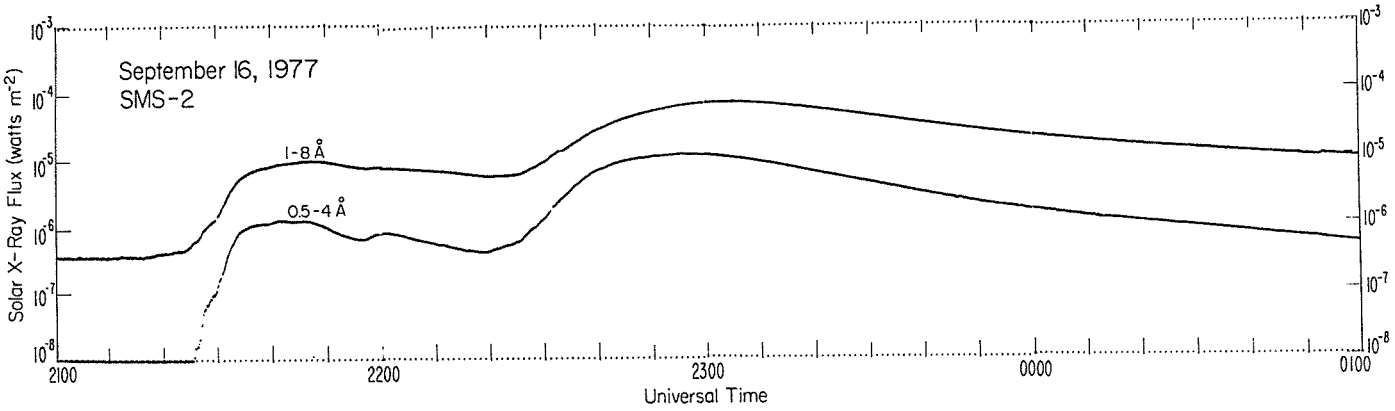

Fig. 3. Solar X-rays from SMS-2 Sept. 16, 1977.

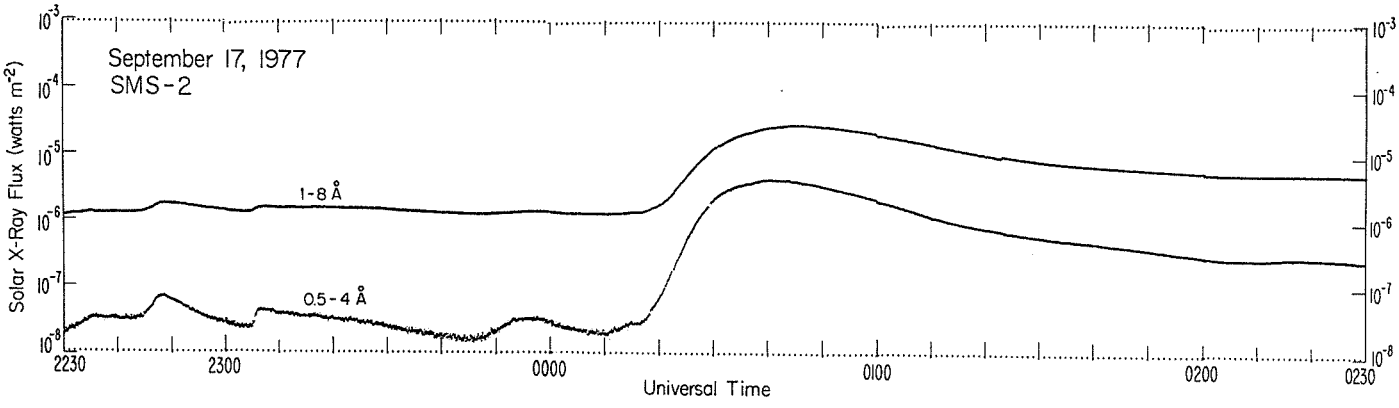

Fig. 4. Solar X-rays from SMS-2 Sept. 17, 1977.

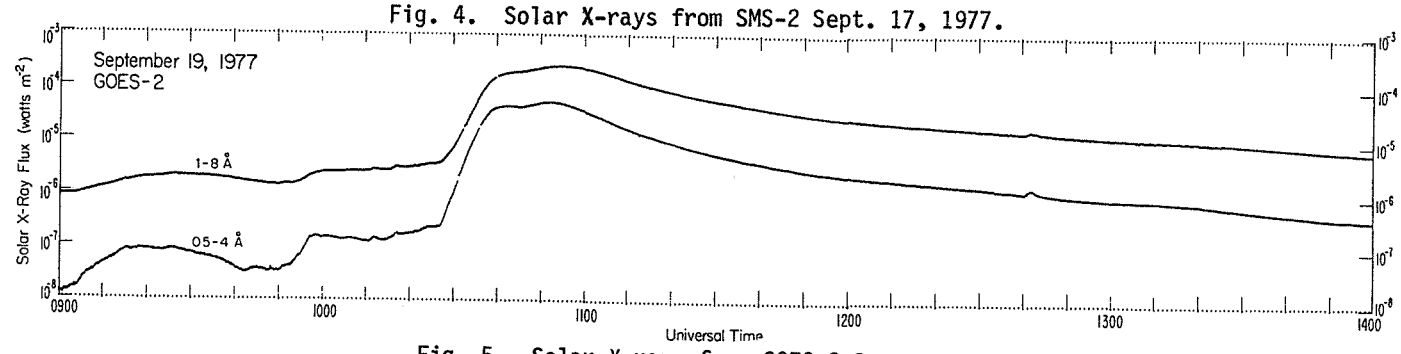

Fig. 5. Solar X-rays from GOES-2 Sept. 19, 1977.

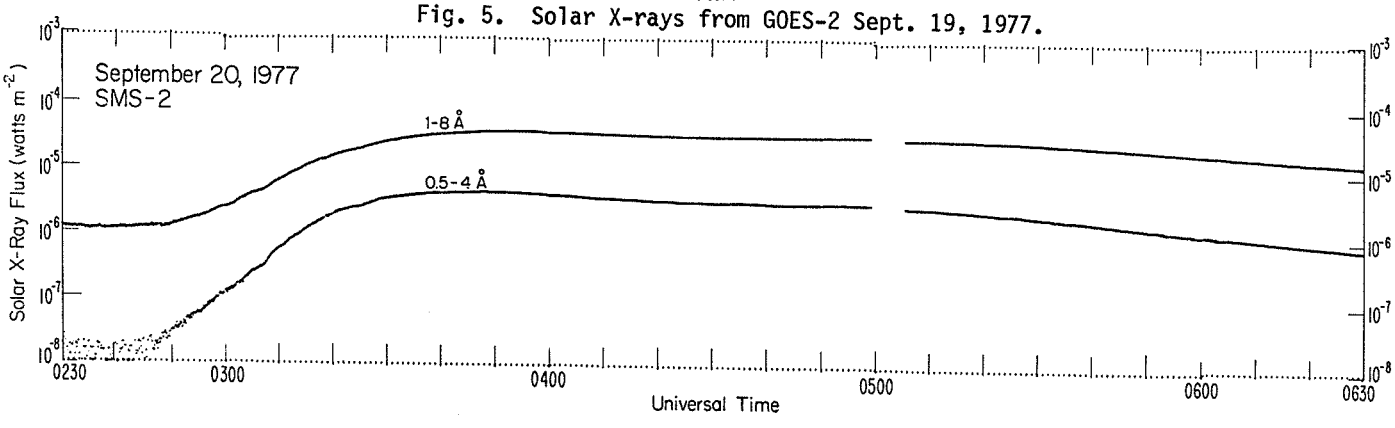

Fig. 6. Solar X-rays from SMS-2 Sept. 20, 1977.

The decay time constant, τ, is defined by the relationship

$$\Phi(t_2) = \Phi(t_1)\exp[-(t_2-t_1)/\tau]\text{Wm}^{-2}$$

where $\Phi(t)$ is the value of flux at times t. In Table 1, the "a" and "b" columns under Exponential Decay Time Constant denote Φ for the early and late phases of the flare's decay.

The amplitude difference, defined by Φ(1-8 Å) - Φ(½-4 Å), was determined for two times of interest, namely the peak time for Φ(½-4 Å) and the peak time for Φ(1-8 Å). Since the contribution by energies of wavelengths ½-1 Å to the overall flux levels of the ½-4 Å detector is small, this band of energies, ½-1 Å, was neglected. The results of this computation gave a general indication of the energy contained in the flare. The larger Φ(½-4Å) is relative to Φ(4-8 Å), the more energetic the X-ray flare. The time when the ratio of the output of the ½-4 Å channel to the 1-8 Å channel has reduced to 0.1 is an indication that the ½-4 Å spectral distribution is not reliable.

Flares with X-ray levels equal to or less than 1 x 10^{-6}Wm^{-2} have an undetectable effect on the ionospheric D region [Donnelley, 1976]. Therefore, the times when the 1-8 Å level decays to 1 x 10^{-6}Wm^{-2}, or to that point in time where there is a marked increase in the ½-4 Å level indicating the beginning of a new flare, were defined as flare end times and are included in Table 1. The flare duration is the difference between flare start time and this end time.

Many smaller flares occurred during September 1977. An example of these flares is found in Figure 7. The following features were scaled for small flares and are listed in Table 2.

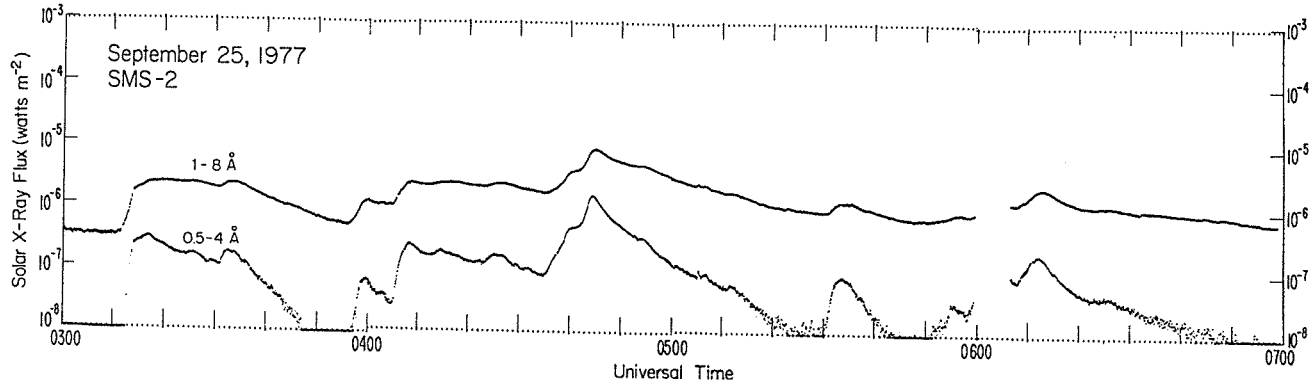

Fig. 7. Solar X-rays from SMS-2 Sept. 25, 1977.

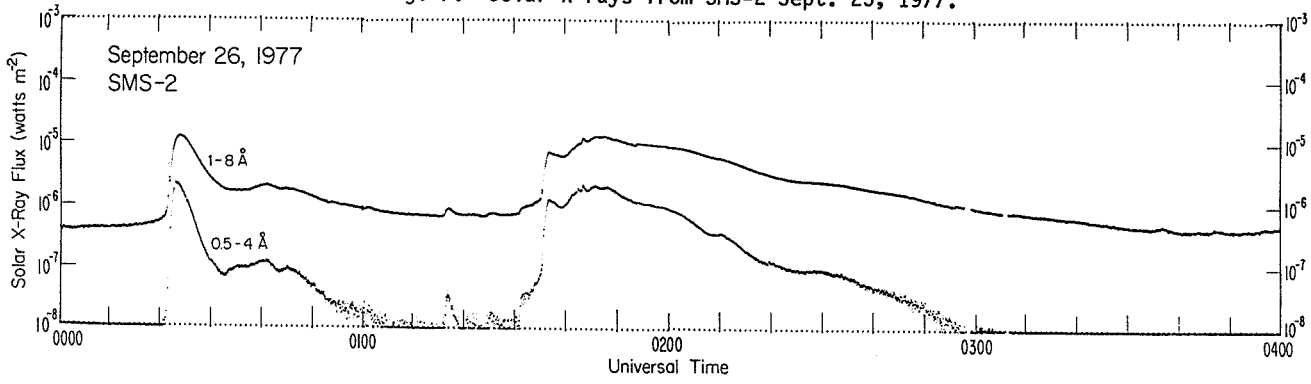

Fig. 8. Solar X-rays from SMS-2 Sept. 26, 1977.

Table 2. Examples of Minor Flares During September 1977

Date of Flare	Start Time (UT)	Peak Amplitude (Wm^2) 1/2-4 A	Peak Amplitude (Wm^2) 1-8 A	Time of Occurrence of Peak (UT) 1/2-4 A	Time of Occurrence of Peak (UT) 1-8 A	Flare Duration (min) 1-8 A
Sept. 25, 1977	0312	3×10^{-7}	2.4×10^{-6}	0317	0318	44
	0356	1.7×10^{-6}	9×10^{-6}	0444	0445	94
	0430	8×10^{-8}	1.4×10^{-7}	0533	0533	13
	0550	2×10^{-7}	2.5×10^{-6}	0612	0613	60
Sept. 26, 1977	0021	1.1×10^{-6}	1.3×10^{-5}	0023	0024	39
	0116	3.4×10^{-8}	9×10^{-7}	0117	0117	4
	0131	2×10^{-6}	1.3×10^{-5}	0146	0147	87

a. Start time. Peak fluxes for many minor flares do not have large increases over background flux levels in the 1-8 Å wavelength range; therefore the start time of these flares will be determined primarily as the time of a major increase in the ½-4Å flux level.
b. Peak flux.
c. Duration of flare. For small flares the time period begins with the flare start time, as described above, and continues until either the 1-8 Å flux level decays to 10% above the background level or the ½-4 Å flux level begins a definite increase in flux level.

Results

The flares that occurred during the September 1977 time period originated in one active region on the Sun. All of the major eruptions, Figures 1-8, had similar characteristics. One characteristic immediately observed was the long decay times for both the 1-8 Å and ½-4 Å wavelength bands. The decay times for these flares were on the order of hours. A second observed characteristic was the step or precursor in the leading edge of each event. As solar rotation moved this active region westward the step that was very pronounced in the September 9 event became more reduced and preceded the main portion of each flare by longer spans of time. A third characteristic of these major bursts is the progressive decrease in flare duration time. The major exception to this trend was the event of September 20.

The November 22 event, Figure 9, follows somewhat the same characteristics as the ones in September. A definite step at the leading edge of the flare exists in conjunction with a long decay time of the 1-8 Å wavelength. The difference from the September flares was the peak duration time. For this flare this period was much shorter than the September events.

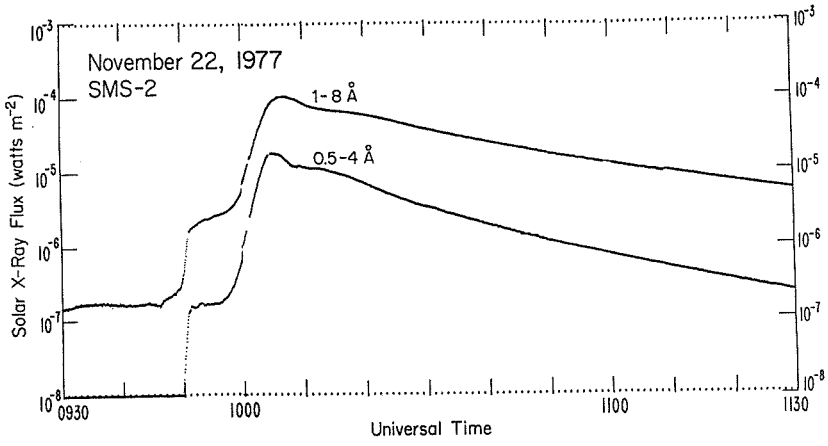

Fig. 9. Solar X-rays from SMS-2 Nov. 22, 1977.

Acknowledgments

The authors of this report thank Mr. Robert Hines of the Real Time Data Services and Mr. Frank Cowley of the Analysis Group in the Space Environment Laboratory, NOAA, for help in data processing. The data presented in this report were originally lost due to mechanical failure of the computer system used in collecting SMS/GOES X-ray data. Due to Mr. Hines' programming efforts of the backup system at Table Mountain, Boulder, Colorado, the data for this report were retrieved.

REFERENCES

BAKER, DONALD M. 1970 Flare classification based upon X-ray intensity, *AIAA Observation and Prediction of Solar Activity Conference*, November 16-18, 1970, Huntsville, Alabama.

DONNELLY, RICHARD F. 1976 Solar flare X-ray and EUV emission: A terrestrial viewpoint, *Physics of Solar Planetary Environments, Vol. I*, Proceedings of the International Symposium on Solar-Terrestrial Physics, June 7-18, 1976, Boulder, Colorado, ed. Donald J. Williams.

UNZICKER, ARLYN and RICHARD F. DONNELLY 1974 Calibration of X-ray ion chambers for Space Environment Monitoring System, *NOAA Technical Report, ERL 310-SEL 31*.

A Summary of Lockheed X-Ray Data for McMath 14943 and for the Flare of November 22, 1977

by

J.M. Mosher, G.H. Bruner, and C.J. Wolfson
Lockheed Palo Alto Research Laboratory
Palo Alto, California

Introduction

Since June 1975, the Lockheed Mapping X-Ray Heliometer (MXRH) onboard OSO-8 has provided essentially continuous coverage of solar activity in the 2-15 keV X-ray band via one-dimensional collimators and proportional counter detectors. The present contribution summarizes the data obtained for McMath 14943, during September 1977, and for the flare of November 22, 1977.

Instrumentation

The design and operation of the MXRH instrument were described in our submission to UAG Report 61 [Wolfson et al., 1977]. More detailed information is provided in Wolfson et al. [1975]. For the present purpose, it is sufficient to know that the data are collected in a manner such that count rates can be extracted in various combinations of arc-minute wide linear strips laid across the Sun in three orientations at 120° to one another. With any strip the counts can be further subdivided into 15 pulse-height (i.e., energy) channels, on the basis of which the effective temperature and emission measure of a source with the strip can be determined.

The 550-km altitude of the OSO-8 orbit limits data collection to 60-minute daylight segments separated by 30-min periods of darkness. Additional intervals of up to 32 min are lost when the detector high voltages are switched off as the spacecraft passes through the South Atlantic Anomaly. The resultant average coverage is about 50 percent, with a measurement every 10 sec in one of the three collimator systems during the active periods.

General Nature of X-Ray Observations for September 1977

An examination of MXRH maps from September 8 to September 22, 1977, shows that the intense magnetic complex formed by McMath 14943 and its smaller companion region McMath 14942 was the dominant X-ray source on the Sun during the entire course of its disk passage. No attempt has been made to separate the signals from the two, since at the resolution of the MXRH the sources are essentially unresolved. McMath 14943 is presumably the main contributor based on H-alpha flare reports.

Next to this complex, the second most important producer of X-ray emission was McMath 14952, in the opposite hemisphere. While in its non-flaring state it was roughly an order of magnitude dimmer than McMath 14943, it could, during flares, briefly dominate the Sun. On two occasions (September 18 at 1822 UT and September 19 at 1937 UT) the MXRH shows it reaching four times the brightness of McMath 14943 in the 2 - 14 keV band. On a number of other occasions it achieved approximate equality (e.g.: September 18 at 2326 UT, September 19 at 1534 UT, and September 22 at 0820 UT). The only other region to achieve this distinction was McMath 14930. On September 13 at 1125 UT when it was on the NW limb and McMath 14943 was at a low ebb, it reached about two-thirds of the intensity of McMath 14943.

Observations of McMath 14943

A. Light Curve

Variations in the X-ray intensity of McMath 14943 (or, more properly, of the unresolved activity complex formed by McMath 14943 and its companion region McMath 14942) from September 5 through September 25, 1977, were investigated by constructing eighty-four 6-h light curves using the Vertical detector system. Data in this system are collected once every 20 sec; using the Vertical Large detector for count rates below 15,000 cps, and the 15 time less sensitive Vertical Small Flare detector for count rates above that level. The approximate energy coverage is 2 - 15 keV for either detector, with most of the counts coming at the low-energy end. Two small data gaps, one of 5 h on September 10 and the other of 4 h on September 11 were introduced by operational errors.

For an example of a typical Vertical collimator light curve, see Figure 3. A summary presentation of all individual light curve results for McMath 14943 is given in Figure 1, where each vertical bar represents the span of count rates encountered in a 90-min orbit, and the connected dots are orbital averages. In preparing this plot, the problem of detector switching discussed in Wolfson et al. [1977] has been avoided by manually sliding the Small Flare data by a factor of 15 to obtain an effective count rate in Vertical Large. Even so, the magnitudes of five of the major flare events are not accurately represented since they were sufficiently intense to produce overflow and saturation even in this least sensitive of the MXRH detectors. The maxima of smaller flares will also be underestimated whenever their peaks happen to fall in MXRH data gaps.

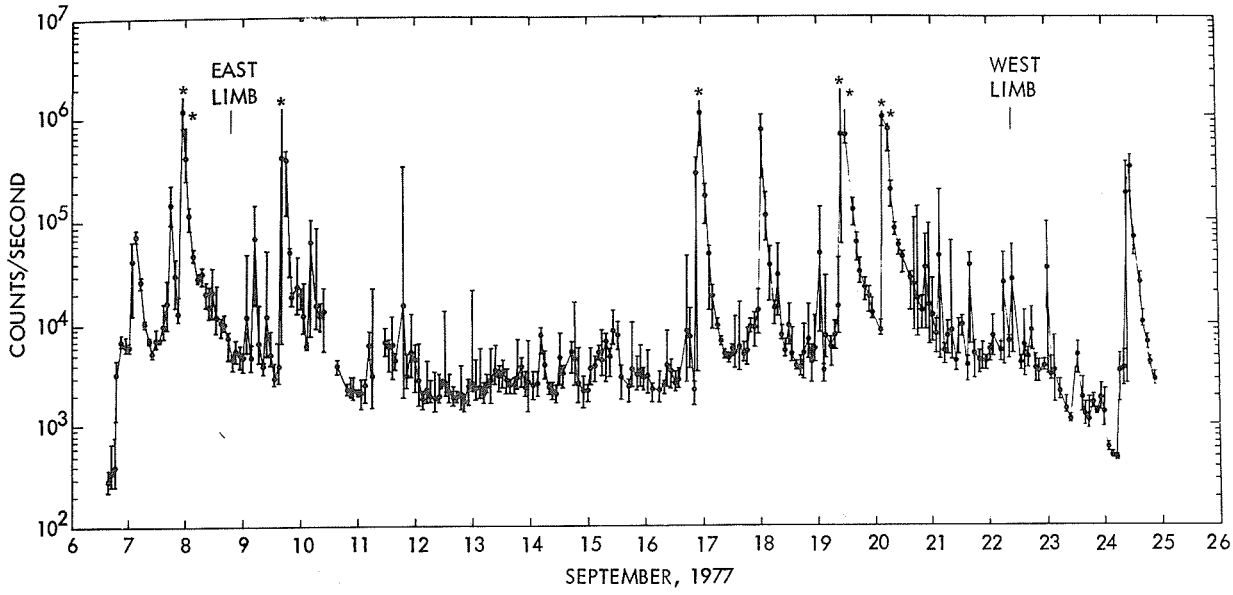

Fig. 1. Summary of 2-15 keV X-ray light curve data for McMath 14943. In orbits marked by asterisks the upper level is limited by saturation. Count rates are expressed in terms of an effective rate in Vertical Large for the peak area segment. The Vertical Small Flare detector is used above 15,000 cps.

Data have been shown only from September 6 through September 24, since before and after these dates the weakening signal from the source behind the limb became blended with comparable signals from smaller sources on the visible disk (McMath 14941 in the East and McMath 14943 in the West) in such a way that the two signals could not be easily disentangled at the resolution of the MXRH. For the interval shown, observations of McMath 14943 in the Vertical system should be clean.

One of the main observational results illustrated by Figure 1 is the sporadic nature of the flare occurrences, with two periods of distinct activity separated by a relatively long dry spell. This variation does not appear to be related to any obvious change in the photospheric magnetic structure.

In general the timings of the X-ray flares (particularly the start and peak times) coincide very well with the H-alpha times reported in Solar-Geophysical Data, but there can be a considerable variation in the magnitudes of X-ray events corresponding to a given H-alpha class, particularly subflares. For example, a class -N subflare reported by three observatories at 1850 UT on September 11 produced more than a hundred-fold enhancement in the 2 - 15 keV X-ray intensity, whereas other events in this class may cause scarcely a ripple.

In relating MXRH observations to terrestrial effects, it should be noted that for an average solar active region producing a count rate R (cps) in the Vertical Large detector, the 1-8 Å X-ray energy flux (I) it creates at the top of the Earth's atmosphere is given approximately by:

$$I_{1\text{-}8\text{Å}} = 10^{-9} \times R^{0.75} \ W/m^2$$

Individual regions, with distinctive spectral characteristics, deviate from this empirical relationship by factors on the order of 2 or 3.

B. Identification of Behind-the-Limb Bursts

Since for the bulk of its disk passage McMath 14943 was the dominant solar X-ray source, the data provided in Figure 1 are largely redundant with those provided by full-disk X-ray monitors, such as the ones on NOAA's SMS and GOES satellites. The MXRH is particularly useful, however, in the identification of behind-the-limb bursts.

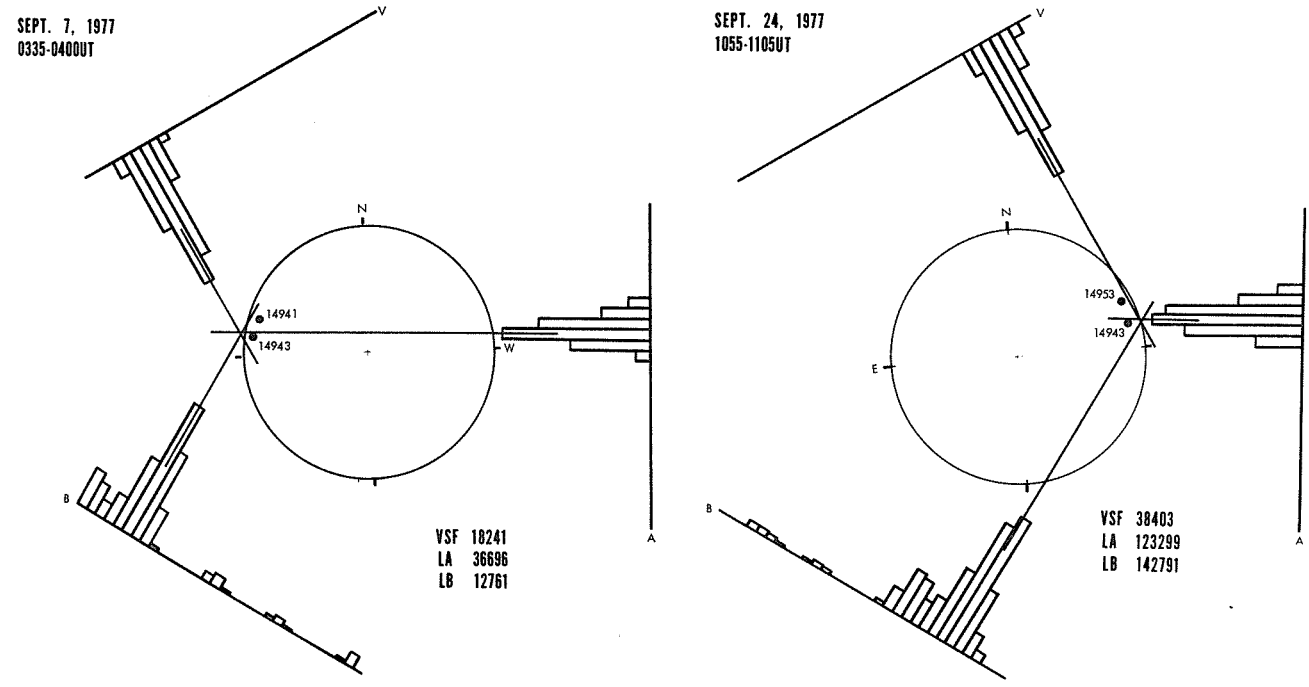

Fig. 2. Typical X-ray maps for behind-the-limb bursts. For each detector the histogram is normalized to the peak count rate as indicated on the map. The dots for McMath 14943 represent its approximate position behind-the-limb, while the second dot represents the position of a region on the visible disk. The secondary peak in the Large B histograms is due to a flaw in the collimator.

Figure 2 shows MXRH maps for the first and last bursts that could definitely be attributed to McMath 14943 (and which terminate the plot in Figure 1). In each case, the approximate position of this source on the backside of the Sun is indicated, along with the location of the most plausible alternative source on the visible disk. The fact that no associated H-alpha activity was reported in these alternate sources, together with the fact that the location of the observed X-ray emission on the limb coincides with that of a source suspended radially above McMath 14943 would seem to confirm our identification, although a considerable height is implied. At the time of the September 7th burst, the center of McMath 14943 is 21° behind-the-limb, requiring that the detected X-ray emission comes from heights on the order of 50,000 km or more above the photosphere. For the September 24th event, the region is 27° behind-the-limb, giving heights of at least 82,000 km.

MXRH Data for the Flare of November 22, 1977

The light curve of McMath 15031 on the day of November 22, 1977, the main feature of which is a beautiful 2B flare around mid-day, is shown in Figure 3. Again the Vertical Collimator was chosen, with Small Flare data (which appear at intensities of greater than 15,000 cps) being shifted by a factor of 15.

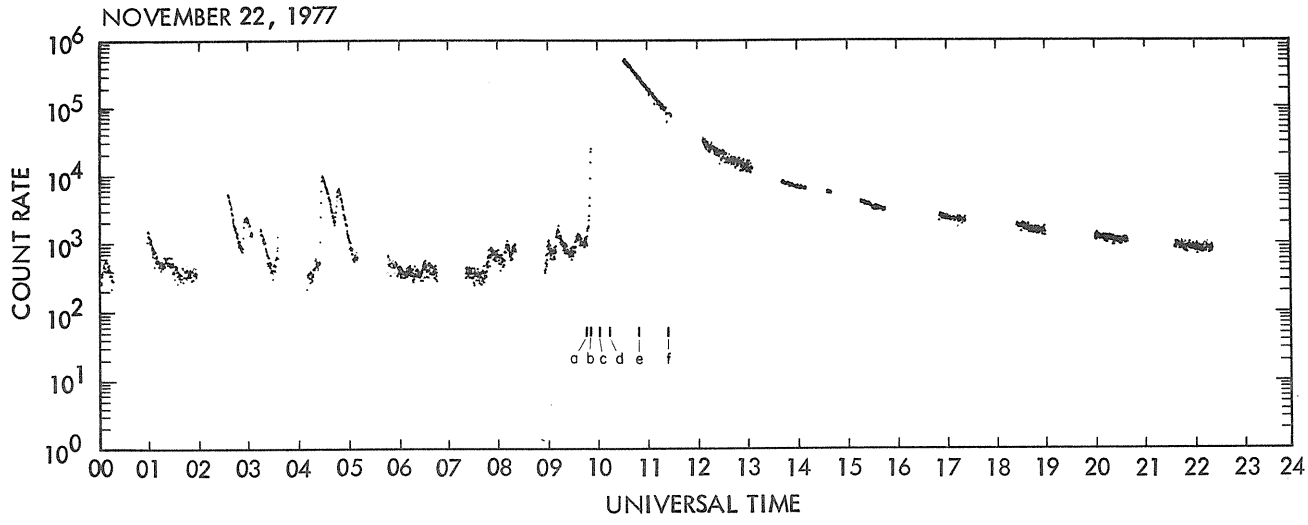

Fig. 3. X-ray light curve for McMath 15031 on November 22, 1977. Times corresponding to the H-alpha photographs of Figure 4 are indicated. Frame (b) corresponds to the second to last MXRH point shown on the rising slope. Detectors and energy coverage are as in Figure 1.

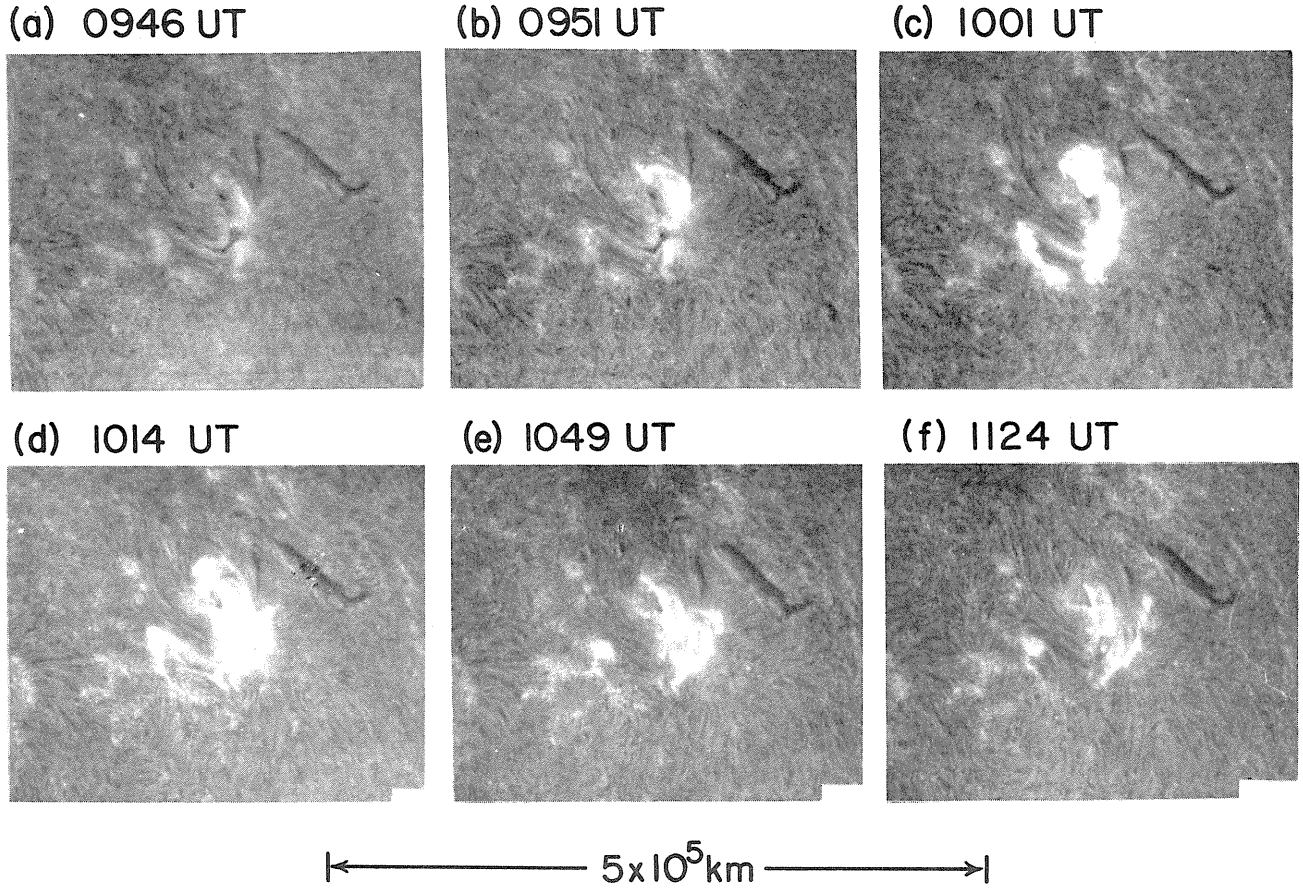

Fig. 4. On-band H-alpha photographs of the flare of November 22, 1977, taken at Tel Aviv (courtesy H. Zirin, Big Bear Solar Observatory). North is at the top, and east is to the left.

The flare is a classic, both in X-rays and in hydrogen light, a sequence of which is shown in Figure 4. The timing of the first enhancement in H-alpha at 0946 UT coincides quite precisely with the onset of the X-ray burst. The flash phase appears to be simultaneous with the disruption of a small filament along the neutral line, the brightening occuring primarily in two discrete ribbons situated over the opposite polarity plages, and lighting up in different places so as to produce an apparent spreading at about 10 km/sec during the first h. In X-rays, the initial cooling is exponential, with a time consistant of 29 min.

Summary

The present report is intended to summarize MXRH data for McMath 14943 and for the flare of November 22, 1977. More detailed information for selected times, including high-resolution light curves, temperature and emission measure profiles and X-ray maps can be supplied on request.

Acknowledgments

Operation of the Mapping X-Ray Heliometer is made possible by NASA Contract NAS5-22411. The analysis program is supported both by this contract and by the Lockheed Independent Research Program. Loren W. Acton is Principal Investigator on the MXRH experiment. The preparation of this report benefitted materially from the extensive analysis of quick-look data performed by Kermit L. Smith. Special thanks are due to H. Zirin for providing the H-alpha photographs.

REFERENCES

WOLFSON, C.J., L.W. ACTON and C.W. GILBRETH — 1975 — Mapping X-Ray Heliometer for Orbiting Solar Observatory-8, Final Report, NASA-CR-144710.

WOLFSON, C.J., L.W. ACTON, D.T. ROETHIG and K.L. SMITH — 1977 — 2-30 keV X-Ray Data From OSO-8, Report UAG-61, (World Data Center A), p. 187.

4. COSMIC RAYS

Observations of September 1977 Cosmic Ray Events at High Rigidity

by
Derek B. Swinson
Department of Physics and Astronomy
The University of New Mexico
800 Yale Boulevard NE, Albuquerque, NM 87131

In this report data are presented from the large underground muon telescopes at Embudo and Socorro for September 11-25, 1977. These data, at relatively high rigidity, are compared to observations from the Deep River neutron monitor at low rigidity.

The two underground detectors are large multidirectional muon telescopes that use plastic scintillators [Regener et al., 1970]. These telescopes are located at Embudo Cave, near Albuquerque, New Mexico (N35.2 W106.4) and at Socorro, New Mexico (N34.0 W106.6). The Embudo detector has a depth below the top of the atmosphere of 35 mwe, a threshold rigidity of 19 GV and a vertical telescope counting rate of 333,000/h. For the Socorro instrument these same quantities have the values 82 mwe, 45 GV [H.S. Ahluwalia, private communication] and 67,000/h. A third underground telescope at Mt. Chacaltaya, Bolivia, which had operated since 1965, was permanently discontinued at the end of 1976.

In Figure 1 the pressure-corrected cosmic ray intensities recorded between the 11th and the 25th of September 1977 are displayed for the Embudo telescope, together with Socorro data from the 13th to the 25th of September (Socorro was closed September 11th and 12th). For comparison Figure 1 also includes the Deep River neutron monitor data for the same period [*SGD*, 1977a]. All data are plotted as a function of Universal Time (UT). The Deep River intensity scale marked in percent is the scale provided with the original data. For Embudo and Socorro, the intensity corresponding to the first datum point in each series is labeled 100%. The scale differs for each detector.

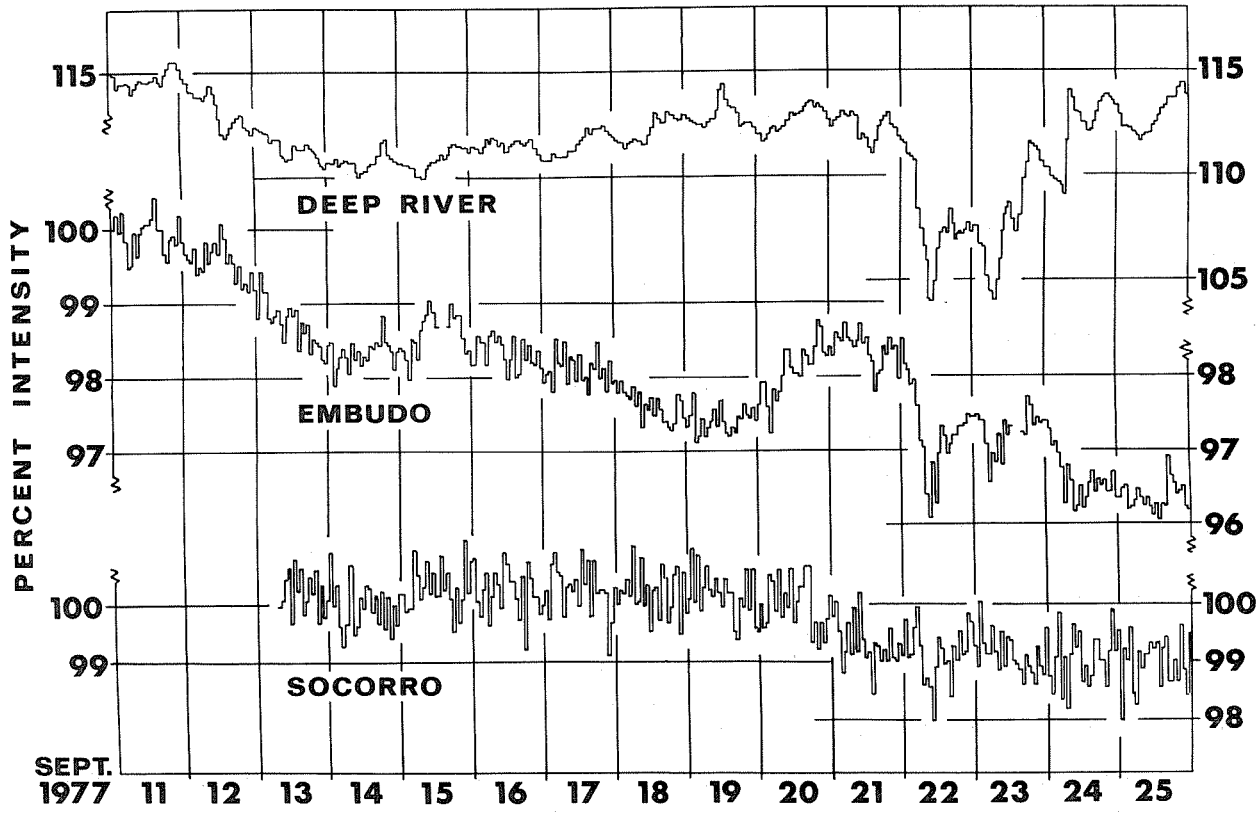

Fig. 1. Cosmic ray intensity in Universal Time recorded by the Deep River neutron monitor, and by underground muon telescopes at Embudo and Socorro in September 1977.

The most interesting features are a series of Forbush decreases between September 21st and 24th that appear to be present in the profiles from all three stations.

First Event.

The first decrease occurs on September 21st. In the Deep River data this is a decline of about 2% to a minimum between 1500 and about 1600 UT; it is followed by a recovery to the original intensity over the next 5 h. The Embudo data reach a minimum at about 1600 UT: the decrease being ~ 0.9% and the recovery taking 3 h. Because the counting rate at Socorro is much less than at Embudo, the "noise" is greater; also, because of its high threshold rigidity, the "signal" is usually smaller. Nevertheless, there is an intensity minimum in the Socorro data at approximately 1400 UT--a decrease of ~ 1% below the mean counting rate.

Second Event.

The most spectacular decrease starts about 2000 UT on September 21st in the Deep River data; here the intensity drops 9%, reaching a minimum between 1000 and about 1100 UT on September 22nd. This is followed by a 4.5% intensity increase over the next 6 h. At Embudo the decrease starts at 0100 UT on September 22nd, the intensity drops by 2.4% to a minimum at about 1000 UT, and then it gradually increases again by 1.4% by the end of September 22nd. At Socorro there is a clearly apparent minimum at approximately 1000 UT, the intensity being ~ 1.5% below the mean surrounding values.

Third Event.

The third decrease starts at about 0200 UT, September 23rd, in the Deep River data, and the intensity falls about 3.5% to a minimum between 0600 and about 0700 UT. This response is followed by a rapid recovery and another small decrease near 1500 UT on September 23rd. The decrease at Embudo also starts at 0200 UT, drops 0.9% to a minimum at 0600 UT, and then begins its recovery. There are no Embudo data for 1400, 1500 and 1600 UT on September 23rd. The decrease is not distinguishable in the Socorro data.

Fourth Event.

The fourth decrease starts around 2000 UT on September 23rd in the Deep River data. The intensity decreases slowly by 2.5% until about 0700 UT, at which time the decline is interrupted by a GLE that causes a rapid 5% increase in the counting rate. After that, the previous slow decrease appears to continue at about the same rate for a further decrease of 2% until about 1200 UT on September 24th. At Embudo the fourth decline begins about 0100 UT on September 24th and falls some 1.5% to an initial minimum by 0700 UT on the same day. There is then a rapid increase of 0.5%, but the intensity again falls to a level slightly below the 0700 UT minimum by 1000 UT; afterwards, the intensity continues to fluctuate near that level over the next 36 h. At Socorro there appears to be an intensity decrease of ~ 1% at 0700 UT on September 24th.

The decreases at each of the three detectors are listed in Table 1.

Table 1. The September 1977 Forbush Decreases

Time of Min (UT)	1400-1600 Sept. 21	1000-1100 Sept. 22	0600-0700 Sept. 23	0700 Sept. 24
Deep River Decrease	2%	9%	3.5%	2.5%*
Embudo Decrease	0.9±0.2%	2.4±0.2%	0.9±0.2%	1.5±0.2%
Socorro Decrease	1.0±0.4%	1.5±0.4%	---	1.0±0.4%

*followed by a further decrease of 2% after the GLE

The threshold rigidity at Deep River is 1.1 GV, and at Embudo and Socorro they are 19 and 45 GV, respectively [H.S. Ahluwalia, private communication]. The threshold rigidities for Embudo and Socorro have been revised downward from those values quoted previously by Swinson [1973].

The November 22, 1977 GLE, which is apparent in neutron monitor data from Kiel and Climax [*SGD*, 1977b] is not present in either the Embudo or Socorro profiles.

Acknowledgments

I am indebted to Professor H.S. Ahluwalia for calculating the threshold rigidities for the Embudo and Socorro telescopes. This work was supported by the Atmospheric Sciences Section, National Science Foundation, under grant ATM76-11743.

REFERENCES

REGENER, V.H., D.B. SWINSON, J.H. ERICKSEN and H.S. AHLUWALIA — 1970 — The Solar Diurnal Variation of Cosmic Rays Underground Since 1958," *Acta Phys. Acad. Sci. Hungaricae, 29,* Suppl. 2, 133.

SGD — 1977a — *Solar Geophysical Data,* 399 Part I, 116-119, November 1977, U.S. Department of Commerce (Boulder, Colorado, 80303 U.S.A.).

SGD — 1977b — *Solar Geophysical Data*, 401 Part I, 107, January 1978, U.S. Department of Commerce (Boulder, Colorado, 80303 U.S.A.).

SWINSON, D.B. — 1973 — Observations of the August 1972 Cosmic Ray Storm at High Rigidities," *J. Geophys. Res., 78,* 1707.

Solar Cosmic Ray Measurements in the Stratosphere in September and November 1977

by

A. N. Charakhchyan, G. A. Bazilevskaya, L. P. Borovkov,
T. N. Charakhchyan, Yu. I. Stozhkov, N. S. Svirzhevsky and E. V. Vashenjuk
P. N. Lebedev Physical Institute
The Academy of Sciences of the USSR
Moscow, USSR

On September 19-20 and 24-25 and on November 22-24, 1977, solar cosmic rays were measured in the stratosphere with radiosondes over Murmansk Region (N68.95 E33.05) and Mirny, Antarctica (S66.92 E93.00). The detector consisted of two Geiger-Müller tubes arranged to form a telescope and interlaid with an aluminum plate 2 g cm^{-2} thick. The wall thickness of each Geiger-Müller tube was 0.05 g cm^{-2} of steel. The pulse rate of a single counter and of both counters in coincidence were recorded.

The energy spectra of solar particles are obtained from absorption of the charged particle flux in the air. The following assumptions are used: (1) the solar cosmic rays are protons; (2) the flux of charged particles is isotropic at the boundary of the atmosphere, and the Gross procedure is valid; and (3) there are no rapid changes in solar cosmic ray flux during the radiosonde ascent.

Examples of energy spectra taken in the stratosphere are given in Figure 1. Tables 1-3 present data on integral energy spectra using a power-law function $N(\geq E) \sim E^{-\gamma}$ for the intensity of solar protons with energies more than 150 MeV.

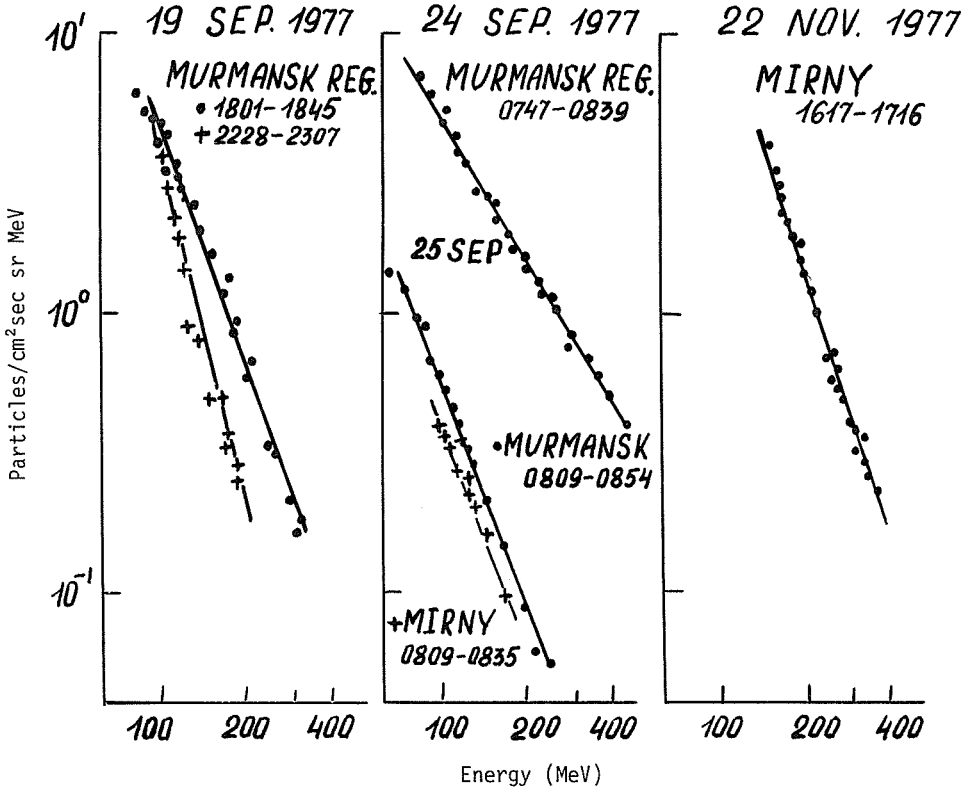

Fig. 1. Energy spectra measured in the stratosphere over Murmansk Region and Mirny, Antarctica during the particle events of September 19 and 24 and November 22, 1977. Shaded entries in Tables 1-3 represent the integrals of the spectra plotted above.

Table 1. Solar Cosmic Ray Integral Energy Spectra Measured in the Stratosphere During the September 19, 1977 Event.

No.	Day	Time (UT)	Location	ΔE (MeV)	γ	N(≥ 150 MeV) /cm²sec sr
1	19	1101-1150	Murmansk	100-400	2.7	0.820*
2	19	1244-1330	Murmansk	95-435	2.5	1.47
3	19	1506-1542	Murmansk	130-400	3.0	2.00*
4	19	1547-1610	Murmansk	135-275	2.9	2.14
5	19	1717-1744	Murmansk	170-300	3.1	--
6	19	1801-1845	Murmansk	85-310	2.8	1.49
7	19	2018-2041	Murmansk	100-235	3.2	0.83
8	19	2142-2228	Murmansk	90-250	3.5	0.70*
9	19	2228-2307	Murmansk	95-250	4.5	0.71
10	20	0045-0110	Murmansk	120-250	3.1	1.00*
11	20	0245-0319	Murmansk	135-250	4.1	1.40*
12	20	0700-0735	Murmansk	95-200	3.0	0.30*
13	20	0748-0817	Murmansk	80-170	3.3	0.14
14	20	0816-0827	Mirny	90-120	4.7	--
15	20	0936-1006	Murmansk	90-170	3.0	0.30*
16	20	1045-1105	Murmansk	90-175	3.2	0.18
17	20	1129-1158	Murmansk	100-175	3.4	0.30*
18	20	1322-1340	Murmansk	100-125	4.4	--
19	20	1348-1455	Murmansk	100-130	4.0	--

* Preliminary data because of uncertainty of the calibration.

Table 2. Solar Cosmic Ray Integral Energy Spectra Measured in the Stratosphere During the September 24, 1977 Event.

No.	Day	Time (UT)	Location	ΔE (MeV)	γ	N(≥150 MeV) /cm²sec sr
1	24	0747-0839	Murmansk	85-440	1.7	2.53
2	24	0823-0948	Mirny	80-460	1.5	2.58
3	24	1043-1151	Murmansk	130-450	2.2	4.20*
4	24	1113-1151	Mirny	165-450	2.9**	--
					2.1**	--
5	24	1236-1306	Murmansk	125-400	2.2**	2.90
					2.3**	1.90
6	24	1447-1527	Murmansk	120-400	2.5	1.45*
7	24	1658-1733	Murmansk	120-325	2.3	1.30
8	24	1806-1844	Mirny	100-300	1.8	0.69
9	24	1906-1957	Murmansk	120-300	2.2	1.00*
11	24	2205-2256	Murmansk	135-300	2.0	1.60*
12	25	0026-0050	Murmansk	120-225	2.2	0.46
13	25	0441-0532	Murmansk	80-200	2.0	0.40*
14	25	0749-0841	Murmansk	80-200	2.0	0.40*
15	25	0809-0835	Mirny	100-170	2.5	0.15
16	25	0809-0854	Murmansk	70-235	2.7	0.18
17	25	1216-1245	Murmansk	70-185	2.1	0.13
18	25	1232-1306	Mirny	100-165	3.6	0.16
19	25	1325-1412	Murmansk	100-165	3.5	0.15*
20	25	1653-1703	Murmansk	100-120	3.3	--

* Preliminary data because of uncertainty of the calibration.

** Discrepancies occurred between the single counter and both counters in coincidence because the particle flux failed to satisfy completely the three assumed conditions mentioned in the text.

Table 3. Solar Cosmic Ray Integral Energy Spectra Measured in the Stratosphere During the November 22, 1977 Event.

No.	Day	Time (UT)	Location	ΔE (MeV)	γ	N(≥150 MeV) /cm²sec sr
1	22	1617-1716	Mirny	150-480	3.3	3.79
2	23	0033-0109	Mirny	100-175	3.1	0.30
3	23	0337-0411	Mirny	70-205	3.0	0.19
4	23	0802-0820	Mirny	95-140	3.8	--
5	23	1142-1150	Mirny	135-170	3.2	0.11
6	23	1428-1441	Mirny	100-160	2.5	0.06
7	24	0305-0319	Mirny	70-120	1.5	--

Cosmic Ray Variations in September and November 1977 at Sverdlovsk

by

V.A. Belyaev, S.F. Nosov and V.F. Zakharchenko
Institute of Geophysics
Urals Scientific Center
Academy of Sciences of the USSR

In this paper observations of cosmic ray neutron intensity during the period September 7-24 and November 21-30, 1977, at Sverdlovsk are reported. The neutron supermonitor "Sverdlovsk" consisting of eighteen BF_3 counters was used. It is located at geographic coordinates N58.34 E56.26 at an altitude of 300 m and has a cut-off rigidity of 2.3 GV. The recorded data were corrected for atmospheric pressure.

Figure 1 shows the per hour data of the neutron intensity observed during the period September 7-24, 1977. During these 15 days two Forbush decreases of cosmic ray intensity were observed: the first one began on the 12th of September and the second one began on the 21st. Sverdlovsk did not record the increase in intensity observed at high latitude stations on the 19th and 24th of September. The daytime variations, however, on the 24th of September attract attention because the neutron intensity increased about 5% during 1 hour and then slowly decreased. Figure 2 shows this increase and subsequent decay at 5-min resolution.

On the 22nd of November 1977, the cosmic ray increase shown in Figure 3 was recorded by the Sverdlovsk station. This ground level event started at 1025 UT ± 5 min and in 15 min reached its maximum of 8.3% above the background counting rate in 15-min intervals. Figure 4 shows hourly intensities of the neutron monitor data in the period 1 day before to 8 days following the November 22 cosmic ray increase.

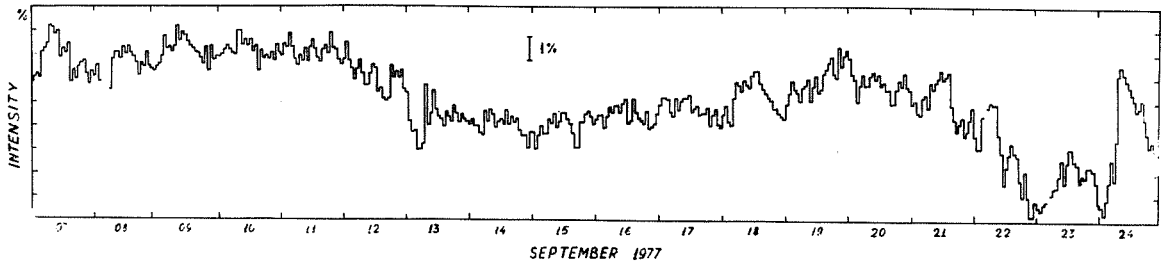

Fig. 1. Sverdlovsk cosmic ray neutron intensity for the period September 7-24, 1977. Forbush decrease began on the 12th and 21st.

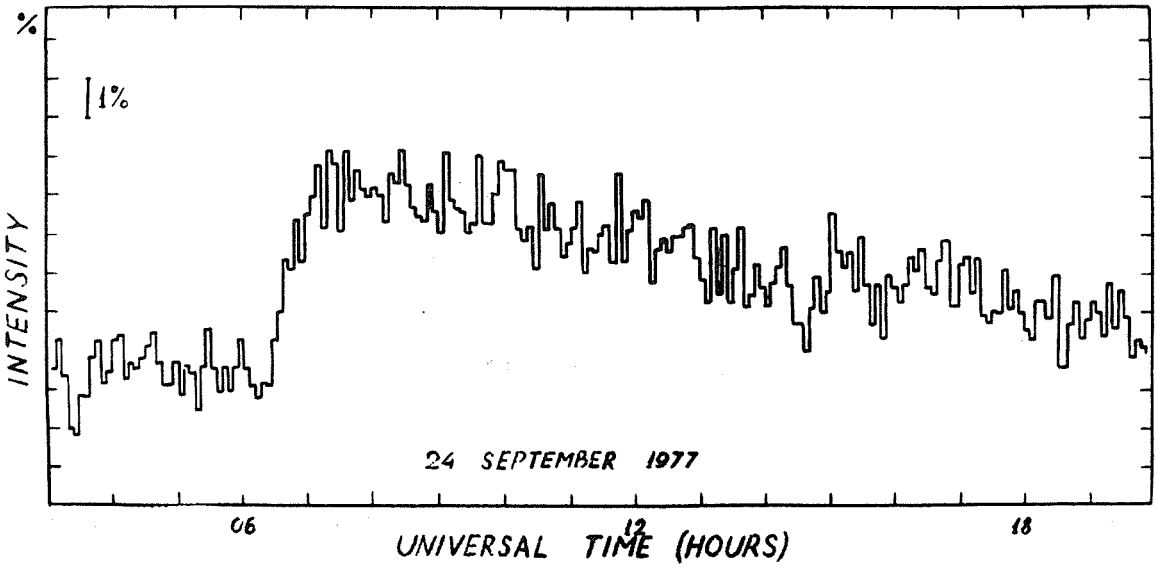

Fig. 2. Sverdlovsk cosmic ray neutron intensity in 5-min intervals on the 24th of September 1977.

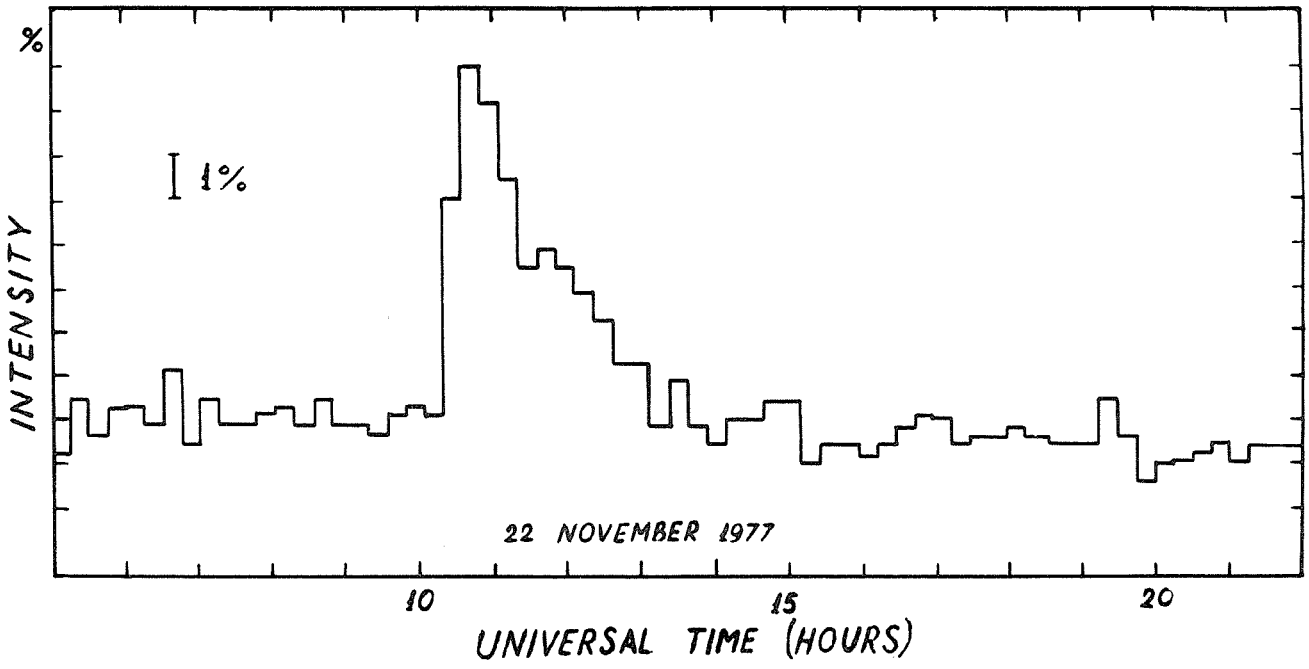

Fig. 3. Sverdlovsk cosmic ray neutron intensity in 15-min intervals on the 22nd of November 1977.

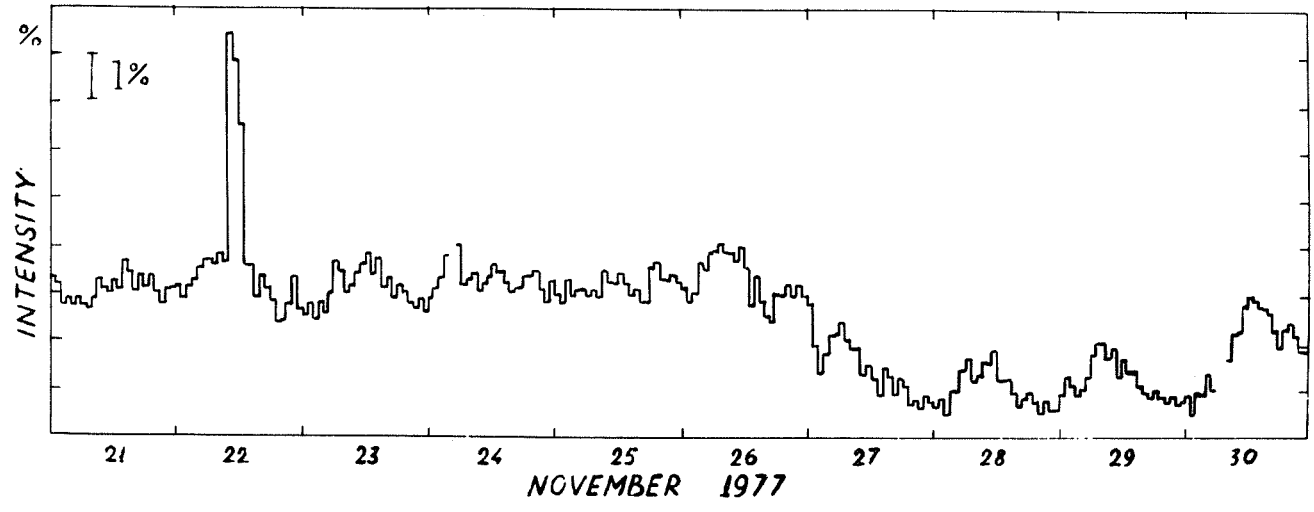

Fig. 4. Sverdlovsk cosmic ray neutron intensity for the period November 21-30, 1977.

Cosmic Ray Variations from September 7 to 25, 1977 According to Neutron Component Data

by

A. V. Belov, Ya. L. Blokh, L. I. Dorman, E. A. Eroshenko,
R. T. Gushchina, O. I. Inozemtseva and N. S. Kaminer
Institute for Terrestrial Magnetism and Radiowave Propagation
The Academy of Sciences of the USSR (IZMIRAN)
P.O. Akademgorodok, Moscow Region 142092, USSR

The variations in ground-level cosmic ray intensity associated with active region McMath 14943 became the first significant manifestation of solar activity in the 21st cycle. The general behavior of the neutron and meson components during September 7-25, 1977, is represented in Figure 1. During this 19-day period, two considerable decreases in cosmic ray intensity occurred--one beginning on September 11 and lasting 6 days (Forbush decrease 1), another beginning on September 21 and lasting 4 days (Forbush decrease 2). The arrival of solar particles at Earth on September 19 and September 24 also produced two increases (designated here as I1 and I2, respectively) in the neutron component intensity. The magnitudes of all these effects may be characterized as average. At the same time, however, the second Forbush decrease late in September 1977 (FD2) was the deepest event recorded between July 1974 and February 1978, while the intensity increase of September 24 was at that time the largest such event since August 1972.

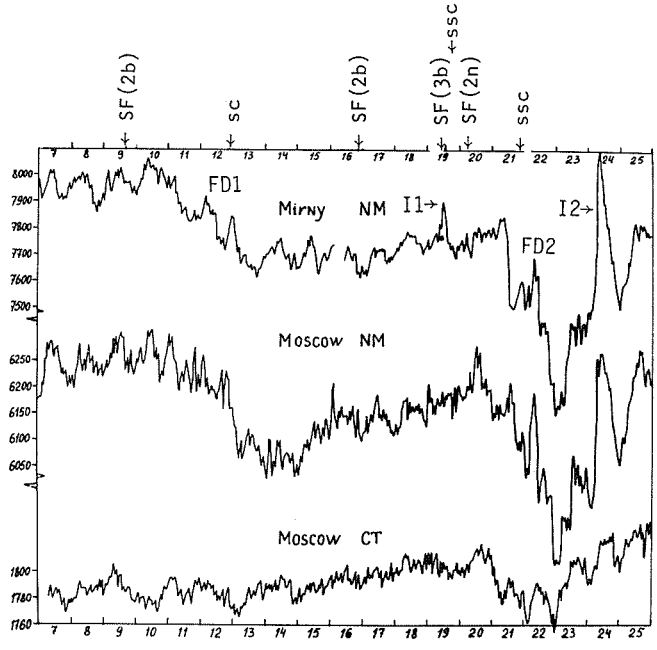

Fig. 1. Variations in the neutron monitor counting rates at Mirny and Moscow stations and in the cubical meson telescope at Moscow from September 7 to 25, 1977. The arrows along the top of the figure indicate the moments of solar flares and commencements of geomagnetic disturbances.

Apart from the data of the neutron monitor and meson telescope at Moscow station, the present work is also based on observations from Apatity, Sverdlovsk, Kiev, Tbilisi, Tashkent, Alma-Ata (806 m above sea level), Alma-Ata (3340 m), Mirny, Novosibirsk, Oulu, Kiel, Durham, Tokyo (Itabashi), Alert and Deep River.

First of all, region 14943 appeared on the solar disk after 5 days (September 3-7) of increased amplitude in the solar-diurnal variation of cosmic ray counting rates. By using the variational coefficients of McCracken et al. [1965] and Shea et al. [1968] for the diurnal wave in the neutron component at various stations, we determined that the ecliptic component of the first harmonic of the cosmic ray intensity anisotropy near Earth had an amplitude of 1.6±1% for particles with a 10-GV rigidity and a propagation direction 70° ± 20° west of the Sun-Earth line. At the same time, the first harmonic amplitude showed an $R^{-\beta}$ dependence on rigidity, where $\beta=0.3\pm0.2$.

A gradual decrease in the intensity began on September 11 and lasted until September 14 at almost all stations. The maximum depth of the decrease at the high-latitude stations was about 4%. FD1 was

not accompanied by a significant increase of anisotropy. We took the difference in the daily average intensities of September 10 and 14 as the decrease depth and studied the latitude dependence of the effect (see Figure 2a). For FD1 the cosmic ray intensity variation followed a power law of the form

$$\Delta I/I = a/R^{\gamma}$$

where $\gamma = 0.7 \pm 0.1$. It is assumed in the calculations here and elsewhere in this paper that the coupling coefficients are functions of rigidity, namely, that

$$W(R) = \alpha K \exp(-\alpha/R^{K}) / R^{K+1},$$

where $K = 0.85$ and $\alpha = 7.6$ [Bednazhevsky, 1973].

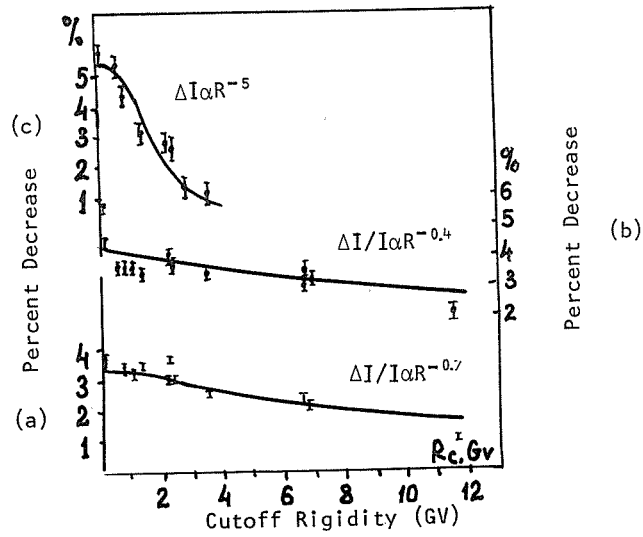

Fig. 2. The value of the Forbush decrease effects during September 1977 as a function of cutoff rigidity for the event beginning on September 11 (FD1) in part (a) and for the event beginning on September 21 (FD2) in part (b). Part (c) shows the cutoff rigidity dependence for the ground level event of September 24, 1977 (I2).

Intensity decrease FD2 was deeper and much more complex than FD1. Figure 3 shows the counting rate variations with respect to the average value of September 20 for various neutron monitors and for the cubic meson telescope at Moscow station. FD2 began at midday on September 22, approximately 2 days after the class 3b flare on September 19. The time of the FD2 commencement differs at various stations. In general, the behavior of the cosmic ray intensity on September 21-22 at the European stations was significantly different from that at the American stations, while the variations in the Northern Hemisphere were dissimilar to those in the Southern Hemisphere. These asymmetries probably indicate the existence of a strong variation in galactic cosmic ray intensity with direction, during the FD2 intensity decrease phase on September 21-22. The moment of the FD2 commencement coincides neither with the ssc detected on September 19 at 1143 UT nor with the one on September 21 at 2044 UT [*SGD*, 1977]. The FD2 depth reached 9% at high-latitude stations.

Figure 2b shows the cutoff rigidity dependence of the average depth of the decrease for September 23 relative to the average counting rate for September 20. The latitude distribution of the effect corresponds approximately to a power-law variation spectrum with exponent $\gamma = 0.4 \pm 0.1$ and implies a very rigid spectrum for FD2. Moreover, the ratio of the Forbush decreases in the meson and neutron components for FD2 is 0.52 ± 0.04, according to data from Moscow station. On the other hand, FD2 occurred against the background of a strong magnetic storm and, therefore, the true cutoff rigidities may be somewhat different from those used [Shea, 1972].

A large solar-diurnal variation was observed during the FD2 recovery phase on September 23-25. We found from the data of stations with high cutoff rigidities (Tokyo, Tashkent and Tbilisi) that the ecliptic component amplitude (A) was about 1.5-2% on September 23-25 for rigidities of 10-20 GV (at some hours A was probably >2%), while the flux was directed almost precisely to the west ($\phi = 90 \pm 20°$). Such anisotropy is characteristic of Forbush decreases from flares west of the central meridian in which the region of maximum decrease is located west of Earth. Consider, for example, the Forbush effect of August 9, 1972.

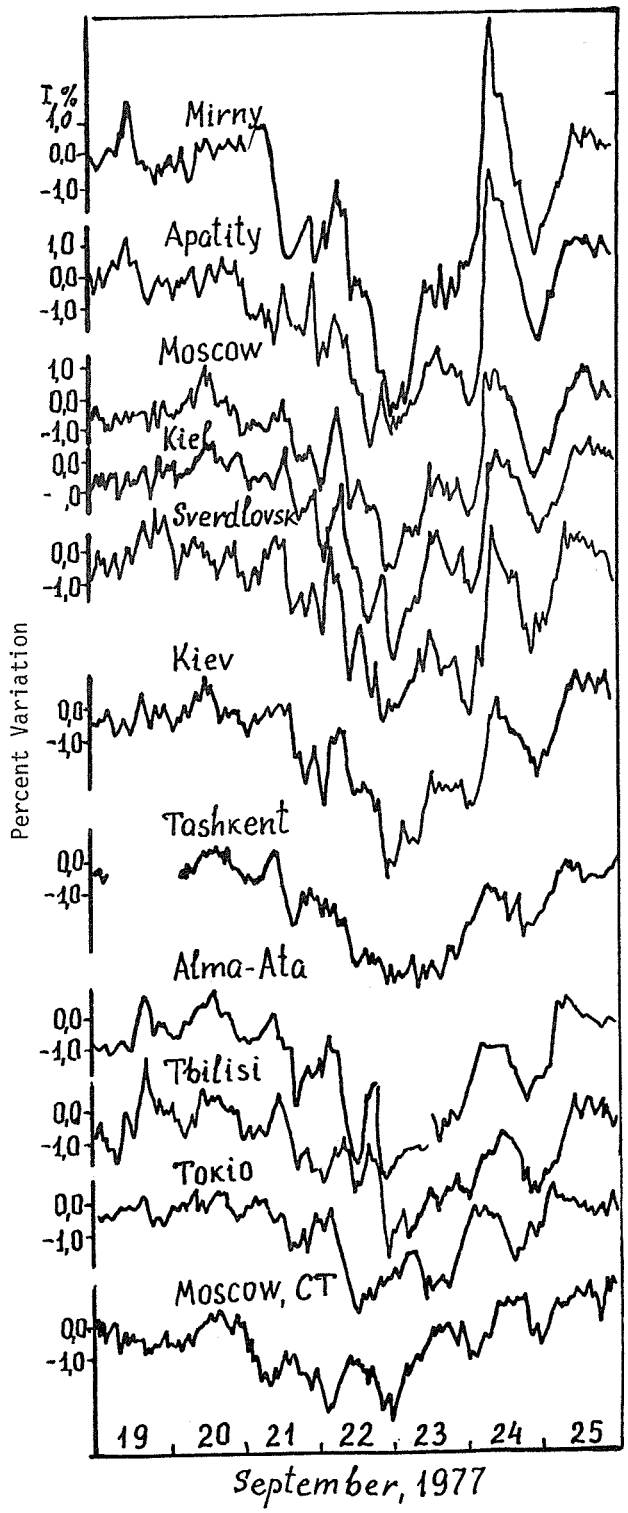

Fig. 3. Variations in the neutron component intensity observed at several stations and in the meson component measured at Moscow station for the period September 19-25, 1977. Units along the y axis denote percent variation in the particle counting rate with respect to the average counting rate observed on September 20, 1977. Profiles for the event FD2 and I2 are shown.

The cosmic ray intensity burst of September 19 was detected at high latitudes only (Mirny, Apatity, Oulu and Durham), and even at these stations the value of the effect was only about 1%. The increase of September 19 was not noted at stations with cutoff rigidities R_c >2 GV. The 5-min data of Mirny station show that solar particles began to arrive at Earth not later than 1105 UT.

The September 24 increase offers more data for analysis. The study of the event, however, is difficult, since it is superposed on significant variations in the intensity of galactic cosmic rays. To distinguish between the effects of galactic and solar cosmic rays during September 23-25, we found the separate time dependences of the recoveries of the isotropic intensity component and of the solar-diurnal variation. After that, we introduced a correction for galactic particle variation in the daily average data for September 24. Figure 4 presents the solar cosmic ray effect obtained in that way from the data of various stations. The value of the increase varied from 1.5% at Kiev to 6% at Mirny.

The cutoff rigidity dependence of the mean value of the increase at 0700-1000 UT is shown in Figure 2c. The latitude dependence of the effect corresponds to a rigidity spectrum of solar particle intensity ΔI proportional to $R^{-\gamma}$, where $\gamma=5\pm0.5$. A more accurate value of the exponent γ can be found by specifying the cutoff rigidities at the stations, since the Dst variation of the Earth's magnetic field was about 60 γ at the moment of the increase on September 24.

Note the extremely slow decrease of intensity in the burst of September 24. We found from the data of Apatity station that the decrease was exponential, namely, exp(-t/to), with a characteristic fall time $t_0=270\pm20$ min. Such a slow decrease is probably associated with the difficulty solar particles have in leaking from the Forbush-decrease zone, where they are confined in an enhanced magnetic field.

Figure 5 presents the pressure-corrected 5-min data of the neutron monitors from Moscow and Mirny and 15-min data of the neutron monitor from Apatity. We found from the presented data and from observations at Kiev and Novosibirsk over short monitoring intervals that the most probable start time of solar particle detection on Earth was 0615±05 UT. If it is agreed that the solar flare in which the detected particles were generated occurred behind the west limb, and that the radio burst commencement at 0550 UT [*SD*, 1977] represents the start time of the flare, then the beginning of the ground level event was delayed relative to the solar flare onset by 20-30 min and relative to the flare's maximum by 90-110 min.

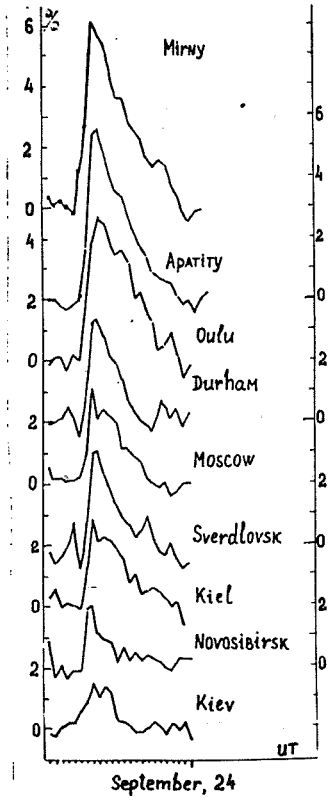

Fig. 4. Intensity increase of September 24, 1977 at various stations. The data are corrected for variations of galactic cosmic rays. Units along the y axis denote present variation in the particle counting rate. Profiles for event I2 are shown.

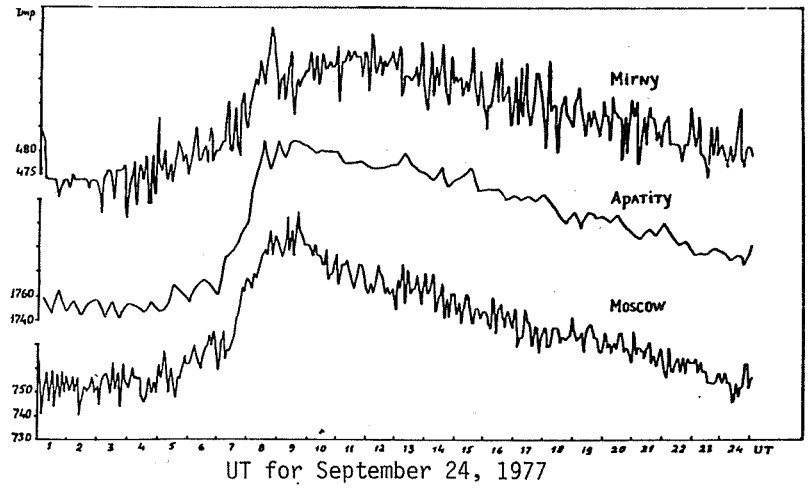

Fig. 5. Variations in the neutron component counting rate on September 24, 1977 according to 5-min data from Mirny and Moscow stations and 15-min data from Apatity. Note the extremely slow decrease in intensity.

REFERENCES

BEDNAZHEVSKY, V.M. 1973 Studies of Cosmic Rays Onboard Research Ship "Academik Kurchatov," thesis (Institute of Nuclear Physics, Moscow State University, Moscow).

McCRACKEN, K.G., V.R. RAO, M.A. SHEA and D.F. SMART 1965 *Cosmic Ray Tables--Asymptotic Directions, Variational Coefficients and Cut-Off Rigidities, IQSY Instruction Manual No. 10* (Report No. NASA-CR-75779, Southwest Center for Advanced Studies, Dallas, Texas).

SHEA, M.A. 1972 *Ground-Based Cosmic-Ray Instrumentation Catalog* (Air Force Cambridge Research Laboratories, L.G. Hanscom Field, Bedford, Massachusetts).

SHEA, M.A., D.F. SMART, K.G. McCRACKEN and V.R. RAO 1968 *Supplement to IQSY Instruction Manual No. 10, Cosmic Ray Tables: Asymptotic Directions, Variational Coefficients and Cutoff Rigidities* (Special Report No. 71, Air Force Cambridge Research Laboratories, L.G. Hanscom Field, Bedford, Massachusetts).

SD 1977 *Solar Data*, No. 9, September 1977 (Nauka, Leningrad). In Russian

SGD 1977 *Solar-Geophysical Data*, 399 Part I, 126, November 1977, U.S. Department of Commerce (Boulder, Colorado 80303 U.S.A.)

Cosmic Ray Variations with Energy 1-100 GeV on September 19-26, 1977

by

A.T. Filippov, V.A. Filippov, N.P. Chirkov, G.V. Skripin, A.N. Prikhod'ko and A.M. Novikov
Institute of Cosmophysical Research and Aeronomy, Yakutsk Branch
Siberian Department of the USSR Academy of Sciences, Yakutsk, USSR

A.V. Sergeev and V.P. Karpov
Siberian Institute of Terrestrial Magnetism, Ionosphere and Radio Wave Propagation
Siberian Department of the USSR Academy of Sciences, Irkutsk, USSR

V.L. Yanchukovsky
Institute of Geology and Geophysics
Siberian Department of the USSR Academy of Sciences, Novosibirsk, USSR

T.T. Sokolova
Northeast Complex Research Institute
Far East Scientific Center of the USSR Academy of Sciences, Magadan, USSR

Introduction

During Sept. 15-21, 1977, a large active region designated McMath 14943 [*SGD*, 1977a] passed across the western half of the Sun's visible disk. Some intense chromospheric flares were observed in this active region--ones generating high-energy protons and shock waves. The shock fronts were responsible for the magnetospheric storms and Forbush decreases in galactic cosmic rays (c.r.) that were observed during this period. Moreover, on Sept. 24, 1977, the Siberian neutron supermonitors registered a c.r. flare with E>1 GeV. This paper presents a short analysis of the c.r. temporal variations at 1-100 GeV energies and uses data obtained by the Siberian neutron supermonitors network and the complex of underground meson telescopes at Yakutsk.

Observations

Those chromospheric flares of importance 1 or greater observed during Sept. 15-21, 1977 are presented in the upper half of Table 1. Some were followed by protons with energies of more than 10 MeV [*SGD*, 1977b]. Geomagnetic storm sudden commencements and proton flux increases, ΔI, for different ranges of particle energy are also given in the upper half of this table. The lower half of Table 1 includes all flares observed on Sept. 24.

Table 1. Significant Flare Activity and Inactivity During Sept. 15-24, 1977

Sept. Date	Start (UT)	End (UT)	Position	Imp.	SSC Date/Time (UT)	ΔI (MeV)
16	<2140	0215	N07 W21	2b	19/1140	E>40
18	0019	>0054	N07 W33	1b		
19	0955	1125	N05 W57	3b	21/2045	E>30
20	0605	0650	N08 W60	1b		
24	<0446	0508	S20 E61	Sf	26/0732	E>30
24	1100	1100	N15 E90	Sf		$E>10^3$
24	1943	1950	S18 E69	Sf		

Figure 1 shows temporal variations in the hourly averages of c.r. intensity recorded by the Siberian network of supermonitors and at four underground depths at Yakutsk. N.P. Chirkov et al. and V.A. Filippov et al. [1973] have described the energy characteristics of this apparatus elsewhere. Figure 1 contains several Forbush decreases of galactic cosmic rays and two c.r. intensity increases--one on Sept. 22 and another on the 24th. The characteristics of these events are given below.

Sept. 19 event. This c.r. intensity decrease was observed up to energies of about 5 GeV (see Figure 1), i.e., the meson telescope registered the decrease at 0 mwe. The latitudinal dependence of the decrease amplitude is described by $R^{-\gamma}$, where R is the geomagnetic cutoff rigidity and γ is a spectral parameter of value 0.37.

Sept. 21 event. As is seen from Figure 1, a c.r. Forbush decrease up to energies ~ 15 GeV is clearly observed. Preliminary analysis shows that, in this case, γ is ~ 0.54 in the energy range 2-15 GeV.

Sept. 22 event. This event was the largest Forbush decrease registered by neutron supermonitors during this period. At Tixie Bay the c.r. intensity decreased ~ 6%. Here the exponent γ in the expression for the latitudinal dependence of the c.r. decrease equaled ~ 0.6 over the energy range 2 to 80 GeV.

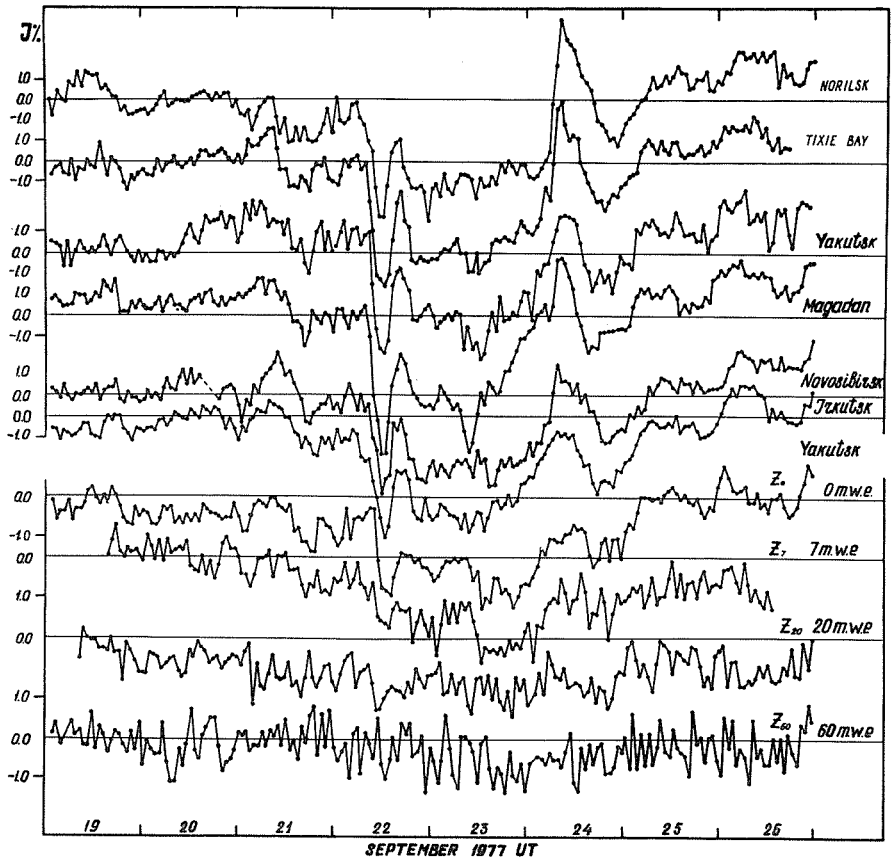

Fig. 1. The c.r. intensity variations on September 19-26, 1977, as observed by the Siberian network of neutron supermonitors and by the underground complex of meson telescopes at Yakutsk.

The c.r. intensity increase on Sept. 22. Here an unusual intensity increase occurred, up to energies of ~ 35 GeV, during the deep Forbush decrease minimum recorded on the 22nd. From Figure 1 it is seen that the underground meson telescope registered an amplitude increase of ~ 0.6% at 20 mwe. The magnitude of γ was found to be 0.2 in the energy range 1-3 GeV, 1.5 in the energy range 3-7 GeV, and 0.5 in the range 7-35 GeV. During this time no energetic chromospheric flares were observed.

The c.r. intensity increase on Sept. 24. Note the latitudinal dependence in the response of the neutron supermonitor, shown in Figure 1. The exponent γ in the latitudinal dependence of the c.r. flare amplitude was 0.9 between 1 and 2.5 GeV and 3.9 in the energy range 2.5-4 GeV.

Figure 2 presents 5-min data recorded by the Tixie Bay neutron supermonitor on Sept. 24. The rapid increase to the intensity maximum (~ 40 min) and the slow decay to the pre-flare c.r. level indicate that this event is of solar origin.

Discussion

As is seen from Table 1, some intense chromospheric flares with generation of high-energy protons erupted as active region McMath 14943 crossed the western half of the visible solar disk. The Forbush decrease in galactic cosmic rays on Sept. 19, 1977, was probably caused by the flare that began at 2140 UT on the 16th; the c.r. intensity decrease on the 21st undoubtedly resulted from the shock wave generated by the importance 1b flare that occurred on Sept. 18 at 0019 UT; and the third and largest Forbush decrease, which began on Sept. 22, was most probably caused by the shock wave, associated with the 3b flare of the 19th, "sweeping" galactic cosmic rays from the inner heliosphere.

Although the nature of the c.r. intensity increase on Sept, 22 requires additional analysis, the c.r. flare on the 24th displayed those characteristics that imply a solar origin. The anisotropic diffusion model of Burlaga [1967] was applied to the Tixie Bay data (see Figure 2) to determine the flare's coordinates. As is seen from Figure 3, the beginning of the particle injection t_0 was 0520 UT. Taking into account that the $\Sigma Kp = 21$ on Sept. 24 [*SGD*, 1977c], we computed the flare longitudinal coordinate Θ_f to be approximately 140° W. Thus, the source of relativistic particles lay behind the solar limb.

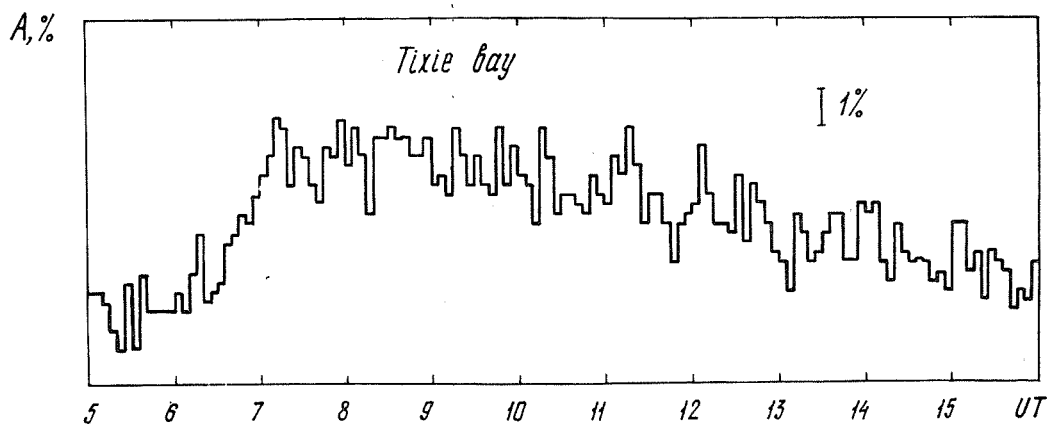

Fig. 2. The c.r. intensity variations on Sept. 24, 1977, generated from 5-min data recorded by the Tixie Bay neutron supermonitor.

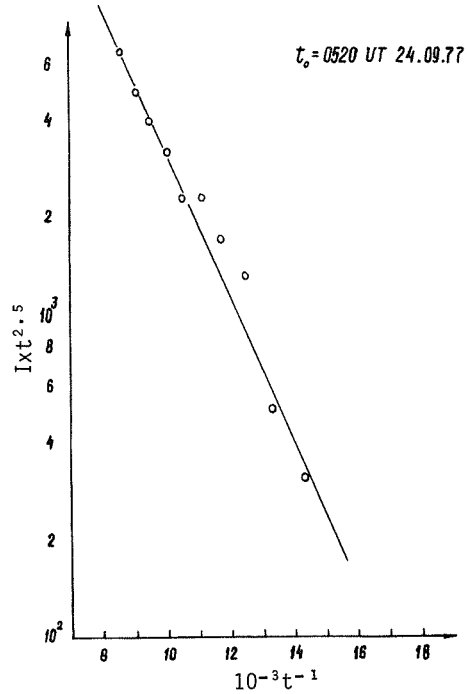

Fig. 3. Results of applying the anisotropic diffusion model of Burlaga [1967] to observations of the Sept. 24, 1977 GLE at Tixie Bay. Particle injection began at 0520 UT.

In fact, as is seen from Table 1, no chromospheric flare that could have been a source of relativistic particles was observed on the visible side of the sun.

Moreover, on Sept. 21 the highly active and proton-producing region McMath 14943 [*SGD*, 1977a] "escaped" behind the west limb of the sun. If this region is assumed to be the source of the c.r. intensity increase on the 24th, then the W140 computed for its central meridian distance emerges as quite reasonable.

Conclusion

During the period investigated, three Forbush decreases and two c.r. intensity increases were recorded. The short analysis above allows us to confirm that the observed decreases were caused by the arrival of flare-generated shock waves at Earth. The c.r. intensity increase on Sept. 24 was probably due to particles accelerated in a flare located behind the west limb.

REFERENCES

BURLAGA, L.F. 1967 Anisotropic Diffusion of Solar Cosmic Rays, *J. Geophysical Res., 72,* 4449-4466.

CHIRKOV, N.P., A.M. NOVIKOV, I.S. SAMSONOV, A.A. UPOLNIKOV, A.A. LUZOV, A.V. SERGEYEV, Yu.A. KURCHENKO, V.N. NIKOLAYEV, V.L. YANCHUKOVSKY and G.G. TODIKOV 1973 Cosmic Ray Variations on August 1-14, 1972 from Data of Neutron Supermonitors in Siberia and Far East, *Collected Data Reports on August 1972 Solar-Terrestrial Events,* H.E. Coffey, Ed. (Report UAG-28 Part II, World Data Center A for Solar-Terrestrial Physics, Boulder, Colorado U.S.A. 80303) pp. 465-468.

FILIPPOV, V.A., A.I. KUZMIN, A.N. PRIKHODKO, I.S. SAMSONOV, G.V. SKRIPIN, G.V. SHAFER and A.A. UPOLNIKOV 1973 Data of the Events of August 1972 from the Cosmic Ray Installation Complex in Yakutsk," *Collected Data Reports on August 1972 Solar-Terrestrial Events,* H.E. Coffey, Ed. (Report UAG-28 Part II, World Data Center A for Solar-Terrestrial Physics, Boulder, Colorado, U.S.A. 80303) pp. 469-474.

SGD 1977a *Solar-Geophysical Data,* 399 Part I, 62-93, November 1977, U.S. Department of Commerce (Boulder, Colorado, U.S.A. 80303).

SGD 1977b *Solar-Geophysical Data,* 398 Part I, 31-32, October 1977, U.S. Department of Commerce (Boulder, Colorado, U.S.A. 80303).

SGD 1977c *Solar-Geophysical Data,* 399 Part I, 120, November 1977, U.S. Department of Commerce (Boulder, Colorado, U.S.A. 80303).

Variations of Cosmic Ray Intensity of Magnetospheric and Interplanetary Origin during Forbush Effect Recorded on September 19-25, 1977 with the Sayan Spectrograph

by

Yu.Ya. Krestyannikov, A.V. Sergeev, V.I. Tergoev, and L.A. Shapovalova
Siberian Institute of Terrestrial Magnetism,
Ionosphere and Radio Wave Propagation
Siberian Department of the USSR Academy of Sciences
Irkutsk, USSR

In this paper the data are given for the Forbush effect in the intensity of cosmic rays recorded with the cosmic ray spectrograph in Irkutsk (R_c = 3.81 GV). The spectrograph consists of the secondary cosmic ray detectors recording neutron and charged components. The data are shown in Figure 1a. These data were corrected for the barometer and temperature effects and are expressed in percent with respect to Sept. 20, 1977. The curves 3 and 4 correspond to the variations of the neutron component intensity for sea level and the altitude 2000 m, while the curves 1 and 2 correspond to the observations for μ-méson hard component and soft ionizing component. Using these data the variations ΔD/D (R) spectrum of the primary cosmic rays and the variations of the geomagnetic cut-off R_c were determined by the spectrographic method [Sergeev, 1973].

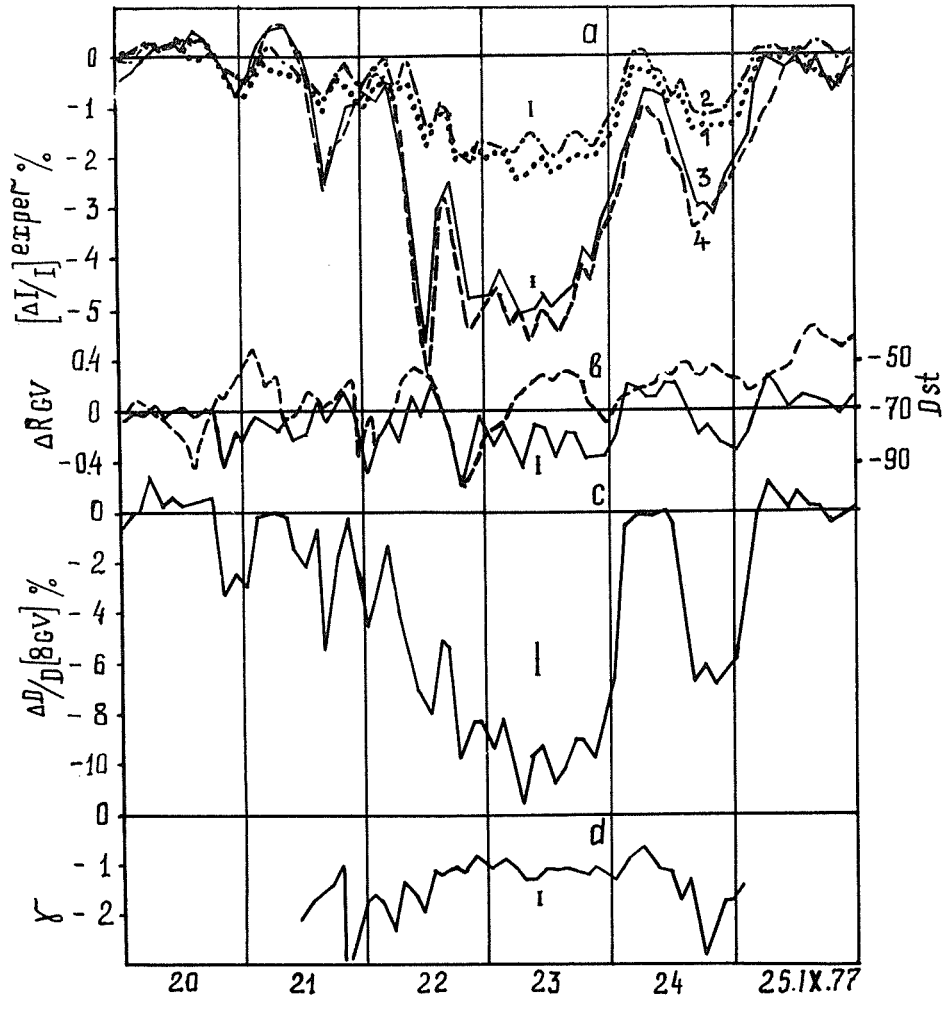

Fig. 1. Cosmic Ray Variations, Irkutsk, September 20-25, 1977.

The analyzed period, Sept. 20-25, 1977, is characterized by the presence of unstable geomagnetic disturbances. This is confirmed by the change of the D_{st}-variation from 50 to 90 γ (the dashed curve in Figure 1b). Similar changes were observed in the behavior of the geomagnetic cut-off R_c (the solid curve in Figure 1b).

The primary cosmic ray intensity of $\Delta D/D$ (8 GV)% are shown in Figure 1c. The rigidity R = 8 GV corresponds to the middle spectral sensitivity of the Sayan spectrograph. The values of $\Delta D/D$ (8 GV)% are given in Table 1 (the error is $\pm$ 0.7%). These data show that the decrease of the cosmic ray intensity had started at 2300 UT on Sept. 20, 1977. The largest magnitude of the modulation was recorded at 0700 UT on Sept. 23, 1977, and equals -11.5%. The recovery of the intensity to its earlier level took place at 0300 UT on Sept. 25, 1977. The recovery of the intensity for primary cosmic rays was recorded on Sept. 24, 1977.

Table 1

UT	Sept. 20	Sept. 21	Sept. 22	Sept. 23	Sept. 24	Sept. 25
0100	-1.1	-3.0	-4.6	-9.7	-6.8	-5.9
0300	0	0.3	-2.7	-8.4	-0.7	-3.0
0500	0.1	0	-1.3	-9.5	-0.2	0
0700	1.5	0	-4.1	-11.5	0	1.4
0900	0.3	0	-2.6	-9.8	-0.2	0.5
1100	0.6	-1.5	-7.2	-9.5	0	0
1300	0.3	-2.3	-8.2	-11.0	-0.8	0.8
1500	0.4	-0.6	-5.2	-10.3	-4.0	0.1
1700	0.5	-5.4	-5.4	-9.3	-6.9	0
1900	0.5	-2.0	-10.1	-9.2	-6.3	-0.6
2100	-3.4	0	-8.5	-9.6	-7.1	-0.5
2300	-2.4	-2.8	-8.4	-8.3	-6.5	0

The behavior of the parameter γ is shown in Figure 1d. This parameter γ characterizes the magnitude dependence of the modulation $\Delta D/D$ (R) of primary cosmic rays with the particle rigidity R if one assumes that $\Delta D/D$ (R) $\approx BR^{-\gamma}$. The average value γ for the whole period of the Forbush effect is equal to -1.4 and changed from -0.7 to -2.4. This is in part caused by the dependence of the cosmic ray modulation on the particle angle in the interplanetary magnetic field [Dvornikov et al., 1978].

REFERENCES

DVORNIKOV, V.M., V.P. KARPOV, and A.V. SERGEEV — 1978 — *Izv. Akad. Nauk USSR, Ser. Geofiz., 42,* No. 7.

SERGEEV, A.V. — 1973 — "The Spectrographic Method for the Study of Cosmic Ray Variations of Magnetospheric and Interplanetary Origin," *Thesis,* Moscow.

Jungfraujoch Neutron Monitor Data for September 7-24 and November 22, 1977

by

E. Born, H. Debrunner, E. Flückiger, and P. Zgraggen
Physikalisches Institut, University of Berne
3012 Berne, Switzerland

Geographic coordinates N46.5 E8.0, a 3550-m altitude, and an effective vertical cutoff rigidity of 4.48 GV characterize the IGY neutron monitor at Jungfraujoch [Shea, 1972]. The recordings made with this instrument have been analyzed for September and November 1977.

The pressure-corrected hourly data for September 7-24, 1977, are listed in Table 1. Figure 1 shows the pressure-corrected intensity for the whole month. Unusual fluctuations occurred after September 12. Uncorrected and corrected 6-min data for September 7-24 are available on request.

Figure 2 shows the ground level event of November 22, 1977. The corresponding pressure-corrected, 6-min data are given in Table 2. The amplitude of the increase amounts to ~3.7%.

Table 1. Pressure-Corrected Hourly Data of the Neutron Monitor at Jungfrau for the Period September 7-24, 1977 (Standard Pressure = 482 mm Hg; Scaling Factor = 100).

Y	M	D	UT= 1	2	3	4	5	6	7	8	9	10	11	12
1977	9	7	5924.9	5939.8	5927.0	5938.0	5951.2	5973.6	6001.2	6012.7	6032.7	6043.3	6026.4	6020.6
1977	9	8	5973.2	5948.8	5979.9	5973.2	5977.0	6013.6	5994.8	6005.4	6001.7-	5991.1	6005.4	5998.6
1977	9	9	5974.0	5973.7	5973.2	5979.2	5976.0	5966.0-	5966.2	5950.7	5977.8	5975.7-	6017.5	5995.5-
1977	9	10	5991.5	5993.8	5997.3	5978.9	6001.9	6028.5	6020.4	5994.7	6000.3	6046.8	6062.0-	6072.5
1977	9	11	6014.9	6017.6	6039.0	6046.0	6051.7	6045.4	5994.0	5984.1	5979.9	5993.7	5981.3	6005.0
1977	9	12	5957.9	5957.3	5992.3	5980.3	5964.1	5943.4	5944.6	5932.4	5919.7	5936.2	5947.1	5935.4
1977	9	13	5935.6	5919.7	5915.4	5872.6	5855.8-	5868.4	5850.9	5851.8	5862.1	5894.9	5885.5	5897.4
1977	9	14	5824.0	5831.0	5821.6	5865.2	5828.7	5799.4	5818.9	5809.9	5831.4	5856.6	5847.9	5842.7
1977	9	15	5805.3	5791.8	5794.6	5815.8	5829.2	5805.9	5827.5	5806.2	5806.2	5833.7	5849.3	5827.5
1977	9	16	5846.9	5830.1	5859.6	5846.1	5820.3	5841.6	5837.1	5844.9	5838.1	5855.9	5869.2	5858.0
1977	9	17	5859.7	5867.3	5873.4	5880.4	5880.5	5891.8	5882.2-	5911.8	5938.2	5940.9	5961.6	5972.1-
1977	9	18	5905.8	5906.4	5900.8	5904.5	5911.3	5926.8	5951.2	5931.4	5921.9	5918.1	5915.8	5958.1
1977	9	19	5931.7	5915.1-	5947.3	5955.7	5943.7	5943.4	5955.1-	5919.1	5897.4	5894.8	5892.2	5924.7
1977	9	20	5979.8	5971.5	5983.2	5954.2	5967.9	5955.3	5980.6	5978.9	5993.1	6043.3	6019.5	6020.6
1977	9	21	5962.8-	5921.9-	5931.1-	5962.6-	5964.2-	5947.0-	5963.6	5994.5	5961.0-	5973.5-	5984.5-	5993.4
1977	9	22	5818.7	5781.6	5786.1	5794.0	5777.9	5888.9	5867.7	5877.9	5883.8	5868.1	5854.2	5816.0
1977	9	23	5619.3	5617.2	5635.4	5676.2	5679.3	5666.6	5713.9	5692.6	5670.1	5647.5	5690.8	5761.2
1977	9	24	5741.1	5723.6	5710.5	5722.4	5767.9	5760.4	5816.9	5886.7	5880.6	5898.2	5921.1	5944.0

Y	M	D	UT=13	14	15	16	17	18	19	20	21	22	23	24
1977	9	7	6029.0	6006.5	6007.9	6004.5	6009.5	5976.3-	5993.7	5986.6	5962.9	5981.0	5962.4	5967.9
1977	9	8	5997.6	6009.4	6006.0	6008.5	5988.8	6006.4	5996.1	5973.0	5978.8	5985.8	5999.6	5985.7
1977	9	9	6043.5-	6078.7-	6099.9-	6036.2-	6002.3-	6031.1-	6000.5	5985.8-	5984.7	5982.3	5965.0	5977.6
1977	9	10	6098.3	6069.1-	6093.6-	6044.3-	6025.5	5995.7-	5984.6	5981.7	5991.0	5942.2	5976.6	5986.3
1977	9	11	5989.4	5989.4	6010.8	5990.4	6032.2	6015.4	5976.6	5994.4	6005.2	5969.0	5973.9	5966.9
1977	9	12	5943.1	5922.2	5929.6	5939.5	5944.5	5929.0	5931.4	5967.2	5984.5	5951.9	5960.4	5963.4
1977	9	13	5860.2	5880.4	5851.5	5872.3	5869.8	5877.9	5903.4	5884.3	5849.3	5857.0	5826.0	5823.1
1977	9	14	5869.9	5847.5	5845.1	5841.9	5837.5	5822.8	5816.5	5819.7	5821.7	5783.8	5803.3	5775.1
1977	9	15	5869.4	5851.4	5867.2	5841.3	5823.3	5830.8	5841.4	5847.5	5828.5	5825.5	5828.0	5846.7
1977	9	16	5872.2	5869.7	5857.4	5870.2	5875.6	5869.8	5860.9	5872.7	5873.3	5860.8	5864.5	5862.6
1977	9	17	5958.6-	5947.0	5938.2	5940.8	5921.1	5936.8	5960.9	5924.2	5926.9	5887.3	5892.1	5891.7
1977	9	18	5987.0	5959.2	5973.8	5921.7	5926.4	5915.6	5929.5	5943.0	5920.8	5897.4	5940.2	5908.4
1977	9	19	5875.4	5915.0	5942.9	6007.4	5993.9	5999.3	5962.9	5959.0	5991.1	5995.3-	5976.5	5995.4-
1977	9	20	6054.9	6072.9	6078.2-	6062.8	6032.7	6009.4	5991.5	5979.8	5984.7	5976.8	5982.7	5988.5-
1977	9	21	5989.2	6013.3	5992.2	5967.5	5914.2	5862.5	5893.2	5887.2	5880.8	5821.6	5870.2	5884.4
1977	9	22	5781.6	5774.3	5791.4	5815.4	5777.0	5803.8-	5734.2-	5756.0	5795.8	5734.5-	5653.7-	5601.1
1977	9	23	5813.2	5810.1	5803.8	5828.7	5801.7	5828.1	5803.0	5784.6	5783.6	5803.2	5790.3	5770.6
1977	9	24	5936.9	5921.5	5946.7	5930.7	5929.6	5920.0	5880.6	5856.8	5858.2	5811.3	5798.2	5788.4

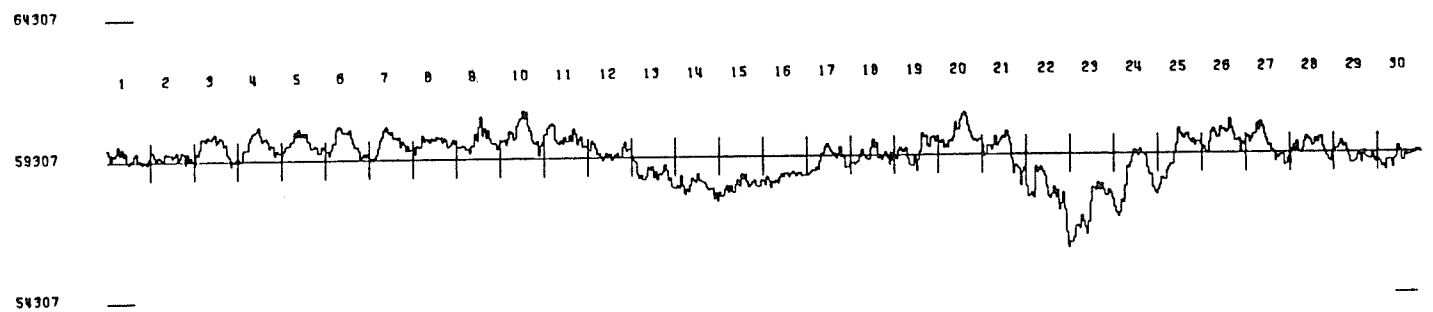

Fig. 1. Scaled pressure-corrected hourly data of the neutron monitor at Jungfraujoch for September 1977 (Standard Pressure = 482 mm Hg; Scaling Factor = 10).

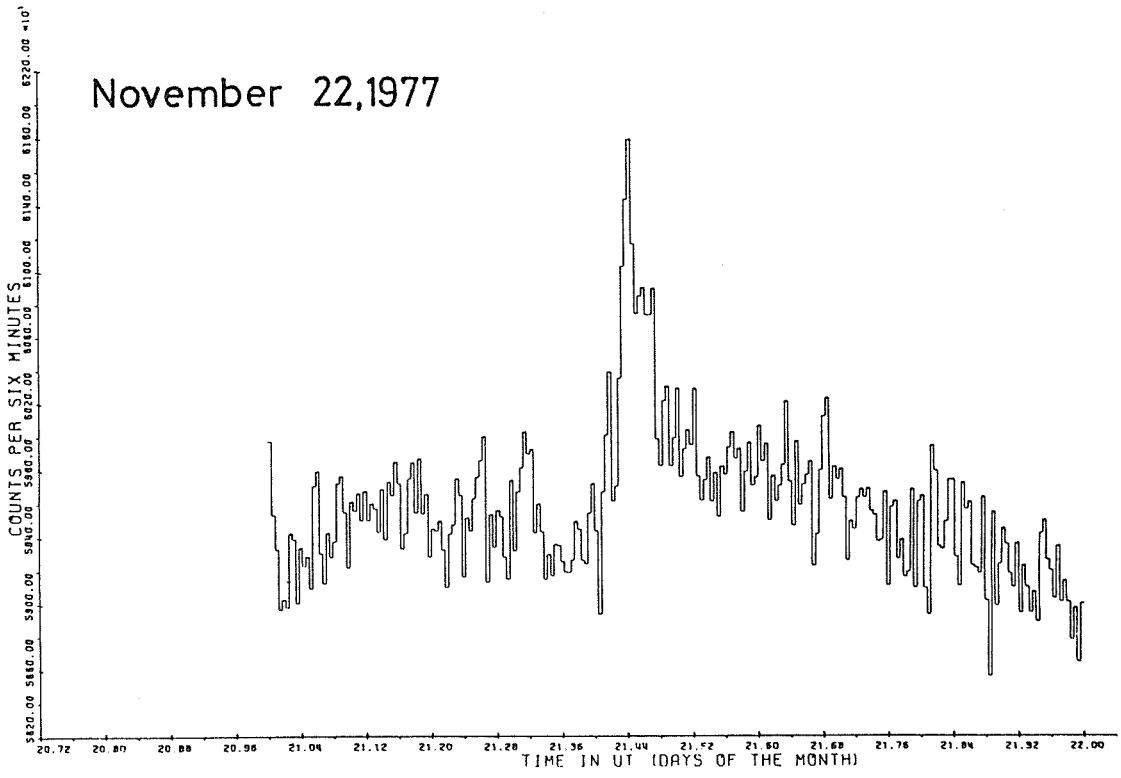

Fig. 2. Pressure-corrected, 6-min data of the neutron monitor at Jungfraujoch for November 22, 1977. Standard pressure = 482 mm Hg; scaling factor = 10. Ground level event shown rose to about 3.7% above background.

Table 2. Pressure-Corrected, 6-min Data of the Neutron Monitor at Jungfraujoch for November 22, 1977 (Standard Pressure = 482 mm Hg).

DAY	HOUR	6	12	18	24	30	36	42	48	54	60	MINUTES
22	0	59972.4	59528.8	59325.8	58961.3	59025.0	58975.1	59422.1	59386.2	59001.8	59337.0	
22	1	59225.6	59294.1	59090.5	59703.9	59793.2	59302.1	59123.1	59426.1	59279.5	59375.0	
22	2	59720.9	59763.6	59545.4	59216.4	59611.1	59554.7	59659.3	59498.1	59671.7	59498.0	
22	3	59597.1	59567.9	59427.5	59685.0	59385.2	59729.1	59646.0	59848.2	59718.6	59330.3	
22	4	59422.7	59749.7	59844.2	59543.3	59867.0	59537.8	59654.1	59282.9	59449.3	59436.7	
22	5	59495.2	59323.7	59097.8	59419.2	59472.2	59748.4	59648.6	59160.7	59515.8	59435.2	
22	6	59630.1	59756.3	59858.0	59999.9	59130.1	59534.7	59340.9	59558.2	59518.8	59280.5	
22	7	59148.7	59737.2	59318.7	59669.7	59814.4	60026.9	59894.8	59923.2	59425.1	59595.8	
22	8	59431.1	59144.4	59297.5	59166.5	59358.3	59350.1	59252.8	59189.3	59187.4	59265.9	
22	9	59493.5	59445.0	59262.1	59240.5	59542.1	59717.9	59434.9	58934.3	59670.0	60010.6	
22	10	60398.4	59610.5	59703.5	60349.5	61027.0	61432.1	61788.1	61159.2	60736.3	60847.6	
22	11	60897.8	60729.0	60730.8	60891.4	59982.4	59823.3	60211.7	60300.0	59821.6	59993.2	
22	12	60286.6	59753.8	59924.3	60038.5	59946.9	60285.3	59760.0	59615.9	59740.6	59874.6	
22	13	59610.3	59782.9	59518.6	59820.7	59770.0	59934.4	60025.0	59866.1	59924.8	59548.2	
22	14	59790.5	59962.8	59703.9	59756.1	60062.4	59850.1	59955.5	59496.3	59763.4	59609.8	
22	15	59706.2	59829.9	60208.2	59726.9	59464.2	59969.3	59508.1	59712.9	59770.5	59850.5	
22	16	59224.7	59418.6	59800.2	60121.0	60226.8	59623.6	59818.7	59742.4	59805.5	59633.1	
22	17	59257.3	59492.2	59445.2	59632.0	59683.5	59631.5	59687.9	59553.2	59527.9	59370.8	
22	18	59380.8	59668.7	59106.0	59578.3	59612.3	59268.6	59392.4	59156.3	59190.6	59682.3	
22	19	59093.4	59611.7	59644.9	59090.0	58930.2	59945.5	59792.1	59342.4	59325.0	59492.9	
22	20	59743.0	59742.4	59281.0	59102.0	59722.8	59565.9	59607.6	59230.4	59215.6	59180.7	
22	21	59636.4	59015.9	58555.7	59546.8	58985.6	59240.0	59451.9	59358.6	59178.9	59095.5	
22	22	59362.5	58941.1	59230.4	59098.5	58943.4	59069.1	58888.6	59424.8	59499.3	59263.3	
22	23	59201.2	59027.1	59347.2	59007.8	59137.1	59007.7	58778.3	58972.0	58643.2	58999.2	

Acknowledgments

This work has been supported by the Swiss National Science Foundation under grant 2.656-0.76.

REFERENCES

SHEA, M.A. 1972 *Ground-Based Cosmic-Ray Instrumentation Catalog*, (AFCRL-72-0411, Air Force Cambridge Research Laboratories, Bedford, Massachusetts).

Predigtstuhl Hourly Super Neutron Monitor Data for September 1977 and November 1977

by

R. Reiter
Institute for Atmospheric Environmental Research
Garmisch-Partenkirchen, G.F.R.

In addition to the usual hourly tabulations submitted to World Data Center A for Solar-Terrestrial Physics, the corrected neutron rates are presented in graphical form. Figure 1 is for September 1977 and Figure 2 is for November 1977. These are the observations at Predigtstuhl (47.70N 12.88E), 1614 m above sea level. The real counts are 100 times the plotted values.

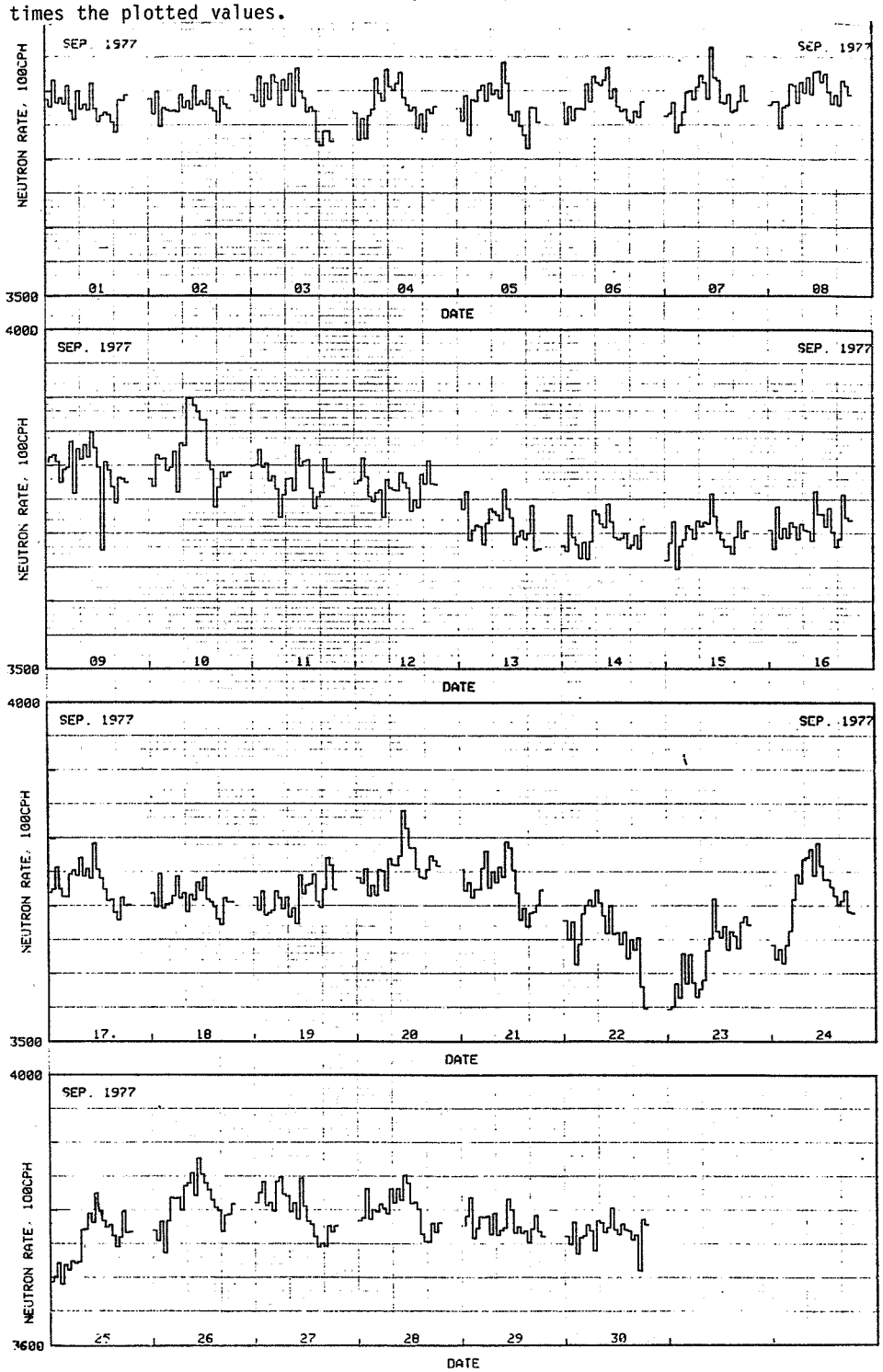

Fig. 1. Super neutron monitor hourly values, Predigtstuhl, September 1977.

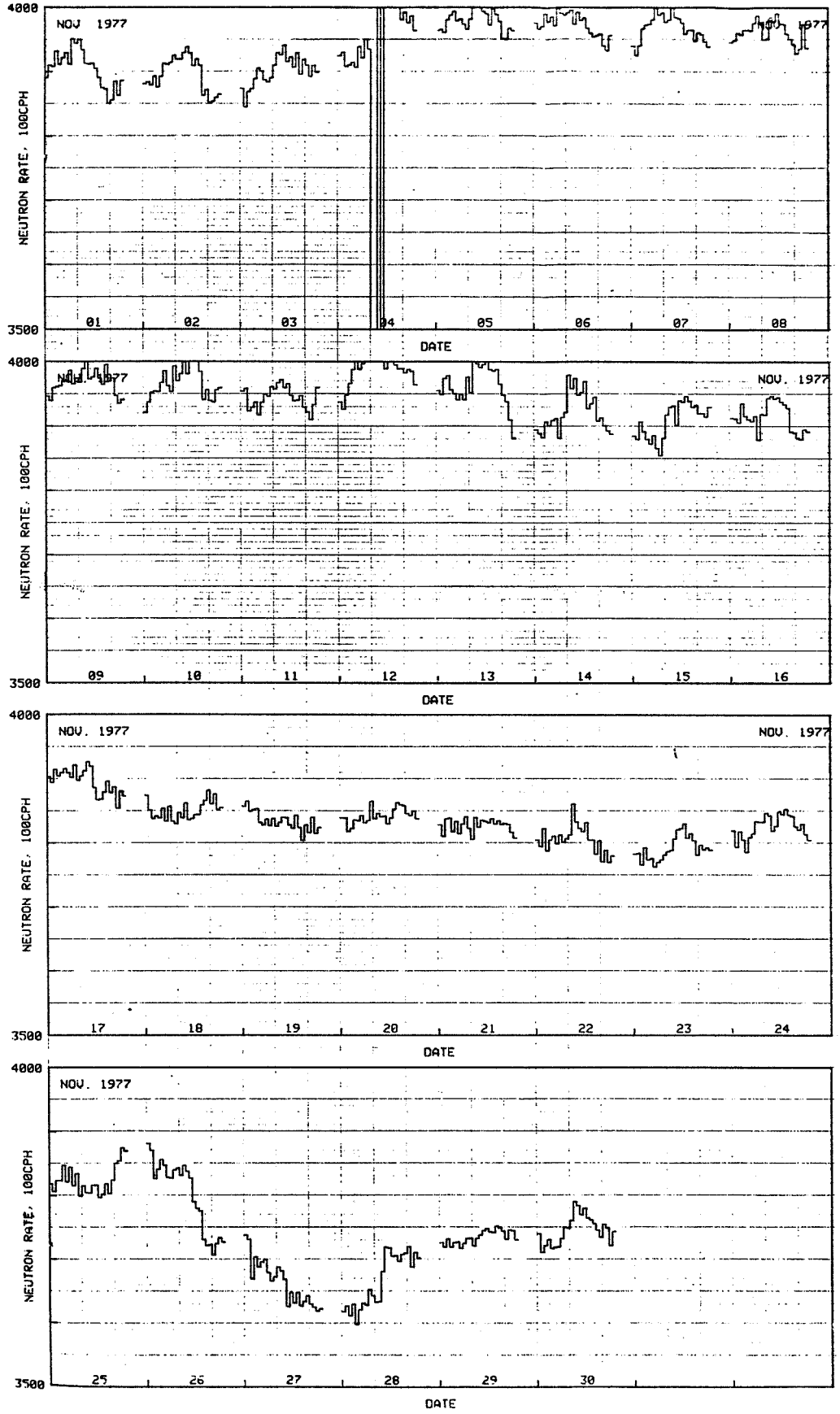

Fig. 2. Super neutron monitor hourly values, Predigtstuhl, November 1977.

Five-Minute Data from the Utrecht Neutron Monitor for September 7-24, 1977 and for November 22, 1977

by

S. Arlman, M. Arena, D.P. Huijsmans and H.F. Jongen
Natuurkundig Laboratorium der Universiteit van Amsterdam
Amsterdam 1018 XE, The Netherlands

The air-pressure-corrected, 5-minute recordings of the Utrecht 18 NM Supermonitor (N52.10 E5.12) are presented in numerical and graphical form for the period September 7-24, 1977, and for November 22, 1977. The reference level for the plots of September 7-24 is the hourly average counting rate of September 1977 reduced to its 5-minute value. The reference level for the plot of November 22 is the hourly average counting rate of the first 5 hours of the same day reduced to its 5-minute value.

UTRECHT THE NETHERLANDS NM64 NEUTRON MONITOR

DATE: 7 9 77 CORRECTED FOR AIRPRESSURE COEFFICIENT: 0.99 PCT PER MM HG

HOURS	05	10	15	20	25	30	35	40	45	50	55	00
0.05 - 1.00	52646	53534	53123	53310	52840	52787	53509	52861	52819	53526	52962	53713
1.05 - 2.00	52834	53270	52973	52658	52953	53292	52956	52802	52944	53463	53590	53187
2.05 - 3.00	53671	53608	53548	53505	53303	52379	53588	53434	53202	53521	53683	52976
3.05 - 4.00	53377	53400	52548	53452	53119	52895	52996	52933	52839	53481	53499	53432
4.05 - 5.00	53015	52821	53739	53243	53569	53375	53080	53362	53216	53967	52845	53157
5.05 - 6.00	52589	52952	53054	53768	53249	53820	53068	53627	53472	53339	53170	53475
6.05 - 7.00	53265	53032	52794	53315	53123	53383	53736	53217	52979	53598	53484	53326
7.05 - 8.00	53531	52763	53454	53405	53168	54181	53023	54082	53346	54638	54093	53855
8.05 - 9.00	54072	54140	53683	54034	54196	53937	53630	53403	53530	53964	53016	53673
9.05 - 10.00	54016	54022	53443	53990	54358	53821	54049	53841	54008	54460	53793	54640
10.05 - 11.00	54899	54454	53773	54468	54098	54304	54533	54432	53272	53922	54239	53884
11.05 - 12.00	53887	53892	53660	54611	53804	53751	54186	54069	53910	54024	53767	53573
12.05 - 13.00	54147	53796	54292	53783	53996	54129	54212	53727	54079	53631	53805	54089
13.05 - 14.00	53583	54070	53491	54125	53894	54028	53211	54199	54160	54835	53897	53962
14.05 - 15.00	53686	53666	53905	53405	53881	53512	53783	54283	54685	54017	53756	53604
15.05 - 16.00	53381	53788	53550	53782	53831	53840	53526	53573	54004	54210	53872	54150
16.05 - 17.00	53877	53827	54344	54173	54065	54060	53437	53488	54215	54223	53930	53518
17.05 - 18.00	53686	53591	53557	53902	53475	53428	53201	53804	53443	53332	54114	53643
18.05 - 19.00	53171	54012	53200	53861	53380	53552	53727	53862	52958	53865	52916	53306
19.05 - 20.00	53982	53316	53456	53935	53094	53770	53548	53380	54102	53316	53877	54304
20.05 - 21.00	53952	53129	53794	53437	54249	53159	53715	53250	53893	53297	53713	53358
21.05 - 22.00	53642	54044	54154	53212	52876	53528	53835	53374	53494	53620	53231	53266
22.05 - 23.00	53275	53585	53305	53328	53010	53374	52993	53355	53935	53177	53125	53400
23.05 - 24.00	53299	53533	53053	53173	52991	53332	53447	53606	53810	53527	53714	53711

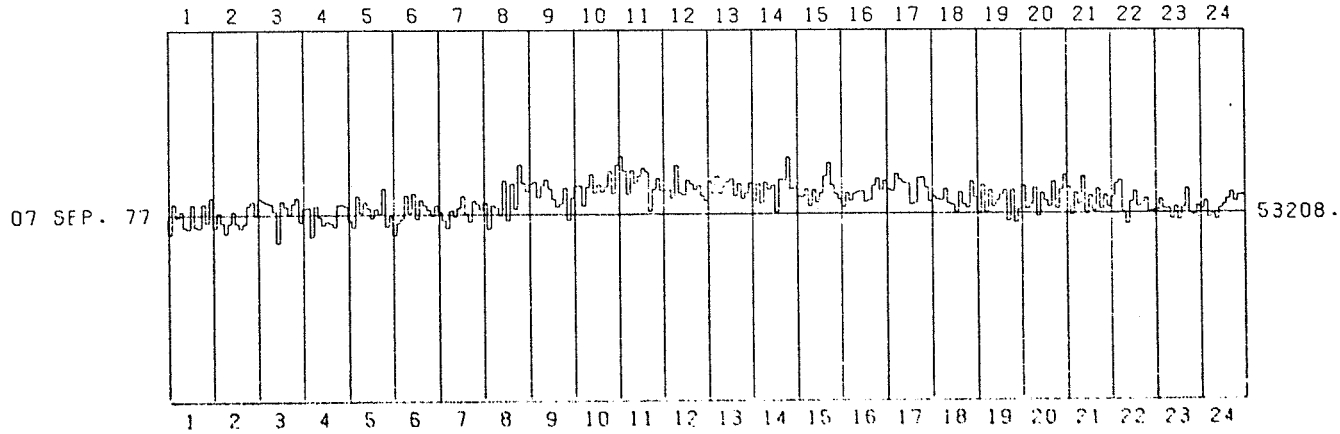

EACH VERTICAL DIVISION REPRESENTS 10 PERCENT DEVIATION

UTRECHT THE NETHERLANDS NM64 NEUTRON MONITOR

DATE: 8 9 77 CORRECTED FOR AIRPRESSURE COEFFICIENT: 0.99 PCT. PER MM HG

HOURS	05	10	15	20	25	30	35	40	45	50	55	00
0.05 - 1.00	53987	54147	53906	54495	53795	53696	53160	54465	53709	53264	53317	53403
1.05 - 2.00	53840	53744	53543	52853	53789	53539	54187	53738	53440	53356	53668	54099
2.05 - 3.00	53972	52861	53372	53627	53257	53378	53242	53054	54199	53357	53668	53309
3.05 - 4.00	53558	53198	53352	53025	52902	53332	52955	53263	53882	53794	53646	53035
4.05 - 5.00	53718	53358	53598	53416	53655	53005	53336	53624	53326	54042	53350	53530
5.05 - 6.00	53408	53546	53643	53574	54761	52945	52991	53871	54001	53928	54175	53157
6.05 - 7.00	54254	53713	53851	53782	53530	53633	53924	53824	53256	53270	54274	53519
7.05 - 8.00	54207	53950	54158	53919	53541	53330	53732	54212	54090	54411	53255	53580
8.05 - 9.00	54206	53742	54043	53503	53973	53475	53193	54596	54035	53444	54281	54192
9.05 - 10.00	53464	53805	53670	54431	53607	54054	53523	53790	53253	53633	53804	54571
10.05 - 11.00	53408	54140	53560	54280	54061	53626	53498	54064	53555	54368	54032	53959
11.05 - 12.00	54179	53834	53838	53626	53958	53462	54869	53732	53933	54367	53632	53844
12.05 - 13.00	54343	53935	54203	53568	53849	54053	54388	53781	53902	54232	53538	54211
13.05 - 14.00	53488	54025	53759	53728	53471	53857	54263	54322	54132	54898	54628	54043
14.05 - 15.00	53856	54046	53983	54044	53825	54519	54315	53940	53838	53770	53887	53925
15.05 - 16.00	53361	54195	54008	54089	54298	54421	54498	53874	53338	54092	53818	53998
16.05 - 17.00	54074	53373	53983	54357	54310	54012	53804	53896	54163	53715	53822	53895
17.05 - 18.00	54150	54006	54562	54353	54089	54112	53897	53739	53539	54046	53573	53842
18.05 - 19.00	54040	53769	53868	53709	53653	53708	54074	53957	53991	54218	54014	53553
19.05 - 20.00	54107	53709	54059	53725	54037	53031	54085	54043	54042	54112	53450	53828
20.05 - 21.00	53979	54531	54607	53390	53996	53874	54273	53886	53844	54015	53900	53691
21.05 - 22.00	53586	54002	53836	53653	53644	54371	53885	54251	53977	54137	54079	54053
22.05 - 23.00	53530	53776	54285	53987	53738	53966	53787	53290	53979	53591	53788	54386
23.05 - 24.00	53909	53959	54033	54322	53800	53823	53788	53493	53773	54276	53902	53542

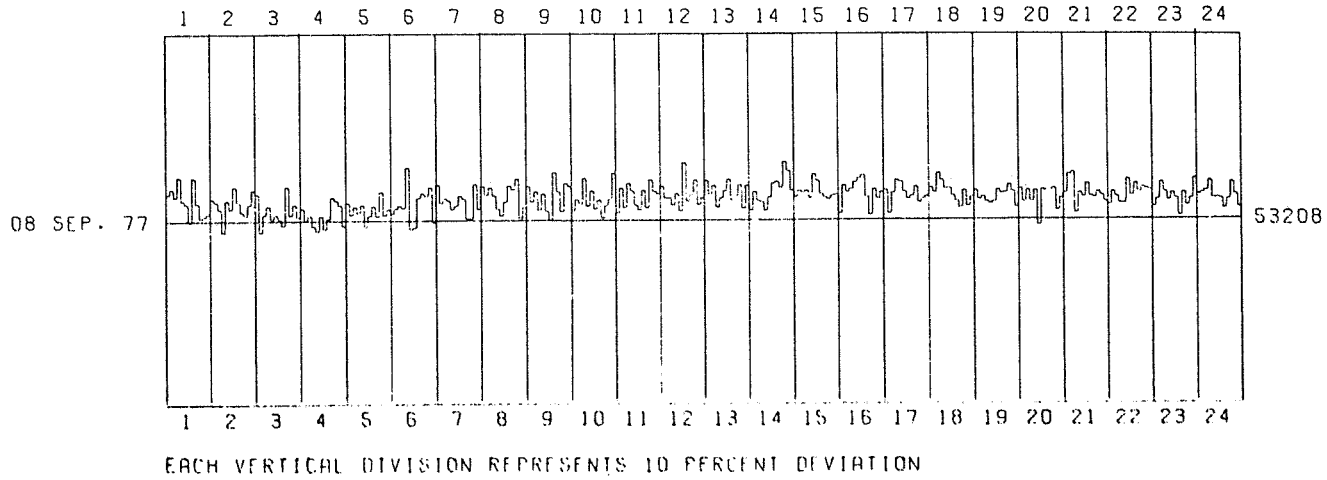

UTRECHT THE NETHERLANDS NM64 NEUTRON MONITOR

DATE: 9 9 77 CORRECTED FOR AIRPRESSURE COEFFICIENT: 0.99 PCT PER MM HG

HOURS	05	10	15	20	25	30	35	40	45	50	55	00
0.05 - 1.00	53355	53993	54007	54200	53870	53611	53601	53925	53282	54380	53731	53506
1.05 - 2.00	54044	53597	54115	54070	53393	54295	54242	54124	54760	54319	53754	54105
2.05 - 3.00	53737	53591	54200	54578	54261	53517	53544	54080	54241	53885	53874	53598
3.05 - 4.00	54656	54087	53894	53765	53876	53343	54067	54108	54076	53920	53750	54107
4.05 - 5.00	54398	54447	53900	54460	53441	54216	54209	54090	54133	53598	53853	54203
5.05 - 6.00	54089	54029	54041	53563	53820	54282	53864	53567	53284	53969	53998	54251
6.05 - 7.00	53520	53791	53757	54160	54279	54410	54086	53899	53839	53574	54153	54125
7.05 - 8.00	53616	54226	53707	53992	53681	54095	54142	54258	54046	53844	54371	53940
8.05 - 9.00	53735	54036	54186	54135	54398	54200	53943	54478	54394	54755	54466	54149
9.05 - 10.00	53731	54233	54508	54283	53697	53426	54104	53512	53948	54335	54146	54675
10.05 - 11.00	54722	54223	54277	54505	53770	53970	53897	54506	54416	54280	54268	54653
11.05 - 12.00	54348	54305	54445	53343	53882	53893	54229	53612	54395	54548	54479	54251
12.05 - 13.00	54497	54975	54088	53864	53956	54630	53600	54190	54696	53791	54545	54375
13.05 - 14.00	54174	54051	54071	54808	54185	54878	54287	54604	54023	55061	54311	54725
14.05 - 15.00	53676	54241	53900	54074	54242	54223	53942	54043	54096	54137	54154	53793
15.05 - 16.00	53908	54376	53845	54157	53976	53714	53562	53758	54134	53908	54072	54900
16.05 - 17.00	53866	54111	54042	53797	54303	53854	54609	54115	54018	54076	53574	54539
17.05 - 18.00	53287	54239	54480	54017	54355	54192	54734	54860	54019	53895	53413	54571
18.05 - 19.00	53644	53834	54077	54092	53589	54211	54181	53777	53954	53654	54387	53900
19.05 - 20.00	53934	54288	54394	54217	54140	53776	54159	54035	53506	53420	54063	54156
20.05 - 21.00	53341	53503	53764	53719	53717	53912	53946	54045	53653	53183	53598	53592
21.05 - 22.00	53825	53901	53592	54017	53534	53616	54360	53795	53888	53533	53828	53723
22.05 - 23.00	53935	53632	53791	53946	53472	54044	54538	53771	52820	53659	53560	53391
23.05 - 24.00	53676	53826	53771	53929	54067	52826	53962	53491	54033	53391	53744	54190

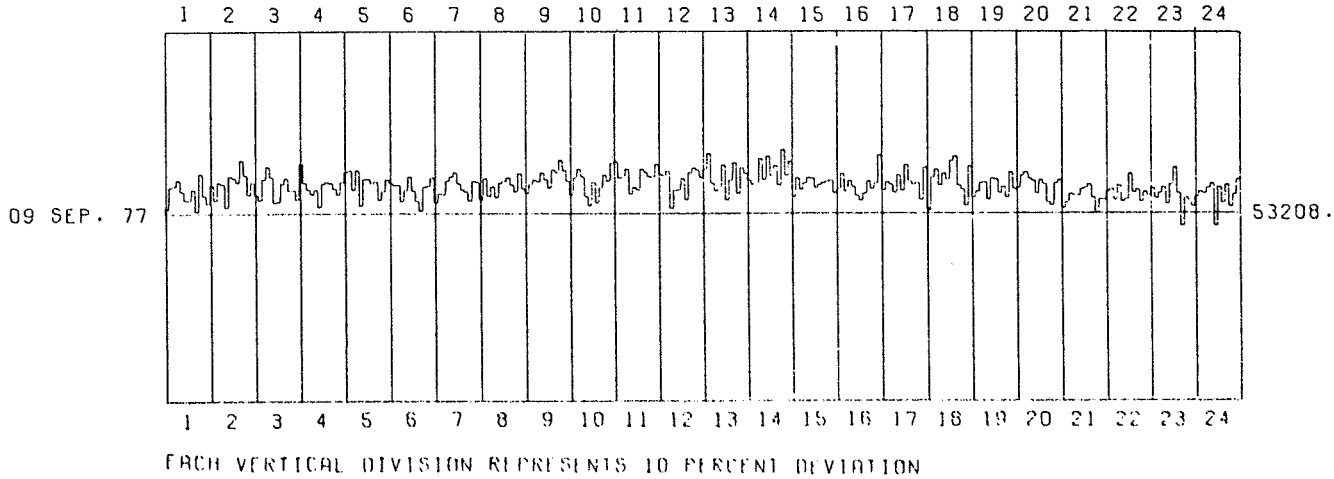

EACH VERTICAL DIVISION REPRESENTS 10 PERCENT DEVIATION

UTRECHT THE NETHERLANDS NM64 NEUTRON MONITOR

DATE: 10 9 77 CORRECTED FOR AIRPRESSURE COEFFICIENT: 0.99 PCT PER MM HG

HOURS	05	10	15	20	25	30	35	40	45	50	55	00
0.05 - 1.00	53638	53351	54028	53394	53619	53381	54372	53812	53608	54166	53266	53224
1.05 - 2.00	53685	53655	53939	52908	54346	53834	54196	54080	53720	53584	53358	53971
2.05 - 3.00	53417	53704	53799	53413	53703	53471	53376	53643	53735	53930	54100	54139
3.05 - 4.00	54016	53532	54532	54114	53646	53880	54324	53812	54351	54069	53550	53803
4.05 - 5.00	53775	53633	54167	54424	54511	54447	54144	54348	54237	54829	54192	54256
5.05 - 6.00	54064	53884	54419	54665	54705	54383	53781	53406	53654	54317	54859	54053
6.05 - 7.00	53851	53645	53958	54306	53716	54798	54268	54234	54286	54864	54435	54036
7.05 - 8.00	53962	53610	53984	54314	53578	54277	53854	53834	53888	54619	53967	54385
8.05 - 9.00	53909	53278	53722	54488	53863	53542	53442	53865	54164	54267	54596	53797
9.05 - 10.00	54356	53773	54406	54242	54499	54119	54159	54017	54151	53826	53780	54484
10.05 - 11.00	54201	54045	54334	54365	53933	54280	54592	54106	53952	54680	54663	54571
11.05 - 12.00	54001	54342	54894	54656	54586	54451	54309	54587	54279	53974	54212	54125
12.05 - 13.00	54548	54470	54047	54167	54692	54421	54153	54329	54621	54442	54580	55059
13.05 - 14.00	54085	54298	53960	54008	55071	53786	54456	54584	53917	53923	53916	54242
14.05 - 15.00	53996	54580	53948	54105	53982	54377	53834	54081	54307	53937	53440	54535
15.05 - 16.00	54128	53978	54447	54257	54104	53526	54274	53846	53737	54436	54085	54042
16.05 - 17.00	52935	53874	54032	53979	53239	54012	53279	53914	53080	54409	54342	53733
17.05 - 18.00	53899	53993	54220	53966	54193	53752	53536	54136	54117	53611	53559	53994
18.05 - 19.00	53730	54090	53350	53296	53936	53754	53373	53443	53977	53339	53233	53735
19.05 - 20.00	53616	53647	53550	53740	52621	53750	53093	53892	53615	53371	53372	53236
20.05 - 21.00	53307	53484	54035	53489	53741	54370	54108	53339	53612	53911	53250	53437
21.05 - 22.00	53431	53792	53636	53111	53508	53080	52775	53462	53169	53239	53746	53671
22.05 - 23.00	52919	53442	54009	54191	52995	53164	52812	53256	53556	53059	53277	54098
23.05 - 24.00	53613	53757	53543	53622	53257	53208	53466	53613	52944	53377	53455	53869

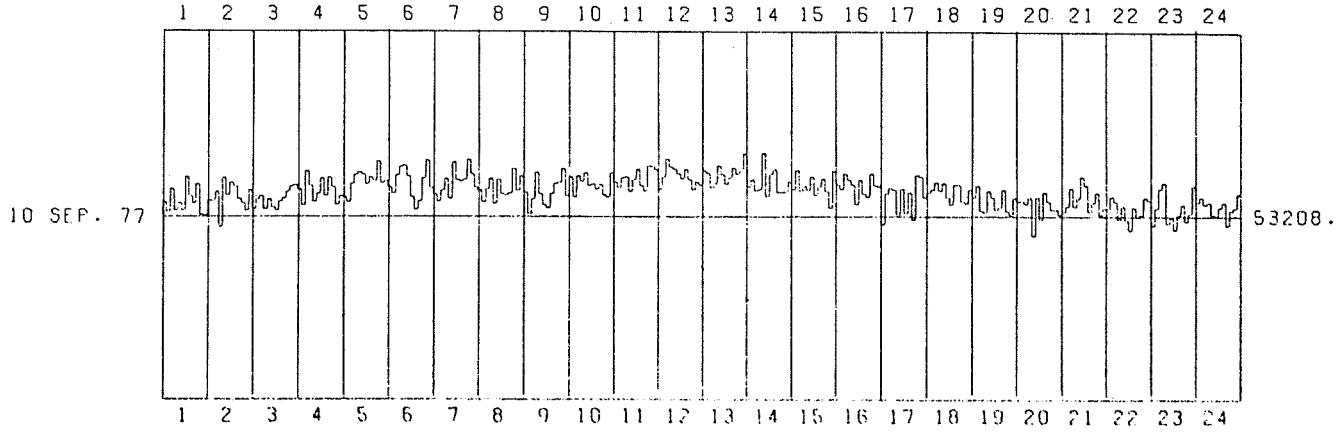

EACH VERTICAL DIVISION REPRESENTS 10 PERCENT DEVIATION

UTRECHT THE NETHERLANDS IMG4 NEUTRON MONITOR

DATE: 11 9 77 CORRECTED FOR AIRPRESSURE COEFFICIENT: 0.99 PCT PER MM HG

HOURS	05	10	15	20	25	30	35	40	45	50	55	00
0.05 - 1.00	53239	53288	53877	53543	53828	53548	54263	53660	54217	54077	53821	53477
1.05 - 2.00	54077	53745	54080	53821	53758	53688	54000	53968	54046	54250	54351	53442
2.05 - 3.00	54334	53984	54460	53775	54171	53863	54119	54008	53923	54067	54387	53958
3.05 - 4.00	53927	54046	54380	53762	54464	54701	54030	53783	54252	54270	54005	54084
4.05 - 5.00	54104	54650	54129	54778	54294	53548	54242	53256	53717	54116	53460	54351
5.05 - 6.00	53704	53836	53678	53915	53411	54026	53950	53973	53535	53818	53679	53577
6.05 - 7.00	53408	53432	53700	53353	54299	53501	53799	53877	54453	53140	54073	53674
7.05 - 8.00	53705	53127	53485	53979	54022	53942	53893	53925	53729	53539	53707	53672
8.05 - 9.00	53273	53975	53246	53592	53914	53492	53840	53431	53645	53272	53069	53381
9.05 - 10.00	53904	53639	53294	53663	54080	53131	53977	53376	53622	53697	53147	53066
10.05 - 11.00	53242	53073	53593	53917	53725	53450	53474	53816	53701	53329	52957	53703
11.05 - 12.00	54472	53890	53330	53160	53023	53664	53298	53191	53582	53924	54001	52467
12.05 - 13.00	53095	53110	53708	53657	53583	54102	53469	53518	54070	53539	53841	53253
13.05 - 14.00	53395	53233	53302	54024	52642	53720	53769	53742	52976	53528	53492	53905
14.05 - 15.00	53594	53469	54096	53481	53250	53527	53055	53573	54082	53658	53685	53355
15.05 - 16.00	53950	53576	53661	53244	53356	53325	54067	53203	54143	53213	53655	54436
16.05 - 17.00	53616	52952	53268	53800	53792	53553	53206	54380	53617	53948	53548	53818
17.05 - 18.00	53656	53584	53868	53232	53810	53304	53835	53941	53918	53683	53050	54218
18.05 - 19.00	53375	53786	53494	53816	53526	53298	52950	52580	52763	53525	53625	53709
19.05 - 20.00	52831	53589	53603	53023	53544	53229	52435	53195	53361	53458	53220	52889
20.05 - 21.00	53384	53554	53111	53266	53236	53352	53703	53258	53374	53408	53701	53182
21.05 - 22.00	53185	53452	53355	53064	53863	53023	53294	53607	53515	53690	53353	53439
22.05 - 23.00	54181	53254	53209	53559	53167	53611	53893	53715	53729	53307	54157	53752
23.05 - 24.00	53869	53670	53854	53561	52994	53847	53448	53456	54046	53323	53667	52850

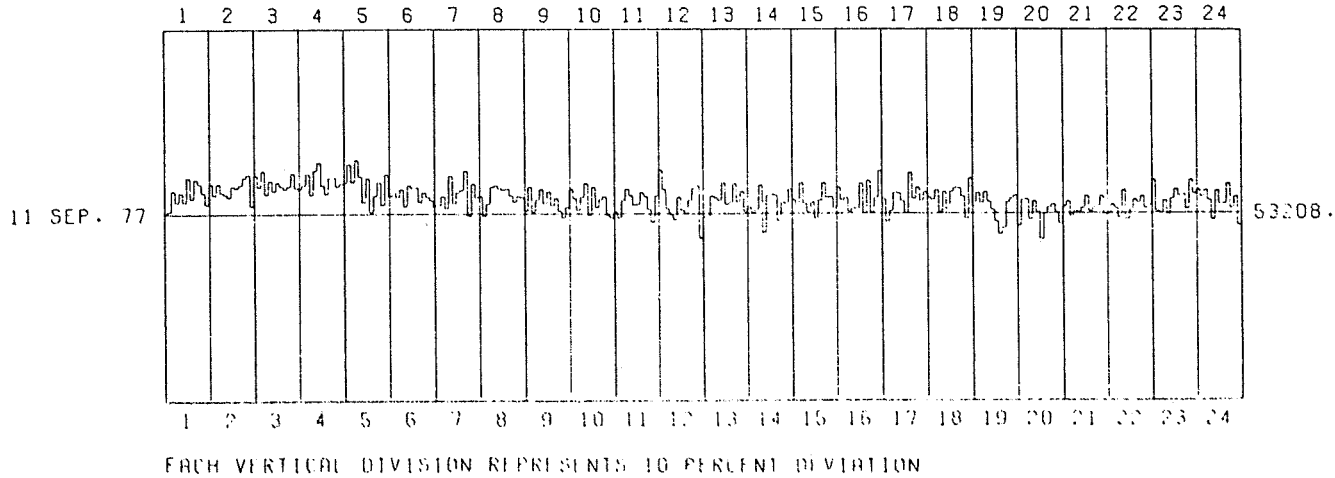

UTRECHT THE NETHERLANDS NM64 NEUTRON MONITOR

DATE: 12 9 77 CORRECTED FOR AIRPRESSURE COEFFICIENT: 0.99 PCT PER MM HG

HOURS	05	10	15	20	25	30	35	40	45	50	55	00
0.05 - 1.00	53349	53509	53215	53823	53635	53591	53895	54124	53411	54070	53133	53107
1.05 - 2.00	53319	53466	53128	54039	53421	53697	53111	53713	53686	53597	53422	53688
2.05 - 3.00	53600	53007	52699	53515	53897	53598	53556	53942	53107	53165	54599	53065
3.05 - 4.00	53890	53571	53379	53463	53144	53773	53745	52993	53322	53576	53513	53744
4.05 - 5.00	53658	53270	53619	53472	52969	53004	53501	52975	53574	53484	53604	53461
5.05 - 6.00	53593	53181	53260	53353	53226	53592	53475	53312	53110	52991	53598	53637
6.05 - 7.00	53599	52889	53436	53607	53323	52921	53652	53605	53085	53068	53468	53236
7.05 - 8.00	53120	53441	52888	53451	53512	53363	53503	52967	53397	53301	53121	52909
8.05 - 9.00	53122	53176	52681	53454	53152	53467	53225	52918	53625	53218	53332	52686
9.05 - 10.00	53812	52629	53299	53372	53404	53468	53164	53032	53315	53620	53188	53266
10.05 - 11.00	52862	53174	53561	53604	53041	53437	53460	52942	53129	54039	53271	53453
11.05 - 12.00	53613	53114	53344	52966	52581	53137	53192	53015	53470	53397	53562	53202
12.05 - 13.00	53893	53513	52929	52976	53368	53175	52634	52952	53389	53036	53243	52789
13.05 - 14.00	52932	52848	53279	53742	52494	53321	53141	52709	52784	53020	53630	53423
14.05 - 15.00	52807	53353	52730	52763	53334	53255	53372	53503	53781	53273	53278	52712
15.05 - 16.00	53362	53089	53068	53489	52407	52980	52711	53050	53115	52781	53160	52926
16.05 - 17.00	53016	53296	52771	52664	53002	53241	52900	52937	53283	52542	52893	52938
17.05 - 18.00	53516	53343	53372	52901	52895	53756	53698	53376	53314	53408	53375	53333
18.05 - 19.00	52971	53534	53514	52857	52871	52782	52944	52780	53071	53456	53589	53404
19.05 - 20.00	53558	52718	53270	52880	52608	53044	53179	52594	52830	53812	53272	53169
20.05 - 21.00	53250	53214	52466	52587	54267	53090	52949	53129	53086	53289	53068	52895
21.05 - 22.00	52922	53248	53107	52785	53588	53440	53437	53152	52901	52841	53699	53279
22.05 - 23.00	52878	53280	53310	53223	53758	52947	53709	53309	53400	53268	53487	53265
23.05 - 24.00	53615	53784	53130	53135	53753	53455	53770	53531	53292	53769	53748	53254

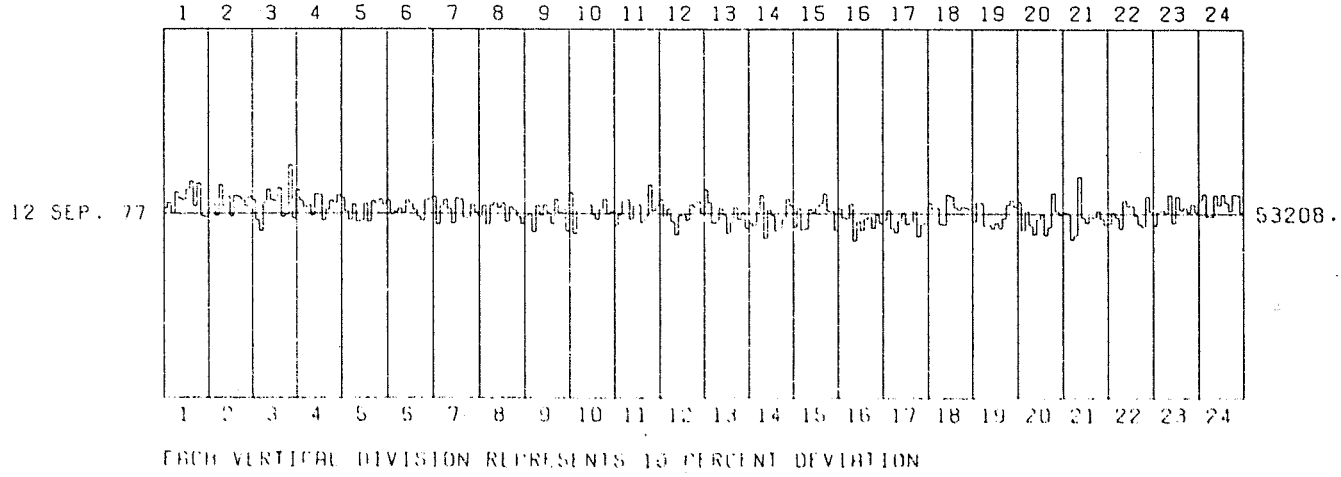

UTRECHT THE NETHERLANDS NM64 NEUTRON MONITOR

DATE: 13 9 77 CORRECTED FOR AIRPRESSURE COEFFICIENT: 0.99 PCT PER MM HG

HOURS	05	10	15	20	25	30	35	40	45	50	55	00
0.05 - 1.00	53613	54037	54072	53797	53184	53988	53789	52622	53736	54257	53698	53298
1.05 - 2.00	52619	53206	52709	52387	53351	52970	52798	52659	52434	52557	52322	52403
2.05 - 3.00	52452	52153	52775	52699	53149	52593	52911	52804	52575	52160	52760	53038
3.05 - 4.00	53020	52834	52610	52515	53053	53324	52699	52552	53049	52467	53279	52401
4.05 - 5.00	52291	52688	52504	51924	53036	52497	52202	52376	52698	52213	52895	52089
5.05 - 6.00	53036	52357	52125	52157	53105	52591	52606	52464	51992	52416	52279	52313
6.05 - 7.00	52784	52246	51862	52736	52502	51930	52390	51956	52915	52316	52865	52780
7.05 - 8.00	51807	51845	52366	52462	52282	52128	52190	52041	52462	52453	52383	51759
8.05 - 9.00	52099	52170	52619	52428	52195	51919	52412	52117	52243	51710	52530	51940
9.05 - 10.00	52561	52635	52877	52639	52939	52334	52634	52709	53148	52618	52871	52418
10.05 - 11.00	52202	52394	52899	52668	52467	52707	52993	52773	52994	53182	52773	53307
11.05 - 12.00	53071	53053	53445	53243	52431	52876	52570	53103	52740	53073	52503	52502
12.05 - 13.00	52639	52599	53051	53067	52636	52622	53226	52467	52579	52641	53029	52737
13.05 - 14.00	52768	52283	52764	52648	52928	52505	52443	52331	52345	53119	52443	53370
14.05 - 15.00	52187	52970	52853	52834	53108	53054	53081	52283	53441	52222	52589	53094
15.05 - 16.00	52914	53596	52598	51974	52898	52818	52770	52895	52452	52737	52533	52932
16.05 - 17.00	52525	52128	52911	52339	53081	52144	52090	52193	52442	52681	52363	52539
17.05 - 18.00	52672	51740	51710	52180	52006	52171	52137	52271	51959	52651	51915	52846
18.05 - 19.00	52486	52256	52143	52404	52404	51887	52284	52526	52445	52834	52431	52927
19.05 - 20.00	52243	52641	52189	51775	52903	52219	52075	52602	52116	52204	52185	53090
20.05 - 21.00	52057	52392	52342	52481	52745	52216	52495	51971	52247	51820	51752	51975
21.05 - 22.00	51912	51514	51585	52543	52505	52367	52300	52582	51807	52324	52979	52793
22.05 - 23.00	53025	52217	52470	52900	51907	52208	52084	51612	51963	52294	52421	52401
23.05 - 24.00	52190	52030	52252	51837	51680	51779	51917	52090	51649	51993	51653	51793

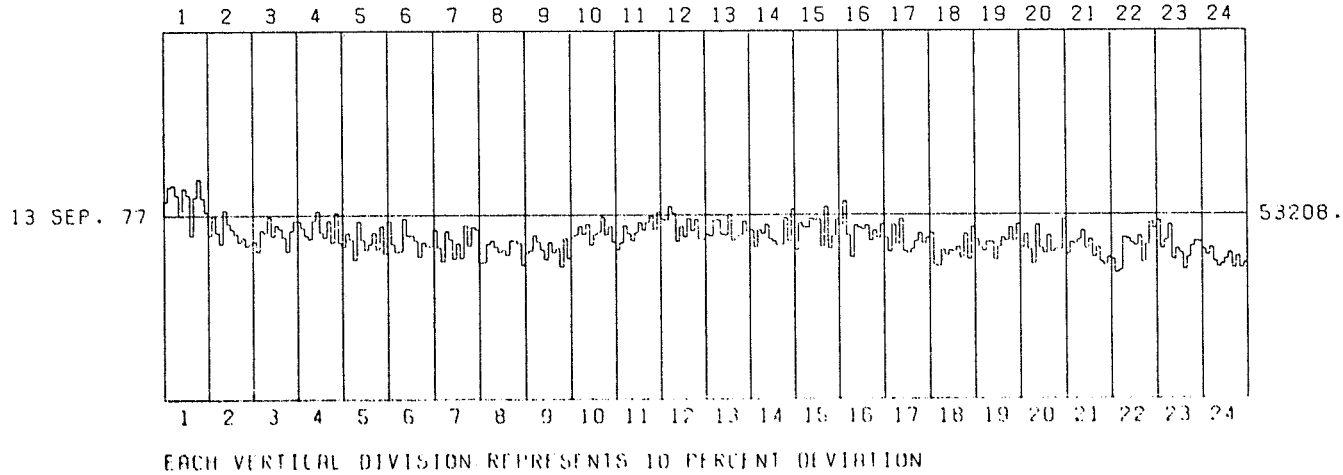

EACH VERTICAL DIVISION REPRESENTS 10 PERCENT DEVIATION

UTRECHT THE NETHERLANDS NM64 NEUTRON MONITOR

DATE: 14 .9 77 CORRECTED FOR AIRPRESSURE COEFFICIENT: 0.99 PCT PER MM HG

HOURS	05	10	15	20	25	30	35	40	45	50	55	00
0.05 - 1.00	51930	52018	52269	51514	52136	51968	52325	51879	52064	51288	52107	52320
1.05 - 2.00	52136	52209	52430	51931	52144	51955	52254	51669	52313	51332	51906	52346
2.05 - 3.00	52307	52324	52236	52387	52523	51880	51773	52186	53081	52542	52123	51961
3.05 - 4.00	51843	52131	52345	52037	52812	52452	51749	52169	52468	52419	52103	52387
4.05 - 5.00	52498	51946	53065	52555	51752	51921	52297	51923	52112	52464	51765	52167
5.05 - 6.00	51301	52279	51970	51991	51657	51980	51632	51231	51465	51758	51288	51821
6.05 - 7.00	51520	51666	51620	51624	51264	52123	51330	52270	52220	51608	52344	51681
7.05 - 8.00	52033	51959	51748	52191	51632	52019	52081	51728	52626	51869	52002	52029
8.05 - 9.00	51921	52189	51686	51957	52867	51412	51530	52021	51987	52053	52351	52152
9.05 - 10.00	52153	52336	52000	52566	52410	51684	52235	52356	51854	52644	52382	52660
10.05 - 11.00	51388	52029	51756	52295	52395	52596	52443	52089	52309	52735	52592	52302
11.05 - 12.00	52427	52295	52667	52177	52068	52025	52501	52435	51971	51904	52641	52308
12.05 - 13.00	51999	52569	52574	52415	52089	52157	52400	53030	51898	51943	51926	52481
13.05 - 14.00	52037	53030	52343	52468	52312	52371	52368	52267	52232	51528	52211	52059
14.05 - 15.00	51975	52363	52649	52999	51830	52526	52488	52847	52096	51808	51713	52090
15.05 - 16.00	52647	51409	52415	52773	52083	52414	52576	52017	52456	51782	51957	51963
16.05 - 17.00	52589	52399	51992	52433	51794	51905	51794	51893	51990	52680	52722	52345
17.05 - 18.00	52365	52503	52424	52233	52293	52359	51916	51742	52161	51949	52013	51908
18.05 - 19.00	52507	52267	52098	51669	52273	51824	52164	52581	51861	51893	52174	51678
19.05 - 20.00	52251	52011	52350	51864	52040	52779	52138	51865	51935	51876	52310	52201
20.05 - 21.00	52126	51786	51733	51453	52009	52490	51788	52367	51997	51938	52137	51965
21.05 - 22.00	52566	51687	52415	51891	52308	52031	51843	51684	52111	52370	52565	51963
22.05 - 23.00	52467	52271	52447	52086	51763	51926	52478	52233	51975	51247	52286	51563
23.05 - 24.00	52383	52224	52578	51103	52495	51657	51169	51710	51473	51844	51086	52348

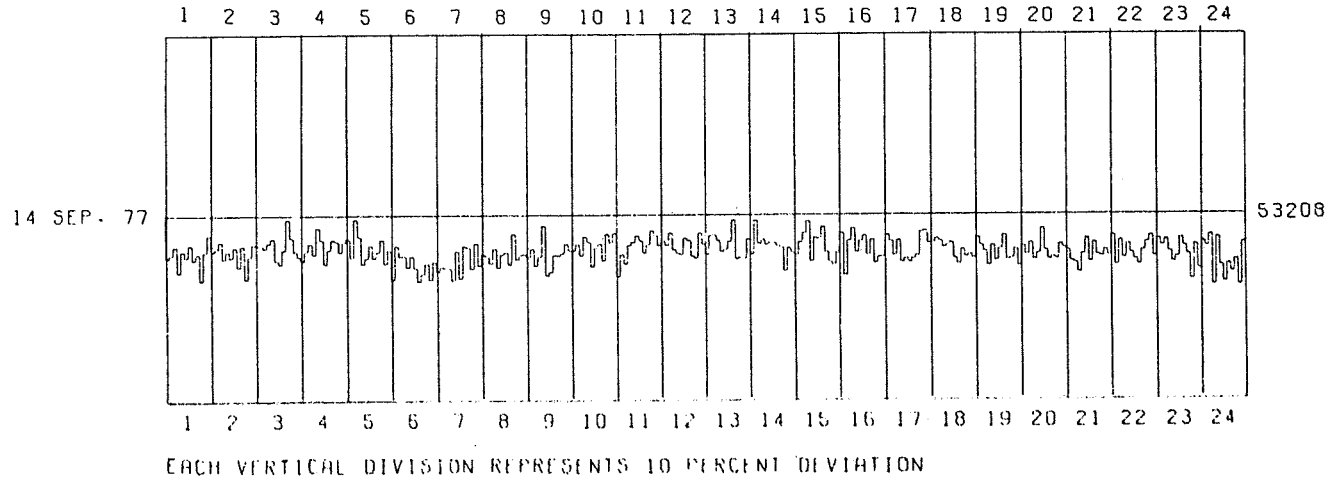

EACH VERTICAL DIVISION REPRESENTS 10 PERCENT DEVIATION

UTRECHT THE NETHERLANDS NM64 NEUTRON MONITOR

DATE: 15 9 77 CORRECTED FOR AIRPRESSURE COEFFICIENT: 0.99 PCT PER MM HG

HOURS	05	10	15	20	25	30	35	40	45	50	55	00
0.05 - 1.00	51701	51785	51375	51816	52026	52064	52326	51523	51323	51987	51705	51764
1.05 - 2.00	51661	51323	51857	52588	51865	51881	51730	51610	51306	51860	52113	51785
2.05 - 3.00	51770	52173	51926	52371	51927	51237	51722	51976	51703	52061	52067	51879
3.05 - 4.00	52059	51988	50990	51779	52074	52501	52010	51906	52038	52035	51963	51396
4.05 - 5.00	52086	52137	51794	52075	51721	51952	51976	51500	51776	51572	52109	51740
5.05 - 6.00	52068	51466	52177	51719	52295	51993	52013	51256	52019	51994	51979	52009
6.05 - 7.00	51987	52608	51911	52037	51818	52073	51716	51724	51924	52105	52329	51922
7.05 - 8.00	51945	51954	52011	52378	51813	51604	51927	51968	51474	52303	52237	51984
8.05 - 9.00	52196	52105	51957	51710	52657	51982	52111	51875	51777	52242	52020	52111
9.05 - 10.00	51860	52060	51778	51950	51838	52163	52004	52649	52167	52242	51573	51979
10.05 - 11.00	52404	52224	51842	52387	52098	52207	52637	52456	52036	51920	52058	52191
11.05 - 12.00	52183	52238	52259	52065	51750	52543	51740	52642	51984	51841	52841	52350
12.05 - 13.00	52165	51611	52044	52009	52197	52096	52205	52345	52842	52835	51837	53062
13.05 - 14.00	52003	52270	52737	52297	52436	52011	52627	52391	52873	52780	52186	52029
14.05 - 15.00	52461	51986	52469	52026	52260	52339	52570	52391	52123	52543	52649	52178
15.05 - 16.00	52612	51859	52283	52720	52617	52574	51845	52178	51694	52432	51992	51680
16.05 - 17.00	51761	51777	52536	52990	52431	52576	52342	51504	52419	52006	52407	52489
17.05 - 18.00	52584	52350	51612	52063	51969	51754	51954	51889	51974	51604	51876	52223
18.05 - 19.00	52331	51685	52403	51647	52679	52273	52017	52358	51877	52727	52056	52576
19.05 - 20.00	51998	52611	52510	52717	51911	52512	52202	51890	52477	52063	52199	52096
20.05 - 21.00	52427	52620	52117	52610	52251	52450	52756	51839	52072	52560	51743	52263
21.05 - 22.00	52482	52336	51959	52479	52700	51565	51844	52946	52143	52905	52293	51989
22.05 - 23.00	52431	52331	52879	52498	52742	52466	52392	51824	52201	52189	52155	52030
23.05 - 24.00	51982	52372	52361	52031	52063	52179	52604	52305	52255	53100	52258	52793

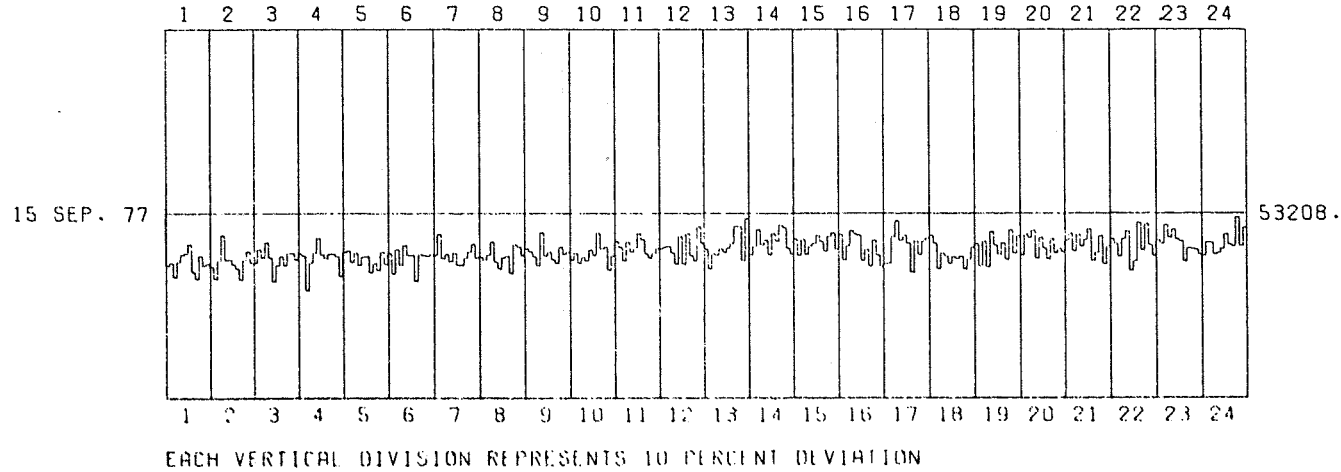

EACH VERTICAL DIVISION REPRESENTS 10 PERCENT DEVIATION

UTRECHT THE NETHERLANDS NM64 NEUTRON MONITOR

DATE: 16 9 77 CORRECTED FOR AIRPRESSURE COEFFICIENT: 0.99 PCT PER MM HG

HOURS	05	10	15	20	25	30	35	40	45	50	55	00
0.05 - 1.00	52330	51991	52808	52321	52712	52508	52129	52984	52863	52893	51961	52692
1.05 - 2.00	52485	52015	53242	52366	53089	52618	52223	52985	52623	52186	53065	52910
2.05 - 3.00	52641	52798	52923	53230	52651	52724	53293	52703	52456	52588	52686	52623
3.05 - 4.00	52397	52059	52925	53061	52456	52578	52191	52372	52508	52988	52424	52346
4.05 - 5.00	51994	52529	52360	52335	52252	52330	52239	52405	52629	52210	53169	52619
5.05 - 6.00	52586	52336	52503	52246	52844	52655	52022	52277	52251	52151	52447	52576
6.05 - 7.00	52218	52405	52970	52645	52800	52574	52381	52712	52674	52449	52682	52414
7.05 - 8.00	52171	51930	52539	53131	52851	52430	52593	51909	52575	52653	51781	52521
8.05 - 9.00	52894	52500	53242	52252	52273	53130	52492	53133	52497	52167	53278	53110
9.05 - 10.00	53308	52724	52566	52862	52777	53010	52728	52603	52709	52584	52365	52667
10.05 - 11.00	52375	53228	52094	52652	52299	52767	52760	52897	53299	52986	52950	52814
11.05 - 12.00	52581	52943	52201	52751	52749	52612	52395	52950	53140	52575	52523	52780
12.05 - 13.00	52668	52810	53534	53199	52501	52853	52688	52632	52935	52277	52779	52346
13.05 - 14.00	52846	52730	52324	52582	52237	52784	53233	52455	52901	52934	52409	52792
14.05 - 15.00	53062	52339	52199	52954	52659	52534	52386	52813	52800	53149	52541	52517
15.05 - 16.00	52125	52560	53186	53034	53027	52654	52785	53012	53281	52570	52643	52533
16.05 - 17.00	53021	52239	53155	52740	53056	52744	51826	52538	52255	52814	53149	52689
17.05 - 18.00	52040	52651	52554	52647	52692	52041	52422	52888	52563	52829	52928	51514
18.05 - 19.00	51893	52888	52868	52824	52750	52188	52582	52417	52881	52391	52932	52395
19.05 - 20.00	52611	52073	52556	52441	52866	52676	52598	52607	53237	52597	52686	53137
20.05 - 21.00	51712	52841	52793	53182	52656	52517	52269	52329	52804	52316	52879	52451
21.05 - 22.00	52753	52174	52943	52750	52694	52582	51785	52058	52680	52809	53315	52919
22.05 - 23.00	52867	53096	52200	51874	52181	52597	52413	52743	52090	51931	52664	52510
23.05 - 24.00	52179	52956	52447	52481	52579	52567	52671	52526	52774	52818	52685	52779

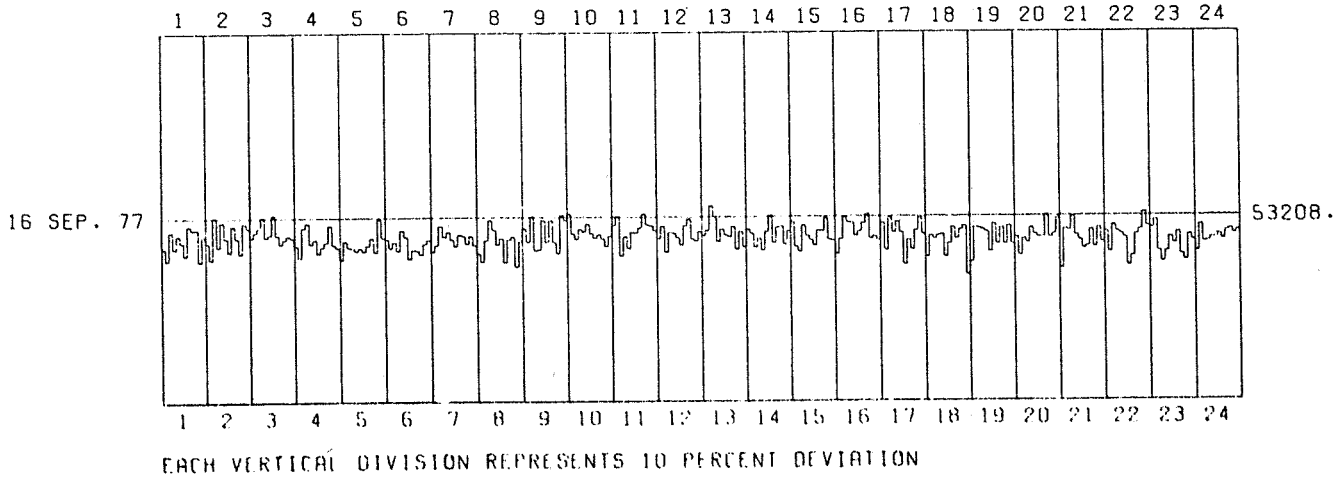

EACH VERTICAL DIVISION REPRESENTS 10 PERCENT DEVIATION

UTRECHT THE NETHERLANDS NM64 NEUTRON MONITOR

DATE: 17 9 77 CORRECTED FOR AIRPRESSURE COEFFICIENT: 0.99 PCT PER MM HG

HOURS	05	10	15	20	25	30	35	40	45	50	55	00
0.05 - 1.00	52700	52415	52956	52368	52640	52347	52225	52773	51807	52755	52301	52812
1.05 - 2.00	52132	52678	52623	52717	52688	52400	53057	52466	52911	52659	51891	52650
2.05 - 3.00	52372	52531	52424	52724	52672	52873	51925	52752	52603	52407	53375	52351
3.05 - 4.00	52176	52609	52757	52656	52628	52423	52908	52492	53189	51891	52864	51935
4.05 - 5.00	53088	52851	53085	52234	52518	52672	52590	52789	53228	52624	52697	52709
5.05 - 6.00	53012	52694	52302	52840	52907	53174	53081	52837	52930	52180	53133	53192
6.05 - 7.00	53281	52311	52506	53070	52412	53010	53306	52553	52925	52411	53362	52832
7.05 - 8.00	52298	53094	52313	52677	52563	52890	52358	52964	53149	53424	52620	52377
8.05 - 9.00	53269	53055	52376	52510	53259	53303	53159	52931	53263	52940	52752	53579
9.05 - 10.00	52946	53205	53386	53032	53202	52993	52669	52582	53254	52624	52575	52677
10.05 - 11.00	53138	53498	52928	53546	53242	53233	53601	53494	52982	52668	53363	52961
11.05 - 12.00	53642	53215	53024	53150	53627	53136	52896	52439	53744	53144	53102	53348
12.05 - 13.00	53456	52591	53449	53456	53572	53414	53223	52721	53133	53674	53474	53185
13.05 - 14.00	53572	53246	53633	52712	52950	52817	53592	53146	52797	54187	52702	52940
14.05 - 15.00	53609	52905	53608	53784	52715	52597	52855	53391	52962	53298	53023	53081
15.05 - 16.00	53281	53534	53094	53360	53444	53020	52976	52979	53072	53304	53524	52935
16.05 - 17.00	53179	52922	53373	52764	53001	53436	52200	52885	52487	52946	53365	53259
17.05 - 18.00	52865	53212	52590	53417	53143	53003	52895	52747	52846	52117	52754	52861
18.05 - 19.00	52945	53424	52963	53400	53366	53913	52594	53090	52247	52802	52739	52826
19.05 - 20.00	53076	52981	51851	53002	52532	52531	52865	53138	53100	53187	52842	52693
20.05 - 21.00	52972	52506	52366	52965	52782	52710	52939	52429	52859	52950	53050	52898
21.05 - 22.00	52522	52718	52959	52830	52445	52855	52778	52904	52830	52387	53126	52066
22.05 - 23.00	52905	53130	53017	52825	52730	52287	52366	52514	53006	52978	52952	52738
23.05 - 24.00	52144	52807	53007	52614	53628	52228	52758	53241	51820	52820	52892	53237

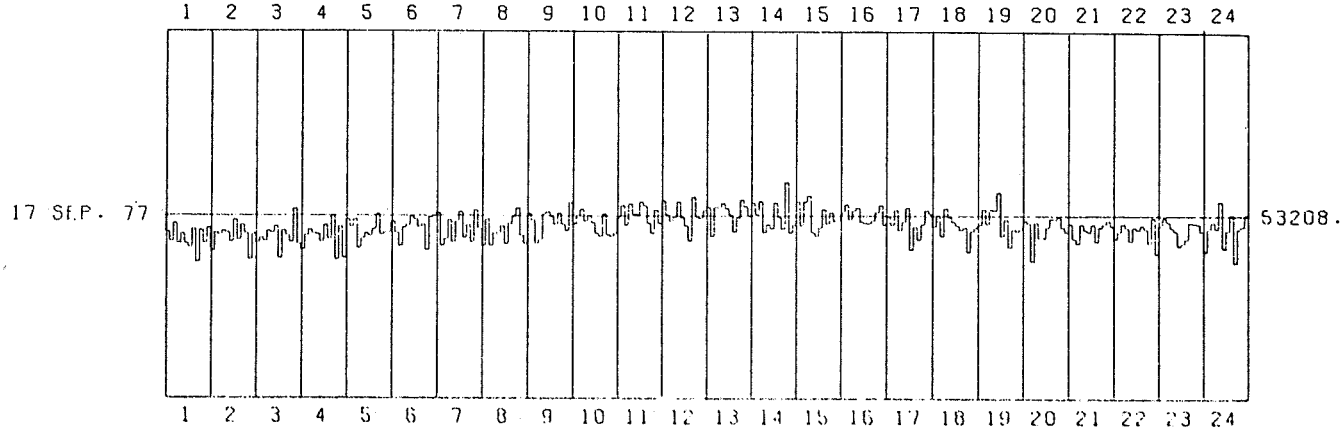

EACH VERTICAL DIVISION REPRESENTS 10 PERCENT DEVIATION

UTRECHT THE NETHERLANDS NM64 NEUTRON MONITOR

DATE: 18 9 77 CORRECTED FOR AIRPRESSURE COEFFICIENT: 0.99 PCT PER MM HG

HOURS	05	10	15	20	25	30	35	40	45	50	55	00
0.05 - 1.00	53206	52285	51853	52496	52071	52826	52512	53238	53184	52752	51937	52876
1.05 - 2.00	53326	52945	52304	52895	52734	52855	52961	53245	53682	53158	52881	53209
2.05 - 3.00	52672	52943	52822	52588	52744	53297	53055	53265	52527	52585	53116	52859
3.05 - 4.00	52547	53676	53291	52731	52809	52971	53175	53195	52406	52924	52705	53051
4.05 - 5.00	53274	52521	52336	52619	52225	52947	53030	52894	52627	52373	52521	52521
5.05 - 6.00	52752	52807	53565	52360	52594	52692	52651	52724	52692	52905	53426	53298
6.05 - 7.00	53188	52880	52756	53220	53219	52981	52507	52899	53101	53196	53063	53424
7.05 - 8.00	53625	52745	52823	53600	53781	53397	53195	52894	53221	53264	53559	53740
8.05 - 9.00	53371	53308	52852	52702	52924	53257	53487	53451	53537	53426	53070	53422
9.05 - 10.00	53547	53257	53694	52897	53166	53468	53696	53913	52950	53559	53995	53600
10.05 - 11.00	53457	53124	53511	53455	53092	53558	53116	53250	53528	53268	53374	53209
11.05 - 12.00	53898	53806	53188	53024	53410	53238	53316	52661	53868	53663	52976	53603
12.05 - 13.00	53021	53178	53490	52488	53732	53184	53180	53690	52945	53836	53597	52924
13.05 - 14.00	53365	53544	54270	52401	53259	53005	53240	53444	53690	53670	53746	53684
14.05 - 15.00	53926	53231	52811	53403	53234	53749	53629	53757	53521	53943	53123	53607
15.05 - 16.00	53228	53297	53249	53167	54279	53482	53282	53381	53556	52764	53946	53525
16.05 - 17.00	53072	53675	53051	53715	53198	53509	52805	53242	53458	53220	52500	53758
17.05 - 18.00	53314	53853	54063	53307	53265	53454	53123	53776	53383	52826	53642	53207
18.05 - 19.00	53587	53566	53085	53514	52945	53543	53455	53678	53832	53561	53287	53937
19.05 - 20.00	53591	53247	53333	53333	53408	53050	52924	53570	53252	52697	53492	54332
20.05 - 21.00	53336	53336	52914	53191	53360	53376	53830	53189	53372	53350	52850	53540
21.05 - 22.00	52861	53395	53218	53195	53340	52908	52951	53316	52874	52813	53263	52948
22.05 - 23.00	53167	53002	53778	53089	53458	52802	53696	52837	53391	53102	52296	53701
23.05 - 24.00	53262	53250	52962	53643	53371	53007	53556	52822	53191	52687	52480	52905

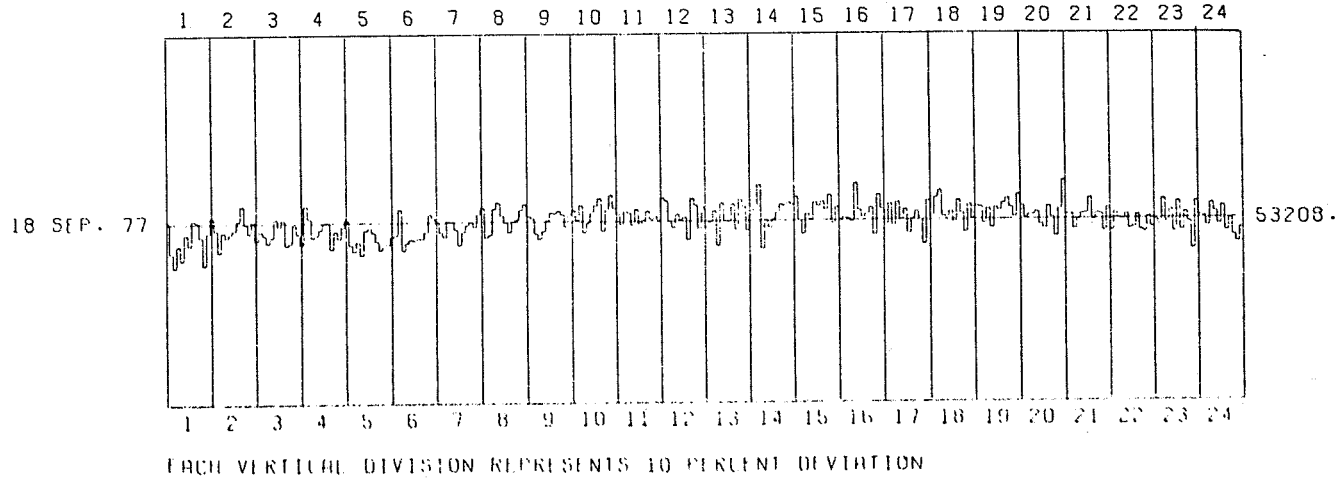

EACH VERTICAL DIVISION REPRESENTS 10 PERCENT DEVIATION

UTRECHT THE NETHERLANDS NM64 NEUTRON MONITOR

DATE: 19 9 77 CORRECTED FOR AIRPRESSURE COEFFICIENT: 0.99 PCT PER MM HG

HOURS	05	10	15	20	25	30	35	40	45	50	55	00
0.05 - 1.00	53476	52881	52979	53296	53547	53773	52644	53254	52794	52714	52390	53290
1.05 - 2.00	53480	53282	53279	54484	53085	53071	52903	53102	53615	53308	53038	53692
2.05 - 3.00	52609	53286	52987	53170	53646	53103	52937	52884	53048	53559	53144	53627
3.05 - 4.00	52922	53023	53302	53297	53680	53478	53232	53804	52693	53243	53696	53234
4.05 - 5.00	53653	52755	53236	53106	54011	53251	53818	53132	53086	52824	53975	52882
5.05 - 6.00	53252	52580	52984	53491	53146	53619	53357	53657	52866	53679	53320	53310
6.05 - 7.00	53000	52551	52790	53077	53148	53283	53108	52748	53603	53524	53567	53224
7.05 - 8.00	53375	53148	53275	53545	52726	53036	52941	53467	53166	52877	52737	53068
8.05 - 9.00	52690	53164	53315	52662	53068	52682	53785	52835	53022	53663	53051	53340
9.05 - 10.00	53480	53001	53151	53409	52857	52822	52926	53298	53047	53713	52758	53393
10.05 - 11.00	53031	53047	52705	53161	52596	52938	52476	52641	53383	53082	53337	52881
11.05 - 12.00	53060	53597	53149	53049	53010	52823	52931	53441	53448	52934	53375	53175
12.05 - 13.00	52916	52923	53161	52196	53423	53776	52738	52905	52593	52612	53592	53733
13.05 - 14.00	52417	53697	53012	53455	53752	53191	53134	53291	53159	53058	52758	53312
14.05 - 15.00	52908	52869	53118	52934	53103	53085	52601	52538	53580	53183	53556	53134
15.05 - 16.00	53300	52988	53850	52993	53041	52753	53863	54142	53719	53794	53152	52951
16.05 - 17.00	53382	53416	53326	53313	53273	53882	53165	53104	53155	53737	53370	52825
17.05 - 18.00	53187	53429	53748	53461	53119	53266	53611	53494	53146	53229	53338	53027
18.05 - 19.00	52835	52793	53663	53402	53617	53355	52883	53354	53492	52982	53420	53183
19.05 - 20.00	53066	53097	53086	53255	53829	53541	52941	53059	52730	53233	52737	52655
20.05 - 21.00	53487	53143	53538	53204	53338	53114	53389	53370	53312	53471	52912	53393
21.05 - 22.00	52632	53516	53998	53273	53664	53561	53348	53941	52958	53526	52925	53514
22.05 - 23.00	53460	53269	53459	53324	53395	53467	53414	53178	53481	54269	53686	53195
23.05 - 24.00	53346	53013	53225	53427	53229	53001	53498	52675	53336	53698	53673	53467

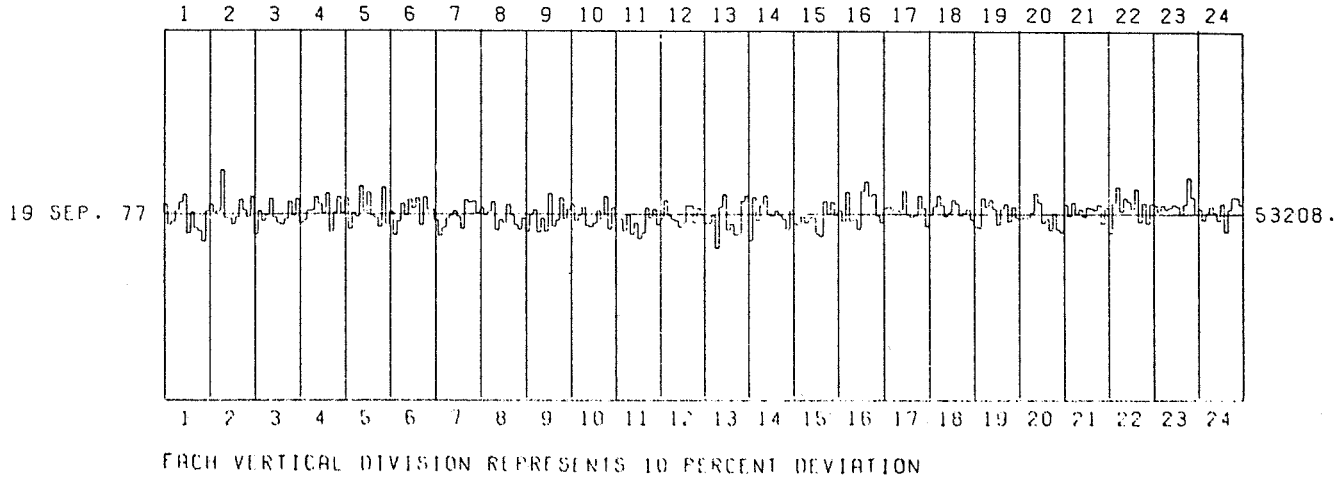

EACH VERTICAL DIVISION REPRESENTS 10 PERCENT DEVIATION

UTRECHT THE NETHERLANDS NM64 NEUTRON MONITOR

DATE: 20 9 77 CORRECTED FOR AIRPRESSURE COEFFICIENT: 0.99 PCT PER MM HG

HOURS	05	10	15	20	25	30	35	40	45	50	55	00
0.05 - 1.00	53515	53036	52954	53358	53489	53710	53107	53605	53270	52936	53327	53437
1.05 - 2.00	54276	53161	52752	53811	53672	53926	53706	52892	53654	53972	53372	53680
2.05 - 3.00	53307	53685	53577	53994	53488	53227	53793	53590	53255	53006	53382	53341
3.05 - 4.00	53741	53376	53249	53090	52851	52723	53373	53274	53678	53492	53102	52775
4.05 - 5.00	52867	53103	53901	53549	53342	53405	53039	52755	53532	53735	52870	53991
5.05 - 6.00	53792	53258	53218	53405	53433	53366	53159	53865	53084	53137	53629	53395
6.05 - 7.00	52905	53144	53296	52366	53831	53507	53307	53132	53574	53092	53534	53792
7.05 - 8.00	52590	53310	53319	53219	53238	52953	53665	53629	53448	53305	53689	53492
8.05 - 9.00	53058	53431	53340	53075	53736	53266	53154	53996	53714	53591	53341	53087
9.05 - 10.00	53580	53514	54234	53782	53762	53428	53365	54281	53647	53734	53343	53285
10.05 - 11.00	53388	53445	53385	53817	53491	53570	53356	53901	53454	53558	53660	53495
11.05 - 12.00	53354	53851	53703	53675	53560	54130	53495	53916	53633	53995	53322	53736
12.05 - 13.00	53577	54144	52906	53825	53736	53538	54425	53883	54373	53777	53823	53642
13.05 - 14.00	53216	53645	54065	54236	53501	53491	53770	53905	54168	54032	54037	54497
14.05 - 15.00	53496	54762	53846	53987	54443	54040	53662	53691	53926	54163	54072	53652
15.05 - 16.00	53673	53966	53525	53984	53657	54469	53709	53328	53539	53609	53509	54006
16.05 - 17.00	53502	53837	54164	53618	54084	53659	53677	53594	53688	53125	53574	54344
17.05 - 18.00	54029	53662	53778	53539	53006	53483	53221	53493	53093	53507	53712	53137
18.05 - 19.00	53611	53265	52982	53733	53984	53313	53326	53276	53789	53260	53601	53269
19.05 - 20.00	53108	52940	53284	53212	53079	53137	53732	53832	53324	52947	53548	53690
20.05 - 21.00	53877	53291	53400	52935	53341	52977	53486	53365	53075	53380	53837	53132
21.05 - 22.00	53562	52365	53362	53225	53773	53452	53774	53225	53510	53159	53370	54114
22.05 - 23.00	53880	53174	52891	53391	53730	53931	53865	53870	53502	54346	52663	53359
23.05 - 24.00	53424	53721	53290	53142	53209	53435	53612	53421	53635	53555	53704	52985

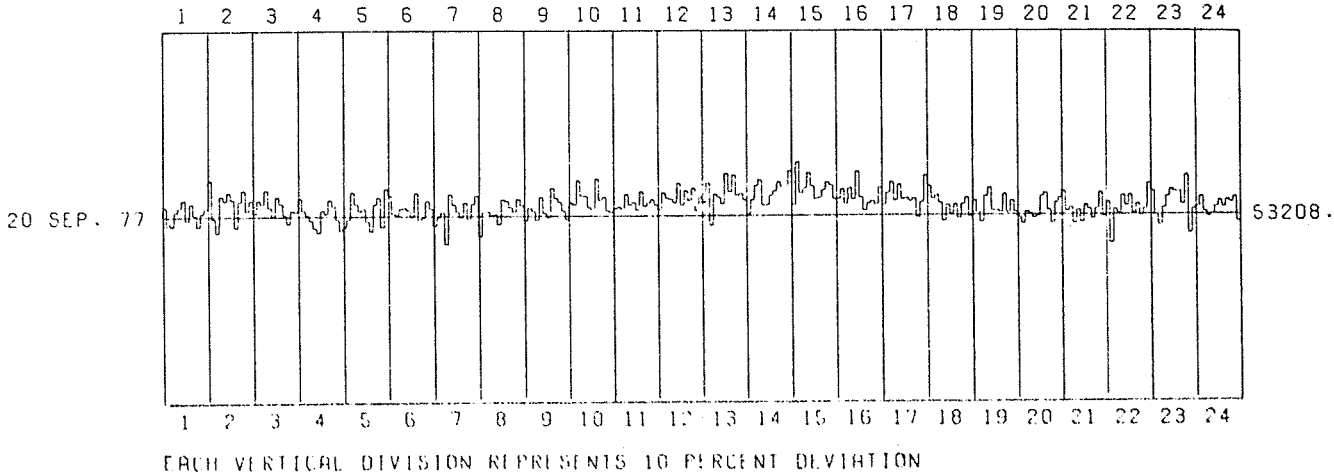

UTRECHT THE NETHERLANDS NM64 NEUTRON MONITOR

DATE: 21 9 77 CORRECTED FOR AIRPRESSURE COEFFICIENT: 0.99 PCT PER MM HG

HOURS	05	10	15	20	25	30	35	40	45	50	55	00
0.05 - 1.00	53475	53569	52895	53607	54108	53281	53240	53560	53111	52672	53118	53403
1.05 - 2.00	53172	53671	53127	53012	53162	53702	53723	53335	53261	53105	53073	53226
2.05 - 3.00	53148	52992	52991	53329	52572	52273	53004	52704	53275	52595	53255	53318
3.05 - 4.00	53043	52830	52773	53106	52941	53554	53076	52759	53417	53178	53059	53983
4.05 - 5.00	52224	53104	53308	53671	53050	53416	53682	53266	53819	52968	53267	52706
5.05 - 6.00	52757	53287	52551	52780	52908	53258	53110	52464	53105	53120	53129	53073
6.05 - 7.00	53346	52716	53200	53197	52813	52229	53390	53099	53098	53274	53344	53701
7.05 - 8.00	53438	53088	52858	53438	53269	53120	53011	52905	52810	53392	53993	53591
8.05 - 9.00	53754	54054	53260	53346	53395	52936	53833	53519	52810	53708	53514	53901
9.05 - 10.00	53067	52514	53141	52949	52644	52867	52910	52703	53526	53425	53018	53039
10.05 - 11.00	52547	53059	53072	53200	53188	53287	53079	52928	53522	52760	53044	53085
11.05 - 12.00	53117	53239	53068	53227	52743	53224	52776	52465	52910	53213	53231	52242
12.05 - 13.00	53140	53252	52422	53044	52761	53571	52767	53495	53026	53583	53716	53592
13.05 - 14.00	53467	53965	53783	53795	53487	53916	53512	53687	53887	53528	53883	53465
14.05 - 15.00	53689	53588	53643	53297	53819	53149	53318	53679	53238	53360	53479	53307
15.05 - 16.00	53286	53072	53420	53400	54248	52877	53439	52832	52960	53754	53623	52920
16.05 - 17.00	52815	52883	53669	53304	53740	52741	53513	53421	52412	52871	53118	52310
17.05 - 18.00	52337	52181	53052	52645	52194	52728	52581	52920	52823	52398	53270	53146
18.05 - 19.00	51869	52192	52470	52932	52309	51908	53604	52623	52686	53075	52447	53119
19.05 - 20.00	52874	52856	52675	52697	53151	52806	53156	52680	52315	52487	52479	52696
20.05 - 21.00	52210	52616	51754	53132	52691	52466	53059	52736	53425	52340	52356	52164
21.05 - 22.00	52050	52917	52669	52416	53119	51981	52715	52346	52286	52309	52660	52357
22.05 - 23.00	53291	52218	52612	52573	52902	52892	52490	52682	52680	52876	52803	52753
23.05 - 24.00	52822	53611	52652	53210	52847	53065	53707	53372	52472	52592	52701	52710

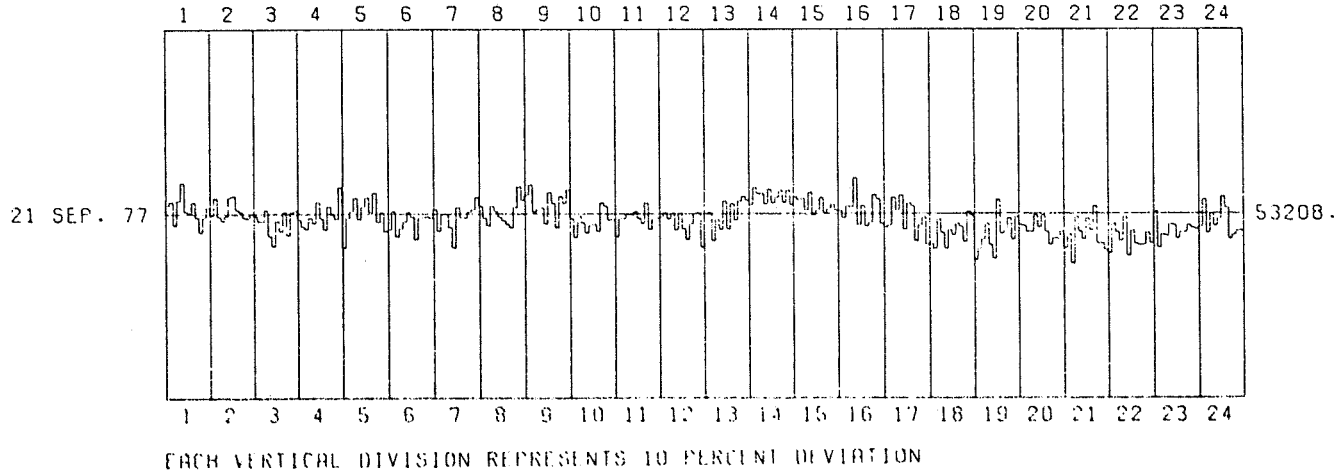

UTRECHT THE NETHERLANDS NM64 NEUTRON MONITOR

DATE: 22 9 77 CORRECTED FOR AIRPRESSURE COEFFICIENT: 0.99 PCT PER MM HG

HOURS	05	10	15	20	25	30	35	40	45	50	55	00
0.05 - 1.00	53381	52694	52944	52895	52578	52330	51829	51629	52240	52287	52643	52176
1.05 - 2.00	52096	52010	52287	52188	52628	52086	51759	51794	51815	51115	51864	51646
2.05 - 3.00	51599	51666	51651	51321	51424	51508	51574	52110	52443	51875	51889	51716
3.05 - 4.00	51892	51102	52036	52206	51650	51497	51726	51728	51257	52071	51402	51791
4.05 - 5.00	51795	51786	51530	51216	51780	51438	51829	51978	51979	51787	51836	52157
5.05 - 6.00	52494	52352	51977	51794	52590	52705	52751	52364	52550	52327	52162	52620
6.05 - 7.00	52353	52844	52563	53065	52063	52793	51811	52450	52237	52048	52500	52048
7.05 - 8.00	52442	52797	52343	52969	52750	52572	52174	52553	52619	52637	52631	53436
8.05 - 9.00	52602	52930	52623	53308	52828	52766	52743	53136	53346	52883	53364	52561
9.05 - 10.00	52815	53083	52836	53066	53260	53263	52674	52657	52858	53216	52548	52386
10.05 - 11.00	52442	52519	52506	52801	52570	52732	52410	53008	53237	53076	52870	52642
11.05 - 12.00	52623	53281	52416	52540	52879	52511	52479	52104	52254	51827	52247	52331
12.05 - 13.00	52583	52249	51826	52050	51425	51940	52302	51042	51141	51524	51603	51081
13.05 - 14.00	51444	52114	51311	51540	51755	51854	52020	51167	52105	51456	51533	51268
14.05 - 15.00	51763	51738	51491	51808	51513	51937	51500	51167	51926	51411	51785	51633
15.05 - 16.00	51552	51843	51575	51756	51380	51223	51643	51959	52170	51598	51802	51277
16.05 - 17.00	51487	51335	51083	51315	51146	50805	51773	51422	50786	50868	50690	51140
17.05 - 18.00	50771	51381	51661	50681	51287	50918	51684	50251	50572	50791	51213	50950
18.05 - 19.00	50668	51173	50651	51174	51279	51144	51094	50699	50993	51328	51334	51152
19.05 - 20.00	51242	51395	51058	51304	51691	51287	50832	51200	51402	50966	51071	50870
20.05 - 21.00	51016	50846	51551	50727	51522	51368	51816	51537	51918	51685	51208	51735
21.05 - 22.00	51479	50745	51892	51760	51455	51274	51678	51175	51510	51801	52156	51808
22.05 - 23.00	51772	51403	51371	51335	51476	51054	51018	50479	51532	50947	50374	50891
23.05 - 24.00	51999	51903	51607	50270	50881	50362	50551	50061	50689	49971	50153	50105

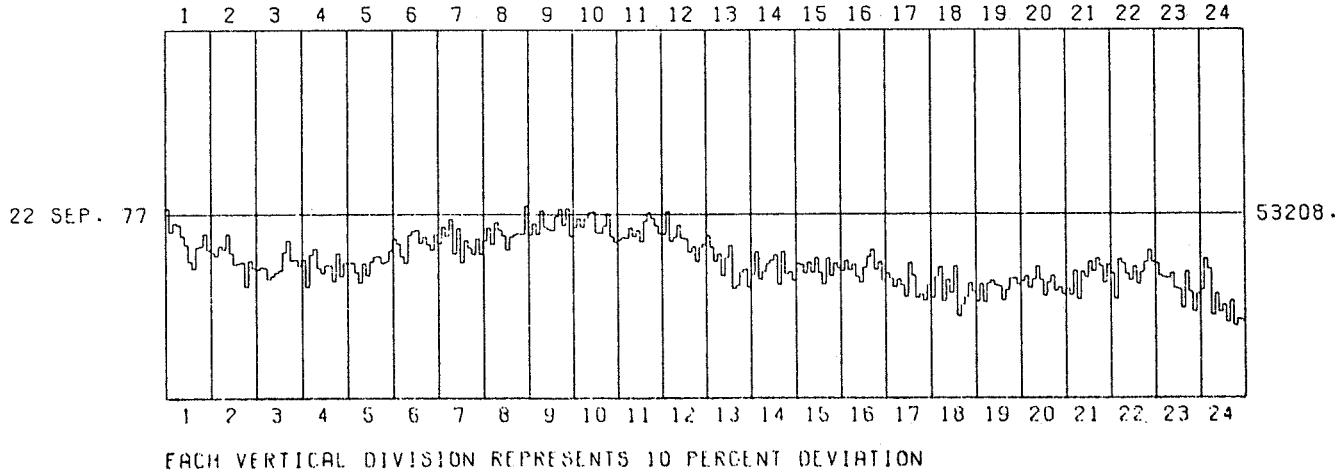

EACH VERTICAL DIVISION REPRESENTS 10 PERCENT DEVIATION

UTRECHT THE NETHERLANDS NM64 NEUTRON MONITOR

DATE: 23 9 77 CORRECTED FOR AIRPRESSURE COEFFICIENT: 0.99 PCT PER MM HG

HOURS	05	10	15	20	25	30	35	40	45	50	55	00
0.05 - 1.00	50739	50318	50726	50248	50100	49696	50632	49969	49871	50056	49819	50149
1.05 - 2.00	50236	49798	50492	49786	50020	51702	50784	50129	49682	50025	49429	50291
2.05 - 3.00	51746	50575	49564	50216	50921	50098	50310	50468	49628	50138	50538	50015
3.05 - 4.00	50871	51097	50968	50548	50875	50814	50334	49986	50408	50937	50874	50984
4.05 - 5.00	50942	50915	50547	51834	50738	51102	51228	50773	50892	50944	51272	51381
5.05 - 6.00	51647	50822	50675	50968	51477	51348	50866	50617	51117	51333	50694	50924
6.05 - 7.00	51360	51341	50831	50973	51044	51583	50392	50748	50922	50389	50591	50931
7.05 - 8.00	51315	50899	50873	51531	50957	51053	50892	50829	51125	50834	51003	51162
8.05 - 9.00	51139	51380	51510	51302	51056	51326	50986	51466	50482	51108	51211	51005
9.05 - 10.00	51350	50933	51185	50908	50345	51156	51023	50741	50756	50718	50840	51069
10.05 - 11.00	51358	51573	50735	50457	51166	50661	51291	51061	50613	51054	51252	51160
11.05 - 12.00	51646	51411	51188	51312	50932	50978	51556	51621	51837	51853	51816	50645
12.05 - 13.00	51342	51243	51707	51321	51684	51454	51982	51745	51258	51578	51638	51607
13.05 - 14.00	52648	51920	52613	52348	52331	52214	51652	52029	52095	52588	52592	52390
14.05 - 15.00	51844	52468	52072	52264	51867	51608	52290	52191	51824	52120	52375	51335
15.05 - 16.00	51699	52249	52034	52105	51690	51819	52417	52288	52211	53016	52341	52190
16.05 - 17.00	52141	51398	51409	51689	52026	52297	52503	52096	52380	52046	51812	52167
17.05 - 18.00	52169	52265	52028	52351	51887	52299	52527	51600	51981	52238	51999	51754
18.05 - 19.00	51295	51109	52029	52228	52145	51518	52377	52276	51835	52011	52069	51549
19.05 - 20.00	52073	51915	51677	51982	51764	51328	52130	51798	51850	51487	52168	51721
20.05 - 21.00	52293	51982	51195	52140	51627	51969	51586	51773	52113	51511	51558	51404
21.05 - 22.00	51351	51805	51229	51631	51402	51048	52034	52158	51677	52010	52168	51789
22.05 - 23.00	51196	52062	51853	52337	51793	51821	51452	51373	51663	51884	52191	51992
23.05 - 24.00	52628	52187	52088	52397	52003	52108	51316	51940	51809	51878	51878	52047

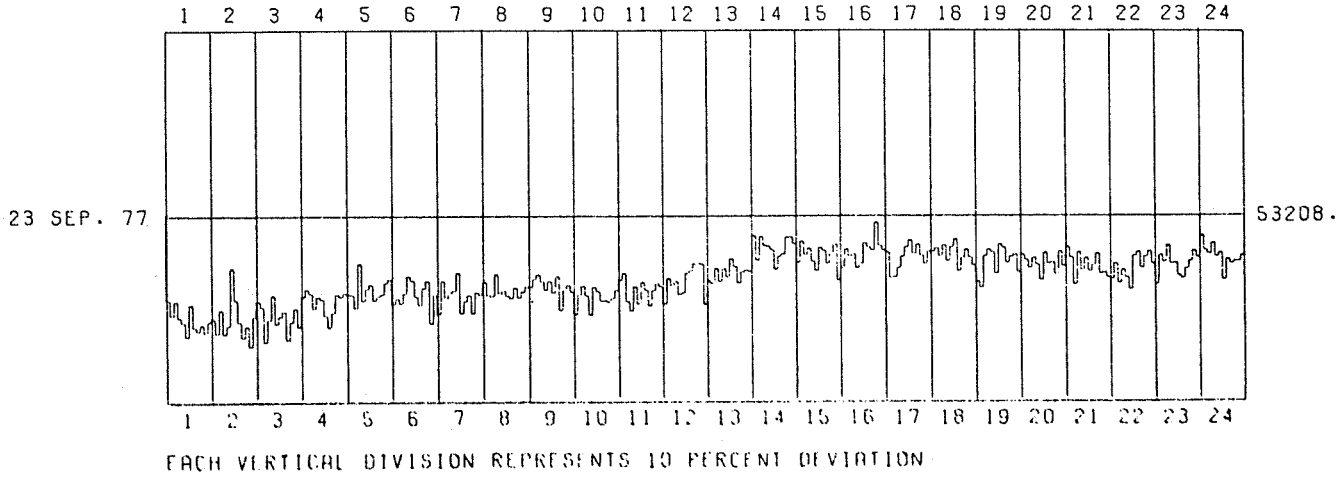

EACH VERTICAL DIVISION REPRESENTS 10 PERCENT DEVIATION

UTRECHT THE NETHERLANDS NM64 NEUTRON MONITOR

DATE: 24 9 77 CORRECTED FOR AIRPRESSURE COEFFICIENT: 0.99 PCT PER MM HG

HOURS	05	10	15	20	25	30	35	40	45	50	55	00
0.05 - 1.00	51691	51470	52220	51435	52161	51621	51417	51116	51641	51119	51662	51288
1.05 - 2.00	51897	51547	51764	51193	51079	50846	51333	51335	51391	50942	50865	51074
2.05 - 3.00	51345	51437	50973	51382	51285	51267	50736	51372	51781	51665	51126	50872
3.05 - 4.00	51694	51687	51881	51210	51641	51204	51184	51792	51030	50939	51470	51442
4.05 - 5.00	51289	51245	50856	51282	52242	51626	51607	50762	51665	51794	51797	51544
5.05 - 6.00	51884	51733	52022	51164	51789	51379	51625	51371	51715	52343	51518	51616
6.05 - 7.00	51419	51719	51487	52183	51742	52601	52512	52048	52644	52600	52811	52321
7.05 - 8.00	52803	52987	52619	52487	53848	53005	53112	52857	52987	52874	53738	53174
8.05 - 9.00	52890	52799	52970	52534	52486	52944	52400	52843	53167	52676	53170	52851
9.05 - 10.00	52641	52969	52821	52587	53601	52312	53287	52630	52774	52806	53434	53529
10.05 - 11.00	53363	53650	53066	54031	53499	53136	53539	53684	53641	53843	53758	53769
11.05 - 12.00	53688	53545	54066	53228	53650	53485	53670	53445	53584	53123	53423	52730
12.05 - 13.00	53253	53668	53651	53648	53222	53061	53474	53125	53102	53054	53150	53682
13.05 - 14.00	53800	53057	53368	53566	53146	53208	53372	53289	53423	52709	52711	53343
14.05 - 15.00	53116	53529	53466	53078	53495	53434	53370	52859	53516	53656	53396	53181
15.05 - 16.00	53093	53383	52735	53370	53144	53039	53241	53383	53215	53148	54165	53461
16.05 - 17.00	53219	53376	53817	53126	53586	53588	52961	53204	52876	53029	53645	53607
17.05 - 18.00	53190	53364	52982	53042	52899	53015	53065	53040	53703	53076	52871	52993
18.05 - 19.00	53279	53132	53570	53642	53406	53500	52353	53689	53786	52753	53244	53019
19.05 - 20.00	52979	53465	53029	53486	53407	53284	52738	52822	52691	52650	53471	52648
20.05 - 21.00	53368	53007	53489	52309	53002	52917	53190	52948	52780	52711	52749	52735
21.05 - 22.00	52810	52832	52973	52721	52613	52939	52848	52832	52609	52430	52890	52530
22.05 - 23.00	52939	52731	52233	52192	52504	52298	53317	52414	52739	52344	52519	53084
23.05 - 24.00	52336	52630	52916	52758	52834	52273	52628	52246	51515	51811	52183	52542

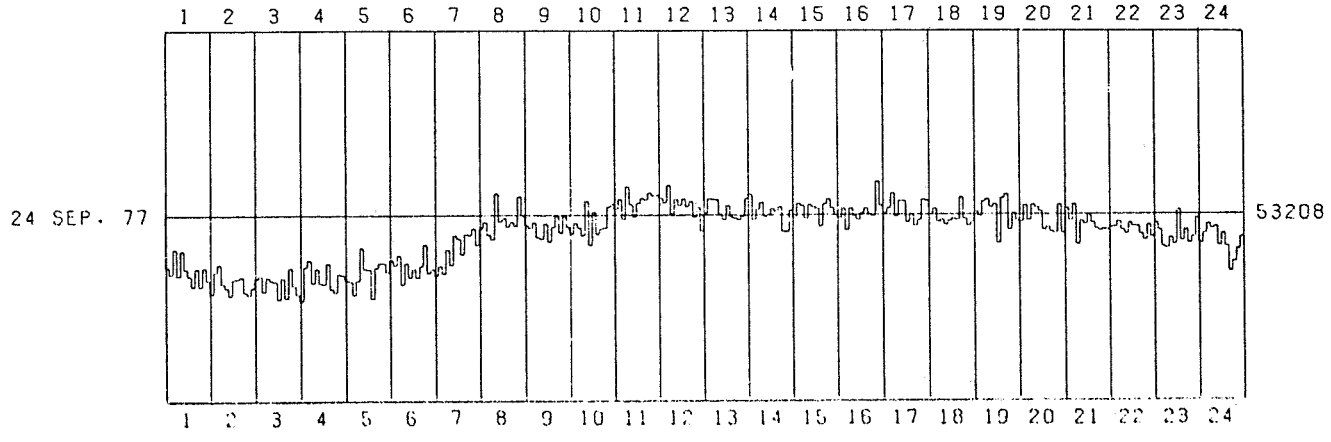

EACH VERTICAL DIVISION REPRESENTS 10 PERCENT DEVIATION

UTRECHT THE NETHERLANDS NM64 NEUTRON MONITOR

DATE: 22 11 77 CORRECTED FOR AIRPRESSURE COEFFICIENT: 0.99 PCT PER MM HG

HOURS	05	10	15	20	25	30	35	40	45	50	55	00
0.05 - 1.00	53555	53712	53799	53865	53498	53655	53985	53401	53583	54127	53829	54265
1.05 - 2.00	53807	53876	54245	54052	54475	53803	53993	54074	54746	53463	53798	54015
2.05 - 3.00	54506	53988	53761	53796	54475	54086	53827	53707	53930	54127	54366	54007
3.05 - 4.00	54354	53790	54834	54163	54567	54339	54013	54277	54377	54269	53852	54579
4.05 - 5.00	53753	53953	54339	53846	54071	54071	54532	53439	53864	54016	53948	53800
5.05 - 6.00	54079	54114	53999	54202	54325	54527	53757	54248	53815	54357	54216	53944
6.05 - 7.00	53923	53580	54715	53743	54171	54310	54102	54050	54889	54228	54133	53843
7.05 - 8.00	54239	53954	54613	54321	54160	54355	54594	54125	54139	54227	54003	54365
8.05 - 9.00	54381	54309	54522	54875	54159	53903	53770	54738	54176	54043	54148	54479
9.05 - 10.00	54715	53780	53963	54270	54078	54291	54382	54388	54197	54087	54560	54251
10.05 - 11.00	54128	54263	54827	54888	56118	56400	57007	57217	56938	56795	57065	56867
11.05 - 12.00	57076	56168	56908	56574	55892	55830	55807	55444	55239	55135	55530	55549
12.05 - 13.00	54907	54967	55213	54410	54715	55201	54721	54788	54342	54453	55031	54966
13.05 - 14.00	54423	54724	54694	54936	54569	54358	54502	53436	54384	54411	54624	54163
14.05 - 15.00	54185	53900	53903	53954	54469	53986	54190	53646	54001	54824	54275	54703
15.05 - 16.00	54325	53863	54158	53926	54599	53806	54735	54355	54557	53491	53522	55026
16.05 - 17.00	53637	53909	54596	54305	53529	53823	54470	53614	54384	54332	53666	54325
17.05 - 18.00	54049	54291	54124	54224	54356	53347	54108	53679	53936	53821	53827	53405
18.05 - 19.00	54181	54257	53668	54260	54260	53879	54304	54332	53932	53942	54778	54374
19.05 - 20.00	53897	54742	54215	54128	53650	54321	53768	53298	54053	53564	53870	54398
20.05 - 21.00	54425	54318	54600	53917	53930	54166	53663	54053	53946	54133	54126	54408
21.05 - 22.00	54961	53830	53909	54454	53797	53829	53257	53833	53717	54244	53973	54292
22.05 - 23.00	54079	54087	53700	53504	54707	53908	54042	54047	54748	53453	53391	53419
23.05 - 24.00	53540	54222	53866	53664	53689	53939	54446	54127	53793	53866	53986	53690

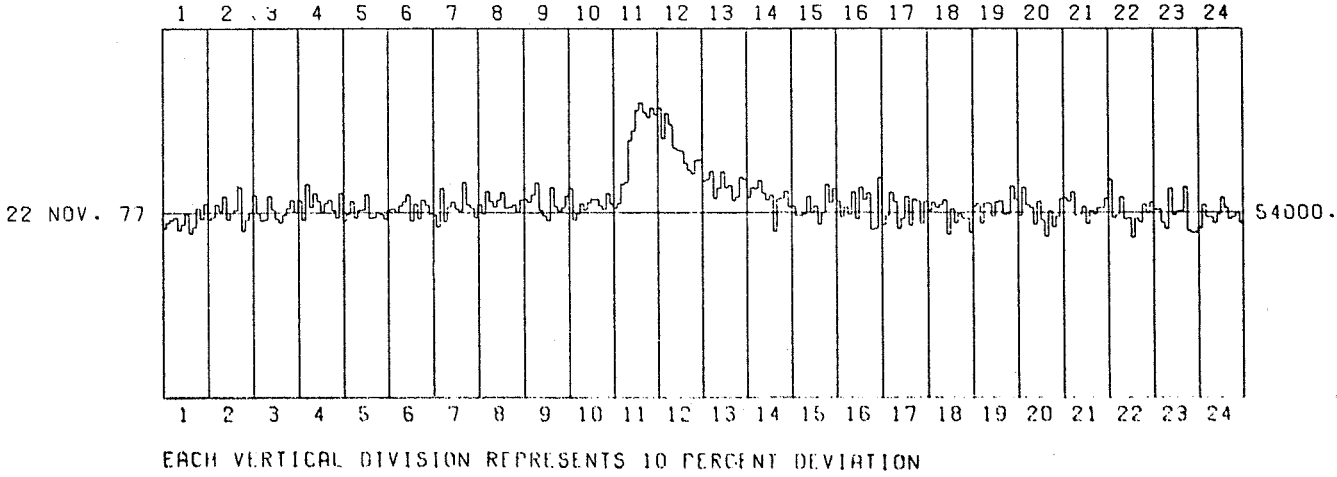

EACH VERTICAL DIVISION REPRESENTS 10 PERCENT DEVIATION

Dourbes Neutron Monitor Data for the September 7-24, 1977 Period and the Event of November 22, 1977

by

J.C. Jodogne
Institut Royal Meteorologique
3, Avenue Circulaire
1180 Bruxelles, Belgium

The Dourbes neutron monitor data are briefly reviewed in this report. Located at N50.10 E4.60 this station lies at an altitude of 225 m and has a 3.24 GV rigidity cutoff, a barometric coefficient equal to 0.99% mm of Hg, a barometric reference of 740 mm of Hg, and a quiet-day counting rate of 374000 cts/h. The horizontal component of the geomagnetic field at Dourbes has a baseline equal to 19840 nT.

The graph in Figure 1 shows a plot of the 15-min data on November 22, 1977. The horizontal magnetic field component displays a small variation that does not exceed 20 nT.

The hourly values of the recordings listed in the *Bulletin Mensuel* [1977] are plotted in Figure 2 together with the horizontal component of the Earth's magnetic field measured at the station. Note the Forbush decreases of September 11 and 21. Small decreases in the horizontal magnetic field component may have changed slightly the rigidity threshold. Although the inferred interplanetary magnetic field polarity [*SGD*, 1977] during this period was mixed, for the November 22 event, it pointed toward the Sun.

The ground level events of September 24 and November 22, 1977, clearly seen in the Figures, are not associated with a change in cutoff rigidity. The 15-min data have been published in the *Bulletin Mensuel* [1977]. We welcome special requests for other periods.

Acknowledgment

The horizontal magnetic field component data were supplied by Prof. A. de Vuyst of Dourbes.

REFERENCES

Bulletin Mensuel 1977 Observations iono. et du ray. cosm. (Institut Royal Météorologique, Bruxelles, Belgium).

SGD 1977 *Solar-Geophysical Data*, 399 Part I, 28, November 1977, U.S. Department of Commerce (Boulder, Colorado 80303).

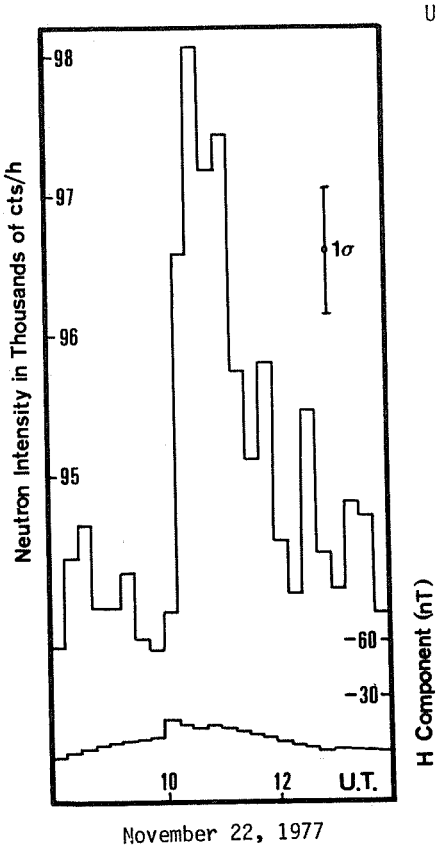

Fig. 1. Fifteen-min averages of the Dourbes neutron monitor and of the geomagnetic field's horizontal component at the same site during the period 0800 to 1400 UT on November 22, 1977.

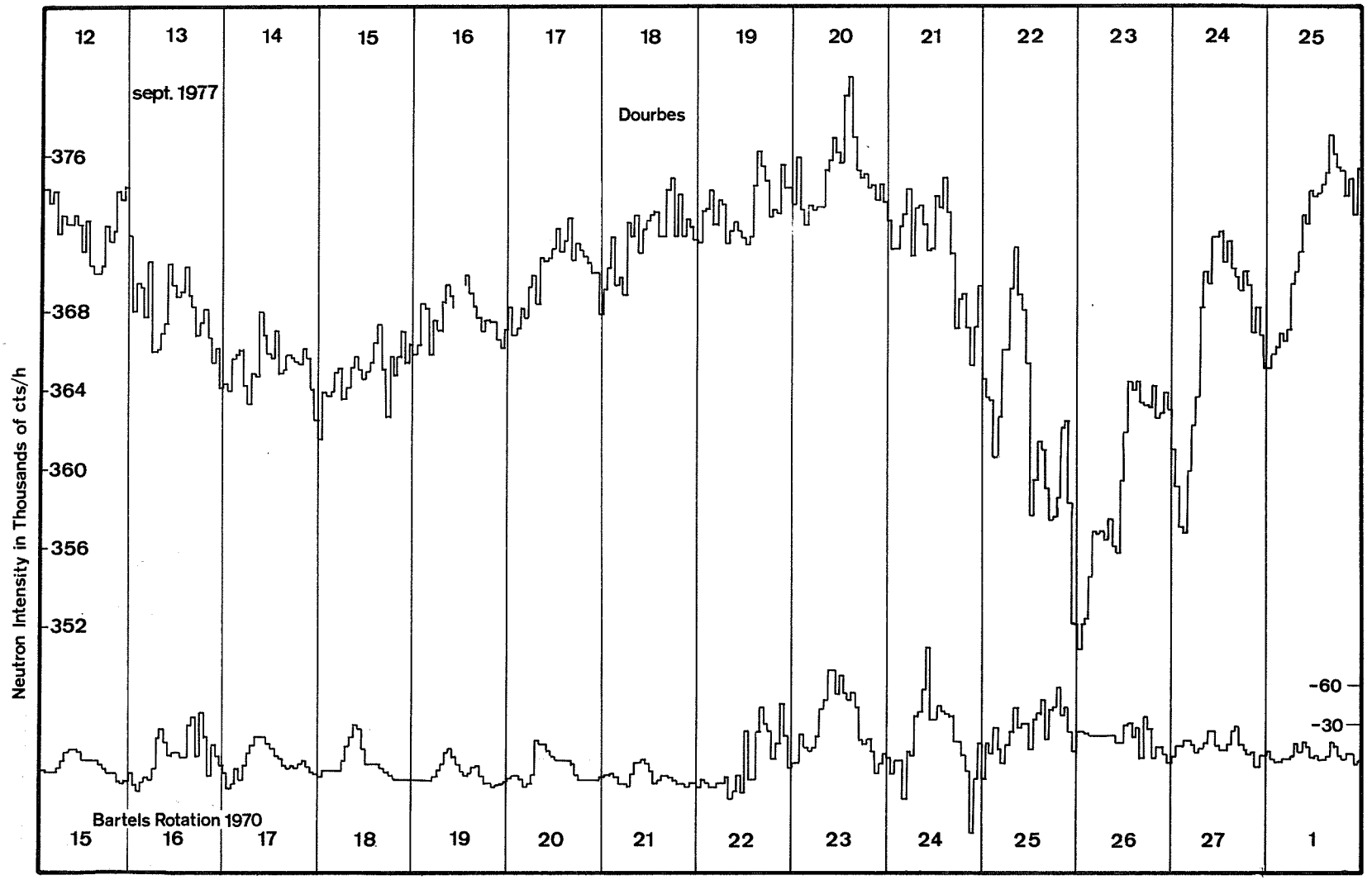

Fig. 2. Time variation of the hourly average intensity of the Dourbes neutron monitor and of the geomagnetic field's horizontal component at the same site during the period September 12-25, 1977. Dates along bottom of figure refer to the days within a Bartels Rotation.

The Intensity Variation of Galactic Cosmic Rays During September 1977

by

N. Iucci, M. Parisi, M. Storini, G. Villoresi and N.L. Zangrilli
Laboratorio Plasma Spazio - C.N.R.
Istituto di Fisica "G. Marconi" - Universita
Piazzale delle Scienze, 5 - 00185 Roma, Italia

Analysis

Perturbations of galactic cosmic ray (c. r.) intensity that occurred in September 1977 have been studied by us with the following kinds of data:

(1) the hourly values of the Rome 9-NM-64 neutron monitor (6.3 GV threshold rigidity) shown in Figure 1;
(2) the IMP 7 and 8 solar wind plasma data (bulk speed V, number density N and temperature T) taken from *SGD* [1978] and shown in Figure 2;
(3) the inferred interplanetary magnetic field polarities [*SGD*, 1978] shown at the bottom of Figure 2; and those
(4) solar flares that were accompanied by Type IV radio emission [*SGD*, 1977 and 1978].

Two large Forbush decreases represent the outstanding events registered in the Rome neutron monitor intensity. Onset days and amplitudes of these events are reported in Table 1 together with their parent Type IV solar flares, because the most probable origin of such decreases has been found to be solar flares accompanied by Type IV radio emission that is sufficiently energetic between millimeter and meter wavelengths [Iucci et al., 1977a and b]. All flares stemmed from active region No. 14943.

The Forbush Decrease of September 11. The parent flares erupted near the east limb of the Sun. The relatively long time interval between flares and Forbush decrease may account for the long descending phase of the event (from the beginning of Sept. 11 to the end of Sept. 14). Moreover, two decreases --one on Sept. 11, another on Sept. 12--form this main phase and they occur in coincidence with two sharp and simultaneous increases in the IMP 7 and 8 solar wind plasma parameters. The latter probably indicate the existence of shock fronts crossing the Earth. After September 14, the c.r. intensity recovered very slowly toward the prestorm level.

The solar wind speed shows a fast stream, lasting from the middle of the descending phase to the beginning of the recovery phase; inside this stream the inferred magnetic field polarity frequently changed sign.

The Possible Forbush Decrease of September 19. This small event which registered only in the high-latitude neutron monitor data, is probably associated with the Type IV solar flare of Sept. 16. In the Rome neutron monitor intensity this event is not visible because the geomagnetic storm (~80nT) of Sept. 19, which was coincident with a sharp increase in the solar wind speed, seemed to cause a small c.r. increase owing to the change in cutoff rigidity.

Table 1. Tentative Association Between Solar Flares and Forbush Decreases

Forbush Decrease		Type IV Solar Flare			
Date 1977	ΔI/I (%)	Date 1977	Active Region	Position	Start UT
Sept. 11	2.5	Sept. 7	14943	N10 E90	(2230)
		8	(14943)	N08 E90	(2244)
		9	14943	N08 E84	(1629)
Sept. 19	?	Sept. 16	14943	N06 W20	(2225)
Sept. 21	4.2	Sept. 19	14943	N08 W57	(1042)
		20	14943	N09 W59	(0250)

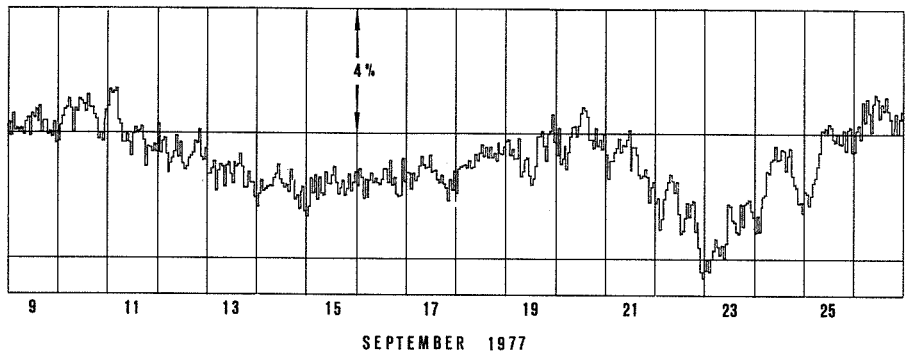

Fig. 1. Plot of the hourly values of the Rome neutron monitor intensity for the period Sept. 9-26, 1977.

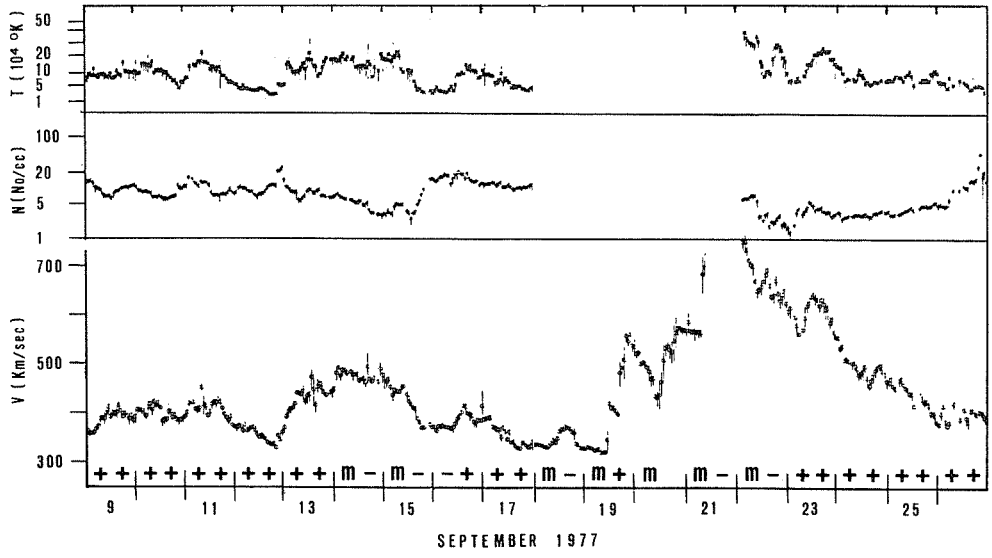

Fig. 2. IMP 7 and 8 solar wind plasma data and the inferred interplanetary magnetic field polarity for the period Sept. 9-26, 1977; m indicates mixed polarity and (+) and (-) denote an interplanetary field directed away from the Sun and toward the Sun, respectively.

The Forbush Decrease of September 20-21. In this case the parent flares were located near W60, and the decreasing phase was formed by subsequent steps. Although measurements of solar wind temperature and density are missing during the event's descending phase, two pronounced and sharp increases in solar wind speed are observed on Sept. 20 and 21. The recovery phase lasted only 3 days.

In the solar wind speed a large fast particle stream, beginning midday on the 19th lasted for the duration of the event. The inferred interplanetary magnetic field polarity changed frequently inside this stream.

Conclusions

During September 1977, a series of flares from McMath region 14943 and accompanied by Type IV radio emissions temporarily depressed the galactic c.r. intensity in a wide region of interplanetary space. The recovery time after each decrease was consistent with the Forbush decrease model derived by Iucci et al. [1977a, b, c, and d], which is briefly summarized here. Whenever an energetic and sufficiently-extended-in-frequency Type IV solar flare occurs, a radially advancing plasma cloud is emitted by the Sun. The sweeping motion of such a perturbation depressed the c.r. intensity over a wide portion of the inner solar system. This modulated region extends from the Sun to the radially-advancing shock wave and follows the interplanetary magnetic field lines. It also corotates with the Sun, and can extend more than 180° in ecliptic longitude. The c.r. intensity inside the modulated region recovers to the unperturbed level with a time constant of ~10 days or until the occurrence of another Type IV solar flare in the same active region. The time behavior of the observed c.r. recovery is mainly due to two combined effects: one accounting for the relative movement of the Earth through the modulated region and the other accounting for the quasi-exponential c.r. recovery inside the disturbed region. The longer recovery times of Forbush decreases associated with Eastern Hemisphere flares and the shorter ones characterizing Western Hemisphere flares agree with this model. For the flare sequence described here the effected region engulfed the Earth between Sept. 11 and Sept. 25-26, thus spanning 200 to 215° of longitude. In addition, the two solar wind streams occurring in the analyzed period were not produced by monopolar cells like coronal holes because of the variability in the interplanetary magnetic field polarity. Their source more likely lay within the intense solar flare activity of McMath plage region No. 14943.

Acknowledgments

This work was supported by the National Research Council of Italy under grant No. 7700902102 - G.I.F.CO.

REFERENCES

IUCCI, N., M. PARISI, M. STORINI and G. VILLORESI — 1977a — A Study of the Forbush Decrease Effect: The Origin and Development in Interplanetary Space, *Internal Report LPS-77-2*, Laboratorio Plasma Spazio, C.N.R. (Rome, Italy).

IUCCI, N., M. PARISI, M. STORINI and G. VILLORESI — 1977b — Type IV Solar Radio Bursts and Forbush Decreases, *Proc. 15th Inter. Cosmic Ray Conference, 3*, 329.

IUCCI, N., M. PARISI, M. STORINI and G. VILLORESI — 1977c — Forbush Decreases not Associated with Type IV Solar Flares in the Visible Hemisphere of the Sun, ibid., 335.

IUCCI, N., S. ORSINI, M. PARISI, M. STORINI and G. VILLORESI — 1977d — The Interplanetary Perturbation Associated with Forbush Decreases, ibid., 341.

SGD — 1977 — *Solar Geophysical Data*, 399 Part I, November 1977, U.S. Department of Commerce (Boulder, Colorado 80303).

SGD — 1978 — *Solar Geophysical Data*, 403 Part I and Part II, March 1978, U.S. Department of Commerce (Boulder, Colorado 80303).

Cosmic Ray Neutron Intensity at Morioka for September 7-27, 1977 and November 20-28, 1977

by

T. Chiba and H. Takahashi
Department of Physics
Iwate University
Morioka, Japan

Ground-based recordings of the neutron component of cosmic rays were made at the Morioka station with a single NM-64 type counter during September 1977 and with two NM-64 type counters during November 1977. The Morioka cosmic ray station lies at geographic coordinates N39.70 E141.13 and at an altitude of 135 m above sea level. Its vertical cutoff rigidity is 10.2 GV and its median rigidity is 41 GV. The counting rates are 2.3 x 10^4/hour for the one-counter monitor and 4.3 x 10^4/hour for the two-counter monitor.

Figure 1 shows the time variations of the hourly values, in percentage, of the neutron intensities for September 7-27, 1977. The digital data for the whole period of September are given in Table 1. In Figure 1, geomagnetic storm sudden commencement observations are also shown in order to indicate the passage of shock fronts over the Earth. A Forbush decrease started around the time of the second ssc and reached its maximum depression about midday on September 22. These observations are almost in accordance with the results given in a paper by Fujii et al. [1978] in which the characteristic features of this Forbush decrease are studied in a wide rigidity range, using data from Japanese cosmic ray stations.

Figure 2 shows the time variations of the hourly values, in percentage, of the neutron intensities for November 20-28, 1977. The digital data for the whole period of November are given in Table 2. As is recognized from the figure, no GLE was observed at Morioka.

REFERENCES

FUJII, Z., K. FUJIMOTO, H. UENO, K. NAGASHIMA, S. MORI, S. YASUE, M. ICHINOSE, M. WADA, K. MURAKAMI, S. KAWASAKI, H. TAKAHASHI, T. CHIBA and N. YAHAGI 1978 Solar-Terrestrial Disturbances Associated with McMath Region 14943--The September 1977 Cosmic Ray Storm Observed in a Wide Rigidity Range, *Solar Terrestrial Environmental Research in Japan, 2,* 55-61.

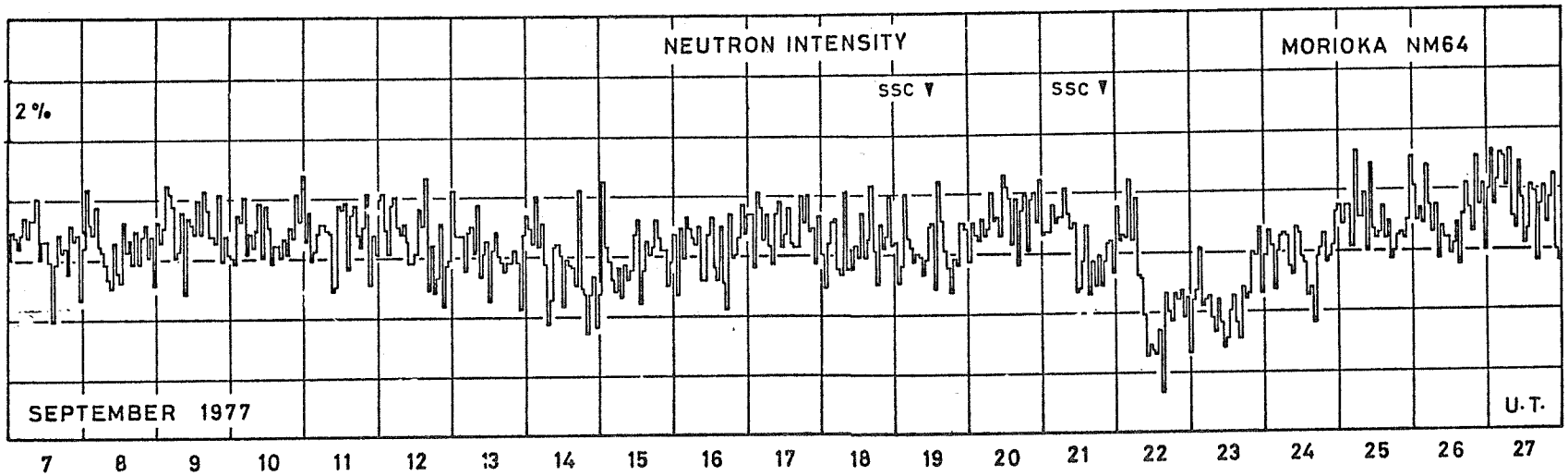

Fig. 1. Time variations of the hourly neutron intensity observed at Morioka, Japan, and expressed as a percentage of the background counting rate.

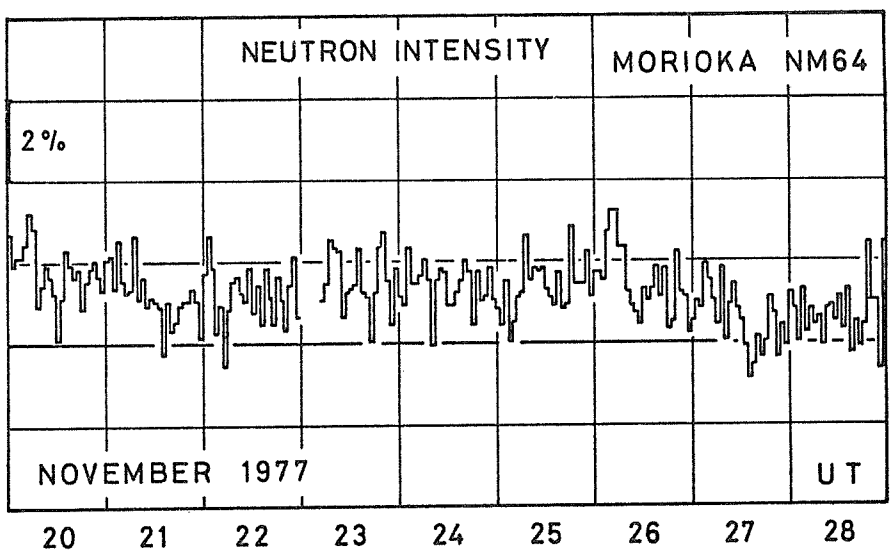

Fig. 2. Time variations of the hourly neutron intensity observed at Morioka, Japan, and expressed as a percentage of the background counting rate. Note the absence of a ground level event in the record on November 22.

Table 1. Morioka, Japan, Hourly Neutron Data for September 1977

Y	M	D	365	1	2	3	4	5	6	7	8	9	10	11	12	13	14	15	16	17	18	19	20	21	22	23	24	SUM	N	MEAN	D
77	9	1	244	367	363	383	365	367	371	352	368	365	372	365	358	367	361	385	382	359	354	369	376	374	353	375	364	8815	24	367.3	1
77	9	2	245	379	357	371	356	372	371	365	364	375	381	360	353	367	359	365	348	360	389	366	372	370	377	357	360	8794	24	366.4	2
77	9	3	246	365	339	368	379	999	999	999	354	370	356	356	369	368	362	364	358	358	364	378	376	376	372	368	360	7660	21	364.8	3
77	9	4	247	366	361	363	368	362	366	359	374	358	377	367	366	360	374	378	365	367	374	365	363	372	365	368	383	8821	24	367.5	4
77	9	5	248	375	378	373	369	382	357	375	373	370	378	352	363	357	370	369	354	351	359	364	382	367	371	374	365	8828	24	367.8	5
77	9	6	249	363	363	371	377	376	380	363	372	372	374	358	365	375	371	361	362	381	364	355	367	355	379	352	367	8823	24	367.6	6
77	9	7	250	360	369	367	365	368	374	367	373	373	380	360	366	366	359	339	358	368	362	363	355	371	366	368	346	8743	24	364.3	7
77	9	8	251	363	383	371	368	377	364	362	358	353	350	365	355	352	372	362	366	358	369	358	367	371	360	367	351	8722	24	363.4	8
77	9	9	252	372	365	370	384	381	377	360	362	375	348	373	371	368	379	368	382	376	367	367	365	381	359	367	361	8878	24	369.9	9
77	9	10	253	360	358	374	372	380	361	368	363	369	378	360	377	370	358	364	364	360	366	361	370	366	381	372	387	8839	24	368.3	10
77	9	11	254	365	375	359	362	368	371	371	369	368	349	350	377	376	378	356	374	377	367	363	370	381	351	367	361	8805	24	366.9	11
77	9	12	255	379	381	369	361	377	380	370	367	371	365	358	358	361	376	370	386	349	364	348	353	371	343	357	359	8773	24	365.5	12
77	9	13	256	382	367	367	367	355	368	370	361	377	353	361	365	345	362	368	360	358	355	358	358	362	358	342	367	8686	24	361.9	13
77	9	14	257	373	369	364	380	363	371	357	337	345	363	364	360	343	359	357	356	350	382	349	347	334	347	353	336	8559	24	356.6	14
77	9	15	258	347	385	363	358	352	348	356	346	357	352	355	367	372	344	355	365	360	363	372	366	362	362	350	358	8615	24	359.0	15
77	9	16	259	367	347	369	359	373	369	366	364	370	352	352	367	373	356	352	370	351	342	374	359	360	366	377	367	8702	24	362.6	16
77	9	17	260	374	374	356	381	376	365	374	363	357	374	378	363	367	376	364	363	363	380	371	380	368	369	357	373	8866	24	369.4	17
77	9	18	261	360	349	364	371	372	355	353	381	355	362	355	363	359	374	359	365	383	361	350	370	362	366	379	363	8731	24	363.8	18
77	9	19	262	364	350	356	370	365	362	357	360	359	353	358	369	370	348	384	371	361	355	347	358	356	370	370	368	8681	24	361.7	19
77	9	20	263	357	370	366	364	371	366	368	380	371	372	366	386	382	378	363	378	356	374	379	361	378	380	370	384	8920	24	371.7	20
77	9	21	264	366	367	367	376	370	372	372	381	373	368	370	347	348	357	369	346	357	349	359	349	357	363	364	353	8700	24	362.5	21
77	9	22	265	375	364	366	365	384	364	378	352	351	339	325	329	327	326	334	313	346	340	337	346	344	347	338	345	8335	24	347.3	22
77	9	23	266	326	344	347	361	342	344	345	339	333	344	336	328	331	340	345	336	331	348	344	346	360	359	368	346	8242	24	343.4	23
77	9	24	267	359	367	362	347	360	365	366	365	355	352	368	366	358	356	345	348	336	358	361	366	356	358	362	373	8609	24	358.7	24
77	9	25	268	375	369	375	375	361	393	371	371	379	360	389	367	364	366	375	364	370	357	360	365	366	364	370	391	8897	24	370.7	25
77	9	26	269	381	370	374	369	388	375	366	375	357	368	364	364	359	362	369	355	372	382	374	366	391	375	382	360	8898	24	370.8	26
77	9	27	270	380	393	375	383	392	391	381	393	371	367	389	377	362	367	381	379	356	375	381	369	377	385	360	356	9040	24	376.7	27
77	9	28	271	359	384	365	371	359	364	369	367	360	356	373	376	372	380	372	381	365	379	362	392	373	366	379	364	8888	24	370.3	28
77	9	29	272	374	362	353	367	353	362	372	382	376	368	373	375	395	379	365	374	379	381	372	368	367	372	368	383	8920	24	371.7	29
77	9	30	273	999	999	999	999	999	999	999	999	999	999	999	999	999	999	999	999	999	999	999	999	999	999	999	999	0	0	999.0	30

NOTE: For the Morioka cosmic ray station the geographic coordinates = N39.70 E141.13; altitude = 135.0 m; instrument = 1-NM64 neutron monitor; vertical cutoff rigidity = 10.16 GV; standard pressure = 995.5 mb; coefficient = -0.700%/mb; and counting rate = 24000/hour. Each tabulated entry = $10^3[\ln(\text{counts}/16/10^3)]$ in units of 0.1% and has been corrected for the barometric effect; 999 stands for no observation.

Table 2. Morioka, Japan Hourly Neutron Data for November 1977

Y	M	D	365	1	2	3	4	5	6	7	8	9	10	11	12	13	14	15	16	17	18	19	20	21	22	23	24	SUM	N	MEAN	D
77	11	1	305	362	372	374	379	362	355	369	356	362	374	365	375	365	370	371	342	370	362	362	353	385	371	380	394	8830	24	367.9	1
77	11	2	306	404	380	369	379	362	377	371	359	380	362	371	375	370	375	379	375	363	371	372	379	377	388	367	356	8961	24	373.4	2
77	11	3	307	373	374	394	374	372	383	361	375	367	394	374	360	379	373	376	374	387	361	380	367	366	363	387	390	9004	24	375.2	3
77	11	4	308	385	385	375	405	394	387	392	375	345	368	379	360	379	381	382	383	370	391	364	382	374	384	391	379	9110	24	379.6	4
77	11	5	309	383	386	398	372	385	382	388	369	384	392	389	374	378	378	377	397	386	390	359	383	382	385	396	378	9191	24	383.0	5
77	11	6	310	391	391	386	383	381	388	381	392	398	359	379	372	383	375	375	380	391	388	391	366	382	377	378	392	9179	24	382.5	6
77	11	7	311	370	386	383	378	386	377	378	395	393	380	378	375	387	370	381	376	377	379	398	381	384	375	374	377	9138	24	380.8	7
77	11	8	312	379	384	402	381	382	366	390	377	367	366	360	358	383	382	380	380	390	377	365	376	371	383	381	367	9047	24	377.0	8
77	11	9	313	413	400	386	377	392	390	385	384	391	391	399	384	384	371	402	383	379	376	379	381	372	403	363	373	9258	24	385.8	9
77	11	10	314	391	393	380	398	375	388	383	402	386	385	387	378	381	367	383	402	390	373	382	381	380	384	389	384	9242	24	385.1	10
77	11	11	315	391	391	391	391	385	391	388	386	395	394	354	379	372	383	390	394	392	380	377	385	386	378	384	378	9235	24	384.8	11
77	11	12	316	999	999	999	999	999	999	999	999	999	999	999	999	999	999	999	999	999	999	999	999	999	999	999	999	0	0	999.0	12
77	11	13	317	999	999	999	999	999	999	999	999	999	999	999	999	999	999	999	999	999	999	999	999	999	999	999	999	0	0	999.0	13
77	11	14	318	374	380	379	380	373	376	383	380	387	370	372	382	371	384	372	369	379	375	369	369	362	380	372	381	9019	24	375.8	14
77	11	15	319	372	375	377	382	370	370	367	390	382	384	376	377	370	367	379	363	373	368	374	362	382	367	364	371	8962	24	373.4	15
77	11	16	320	373	365	384	382	380	376	380	372	365	364	385	374	361	373	369	370	376	366	357	368	349	371	365	370	8895	24	370.6	16
77	11	17	321	379	367	362	365	371	360	371	370	360	366	359	376	373	376	378	368	364	374	360	360	378	370	362	381	8850	24	368.8	17
77	11	18	322	375	373	375	379	381	363	371	381	367	367	375	387	366	382	372	369	372	366	368	383	365	386	366	371	8960	24	373.3	18
77	11	19	323	367	369	364	375	367	360	368	372	364	374	370	371	374	380	376	382	383	373	370	374	369	373	377	386	8938	24	372.4	19
77	11	20	324	387	379	381	381	384	392	388	369	374	379	376	372	361	371	383	379	376	378	368	365	378	380	376	373	9050	24	377.1	20
77	11	21	325	380	381	373	385	375	372	373	386	371	376	369	371	370	369	357	370	363	365	369	370	370	373	370	361	8919	24	371.6	21
77	11	22	326	377	386	378	362	369	354	368	375	376	372	370	378	367	374	364	378	371	364	376	370	363	374	381	366	8913	24	371.4	22
77	11	23	327	999	999	999	999	999	370	374	385	383	382	366	372	373	374	385	372	371	360	372	383	387	375	364	378	7124	19	374.9	23
77	11	24	328	371	369	383	374	374	376	380	375	359	375	378	377	369	369	372	375	380	377	364	377	370	371	378	370	8963	24	373.5	24
77	11	25	329	368	364	375	360	365	371	372	386	375	378	377	378	373	371	369	377	368	369	388	374	374	374	382	371	8959	24	373.3	25
77	11	26	330	377	377	375	387	392	392	383	383	372	369	367	364	373	370	373	378	371	378	363	365	382	372	371	362	8996	24	374.8	26
77	11	27	331	365	370	368	379	375	370	364	378	360	369	374	368	365	359	351	354	361	356	360	371	367	356	364	359	8763	24	365.1	27
77	11	28	332	372	368	360	373	362	368	364	366	359	368	369	365	371	363	373	357	365	359	364	384	370	370	353	384	8807	24	367.0	28
77	11	29	333	374	375	365	383	371	373	357	364	353	355	365	375	367	374	363	369	371	374	361	358	368	362	362	372	8811	24	367.1	29
77	11	30	334	364	368	362	378	366	370	370	379	380	364	360	365	363	371	358	373	355	365	357	367	374	368	374	371	8822	24	367.6	30

NOTE: For the Morioka cosmic ray station the geographic coordinates = N39.70 E141.13; altitude = 135.0 m; instrument = 1-NM64 neutron monitor; vertical cutoff rigidity = 10.16 GV; standard pressure = 995.5 mb; coefficient = -0.700%/mb; and counting rate = 24000/hour. Each tabulated entry = 10^3[ln (counts;16/10^3)] in units of 0.1% and has been corrected for the barometric effect; 999 stands for no observation.

The September 1977 Cosmic Ray Storm Observed at Misato Underground Station

by

S. Mori, S. Yasue and M. Ichinose
Department of Physics, Shinshu University
Matsumoto, Japan

The Forbush decrease in cosmic ray intensity during September 21-24, 1977, that was associated with McMath plage region 14943, is reported as observed at Misato underground station in Japan. Geographically the station lies at coordinates N36.2 E137.83 and geomagnetically at N25.7 E203.6. The observatory has an altitude of 735 m, a cutoff rigidity of 11.39 GV and a water equivalent depth of 34 m. In Table 1 we summarize some details of the Misato muon telescope [Mori et al., 1976].

Table 1. Characteristics of the Misato Underground Muon Telescope

Component	Center Direction of View		Counts	Median Rigidity	Effective
	Azimuth	Zenith Angle	(10^4/h)	(GV)	Depth(m)
V	Vertical		28	145	57
N	NNE	33°	10.7	155	60
S	SSW	33	10.7	155	60
E	ESE	33	14.2	142	56
W	WNW	33	9.8	156	61
WT	Vertical		96	145	60

Figure 1 shows the hourly values of cosmic ray intensity recorded between September 12 and October 8, 1977. They are displayed for five directional components (V, N, S, E, and W), including WT which represents a two-fold coincidence between two layers of 16 scintillator detectors. Each of these layers covers 1 m^2 of area and 153 cm separates them vertically.

The magnitude of the maximum depression, which occurred around midday on September 22, was about 0.3% for the WT component [Fujii et al., 1978]. Note that this Forbush decrease was accompanied by pronounced anisotropic intensity variations.

REFERENCES

FUJII, Z., K. FUJIMOTO, H. UENO, K. NAGASHIMA, S. MORI, S. YASUE, M. ICHINOSE, M. WADA, K. MURAKAMI, S. KAWASAKI, H. TAKAHASHI, T. CHIBA and N. YAHAGI 1978 The September 1977 Cosmic Ray Storm Observed in a Wide Rigidity Range, *Solar Terr. Environ. Res., Japan, 2,* 55-61.

MORI, S., S. YASUE, M. ICHINOSE, S. SAGISAKA, S. AKAHANE and K. CHINO 1976 Mosato Underground Observatory of Shinshu University, *Proc. Int. Cosmic Ray Symp.*, Tokyo, Japan, 78-84.

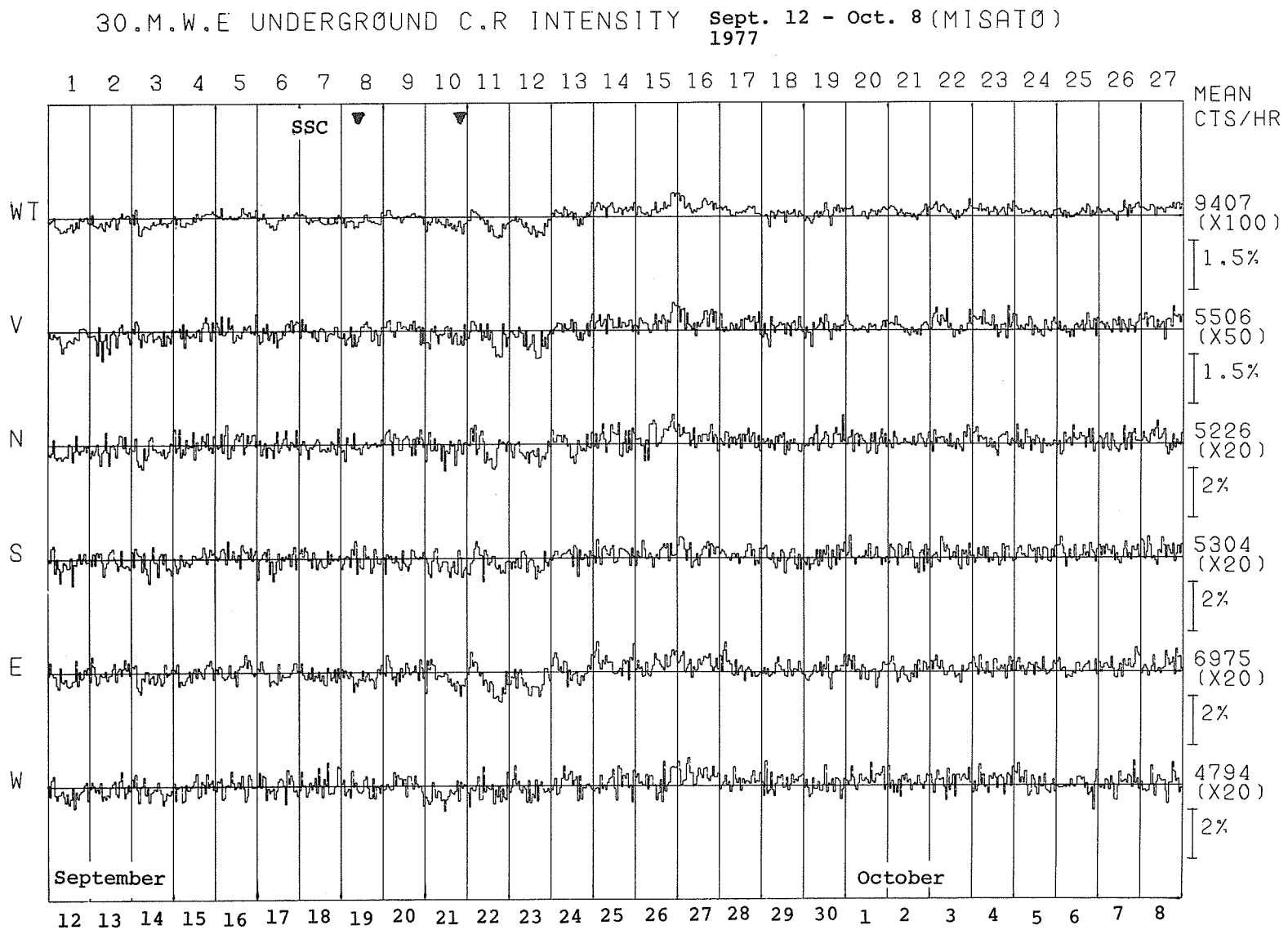

Fig. 1. The 30-m, water-equivalent-depth, underground cosmic ray intensity as a function of UT observed at Misato, Japan, during the period Sept. 12- Oct. 8, 1977. The mean cts/h for five directional components plus a vertical coincidence component are shown. Numbers along the top of the figure denote days within Bartels Rotations No. 1970 and 1971.

Multidirectional Meson Intensities at Nagoya and at Sakashita Underground Station During September 16-30, 1977

by

Z. Fujii, K. Fujimoto, S. Sakakibara, H. Ueno and K. Nagashima
Cosmic Ray Research Laboratory, Nagoya University
Chikusa-ku, Nagoya, Japan 464

A remarkable cosmic ray storm occurred on September 22, 1977, during the activity associated with McMath plage region 14943. In this communication, we report cosmic ray intensity data observed by the Nagoya multidirectional meson telescope [Sekido et al. 1975] and the Sakashita underground telescope (see Table 1) during September 16 to 30, 1977.

In Figure 1 the pressure-corrected hourly values of cosmic ray intensities recorded between the 16th and 30th of September 1977 are displayed for 13 directions monitored by the Nagoya instrument and for the vertical direction observed at Sakashita. In the Figure observations of geomagnetic storm sudden commencements (ssc) are also shown to indicate passages of shock fronts over the Earth at 1142 UT on the 19th and at 2045 UT on the 21st. The cosmic ray storm started about the same time as the second ssc and reached a maximum depression at about midday on September 22. The magnitude of the depression was about 2% for the vertical telescope at Nagoya and decreased with increasing telescope median rigidity. The decrease is not visible in the intensity variations of the Sakashita telescope, which has a primary median rigidity of about 340 GV [Fujimoto et al., 1976]. Note, too, in Figure 1 that the Forbush decrease is accompanied by a pronounced anisotropic intensity variation. The pressure-corrected hourly values are listed in Table 2 for five representative components of Nagoya multidirectional telescope.

To investigate the rigidity dependence of the Forbush decrease, we defined the intensity levels before the decrease to be the intensities averaged over the period September 16 to 20. The intensities averaged for the 24-h period 1200 UT on the 22nd to 1200 UT on the 23rd were derived, and the amounts of intensity depression were denoted as the difference between the averaged and the recorded levels. Assuming a power law spectrum with an upper cutoff rigidity for the variational spectrum of the Forbush decrease, we made the best fit between the observed and the expected intensities. Figure 2 shows our results. It demonstrates that the exponent of the spectral parameter lies close to -1.0 and that the upper cutoff rigidity is less than 100 GV.

To examine the anisotropy associated with the September 22-23 Forbush decrease, differences between intensities measured along two separate directions were computed and plotted in Figure 3 for four representative pairs of directions: vertical and 30° east, 30° west and 30° east, 30° north and 30° east, and 30° south and 30° east. Figure 3 clearly illustrates that the enhanced daily variation appears with the onset of the Forbush decrease and exists for several days, decaying with the recovery of the Forbush decrease. A preliminary analysis shows that the enhanced diurnal variation was due to a flow from about the 1700-h direction. The amplitude of flow was about one order of magnitude larger than that of the steady state on September 22--the day on which most enhanced diurnal variations occurred.

Figure 4 shows the hourly values of the second-order differences G and GG, which are defined from the directional intensities as indices that reflect mainly intensity variations of north-south asymmetry [Nagashima et al., 1972]. Note that the pronounced variations of these two indices occurred during September 21 to 23 and thus displayed a different time profile from the daily variations shown in Figure 1. It may indicate a north-south asymmetry increase associated with the Forbush decrease. Further analysis of diurnal variation as well as north-south asymmetry may yield information on cosmic ray flow in interplanetary space during the Forbush decrease.

REFERENCES

FUJIMOTO, K., K. MURAKAMI, I. KONDO, and K. NAGASHIMA — 1976 — Coupling Coefficients of Cosmic Ray Variation for Underground Muon Telescopes *Proc. Int. Cosmic Ray Symposium on High Energy Modulation, 60.*

NAGASHIMA, K., K. FUJIMOTO, Z. FUJII, H. UENO, and I. KONDO — 1972 — Three-Dimensional Cosmic Ray Anisotropy in Interplanetary Space, Part IV-Origin of Solar Semi-diurnal Variation *Rep. Ionos. Space Res., Japan, 26,* 31.

SEKIDO, Y. K. NAGASHIMA, I. KONDO, H. UENO, K. FUJIMOTO, and Z. FUJII — 1975 — Multi-Directional Cosmic-Ray Intensities, Nagoya, 1970-1973 *Rep. Cosmic-Ray Res. Lab., No. 2,* Nagoya Univ., Nagoya, Japan.

Table 1. Characteristics of Nagoya multi-directional meson telescope and Sakashita underground telescope.

Station	Component	Direction	Cutoff Rigidity Pc(GV)	Counting Rate $N \cdot 10^6/h$	Standard Error	Barometric Coefficient -B (%/mb)	Primary Median Rigidity GV
Nagoya	V	Vertical	11.5	2.7	0.06	0.12	61.5
	N	North 30°	13.2	1.2	0.09	0.12	66.9
	E	East 30°	16.6				68.7
	S	South 30°	11.3				65.2
	W	West 30°	9.4				64.4
	NE	North-East 39°	17.7	0.57	0.13	0.12	74.4
	ES	East-South 39°	14.9				72.2
	SW	South-West 39°	9.3				68.7
	WN	West-North 39°	11.1				69.7
	NN	Far-North 49°	13.5	0.47	0.14	0.12	84.0
	EE	Far-East 49°	20.7				88.4
	SS	Far-South 49°	11.0				82.1
	WW	Far-West 49°	9.4				81.1
	NNN	Three-North 55°	10.7	0.13	0.28	0.15	111.
	EEE	Three-East 55°	23.4				118.
	SSS	Three-South 55°	10.9				109.
	WWW	Three-West 55°	8.4				108.
Sakashita Under-ground (80 MWE)	V	Vertical	11.5	0.12	0.29	0.03	340

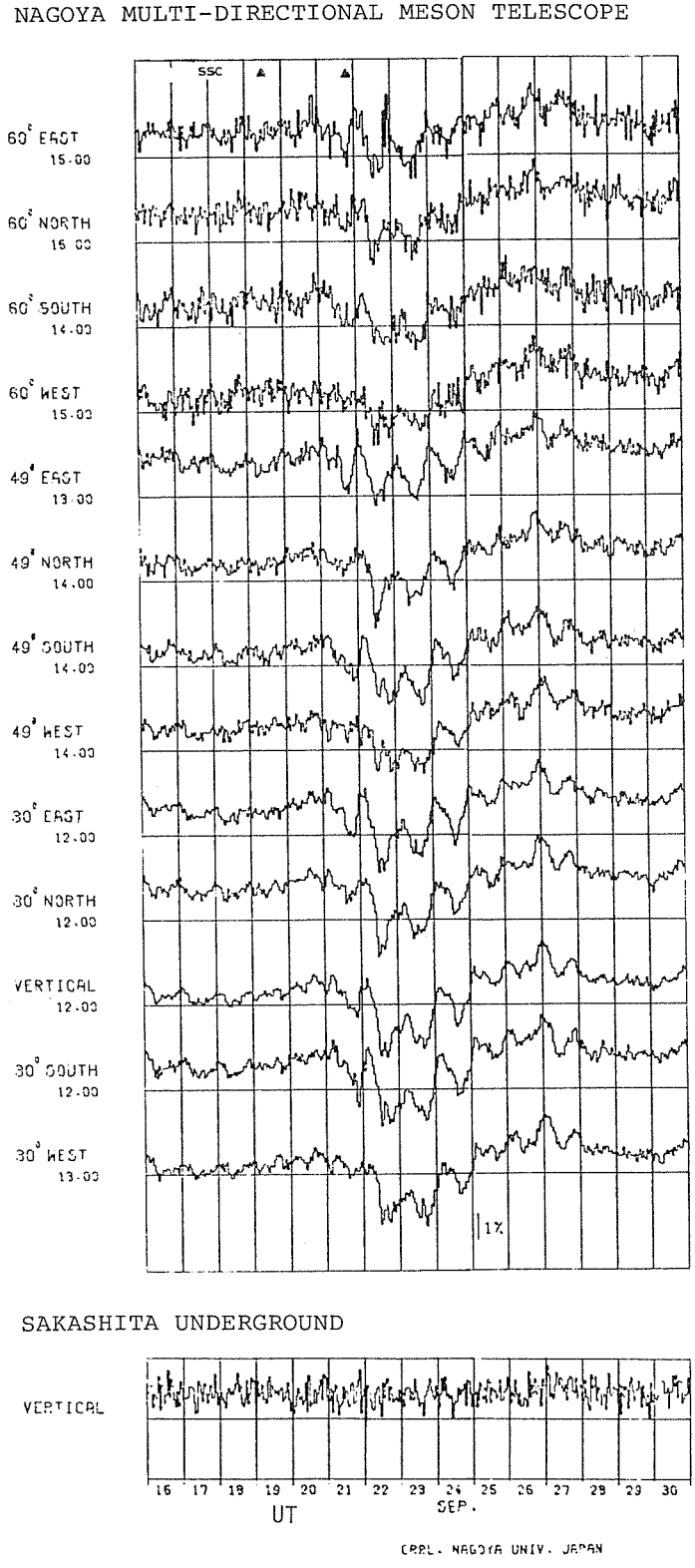

Fig. 1. The pressure corrected hourly values of cosmic ray intensity observed by Nagoya multi-directional meson telescope and Sakashita underground telescope during September 16 to 30, 1977.

Table 2. Pressure-corrected hourly data of cosmic-ray meson intensities observed by Nagoya multi-directional meson telescope in Universal Time during September 16 to 30, 1977. Tabulated values are in units of 0.01% by natural logarithmic representation. Components; Vertical, 30°East, 30°West, 30°South and 30°North.

NAGOYA VERTICAL

DAY OF YR	MN	HOUR(U.T.) 0 - 1	1 - 2	2 - 3	3 - 4	4 - 5	5 - 6	6 - 7	7 - 8	8 - 9	9 - 10	10 - 11	11 - 12	12 - 13	13 - 14	14 - 15	15 - 16	16 - 17	17 - 18	18 - 19	19 - 20	20 - 21	21 - 22	22 - 23	23 - 24	MEAN	N
259	16	1274	1265	1263	1258	1252	1241	1221	1205	1211	1215	1220	1234	1228	1223	1228	1234	1231	1220	1229	1229	1237	1241	1248	1241	12353	24
260	17	1258	1253	1240	1240	1235	1210	1212	1202	1211	1202	1208	1223	1209	1207	1196	1205	1223	1209	1218	1220	1221	1229	1232	1242	12210	24
261	18	1232	1238	1236	1235	1232	1212	1206	1194	1200	1193	1214	1217	1212	1212	1202	1210	1231	1228	1238	1240	1236	1243	1239	1232	12222	24
262	19	1216	1214	1221	1229	1230	1234	1231	1246	1228	1235	1237	1229	1229	1249	1249	1254	1248	1251	1216	1232	1228	1236	1235	1244	12342	24
263	20	1255	1253	1259	1258	1274	1264	1256	1261	1244	1243	1238	1270	1270	1273	1281	1297	1293	1292	1276	1267	1274	1272	1262	1244	12657	24
264	21	1234	1245	1268	1295	1296	1291	1278	1241	1234	1246	1228	1238	1243	1216	1185	1192	1186	1185	1188	1177	1157	1179	1241	1257	12292	24
265	22	1248	1249	1252	1285	1256	1238	1220	1209	1187	1155	1110	1048	1028	1047	1072	1043	1024	1045	1070	1104	1110	1123	1111	1126	11400	24
266	23	1102	1113	1130	1145	1163	1166	1158	1140	1119	1088	1071	1068	1079	1096	1087	1085	1052	1061	1083	1085	1122	1143	1179	1190	11135	24
267	24	1209	1238	1251	1253	1244	1237	1226	1230	1226	1232	1214	1205	1187	1144	1124	1133	1137	1151	1174	1197	1195	1207	1211	1235	12025	24
268	25	1269	1304	1324	1296	1292	1287	1283	1294	1307	1304	1295	1290	1284	1267	1269	1266	1260	1273	1270	1279	1286	1316	1323	1343	12909	24
269	26	1333	1340	1331	1329	1325	1316	1297	1300	1285	1305	1316	1330	1332	1341	1326	1308	1327	1328	1323	1334	1368	1393	1390	1405	13326	24
270	27	1399	1390	1391	1373	1362	1332	1319	1318	1300	1287	1289	1294	1303	1293	1317	1319	1336	1340	1347	1347	1342	1339	1318	1298	13314	24
271	28	1306	1290	1289	1287	1293	1276	1271	1272	1269	1280	1266	1281	1277	1287	1293	1284	1295	1282	1268	1270	1270	1274	1282	1270	12805	24
272	29	1266	1260	1263	1264	1269	1275	1274	1285	1295	1265	1270	1278	1258	1271	1288	1279	1258	1265	1256	1265	1268	1285	1257	1271	12702	24
273	30	1259	1241	1257	1249	1254	1257	1268	1280	1285	1281	1273	1269	1275	1271	1277	1282	1277	1283	1297	1300	1304	1321	1314	1310	12785	24

NAGOYA 30 DEG. EAST

DAY OF YR	MN	HOUR(U.T.) 0 - 1	1 - 2	2 - 3	3 - 4	4 - 5	5 - 6	6 - 7	7 - 8	8 - 9	9 - 10	10 - 11	11 - 12	12 - 13	13 - 14	14 - 15	15 - 16	16 - 17	17 - 18	18 - 19	19 - 20	20 - 21	21 - 22	22 - 23	23 - 24	MEAN	N
258	15	1317	1279	1289	1270	1266	1254	1262	1249	1261	1250	1257	1260	1280	1272	1268	1294	1309	1321	1322	1328	1322	1330	1334	1317	12888	24
259	16	1330	1320	1309	1298	1282	1292	1264	1264	1275	1292	1283	1282	1293	1294	1296	1302	1287	1283	1281	1299	1303	1298	1301	1298	12928	24
260	17	1309	1300	1276	1288	1276	1250	1267	1252	1269	1255	1260	1265	1262	1258	1261	1262	1259	1276	1284	1278	1272	1282	1285	1285	12721	24
261	18	1290	1295	1265	1262	1253	1250	1234	1248	1244	1245	1264	1267	1275	1246	1238	1269	1287	1282	1280	1282	1282	1262	1292	1294	12669	24
262	19	1258	1277	1259	1271	1270	1269	1277	1283	1273	1259	1253	1279	1274	1290	1268	1293	1281	1290	1253	1279	1279	1285	1296	1287	12764	24
263	20	1307	1290	1304	1321	1300	1302	1283	1296	1288	1313	1305	1305	1303	1321	1344	1331	1343	1325	1304	1313	1325	1320	1307	1302	13105	24
264	21	1302	1338	1354	1341	1339	1294	1282	1281	1270	1285	1288	1286	1289	1274	1229	1216	1196	1211	1199	1193	1204	1258	1265	1334	12720	24
265	22	1330	1325	1324	1353	1311	1252	1248	1223	1226	1188	1157	1111	1074	1120	1115	1079	1107	1113	1154	1185	1194	1196	1201	1189	11990	24
266	23	1188	1216	1211	1249	1248	1218	1216	1202	1192	1157	1137	1139	1182	1138	1133	1140	1125	1158	1180	1176	1222	1233	1275	1293	11928	24
267	24	1316	1322	1302	1305	1286	1288	1273	1284	1260	1266	1252	1225	1215	1193	1162	1181	1205	1231	1249	1256	1271	1291	1308	1351	12622	24
268	25	1362	1356	1327	1336	1328	1332	1323	1347	1338	1325	1329	1308	1292	1302	1301	1312	1307	1300	1317	1335	1352	1375	1382	1374	13317	24
269	26	1370	1366	1357	1358	1348	1373	1369	1368	1363	1353	1359	1370	1367	1360	1360	1364	1374	1379	1405	1404	1406	1429	1445	1435	13784	24
270	27	1418	1405	1416	1391	1370	1373	1333	1332	1330	1331	1337	1331	1347	1350	1374	1373	1373	1386	1376	1391	1375	1373	1339	1344	13653	24
271	28	1351	1347	1344	1355	1336	1326	1318	1324	1297	1320	1301	1321	1341	1351	1343	1345	1342	1323	1334	1334	1319	1319	1320	1300	13296	24
272	29	1323	1321	1304	1290	1307	1337	1323	1337	1327	1316	1296	1319	1300	1306	1299	1317	1331	1301	1313	1292	1312	1303	1319	1311	13127	24
273	30	1293	1294	1305	1292	1303	1300	1311	1316	1324	1313	1302	1294	1301	1305	1330	1330	1335	1346	1334	1347	1353	1362	1344	1336	13196	24

Table 2 (Continued)

NAGOYA 30 DEG. WEST

DAY OF YR	MN	HOUR(U.T.) 0	1	2	3	4	5	6	7	8	9	10	11	12	13	14	15	16	17	18	19	20	21	22	23	24	MEAN	N
259	16	1365	1360	1341	1348	1355	1330	1311	1304	1279	1303	1298	1315	1312	1319	1318	1314	1297	1297	1323	1319	1321	1303	1330	1333	13206	24
260	17	1329	1329	1327	1313	1334	1321	1304	1304	1283	1295	1288	1302	1309	1315	1293	1303	1300	1302	1316	1308	1311	1315	1331	1328	13108	24
261	18	1333	1320	1334	1310	1329	1338	1304	1300	1286	1286	1304	1297	1315	1306	1307	1313	1332	1327	1332	1322	1339	1326	1339	1344	13185	24
262	19	1340	1316	1302	1312	1321	1330	1332	1330	1320	1305	1327	1323	1325	1347	1361	1357	1365	1357	1317	1327	1348	1315	1338	1332	13311	24
263	20	1339	1346	1359	1347	1357	1356	1347	1346	1337	1338	1313	1337	1357	1345	1371	1386	1377	1355	1370	1362	1368	1354	1339	1352	13524	24
264	21	1330	1316	1298	1342	1343	1361	1351	1359	1341	1340	1320	1333	1324	1317	1284	1299	1294	1303	1318	1308	1308	1321	1338	1321	13237	24
265	22	1314	1296	1304	1332	1317	1326	1302	1308	1277	1269	1188	1132	1147	1178	1180	1197	1149	1140	1176	1206	1174	1198	1193	1216	12300	24
266	23	1208	1217	1211	1235	1233	1226	1244	1240	1219	1203	1172	1170	1153	1155	1215	1194	1159	1126	1163	1165	1196	1191	1242	1242	11991	24
267	24	1253	1295	1295	1334	1325	1335	1294	1304	1316	1306	1312	1301	1279	1270	1271	1231	1231	1248	1247	1268	1269	1287	1293	1304	12862	24
268	25	1309	1346	1399	1384	1379	1381	1360	1355	1369	1377	1366	1382	1391	1390	1382	1369	1340	1349	1365	1373	1367	1372	1400	1391	13707	24
269	26	1415	1425	1404	1424	1431	1437	1417	1415	1382	1371	1365	1385	1383	1412	1395	1392	1402	1389	1406	1443	1436	1469	1474	1483	14148	24
270	27	1490	1483	1484	1481	1452	1450	1436	1419	1395	1401	1384	1377	1378	1378	1401	1408	1421	1416	1429	1443	1431	1431	1428	1417	14264	24
271	28	1389	1388	1366	1366	1386	1371	1375	1358	1368	1381	1393	1367	1372	1362	1384	1377	1385	1385	1367	1368	1371	1363	1366	1356	13735	24
272	29	1365	1355	1355	1357	1383	1359	1347	1368	1366	1356	1356	1354	1359	1335	1358	1374	1348	1370	1349	1343	1376	1360	1374	1353	13592	24
273	30	1339	1362	1360	1352	1331	1329	1329	1361	1360	1373	1360	1369	1373	1355	1381	1370	1387	1388	1380	1381	1408	1403	1399	1399	13687	24

NAGOYA 30 DEG. SOUTH

DAY OF YR	MN	HOUR(U.T.) 0	1	2	3	4	5	6	7	8	9	10	11	12	13	14	15	16	17	18	19	20	21	22	23	24	MEAN	N
259	16	1328	1322	1305	1299	1302	1269	1243	1265	1237	1278	1251	1269	1270	1271	1272	1274	1297	1276	1284	1259	1277	1278	1295	1282	12793	24
260	17	1291	1296	1306	1284	1291	1272	1257	1245	1268	1257	1245	1240	1251	1261	1265	1240	1245	1256	1259	1269	1260	1268	1265	1292	12660	24
261	18	1294	1290	1285	1274	1285	1264	1240	1252	1241	1251	1250	1257	1246	1258	1254	1258	1262	1277	1274	1288	1298	1300	1272	1285	12690	24
262	19	1269	1269	1276	1290	1272	1265	1284	1286	1273	1280	1270	1271	1272	1280	1295	1306	1291	1289	1253	1276	1266	1279	1280	1314	12794	24
263	20	1304	1303	1302	1319	1296	1310	1293	1316	1295	1283	1284	1301	1314	1306	1320	1307	1325	1330	1312	1307	1297	1311	1327	1322	13077	24
264	21	1309	1299	1320	1332	1362	1324	1343	1287	1274	1273	1278	1294	1285	1286	1253	1243	1232	1213	1251	1226	1158	1141	1206	1254	12685	24
265	22	1289	1260	1329	1338	1318	1310	1277	1250	1219	1208	1180	1127	1077	1096	1157	1147	1110	1085	1099	1091	1119	1142	1140	1153	11884	24
266	23	1134	1151	1152	1192	1199	1200	1189	1188	1169	1151	1139	1141	1123	1129	1144	1127	1112	1095	1098	1124	1158	1167	1200	1246	11553	24
267	24	1267	1304	1309	1308	1314	1290	1282	1267	1256	1266	1258	1245	1235	1218	1175	1181	1181	1186	1215	1232	1223	1256	1257	1268	12497	24
268	25	1290	1335	1368	1367	1354	1328	1337	1344	1344	1347	1340	1320	1348	1323	1298	1302	1313	1301	1309	1313	1320	1353	1365	1373	13330	24
269	26	1394	1389	1379	1393	1378	1358	1341	1350	1352	1343	1356	1356	1368	1364	1379	1359	1361	1379	1393	1378	1392	1400	1442	1434	13766	24
270	27	1430	1418	1417	1401	1415	1397	1353	1341	1313	1314	1302	1314	1312	1309	1338	1351	1365	1352	1351	1387	1391	1396	1353	1339	13608	24
271	28	1332	1357	1330	1336	1312	1314	1308	1290	1297	1316	1321	1285	1299	1311	1332	1355	1332	1330	1318	1309	1309	1330	1311	1309	13185	24
272	29	1309	1305	1319	1303	1300	1303	1290	1319	1341	1318	1315	1298	1292	1311	1310	1317	1315	1319	1310	1322	1312	1304	1304	1309	13102	24
273	30	1322	1307	1299	1301	1291	1282	1315	1312	1302	1309	1296	1312	1320	1330	1314	1324	1310	1319	1335	1336	1350	1345	1357	1339	13178	24

Table 2 (Continued)

NAGOYA 30 DEG. NORTH

DAY OF YR	MN	HOUR (U.T.) 0 -	1 -	2 -	3 -	4 -	5 -	6 -	7 -	8 -	9 -	10 -	11 -	12 -	13 -	14 -	15 -	16 -	17 -	18 -	19 -	20 -	21 -	22 -	23 -	24	MEAN	N
259	16	1350	1328	1322	1322	1301	1279	1268	1286	1273	1309	1311	1311	1291	1307	1296	1294	1278	1302	1316	1319	1310	1311	1332	1311	13061	24
260	17	1340	1310	1308	1291	1305	1287	1279	1279	1267	1281	1284	1298	1288	1290	1264	1284	1286	1278	1294	1296	1299	1296	1312	1325	12934	24
261	18	1317	1314	1311	1307	1291	1265	1269	1260	1303	1274	1289	1290	1278	1291	1271	1292	1299	1305	1304	1293	1318	1310	1326	1308	12952	24
262	19	1307	1281	1281	1307	1321	1302	1287	1301	1285	1274	1286	1297	1301	1316	1319	1332	1323	1310	1297	1297	1288	1317	1323	1311	13026	24
263	20	1331	1328	1329	1330	1326	1333	1327	1334	1331	1330	1330	1342	1339	1364	1371	1361	1349	1335	1349	1342	1339	1324	1297	1295	13348	24
264	21	1308	1343	1367	1360	1345	1321	1308	1315	1311	1299	1302	1314	1310	1310	1252	1267	1283	1260	1294	1285	1280	1305	1328	1329	13082	24
265	22	1324	1311	1320	1335	1316	1314	1287	1280	1251	1223	1142	1076	1085	1116	1111	1100	1128	1180	1198	1195	1213	1204	1228	1221	12149	24
266	23	1199	1221	1213	1244	1253	1244	1216	1198	1186	1164	1135	1154	1149	1179	1163	1154	1164	1161	1174	1194	1204	1230	1283	1276	11983	24
267	24	1292	1322	1310	1302	1321	1302	1302	1284	1303	1298	1285	1270	1232	1214	1220	1224	1230	1255	1254	1267	1268	1287	1312	1315	12779	24
268	25	1351	1337	1345	1355	1366	1376	1347	1344	1369	1356	1361	1355	1325	1303	1320	1307	1309	1332	1348	1326	1362	1405	1374	1378	13480	24
269	26	1379	1390	1389	1387	1374	1386	1369	1364	1368	1368	1373	1382	1390	1386	1371	1368	1382	1375	1400	1417	1459	1476	1452	1454	13941	24
270	27	1468	1460	1455	1441	1443	1407	1387	1398	1370	1362	1364	1360	1379	1386	1395	1412	1404	1420	1424	1421	1410	1383	1371	1375	14040	24
271	28	1371	1358	1369	1372	1350	1371	1353	1353	1333	1332	1346	1348	1355	1367	1340	1351	1360	1338	1357	1352	1357	1342	1326	1356	13524	24
272	29	1340	1326	1334	1351	1353	1352	1353	1356	1349	1355	1346	1346	1335	1338	1348	1352	1328	1329	1341	1337	1343	1343	1330	1316	13417	24
273	30	1311	1308	1287	1317	1325	1326	1346	1338	1335	1352	1329	1327	1355	1346	1351	1344	1362	1374	1358	1391	1389	1389	1371	1379	13463	24

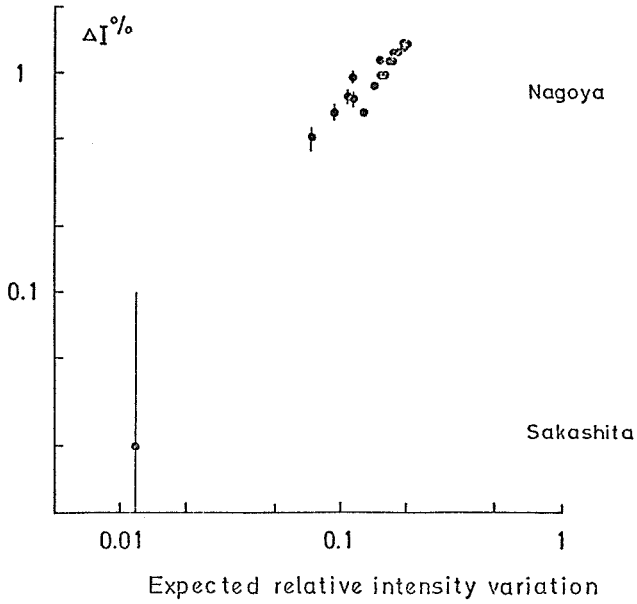

Fig. 2. Correlation between the amounts of cosmic ray intensity depression and those expected for the variational spectrum of power type with exponent of -1 and an upper cutoff rigidity of 100 GV.

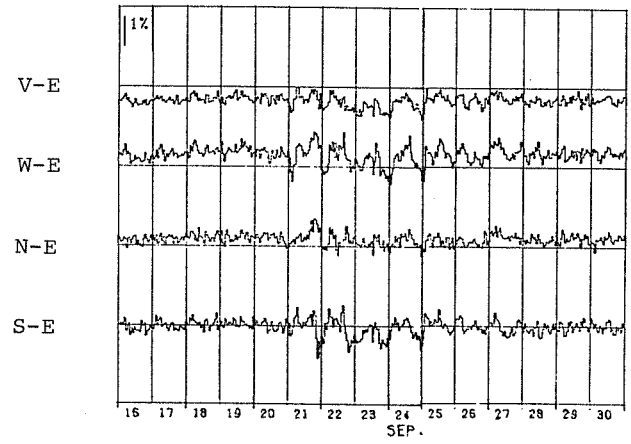

Fig. 3. Difference intensities between selected pairs of components, V-E = Vertical-30°East, W-E = 30°West-30°East, N-E = 30°North-30°East, S-E = 30°South-30°East, during September 16 to 30, 1977.

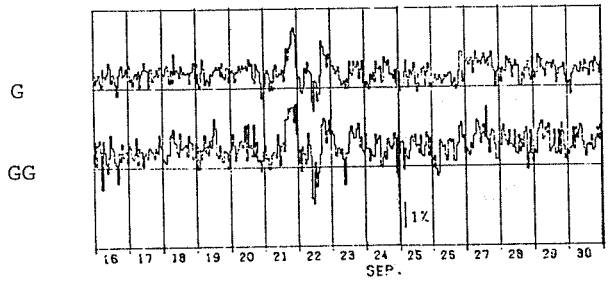

Fig. 4. Hourly values of north-south indices, G and and GG, derived from directional intensities of Nagoya multi-directional meson telescope during September 16 to 30, 1977.

AUTHOR INDEX

UAG SERIES OF REPORTS

Between 4 and 12 UAG Reports are published at irregular intervals each year. Subscriptions may be ordered through the National Geophysical and Solar-Terrestrial Data Center, Environmental Data and Information Service, NOAA, Boulder, CO 80303, USA. The subscription price for the calendar year only is $40.00 ($23.00 additional for foreign mailing). Each year the single copy prices total less than $40.00, the expiration date for all subscriptions will be extended. Back issues may be purchased at the prices shown below plus a $4.00 handling charge per order; some reports, though, are available only on microfiche. Orders must include check or money order payable in U.S. currency to the Department of Commerce, NOAA/NGSDC.

UAG-1 "IQSY Night Airglow Data," by L.L. Smith, F.E. Roach, and J.M. McKennan, ESSA Aeronomy Laboratory, Boulder, CO, July 1968, 305 pp, $1.75.

UAG-2 "A Reevaluation of Solar Flares, 1964-1966," by Helen W. Dodson and E. Ruth Hedeman, McMath-Hulbert Observatory, University of Michigan, Pontiac, MI, August 1968, 28 pp, $0.30.

UAG-3 "Observations of Jupiter's Sporadic Radio Emission in the Range 7.6-41 MHz, 6 July 1966 through 8 September 1968," by James W. Warwick and George A. Dulk, University of Colorado, Boulder, CO, October 1968, 35 pp, $0.55.

UAG-4 "Abbreviated Calendar Record 1966-1967," by J. Virginia Lincoln, Hope I. Leighton and Dorothy K. Kropp, ESSA now NOAA, Aeronomy and Space Data Center, Boulder, CO, January 1969, 170 pp, $1.25.

UAG-5 "Data on Solar Event of May 23, 1967 and its Geophysical Effects," compiled by J. Virginia Lincoln, World Data Center A, Upper Atmosphere Geophysics, ESSA now NOAA, Boulder, CO, February 1969, 120 pp, $0.65.

UAG-6 "International Geophysical Calendars 1957-1969," by A.H. Shapley and J. Virginia Lincoln, ESSA Research Laboratories, now NOAA, Boulder, CO, March 1969, 25 pp, $0.30.

UAG-7 "Observations of the Solar Electron Corona: February 1964 - January 1968," by Richard T. Hansen, High Altitude Observatory, NCAR, Boulder, CO, and Kamuela, HI, October 1969, 12 pp, $0.15.

UAG-8 "Data on Solar-Geophysical Activity October 24 - November 6, 1968," Parts 1 and 2, compiled by J. Virginia Lincoln, World Data Center A, Upper Atmosphere Geophysics, ESSA now NOAA, Boulder, CO, March 1970, 312 pp, $1.75 (includes Parts 1 and 2).

UAG-9 "Data on Cosmic Ray Event of November 18, 1968 and Associated Phenomena," compiled by J. Virginia Lincoln, World Data Center A, Upper Atmosphere Geophysics, ESSA now NOAA, Boulder, CO, April 1970, 109 pp, $0.55.

UAG-10 "Atlas of Ionograms," edited by A.H. Shapley, ESSA Research Laboratories now NOAA, Boulder, CO, May 1970, 243 pp, $1.50.

UAG-12 "Solar-Geophysical Activity Associated with the Major Geomagnetic Storm of March 8, 1970," Parts 1, 2 and 3, compiled by J. Virginia Lincoln and Dale B. Bucknam, World Data Center A, Upper Atmosphere Geophysics, ESSA now NOAA, Boulder, CO, April 1971, 466 pp, $3.00 (includes Parts 1-3).

UAG-13 "Data on the Solar Proton Event of November 2, 1969 through the Geomagnetic Storm of November 8-10, 1969," compiled by Dale B. Bucknam and J. Virginia Lincoln, World Data Center A, Upper Atmosphere Geophysics, ESSA now NOAA, Boulder, CO, May 1971, 76 pp, $0.90.

UAG-14 "An Experimental, Comprehensive Flare Index and Its Derivation for 'Major" Flares, 1955-1969," by Helen W. Dodson and E. Ruth Hedeman, McMath-Hulbert Observatory, University of Michigan, Pontiac, MI, July 1971, 25 pp, $0.30.

UAG-16 "Temporal Development of the Geophysical Distribution of Auroral Absorption for 30 Substorm Events in each of IQSY (1964-65) and IASY (1960)," by F.T. Berkey, University of Alaska, Fairbanks, AK; V.M. Driatskiy, Arctic and Antarctic Research Institute, Leningrad, USSR; K. Henriksen, Auroral Observatory, Tromson, Norway; D.H. Jelly, Communications Research Center, Ottawa, Canada; T.I. Shchuka, Arctic and Antarctic Research Institute, Leningrad, USSR; A. Theander, Kiruna Geophysical Observatory, Kiruna, Sweden; and J. Yliniemi, University of Oulu, Oulu, Finland, September 1971, 131 pp, $0.70 (microfiche only).

UAG-17 "Ionospheric Drift Velocity Measurements at Jicamarca, Peru (July 1967 - March 1970)," by Ben B. Balsley, NOAA Aeronomy Laboratory, Boulder, CO, and Ronald F. Woodman, Jicamarca Radar Observatory, Instituto Geofisico del Peru, Lima, Peru, October 1971, 45 pp, $0.55 (microfiche only).

UAG-18 "A Study of Polar Cap and Auroral Zone Magnetic Variations," by K. Kawasaki and S.-I. Asasofu, University of Alaska, Fairbanks, AK, June 1972, 21 pp, $0.20.

UAG-19 "Reevaluation of Solar Flares 1967," by Helen W. Dodson and E. Ruth Hedeman, McMath-Hulbert Observatory, University of Michigan, Pontiac, MI, and Marta Rovira de Miceli, San Miguel Observatory, Argentina, June 1972, 15 pp, $0.15.

UAG-21 "Preliminary Compilation of Data for Retrospective World Interval July 26 - August 14, 1972," by J. Virginia Lincoln and Hope I. Leighton, World Data Center A for Solar-Terrestrial Physics, NOAA, Boulder, CO, November 1972, 128 pp, $0.70.

UAG-22 "Auroral Electrojet Magnetic Activity Indices (AE) for 1970," by Joe Haskell Allen, National Geophysical and Solar-Terrestrial Data Center, Boulder, CO, November 1972, 146 pp, $0.75.

UAG-23 "U.R.S.I. Handbook of Ionogram Interpretation and Reduction," Second Edition, November 1972, edited by W.R. Piggott, Radio and Space Research Station, Slough, UK, and K. Rawer, Arbeitsgruppe fur Physikalische Weltraumforschung, Freiburg, GFR, November 1972, 324 pp, $1.75.

UAG-23A "U.R.S.I. Handbook of Ionogram Interpretation and Reduction," Second Edition, Revision of Chapters 1-4, edited by W.R. Piggott, Radio and Space Research Station, Slough, UK, and K. Rawer, Arbeitsgruppe fur Physikalische Weltraumforschung, Freiburg, GFR, November 1972, 135 pp, $2.14.

UAG-24 "Data on Solar-Geophysical Activity Associated with the Major Ground Level Cosmic Ray Events of 24 January and 1 September 1971," Parts 1 and 2, compiled by Helen E. Coffey and J. Virginia Lincoln, World Data Center A for Solar-Terrestrial Physics, NOAA, Boulder, CO, December 1972, 462 pp, $2.00 (includes Parts 1 and 2).

UAG-25 "Observations of Jupiter's Sporadic Radio Emission in the Range 7.6-41 MHz, 9 September 1968 through 9 December 1971," by James W. Warwick, George A. Dulk and David G. Swann, University of Colorado, Boulder, CO, February 1973, 35 pp, $0.35.

UAG-26 "Data Compilation for the Magnetospherically Quiet Periods February 19-23 and November 29 - December 3, 1970," compiled by Helen E. Coffey and J. Virginia Lincoln, World Data Center A for Solar-Terrestrial Physics, NOAA, Boulder, CO, May 1973, 129 pp, $0.70.

UAG-27 "High Speed Streams in the Solar Wind," by D.S. Intriligator, University of Southern California, Los Angeles, CA, June 1973, 16 pp, $0.15.

UAG-28 "Collected Data Reports on August 1972 Solar-Terrestrial Events," Parts 1, 2 and 3, edited by Helen E. Coffey, World Data Center A for Solar-Terrestrial Physics, NOAA, Boulder, CO, July 1973, 932 pp, $4.50.

UAG-29 "Auroral Electrojet Magnetic Activity Indices AE(11) for 1968," by Joe Haskell Allen, Carl C. Abston and Leslie D. Morris, National Geophysical and Solar-Terrestrial Data Center, Boulder, CO, October 1973, 148 pp, $0.75.

UAG-30 "Catalogue of Data on Solar-Terrestrial Physics," prepared by NOAA Environmental Data Service, Boulder, CO, October 1973, $1.50. Supersedes UAG-11, 15, and 20 catalogs.

UAG-31 "Auroral Electrojet Magnetic Activity Indices AE(11) for 1969," by Joe Haskell Allen, Carl C. Abston and Leslie D. Morris, National Geophysical and Solar-Terrestrial Data Center, Boulder, CO, February 1974, 142 pp, $0.75.

UAG-32 "Synoptic Radio Maps of the Sun at 3.3 mm for the Years 1967-1969," by Earle B. Mayfield, Kennon P. White III, and Fred I. Shimabukuro, Aerospace Corp., El Segundo, CA, April 1974, 26 pp, $0.35.

UAG-33 "Auroral Electrojet Magnetic Activity Indices AE(10) for 1967," by Joe Haskell Allen, Carl C. Abston and Leslie D. Morris, National Geophysical and Solar-Terrestrial Data Center, Boulder, CO, May 1974, 142 pp, $0.75.

UAG-34 "Absorption Data for the IGY/IGC and IQSY," compiled and edited by A.H. Shapley, National Geophysical and Solar-Terrestrial Data Center, Boulder, CO; W.R. Piggott, Appleton Laboratory, Slough, UK; and K. Rawer, Arbeitsgruppe fur Physikalische Weltraumforschung, Freiburg, GFR, June 1974, 381 pp, $2.00.

UAG-35 "Catalogue of Digital Geomagnetic Variation Data at World Data Center A for Solar-Terrestrial Physics," prepared by NOAA Environmental Data Service, Boulder, CO, July 1974, 20 pp, $0.20.

UAG-36 "An Atlas of Extreme Ultraviolet Flashes of Solar Flares Observed via Sudden Frequency Deviations During the ATM-SKYLAB Missions," by R.F. Donnelly and E.L. Berger, NOAA Space Environment Laboratory; Lt. J.D. Busman, NOAA Commissioned Corps; B. Henson, NASA Marshall Space Flight Center; T.B. Jones, University of Leicester, UK; G.M. Lerfald, NOAA Wave Propagation Laboratory; K. Najita, University of Hawaii; W.M. Retallack, NOAA Space Environment Laboratory and W.J. Wagner, Sacramento Peak Observatory, October 1974, 95 pp, $0.55.

UAG-37 "Auroral Electrojet Magnetic Activity Indices AE(10) for 1966," by Joe Haskell Allen, Carl C. Abston and Leslie D. Morris, National Geophysical and Solar-Terrestrial Data Center, Boulder, CO, December 1974, 142 pp, $0.75.

UAG-38 "Master Station List for Solar-Terrestrial Physics Data at WDC-A for Solar-Terrestrial Physics," by R.W. Buhmann, World Data Center A for Solar-Terrestrial Physics, Boulder, CO; Juan D. Roederer, University of Denver, Denver, CO; and M.A. Shea and D.F. Smart, Air Force Cambridge Research Laboratories, Hanscom AFB, MA, December 1974, 110 pp, $1.60.

UAG-39 "Auroral Electrojet Magnetic Activity Indices AE(11) for 1971," by Joe Haskell Allen, Carl C. Abston and Leslie D. Morris, National Geophysical and Solar-Terrestrial Data Center, Boulder, CO, February 1975, 144 pp, $2.05.

UAG-40 "H-Alpha Synoptic Charts of Solar Activity for the Period of Skylab Observations, May 1973 - March 1974," by Patrick S. McIntosh, NOAA Space Environment Laboratory, Boulder, CO, February 1975, 32 pp, $0.56.

UAG-41 "H-Alpha Synoptic Charts of Solar Activity During the First Year of Solar Cycle 20 October 1964 - August 1965," by Patrick S. McIntosh, NOAA Space Environment Laboratory, Boulder, CO and Jerome T. Nolte, American Science and Engineering, Inc., Cambridge, MA, March 1975, 25 pp, $0.48.

UAG-42 "Observations of Jupiter's Sporadic Radio Emission in the Range 7.6-80 MHz, 10 December 1971 through 21 March 1975," by James W. Warwick, George A. Dulk and Anthony C. Riddle, University of Colorado, Boulder, CO, April 1975, 49 pp, $1.15.

UAG-43 "Catalog of Observation Times of Ground-Based Skylab-Coordinated Solar Observing Programs," compiled by Helen E. Coffey, World Data Center A for Solar-Terrestrial Physics, NOAA, Boulder, CO, May 1975, 159 pp, $3.00.

UAG-44 "Synoptic Maps of Solar 9.1 cm Microwave Emission from June 1962 to August 1973," by Werner Graf and Ronald N. Bracewell, Stanford University, Stanford, CA, May 1975, 183 pp, $2.55.

UAG-45 "Auroral Electrojet Magnetic Activity Indices AE(11) for 1972," by Joe Haskell Allen, Carl C. Abston and Leslie D. Morris, National Geophysical and Solar-Terrestrial Data Center, Boulder, CO, May 1975, 144 pp, $2.10 (microfiche only).

UAG-46 "Interplanetary Magnetic Field Data 1963-1964," by Joseph H. King, National Space Science Data Center, NASA Goddard Space Flight Center, Greenbelt, MD, June 1975, 382 pp, $1.95.

UAG-47 "Auroral Electrojet Magnetic Activity Indices AE(11) for 1973," by Joe Haskell Allen, Carl C. Abston and Leslie D. Morris, National Geophysical and Solar-Terrestrial Data Center, Boulder, CO, June 1975, 144 pp, $2.10 (microfiche only).

UAG-48A "Synoptic Observations of the Solar Corona during Carrington Rotations 1580-1596 (11 October 1971 - 15 January 1973)," [Reissue of UAG-48 with quality images], by R.A. Howard, M.J. Koomen, D.J. Michels, R. Tousey, C.R. Detwiler, D.E. Roberts, R.T. Seal, and J.D. Whitney, U.S. Naval Research Laboratory, Washington, DC, and R.T. Hansen and S.F. Hansen, C.J. Garcia and E. Yasukawa, High Altitude Observatory, NCAR, Boulder, CO, February 1976, 200 pp, $4.27.

UAG-49 "Catalog of Standard Geomagnetic Variation Data," prepared by NOAA Environmental Data Service, Boulder, CO, August 1975, 125 pp, $1.85.

UAG-50 "High-Latitude Supplement to the URSI Handbook on Ionogram Interpretation and Rediction," edited by W.R. Piggott, British Antarctic Survey, c/o Appleton Laboratory, Slough, UK, October 1975, 294 pp, $4.00.

UAG-51 "Synoptic Maps of Solar Coronal Hole Boundaries Derived from He II 304A Spectroheliograms from the Manned Skylab Missions," by J.D. Bohlin and D.M. Rubenstein, U.S. Naval Research Laboratory, Washington, DC, November 1975, 30 pp, $0.54.

UAG-52 "Experimental Comprehensive Solar Flare Indices for Certain Flares, 1970-1974," by Helen W. Dodson and E. Ruth Hedeman, McMath-Hulbert Observatory, University of Michigan Pontiac, MI, November 1975, 27 pp, $0.60.

UAG-53 "Description and Catalog of Ionospheric F-Region Data, Jicamarca Radio Observatory (November 1966 - April 1969), by W.L. Clark and T.E. Van Zandt, NOAA Aeronomy Laboratory, Boulder, CO, and J.P. McClure, University of Texas as Dallas, Dallas, TX, April 1976, 10 pp, $0.33.

UAG-54 "Catalog of Ionosphere Vertical Soundings Data," prepared by NOAA Environmental Data Service, Boulder, CO, April 1976, 130 pp, $2.10.

UAG-55 "Equivalent Ionospheric Current Representations by a New Method, Illustrated for 8-9 November 1969 Magnetic Disturbances," by Y. Kamide, Cooperative Institute for Research in Environmental Sciences, University of Colorado, Boulder, CO; H.W. Kroehl, Data Studies Division, National Geophysical and Solar-Terrestrial Data Center, Boulder, CO; M. Kanamitsu, Advanced Study Program, National Center for Atmospheric Research, Boulder, CO; Joe Haskell Allen, Data Studies Division, National Geophysical and Solar-Terrestrial Data Center, Boulder, CO; and S.-I Akasofu, Geophysical Institute, University of Alaska, Fairbanks, AK, April 1976, 91 pp, $1.60 (microfiche only).

UAG-56 "Iso-intensity Contours of Ground Magnetic H Perturbations for the December 16-18, 1971, Geomagnetic Storm," Y. Kamide, Cooperative Institute for Research in Environmental Sciences, University of Colorado, Boulder, CO, April 1976, 37 pp, $1.39.

UAG-57 "Manual on Ionospheric Absorption Measurements," edited by K. Rawer, Institut fur Physikalische Weltraumforschung, Freiburg, GFR, June 1976, 302 pp, $4.27.

UAG-58 "ATS6 Radio Beacon Electron Content Measurements at Boulder, July 1974 - May 1975," by R.B. Fritz, NOAA Space Environment Laboratory, Boulder, CO, September 1976, 61 pp, $1.04.

UAG-59 "Auroral Electrojet Magnetic Activity Indices AE(11) for 1974," by Joe Haskell Allen, Carl C. Abston and Leslie D. Morris, National Geophysical and Solar-Terrestrial Data Center, Boulder, CO, December 1976, 144 pp, $2.16.

UAG-60 "Geomagnetic Data for January 1976 (AE(7) Indices and Stacked Magnetograms)," by Joe Haskell Allen, Carl C. Abston and Leslie D. Morris, National Geophysical and Solar-Terrestrial Data Center, Boulder, CO, July 1977, 57 pp, $1.07.

UAG-61 "Collected Data Reports for STIP Interval II 20 March - 5 May 1976, edited by Helen E. Coffey and John A. McKinnon, World Data Center A for Solar-Terrestrial Physics, Boulder, CO, August 1977, 313 pp, $2.95.

UAG-62 "Geomagnetic Data for February 1976 (AE(7) Indices and Stacked Magnetograms)," by Joe Haskell Allen, Carl C. Abston and Leslie D. Morris, National Geophysical and Solar-Terrestrial Data Center, Boulder, CO, September 1977, 55 pp, $1.11.

UAG-63 "Geomagnetic Data for March 1976 (AE(7) Indices and Stacked Magnetograms)," by Joe Haskell Allen, Carl C. Abston and Leslie D. Morris, National Geophysical and Solar-Terrestrial Data Center, Boulder, CO, September 1977, 57 pp, $1.11.

UAG-64 "Geomagnetic Data for April 1976 (AE(8) Indices and Stacked Magnetograms)," by Joe Haskell Allen, Carl C. Abston and Leslie D. Morris, National Geophysical and Solar-Terrestrial Data Center, Boulder, CO, February 1978, 55 pp, $1.00.

UAG-65 "The Information Explosion and Its Consequences for Data Acquisition, Documentation, Processing," by G.K. Hartmann, Max-Planck-Institut fur Aeronomie, Lindau, GFR, May 1978, 36 pp, $0.75.

UAG-66 "Synoptic Radio Maps of the Sun at 3.3 mm 1970-1973," by Earle B. Mayfield and Fred I. Shimabukuro, Aerospace Corp., El Segundo, CA, May 1978, 30 pp, $0.75.

UAG-67 "Ionospheric D-Region Profile Data Base, A Collection of Computer-Accessible Experimental Profiles of the D and Lower E Regions," by L.F. McNamara, Ionospheric Prediction Service, Sydney, Australia, August 1978, 30 pp, $0.88 (microfiche only).

UAG-68 "A Comparative Study of Methods of Electron Density Profile Analysis," by L.F. McNamara, Ionospheric Prediction Service, Sydney, Australia, August 1978, 30 pp, $0.88 (microfiche only).

UAG-69 "Selected Disturbed D-Region Electron Density Profiles. Their relation to the undisturbed D region," by L.F. McNamara, Ionospheric Prediction Service, Sydney, Australia, October 1978, 50 pp, $1.29 (microfiche only).

UAG-70 "Annotated Atlas of the H-alpha Synoptic Charts for Solar Cycle 20 (1964-1974) Carrington Solar Rotations 1487-1616," by Patrick S. McIntosh, NOAA Space Environment Laboratory, Boulder, CO, February 1979, 327 pp, $3.50.

UAG-71 "Magnetic Potential Plots over the Northern Hemisphere for 26-28 March 1976," A.D. Richmond, NOAA Space Environment Laboratory, Boulder, CO; H.W. Kroehl, National Geophysical and Solar-Terrestrial Data Center, Boulder, CO; M.A. Henning, Lockheed Missils and Space Co., Aurora, CO; and Y. Kamide, Kyoto Sangyo University, Kyoto, Japan, April 1979, 118 pp, $1.50.

UAG-72 "Energy Release in Solar Flares, Proceedings of the Workshop on Energy Release in Flares, 26 February - 1 March 1979, Cambridge, Massachusetts, U.S.A.," edited by David M. Rust, American Science and Engineering, Inc., Cambridge, MA, and A. Gordon Emslie, Harvard-Smithsonian Center for Astrophysics, Cambridge, MA, July 1979, 68 pp, $1.50 (microfiche only).

UAG-73 "Auroral Electrojet Magnetic Activity Indices AE(11-12) for January - June 1975," by Joe Haskell Allen, Carl C. Abston, J.E. Salazar and J.A. McKinnon, National Geophysical and Solar-Terrestrial Data Center, NOAA, Boulder, CO, August 1979, 114 pp, $1.75.

UAG-74 "ATS-6 Radio Beacon Electron Content Measurements at Ootacamund, India, October - July 1976," by S.D. Bouwer, K. Davies, R.F. Donnelly, R.N. Grubb, J.E. Jones and J.H. Taylor, NOAA Space Environment Laboratory, Boulder, CO, and R.G. Rastogi, M.R. Deshpande, H. Chandra and G. Sethia, Physical Research Laboratory, Ahmedabad, India, March 1980, 58 pp, $2.50.

UAG-75 "The Alaska IMS Meridian Chain: Magnetic Variations for 9 March - 27 April 1978," by H.W. Kroehl and G.P. Kosinski, National Geophysical and Solar-Terrestrial Data Center, Boulder, CO; S.-I Akasofu, G.J. Romick, C.E. Campbell and G.K. Corrick, University of Alaska, Fairbanks, AK; and C.E. Hornback and A.M. Gray, NOAA Space Environment Laboratory, Boulder, CO, June 1980, 107 pp, $3.00.

UAG-76 "Auroral Electrojet Magnetic Activity Indices AE(12) for July - December 1975," by Joe Haskell Allen, Carl C. Abston, J.E. Salazar and J.A. McKinnon, National Geophysical and Solar-Terrestrial Data Center, NOAA, Boulder, CO, August 1980, 116 pp, $2.50.

UAG-77 "Synoptic Solar Magnetic Field Maps for the Interval Including Carrington Rotations 1601-1680, May 5, 1973 - April 26, 1979," by J. Harvey, B. Gillespie, P. Miedaner and C. Slaughter, Kitt Peak National Observatory, Tucson, AZ, August 1980, 66 pp, $2.50.

UAG-78 "The Equatorial Latitude of Auroral Activity During 1972-1977," by N.R. Sheeley, Jr. and R.A. Howard, E. O. Hulbert Center for Space Research, U.S. Naval Research Laboratory, Washington, DC and B.S. Dandekar, Air Force Geophysics Laboratory, Hanscom AFB, MA, October 1980, 61 pp, $3.00.

UAG-79 "Solar Observations During Skylab, April 1973 - February 1974, I. Coronal X-Ray Structure, II. Solar Flare Activity," by J.M. Hanson, University of Michigan, Ann Arbor, MI; and E.C. Roelof and R.E. Gold, The Johns Hopkins University, Laurel, MD, December 1980, 43 pp, $2.50.

UAG-80 "Experimental Comprehensive Solar Flare Indices for 'Major' and Certain Lesser Flares, 1975-1979," compiled by Helen W. Dodson and E. Ruth Hedeman, The Johns Hopkins University, Laurel, MD, July 1981, 33 pp, $2.00.

UAG-81 "Evolutionary Charts of Solar Activity (Calcium Plages) as Functions of Heliographic Longitude and Time, 1964-1979," by E. Ruth Hedeman, Helen W. Dodson and Edmond C. Roelof, The Johns Hopkins University, Laurel, MD 20707, August 1981, 103 pp, $4.00.

UAG-82 "International Reference Ionosphere - IRI 79," edited by J. Virginia Lincoln and Raymond O. Conkright, National Geophysical and Solar-Terrestrial Data Center, NOAA, Boulder, CO, November 1981, 243 pp, $4.50.

UAG-83 "Solar-Geophysical Activity Reports for September 7-24, 1977 and November 22, 1977," Parts 1 and 2, compiled by John A. McKinnon and J. Virginia Lincoln, World Data Center A for Solar-Terrestrial Physics, NOAA, Boulder, CO, February 1982, 553 pp, $10.00.